University of Southampton

Faculty of Engineering and Physical Sciences

School of Chemistry

NOVEL HYBRID REACTIVATORS OF ACETYLCHOLINESTERASES INHIBITED BY ORGANOPHOSPHORUS CHEMICAL WARFARE AGENTS

by

Alexander John Maryan-Instone

Thesis for the degree of Doctor of Philosophy in Chemistry

April 2019

Abstract

Since their development as pesticides in the 1930s, organophosphorus nerve agents (OPNA) have been weaponised and declared weapons of mass destruction. Their production and stockpiling have been forbidden since 1992, however their presence persists and they have since been employed in several acts of terror. OPNA poisoning also continues to claim lives globally through the use of the agents in the agrochemical sector of developing countries. OPNA poisoning proceeds *via* the irreversible inhibition of the human acetylcholinesterase (*h*AChE) enzyme, a key biomolecule found ubiquitously within the body, responsible for nerve impulse propagation.

This research addresses the current unmet need for universal remediation for OPNA inhibited *h*AChE and shortcomings of existing antidotes. We describe the development of 'hybrid reactivators' that incorporate a peripheral site ligand (PSL) and a reactivator component. The PSL offers initial binding on the surface of AChE, in close proximity to the inhibited active site; found buried within the enzyme. The reactivator, bearing a highly nucleophillic functionality is then able to pass down towards the inhibited active site where it is able to remove the nerve agent, reactivating the enzyme.

Nineteen novel hybrid reactivators based on the quinoline, theobromine, naphthalene and benzylpiperazine PSL scaffold were designed, synthesised and evaluated against sarin, VX, tabun and paraoxon-inhibited human acetylcholinesterase. A simplified, dehydroxylated pyridine aldoxime reactivator functionality was explored and a novel *in silico* evaluation assay was developed. A streamlined synthesis has been established towards the development of these compounds, which is able to deliver much larger amounts for biological studies. We have been able to develop a better understanding of structure-activity relationships of novel hybrid reactivators and are now equipped with a computational model for assessing potential new structures without necessitating arduous synthetic efforts.

Table of Contents

Declaration of Authorship

Print name:	ALEXANDER JOHN MARYAN-INSTONE

Title of thesis:	Novel Hybrid Reactivators of Acetylcholinesterases Inhibited by Organophosphorus Chemical Warfare Agents

I declare that this thesis and the work presented in it are my own and has been generated by me as the result of my own original research.

I confirm that:

1. This work was done wholly or mainly while in candidature for a research degree at this University;
2. Where any part of this thesis has previously been submitted for a degree or any other qualification at this University or any other institution, this has been clearly stated;
3. Where I have consulted the published work of others, this is always clearly attributed;
4. Where I have quoted from the work of others, the source is always given. With the exception of such quotations, this thesis is entirely my own work;
5. I have acknowledged all main sources of help;
6. Where the thesis is based on work done by myself jointly with others, I have made clear exactly what was done by others and what I have contributed myself;
7. Parts of this work have been published as:

A. J. Maryan-Instone, R. C. D. Brown, R. Baati, J. Dias, Y. Jagadeesh, EU. Pat., 1930585.1, 2019 (Patent deposited)

Signature:		Date:	30/04/2019

Acknowledgements

Firstly, I would like to thank my supervisors, Professor Richard Brown and Dr Rachid Baati. I am incredibly grateful and honoured to have had the opportunity to undertake this research under your supervision. I am confident that this experience has made me a strong and confident chemist and that is no doubt a testament to your excellent supervision and support. Thank you Richard for putting up with my strops when reactions failed and for always being a level-headed presence! Rachid, I thank you for you continued confidence and trust in me throughout this research – and for all the wonderful trips to Strasbourg.

I would also like to extend my huge gratitude to Dstl (British Defence Science and Technology Laboratories) and DGA (French Direction Générale de l'Armement) for funding this research and offering incredible conferences in amazing places.

Next, I would like to thank all members of the Brown group, past and present. Rob Green, thank you for being around towards the start of my PhD and showing me the ropes. Katie Jolley, your expertise and experience have been so valuable during my time in the group. Thank you for always being around to help out and make everything so much more bearable – especially when my reactions were not working, at all. Alex Leeder, thanks for letting me be sassy. Lynda, you have always been such a great support and provided hours of entertaining chats during long and boring columns! Thank you to everyone for making the lab a fun place to work.

Enormous thanks go to Mabel Wong of the Essex group at the University of Southampton, thank you so much for all your patience and hard work during the development of the computational chemistry model. You're such a hard worker and I wish you all the best. Extended thanks go to the rest of the Essex group and Professor Jon Essex for agreeing to offer assistance in the computational part of this work.

To all academic and technical staff at the University of Southampton, I would like to express my gratitude. Julie Herniman and Dr Neil Wells for all of your help and hard work with MS and NMR.

From the other side of the Channel, I would like to thank Dr José Dias and all of the team under the supervision of Dr Florian Nachon at IRBA. Thank you for extending your kindness and adopting me into the IRBA team. Dr Guilhelm Calas for his hard work with *in vivo* studies. Professor Marie-Pierre Dehouck and Dr Caroline Coisne for their very useful blood brain barrier permeability studies.

No real combination of lovely words can truly express my enormous appreciation for my amazing parents Fiona and Adam. I can't tell you both how wonderful you are and how much I have always appreciated your endless love and support. Mum, thank you for talking to me on the phone at least two times every day – some days it was the only thing I was looking forward to (that's when the

chemistry was not on my side!) and for your understanding when I just wanted to be left alone. Ads, thank you for always being true to yourself and giving incredible advice. To my brother, Ben, you will always be an amazing person and your hard work and perseverance is nothing short of incredible. Thank you for being there for me.

To Jack, you're my rock. Thank you for being there for me no matter what. I am not sure I would be in this position today, writing this thesis, if it were not for you. The times I wasn't sure I could do this were only ever fleeting with your continued love and encouragement. I loved the memories we made in Southampton and I can't wait to make more with you.

Finally, I would like to dedicate this work to my father Richard Maryan. Although our time together was short, it's undeniable that you taught me everything I needed to know to become a kind, brave and strong man.

Abbreviations

Ac	Acetyl
ACh	Acetylcholine
AChE	Acetylcholinesterase
ADDP	1,1'-(Azodicarbonyl)dipiperidine
API	Active pharmaceutical ingredient
aq.	Aqueous
Ar	Aryl
atm	Atmosphere
BBB	Blood brain barrier
BChE	Butyrylcholinesterase
BINAP	2,2'-Bis(diphenylphosphino)-1,1'-binapthyl
Bn	Benzyl
Boc	*tert*-Butoxycarbonyl
br.	Broad
^{n}Bu	*n*-Butyl
^{t}Bu	*tert*-Butyl
Bz	Benzoyl
CAS	Catalytic active site
Cbz	Benzyloxycarbonyl
cf.	*Conferatur*, compared to
ChE	Cholinesterase(s)
CNS	Central nervous system
CWA	Chemical warfare agent(s)
dba	Dibenzylidineacetone
d	Doublet
dd	Double doublet
ddd	Doublet of doublet of doublets
dt	Doublet of triplets
DIAD	Diisopropyl azidodicarboxylate
DIBAL-H	Diisobutyl aluminium hydride
DIPEA	Diisopropylethylamine
DGA	Direction Générale de l'Armement (France)
DMAP	4-Dimethylaminopyridine
DMF	Dimethylformamide

DMSO	Dimethylsulfoxide
dppf	1,1'-Bis(diphenylphosphino)ferrocene
Dstl	Defence Science and Technology Laboratory (UK)
equiv.	Equivalents
ESI^+	Electrospray ionisation (positive ion)
ESP	Electrostatic potential
Et	Ethyl
FCC	Flash column chromatography
FF	Force field
Glu	Glutamic acid
*h*AChE	*Human* Acetylcholinesterase
His	Histidine
HRMS	High resolution mass spectrometry
IC_{50}	Half maximal inhibitory concentration
IPA	Isopropyl alcohol
IR	Infrared
IRBA	Institut de Recherche Biomédicale des Armées (France)
J	Coupling constant
K_D	Dissociation constant
k_r	Reactivation rate constant
k_{r2}	Second-order rate constant
L	Litre(s)
LRMS	Low resolution mass spectrometry
m (IR)	Medium
m (NMR)	Multiplet
m	*meta*
M	Molar
MD	Molecular dynamics
Me	Methyl
MHz	Megahertz
min	Minute(s)
mol	Mole(s)
MPt	Melting point
MS	Molecular sieves
Ms	Methanesulfonyl
MWt	Molecular weight
NEDPA	4-Nitrophenylethyldimethylphosphoramidate

NMR	Nuclear magnetic resonance
o	*ortho*
OP	Organophosphorus
OPNA	Organophosphorus nerve agent(s)
p	*para*
PAS	Peripheral anionic site
PD	Pharmacodynamics
pdb	Protein data bank
Ph	Phenyl
Piz	Piperazine
PK	Pharmacokinetics
pK_a	Acid dissociation constant
PMB	*para*-methoxybenzyl
ppm	Parts per million
Pr	Propyl
PSL	Peripheral site ligand
q	Quartet
QM	Quantum mechanics
quin	Quintet
RESP	Restrained electrostatic potential
RMSD	Root mean squared deviation
RMSF	Root mean squared fluctuation
R_f	Retardation factor
rt	Room temperature
s (IR)	Strong
s (NMR)	Singlet
SAR	Structure-activity relationship(s)
sept	Septet
Ser	Serine
S_N	Nucleophillic substitution
S_NAr	Nucleophillic aromatic substitution
sat.	Saturated
sext	Sextet
t	Triplet
td	Triplet of doublets
tert/*t*	Tertiary
T	Temperature

TBAHS	*Tert*-butylammonium hydrogen sulfate
TBS	*Tert*-butyldimethylsilyl
*Tc*AChE	*Torpedo Californica* acetylcholinesterase
Tf	Trifluoromethanesulfonyl
THF	Tetrahydrofuran
TIPS	Triisopropylsilyl
TLC	Thin layer
TMS	Tetramethylsilane
Tol	*p*-Toluene
Ts	*p*-Toluenesulfonyl
UV	Ultraviolet
w (IR)	Weak
WW (I, II)	World War (I, II)
Å	Angstrom
∂	Chemical shift
µ	Micro
µW	Microwave
λ	Wavelength(s)

Chapter 1 Introduction

This chapter will introduce the history of chemical weapons, specifically the organophosphorus nerve agents, including their initial development as pesticides to their later weaponisation. Subsequent sections of this chapter will focus on the enzyme, acetylcholinesterase, the biological target of these nerve agents. The enzyme's structure and intended function will be discussed before the effects of organophosphorus nerve agent inhibition of this target are explained, including the mechanism and physiological effects. Focus will then be placed upon the history of the development of antidotes, or so-called "reactivators" of organophosphorus nerve agent-inhibited acetylcholinesterase. The mechanism and enzyme kinetics of reactivation will be explored, followed by the range of shortcomings experienced by currently available treatments. Finally, this research will be introduced with an overview of the "hybrid reactivator", a structural scaffold for novel antidotes, able to offer superior protection against the effects of organophosphorus nerve agents.

1.1 The History of the Use of Chemical Weapons

Chemical weapons (CW) were first employed extensively during the World War I (WWI), when in 1915, German industrial chemists at Ypres in Belgium began to develop new methods for the incapacitation, demoralisation and destruction of their enemies on the Western Front. Their research led to campaigns by many nations to devise new, more effective poisons. Between WWI and the Second World War (WWII), much research and development was undertaken towards new candidates and an entire arsenal of chemical compounds were in the hands of the world militaries for use in combat. Among this arsenal were the organophosphorus nerve agents (OPNA).

1.1.1 Early Development of Organophosphorus Compounds: Pesticides

Organophosphorus (OP) compounds have become ubiquitous within the agrochemical industry since their original discovery in 1848 by Franz Anton Voegeli. Following the hypothesis of the existence of phosphoric acid monoethyl ester (**1.1**) by Jean Louis Lassainge[1] in 1820 and its subsequent synthesis by Jules Pelouze[2] in 1833, Voegeli became the first chemist to synthesise triethyl phosphate (TEP, **1.2**).[3]

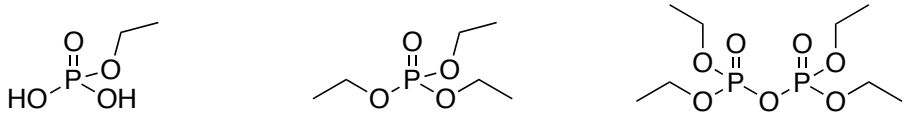

1.1 **1.2** **1.3**

Figure 1.1. Chemical structures of phosphoric acid monoethyl ester (**1.1**), triethyl phosphate (TEP) (**1.2**) and tetraethyl pyrophosphate (TEPP) (**1.3**)

Shortly after this, in 1854, Phillipe de Clermont reported the synthesis of tetraethyl pyrophosphate (**1.3**, TEPP), the first documented OPNA to exhibit anticholinesterase behaviour.[4] It wasn't until 1932 that the toxic properties of these OP compounds became apparent. German industrial chemists, Willy Lange and Gerda Von Krueger, inadvertently exposed themselves to phosphorus esters and experienced some unpleasant toxic effects.[5] They noted difficulty in breathing, photophobia and disturbance to their consciousness after exposure to very small amounts of monofluoroorganophosphate esters.

Following this discovery a chemist at IG Farben, Gerhardt Schrader was enlisted to incorporate organophosphates into a campaign towards more efficient pesticides in an effort towards tackling global hunger.[6] Schrader noted that TEPP could be used as an insecticide since it exhibited the same toxic characteristics experienced by Lange and Von Krueger. In 1944, TEPP became the first commercialised OP insecticide. Schrader's research also led him to the discovery of parathion (**1.4**), which upon metabolism in animals, is converted into paraoxon (**1.5**), which shows extremely high toxicity in insects and animals.[7]

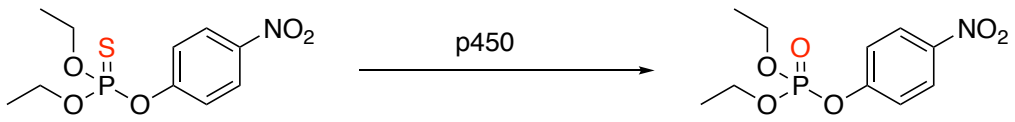

1.4 **1.5**

Scheme 1.1. Metabolic pathway of parathion (**1.4**) to paraoxon (**1.5**), catalysed by cytochrome p450 (cyp450)

Today, parathion is still employed as a pesticide within the agrochemical industry, particularly in developing countries, where agriculture represents a large proportion of gross national product (GNP).[8] Since the invention of parathion, a range of OP pesticides have been developed. There are 76 current commercial OP pesticides, which are comprised of 58 insecticides, 16 herbicides, fungicides and nematicides and two plant growth regulators.[9] The use of OP pesticides is linked to a remarkable number of human poisonings, as demonstrated below in Table 1.1.

Table 1.1. Examples of poisonings from parathion

Country	Year	Poisoned Commodity	Individuals Poisoned	Individuals Killed
India[10]	1958	Wheat	360	102
Colombia[11]	1967	Flour	600	88
Mexico[12]	1968	Sugar	300	17
Egypt[13]	1958	Flour	200	8

The World Health Organisation (WHO) estimate around three million acute intoxications by OPNA and approximately 300,000 deaths annually (2018).[14] Of the three million, suicidal, intentional and accidental poisonings are accounted for, the latter arising predominantly from pesticides employed within the agrochemical sector.[15]

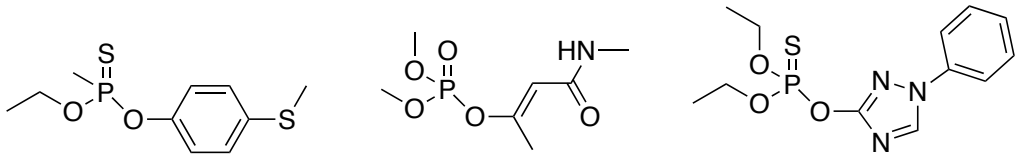

1.6 **1.7** **1.8**

Figure 1.2. Structures of other popular OP pesticides; BAY 29952 (**1.6**); monocrotophos (**1.7**) and triazophos (**1.8**)

1.1.2 Development of OP Pesticides into Chemical Warfare Agents

The expression "chemical warfare agent" (CWA) is an umbrella term for a spectrum of chemical agents that seek to cause harm by exploiting their toxic properties. CWAs are often categorised according to their effect and include the following:[16]

1.1.2.1 Riot Control Agents

These CWAs are irritants and are only lethal in very high concentrations. These agents are designed to incapacitate humans without causing lasting damage. Examples of these agents are lachrymators (tear gas) such as bromobenzyl cyanide (**1.9**) and chloroacetophenone (**1.10**), which irritate the eyes and skin.

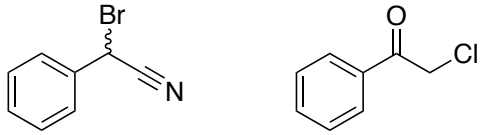

1.9 **1.10**

Figure 1.3. Examples of riot control agents, bromobenzyl cyanide (**1.9**) and chloroacetophenone (**1.10**)

1.1.2.2 Choking Gases

Choking gases, such as phosgene (**1.11**) and diphosgene (**1.12**), are designed to irritate the lower respiratory tract. Unlike the aforementioned riot control agents, choking gases work to destroy the membranes of the respiratory system. This can result in infection of the lungs (pneumonia) or in extreme cases, death by asphyxiation due to poor oxygen uptake as a result of damage to the lungs.

1.11 **1.12**

Figure 1.4. Examples of choking gases, phosgene (**1.11**) and diphosgene (**1.12**)

1.1.2.3 Blood Gases

These agents are principally absorbed by inhalation. Once they have been inhaled, they rapidly enter the bloodstream, where they interfere with oxygen exchange processes within the blood. This results in inefficient oxygen transfer, leading to cell death due to oxygen starvation. The blood gases, for example cyanogen chloride (**1.13**) and hydrogen cyanide (**1.14**), cause death incredibly rapidly by acute oxygen starvation.

1.13 **1.14**

Figure 1.5. Examples of blood agents, cyanogen chloride (**1.13**) and hydrogen cyanide (**1.14**)

1.1.2.4 Blister Agents

Blister agents are extremely irritating chemicals, such as Lewisite (**1.15**) and mustard gas (**1.16**), which are designed to inflict damage to the skin and eyes, resulting in painful blistering through which the agents can enter the bloodstream. These agents also target the eyes, which can lead to conjunctivitis and severe corneal damage.

1.15 **1.16**

Figure 1.6. Examples of blister agents, Lewisite (**1.15**) and mustard gas (**1.16**)

1.1.2.5 Vomiting Agents

Vomiting agents attack the alimentary canal, irritate eyes and nose mucous membranes leading to vomiting. Examples include diphenylchloroarsine (**1.17**) and diphenylcyanoarsine (**1.18**), which act as violent vomiting agents.

1.17 **1.18**

Figure 1.7. Examples of vomiting agents, diphenylchloroarsine (**1.17**) and diphenylcyanoarsine (**1.18**)

1.1.2.6 Nerve Agents

Nerve agents attack the human acetylcholinesterase (*h*AChE) enzyme. They block the enzyme, which results in the arrest of skeletal muscle and in severe cases leads to death by asphyxia due to the paralysis of respiratory muscles, such as the diaphragm.

During Dr Gerhard Schrader's research towards novel OP pesticides, the Nazi government tasked him with the development of OP-containing chemical weapons, more specifically, nerve agents. In 1937,[17] the first OPNA designed specifically as a chemical weapon was synthesised. Tabun (**1.19**) was discovered and shorty after, in 1938, sarin (**1.20**) was synthesised. These discoveries were punctuated with the formulation of soman (**1.21**) and cyclosarin (**1.22**) in 1944[18] and 1949[19] respectively.

1.19 **1.20** **1.21** **1.22**

Figure 1.8. The German Agents; tabun (**1.19**), sarin (**1.20**), soman (**1.21**) and cyclosarin (**1.22**)

These compounds comprised the "G" (German) agent family. This group of OP neurotoxins had similar characteristics, and were all obtained as colourless, volatile liquids, resulting in non-persisting behaviour but heightened risk of inhalation.

Table 1.2. Lethal doses of the G agents in 50% of the population (LD_{50}) and LCt_{50} (a measurement for mean dose, causing incapacitation from exposure) in rats. Data for cyclosarin was not available (Source: Federation of American Scientists)[20,21]

G Agent	LD_{50} (skin) / mg	LD_{50} (oral) / mg/kg	LCt_{50} (inhalation) / mg min m^{-3}
tabun	4000	3.6	70
sarin	1700	0.7	35
soman	300	0.4	35
cyclosarin	30	*n.a.*	*n.a.*

Following WWII, OPNAs became of interest amongst industrial research chemists around the world. The next notable agent was developed in Great Britain, and began a new generation of nerve agents, termed the "V" (vesicant) Agents. VX was synthesised in 1953 by Ranajit Ghosh at ICI, during research towards more effective OP-containing pesticides.[22] VX displays a much higher viscosity and lower volatility; these characteristics contribute towards a higher persistence in the environment, thus dramatically increasing their toxicity. Unlike the G Agents, the V Agents' low volatility and high biological and chemical stability allows for high percutaneous toxicity.[23]

Following the discovery of VX (**1.23**), various analogues of the V agents were synthesised, most notably, Russian VX (**1.24**) in 1963,[24] by the Soviet Union's Scientific Research Institute No. 42 and Chinese VX (**1.25**).

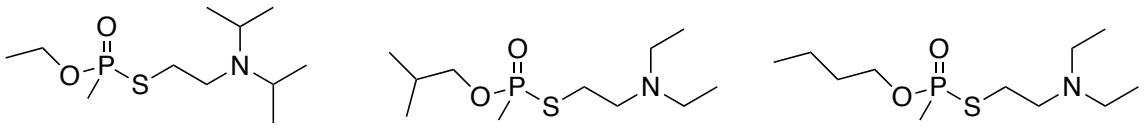

1.23 **1.24** **1.25**

Figure 1.9. The Vesicant Agents; VX (**1.23**), Russian VX (**1.24**) and Chinese VX (**1.25**)

Table 1.3. Lethal doses of the V agents, VX, Russian VX (information for Chinese VX was not available) in rats[19,20]

V Agent	LD_{50} (skin) / mg	LD_{50} (orally) / mg/kg	LCt_{50} (inhalation) / mg min m^{-3}
VX	0.2	0.2	15
Russian VX	0.5	1.4	10
Chinese VX	*n.a.*	*n.a.*	*n.a.*

Table 1.2 and Table 1.3 clearly shows the increased toxicity of the V agents compared to the G agents in rats. For example, the lethal dose *via* skin absorption of VX is incredibly small at only 0.2 mg whereas the lethal dose of tabun is 4000 mg in rats.

1.1.3 History of the Use of Nerve Agents as Chemical Weapons during the 20th Century

Thankfully, this battery of nerve agents (G agents, V agents and early OP agents) developed throughout the years between WWI and WWII and beyond, was never employed in Europe during the armed conflict of WWII. The G agents were never employed in combat, despite their rigorous testing at Spandau Citadel, Berlin, where a gas laboratory had been integrated into a former military fort. Stockpiles of predominantly sarin were produced on mass during the early 1940s, estimated to be anywhere between 500 kg and 10 tonnes.

The reason for sidestepping the use of these nerve agents is still a point of contention. Many argue that Adolf Hitler was warned by intelligence at IG Farben that Germany was not the sole owner of the nerve gas capability and that the Allies may be able to produce these gases with much higher productivity and of a better quality.[25]

It wasn't until the 1980's when the first large-scale use of nerve gases was reported. During the Iraq-Iran war of 1980-1988, the Iraqi military employed an offensive chemical weapons program led by Iraqi president, Saddam Hussein. Throughout the duration of the war, CWAs were employed and current research estimates that more than 100,000 people have died as a direct result of chemical warfare, due to immediate and long-term effects of the agents employed.[26] The most notorious event was the Halabja massacre of 1988, where Iraqi soldiers utilised CWAs including sarin, tabun and mustard gas[27] against Kurdish and Iranian civilians, killing 5,000 people.[28]

During the mid-1990s, the Japanese doomsday cult, Aum Shinrikyo, gained international notoriety for the employment of nerve agents in two separate terrorist events. In Matsumoto, 1994, seven[29] people were killed after the release of sarin into the air in a residential area. [30] Nine months later, 11 people died in Tokyo,[31] where sarin was released on several lines of the Tokyo subway.[32]

1.1.4 History of the Use of Nerve Agents as Chemical Weapons during the 21st Century

More recently, during the Syrian Civil War in August 2013, Ghouta, a suburb of Damascus, was struck by several rockets containing sarin.[33] It is estimated that more than 1,400 people died as a result of the attack.[34]

On 13th February 2017, whilst travelling through Kuala Lumpur International Airport, two young women attacked Kim Jong-nam with a sample of VX. Kim was reported to have alerted airport personnel that "someone had grabbed him from behind and splashed a liquid on his face" and that a woman "covered his face with a cloth laced with the liquid".[35] Following the attack Kim was treated in the airport clinic before being transferred by ambulance to a nearby hospital, where he died in transit.

In March 2018, another use of nerve agents emerged, this time in the United Kingdom. On 4th March 2018, former Russian military officer and spy, Sergei Skripal and his daughter Yulia were exposed to the Novichok agent, A-234 (Figure 1.10), in Salisbury, Wiltshire. Reports suggest the movements of the pair were followed and they were targeted throughout the day. They first came into contact with the nerve agent at the front door of their home and traces of the chemical were found at various destinations they visited throughout the day, including a pub and a restaurant.[36] Sergei and Yulia Skripal were later found unconscious in a public park, in Salisbury City Centre, from where were transported by air ambulance to Salisbury District Hospital. Both Yulia and Sergei Skripal regained consciousness after a month and were both discharged from the hospital on

9th April and 18th May respectively. A police officer was also taken into Salisbury District Hospital in a critical condition following investigations into the attack. Fortunately, he was reported to have made a full recovery by the 22nd March.[37]

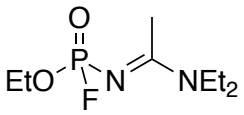

Figure 1.10. Chemical structure of A-234 as disclosed by Mirzayanov, a Russian chemist, formerly involved in the development of weaponised organophosphorus chemical warfare agents, notably, the Novichok Agents[38]

Several months later, on 30th June, two people found a perfume bottle that had been used to contain the nerve agent. The woman, Dawn Sturgess, sprayed some of the contents of the bottle onto her wrist and shortly after exposure, fell ill and died soon after on 8th July. The man, Charlie Rowley, remained in a critical condition until he was discharged from hospital on 20th July.[39]

1.1.5 History of Chemical Weapon Prohibition

On the 27th August 1675, a treaty was signed between the French and the Holy Roman Empire. The treaty was the first example of the prohibition of chemical warfare, with specific regard to the sanction of poisoned bullets.[40]

Despite the extended use of nerve agents, the Geneva Protocol of June 1925 forbade the use in war, of "asphyxiating, poisonous or other gases, and of bacteriological methods of warfare". The treaty also prohibits the use of all analogous liquids and devices. The treaty did not, however, mention the prohibition of production, storage, stockpiling and transfer of these agents. Additionally, a number of signing states of the treaty reserved the right to use CWAs against non-signing countries as retaliation to those using chemical weapons against them.

During the Cold War (1947-1991), significant progress towards chemical weapon armament and stockpiling was made by several states around the world. Following events in Halabja, Iran (1988), the Chemical Weapons Convention (CWC) was assumed at the Conference on Disarmament in Geneva (1992). The CWC was to be an international and multilateral arms control treaty to strictly outlaw the production, stockpiling and use of chemical weapons and their precursors.[41] The Organisation for the Prohibition of Chemical Weapons (OPCW) was established to prepare for the entry-into-force of the CWC in 1997. Since its establishment, the CWC has been managed by the OPCW and as of April 2016, 192 states have signed the treaty, promising to abide by the conditions of the CWC, leaving only South Sudan, Egypt, Israel and North Korea, who are not signatories or a party to the agreements outlined by the convention.

As of October 2015, the OPCW quantified that over 90% of the worlds declared stockpiles of CWAs had been destroyed. This accounts for over 66,000 metric tonnes of a total of 72,525 tonnes of extremely toxic chemicals.[42]

Unfortunately, there is still much work to do in the destruction of the remaining 10% of declared chemical weapons, as well as undeclared stockpiles and those, which may exist under states who are not a party to the CWC agreements. Therefore, efforts must continue towards effective reactivators of OP-inhibited acetylcholinesterases (AChE), in order to protect against possible future acts of terrorism and military warfare.

1.2 The Biological Targets of OPNAs

In order to design suitable reactivators of OP-inhibited human acetylcholinesterase (*h*AChE), it is important that the biological targets are understood. The acute toxicity of OPNAs arises from the irreversible inhibition of the human cholinesterases: human acetylcholinesterase (*h*AChE) and human butylcholinesterase (*h*BChE). This has been understood since 1940,[43] and it has been proven that the cholinesterases play a key role within the human nervous system.[44]

1.2.1 Human Acetylcholinesterase (*h*AChE)

*h*AChE is an enzyme, which catalyses the specific breakdown of acetylcholine (ACh). ACh is a neurotransmitter that is responsible for the transmission of nervous impulses across synapses at neuromuscular junctions, to adjacent neurons. The cholinergic system contains the components that are necessary for the synthesis of ACh, its transport and hydrolysis (the cholinesterases). The function of *h*AChE is to cleave the ACh and terminate neurotransmission. *h*AChE has an incredibly high catalytic turnover, one molecule of AChE is able to catalyse the breakdown of 25,000 molecules of ACh per second.[45] Otto Loewi first described Normal ACh function in 1921,[46] which is summarised in Figure 1.11.

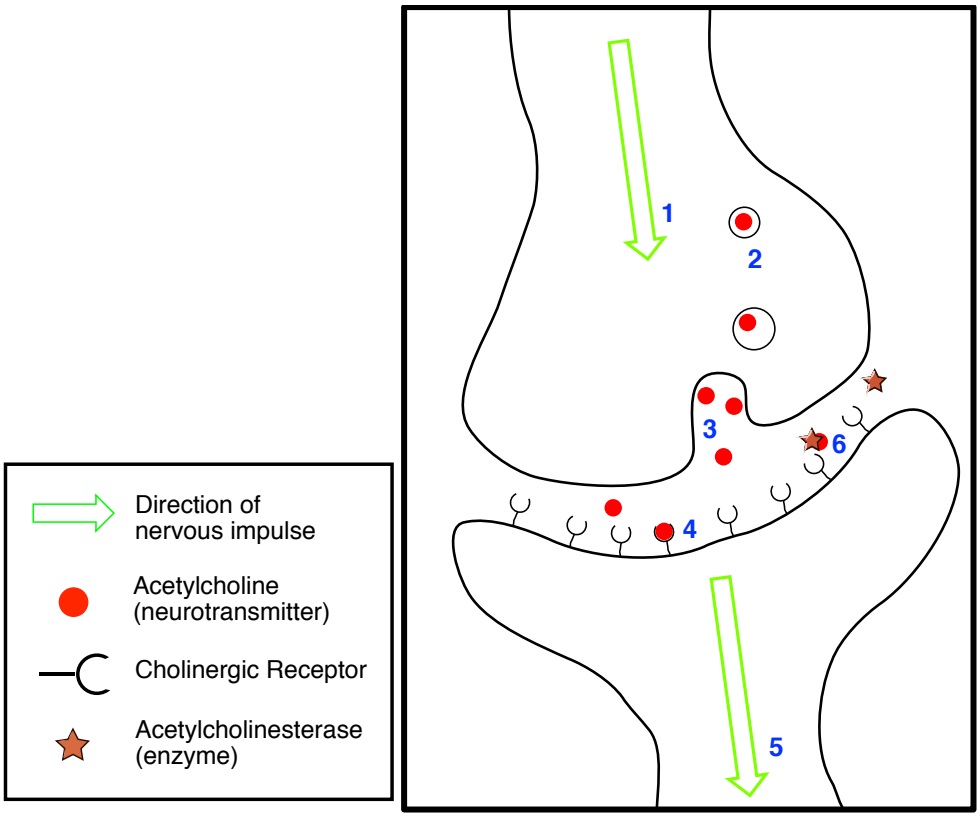

Figure 1.11. Steps towards synaptic transmission

The combination of choline and acetylcoenzyme A (Acetyl-CoA) within neurons, to form ACh (represented by ●), is catalysed by choline acetyltransferase (ChAT).[47] Upon the arrival of a nervous impulse (**1**) at the pre-synaptic neuron, a cascade of biochemical reactions occurs involving the release of Ca^{2+} from voltage-gated channels, which results in the transport of vesicles (**2**) containing ACh (●) towards the edge of the pre-synaptic neuron. Once there, ACh is released into the synaptic cleft (**3**) by exocytosis. Once, released, the neurotransmitter is able to bind with cholinergic receptors on the surface of the post-synaptic neuron (**4**). This binding event results in another cascade of biochemical reaction involving Na^{+} and Ca^{2+} regulation into the post-synaptic neuron, which in turn polarises the nerve, resulting in the propagation of the nervous impulse (**5**). Upon completion of the nervous impulse propagation, AChE (represented by an orange star), within the synaptic cleft catalyses the breakdown of ACh (**6**) to arrest the polarisation of the post-synaptic neuron.

Overall, this cascade of biochemical interactions allows for the termination of the propagation of nervous impulses from the brain to muscles. This results in the relaxation of muscles, an integral role of the human body. The diaphragm is a classic example of essential muscle movement. Upon inhalation, the diaphragm must relax such that the lungs can expand and oxygen transfer can take place. Upon exhalation, the diaphragm contracts in order to expel all carbon dioxide from the lungs. This is a key biological process that is affected by OPNAs and often, in severe cases of poisoning, suffocation due to arrested diaphragm activity is the primary cause of death.

1.2.2 Human Butyrylcholinesterase (*h*BChE)

*h*BChE is a non-specific cholinesterase, formed in the liver and is found predominantly within the blood plasma,[48] it is responsible for the hydrolysis of butyrylcholine (BCh). It is very similar to hAChE, with sequence similarity of 70-72% and 51-54% sequence identity between the two cholinesterases.[49] *h*BChE does not appear to be essential in cholinergic neurotransmission,[50] however, it is able to hydrolyse a wide range of substrates; BCh; benzoylcholine; aspirin and even cocaine, which suggests the *h*BChE may be involved in other critical biological functions.[51] It has been suggested that it is possible to harness this non-specificity and exploit hBChE in biosensors for the detection of OP compounds[52] and other anticholinesterases.[53]

This introduction will focus on reactivators as treatment for the remediation of OP-inhibited AChE. However, BChE has also been employed for the treatment of cases of OP intoxication. Generally a benign biomolecule in cholinergic nerve transmission, BChE is also inhibited by OPNA compounds. Studies have indicated that prophylactic administration of BChE prior to intoxication has minimised toxic effects of OPNAs. The bioscavenger approach is based on the more favourable inhibition of BChE compared to AChE, this results in the "mopping up" of inhibitors and reducing the effect of AChE inhibition[54] Lenz *et al.* demonstrated that following pre-treatment with BChE, guinea pigs were able to survive 5.5 lethal doses of soman and VX.[55] This effect is hypothesised to proceed due to the raised propensity of BChE to act as a highly reactive bioscavenger and intercept OP compounds before reaching AChE.[56] Various methods of BChE administration have been proposed since its initial emergence as a prophylactic treatment of OPNA poisoning, including the introduction of large excesses of stoichiometric BChE[57] and the co-administration of BChE and oxime-containing reactivators, also termed "pseudo-catalytic bioscavengers". The latter was shown to increase the efficacy of current reactivators (HI-6 and Obidoxime) when co-delivered with BuChE (from blood products) by Wille *et al.*, where the concentration of VX showed a comparable decrease when treated with the combined bioscavengers and reactivators compared to the reactivators alone.[58]

1.2.3 Cholinesterase Structure

Throughout the past six decades, much progress has been achieved towards the elucidation of the three-dimensional structure of the cholinesterases. Irwin Wilson, following his pioneering work towards reactivators of inhibited AChE by OPNAs, undertook preliminary research into the structure of the AChE target's active site.

1.2.3.1 Serine Hydrolases

Cholinesterases fall under the serine hydrolase family of enzymes, amongst approximately 200 other human enzymes.[59] AChE, a serine hydrolase, is one of the body's most efficient enzymes

with a catalytic turnover of 25,000 molecules of ACh hydrolysed per second per molecule of AChE, a rate close to the limit allowed by the diffusion of the substrate.[60] These enzymes hydrolyse ester functionality *via* characteristic catalytic amino acid residues (**Figure 1.12**). The first step (**1**) involves the deprotonation of a serine residue by a basic histidine residue, which is driven by an acidic glutamic acid residue (not shown). The nucleophillic serine oxygen attacks the carbonyl of the ACh ester. The resulting anionic carbonyl oxygen attacks back and picks up a proton from the cationic, protonated histidine residue, to liberate choline (**2**). A molecule of water is deprotonated by the basic histidine residue; the nucleophillic oxygen of water attacks the acetylated serine residue and opens the carbonyl (**3**). The carbonyl group collapses and the serine residue is protonated by the protonated histidine residue (**4**) to liberate acetic acid (**5**).

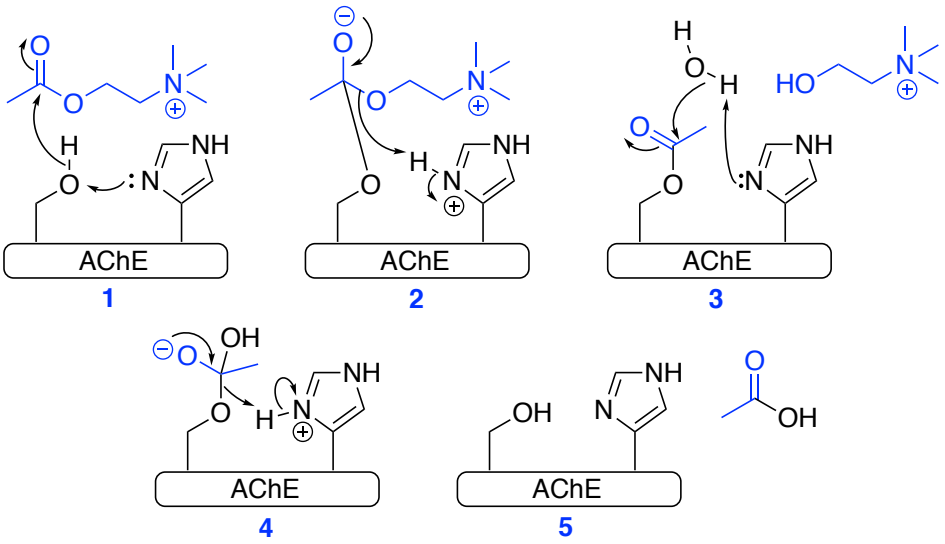

Figure 1.12. AChE serine hydrolase mechanism with ACh

1.2.3.2 The Wilson Brassiere

Irwin Wilson, in 1966,[61] postulated the structure of the active site of the AChE enzyme. The model shows two distinct pockets of specific binding. The first, the esteratic site contains the nucleophillic serine residue (the catalytic machinery) and the histidine residue, while the second pocket contains an anionic residue (the anionic choline binding pocket), which forms an intermolecular ionic bond with the quaternary nitrogen of ACh (**Figure 1.13**).

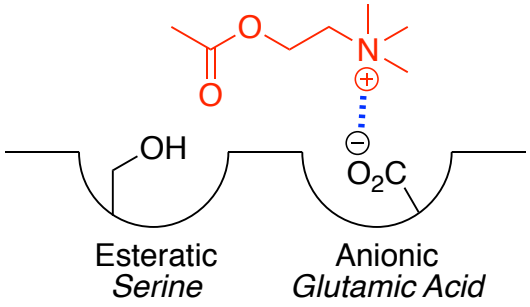

Figure 1.13. The Wilson Brassiere representation of the AChE active site

This schematic representation of the active site seemed to be an accurate representation of the interactions that occur during hydrolysis of ACh into choline and acetic acid.

1.2.3.3 Atomic Structure of AChE

The first three dimensional structure of *Torpedo Californica* Acetycholinesterase (*Tc*AChE) was solved in 1986[62] and *h*AChE was elucidated in 1990.[63] In 1991, Sussman *et al.* solved the atomic structure of AChE (*Tc*AChE) to a 2.8 Å resolution.[64] The results of this research illuminated some interesting differences between the proposed model by Wilson in 1966, and the XRD (X-ray diffraction) data.

AChE (Enzyme Commission number 3.1.1.7) exists in a monodimeric form. The globular enzyme monomer contains 537 amino acid residues, comprising 12-stranded β-sheets surrounded by 14 α-helices. Each dimer possesses an active site, highlighted in cyan and indicated by a black arrow (**Figure 1.14**).

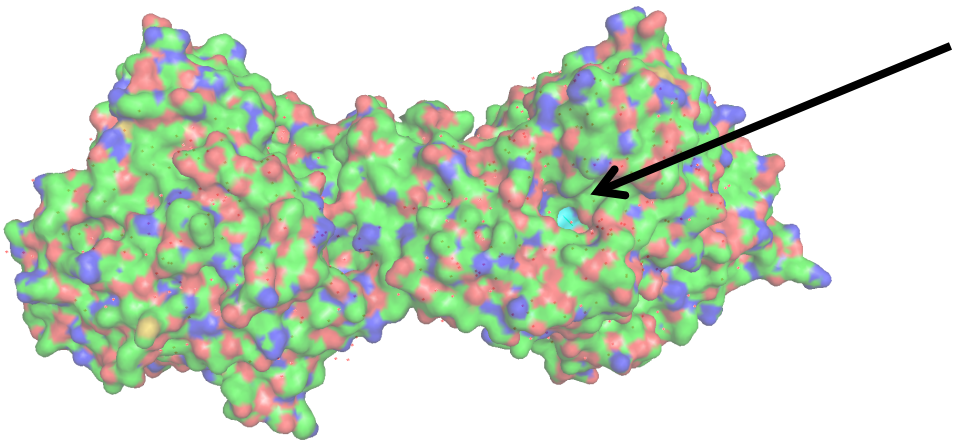

Figure 1.14. The dimeric structure of AChE (pdb: 2GYW), with two distinct globular monomers

The XRD data showed that the characteristic catalytic residues of the active site were located at the bottom of a deep, narrow gorge, embedded in the enzyme. The group suggested that the cationic moiety within ACh was not bound to the anionic site, as suggested by Wilson, but rather, the quaternary ammonium ion of the neurotransmitter was forming hydrophobic interactions with the aromatic residues, which line the gorge (Figure 1.15).[65]

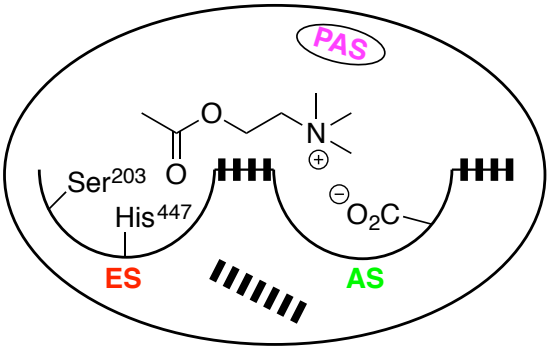

Figure 1.15. Later model proposed by Sussman, with additional peripheral anionic site (PAS) and hydrophobic residues shown as hatched black lines and ACh docked within the active site

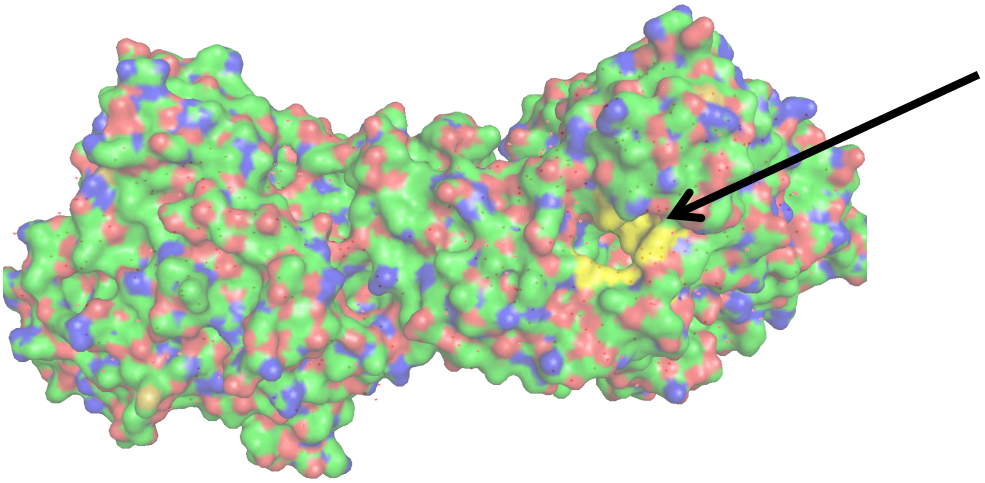

Figure 1.16. Dimeric structure of AChE (pdb: 2GYW), with the hydrophobic residues of the PAS highlighted in yellow and indicated by a black arrow

Sussman *et al.* suggested that the peripheral anionic site (PAS) is a significant site with regards to substrate binding to AChE, whose separate existence from the active site has been resolutely proven by the employment of fluorescence probes (Figure 1.16).[66] The PAS is responsible for "substrate trapping" in close proximity to the mouth of the gorge. Principal residues Trp 279, Asp72 and Tyr70, are involved in this and exist in the PAS, at the mouth of the gorge (Figure 1.17).[67]

The substrate is then able to pass down the gorge towards the active site.[68] Hence, the PAS provides allosteric modulation for the substrate towards the enzyme active site.[69] Upon meeting a molecule of ACh, an initial interaction between the quaternary ammonium terminal of the ACh and the PAS is made. The high concentration of highly hydrophobic residues around the entrance to the gorge increases the affinity of the quaternary ammonium to the PAS by cation-π interactions, which subsequently directs the substrate to the active site.[70]

Once it has passed through the gorge, residue Trp84, is responsible for the orientation of ACh, *via* its trimethylammonium group, into the active site. As suggested by Wilson, the active site is comprised of two sites: the esteratic (ES) or catalytic site (where ACh hydrolysis occurs) and the catalytic anionic site (CAS), where the quaternary ammonium ion is fixated, principally by π-cation interactions (Figure 1.17). A major contribution to binding comes from the *oxyanion hole*, which contains residues; Gly118; Gly119 and Ala201. These residues provide stabilisation *via* hydrogen bonding to the ACh carbonyl oxygen and for the developing charge in the transition state for hydrolysis. In addition to the catalytic site and the oxyanion hole, exists the acyl pocket, which contains residues Trp233, Phe288, Phe290 and Phe331.[71] These predominantly hydrophobic residues work to anchor acetylcholine into the active site.[72]

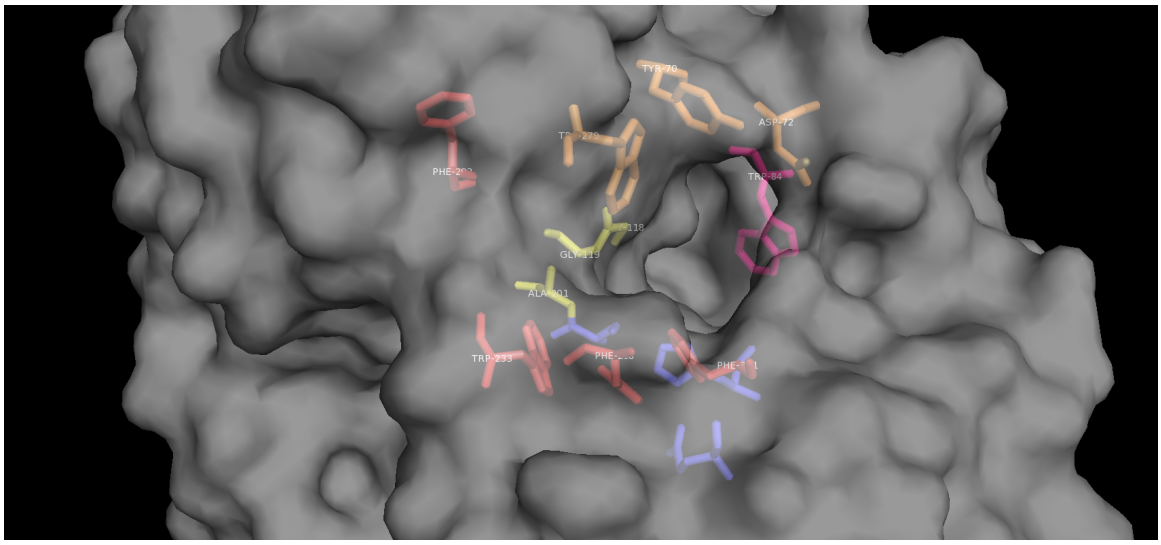

Figure 1.17. Important residues around the gorge in the PAS (orange), Trp84 (pink), the oxyanion hole residues (yellow), the acyl pocket residues (red) and the catalytic triad (purple)

1.2.3.3.1 Atomic Structure of BChE

The differences in the cholinesterases are thought to have resulted from gene duplication during the early evolution of vertebrates.[73] BChE (Enzyme Commission number 3.1.1.8), shares a very similar tertiary structure to AChE, however the active site of BChE is much larger than that of AChE (500 $Å^2$ in BChE *cf.* 300 $Å^2$ in AChE). This increase in active site size results in much lower specificity, as the site is able to accommodate much larger and bulkier substrates and facilitate their hydrolysis.[74] Other notable differences include the replacement of key amino acid residues within the lining of the gorge, 6 of the 14 aromatic residues are replaced with smaller aliphatic amino acids. In addition, within the acyl pocket, the Phe331 is replaced with Ala328, a much less hydrophobic residue. This change results in much less effective anchoring of substrate towards the catalytic triad.

1.3 OPNA Poisoning and its Effects on AChE

OPNA poisoning proceeds *via* the irreversible inhibition of AChE, and OPNAs such as sarin, tabun and soman are excellent drivers for this inhibition. Anticholinesterase OP compounds can be given the following general formula:[75]

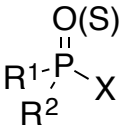

Figure 1.18. General formula for anticholinesterase OPNAs, where X represents a leaving group and R^1 and R^2 are capable of virtually infinite variation

The range in variation of the R groups within OPNAs has allowed for the development of devastatingly effective candidates, specifically in their ability to cross the blood brain barrier (BBB) and enter the CNS.[76] The ability to fine-tune the balance of lipophilicity and hydrophilicity has been key in the development of effective OP CWAs.[77] The presence of a "good" leaving group is important to the structure of these candidates as this modulates the propensity of nucleophillic attack at the phosphorus (V) atom. In some cases, thiophosphate moieties are present, which are metabolised upon entering the body, by the cyp450 enzymes into their corresponding phosphates, which are highly toxic.

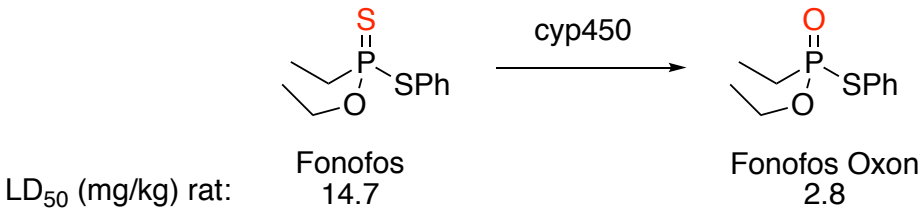

Scheme 1.2. cyp450 mediated metabolism of fonofos into the OPNA fonofos oxon, in a similar way to parathion

The mechanism by which OPNA poisoning proceeds in similar manner to that of the first stages of the normal function of AChE with ACh and is shown in the scheme below:

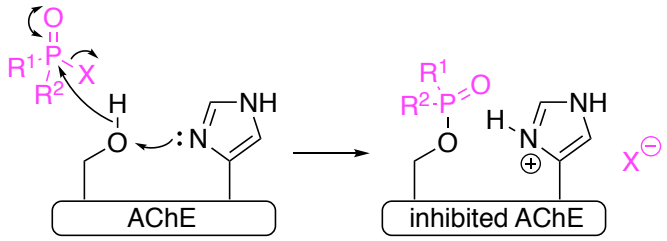

Scheme 1.3. Mechanism of irreversible inhibition of AChE by OPNA

The mechanism of inhibition proceeds as the nitrogen lone pair from the histidine residue accepts the proton of the serine residue, activating the oxygen as a nucleophile. Nucleophillic attack on the phosphorus atom of the OPNA ensues, which liberates the leaving group (X). The result is a

covalently modified enzyme, as the newly formed P-O bond is resistant to hydrolysis. Upon inhibition of the enzyme, AChE is no longer able to undertake its typical function and as a result, the neurotransmitter, ACh, accumulates within the synaptic cleft. In addition to the above mechanism, if left untreated, the inhibited enzyme can proceed to undergo another transformation, known as ageing (Scheme 1.4).[78,79] The ageing process results in the dealkylation of one of the R groups (alkoxy) leaving a negatively charged oxygen substituent, which is able to form an intramolecular salt bridge between the phosphorylated serine residue and the nitrogen cation of the protonated histidine residue. Consequently, the aged complex is stabilised and the serine residue can no longer be dephosphorylated. The mechanism of dealkylation is still disputed, but is commonly suggested to proceed through protonation of an alkoxy oxygen by the histidine residue.[80] Current treatments for the remediation of OPNA poisoning are not effective for aged AChE, however, rapid treatment of poisoning is a method for circumventing the ageing phenomenon.[81]

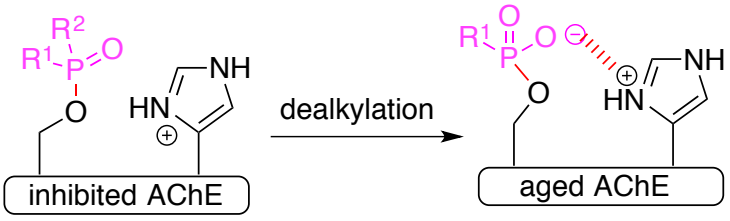

Scheme 1.4. The ageing phenomenon, where R^2 = an alkoxy substituent

1.3.1 Clinical Aspects of OPNA Poisoning

Upon inhibition of AChE, an array of biological consequences can arise, depending upon the dose and class of the OPNA. Accumulation of ACh at the neuromuscular junctions results in overstimulation of cholinergic receptors within the CNS,[82] also known as cholinergic crisis. This overstimulation can feature biological effects, such as tachycardia and high blood pressure. Research has suggested that after exposure to any dose of OP compound, miosis is universal and paralytic symptoms are common.[83] The severity, duration and specific effect of OP poisoning are determined principally by the properties of the nerve agent, such as stability of the phosphorylated AChE and lipophilicity. OPNA-mediated AChE inhibition can manifest itself three chief types of biological effects, for each of the cholinergic receptors and the CNS:

Table 1.4. Symptoms resulting from local exposure to OPNA with regards to the cholinergic receptor[84]

Site of Action	Signs and symptoms following local exposure
Muscarinic	Frontal headache; tightness in the chest; cough; vomiting; excessive sweating; prolonged wheezing and blurred vision
Nicotinic	Fasciculation of muscle fibres resulting in muscular twitching[85]

Table 1.5. Symptoms resulting from systemic exposure to OPNA with regards to the cholinergic receptors[86]

Site of Action	Signs and symptoms following systemic exposure
Muscarinic	Prolonged wheezing; increased lachrymation; increased salivation; bradycardia; involuntary defecation
Nicotinic	Elevation of blood pressure; fatigue; cramps; dyspnoea and tachycardia
CNS	Giddiness; restlessness; headache; tremor; drowsiness; confusion; slurred speech; coma; convulsions and cyanosis

Paralysis is a common symptom of OP poisoning and can also range from reversible symptoms in mild poisoning to paralytic symptoms in very severe cases. In these severe cases, death can proceed due to asphyxia as a result of the paralysis of the respiratory muscles (diaphragm).

Neuropsychiatric side effects also exist among the aforementioned acute muscarinic, nicotinic and CNS side-effects of OP poisoning. Neurobehavioural changes have been reported following acute and chronic OP exposure.[87] Neurological manifestations can range from twisting and writhing to painful muscle spasms and tongue protrusion.[88]

Finally, intermediate syndrome,[89] can occur between 24 and 96 hours following exposure to OPNA and manifests itself in increased muscle weakness of respiratory and flexor muscles. This muscle weakness can result in the abovementioned heavy breathing and asphyxia.

1.4 History of OPNA-Inhibited AChE Reactivators

For the last six decades, considerable research has been focussed upon the remediation or reactivation of inhibited AChE. In order to understand how these reactivators work in delivering a therapeutic effect, it is first important to understand the mechanism of reactivation and the enzyme kinetics of the reaction.[90]

1.4.1 Enzyme Kinetics of OPNA Inhibition and Reactivation

As previously explained, OP poisoning proceeds *via* the phosphorylation of a serine residue, within the active site of the hAChE enzyme. The removal of the phosphoryl group from this residue is considered the primary role of the oxime moiety within reactivator compounds.[91]

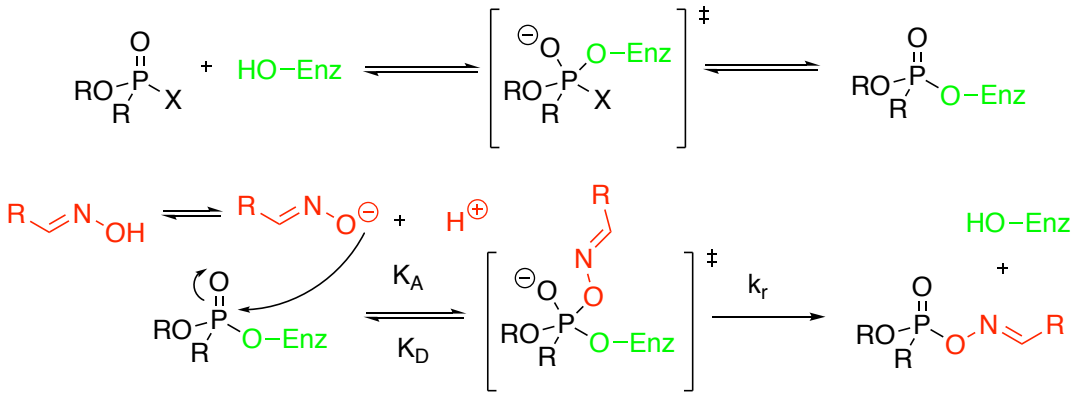

Scheme 1.5. Mechanism of inhibition of AChE (in green) by OPNA (above) and the reactivation mechanism (below) with an oxime reactivator (in red)

The mechanism for reactivation of OP-inhibited AChE follows the physiological oxime deprotonation, assuming that the pK_a of the oxime is sufficiently low (<8, *e.g.* 2-PAM pK_a 5.78) to facilitate an adequate proportion of the oximate anion. The highly nucleophilic oximate attacks at the phosphorus atom, forming a high energy intermediate, which immediately collapses into the reactivated enzyme and the phosphorylated oxime.[92]

Scheme 1.6. Kinetic equation of the reactivation of OPNA-inhibited AChE by an oxime reactivator

The enzyme kinetics are treated using a classic Michaelis-Menten model,[93] as indicated in the scheme above. The oxime reactivator (Ox) is reversibly associated with the phosphorylated enzyme (EP) to give the Michaelis-type phosphoryl-enzyme-oxime complex ([EPOx]). The constant K_D represents the dissociation constant, which is inversely propotional to the affinity of the oxime to the phosphorylated enzyme. Following the formation of the Michaelis-type complex, the phosphorylated oxime is displaced to generate the liberated enzyme (E) and the oxime-phosphoryl complex (POx). This displacement step is represented by another rate constant (k_r). This constant effectively describes the rate at which the phosphoryl functionality is removed from the enzyme active site.

The entire reaction can, itself, be thought of a pseudo-first order reaction by the application of the steady state assumption, such that the concentration of the inhibited enzyme is negligible compared to the concentration of the oxime reactivator.[94]

$$k_{obs} = \frac{k_r[Ox]}{K_D + [Ox]}$$

Equation 1.1. Pseudo-first order equation for the reactivation process, where k_{obs} represents the observed first order rate constant for any given oxime reactivator concentration

When [Ox] << K_D, it is possible to simplify the above equation and evaluate a second order rate constant (k_{r2}). This rate constant represents reactivation as one single step and corresponds to the ratio of k_r and K_D

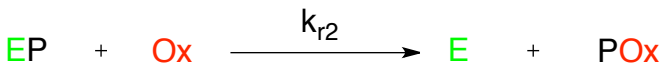

$$k_{r2} = \frac{k_r}{K_D}$$

Scheme 1.7. (above) Second order rate reaction and Equation 1.2. (below) the associated equation (k_{r2})

These metrics are used throughout this work to describe the efficiency of oxime reactivators, as they are effective measures of the rate (k_r) and efficiency (k_{r2}) of reactivation.

1.4.2 pK_a of α-Nucleophiles

An alpha nucleophile describes a molecule containing a nucleophilic atom, adjacent to another electronegative atom bearing a lone pair of electrons. The nucleophilic atom displays enhanced nucleophilicity, however, the origin of this "alpha effect" is not fully understood. It has been proposed that the alpha effect increases nucleophilicity and rate of reactions (e.g. S_N2) due to a lower energy requirement during reactions containing α-nucleophiles to make and break bonds.[95]

Oximes are α-nucleophiles, and their increased nucleophilicity is pivotal in their ability to reactivate OPNA-inhibited *h*AChE. In addition, the ability of the oxime to become ionised under physiological conditions is also important. The pK_a of the oxime group determines the concentration of the oximate ion under a specific pH, which correlates to the overall reactivation rate of reactivation. pK_a studies of various reactivators have been undertaken to assess their propensity to hydrolyse OPNA compounds and Timperley *et al.* proposed that an ideal oxime pK_a value should be around 8. The group noted that reactivator candidates with very high oxime pK_a values exceeding 10 would either demonstrate very poor reactivation efficiency or be ineffective as reactivators entirely.[96]

1.4.3 Irwin Wilson: Initial Development of Reactivators of OPNA-Inhibited AChE

Irwin Wilson could be described as the forefather of OPNA poisoned AChE reactivation. His efforts began in 1951 when he was able to demonstrate the rapid and reversible reactivation of TEPP-inhibited AChE with hydroxylamine (and choline).[97] Wilson noted that the nucleophilic oxygen of hydroxylamine was able to attack the central phosphorus (V).

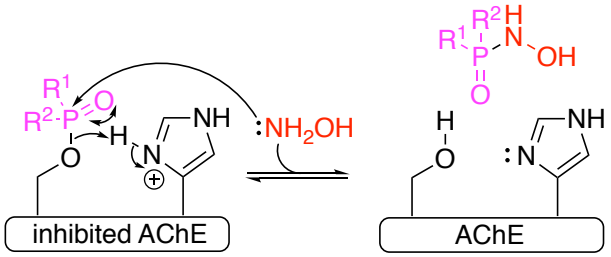

Scheme 1.8. Mechanistic reversible reactivation of phosphorylated AChE by hydroxylamine

This research was the first breakthrough for the potential development of so-called reactivators, or pharmacological candidates with the ability of liberating AChE from OPNAs. While the discovery was useful in gaining proof that inhibited cholinesterases can be reactivated by hydroxylamine and that it is much more effective than water, the enzyme kinetics were still far too slow to allow for efficient reactivation.[98]

Wilson's attention therefore turned to pyridinium oximes in 1955, and alongside his colleague, Sara Ginsburg, the first powerful, clinically relevant reactivator 2-pyridine aldoxime methiodine (2-PAM) was synthesised.[99] The oxime functionality within the candidate is key, as it provides an extremely nucleophillic oxygen to react with the less electrophilic phosphate of the inhibited enzyme.

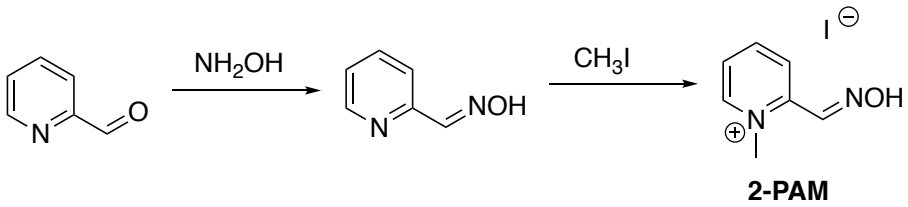

Scheme 1.9. Synthesis of 2-PAM: reaction of 2-formyl pyridine with hydroxylamine to give pyridine-2-aldoxime, which is methylated to afford 2-PAM[100]

Wilson stated that "[2-PAM] reacts a million times faster than hydroxylamine and has proved to be an effective antidote for OP poisoning in animals and in man". The quote still rings true today, as 2-PAM remains in use as a treatment since its first use in 1956. This landmark was acclaimed as the first design process of a clinical candidate that was developed without serendipity and luck, but with "paper and pencil calculations".[101] Rather, Wilson *et al.* developed a candidate together with their knowledge of cholinesterase enzyme kinetics,[102] and alongside the aforementioned model for the active site of AChE, the Wilson Brassiere.

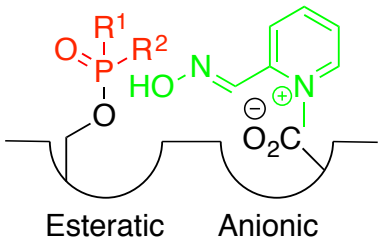

Figure 1.19. 2-PAM docked in the theoretical Wilson Brassiere model of the active site AChE

It was postulated that 2-PAM, shown in green (Figure 1.19), would rest with its pyridinium cationic nitrogen alongside the negatively charged carboxylate, to form a strong affinity through an ionic interaction. The geometry of the 2-PAM would therefore be arranged in such a way that the oxime moiety is placed in close proximity to the phosphorylated (in red) serine residue of AChE.

1.4.4 Development of the Most Potent Bis-pyridinium Oximes

Shortly after the release of 2-PAM, Wilson *et al.* synthesised Trimedoxime (TMB-4) in 1959. This marked the first case of structural modifications of the pyridinium oximes in an attempt to improve the candidate's reactivation efficiency. TMB-4 (K_D 159 µM) showed increased affinity towards the VX-inhibited AChE active site compared to 2-PAM (K_D 215 µM). The synthesis of TMB-4 also celebrated the first example of bis-pyridinium candidates employed as OP-inhibited AChE reactivators.[103]

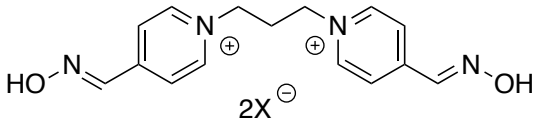

Figure 1.20. Trimedoxime (TMB-4), the first bis-pyridinium reactivator of OP-inhibited AChE. Where X = halide, mesylate or methylsulfate

TMB-4 showed efficient reactivation [104] of AChE inhibited by VX, tabun and sarin. [105] Unfortunately, TMB-4 showed much higher toxicity with dramatically lower LD_{50} values at 70 mg/kg compared to 120 mg/kg for 2-PAM. TMB-4 also showed poor prophylactic reactivation against soman poisoning, giving a 100% mortality rate of a sample population of mice following a 270 µg/kg dose of soman.[106] None the less, TMB-4 has been reported to be the most efficient remediation for poisoning by OP pesticides.[107]

Subsequent structural modification of TMB-4 was aimed at reducing its toxicity while maintaining its reactivation efficiency. Lüttringhaus and Hagedorn made a notable modification in 1964.[108] The central methylene within the linker between the bis-pyridinium rings was replaced with an ether functionality.[109]

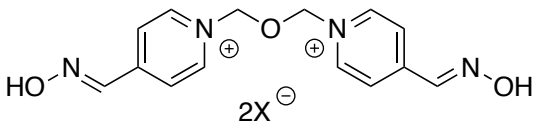

Figure 1.21. Obidoxime (LüH-6), features a central ether functionality within the linker

LüH-6 showed much better toxicity results with LD_{50} values increasing two-fold as well as being able to weakly reactivate soman intoxication, with an 80% mortality rate following a 270 µg/kg dose. LüH-6 showed excellent potential however, it was not able to efficiently reactivate tabun-inhibited AChE.[110] In addition, though LüH-6 showed reduced LD_{50}, it did later show hepatotoxic potential.[111]

Work continued towards fine-tuning the reactivation efficiency of LüH-6. Five years after its discovery, Hi-6 was synthesised with the manipulation of the position of the oxime moiety as well as the integration of additional functionality on the pyridinium rings.[112]

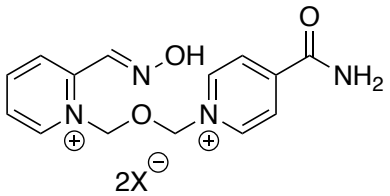

Figure 1.22. Asoxime (Hi-6) features the oxime moiety at the 2 position and an amide functionality at the 4 position of the opposite pyridinium ring

Hi-6 showed the best toxicity results, with a lethal doses of up to 514 mg/kg in mice. In addition, Hi-6 was the first oxime to effectively reactivate soman[113] inhibited AChE, as well as, VX[114] and sarin.[115] Unfortunately, the oxime was not efficient in the reactivation of tabun-inhibited AChE.[116,117] More recent research has revealed that Hi-6 is also effective against cyclosarin poisoning.[118]

Table 1.6. Lethal dose in 50% of population of rats (LD_{50}) of pyridinium oxime reactivators alongside their reactivation as expressed in mortality rates following soman intoxication[116-117]

Reactivator	**LD_{50} (mg/kg)**	**Mortality following 270 µg/kg dose of soman (%)**
2-PAM	120	100
TMB-4	70	100
LüH-6	145	80
Hi-6	514	0

The final bis-pyridinium oxime of significant note, HLö-7, was synthesised in 1986 by Ilse Hagedorn and Marianne Löffler.[119]

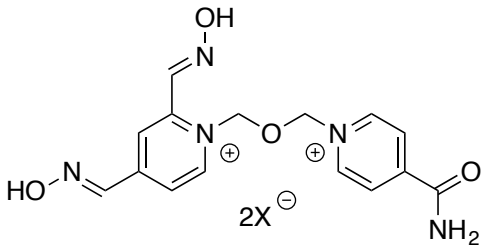

Figure 1.23. HLö-7, similar to Hi-6, features an additional oxime moiety at the 4-position of one pyridinium ring

HLö-7 showed good reactivation for all G agents[120,121,122,123] and VX.[124] Research also suggested that HLö-7 more efficiently restored normal neuromuscular transmission following intoxication with the G agents *cf.* 2-PAM, LüH-6 and Hi-6.[125]

2-PAM, TMB-4, LüH-6, Hi-6 and HLö-7 represent the most potent oxime-containing reactivators with regards to their *in vivo* and *in vitro* reactivation. Their reactivation efficiencies are shown below with respect to their reactivation constants: k_r (min^{-1}), K_D (μM) and k_{r2} ($min^{-1}M^{-1}$). The lower the value of K_D, the higher the affinity of the reactivator to the site of action.

Table 1.7. Reactivation constants (k_r [min^{-1}] and K_D [μM]) for various OP-inhibited hAChE by most effective oxime reactivators (n.a. not available)[126]

	2-PAM		*TMB-4*		*LüH-6*		*Hi-6*		*HLö-7*	
OPNA	**k_r**	**K_D**	**k_r**	**K_D**	**k_r**	**K_D**	**k_r**	**K_D**	**k_r**	**K_D**
VX	0.06	215	0.13	159	0.60	54	0.24	11.5	0.49	7.8
VR[127]	0.06	30.7	0.06	100	0.63	106.0	0.44	50	0.84	5.3
sarin	0.25	27.6	n.a.	n.a.	0.94	31.3	0.68	50.1	0.85	24.2
tabun[128]	0.01	706	0.08	460	0.04	97.3	none	none	0.02	106.5
cyclosarin[129]	0.18	3159	0.06	1585	0.40	945.6	1.30	47.2	1.66	17.9
paraoxon	0.17	187.3	0.97	62	0.81	32.2	0.63	210	0.34	47.8

Table 1.7 shows that there are no reactivators that show consistently high k_r across the range of OPNAs, thus no single reactivator is effective against the broad spectrum of poisons listed above. Indeed, some reactivators are completely ineffective, such as Hi-6 against tabun.

Table 1.8. Second order reactivation constants (k_{r2}) for various OP-inhibited hAChE by most effective oxime reactivators (n.a. indicates data not available)[130,131,132,133]

	2-PAM	*TMB-4*	*LüH-6*	*Hi-6*	*HLö-7*
OPNA			**k_{r2} ($mM^{-1}min^{-1}$)**		
VX	0.28	0.50	11	9	63
VR	2	0.6	5.9	8.8	158
sarin	9.1	n.a.	29.9	13.5	66.58
tabun	0.01	0.6	0.16	none	0.044
cyclosarin	0.05	0.04	0.4	28	93
paraoxon	0.91	16	19	3	n.a.

1.4.5 Structural Modifications of Mono-pyridinium Oximes

Mono-pyridinium oximes are known to be weaker reactivators of OP-inhibited AChE compared to bis-pyridinium oximes.[134] However, structural manipulations of monoquaternary oximes has been undertaken, notably, pralidoxime (PAM).

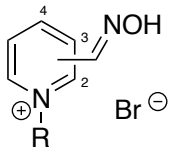

Figure 1.24. Structural modifications undertaken on pralidoxime template

Okonu *et al.* [135] explored some substitutions at the pyridinium nitrogen of pralidoxime where the oxime position was also varied. Six alkyl-PAM structural variations were synthesised, ranging from saturated decyl (**1.26**) and dodecyl chains to functionalised benzyl moieties (**1.27**).

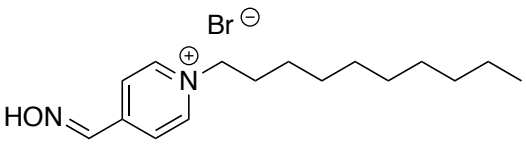

1.26

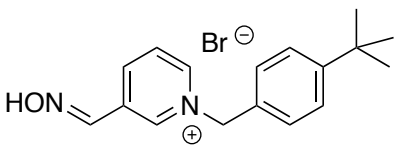

1.27

Figure 1.25. Alkyl substituted PAM structural variants, synthesised by Okonu *et al.*

These analogues were synthesised in an attempt to improve the lipophilicity of the candidates and/or integrate additional π-π stacking interactions. The six structures displayed higher toxicity with dramatically lower LD_{50} values than existing reactivators (as low as 4.3 mg/kg *cf.* 120 mg kg^{-1}

for 2-PAM). In addition, pyridinium oximes **1.26** and **1.27** showed relative activities of 59% and 15% when compared to 2-PAM.

Musilek *et al.*[136] reported similar structural manipulations upon PAM structures, with the incorporation of heterocyclic functionalities at the terminal end of an *N*-pyridinium propyl chain, attached *via* the nitrogen of heterocycle (**1.28**). Where R = 1-pyridinium, 1-pyridazinium, 1-quinolinium and 1-isoquinolinium. However, these novel oximes showed very limited reactivation of tabun-inhibited AChE.

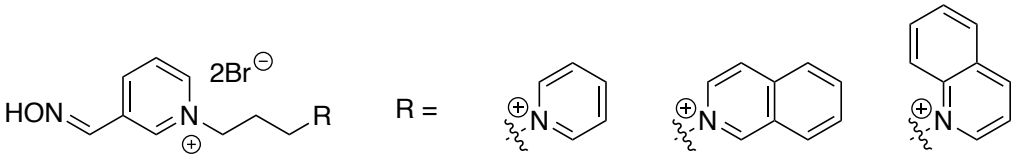

1.28

Figure 1.26. *N*-substituted PAM structural variants, synthesised by Musliek *et al.*

Acharya *et al.*[137] also achieved the synthesis and bioevaulation of a range of novel monoquaternary pyridinium oximes **1.29**. These analogues included the integration of an oxygen atom within the *N*-pyridinium alkyl chain. Structural variation at the R position ranged from alkyl chains with 6-12 carbons to functionalised benzyl rings. The position of the oxime was also varied at the 4 and 3 positions. These analogues were ineffective as reactivators of sarin-inhibited AChE, however, the benzyl substituted candidates were equipotent with Obidoxime for the reactivation of VX-inhibited AChE.

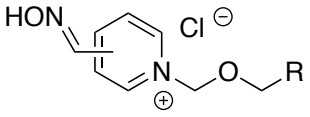

1.29

Figure 1.27. *N*-substituted PAM structural variant, synthesised by Acharya *et al.*

1.4.6 Structural Modifications of Bis-pyridinium Oximes

As previously mentioned in section 1.4.3, the bis-pyridinium oximes generally show improved reactivation of OP-inhibited AChE and have therefore been studied more extensively.

1.4.6.1 Oxime Position

As with the monoquaternary pyridinium oximes, the position of the oxime functionality has been investigated for some bis-pyridinium candidates. Published work by Musilek *et al.*[138] reported the

synthesis of unsymmetrical TMB-4 analogues, substituted with a cyano moiety. The oxime position was varied in **1.30**.

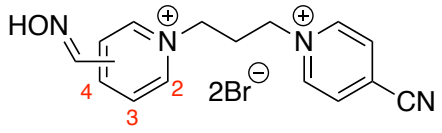

1.30

Figure 1.28. Bis-pyridinium oxime, synthesised by Musilek *et al.*

The asymmetric TMB-4 analogues were tested against tabun-inhibited AChE and showed no reactivation. However, the 4-substituted candidate showed promise against paraoxon-inhibited AChE.

1.4.6.2 Length of Linker

Kuča *et al.*[139] explored the effect of varying the length of the linking alkyl chain between the pyridinium rings (**1.31**).

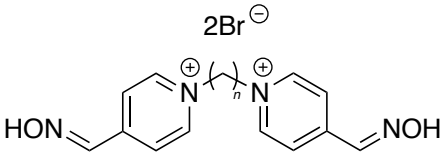

1.31

Figure 1.29. Bis-pyridinium oximes bearing varied length linkers, synthesised by Kuča *et al.*

The group noted the importance of the chemical composition of the bridging linker between the two pyridinium rings. The reactivation data indicated that the most efficient candidates had oxime substituents at the 4 positions and had a linker containing 3 or 4 carbons.

1.4.6.3 Functionality in Ring

Exploration of candidates with additional functionality integrated into the non-oxime pyridinium ring was performed by Musilek *et al.*[140] A range of variations of TMB-4 **1.32** were synthesised with differently substituted non-oxime functionalities at the 4-position. Substituents included esters, carboxylic acids, cyanides and amides. All candidates showed similar or slightly reduced efficiency compared to TMB-4 against sarin and paraoxon.

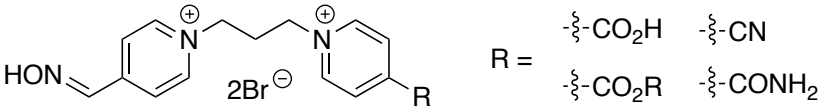

1.32

Figure 1.30. Bis-pyridinium oximes synthesised by Musilek *et al.*

1.4.6.4 Functionality in Linker

Several studies have explored the possibility of incorporating further functionality within the linker. Acharya *et al.*[141] generated candidates **1.33** possessing a methoxyalkane linker of different lengths. Where the oxime moieties were in position 3 and $n = 2$ or 3, reactivation reached 80% and 69% respectively. It is postulated that the addition of heteroatoms increase the reactivators' affinity to the phosphorylated active site, by means of additional intermolecular hydrogen bonding interactions.

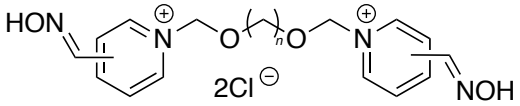

1.33

Figure 1.31. Bis-pyridinium oximes bearing varied length methoxymethane linkers, synthesised by Acharya *et al.*

Kuča *et al.*[142] synthesised candidates with unsaturated linkers and additional functionality within the non-oxime ring (**1.34**), which showed improved *in vitro* reactivation compared to any previously developed reactivators. It is also noteworthy that the compound **1.34**, containing a *trans*-butenyl linker showed a 2.5-fold improvement compared to its corresponding saturated analogue.[143] The integration of amide functionality also has a big impact on the efficiency of the reactivator; compared to TMB-4, the analogue containing the amide shows 6-fold increase in reactivation efficiency. The amide functionality contains both a hydrogen bond donor and acceptor, which is suggested to improve the interactions between the reactivator and the active site, thus increasing its affinity and subsequent efficiency.[144]

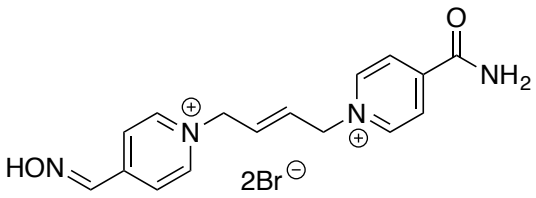

1.34

Figure 1.32. Bis-pyridinium oximes bearing an unsaturated linker, synthesised by Kuča *et al.*

Musilek *et al.*[145] also investigated the idea of conformational restriction with the synthesis of a library of 26 asymmetric bis-pyridinium compounds with xylene connecting linkers in an attempt to increase π-π and cation-π interactions. Compound **1.35** was able to reactivate 45% of sarin inhibited AChE compared to 34% and 24% by 2-PAM and Obidoxime, respectively.

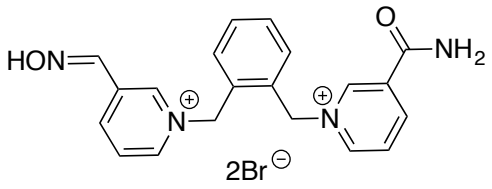

1.35

Figure 1.33. Bis-pyridinium oximes bearing a xylene linker, synthesised by Musilek *et al.*

Interestingly, Musilek concluded that the integration of the xylene linker decreased the reactivation potential of **1.35** due to the restriction the linker placed on the distance between the pyridinium rings, thus a longer or more flexible linker is necessary to exhibit superior reactivation.

1.5 Current Treatment of OPNA Poisoning

The current treatment for the remediation of OP-inhibited depends heavily upon the mechanism of intoxication. In very mild cases with local exposure, non-pharmacological treatments are sufficient. Non-pharmacological treatments can range from additional oxygen supply, decontamination and resuscitation.[146]

Upon more severe cases of intoxication, pharmacological treatment becomes necessary. Common therapy involves a polypharmacological approach:[147,148,149]

(i) Application of a competitive AChE inhibitor, such as atropine (**1.36**)

(ii) Application of an anticonvulsant drug, such as diazepam (**1.37**)

(iii) Application of an oxime-containing reactivator, such as Hi-6 (Figure 1.22)

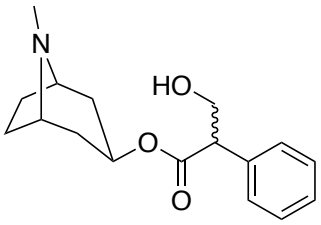

1.36

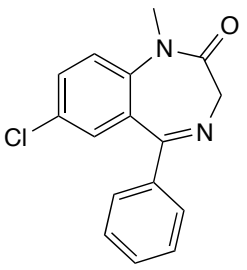

1.37

(±)-Atropine (**1.36**) is responsible for the competitive inhibition of AChE. It is able to reversibly inhibit the muscarinic cholinergic receptors. These muscarinic antagonist drugs are responsible for controlling symptoms such as; bronchospasm;[150] nausea and bronchorrhea.[151]

The benzodiazepine, Diazepam (**1.37**), is responsible for the treatment of seizures, which can be common following intoxication by OPNAs such as tabun and soman.[152] Studies in animals suggest that the treatment of OP-intoxication with Diazepam reduces neural damage[153] and prevents respiratory failure.[154] Finally, the oxime, as previously discussed, is responsible for the reactivation and liberation of the free enzyme, AChE.

1.5.1 Shortcomings of Current Treatment

Although much progress has been made towards newer and more efficient bis-pyridium oxime reactivators, there still exist common drawbacks.

1.5.1.1 Poor BBB Permeability

The blood-brain barrier (BBB) is a barrier that marks the interface between the peripheral blood circulation and CNS. The cells that form the BBB are extremely close together, forming very tight junctions between each cell. The purpose of the BBB is to ensure that foreign bodies such as bacteria and viruses cannot penetrate into the CNS. For penetration, molecules should be small and greasy. In the case of OPNAs, their low molecular weight and relatively lipophilic nature allow passage through the barrier. The oxime reactivators, however, are much larger and more polar molecules, therefore their diffusion through the BBB is substantially reduced. If an oxime is not able to pass through the BBB, remediation of CNS OP-intoxication is incredibly slow and inefficient.

1.5.1.2 Availability of Broad Spectrum Reactivators

There is a huge range of OP nerve agents and pesticides that exist. No single oxime reactivator that has been developed so far is able to reactivate universally. No antidote exists, even for the most common OPNAs and pesticides, therefore it is difficult, particularly within a battlefield environment to administer appropriate pharmacological therapy without elucidating which nerve agent has been employed. This coupled with the time-dependent nature of remediation results in complications with both civilian and military remediation.

1.5.1.3 Reactivation of "Aged" AChE-OPNA Complexes

"Aged" OP-AChE complexes present another issue, such that these complexes are untreatable by reactivating oximes.[155]

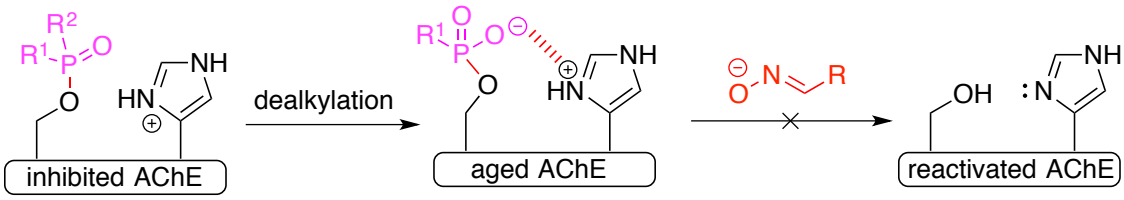

Scheme 1.10. Following dealkylation, the "aged" OP-AChE complex cannot be reactivated by oxime reactivators

1.5.1.4 The Phosphorylated Reactivator Can Act as a Phosphorylating Agent

Also known as the "recapture phenomenon", the phosphorylated reactivator is able to undergo the reverse reaction of reactivation (scheme 1.11).[156] Depending on which OPNA is utilised, the phosphorylated reactivator can become more reactive and electrophilic, allowing for "recapture".

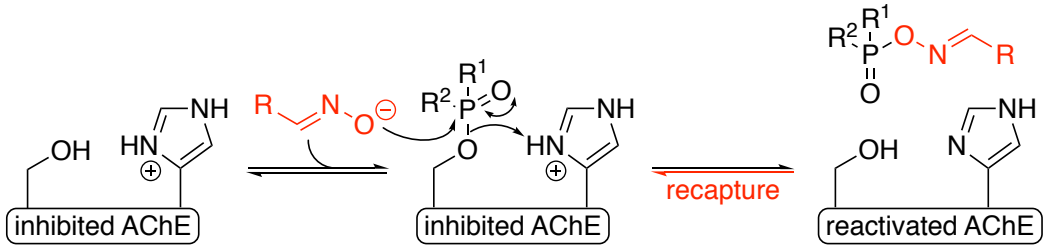

Scheme 1.11. Mechanism of the recapture phenomenon

A proposed solution to this drawback was through the integration of certain reactivators, which form cyclic products that are unable to re-phosphorylate.[157] However, the effectiveness of the isoxazole cyclisation remains a point of debate.

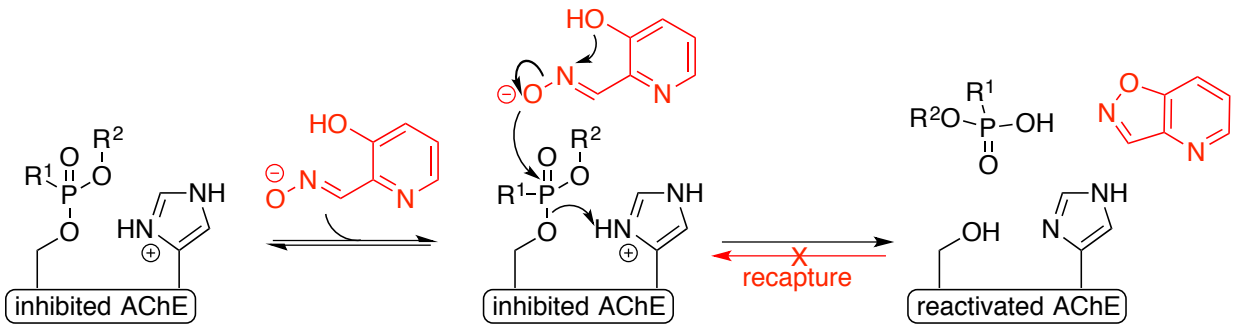

Scheme 1.12. Mechanism of reactivator leading to isoxazole and phosphonic acid

1.5.2 Structural Modifications to Tackle the BBB Problem

Current oxime reactivators are not able to pass through the tight cell junctions of the BBB, this results in the reactivators' ineffective distribution throughout the CNS. Improved BBB penetration of reactivators would enable the design of better and more efficient candidates as antidotes of OP-intoxicated *h*AChE. Various factors have a negative effect upon BBB permeation; the positively charged nitrogen of the pyridinium increases the polarity of the candidates. The highly lipophilic

phospholipid bilayer of the BBB permits less polar molecules to pass through; hence less lipophilic candidates experience reduced transport. Many research groups have focussed their attention upon techniques and structural modifications to improve BBB penetration; some of these techniques are highlighted in this section.

1.5.2.1 Integration of Lipophilic Functionality

As previously mentioned in Section 1.4.4, Okonu *et al.* investigated the substitution of the pyridinium nitrogen with various alkyl and aryl moieties, with a view to increase lipophilicity. The group were able to develop a method to identify BBB penetration using *in vivo* rat brain microdialysis with LC-MS/MS. They reported that one of their compounds, the octyl functionalised 4-PAM, was able to penetrate the BBB by approximately 30%. This indicated that lipophilic functionalisation is an effective means of increasing transport across the BBB.

An alternative method to increase lipophilicity of compounds is by fluorination. Fluorine atom incorporation is commonplace in modern medicinal chemistry and fluorine is present in many highly successful drugs.[158] Jeong *et al.*[159] explored the effect of fluorination on the BBB permeability of 4-PAM and Obidoxime analogues **1.38** and **1.39**. Their investigation showed that fluorinated reactivators showed higher potential to cross the BBB and increased CNS reactivation potential than their non-fluorinated analogues.

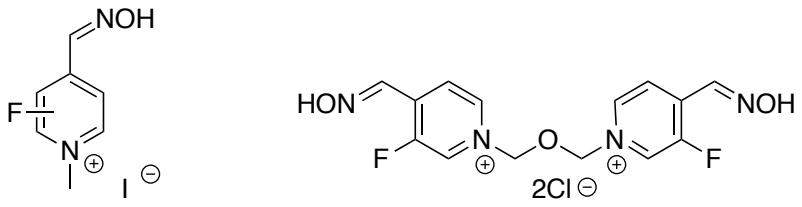

1.38 **1.39**

Figure 1.34. Fluorinated pyridinium oximes synthesised by Jeong *et al.*

1.5.2.2 Integration of Sugars

It has been suggested that glycosylated oximes[160] will reactivate OP-intoxicated AChE more effectively than their parent compounds, due to the active transport of biologically relevant scaffolds, such as sugars, across the BBB. This strategy relies upon biorecognition of sugars by facilitative glucose transporters. Heldman *et al.*[161] undertook the synthesis of a series of novel sugar-based oximes and their results showed that the sugar-conjugated oximes were retained within the blood longer due to reduced clearance and that they were less toxic compared to their non-conjugated analogues. Garcia *et al.,*[162] who synthesised a library of six novel sugar-oximes, continued this research. Glycosylated pyridinium **1.40** showed low toxicity (less than 4-PAM) and good efficiency (almost comparable to 4-PAM) in reactivating paraoxon-inhibited hAChE.

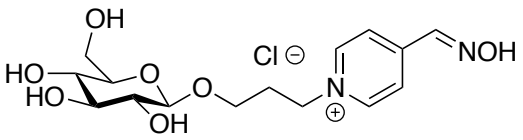

1.40

Figure 1.35. Glycosylated pyridinium oxime synthesised by Heldman *et al.*

1.5.2.3 Uncharged Reactivators

One of the most impeding aspects of all oxime reactivators is the formal positive charge on the pyridinium nitrogen. The highly lipophilic environment of the BBB does not facilitate the transport of very polar molecules; instead it favours passage of less polar and greasier molecules. The removal of this positive charge on reactivators has been suggested and explored with the development of uncharged reactivators. Two uncharged oximes have been reported: monoisonitroacetone (MINA) (**1.41**) and diacetylmonoxime (DAM) (**1.42**).[163]

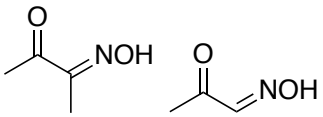

1.41 **1.42**

Figure 1.36. Uncharged oximes: MINA (**1.41**) and DAM (**1.42**)

While these compounds are able to cross the BBB[164] and were able to reactivate AChE inhibited with sarin, cyclosarin and VX, the tertiary, uncharged oximes were much less potent than their quaternary counterparts. In research reported by Shih *et al.*, reactivating doses of monoisonitroacetone were between 3-12 times greater than 2-PAM.[165]

Sainte-André *et al.*[166] have developed uncharged reactivator **1.43**, which displays reactivation efficiency similar (84%) to that of 2-PAM, towards VX-inhibited AChE. The reactivator moiety **1.43** that was developed by Saint-André *et al.* will be used in some of this work as the reactivator portion of the hybrid compounds.

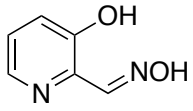

1.43

Figure 1.37. Uncharged pyridine oxime developed by Sainte-André *et al.*

This reactivator is effective due to the oxime's low pK_a value of 8.2, allowing for a reasonable concentration of its corresponding oximate ion under physiological conditions.[167] This leads to enhanced nucleophilicity and reactivity with the phosphorylated enzyme.

1.5.2.4 Peripheral Site Ligands (PSL)

Koning *et al.*[168] suggested the exploitation of the PAS[169] in an attempt to increase affinity to the AChE active site in a 'dual site binding' fashion. During their work, they demonstrated that the integration of a PSL into a "hardly reactivating" oxime **1.44** dramatically increases its reactivation efficiency, providing potent reactivator **1.45**.

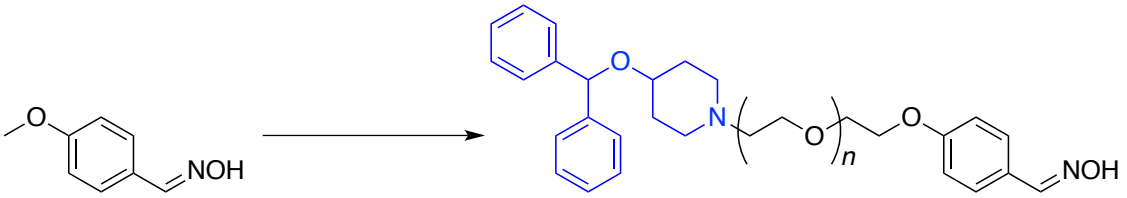

1.44 **1.45**

Scheme 1.13. Development of a weakly reactivating candidate **1.44** into a much more potent reactivator **1.45** by the integration of a **PSL** (highlighted in blue) into the structure by Koning *et al.*

The connection of the oxime reactivator with a linker and a PSL aims to increase the number of interactions and thus affinity towards the target in order to compensate for loss of potency due to the removal of ionic charge from the pyridinium nitrogen. The integration of a PSL can also give an opportunity to incorporate additional functionality to tailor the polarity of the candidate (*i.e.* by means of adding HBA/HBD functionalities) or to add planar moieties to increase π-π or cation-π interactions. It is, however, important to consider the effects of very high affinity PSL. If the interactions of a PSL are very high, it is possible that the candidate can itself, inhibit AChE and become toxic.[170]

Other examples of PSL reactivators have been explored by Kliachyna *et al.* (**1.46**) and Renard *et al.* (**1.47**) showing affinity towards VX-*h*AChE with K_D values of 31 and 885 μM and k_{r2} values of 22 and 6 $mM^{-1}min^{-1}$ respectively.[171,172]

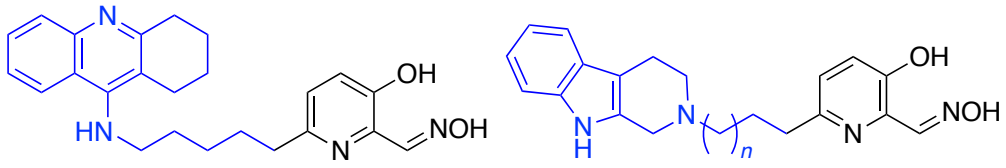

1.46 **1.47**

Figure 1.38. Uncharged hybrid reactivators developed by Kliachyna *et al.* (**1.46**) and Renard *et al.* (**1.47**)

1.5.2.5 Prodrug Reactivators

Bodor *et al.*[173] explored the possibility of administering prodrugs as more lipophilic analogues of common reactivators. Once these modified precursors pass through the BBB, they are converted by

means of enzymic biotransformation by oxyreductases into the active form of the drug. Gordon *et al.* continued this research developing pro-2-PAM (**1.48**).

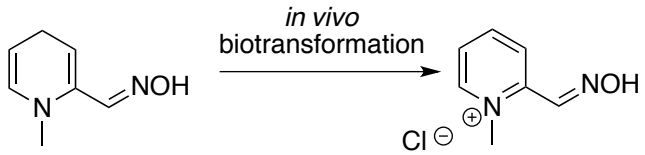

1.48 **1.49**

Scheme 1.14. *In vivo* biotransformation of pro-2-PAM into 2-PAM by oxoreductases

Following administration of pro-2-PAM (**1.48**) and 2-PAM (**1.49**), the concentration of pro-2-PAM within the CNS was much higher than that of 2-PAM, confirming its ability to cross the BBB effectively, where it is subsequently converted to the active 2-PAM.

1.5.2.6 Alternative Strategies

There are several strategies that do not rely upon structural manipulations of the reactivator candidates. The first of these non-structural based strategies involves the employment of nanoparticles, such as liposomes. It has been suggested that nanoparticles prepared from human serum albumin (HSA)[174] can be used in the facilitation of drug delivery across the BBB. Following transport across the barrier, enzymic degradation of the nanoparticle must occur for the embedded drug to be released.[175]

A second non-structural technique is the injection of the reactivator directly into the brain, thus bypassing the penetration step through the BBB. Hatton *et al.* have described intracerebroventricular administration of drugs as a possible method of delivering therapeutic concentrations of drugs into the CNS *via* the brain.[176] There are, however, a range of factors that may hinder this approach including pH and volume.

Another non-structural approach involves the use of low intensity focussed ultrasound (LIFU). LIFU allows for the reversible disruption of the BBB,[177] such that the junctions between the cells of the barrier are less tight and more able to facilitate the transport of larger molecules across it.[178]

1.5.2.7 Non-Oxime Reactivators

In a recent publication, Katz *et al.* report the discovery of new classes of compounds that are able to reactivate AChE inhibited by OPNAs.[179] Following a screen of a library of 2,000 bioactive compounds and medicines, Amodiaquine (ADQ, **1.50**) and scopoletin (**1.51**) were identified as potential non-oxime reactivators of OPNA-inhibited AChE (Figure 1.39). Scopoletin demonstrated reactivation slightly less superior to 2-PAM, however, ADQ was seen to be significantly more active. ADQ showed reactivation of paraoxon-inhibited human, guinea pig and mouse AChE.

Despite its excellent reactivation of inhibited AChE, ADQ has been reported to demonstrate significant toxic effects in high doses,[180] and would therefore be unsuitable as a candidate for prophylactic treatment of OPNA intoxication. Katz reports that the 2-(diethylaminomethyl)phenol (Mannich phenol) portion of ADQ (highlighted in red) was identified as the pharmacophore of the molecule - uncovering the Mannich phenol pharmacophore and 4-amino-2-(diethylaminomethyl)phenol (ADOC, **1.52**) as a new lead non-oxime reactivator of AChE.

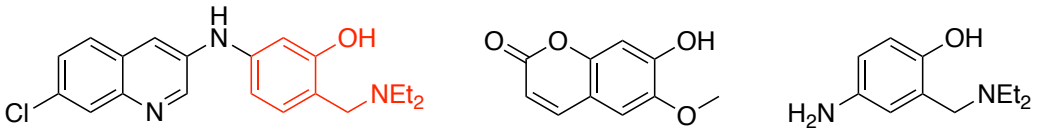

1.50 **1.51** **1.52**

Figure 1.39. Chemical structures of ADQ (**1.50**, in red shows the Mannich phenol template), scopoletin (**1.51**) and ADOC (**1.52**)

Following the discovery of the Mannich phenol pharmacophore, members of the Koning group reported the exciting prospect of the development of potent non-oxime containing reactivators of OP-inhibited AChE. [181] The group synthesised a broad library of 4-amino-2-((diethylamino)methyl)phenol (ADOC, **1.52**) derivatives (Figure 1.40), which had previously shown good reactivation of AChE inhibited by sarin, soman, VX, VR and paraoxon.[182,183]

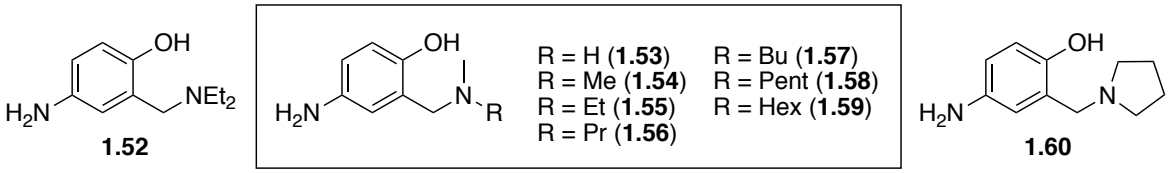

1.52 **1.60**

Figure 1.40. ADOC (**1.52**) and a selection of non-oxime compounds synthesised by de Koning *et al.*

Compound **1.60** was observed to be the most potent non-oxime reactivator known to date. The mechanism by which these compounds reactivate inhibited AChE is currently unknown, however, further research into their kinetic parameters (k_r and K_D) is expected to allow for better understanding in the future.

1.5.3 The Hybrid Reactivator

The compounds that will be prepared in this program of research will be referred to as hybrid reactivators. The so-called hybrid reactivators are comprised of three modules. The first, the reactivator, as mentioned previously was developed by Sainte-André *et al.* and showed extremely similar reactivation to its charged analogue (2-PAM).[166] The reactivator is covalently connected to a linker, whose chief responsibility is to enable access of the reactivator, *via* the gorge, to the active site of AChE. The linker is also attached to the PSL, a group whose role is to form the initial,

favourable interactions with the enzyme, such that the reactivator has an affinity to the general proximity of the entrance to the gorge and hence the active site.

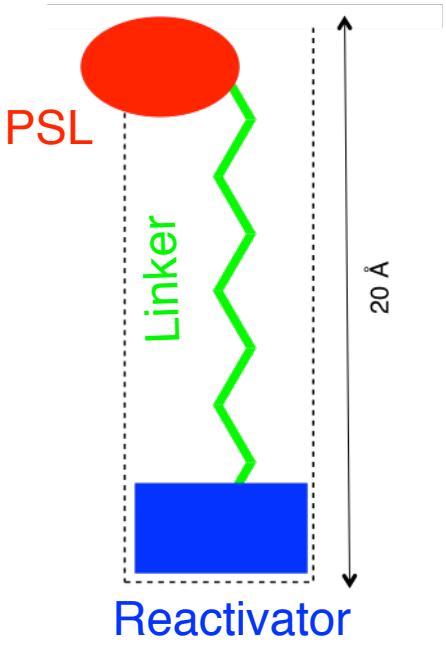

Figure 1.41. Representation of the hybrid reactivator. The PSL is shown in red, the linker is shown in green and the reactivator is shown in blue

Recent research published by Renard *et al.* discussed the synthesis of a series of novel hybrid reactivators bearing various peripheral site ligands (Figure 1.42).[184] Reactivators furnished with the morpholine scaffold proved most effective, providing broad-spectrum reactivation of OP-inhibited *h*AChE. X-ray crystallographic data (Figure 1.43) also showed a productive conformation of compound **1.64** within *Tc*AChE, somewhat exemplifying its apparent potency, with the morpholine moiety anchored within the peripheral site and the reactivator within the gorge.

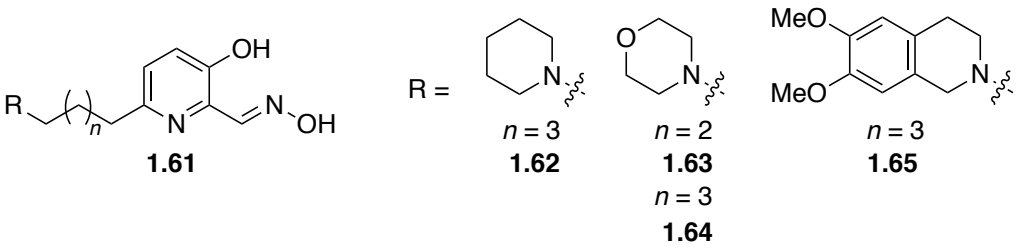

Figure 1.42. Novel hybrid reactivators synthesised by Renard *et al.*[184]

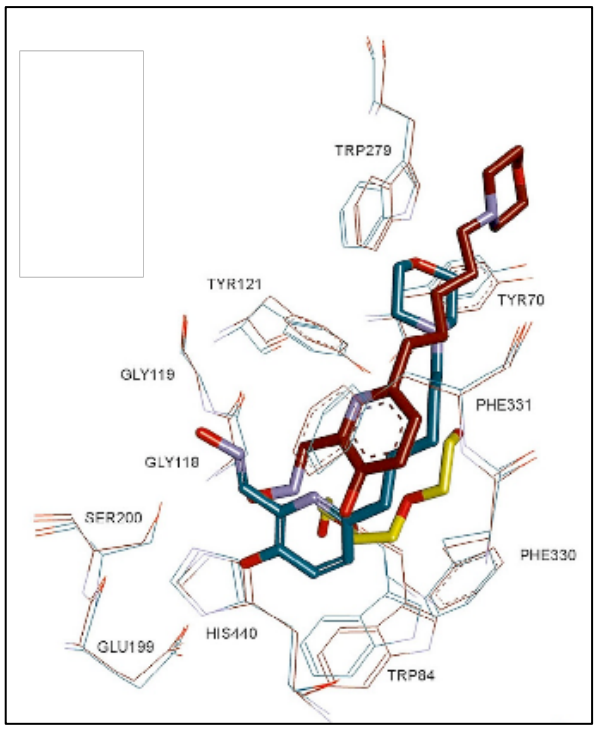

Figure 1.43. X-ray resolution of compound **1.64** within *Tc*AChE[184]

Finally, *in silico* and *in vitro* experiments also confirmed compounds **1.63** and **1.64** ability to permeate the blood-brain barrier.

A library of charged tetrahydroacridine pyridinium oxime hybrid reactivators was recently synthesised by Jung *et al*. (**1.66a-f**, Figure 1.44).[185] The linker length was investigated, where *n* = 2–7. *In vitro* evaluation of the compounds indicated the compound bearing a 4 membered carbon linker gave the best reactivation of paraoxon-inhibited *Tc*AChE (2.5-fold improvement *cf.* 2-PAM and 10-fold improvement *cf.* HI-6). Molecular docking simulations within *Tc*AChE also indicated a binding configuration conducive to successful reactivation of organophosphorus nerve agent-inhibited AChE. The tetrahydroacridine PSL was observed to contribute π-π stacking interations with the tyrosine (Tyr146) and tryptophan (Trp304) residues. A potential cation-π interaction was also noted between the pyridinium nitrogen atom and tyrosine (Tyr359) (Figure 1.45).

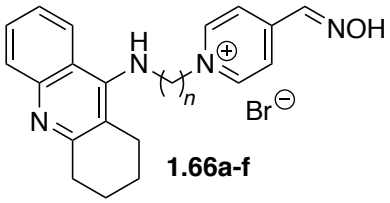

1.66a-f

Figure 1.44. Library of tetrahydroacridine pyridinium oxime hybrid reactivators, where *n* = 2-7

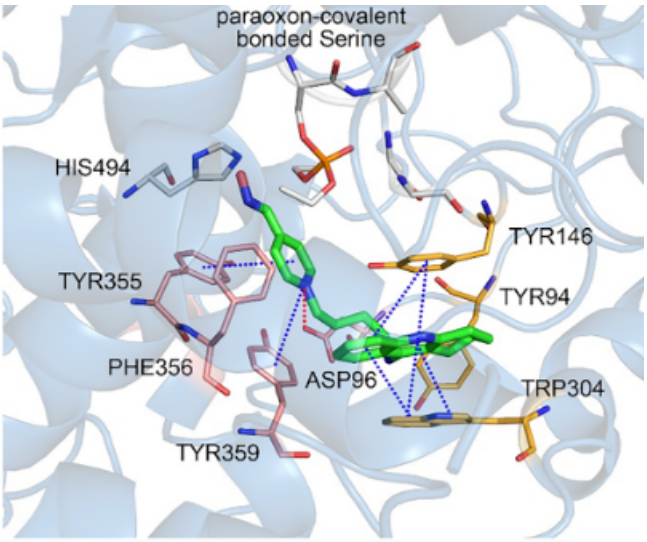

Figure 1.45. Molecular docking of **1.66c** (where $n = 4$, green sticks) within *Tc*AChE, carried out by Jung *et al.*[185] Key residues in pink show potential sites for cation-π interactions and residues in orange show potential π-π stacking

1.6 Previous Research

During the past 10 years, much research has been undertaken, specific to hybrid reactivators. Previously in the Baati and Brown group with collaborative participation of the DGA and dstl, Julien de Sousa prepared a family of novel uncharged, bifunctional reactivator analogues[186] **1.67**, where X = C/N, $n = 1, 2$ and the *a* ring contains 5, 6 and 7 members. These compounds were based around the most potent of the hybrid reactivators developed within this group **1.68**. Two analogues, where $n = 2$ and X = C, where *a* = 5C and 6C, were also synthesised.

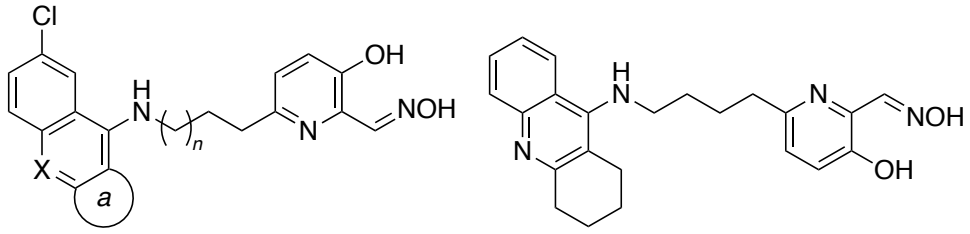

1.67 **1.68**

Figure 1.46. Various hybrid reactivators synthesised by de Sousa

Biological data for compound **1.69** against VX-*h*AChE and sarin-*h*AChE demonstrates k_{r2} values of 51,000 $M^{-1}min^{-1}$ and 25,000 $M^{-1}min^{-1}$, respectively, out-performing all currently available reactivators.

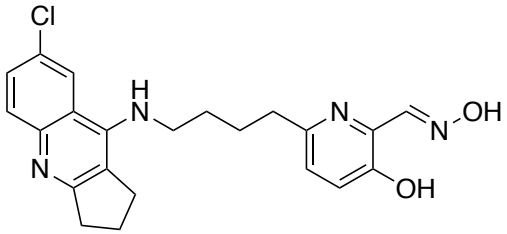

1.69

Figure 1.47. Hybrid reactivator synthesised by de Sousa

Subsequently, a second hybrid reactivator was also synthesised bearing a quinoline (Figure 1.48).

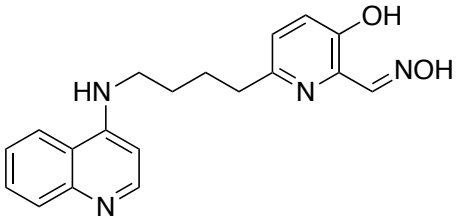

JDS364

Figure 1.48. Quinoline bearing hybrid reactivator synthesised by de Sousa

This compound outperformed all standard reactivators, for both nerve agent and pesticide intoxication (VX, sarin, tabun and ethyl paraoxon), with excellent and efficient, universal reactivation. Quinoline **JDS364** also outperformed the only effective treatment for tabun-intoxication (TMB-4, Figure 1.20) 104-fold (*in* vitro) and is certainly a potential candidate for a universally applicable reactivator (Table 1.9)[186].

This research has provided an exciting starting point to develop a new library of quinoline containing hybrid reactivators in order to work towards an effective and broad-spectrum antidote for OP-intoxicated hAChE.

Table 1.9. *In vitro* reactivation constant (k_{r2}) for quinoline **JDS364** against 4 common OPNAs *cf.* standard reactivators[186]

	k_{r2} ($M^{-1}min^{-1}$)				
OPNA	***JDS364***	***2-PAM***	***TMB-4***	***HLö-6***	***Hi-6***
VX	33,900	280	500	11,000	9,000
sarin	18,300	27,600	*n.d.*	31,300	50,100
tabun	62,400	10	600	160	none
Ethyl paraoxon	20,400	910	16,000	19,000	3,000

1.7 Conclusion

Since Irwin Wilson and Sara Ginsburg laid the foundations of this research in the 1950s, mono- and bis-pyridinium oxime reactivators have remained of great interest with regards to the development of effective management of OP-poisoning. Many programs of research have explored the synthesis, structural manipulation and route optimisation of different potential candidates. However, consistently throughout these groundbreaking publications there have existed many common drawbacks, which have hindered the development of truly universally applicable and efficient reactivators.

Following promising results from Julien de Sousa, this research program will continue to explore novel hybrid reactivators containing the quinoline peripheral site ligand by developing a derivatised library of compounds. Synthetic route optimisation will also be undertaken to improve the throughput of the final hybrid compounds, which historically has been limited to around 10 mg. Later in this program of work, further novel hybrid reactivators will be designed and synthesised with varied peripheral site ligands and a simplified, dehydroxylated reactivator component.

Subsequent *in vitro* evaluation of the compounds synthesised will be discussed with regards to their kinetic parameters (k_r, k_{r2} and K_D) and their permeability across the blood brain barrier. Finally, the development and results of an *in silico* model will be examined. The combined computational and *in vitro* data will be integrated such that the design of future reactivator candidates may be initially validated *in silico*.

Chapter 2 Hydroxylated Substituted Quinoline Hybrid Reactivators

2.1 Introduction

In this chapter, the progress towards hydroxylated substituted quinoline hybrid reactivators will be discussed. This will include the synthetic pathway towards the final compounds and the route development that took place during the synthesis, such that a more streamlined route was achieved. Later in the chapter, attention will focus on computational docking that was undertaken on two hydroxylated substituted quinoline hybrid reactivators.

2.2 Previous Research

The concept of hybrid reactivator compounds, as previously introduced (*vide supra*, Section 1.5.3.), forms a key part of the work that has been undertaken through European collaborative efforts surrounding the development of compounds for superior and broad-spectrum reactivation of OPNA-inhibited *h*AChE. A key shortcoming of compounds developed since 2-PAM, is the low affinity of the reactivator to the active site of *h*AChE. In order to increase this affinity, the reactivator has been conjugated to a ligand that is able to form favourable interactions with residues on the surface of the enzyme, at the mouth of the gorge. The interactions, notably, π–π and cation-π stacking interactions, between the ligand and aromatic residues within *h*AChE greatly increase the affinity of the reactivating molecule towards the active site of AChE.

The initial interactions between the peripheral site ligand (PSL) and the surface of the enzyme bring the conjugate closer in proximity to the gorge. When in this position, it is more likely that the linker and reactivator portion of the hybrid compounds will enter the gorge to improve the reactivation potency. Whilst inside the gorge, the linker also forms favourable interactions with hydrophobic functionality within the gorge (Figure 2.1).

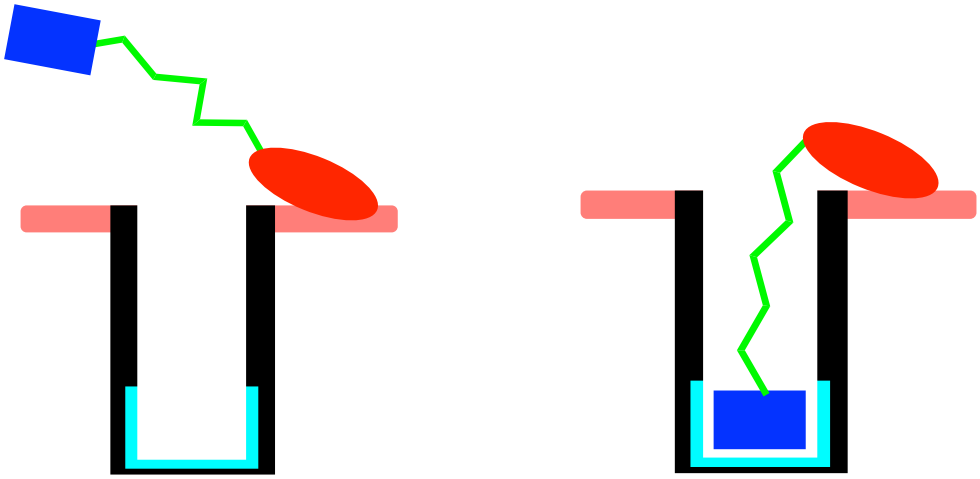

A **B**

Figure 2.1. Allosteric binding of the PSL to aromatic residues on the surface of AChE initially (**A**) and subsequent movement of the linker and the reactivator into the gorge and towards the active site (**B**)

It is also important to understand that the design of hybrid reactivators highly depends on a balance between good affinity towards the active site, such that the reactivator may be placed at the active site, while avoiding very high affinity. Extremely high affinity can cause reactivators themselves to inhibit AChE activity by blocking access to the active site, and functioning as inhibitors themselves. From our international consortium, Nachon *et al.* highlighted this effect in a recent paper where structure-based optimisation was employed to reduce the risk of competitive inhibition[187]. A promising reactivator containing a tetrahydroacridine scaffold **C** demonstrated sub-micromolar inhibition of AChE (Figure 2.2). Data from x-ray crystallography experiments revealed that the reactivator could bind to AChE in an unexpected conformation with the PSL entering the active site, which could be linked to inhibition of the enzyme. It was proposed that integration of a chlorine substituent at the 7-position of the tetrahydroacridine **D** would cause unfavourable steric clashing between the tetrahydroacridine and the active site, removing the possibility of binding in this inhibitory conformation.

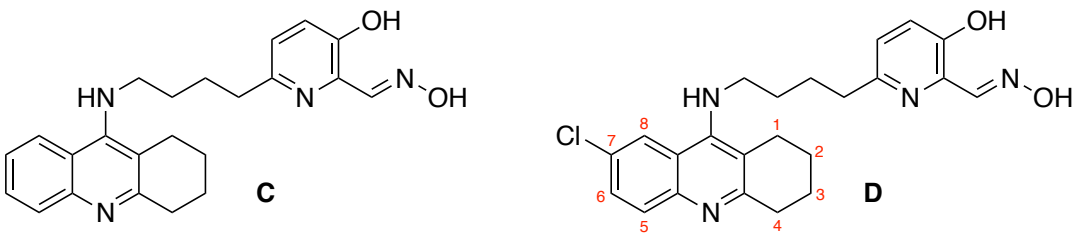

IC_{50} 0.25 µM **IC_{50} 2.3 µM**

Figure 2.2. Tetrahydroacridine-based PSL scaffolds

As predicted, upon *in vitro* analysis of chlorotacrine **D**, a 10-fold decrease in inhibition potency was observed compared to tacrine **C** without any significant reduction in reactivation of OPNA-inhibited AChE.

Throughout the past decade, many examples of hybrid reactivators bearing a PSL have been explored, with promising results. Recently, following a program of work undertaken by de Sousa, a hybrid was synthesised that demonstrated excellent reactivation potency[186]. The hybrid, bearing a quinoline PSL (**2.1**, Figure 2.3), outperformed all existing reactivators for sarin, VX, tabun and paraoxon-inhibited *h*AChE. Excitingly, the quinoline-containing compounds exhibited a millimolar inhibiting potency (IC_{50} 1.4 mM).

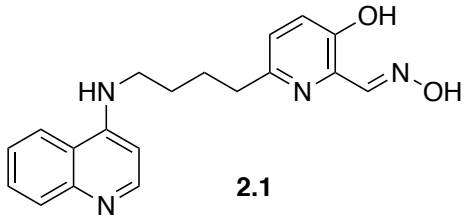

Figure 2.3. Quinoline-bearing hybrid reactivator **2.1**, synthesised by de Sousa

2.3 Initial Development

To begin this research, the synthesis of the 6-bromopyridine reactivator (**2.5**) was undertaken, following the route undertaken by de Sousa[186]. The reactivator was synthesised successfully with yields in accordance to those quoted in the literature (Scheme 2.1).

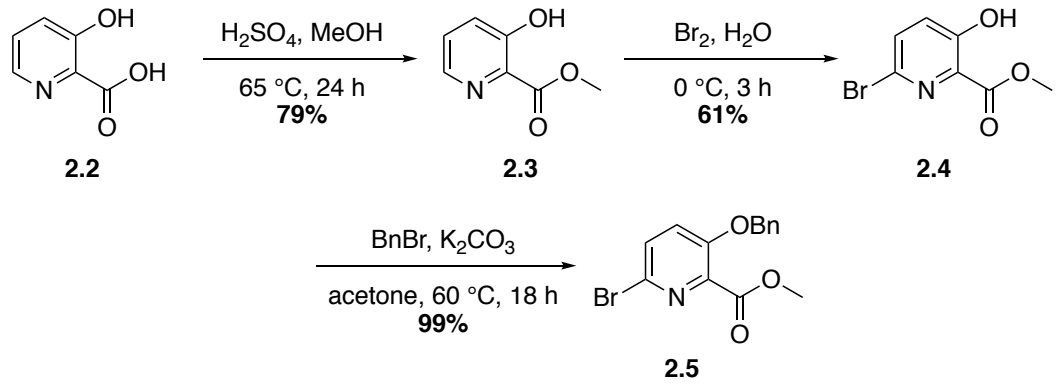

Scheme 2.1. Synthesis of the reactivator analogue, ester **2.5**

Fisher esterification of 3-hydroxypicolinic acid (**2.2**) with methanol under acidic conditions, afforded methyl ester **2.3**. Methyl 3-hydroxypicolinate (**2.3**) was selectively brominated at the 6-position, by electrophilic aromatic substitution to yield compound **2.4**. The pseudo-phenolic hydroxy functionality of methyl ester **2.4** was protected with a benzyl group by treatment with benzyl bromide under mildly basic conditions to afford the hybrid reactivator precursor, methyl 3-benzyloxy-6-bromopicolinate (**2.5**).

Two preliminary quinoline-containing candidates were identified and synthesised in order to evaluate the effect of substitution around the quinoline peripheral site ligand upon the reactivation efficiency of the candidate.

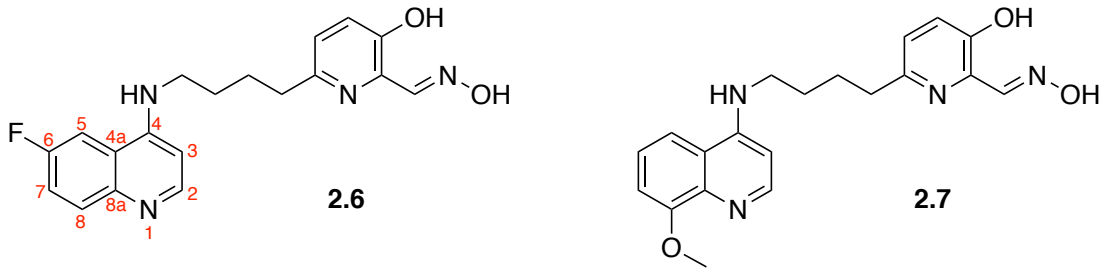

Figure 2.4. Substituted quinoline hybrid reactivators, red numbers represent the quinoline numbering system

Quinoline **2.6** is furnished with a fluorine atom at the 6-position, while quinoline **2.7** bears a methoxy substituent at the 8-position. These compounds were designed to give more information on the effect of adding steric and electronic effects to the quinoline ring, such that the relationships between the chemical structure of these compounds and their biological activity can be probed.

2.4 Preliminary Molecular Docking

Following the development of 6-fluoroquinoline **2.6** and 8-methoxyquinoline **2.7** hybrid reactivators (Figure 2.4), preliminary *in silico* molecular docking experiments were undertaken to validate the design of substituted-quinolines as potential reactivators of OP-inhibited *h*AChE. The docking studies aimed to develop an understanding of the most likely location of reactivator candidates in space, relative to the enzyme (uninhibited AChE, pdb: 4PQE). This was achieved by energy minimisation of both ligand and protein and subsequently running docking algorithms (using a trial license for Maestro LigPrep and Slide package, version 10.5.014, release 2016-1, Schrödinger and generic force field: OPLS_2005).

In silico models (Figure 2.5 and Figure 2.6) demonstrate a conformation that is conducive to π-π stacking interactions between the quinoline PSL and pyridine oxime reactivator aromatic systems of hybrids **2.6** and **2.7** and aromatic residues of *h*AChE, such as tryptophan and phenylalanine. Encouragingly, the interatomic distances between the oxygen atoms of **2.6** and **2.7** and the oxygen atom of serine-203 of AChE are also consistently below 15 Å. This indicates potentially sufficient proximity of the reactivator to the serine residue to elicit reactivation.

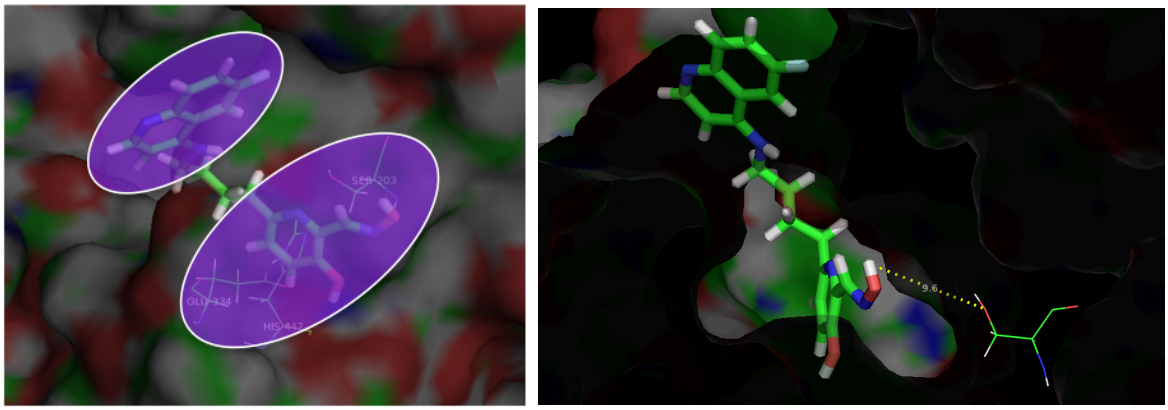

Figure 2.5. (left) shows the two components of the fluorinated hybrid reactivator **2.6**, highlighted in purple. The purple oval at the top of the image shows the PSL and the oval at the bottom shows the pyridine-oxime. The catalytic triad within the gorge is also highlighted. Figure 2.5b. (right) shows the interatomic distance (9.6 Å) between the oxime hydrogen of the hybrid reactivator and the serine-203 oxygen of AChE.

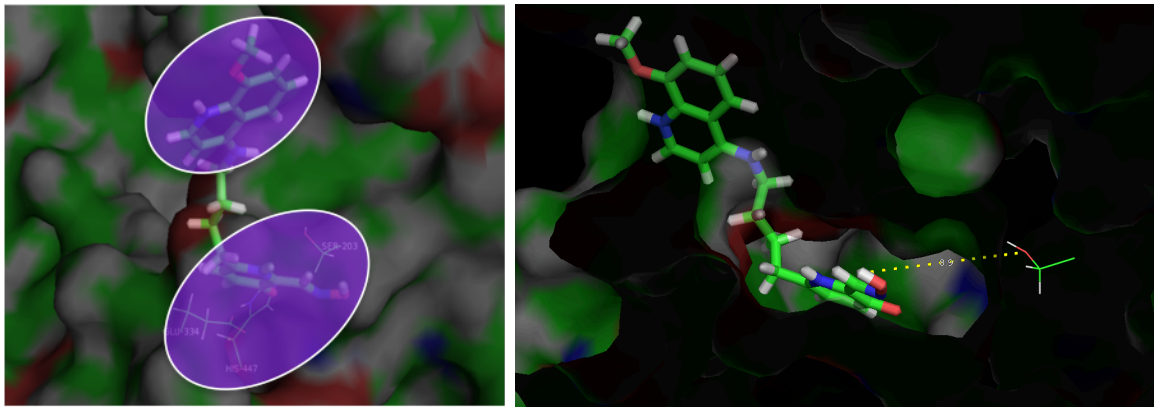

Figure 2.6a. (left) shows the two components of the methoxylated hybrid reactivator **2.7** compound, highlighted in purple. The purple oval at the top of the image shows the PSL and the oval at the bottom shows the pyridine-oxime. The catalytic triad within the gorge is also highlighted. Figure 2.6b. (right) shows the interatomic distance (8.9 Å) between the oxime hydrogen of the hybrid reactivator and the serine-203 oxygen of AChE.

The docking studies reinforced what was expected with respect to binding mode and orientation of the novel hybrid reactivators within the *h*AChE enzyme. Broadly, these preliminary studies showed the potential for interactions expected to be observed in an efficient hybrid reactivator and gave confidence in the design of hybrids **2.6** and **2.7**.

2.5 Development Towards the Synthesis of Substituted Quinolines

Efforts towards an efficient and replicable synthesis of substituted quinolines were undertaken. Initial synthetic work involved the use of a Gould-Jacobs reaction of an aniline (Scheme 2.2). *p*-Fluoroaniline (**2.8**) was treated with diethyl ethoxymethylenemalonate, under neat conditions at 110 °C for 4 hours, to yield enamine **2.9**, which was followed by cyclisation in diphenyl ether at 250 °C to furnish ester substituted quinolin-4-ol **2.10**. Cyclised quinoline **2.10** was heated to 100 °C with NaOH under neat conditions to afford carboxylic acid substituted quinoline **2.11**.

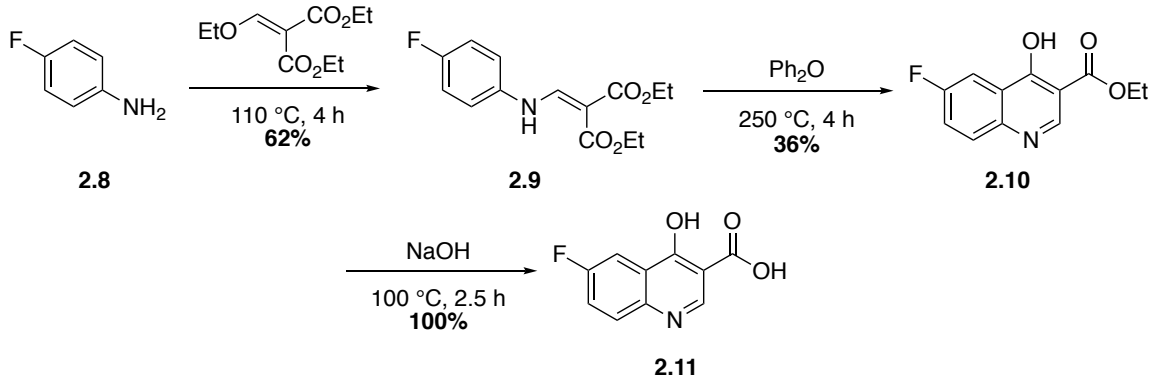

Scheme 2.2. Gould-Jacobs cyclisation of *p*-fluoroaniline

This method was abandoned at this stage due to the number of steps required to access quinoline intermediate **2.11**. In addition, further steps would be required for the decarboxylation to yield the desired substituted quinoline-4-ol. Instead, an alternative method was established with greater efficiency, with the desired substituted quinolin-4-ol obtained over just 2 steps.

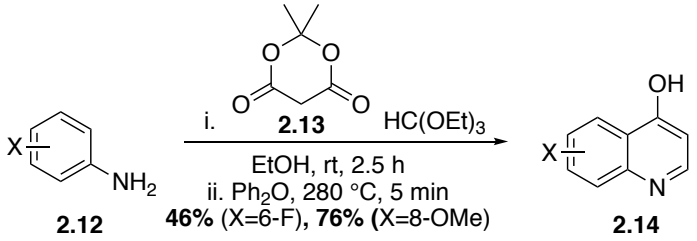

Scheme 2.3. Meldrum's acid facilitated cyclisation (X=6-F **2.14a** (46%) and 8-OMe **2.14b** (76%))

Substituted anilines **2.12a-b** were treated with Meldrum's acid **2.13** and triethyl orthoformate at room temperature for 2.5 hours in EtOH (Scheme 2.3). Intermediates **2.18** were used directly in the next step and heated to 280 °C in diphenyl ether for 5 min (Scheme 2.3). Conveniently, it was possible to crystallise the quinolin-4-ol product **2.14** from the reaction solution during workup, therefore removing the need for chromatographic purification, facilitating large scale reactions (up to 10 g).

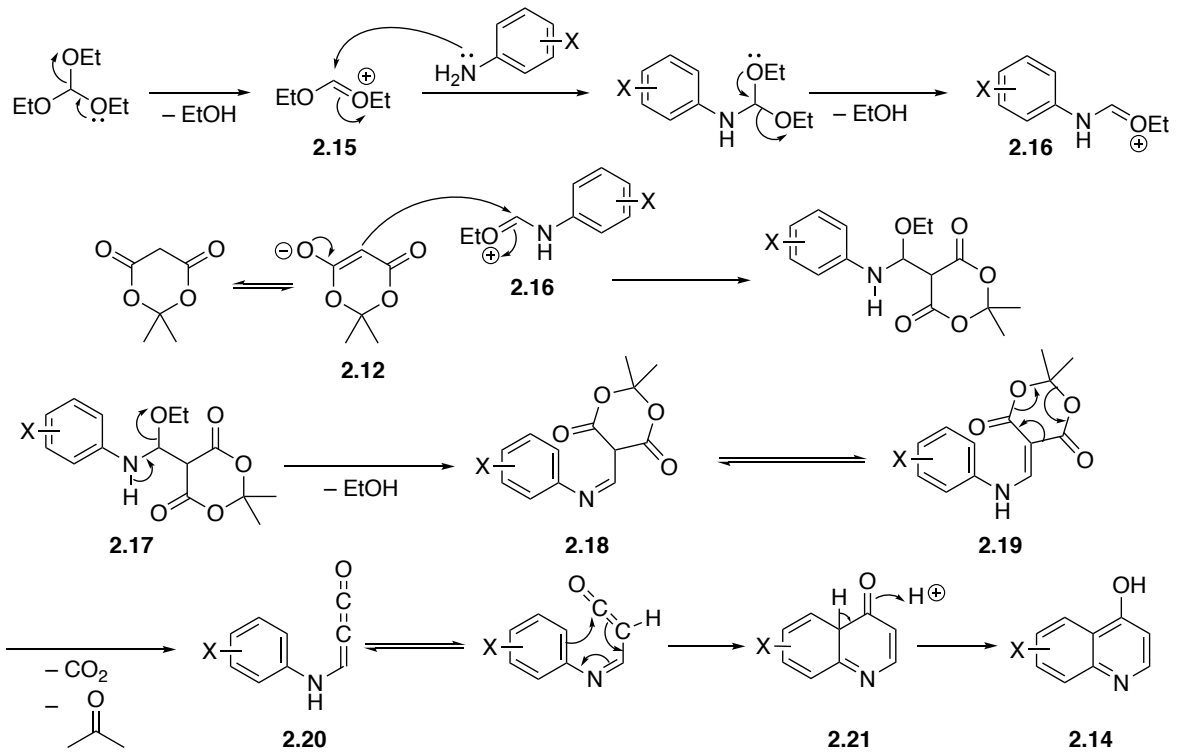

Scheme 2.4. Proposed mechanism of Meldrum's acid facilitated quinoline synthesis

The proposed mechanism (Scheme 2.4) starts with the loss of EtOH and the subsequent attack of the reactive intermediate **2.15** by the aniline nitrogen. Through loss of another equivalent of EtOH, a second reactive intermediate **2.16** is produced, which reacts with the enol or enolate of Meldrum's acid **2.12**. A third equivalent of EtOH is lost from amine **2.17** to afford imine **2.18**. Under thermal conditions, enamine **2.19** undergoes a rearrangement and through loss of CO_2 and CO, ketene **2.20** is formed. The ketene undergoes a cyclisation to furnish bicyclic species **2.21**, which subsequently undergoes tautomerisation to afford the final quinolin-4-ol **2.14**.

The thermally initiated ring closure of the quinoline proved to be effective for the synthesis of 6-fluoroquinolin-4-ol (**2.14a**) and 8-methoxyquinolin-4-ol (**2.14b**) with useful yields of 46% and 76% and easy product isolation over two steps. Following the generation of the substituted quinolin-4-ols, the PSL candidates were brominated by treatment with phosphorus tribromide in yields exceeding 95%. Again, the 4-bromoquinolines were conveniently isolated by crystallisation during workup.

The subsequent step in the synthetic route is the substitution of the quinolin-4-ol with 3-butyn-1-amine (**2.24**). This has previously been achieved by de Sousa (Scheme 2.5), through treatment of quinolin-4-ol **2.22** with triflic anhydride and triethylamine to afford triflate **2.32**.[188] Subsequent Buchwald-Hartwig amination (BHA) furnished the terminal alkyne **2.25** in an overall yield, over two steps, of 11%.

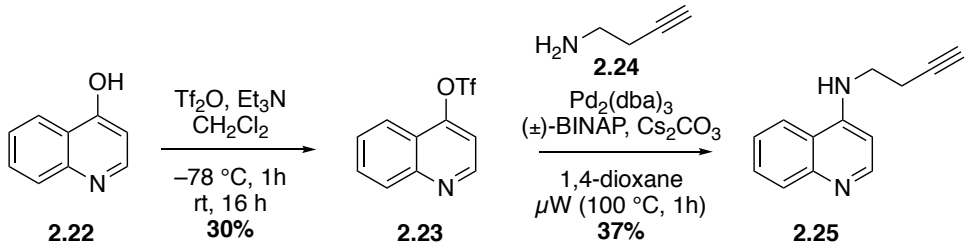

Scheme 2.5. Fomation of homopropargyl substituted quinolin-4-amine reported by de Sousa[188]

Later, de Sousa, starting with commercially available 4-bromoquinoline (**2.26**), modified this sequence to afford terminal alkyne **2.25** without isolation or purification (Scheme 2.6).

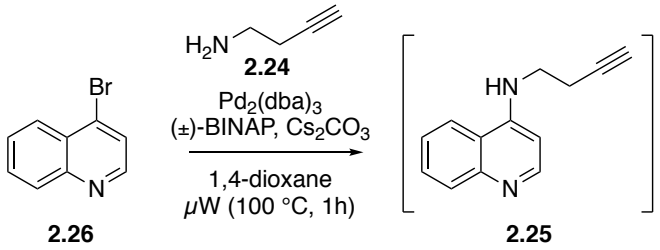

Scheme 2.6. Modified formation of homopropargyl substituted quinolin-4-amine reported by de Sousa[188]

Generally, synthetic steps involving the use of heavy metal catalysts are considered less desirable for the development of medicinal candidates. Metals such as palladium necessitate careful and time-consuming purification steps, and can require special purification techniques, such as the use of expensive resins.[189] With this in mind, synthetic route modification was considered by replacing the palladium-catalysed cross coupling with a simple nucleophillic aromatic substitution (S_NAr) (Scheme 2.7).

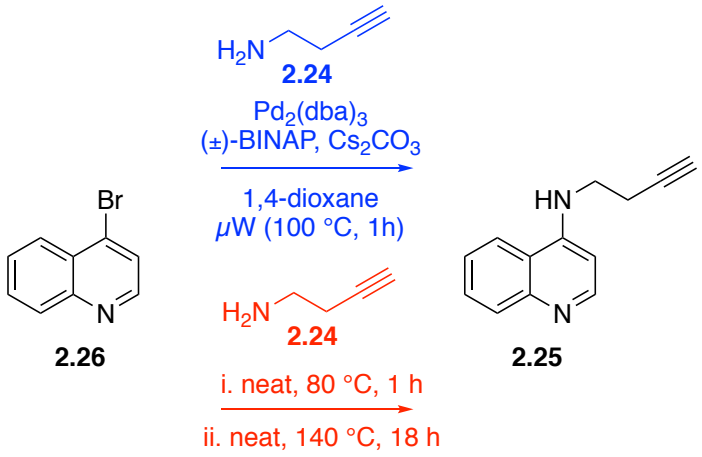

Scheme 2.7. Pd-mediated BHA (blue) and S_NAr metal-free (red) coupling of 4-bromoquinoline with 3-butyn-1-amine

In order to test the efficiency of S_NAr, the 4-chloro and 4-bromo substituted analogues of 6-fluoroquinolin-4-ol (**2.14a**) and 8-methoxyquinolin-4-ol (**2.14b**) were prepared (Scheme 2.8). Treatment of 6-fluoroquinolin-4-ol (**2.14a**) and 8-methoxyquinolin-4-ol (**2.14b**) with phosphorus tribromide afforded 4-bromo-6-fluoroquinoline (**2.26a**) and 4-bromo-8-methoxyquinoline (**2.26b**)

in good yields (67% and 98% respectively). Substituted quinolin-4-ols **2.14a** and **2.14b** were also treated with phosphorus oxychloride to afford 4-chloro-6-fluoroquinoline (**2.27a**) and 4-chloro-8-methoxyquinoline (**2.27b**) in excellent yields of 89% and 100% respectively.

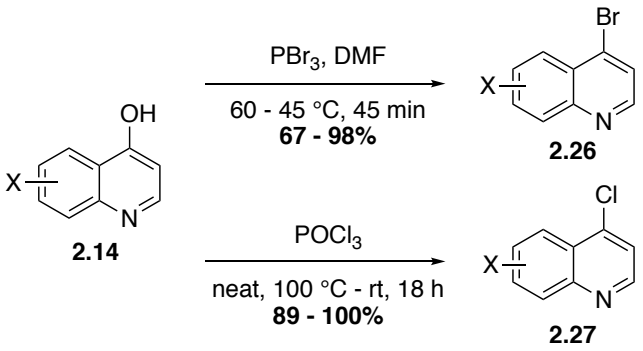

Scheme 2.8. Bromination and chlorination of substituted quinolin-4-ols

A series of preliminary test reactions were undertaken for the substitution of substituted 4-bromoquinolines **2.26** and substituted 4-chloroquinoline with *n*-butylamine and 3-butyn-1-amine (Scheme 2.9, Table 2.1).

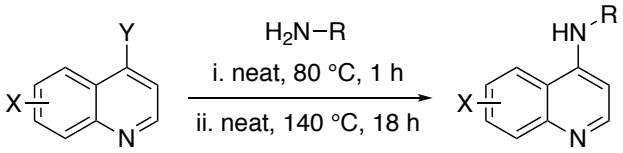

Scheme 2.9. Optimisation of substitution of 4-bromo and 4-chloro substituted quinolines

Table 2.1. Experimental results for the substitution of 4-bromo and 4-chloro substituted quinolines **2.26** and **2.27**. [a]Yields estimated from crude product conversion ratio LCMS (ESI^+) TIC area under curve integration

Entry	Compound	Y	X	R	Estimated Yield[a] (%)
1	**2.28**	Cl	6-F	$(CH_2)_3CH_3$	71
2	**2.29**	Cl	8-OMe	$(CH_2)_3CH_3$	71
3	**2.30**	Br	6-F	$(CH_2)_3CH_3$	83
4	**2.31**	Br	8-OMe	$(CH_2)_3CH_3$	83
5	**2.32**	Cl	6-F	$(CH_2)_2CCH$	30
6	**2.33**	Cl	8-OMe	$(CH_2)_2CCH$	79
7	**2.34**	Br	6-F	$(CH_2)_2CCH$	98
8	**2.35**	Br	8-OMe	$(CH_2)_2CCH$	98

Pleasingly, preliminary S_NAr of 4-bromoquinolines with *n*-butylamine and 3-butyn-1-amine gave good estimated yields up to 98% without purification and with respectable purity. Surprisingly, the bromo-substituted quinolines gave better yields compared to the chloro derivatives. This is unexpected, as the more electronegative halide, chlorine, should create a more electrophilic carbon, onto which the amine nitrogen lone pair can attack and offer greater stabilisation of the Meisenheimer complex (Scheme 2.10).

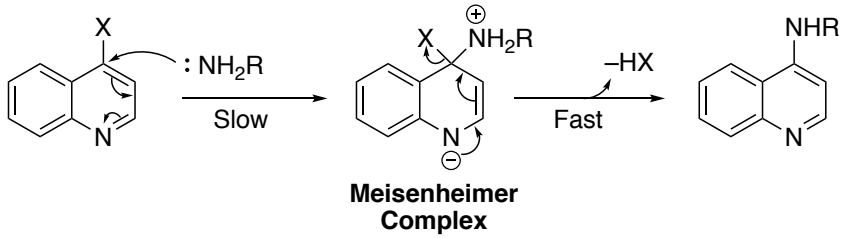

Scheme 2.10. S_NAr amination mechanism *via* Meisenheimer complex

2.6 Synthesis of Hybrid Reactivators

Following a procedure previously described by de Sousa[186], the terminal alkyne was connected to the previously synthesised reactivator portion **2.5** (Scheme 2.11). Both substituted *N*-(but-3-yn-1-yl)-quinolin-4-amines **2.34** and **2.35** were coupled to the 6-bromopyridine reactivator **2.5** moiety using Sonogashira chemistry.

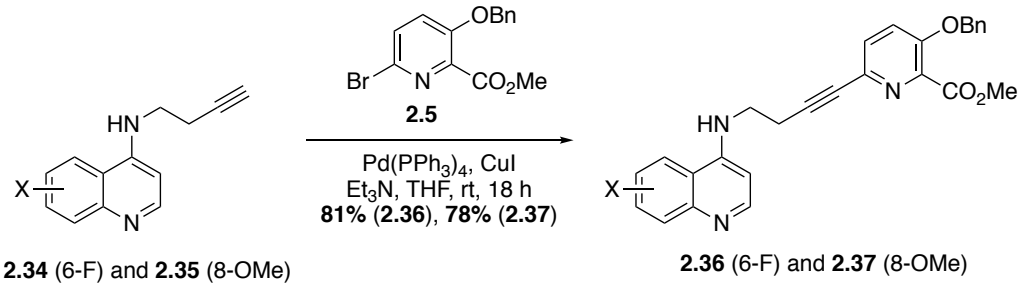

Scheme 2.11. Palladium-catalysed fragment coupling

This step provided very good and replicable yields. Following complete reaction, the compounds were isolated and purified by flash column chromatography (FCC). Subsequent one-pot hydrogenation of the alkyne functionality and hydrogenolysis of the benzyl-protecting group was undertaken, as described by de Sousa (Scheme 2.12).[186]

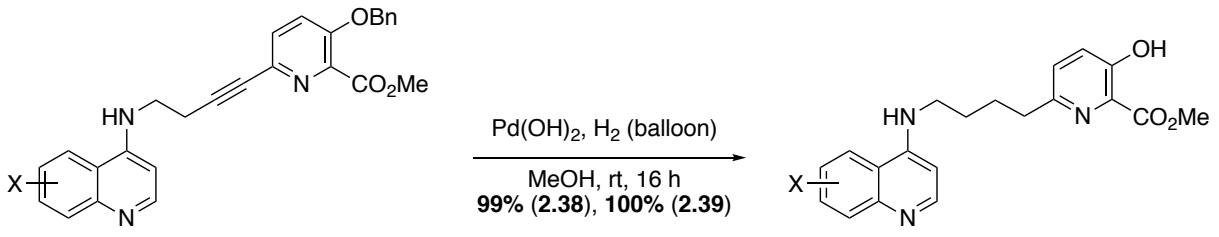

2.36 (6-F) and **2.37** (8-OMe)

2.38 (6-F) and **2.39** (8-OMe)

Scheme 2.12. One-pot hydrogenation and hydrogenolysis of hybrid analogues **2.36** and **2.37**

Esters **2.38** and **2.39** were obtained in high isolated yield by filtration of the reaction solution through a layer of Celite and concentration *in vacuo* without need for further purification.

2.7 Simplification of the Concluding Steps

The proposed concluding synthetic steps towards the final hybrid compounds begin with the treatment of methyl esters **2.38** and **2.39** with TBSOTf and 2,6-lutidine, to afford TBS-protected alcohols **2.40** and **2.41** (Scheme 2.13). Subsequent reduction of crude esters **2.40** and **2.41** with DIBAL-H would then afford aldehydes **2.42** and **2.43**, which are finally reacted with hydroxylamine hydrochloride and sodium acetate to give oximes **2.6** and **2.7**. Initially, attempted purification of the TBS protected esters **2.40** and **2.41** or aldehydes **2.42** and **2.43** were unsuccessful, likely owing their high polarity and the instability of the TBS protecting group. Oximes **2.6** and **2.7** were not obtained *via* this stepwise synthetic route.

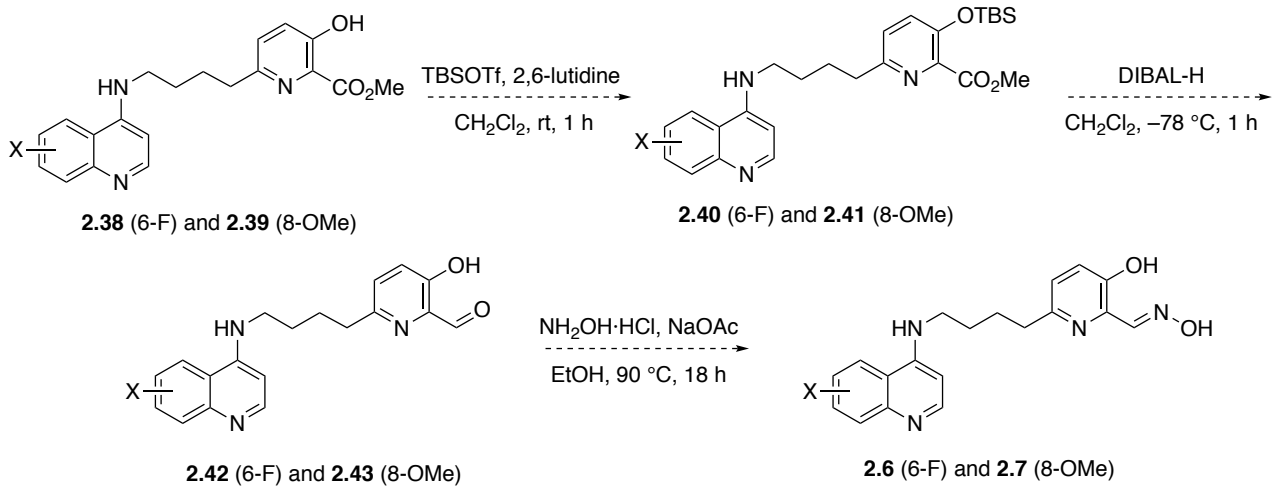

2.38 (6-F) and **2.39** (8-OMe)

2.40 (6-F) and **2.41** (8-OMe)

2.42 (6-F) and **2.43** (8-OMe)

2.6 (6-F) and **2.7** (8-OMe)

Scheme 2.13. Proposed route towards final hybrid reactivators **2.6** and **2.7**

The route was modified such that the intermediate species were not isolated and the final three steps were undertaken as a one-pot process to avoid product loss during purification (Scheme 2.14). Following this modification, oximes **2.6** and **2.7** were obtained in excellent yield.

A TBS-deprotection step is not necessary during the three-step synthesis, an observation first made by de Sousa.[186] It is postulated that the electron deficient nature of the hydroxypyridine ring

weakens the Si-O bond; this is demonstrated by the facile and complete cleavage of the TBS functionality upon treatment with DIBAL-H. This removes the need for an additional deprotection step.

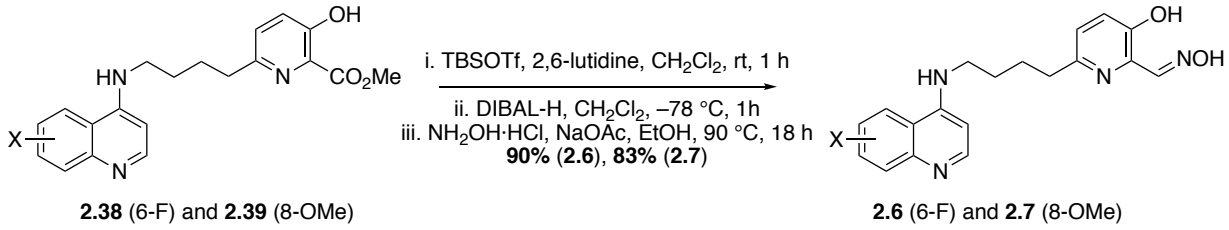

Scheme 2.14. One-pot protocol for synthesis of oximes **2.6** and **2.7** from esters **2.38** and **2.39**

Using the modified approach described above, the final hybrid reactivators **2.6** and **2.7** were obtained over 12 steps in 32% and 29% yield respectively, a reasonable yield to obtain up to 100 mg of reactivator compounds. Biological evaluation of these reactivator candidates is discussed in Chapter 4.

This optimised route was applied to the synthesis of lead hybrid reactivator **2.1** (Scheme 2.15). Previously developed conditions described by de Sousa[186] gave an overall yield of 22% over the final 6 steps of the synthetic route. The optimised route, including simple S_NAr of 4-bromoquinoline (**2.26**) with 3-butyn-1-amine (**2.24**) gave an improved overall yield of 41% over the final 6 steps.

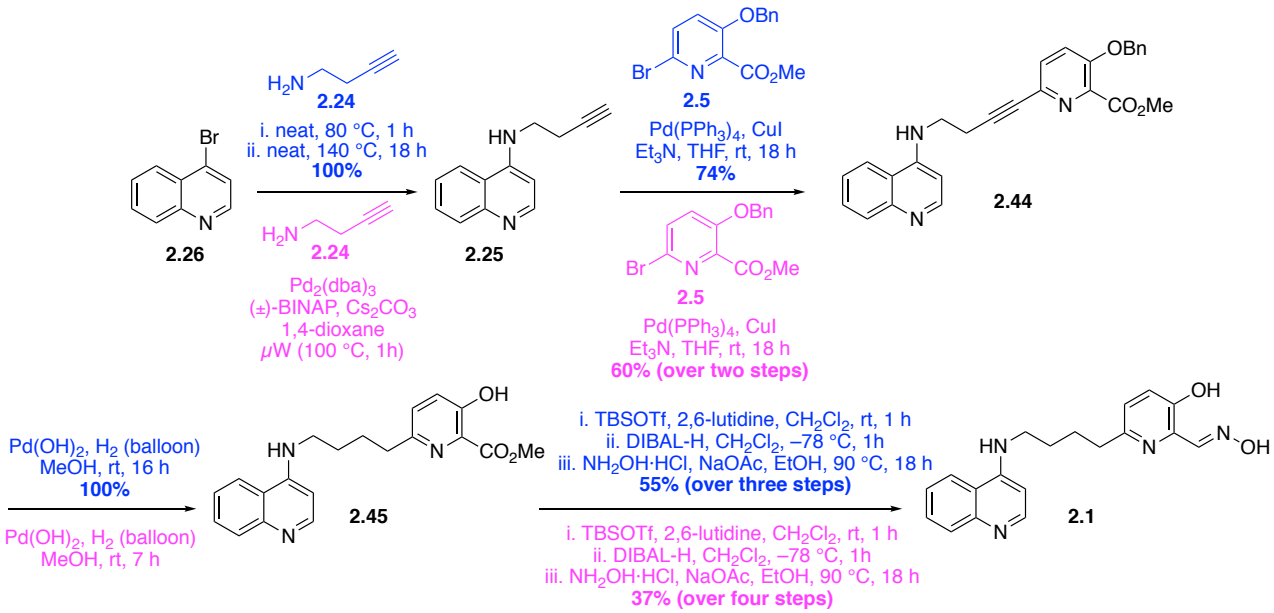

Scheme 2.15. Comparison of synthetic routes towards hybrid reactivator **2.1**, first synthesised by de Sousa.[186] Pink text indicates original route conditions, while blue text shows the optimised route

2.8 Other Substituted Quinolines: Introduction

Following the development of a practical synthetic route towards substituted-quinoline containing hybrid reactivators, efforts shifted to the development of a broader library of differently substituted quinoline compounds. Compounds **2.46**, **2.47**, **2.48** and **2.49** represent further substituted quinoline-containing hybrid reactivators.

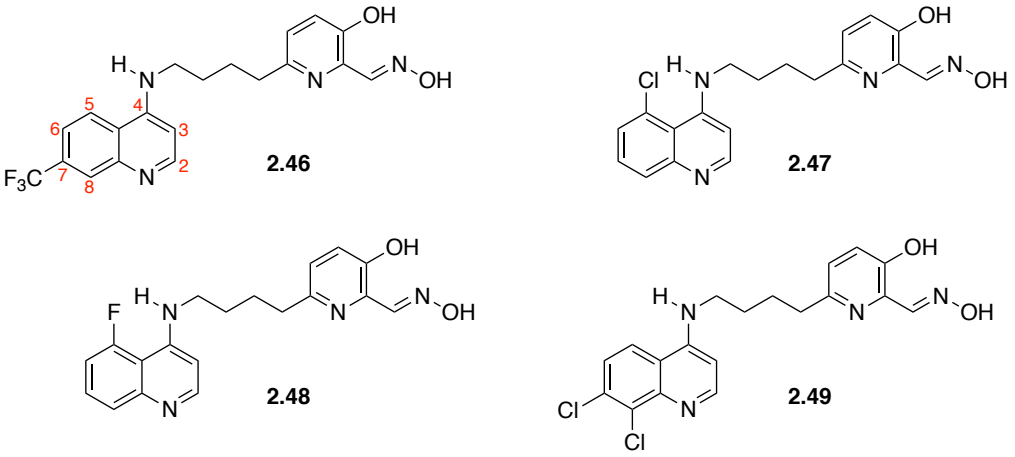

Figure 2.7. Hydroxylated substituted quinoline hybrid reactivators

The new quinoline reactivators (Figure 2.7) were developed with the intention of testing the effect of additional substitution around the quinoline ring to build preliminary structure-activity relationship (SAR) investigations. 7-Trifluoromethylquinoline **2.46** would allow an opportunity to test SAR with substitution at this position. 5-Chloroquinoline **2.47** would allow SAR of 5-substituted quinolines. Sussman *et al.* mention in their paper,[64] in which the crystal structure of *h*AChE was elucidated, that there was a notably density of hydrophobic amino acid residues present in the peripheral and active sites. This compound would offer an opportunity to test the effect of the introduction of hydrophobic functionality within the system. 5-Fluoroquinoline **2.48** represents an opportunity for a comparative study with **2.47**. Finally, 7,8-dichloroquinoline **2.49** presents an additional opportunity to assess the extent to which it is possible to exploit these apparent hydrophobic interactions within the peripheral site of AChE and whether this would be advantageous in terms of increasing the affinity of these potential reactivator candidates to the site of reactivation.

2.9 Further Synthesis of Substituted Quinoline Reactivators

7-Trimethylquinoline **2.46** was synthesised according to the synthetic route as described in Section 2.4. and was obtained in 20% overall yield over 12 steps (Scheme 2.16).

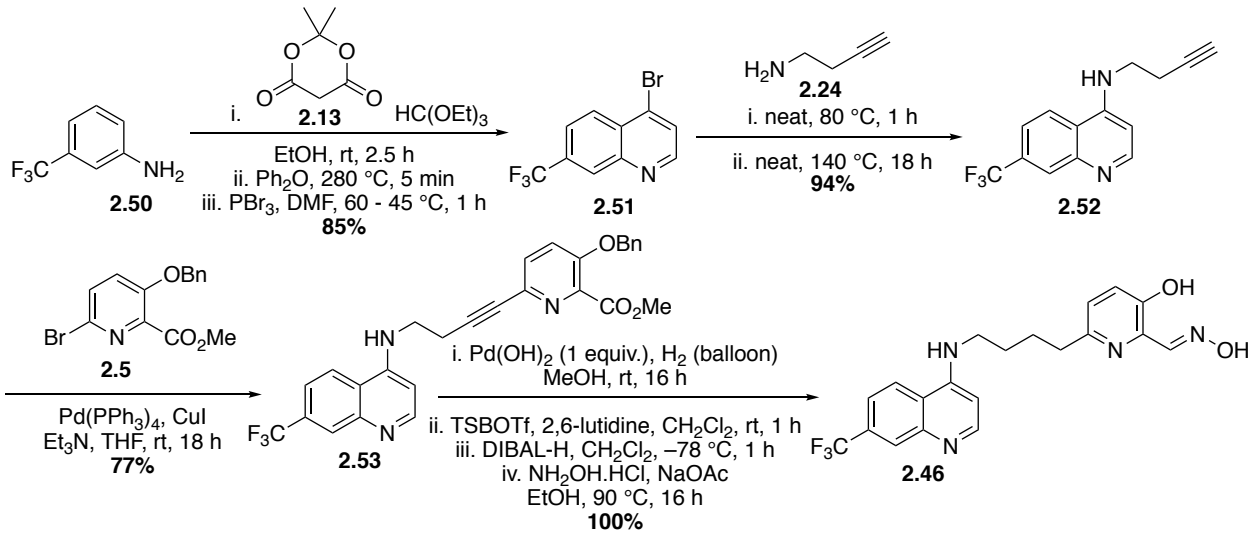

Scheme 2.16. Synthetic route towards 7-trifluoromethylquinoline **2.46** hybrid reactivator

Preparation of the substituted quinolines was achieved using the thermal cyclisation approach described in Section 2.5 from corresponding anilines. *meta*-Anilines have the potential to undergo ring closure at the *ortho* and *para* positions (Scheme 2.17).

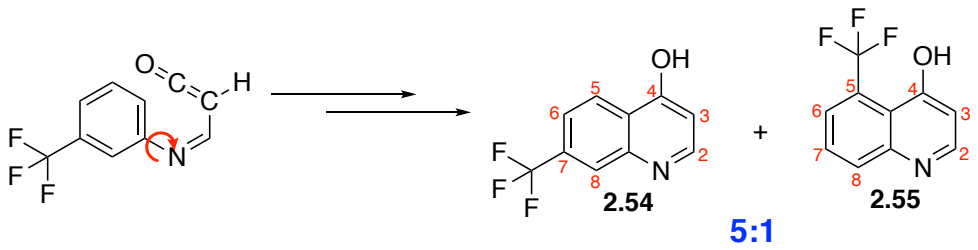

Scheme 2.17. Formation of two regioisomers during thermal cyclisation

Indeed, upon thermal cyclisation of *meta*-directing and ring deactivating *m*-trifluoromethylaniline in the presence of Meldrum's acid, a mixture of regioisomeric products was observed. The ratio of the trifluoromethyl-substituted quinolin-4-ols was determined to be 5:1 (**2.54**:**2.55**) using integration of ^{19}FNMR signals. Purification of the 5:1 mixture by column chromatography allowed further enrichment of the 7-trifluoromethane isomer (9:1, **2.54**:**2.55**).

Following cyclisation of *o/p* directing and ring activating *m*-methylaniline, o*rtho/para* directing and ring deactivating *m*-chloroaniline and *o/p* directing a ring deactivating *m*-fluoroaniline, *m*-anilines bearing *ortho/para* directing groups generally result in *ortho* cyclisation (giving 5-substituted quinolin-4-ols) and *meta* directing groups generally favour *para* cyclisation (giving 7-substituted quinolin-4-ols).

2.9.1 Towards Chloroquinoline-Containing Hybrid Reactivators

Syntheses of 5-chloroquinoline **2.47**, 7,8-dichloroquinoline **2.49** and 6-chloroquinoline analogues were undertaken as described in Sections 2.5 to 2.7 (Scheme 2.18). Substituted anilines **2.56-2.58**

were converted to substituted 4-bromoquinolines **2.59-2.61** and subsequent S_NAr with 4-butyn-1-amine (**2.24**) afforded *N*-homopropargyl substituted quinolines **2.62-2.64**. Sonogashira cross coupling of 5-chloroquinoline **2.62** and 7,8-dichloroquinoline **2.63** with pyridine **2.5** afforded esters **2.65** and **2.66**, both in high yields.

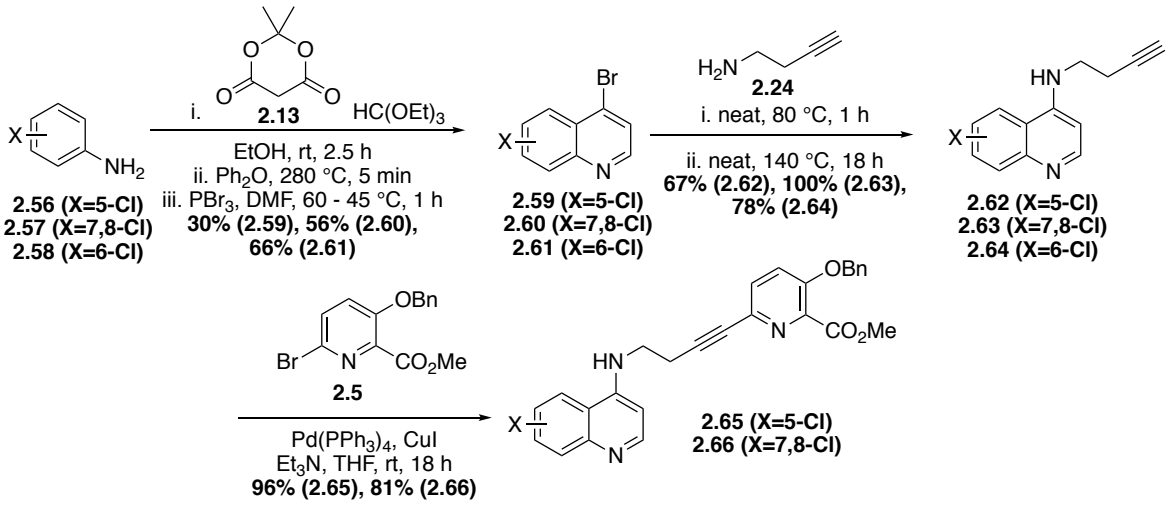

Scheme 2.18. Synthetic route towards chloroquinoline hybrid reactivators

Unfortunately, initial efforts to access the chlorinated reactivators by subjecting the mono- and dichloroquinolines **2.68** and **2.69** to the previously optimised alkyne hydrogenation and *O*-debenzylation conditions were unsuccessful due to complete reduction and cleavage of all carbon-chlorine bonds (Scheme 2.19).

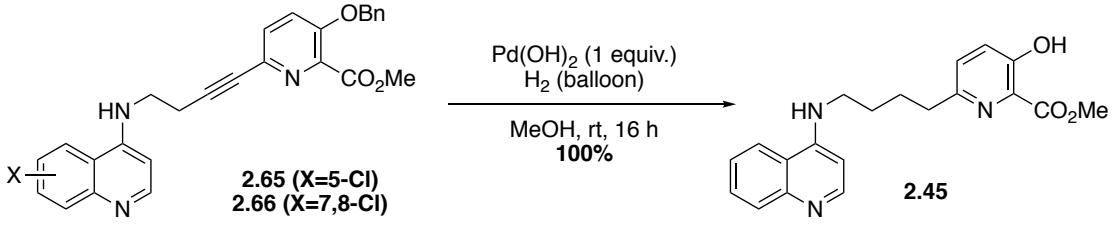

Scheme 2.19. Unselective hydrogenation of chloroquinolines **2.65** and **2.66**

A series of experiments were undertaken to ascertain conditions for selective hydrogenation and *O*-debenzylation without cleavage of chlorine atoms. Reactions were monitored by TLC over time with increasing equivalents of catalyst. Unfortunately, it was not possible to obtain fully hydrogenated and *O*-debenzylated products without observing chlorine cleavage using Pearlman's catalyst. Therefore, alternative hydrogenation methods were explored towards the selective reduction of the alkyne moiety. Wilkinson's catalyst was selected as an alternative to Pearlman's catalyst, and a benzoyl protecting group was added to the pseudo-phenolic hydroxyl functionality of the 6-bromopyridine reactivator moiety **2.4** to afford benzoate **2.67**. Benzoyl ester **2.67** was

subjected to Sonogashira cross-coupling conditions with *N*-homopropargyl quinolines **2.62**, **2.63** and **2.64** to give coupled quinolines **2.68**, **2.69** and **2.70** in excellent yield (Scheme 2.20).

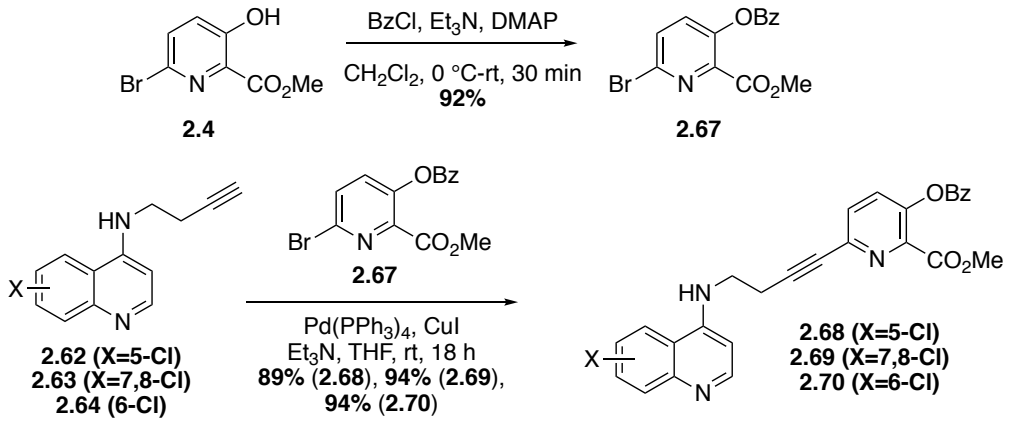

Scheme 2.20. Synthesis of benzoyl-protected alkyne-linked reactivator analogues

Chloro derivatives **2.68-2.70** were treated with 0.45 equivalents of Wilkinson's catalyst for 24 h in EtOAc, however no conversion to the reduced product was observed. Compound **2.69** was also treated with 0.15 equivalents of Wilkinson's catalyst under 10 bar of pressure for 24 h. No conversion was observed and this method of reduction was abandoned (Table 2.2).

Table 2.2. Summary of attempted hydrogenation using Wilkinson's Catalyst ($Rh(PPh_3)_3Cl$)

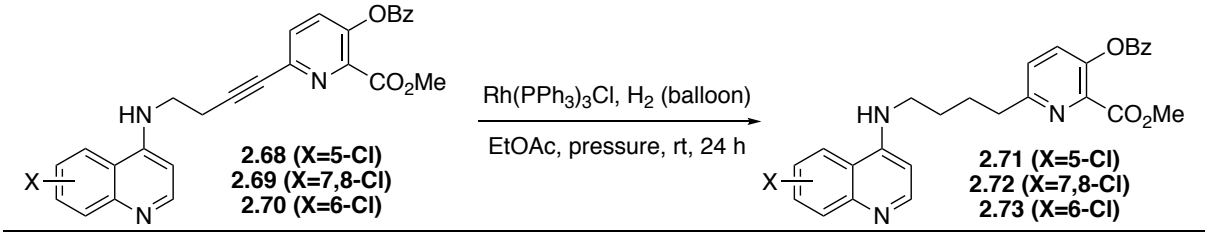

Starting Compound	Catalyst	Equivalents Catalyst	Pressure (bar)	Time (h)	Yield (%)
2.68	$Rh(PPh_3)_3Cl$	0.45	1	24	0
2.69	$Rh(PPh_3)_3Cl$	0.45	1	24	0
2.70	$Rh(PPh_3)_3Cl$	0.45	1	24	0
2.69	$Rh(PPh_3)_3Cl$	0.15	10	24	0

Diimide reduction was next explored. Diimide reduction has been previously used for the reduction of aliphatic unsaturation in compounds containing C-X bonds (Scheme 2.21).[190]

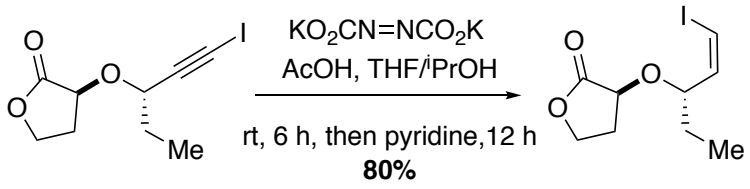

Scheme 2.21. Diimide reduction described by Denmark and Yang

6-Chloro-substituted quinoline **2.70** was treated with tosyl hydrazine ($TsNHNH_2$) and sodium acetate in THF under reflux (Scheme 2.22). After 18 hours a 12% yield of the desired hybrid precursor was obtained, without loss of the chloro group. Although selective reduction was achieved, the low yield of the alkyl-linked compound **2.74** was not satisfactory for further progression, and further development of the chloroquinolines was suspended. Diimide is firstly formed *in-situ* by treatment of $TsNHNH_2$ with sodium acetate, releasing acetic acid and sodium tosylate. Upon formation of diimide, reaction with an alkyne *via* a 6-membered transition state, proceeding through a concerted reaction, releases one equivalent of nitrogen gas and affords reduced alkene.

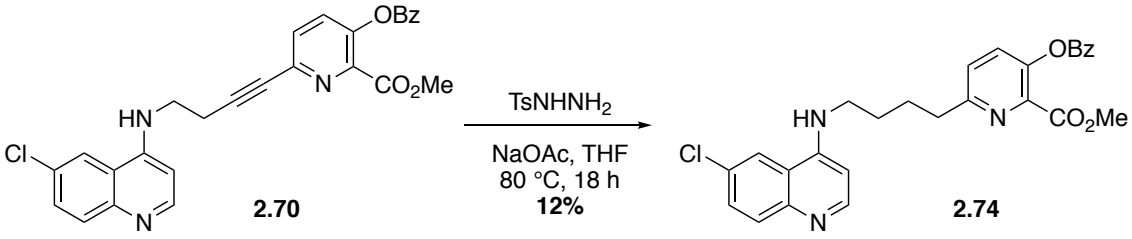

Scheme 2.22. Diimide reduction of alkyne **2.70**

2.9.2 Towards Methyl-Containing Hybrid Reactivators

Although a successful method towards chloro-substituted quinolines was developed, due to time constraints and given the poor yield obtained from the diimide reduction, it was decided that the chlorine-containing compounds should be replaced with their corresponding methyl analogues. The methyl group is often described as a classical isostere of chlorine, due to their comparable lipophilicity and Van der Waals radii.[191]

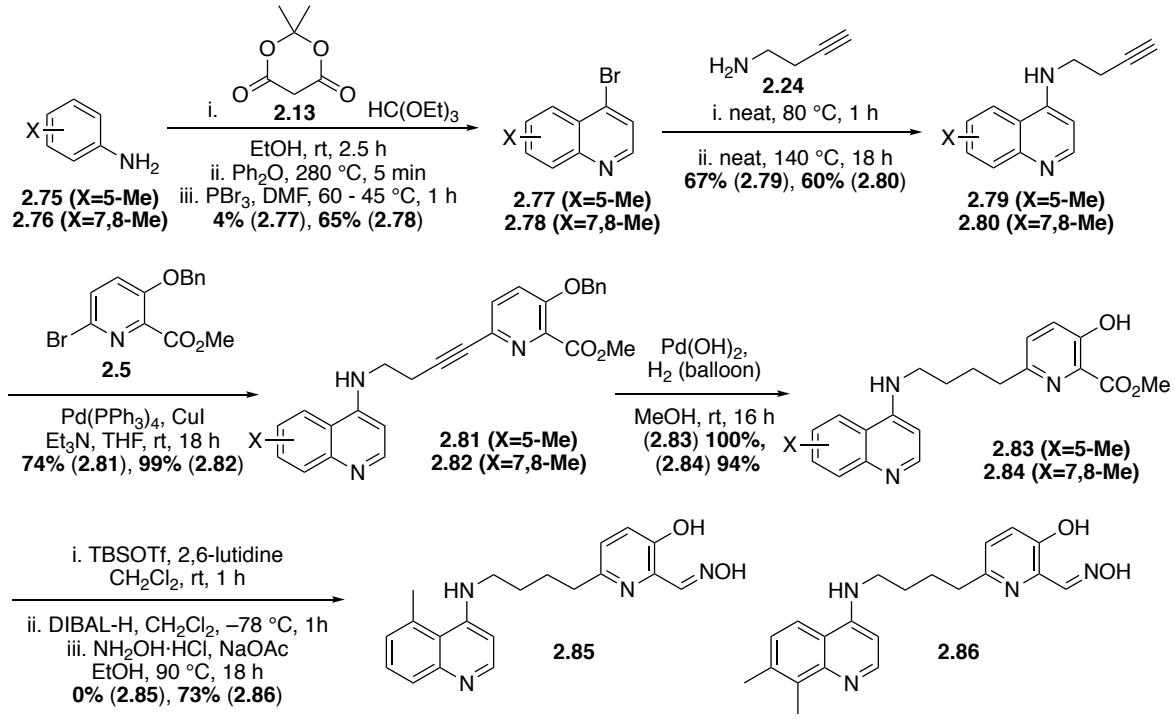

Scheme 2.23. Synthetic route undertaken towards compounds **2.85** and **2.86**

7,8-Dimethylquinoline **2.86** was obtained over 12 steps in 26% yield (Scheme 2.23).

Unfortunately, the final three-stage conversion of the 5-methyl-substituted hybrid compound was unsuccessful, despite several attempts. Due to the length of the synthetic route and time constraints, 5-methylquinoline **2.85** was abandoned and 5-fluoroquinoline hybrid **2.48** was pursued (Scheme 2.24).

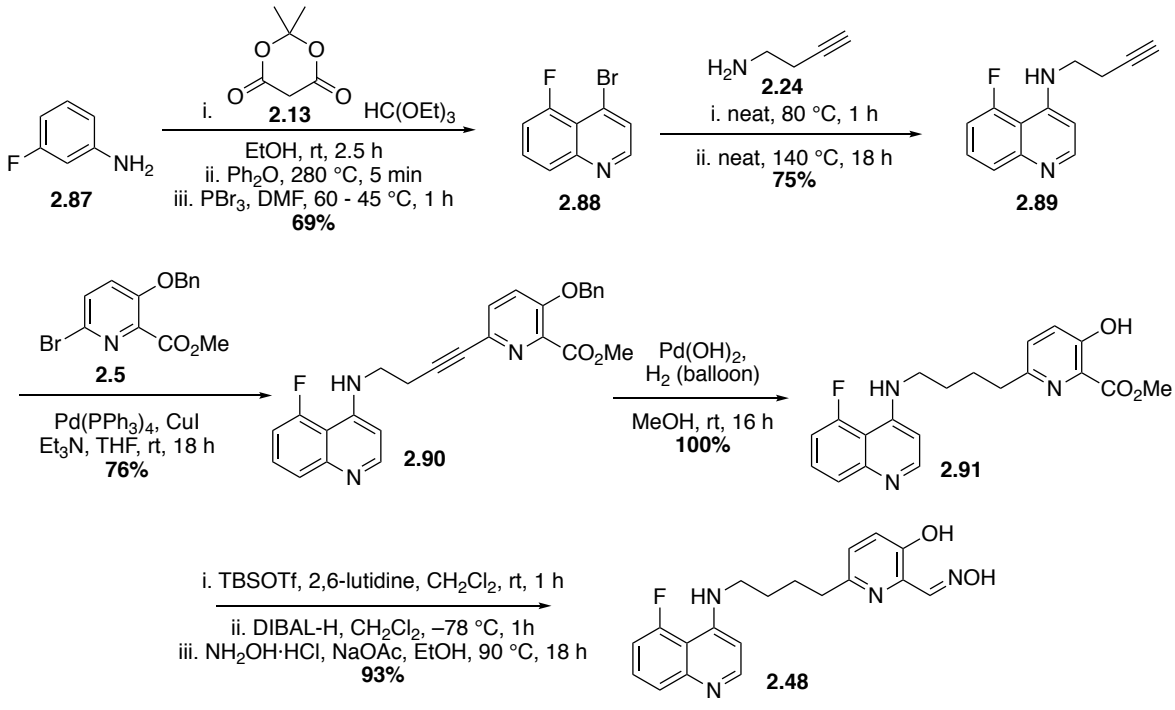

Scheme 2.24. Synthetic route towards compound **2.48**

5-Fluoroquinoline **2.48** was obtained through the synthetic route as described above in Scheme 2.24 in an overall yield of 17% over 12 steps.

2.10 Non-Quinoline Based Reactivators

This section explores efforts towards the integration of 1,8-naphthyridine and indole containing scaffolds as peripheral site ligands. The integration of different PSL scaffolds was envisaged to offer a richer library of compounds and increase understanding of interactions between the PSL and the peripheral site of the inhibited enzyme, during reactivation, such as potential hydrogen bonding. Figure 2.8 shows the three alternative heterocyclic aromatic PSL motifs targeted in this work.

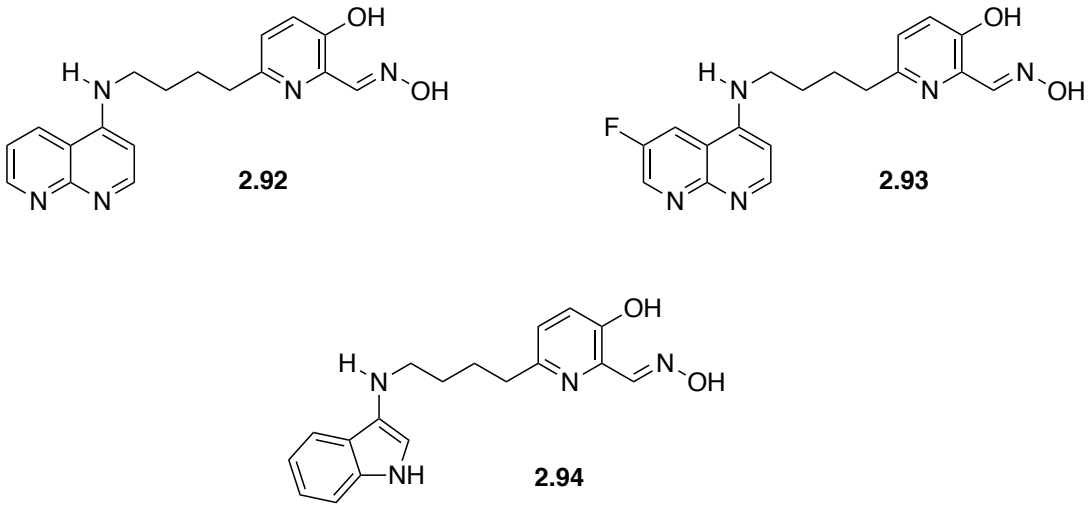

Figure 2.8. Naphthyridine and indole-containing hybrid reactivators

1,8-Naphthyridine hybrids **2.92** and **2.93** represent an opportunity to explore whether any additional hydrogen bonding interactions within the peripheral site can be made by the integration of additional hydrogen bond acceptor functionality within the naphthyridine PSL. This effect may also influence the solubility of the reactivator in water. Indole-containing hybrid reactivators have previously been reported to show reactivation when connected by a 3-membered carbon linker and indole **2.94** was suggested to ascertain whether the reactivation capacity could be improved by the integration of a 4 carbon linkage.

2.10.1 Naphthyridine-Based Reactivators

1,8-naphthyridin-4-ol (**2.97**) has been synthesised previously by Narender and co-workers (Scheme 2.25).[192] They report the treatment of 2-aminopyridine (**2.95**) with methyl propionate (**2.96**) at room temperature in MeOH to afford methyl ester intermediate **2.97** and subsequent cyclisation of intermediate **2.97** at 250 °C in Dowtherm-A yielded 1,8-naphthyridin-4-ol (**2.98**).

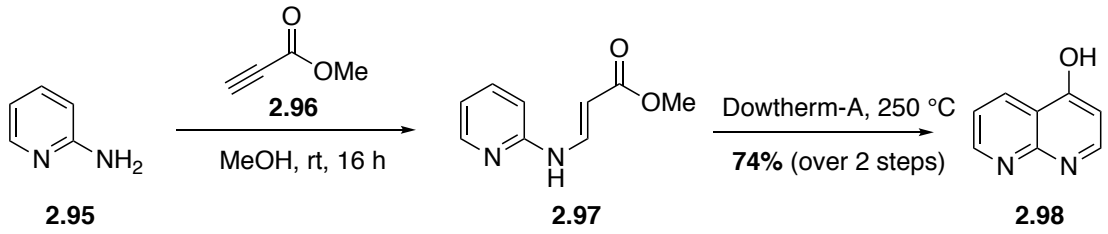

Scheme 2.25. Methyl propionate (**2.96**) mediated thermal cyclisation reported by Narender *et al.*[192]

Narander *et al.* reported a 74% yield over two steps and identified a trough at 3320 cm^{-1} upon characterisation by infrared spectroscopy, indicating the presence of an O–H bond stretching. The literature procedure was repeated using the ethyl derivatised propionate **2.99** and diphenyl ether, due to their availability. Unlike the product reported by Narender *et al.*, plausible product **2.101** was identified by infrared (strong trough at 1690 cm^{-1}) and NMR spectroscopy

Figure 2.9). The ^{1}HNMR spectrum of bicycle **2.101** indicates 6 aromatic proton environments, suggesting the cyclisation of product **2.101**, *via* the pyridine nitrogen.

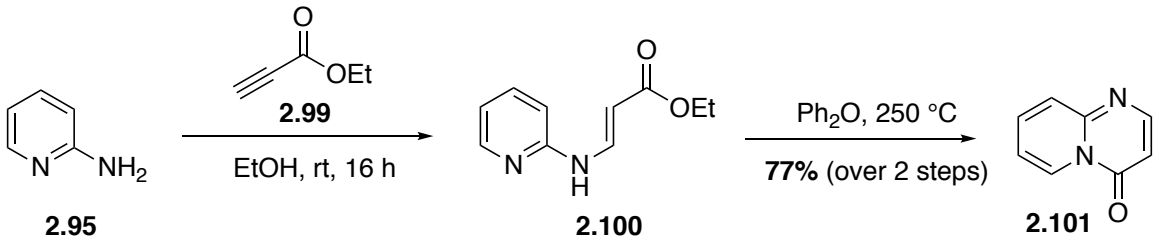

Scheme 2.26. Ethyl propionate (**2.99**) mediated thermal cyclisation

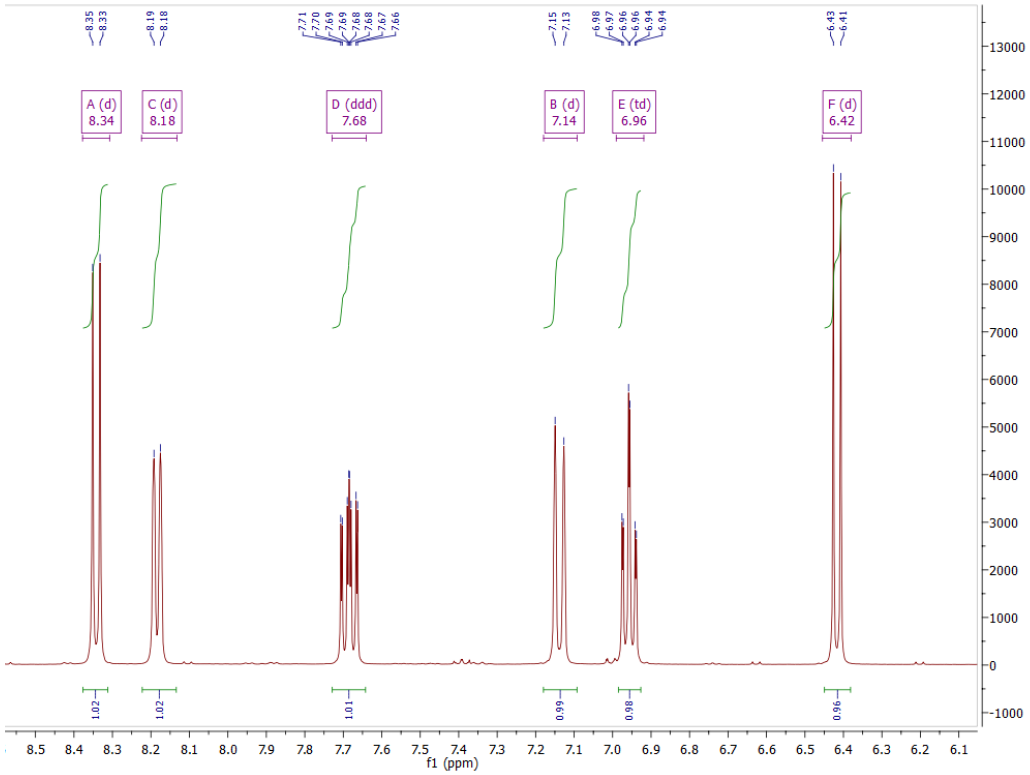

Figure 2.9. ^{1}HNMR of the aromatic region (8.5 to 6.0 ppm) of apparent bicyclic product **2.101** indicates 6 proton environments

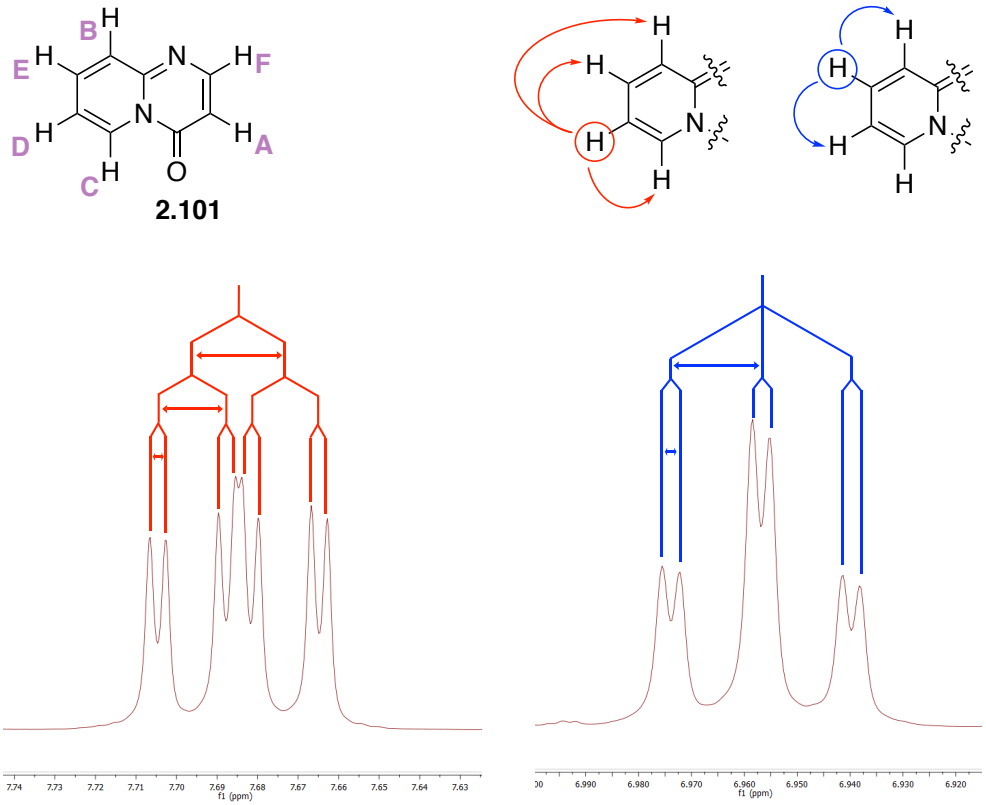

Figure 2.10. Purple letters on structure **2.101** show assignment as per the spectrum above. Multiplets (**ddd** and **td**) are shown with corresponded protons circled and coupling indicated by arrows (top right)

It was subsequently envisaged that 1,8-naphthyridin-4-ol (**2.98**) might be constructed by means of a Meldrum's acid thermal cyclisation. Upon treatment of 2-aminopyridine (**2.95**) with triethyl orthoformate and Meldrum's acid (**2.13**) at room temperature for 2.5 hours, the formation of a new spot was observed by TLC, tentatively assigned to enamine **2.102** (Scheme 2.27). However, subsequent heating to 280 °C in diphenyl ether afforded a brown complex mixture of decomposition products.

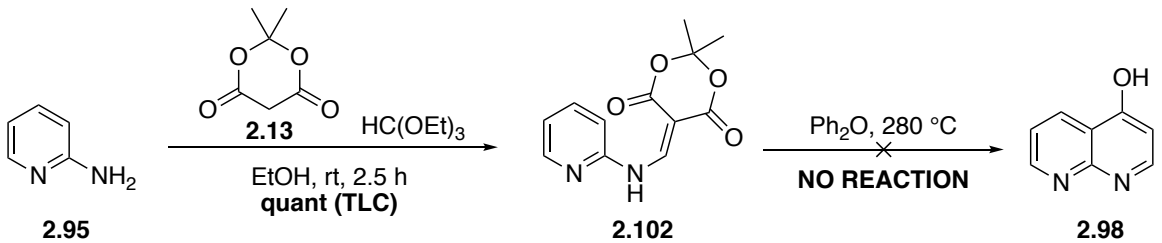

Scheme 2.27. Meldrum's acid (**2.13**) thermal cyclisation of 2-aminopyridine (**2.95**)

Following unsuccessful efforts to synthesise 1,8-naphthyridin-4-ol by thermal cyclisation, feasibly due to the decreased electron density within the pyridine ring compared to the phenyl derivative, the synthesis of hybrid reactivators bearing the naphthyridine PSL was abandoned.

2.10.2 Indole-Based Reactivators

The introduction of a reactive amino handle at the 3-position of indole **2.103** was explored, such that it could be coupled with a homopropargyl linker. It was initially predicted that nitration and subsequent reduction would enable access to 3-aminoindole **2.105** (Scheme 2.28).

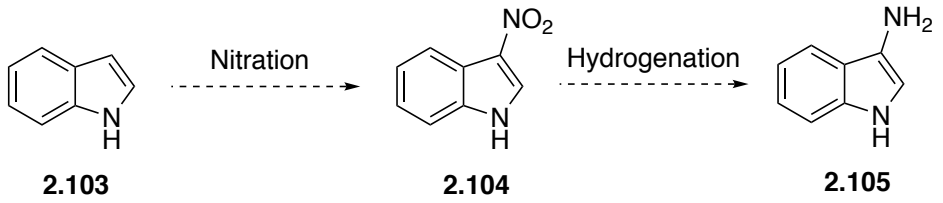

Scheme 2.28. Proposed route towards 3-aminoidole **2.104**

Firstly, toluenesulfonyl-protected indole **2.105** was prepared by treatment of indole **2.103** under basic phase-transfer conditions to give protected indole **2.106** in quantitative yield. Acetyl nitrate was next prepared *in situ* from 70% nitric acid and acetic anhydride, providing the nitronium ion source. Protected indole **2.106** was added to this mixture to afford nitrated indole **2.107** in 26% yield. Finally, nitrated indole **2.107** was hydrogenated over Pd/C to afford *N*-tosyl-3-aminoindole (**2.108**) in 98% yield (Scheme 2.29).

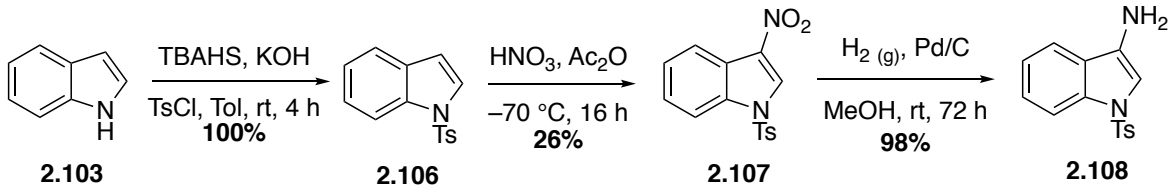

Scheme 2.29. Synthesis of *N*-toluenesulfonyl-3-aminoindole (**2.107**)

The synthesis *N*-homopropargyl aminoindole **2.110** was attempted by *N*-alkylation of aminoindole **2.108** (Scheme 2.30). Unfortunately, the desired alkylated product was no obtained, due to the low electrophilicity of homopropargyl bromide (**2.109**), and its tendency towards elimination (Scheme 2.31).

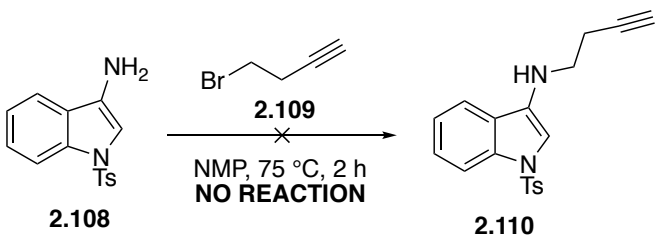

Scheme 2.30. Attempted addition of homopropargyl bromide **2.109**

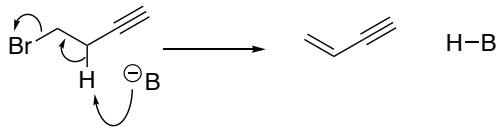

Scheme 2.31. Proposed base-mediated elimination of homopropargyl bromide

An alternative route to *N*-homopropargyl-3-amino-indole (**2.110**) was investigated from 3-bromoindole **2.111** *via* Buchwald-Hartwig palladium mediated amination. *N*-Toluenesulfonyl indole (**2.105**) was treated with bromine at 0 °C to afford 3-bromo-*N*-toluenesulfonyl indole (**2.111**) in quantitative yield (Scheme 2.32).

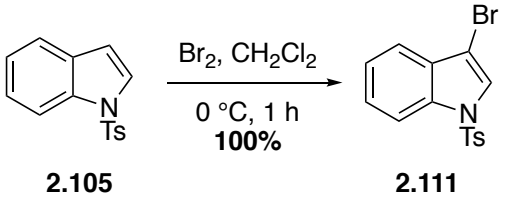

2.105 **2.111**

Scheme 2.32. Bromination of *N*-toluenesulfonyl indole to afford bromoindole **2.111**

Palladium mediated Buchwald-Hartwig amination of 3-bromo-*N*-toluenesulfonyl indole (**2.111**) with 3-butyn-1-amine (**2.24**) was attempted under several different conditions including typical ligands and bases, under microwave irraditation (Table 2.3). Unfortunately, none of the desired product was obtained under any of the conditions investigated.

Table 2.3. Conditions attempted for palladium mediated Buchwald-Hartwig amination of 3-bromo-*N*-toluenesulfonyl indole **2.111** with 3-butyn-1-amine **2.24**

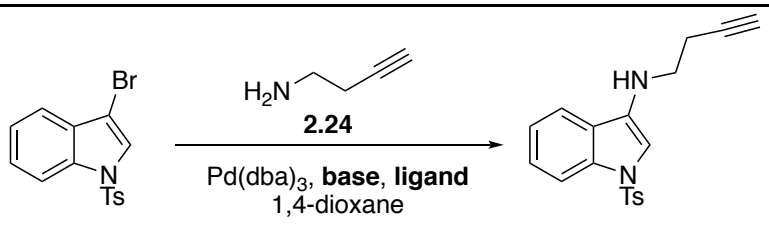

2.111 **2.110**

	Base	Ligand	Conditions	Yield (%)
1	NaO^tBu	Xantphos	90 °C, 16 h	0
2	Cs_2CO_3	(±)-BINAP	100 °C, μW, 1 h	0
3	Cs_2CO_3	(±)-BINAP	90 °C, 16 h	0

Following unsuccessful cross couplings described above, efforts towards indole containing reactivators were abandoned. Recently, Renard and co-workers published the synthesis and *in vitro* evaluation of a similar compound **2.112** containing an indole PSL (Figure 2.11).[193] Indole **2.112**

displayed good reactivation of VX-inhibited *h*AChE, however results of *in vitro* assays indicated the compound was unable to reactivate tabun-inhibited *h*AChE. In view of the synthetic difficulties encountered in the introduction of the aminobutyne linker and the similarity of our targeted PSL reactivator with the reported compound, synthetic efforts were suspended.

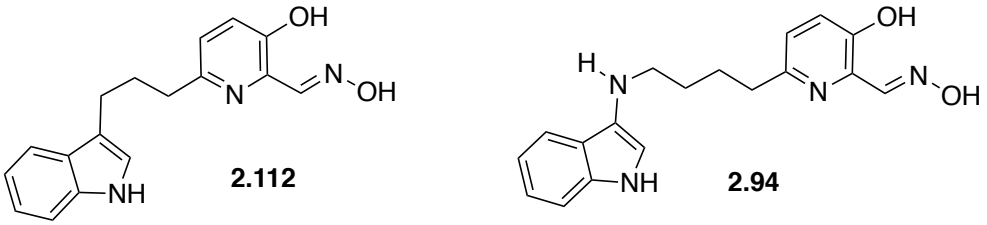

Figure 2.11. Indole reactivator **2.112** prepared by Renard *et al.* and proposed indole-containing reactivator **2.94**

2.11 Conclusions

The design and synthesis of a library of quinoline and non-quinoline hybrid reactivators has been discussed in this chapter. The synthesised compounds (Figure 2.12) will be evaluated for their ability to reactivate OP-inhibited *h*AChE (Chapter 4), and to develop some SAR data. Significantly, the synthetic route towards the quinoline-containing hybrids has been optimised, meaning that greater quantities of material will be accessible for biological evaluation.

The optimised route was applied to previously synthesised quinoline **2.1**, increasing the overall yield from 22% to 41% over the 6 steps of its synthetic route. The key development is the implementation of S_NAr chemistry to replace previously used palladium catalysed microwave-mediated Buchwald-Hartwig cross coupling. This removes the limitation of the capacity of the microwave reactor, and reduces the need for a Pd-catalysed step in the synthesis.

Preliminary *in silico* modelling was undertaken to rationalise and support the development of novel hybrid molecules bearing a substituted quinoline PSL. The computational models demonstrated energy minimised binding modes that would be conducive to OP-inhibited *h*AChE reactivation.

This work has explored various routes towards the homopropargyl-furnished 1,8-naphthyridin-4-amine and 4-aminoindole, however, it has not yet been possible to pursue hybrid reactivators bearing the 1,8-naphthyridine or indole PSL.

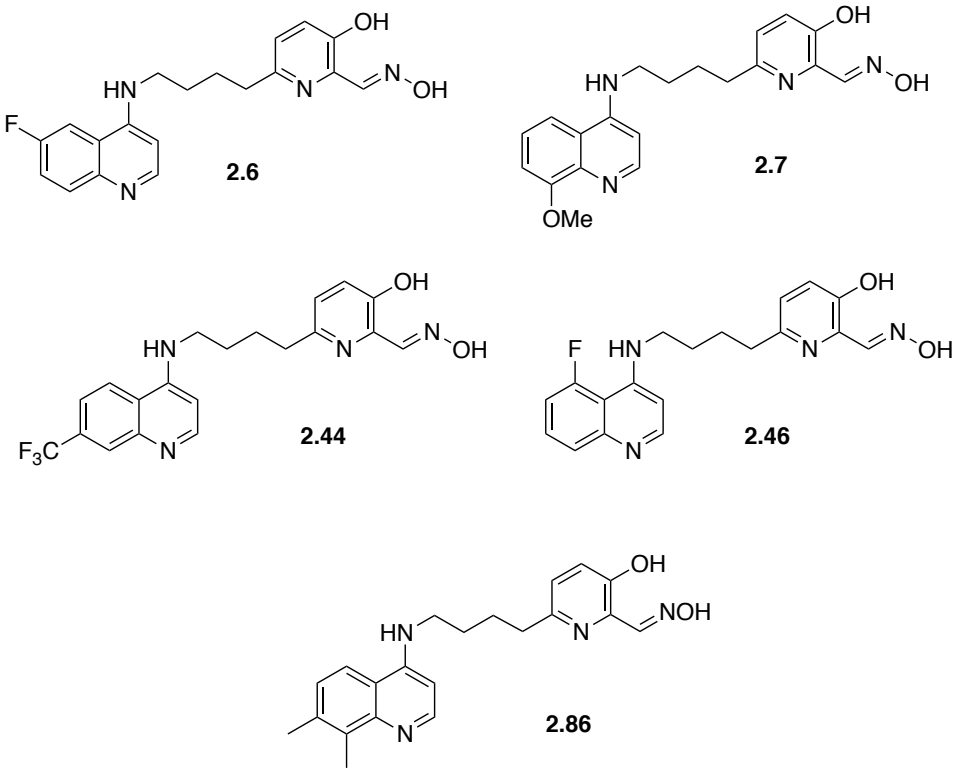

Figure 2.12. Differently substituted quinoline hybrid reactivators synthesised in this chapter

Chapter 3 Structural Simplification and Alternative PSL Hybrid Reactivators

3.1 Structural Simplification of Quinoline Hybrid Reactivators

This chapter will discuss work undertaken towards the synthesis and SARs of hybrid reactivators. A common theme in many medicinal chemistry campaigns is the concept of structural simplification, which has been represented well within the development of bifunctional hybrid reactivators. Julien de Sousa previously undertook the structural simplification of tacrine-bearing hybrid reactivator **3.1** to its corresponding quinoline analogue **2.1**.[186] Whilst simplifying the synthetic route, the strategy also brought about increased efficiency of final quinoline **2.1** (Table 3.1).

Table 3.1. *In vitro* reactivation results from compounds **3.1** and **2.1**

	OPNA	k_{r2} ($mM^{-1}min^{-1}$)
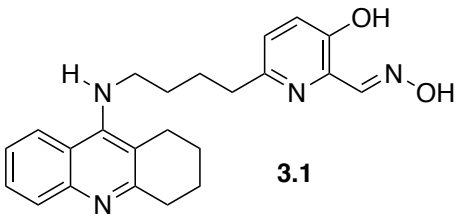 **3.1**	sarin	16
	VX	22
	tabun	3
	paraoxon	31
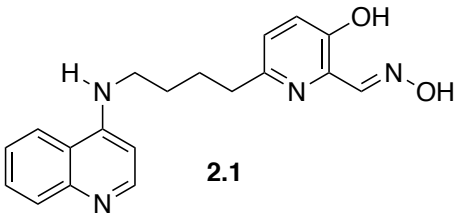 **2.1**	sarin	70
	VX	34
	tabun	62
	paraoxon	20

Table 3.1 demonstrates the effect of structural simplification from tacrine **3.1** to quinoline **2.1**, increasing reactivation efficiency in all but one case (k_{r2} for paraoxon shows a small decrease from 31 $mM^{-1}min^{-1}$ to 20 $mM^{-1}min^{-1}$). For the reactivation of sarin-*h*AChE by quinoline **2.1**, a 4-fold increase in k_{r2} was observed in comparison to tetrahydroacridine **3.1** and a 20 fold increase in k_{r2} was observed for tabun-*h*AChE reactivation in quinoline **2.1** compared to tacrine **3.1.**

It was envisaged that it might be possible to design structurally simplified compounds, such that the synthetic route might be shortened without dramatically reducing the efficiency of the final compounds.

3.2 Dehydroxylated Pyridine Reactivator

Following the success of the simplification of the tacrine PSL, structural simplification was undertaken on the pyridine oxime reactivator component of the hybrid compounds. The hydroxyl functionality at the 3-position of the pyridine ring would be removed (Figure 3.2).

The hydroxy functionality was first reported to be of importance by Sainte-André *et al.* in 2011[166] who demonstrated the cyclisation of phosphorylamidoxime **3.2** to form phosphonic acid **3.4** and isoxazole **3.3** (Scheme 3.1), whilst also demonstrating a low oxime pK_a value (7.96±0.1) to ensure sufficient oximate concentration under physiological conditions. Isoxazole formation was proposed to remove the risk of inhibition through the recapture phenomenon (Section 1.5.1.4). Dehydroxylated phosphorylamidoxime **3.5** is not able to undergo cyclisation and has the potential to phosphorylate AChE (Figure 3.1).

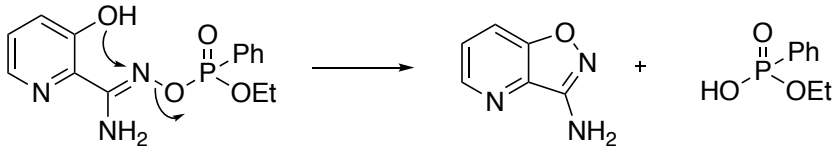

3.2 **3.3** **3.4**

Scheme 3.1. Proposed cyclisation of phosphorylamidoxime **3.2**

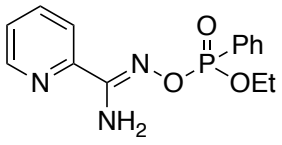

3.5

Figure 3.1. Dehydroxylated phosphorylamidoxime **3.5**

The effect of removing the 3-hydroxy group has not been tested in the context of a hybrid reactivator containing a PSL. Therefore dehydroxylated pyridine oxime **3.6** was proposed (Figure 3.2).

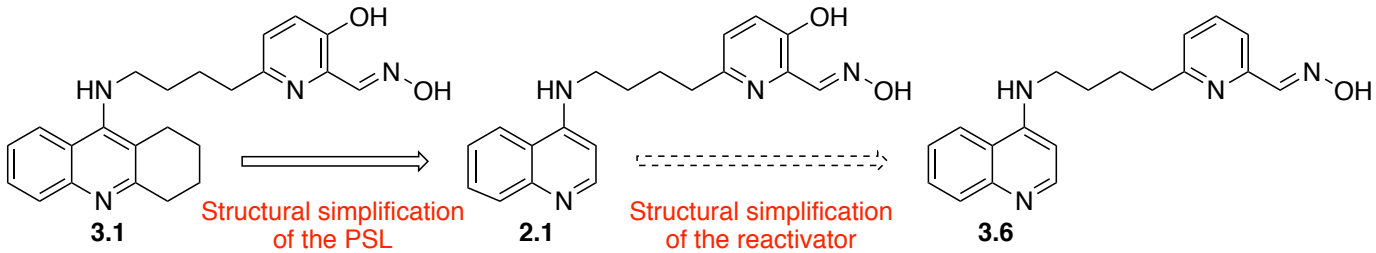

Figure 3.2. Structural simplification tacrine **3.1** to quinoline **2.1** and proposed simplification of the pyridine oxime reactivator to dehydroxylated quinoline **3.6**

A retrosynthetic plan for oxime **3.6** is shown in Scheme 3.2 starting from commercially available 6-bromopyridine-2-carboxaldehyde (**3.8**), which may be oximated to give pyridine oxime **3.9**. Sonogashira cross coupling of homopropargyl quinolinamine **2.25** and bromopyridine oxime **3.9** would afford quinoline **3.7**. Finally, hydrogenation of unsaturated quinoline **3.7** would yield the final hybrid reactivator **3.6**.

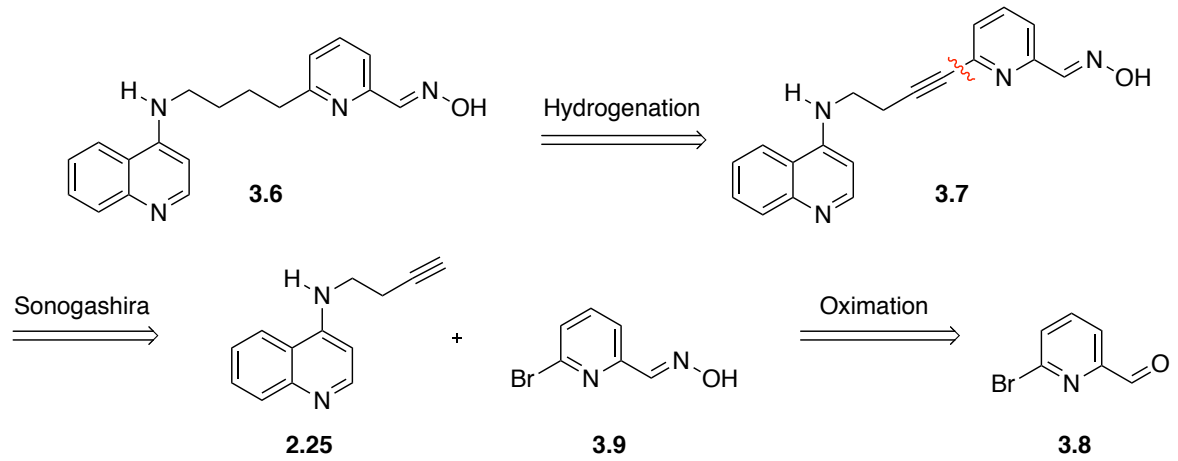

Scheme 3.2. Retrosynthetic plan for dehydroxylated quinoline hybrid reactivator **3.6**

The development of the new synthetic route raised some interesting challenges; it was uncertain whether the oxime functionality would be chemically stable throughout the synthesis. However, early formation of the oxime would be highly advantageous in terms of synthetic efficiency and reducing the number of synthetic steps. The intermediate **3.7**, containing an alkyne linker, offered an interesting opportunity to investigate conformationally restricted compounds for *in vitro* evaluation. Finally, the presence of an *sp* hybridised atom at the 6-position of the pyridine ring should result in a decreased pK_a of the oxime, which should improve the reactivation efficiency.

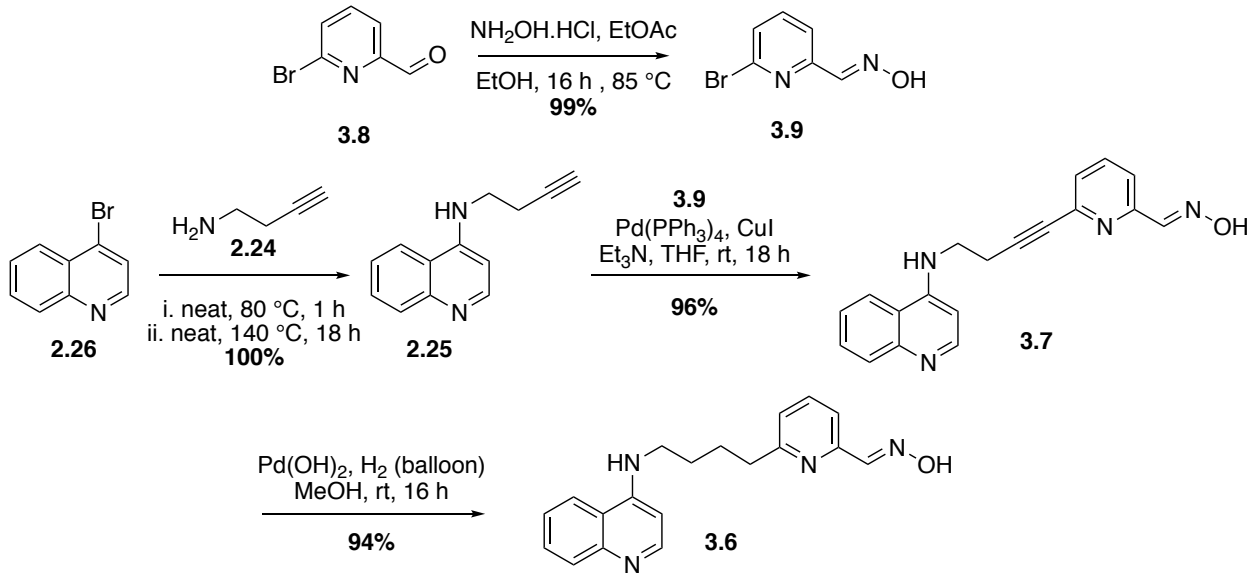

Scheme 3.3. Synthesis of dehydroxylated hybrid reactivators **3.7** and **3.6**

Dehydroxylated hybrid reactivator **3.7** was successfully synthesised over five steps with an overall yield of 95% (Scheme 3.3). Pleasingly, the oxime functionality within alkynyl-linked **3.7** tolerated subsequent hydrogenation conditions over Pearlman's catalyst to afford final alkyl-linked hybrid **3.6** in 94% yield (89% over six steps).

With the development of dehydroxylated quinoline hybrid **3.6**, it was envisaged that the dehydroxylated analogues of selected quinoline-containing hybrids described in Chapter 2 (8-methoxyquinoline **2.6** and 5-fluoroquinoline **2.46**) should be synthesised for comparison in SAR studies.

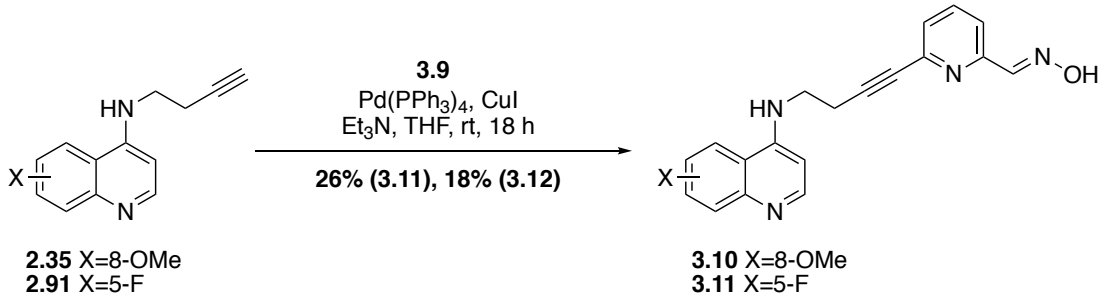

Scheme 3.4. Synthesis of dehydroxylated hybrids **3.10** and **3.11**

Cross coupling between substituted homopropargyl quinolinamines **2.35** and **2.91** and dehydroxylated pyridine oxime **3.9**, gave coupled alkynes **3.10** and **3.11** (Scheme 3.4). Hydrogenation over Pearlman's catalyst afforded saturated hybrid reactivators **3.12** and **3.13** (Scheme 3.5).

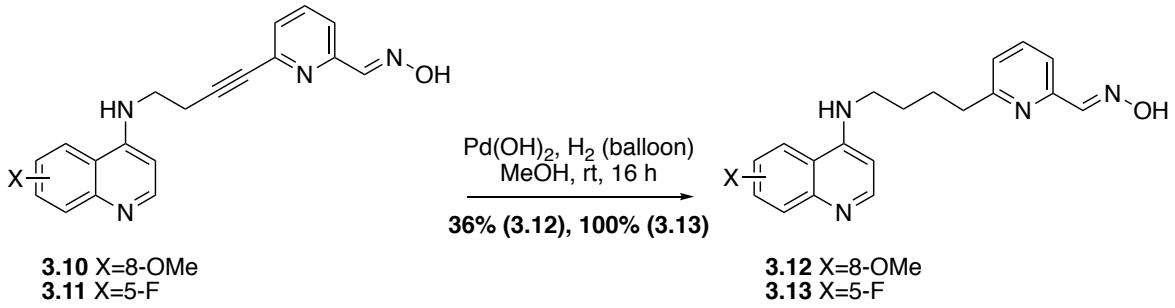

Scheme 3.5. Hydrogenation of unsaturated quinolines **3.10** and **3.11** to afford final hybrids **3.12** and **3.13**

In total, six dehydroxylated hybrid reactivator candidates **3.6**, **3.7**, **3.10**–**3.13** were submitted for *in vitro* evaluation at our collaborator's laboratory. The results of the biological assays will be discussed later in this thesis (Chapter 4).

3.3 Alternative PSL Development

Having established a short route to dehydroxylated quinoline-containing hybrids and successful syntheses of six additional reactivator candidates, our attention turned towards efforts to discover hybrids containing different PSLs.

3.3.1 Theobromine Scaffold

Theobromine is a natural product found within the cacao plant, *Theobroma cacao*. It is commonly found in chocolate and cocoa in levels of between 2-10%. It also exists naturally within the kola nut, the guarana berry and the tea plant, *Camellia sinensis*.[194] Theobromine is a purine and is structurally very similar to caffeine (Figure 3.3).

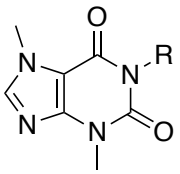

Figure 3.3. General structure of purines; caffeine (R=Me) and theobromine (R=H)

Historically the cola seed, *Cola acuminata*, has been used in indigenous and traditional medicine in the treatment of neurodegenerative disorders and memory loss. In 2008, Niemenak *et al.* discovered that upon analysis of the cola seed, the purines: caffeine and theobromine were present.[195]

It has been reported that both caffeine and theobromine act exclusively on cholinesterases with a high affinity.[196] Nachmansohn *et al* undertook a study where a number of biologically relevant molecules were added to a solution of cholinesterase, as well a mixture of non-specific esterases. Following the introduction of the biomolecules, the enzyme inhibition was recorded. Among this list of biomolecules only caffeine and theobromine showed no inhibitory effect on the non-specific enzyme mix, however they did show some inhibition to cholinesterases. Theobromine might therefore have a specific affinity to AChE and may even bind at the peripheral site, increasing affinity for theobromine-containing hybrid reactivators to the enzyme. Given the potential affinity of theobromine to AChE, three novel hybrid reactivators were proposed (**3.15**, **3.16** and **3.17**, Figure 3.4).

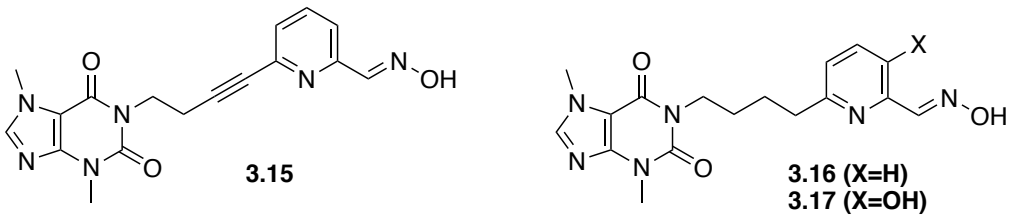

Figure 3.4. Proposed theobromine hybrid reactivators

3.3.2 Theobromine Hybrid Synthesis

The first stage of the design of the theobromine-containing hybrid was the alkylation of the theobromine nitrogen. This could not be achieved, as described earlier in Chapter 2 (Section 2.10.2), by the addition of 4-bromo-1-butyne and a base, due to competing E2 elimination reaction.

The Mitsunobu reaction is the coupling of a primary or secondary alcohol with a pronucleophile (NuH).[197] The process is facilitated by a dialkylazodicarboxylate and a triarylphosphine, commonly diisopropyl azodicarboxylate (DIAD) and triphenylphosphine (PPh_3). The mechanism proceeds through the reduction of the azodicarboxylate to generate a hydrazine derivative, while the phosphine is oxidised to form its corresponding triarylphosphine oxide. The process relies upon pronucleophile being more acidic than betaine **3.20** (pK_a preferably below 11), which results from the reaction between DIAD and triphenyl phosphine.[198] It has been suggested that pronucleophiles with a pK_a >11 are incompatible with the Mitsunobu reaction due to the formation of an undesired alkylated dialkylazodicarboxylate byproduct **3.22**.[199] Given this consideration, theobromine, with a pK_a of 9.9[200] falls within this requisite and should be an appropriate pronucleophile for the Mitsunobu reaction.

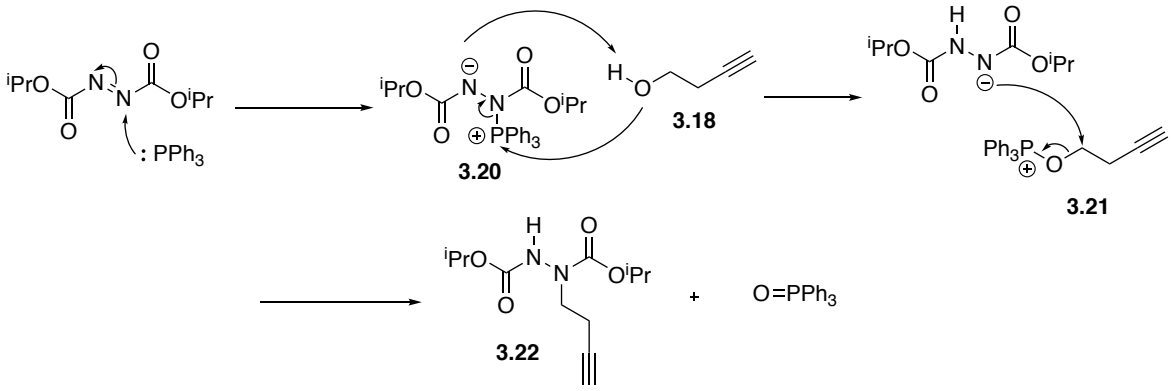

Scheme 3.6. Undesired pathway in Mitsunobu reaction

Research published by Wilhite *et al.* proposed that by-product formation was also dependent on the pK_a of the alcohol (Scheme 3.6).[201] If the pK_a of the alcohol is so high that hydrazo anion **3.20** is not sufficiently basic to deprotonate alcohol **3.18**, then the anion instead attacks the alkoxyphosphonium **3.21** directly to afford the alkylated hydrazine derivative **3.22**.

The reaction of theobromine and 3-buyn-1-ol (**3.18**) in the presence of DIAD and PPh_3 in THF proceeded with poor yields of between 6-12% to afford homopropargyl theobromine **3.19** (Scheme 3.7). The poor yields were attributed in part to product loss during purification by column chromatography due to its co-elution with triphenyl phosphine oxide. In addition, TLC analysis of the reaction mixture indicated that the reaction did not proceed to completion during the 24 hour reaction time.

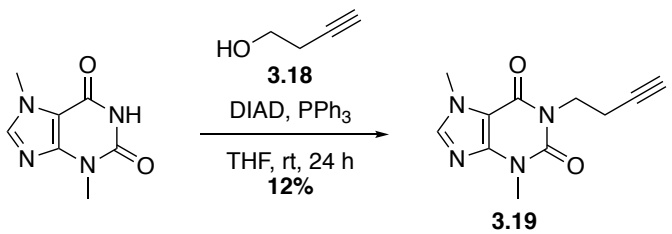

Scheme 3.7. Synthesis of homopropargyl theobromine **3.19**

In an effort to improve the efficiency of the Mitsunobu reaction, a protocol reported by Tsunoda *et al*. using azidodicarbonyldipiperadine (ADDP) and tributylphoshine (PBu_3) was investigated.[202] PBu_3 was used instead of PPh_3 to increase the nucleophilicity of the phosphorus, and enhance the reaction with azodicarboxylate. PBu_3 also facilitates the localisation of the positive charge on the betaine intermediate and the phosphorus derivatised alcohol cation, accelerating nucleophillic attack of deprotonated theobromine in the final step of the reaction. The replacement of the isopropyl group of DIAD with the piperidine group of ADDP increased the basicity of betaine intermediate **3.20**, and subsequent deprotonation of the alcohol. The use of ADDP also increases the basicity of the hydrazo anion reducing the likelihood the undesired route to afford alkylated hydrazine **3.22**. Gratifyingly, under the modified conditions, homopropargyl-substituted theobromine **3.19** was obtained in yields of up to 37% (Scheme 3.8).

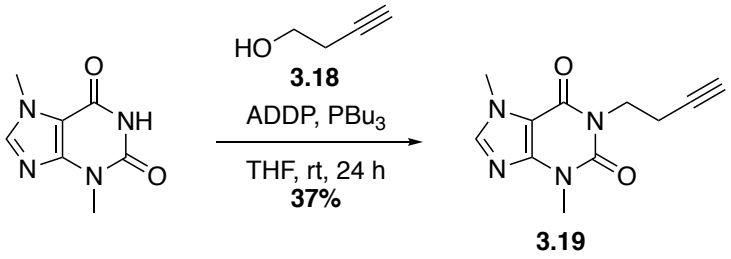

Scheme 3.8 Modified Mitsunobu reaction towards **3.19**

With homopropargyl theobromine **3.19** in hand, it was possible to continue towards the final hybrid reactivators **3.15**, **3.16** and **3.17**. Sonogashira cross coupling was carried out between alkyne **3.19** and bromopyridine analogues **2.5** and **3.9** (Scheme 3.9).

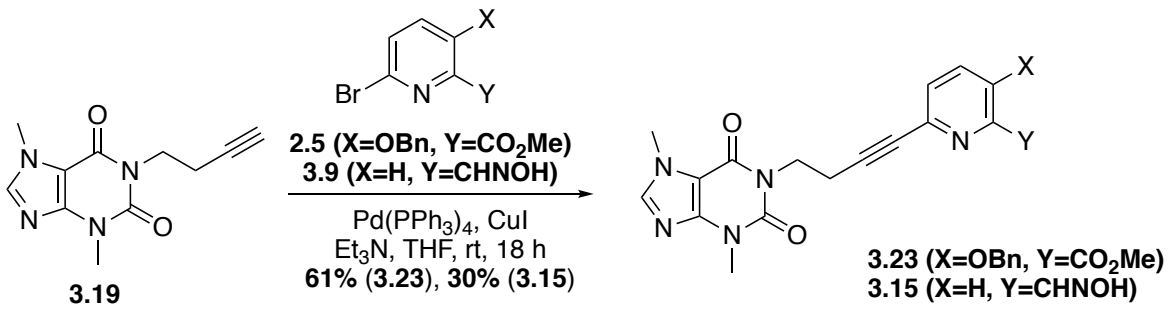

Scheme 3.9. Sonogashira cross coupling between homopropargyl theobromine **3.19** and pyridines **2.5** and **3.9**

Cross coupling of alkylated theobromine **3.19** gave significantly lower yields compared to quinoline-containing analogues. The increase in polarity due to the presence of the theobromine scaffold resulted in some loss of product following purification by column chromatography.

Subsequent hydrogenation of coupled alkynes **3.23** and **3.15** over Pearlman's catalyst was undertaken. Disappointingly, upon purification of dehydroxylated oxime **3.16**, entire loss of compound to the column was observed. Furthermore, the apparent poor solubility of dehydroxylated ethynyl-linked hybrid **3.15** in water, led to termination of further efforts towards

final compound **3.16**. On the other hand, the less polar fully saturated and *O*-debenzylated methyl ester **3.24** was obtained in good yield (Scheme 3.10). Ester **3.24** was subsequently subjected to the established three-step oxime formation protocol. LCMS (ESI+) indicated the presence of the desired oxime product, however, upon purification by column chromatography on silica gel the compound was not recovered. As before, isolation of theobromine oxime hybrid **3.17** was thought to be unsuccessful, at least in part due to the high polarity of the compound.

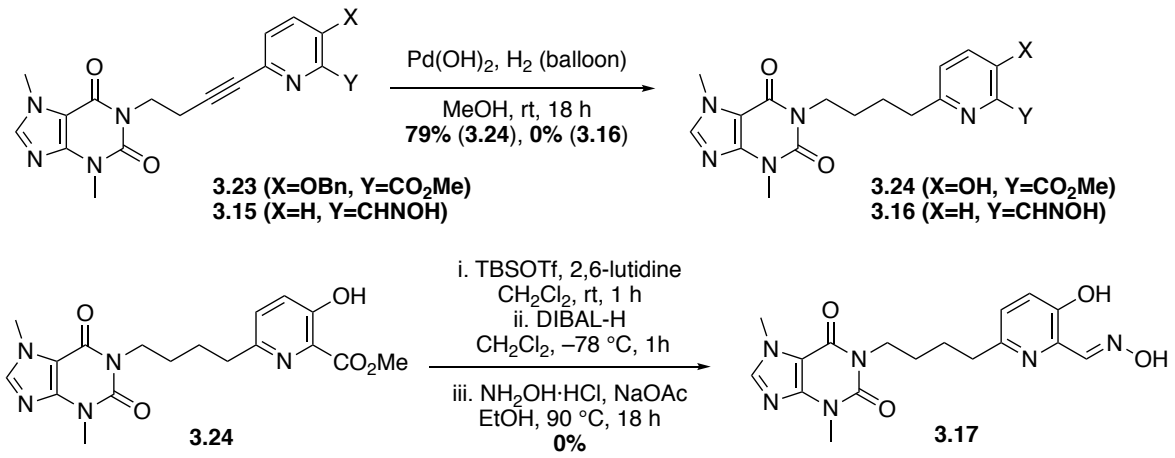

Scheme 3.10. Hydrogenation and hydrogenolysis of compounds **3.15** and **3.23** and subsequent unsuccessful oxime formation of methyl ester **3.24**

To overcome the difficulties due to performing the three-step oximation without purification, the process was repeated with isolation of the intermediate compounds. TBS-protected compound **3.25** was successfully synthesised in 81% yield (Scheme 3.11). With TBS-protected hybrid analogue **3.25** in hand, the DIBAL-H-mediated reduction of the methyl ester was undertaken. Owing to probable side reactions between DIBAL-H and theobromine, the desired product was not observed by TLC or LCMS TIC+. At this stage, efforts towards the development of theobromine hybrids **3.16** and **3.24** were concluded, due to challenging chemical and purification steps, poor aqueous solubility and time constraints.

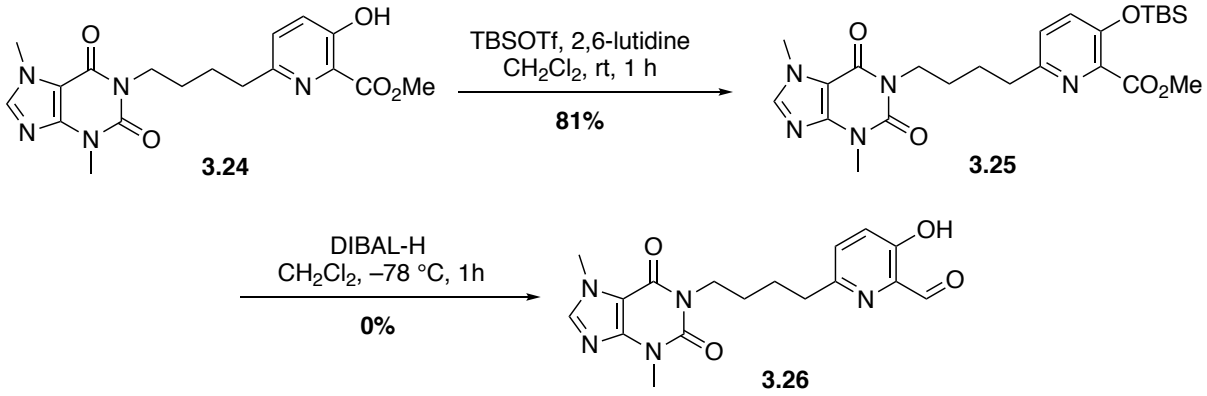

Scheme 3.11. TBS protection of pseudo-phenolic hydroxide **3.24** and subsequent unsuccessful aldehyde formation of TBS ether **3.25**

3.3.3 Naphthalene Scaffold

The significance of the nitrogen atom within the quinoline PSL scaffold was next explored by the development of naphthylamine analogues of dehydroxylated quinolines **3.6** and **3.7** to offer an opportunity to compare the compounds and undertake structure-activity relationship (SAR) investigation into the effect of the nitrogen atom within the quinoline moiety. It may be possible that the nitrogen atom offers increased affinity of the PSL to the peripheral site, by means of forming favourable hydrogen bonding interactions between the nitrogen lone pair of the quinoline and hydrogen bond acceptors within residues of AChE (Figure 3.5).

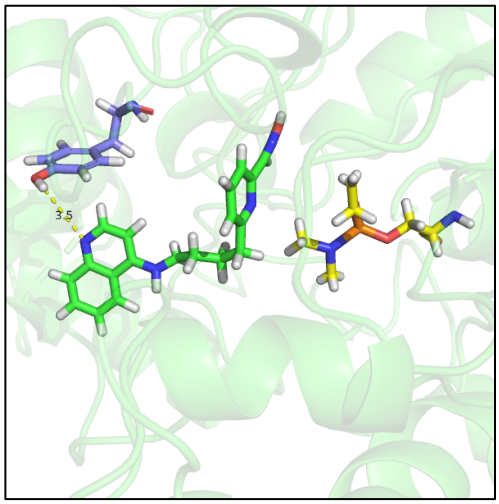

Figure 3.5. Possible mid-range hydrogen bond (dotted yellow line) between the dehydroxylated butyl-linked quinoline reactivator **3.6** (green) quinoline nitrogen and tyrosine (blue) hydroxyl hydrogen. Image taken from computation model developed in Chapter 5

Homopropargylation of naphthylamine was initially explored, firstly, by means of Mitsunobu coupling (Scheme 3.12), which proved unsuccessful.

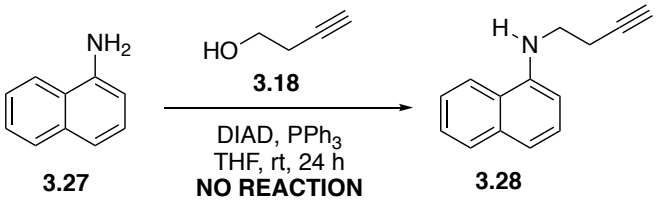

Scheme 3.12. Attempted Mitsunobu reaction between naphthylamine (**3.27**) and 3-butyn-1-ol (**3.18**)

S_NAr amination of the naphthalene system was next explored, as described for the synthesis of *N*-homopropargyl quinolin-4-amines. Upon treatment of 1-bromonaphthalene (**3.29**) with nucleophillic aromatic substitution conditions used previously for the alkylation of bromoquinolines (Section 2.5), no reaction was observed (Scheme 3.13), likely due to the reduced ability of the carbon atom of naphthalene to stabilise the negative charge of the Meisenheimer intermediate, during the S_NAr mechanism compared to quinoline.

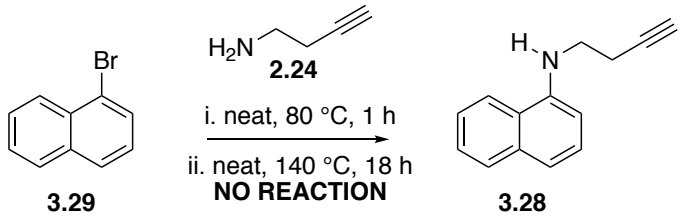

Scheme 3.13. Attempted S_NAr of 1-bromonaphthalene (**3.29**) with 3-butyn-1-amine (**2.24**)

It was proposed that the use of a stronger base might be sufficient to push the substitution reaction. Interestingly, in the presence of four equivalents of caesium carbonate at 100 °C for 48 hours, a very small amount of desired product **3.28** was observed (Scheme 3.14). It is not clear whether the desired product is the result of an S_NAr reaction or an aryne pathway.[203]

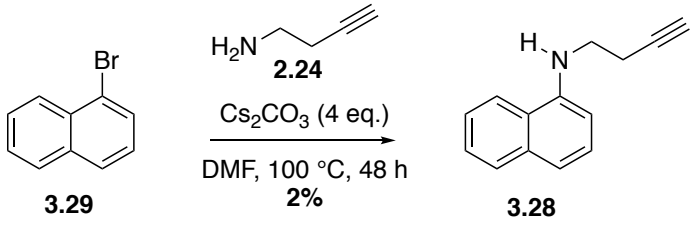

Scheme 3.14. Low yielding amination of 1-bromonaphthylene (**3.29**) with 3-butyn-1-amine (**2.24**)

Following the successful synthesis of tetrahydroacridine substituted hybrid reactivator **3.1** using Buchwald-Hartwig palladium mediated cross coupling (Scheme 3.15), this approach was attempted with the naphthalene scaffold.[188]

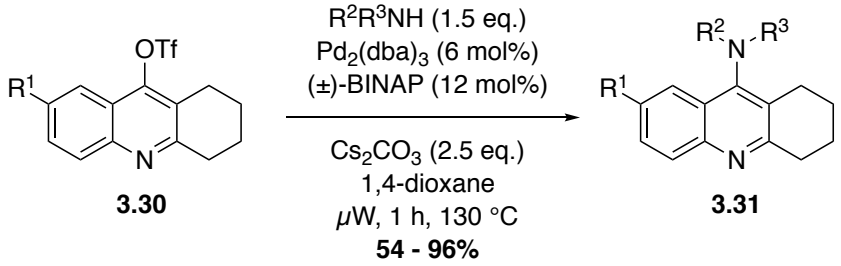

Scheme 3.15. Buchwald-Hartwig conditions developed for the amination of tetrahydroacridines **3.31**

This approach was attempted with the substitution of naphthalene-1-yl trifluoromethylsulfonate (**3.33**) with 3-butyn-1-amine (**2.24**). Firstly, 1-naphthol (**3.32**) was treated with triflic anhydride under basic conditions to afford triflate **3.33** in excellent yield. Treatment of triflate **3.33** under Buchwald-Hartwig amination conditions detailed by de Sousa *et al.*[188] was unsuccessful (Scheme 3.16). *N*-Boc-Naphthylamine was also subjected to basic conditions with homopropargyl bromide **2.110** (Scheme 3.17). Unsurprisingly, under basic conditions, no reaction was observed. This again, may be attributed to base-mediated intermolecular E2 elimination (Scheme 2.31).

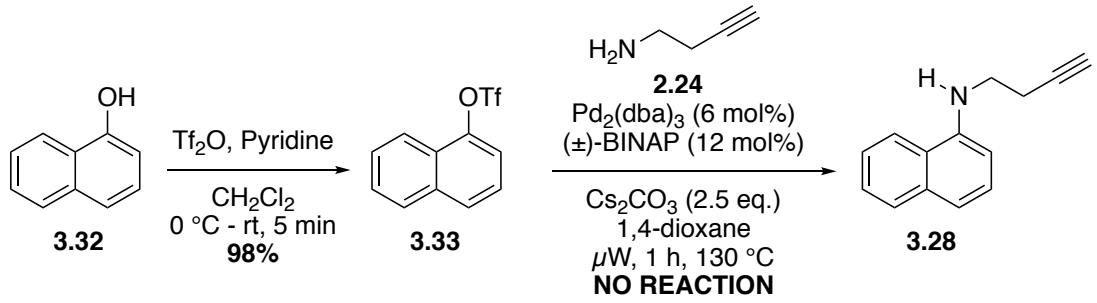

Scheme 3.16. Triflation of 1-naphthol (**3.32**) and subsequent, failed BHA of triflate **3.33** with 3-butyn-1-amine (**2.24**)

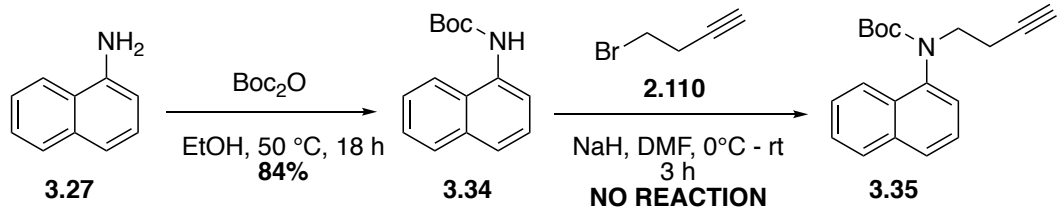

Scheme 3.17. Boc protection of **3.27** and subsequent, unsuccessful alkylation with **2.110**

Following the lack of success with the amination of triflate **3.32**, a revised retrosynthetic plan was considered (Scheme 3.18), incorporating a bromoethyl group into naphthylamine (**3.27**) *via* acylation with bromoacetyl bromide followed by reduction to **3.36**. The simplified pyridine oxime **3.9** and PSL fragments could then be unified by sequential alkyne coupling reaction to afford coupled oxime **3.40**.

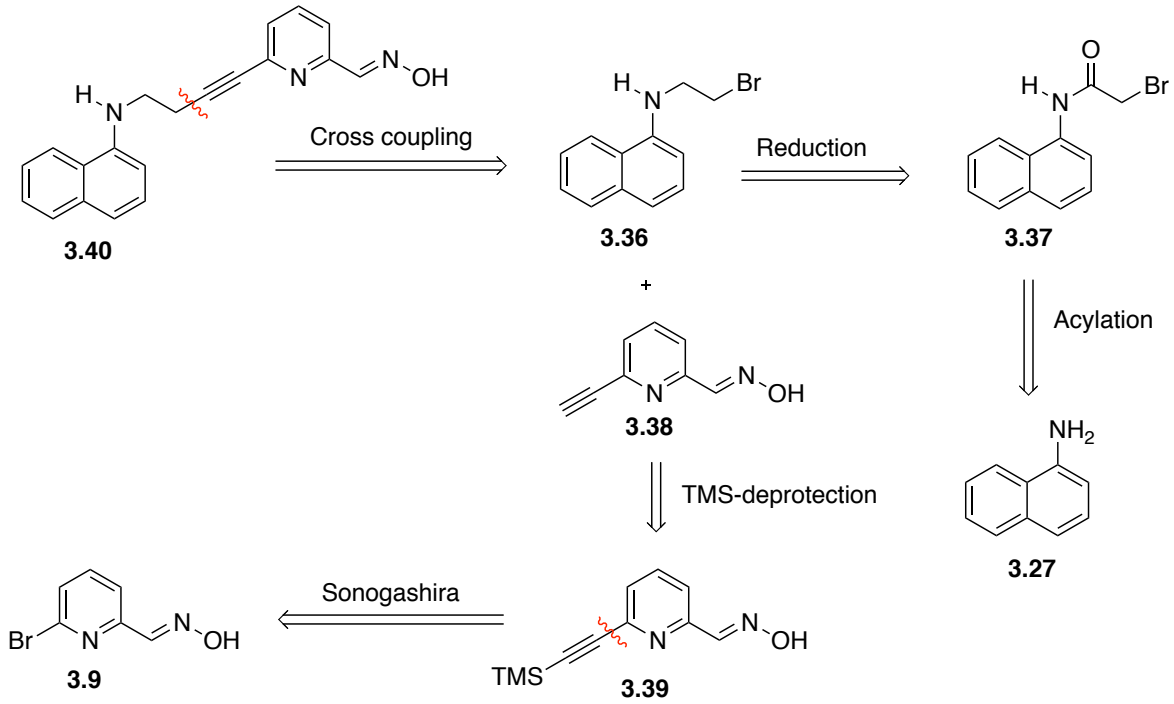

Scheme 3.18. Revised retrosynthetic plan towards dehydroxylated quinoline **3.40**

Acylation and reduction of naphthylamide **3.27** proceeded in modest yields to afford alkyl bromide **3.36** (Scheme 3.19).

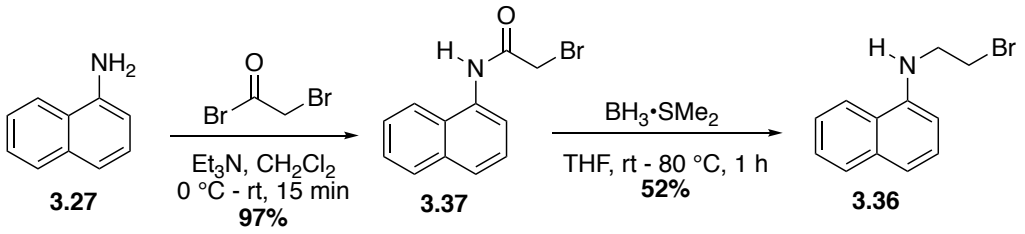

Scheme 3.19. Synthesis of *N*-(2-bromoethyl)naphthalen-1-amine (**3.36**)

Pyridine alkyne **3.38** was successfully synthesised following Sonogashira cross coupling of bromopyridine oxime **3.9** and TMS acetylene, followed by TMS deprotection in moderate yield (Scheme 3.20).

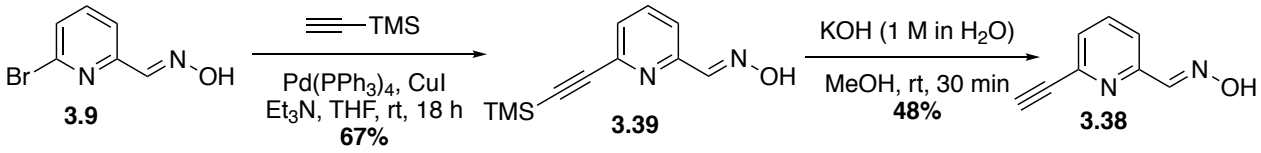

Scheme 3.20. Sonogashira coupling to afford alkyne **3.38**

Subsequent attempted Sonogashira coupling of alkyl bromide **3.36** and acetylene pyridine oxime **3.38** did not proceed and starting materials were recovered (Scheme 3.21). This method for the synthesis of compound **3.40** was not pursued further.

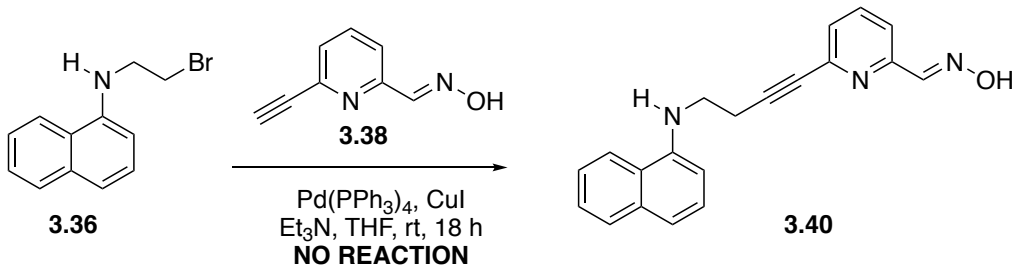

Scheme 3.21. Unsuccessful Sonogashira cross coupling of **3.36** and **3.38**

It was envisaged that this C-C bond formation could be obtained through dianion chemistry (Scheme 3.22) between compounds **3.36** and **3.38**.

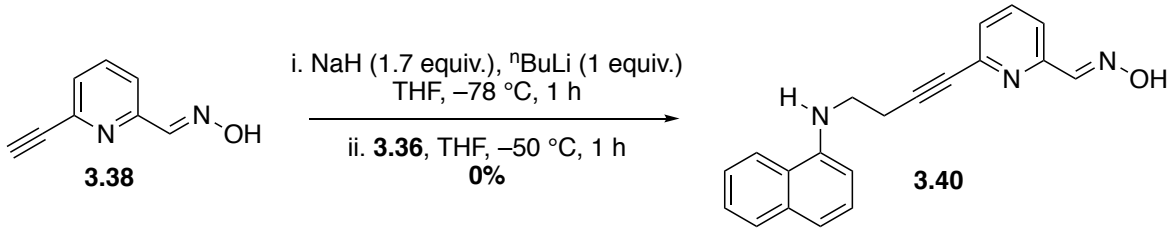

Scheme 3.22. Attempted synthesis of **3.40** *via* dianion chemistry

Interestingly, the formation of aziridine **3.41** was observed and its synthesis was repeated from alkyl bromide **3.36** and sodium hydride (Scheme 3.23). It was proposed that the aziridine might be sufficiently electrophilic to allow coupling with an alkynyl anion to secrure the desired

homopropargylic amine **3.28**. Unfortunately, upon addition of ethynyl magnesium bromide to aziridine **3.41**, none of the desired product was observed and the starting materials were recovered.

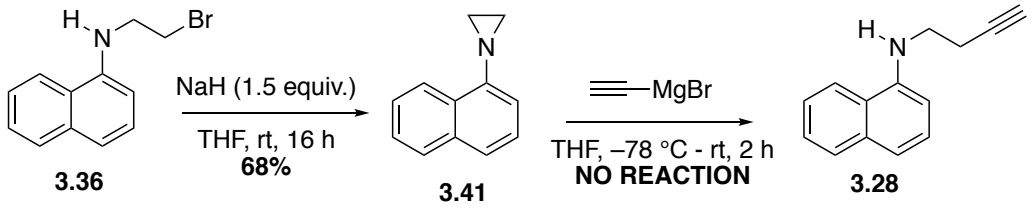

Scheme 3.23. Attempted synthesis of homopropargyl naphthylamine **3.28** *via* aziridine **3.41**

Different strategies for the formation of homopropargyl naphthylamine **3.28** were explored. Firstly, 3-butyn-1-ol (**3.18**) was oxidised to 3-butynoic acid (**3.42**), which was subsequently converted to its acid chloride and added to naphthylamine (**3.27**) in a one-pot process to afford naphthylamide **3.43**. Subsequent reduction of amide **3.43** with borane dimethyl sulfide complex in THF was unsuccessful and homopropargyl naphthylamine **3.28** was not formed (Scheme 3.24).

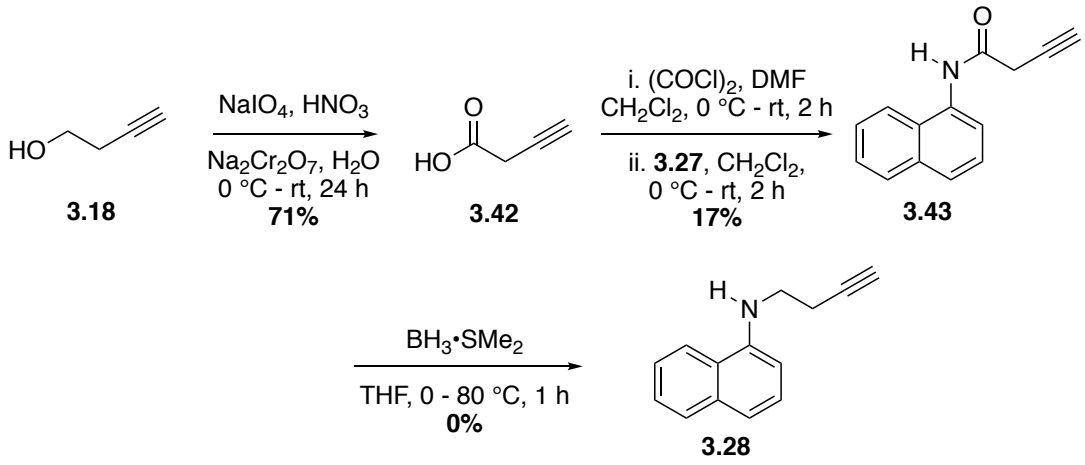

Scheme 3.24. Attempted synthesis of homopropargyl naphthylamine **3.28** by reduction of amide **3.43**

Seyferth-Gilbert homologation chemistry was next explored. The Seyferth-Gilbert reaction proceeds through the reaction of base-promoted Bestmann-Ohira reagent (**3.45**) with aldehyde **3.46**, forming oxaphosphetane **3.47**. [204] Subsequent Wittig-like cycloelimination affords diazoalkene **3.48** and a stable dimethyl phosphate anion (Scheme 3.25). Following the generation of diazoalkene **3.48**, the reaction is warmed to room temperature and nitrogen gas is lost, resulting in the formation of vinylidine carbene **3.52**, which undergoes Fritsch-Buttenberg-Wiechell (FBW) 1,2-migration to afford terminal alkyne **3.28** (Scheme 3.25).

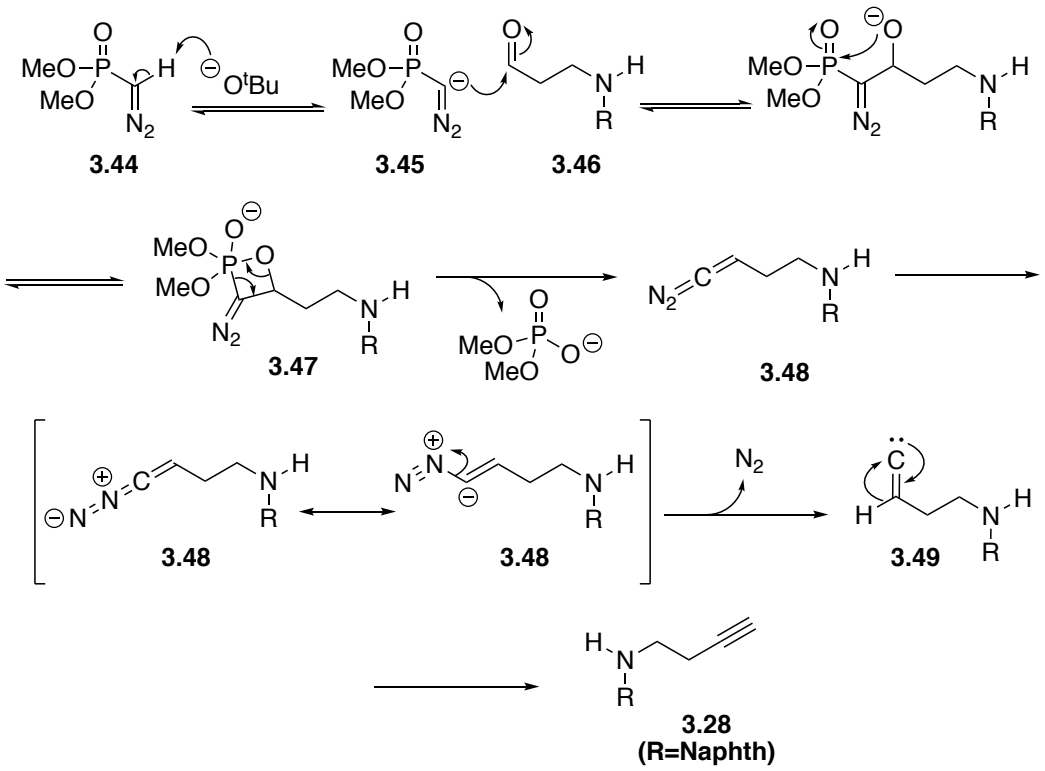

Scheme 3.25. Proposed mechanism of the Seyferth-Gilbert reaction

Initial efforts focussed upon the synthesis of aldehyde **3.52** from ester **3.51** and nitrile **3.54** (Scheme 3.26). However, the presence of aldehyde **3.52** was not observed following the reaction, assumed in part due to the poor stability of aldehyde **3.52**. The desired compound contains a secondary amine and an aldehyde, which have the potential to react with one another. The Seyferth-Gilbert route towards homopropargyl naphthylamine **3.28** was therefore abandoned and other potential routes were explored.

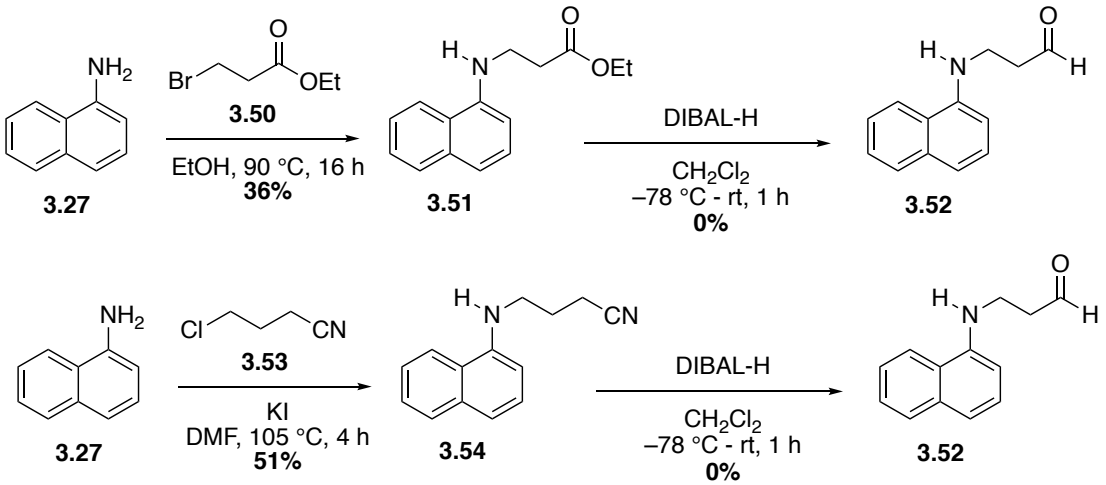

Scheme 3.26 Attempted syntheses of aldehyde **3.52**

Hydrogen "borrowing" has been reported[205,206,207] to be used as an innovative approach to the amination of alcohols, which and has been used to form secondary amines from primary alkyl alcohols.[208] The proposed mechanism is shown below in Scheme 3.27.[209]

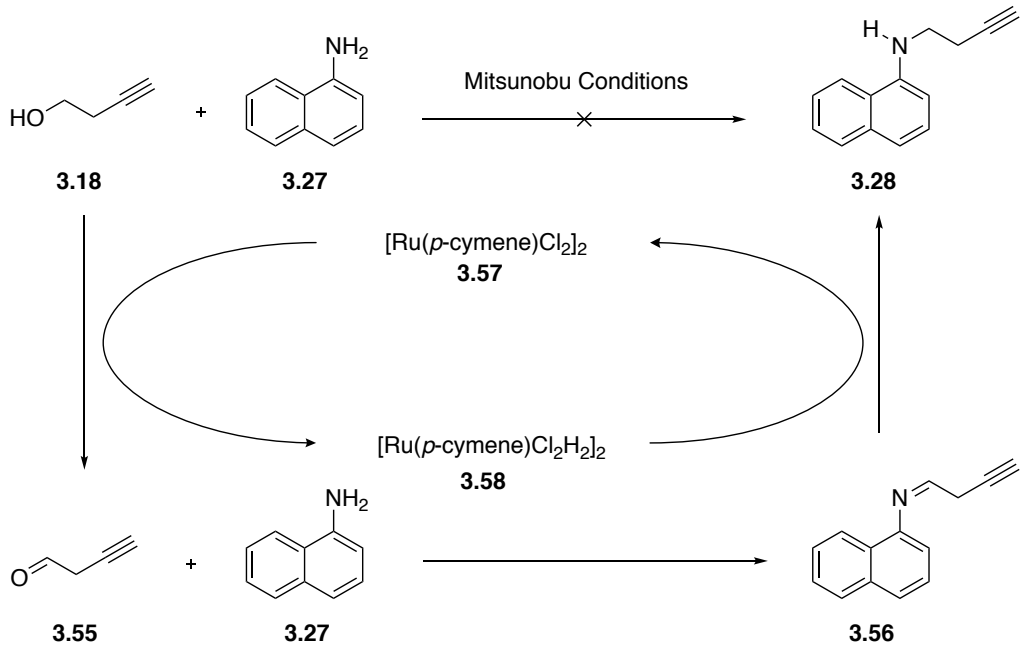

Scheme 3.27. Proposed mechanism for the ruthenium-catalysed hydrogen "borrowing" reaction

The mechanism is proposed to proceed *via* the oxidation of the primary alcohol **3.18** to the corresponding aldehyde **3.55** by ruthenium catalyst **3.57 (**Figure 3.6). The aldehyde then reacts with naphthylamine **3.27** to form imine **3.56**. Selective reduction of the imine by reduced ruthenium catalyst **3.58** may then proceed to afford the desired product **3.28**.

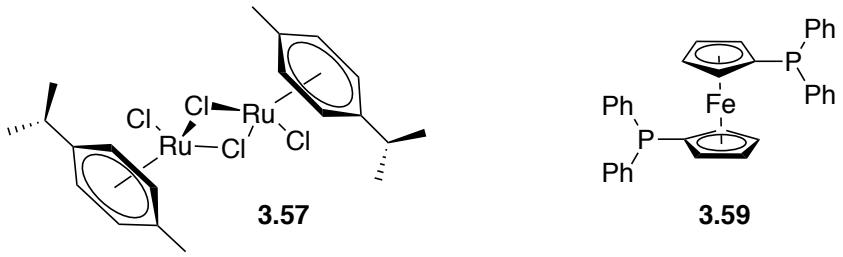

Figure 3.6. Structures of [Ru(*p*-cymene)Cl_2]$_2$ (**3.57)** and dppf (**3.59**)

Following the procedure outlined by Williams *et al.*,[205] the reaction appeared to proceed to imine **3.56**, which was identified from LCMS (ESI+) analysis of the reaction mixture (Scheme 3.28). Curiously, alkylated amine **3.28** was not observed, although TLC analysis indicated complete consumption of amine **3.27**. This would indicate that the final reduction of imine **3.56** by the ruthenium catalyst is problematic; this may be due to the increased steric hindrance of naphthyl-substituted amine.

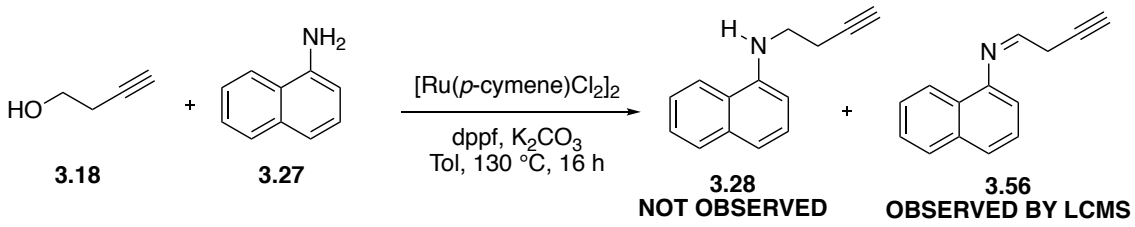

Scheme 3.28. Attempted ruthenium catalysed hydrogen "borrowing" reaction of alcohol **3.18** with naphthylamine **3.27**

Recent research published by Yoshikai *et al.*, suggested an alternative novel approach to the formation of aromatic amines *via* dehydrogenative aromatisation of cyclohexanone imines (Scheme 3.29).[210] This transformation was achieved with the use of palladium catalysis under aerobic conditions.

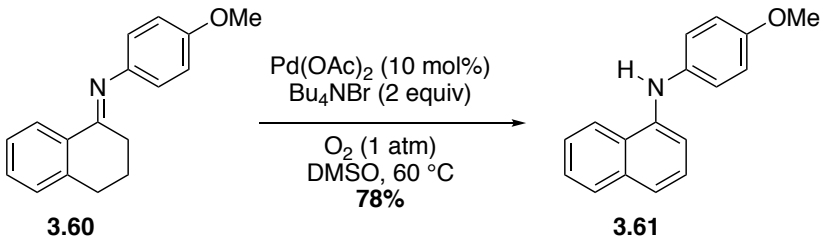

Scheme 3.29. Initial observations from Yoshikai *et al.*[210]

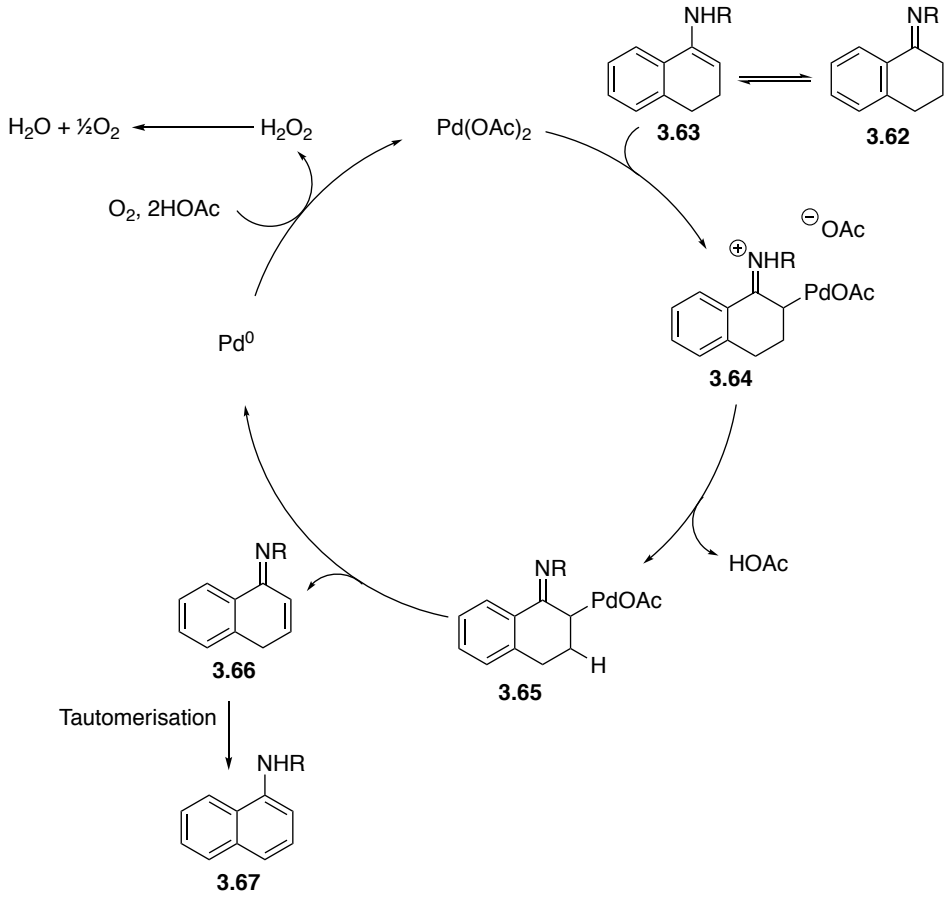

Scheme 3.30. Proposed mechanism for the catalytic dehydrogenative aromatisation of α-tetralone imines, adapted from Yoshikai *et al.*[210]

The mechanism is proposed to proceed *via* catalytic dehydrogenation (Scheme 3.30). Firstly, upon tautomerisation, imine **3.62** forms enamine **3.63**, to which can be added $Pd(OAc)_2$, liberating an acetate anion and iminium **3.64**. Following liberation of an equivalent of acetic acid the resulting imine **3.65** undergoes dehydrogenation to afford imine **3.66**, which itself can tautomerise to afford the final aromatic amine **3.68**. The palladium is reoxidised with one equivalent of molecular oxygen and two equivalents of acetic acid to recover the palladium catalyst.

This literature precedent led us to consider application of the method towards homopropargyl naphthylamine **3.28**. Before exploring the reaction with expensive propargyl amine, initial investigations were undertaken towards the pentyl-substituted naphthylamine **3.72** (Scheme 3.31). Treatment of α-tetralone **3.68** with pentylamine **3.69** and *p*-toluenesulfonic acid in toluene gave imine **3.70** in 81% yield. Subsequent treatment of **3.70** under the conditions described by Yoshikai gave alkylated naphthylamine **3.71** in good yield.

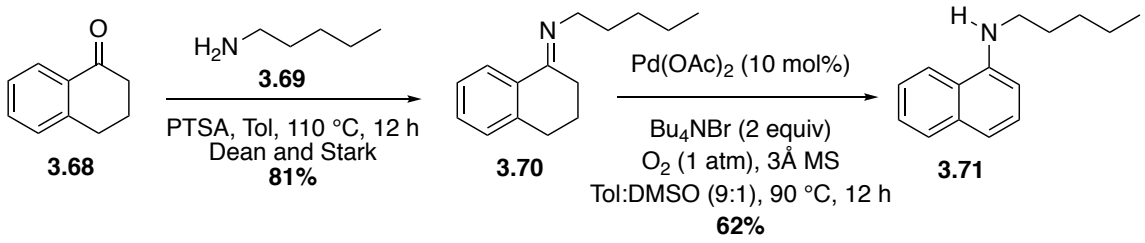

Scheme 3.31. Synthetic route towards alkylated naphthylamine **3.71**

Following the success of the development of alkylated naphthylamine **3.71 (**Scheme 3.32), the homopropargyl substituted tetralone imine was synthesised. Disappointingly, the dehydrogenative aromatisation proved unsuccessful.

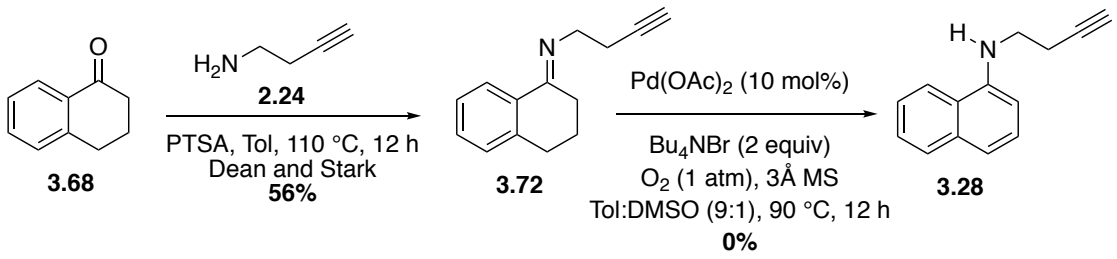

Scheme 3.32. Synthesis of homopropargyl imine **3.72** and subsequent unsuccessful dehydrogenative aromatisation

The failure of the dehydrogenative aromatisation of the homopropargyl analogue was attributed to the presence of the terminal alkyne. It is reasonable to conclude the palladium catalyst would be unavailable to undertake the dehydrogenative aromatisation if it interacts with the terminal alkyne functionality. The aromatisation by dehydrogenation was abandoned in favour of an alternative synthetic route described below.

Recent research published by Couty *et al.*, reported the synthesis of homopropargylamines from 2-cyanoazetidines.[211] This route was previously discounted due to the use of highly toxic reagents

and the length of the synthesis; however, it was reconsidered in light of the failure to develop viable alternatives.

1-Iodonaphthalene (**3.73**) was successfully aminated with 2-aminoethanol (**3.74**) in the presence of CuCl under basic conditions (Scheme 3.33). Subsequent *N*-cyanomethylation of amino alcohol **3.75** proceeds *via* intermediacy of an oxazolidine intermediate with paraformaldehyde and TMSCN. Mesylation and subsequent base-mediated cyclisation of nitrile **3.76** afforded 2-cyanoazetidine **3.77**. Homopropargyl amine **3.28** was obtained following an unusual reaction of azetidine **3.77** with $TMSN_3$ and Bu_2SnO in toluene for 96 hours. Gratifyingly, homopropargyl naphthylamine **3.28** was finally secured over 6 steps with an overall yield of 30%.

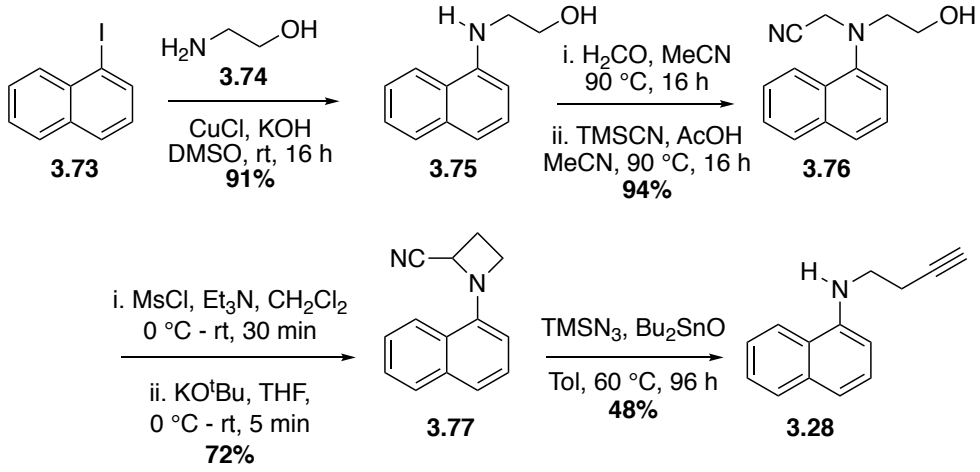

Scheme 3.33. Successful synthesis of homopropragylic amine **3.28**

The *N*-cyanomethylation is a key step and is proposed to proceed *via* the oxazolidine intermediate **3.81**, which is in equilibrium with the iminium **3.80** under acidic conditions (Scheme 3.34). The cyanide nucleophile attacks the iminium carbon and nitrile **3.77** is generated.

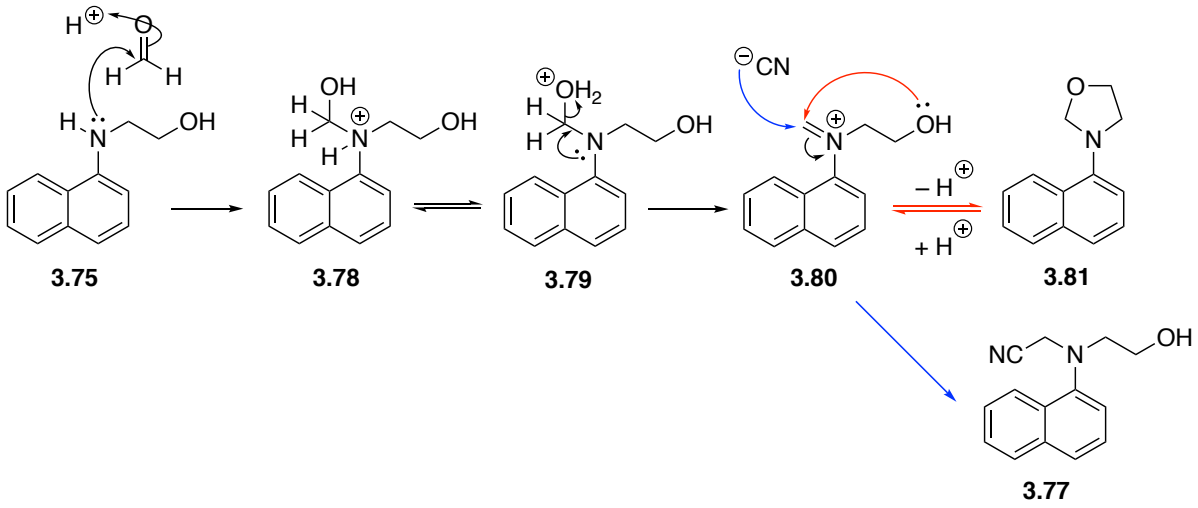

Scheme 3.34. *N*-cyanomethylation of ethanolamine **3.75** *via* oxazolidine **3.81**

The second key step is the $TMSN_3$ and Bu_2SnO mediated formation of the final homopropargylamine. Couty *et al.* proposed a plausible mechanism,[212] starting with the combination of $TMSN_3$ and Bu_2SnO to form the catalytically active species. Tin-catalysed cycloaddition between the azide and nitrile forms tetrazole **3.82**, which can facilitate ring opening of azetidine **3.82** to afford tetraazafulvene **3.83**. Upon decomposition of the latter and liberation of two equivalents of dinitrogen vinyl carbene **3.84** is generated, which can undergo FBW rearrangement to form tin-complex **3.85**. Recombination of $TMSN_3$ and tin-complex **3.85** liberates the homopropargyl naphthylamine **3.28** and the regenerated catalyst (Scheme 3.35).

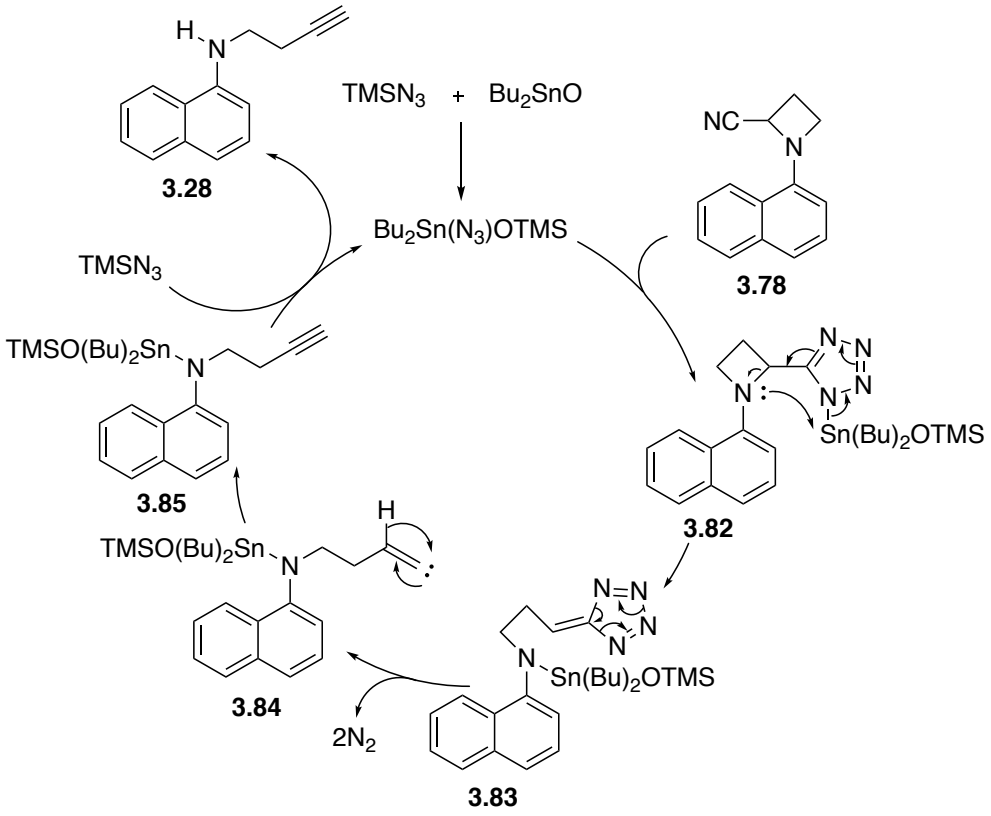

Scheme 3.35. Proposed mechanism for the formation of homopropargyl naphthylamine **3.28**, adapted from Couty *et al.*[212]

Following successful synthesis of alkyne **3.30**, Sonogashira cross coupling was undertaken affording butynyl-linked hybrid **3.40** in 54% yield. Hydrogenation of alkyne **3.40** was achieved over Pearlman's catalyst to afford the final naphthalene containing PSL hybrid reactivator **3.86** (Scheme 3.36).

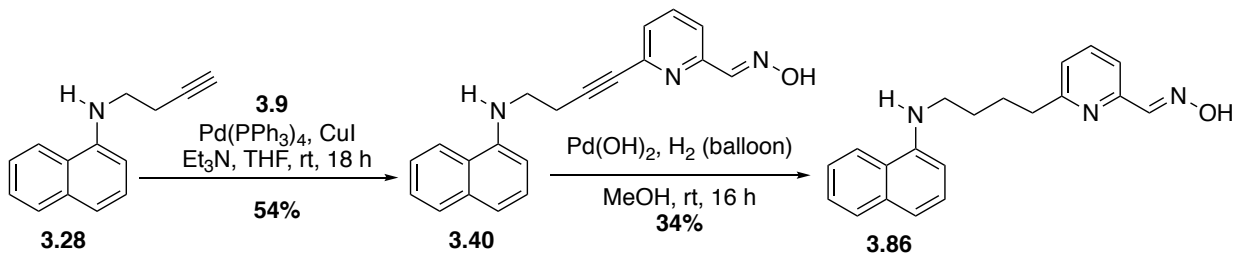

Scheme 3.36. Completing the synthesis of naphthyl oxime **3.86**

3.3.4 Benzylpiperazine Scaffold

The benzylpiperazine (BnPiz) scaffold has become common in drug compounds for the treatment of Alzheimer's disease (AD). AD is a neurodegenerative disorder of the central nervous system that results in premature senile deterioration, anxiety and depression.[213] AD is said to account for 50-60% of overall cases of dementia of people aged 65 and over and has been characterised by a large reduction of acetylcholine (ACh) in the cortex and hippocampus areas of the brain.[214] A key strategy that has been explored for the treatment of AD is the development of inhibitors of AChE in order to decrease the rate of ACh degradation. Tacrine (**3.87**) and Donepezil (**3.88**) represent two AChE inhibitors prescribed for the treatment of AD (Figure 3.7). Tacrine, or tetrahydroacridine (**3.87**) has been explored previously within our team as a PSL in hybrid reactivators. Hence, the benzyl piperidine scaffold of Donepezil (**3.88**) would be explored using BnPiz as a PSL.

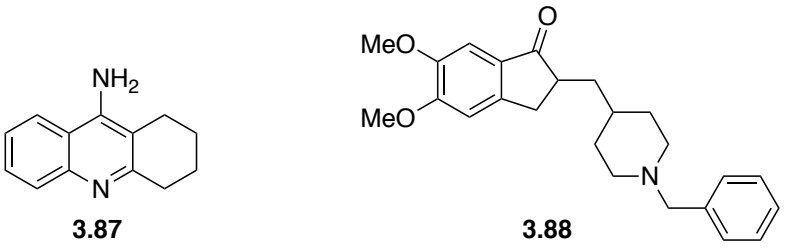

3.87 **3.88**

Figure 3.7. AChE inhibitors Tacrine (**3.87**) and Donepezil (**3.88**)

Recent work by Lui *et al.* focussed on the development of potent AChE inhibitors with a view to treat AD.[215] Benzyl piperazine **3.89** (Figure 3.8) showed excellent *in vitro* potency for electric eel AChE (*ee*AChE) with an IC_{50} (concentration of compound required to reduce enzyme activity by 50%) value of 0.96 ± 0.01 μM.

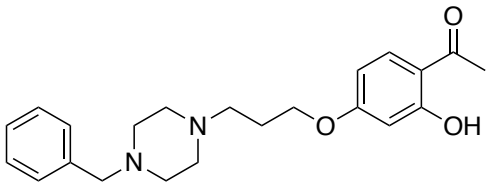

3.89

Figure 3.8. Lead compound developed by Lui *et al.*[215]

The BnPiz scaffold was incorporated into the simplified hybrid reactivator design and four new compounds **3.90**-**3.93** were proposed (Figure 3.9). The new compounds were designed with a 3C and 4C length linker; this decision was made based on the greater size of the BnPiz PSL. The 3C linker was designed to compensate for gain in size of PSL by reducing the length of the linker.

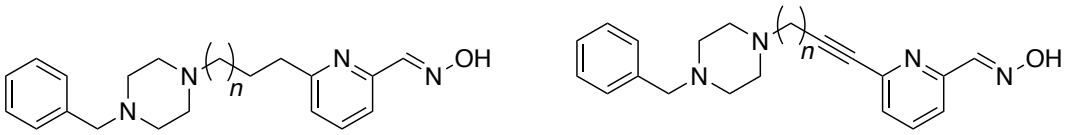

3.90 (*n*=1)
3.91 (*n*=2)

3.92 (*n*=1)
3.93 (*n*=2)

Figure 3.9. New BnPiz containing hybrid reactivator candidates

Piperazine was mono-protected with benzyl (Bn) and *p*-methoxybenzyl (PMB) groups (Scheme 3.37), such that their robustness throughout the synthesis might be tested. Commercially available *N*-Boc piperazine (**3.97**) and *N*-Cbz piperazine (**3.98**) were also used.

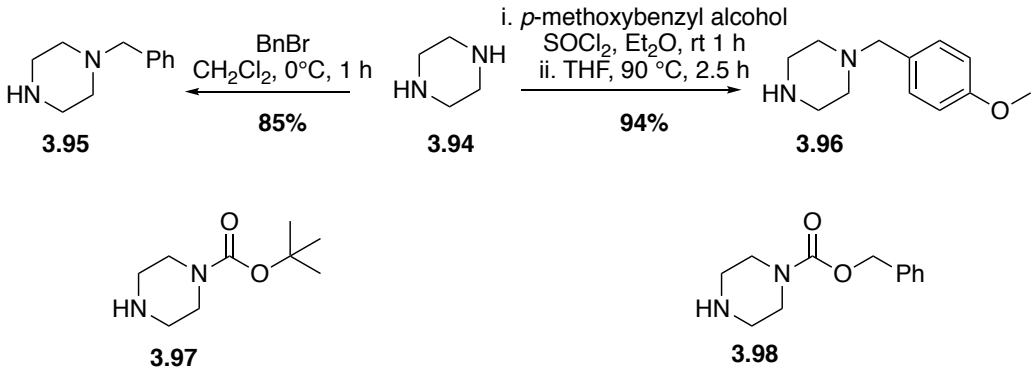

Scheme 3.37. Synthesis of mono-protected piperazines **3.95** and **3.96**, and commercially available protected piperazine **3.97** and **3.98**

Treatment of mono-protected piperazines **3.95-3.98** with but-3-yn-1-yl toluenesulfonate (**3.99**), formed from alcohol **3.18**, under basic conditions to afford homopropargyl substituted protected piperazines **3.100-3.103** in acceptable to good yields (Scheme 3.38).

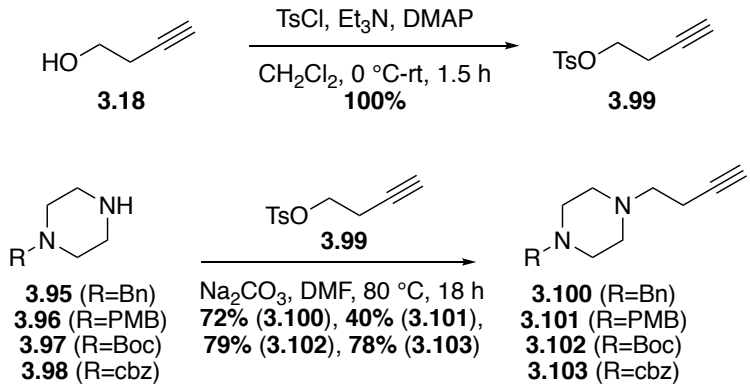

Scheme 3.38. Synthesis of but-3-yn-1-yl *p*-toluenesulfonate (**3.99**) and subsequent homopropargyl substitution of piperazines **3.95-3.98**

Protected piperazines **3.95-3.98** were propargylated by treatment with propargyl bromide (**3.104**) and diisopropylethylamine (DIPEA) (Scheme 3.39).

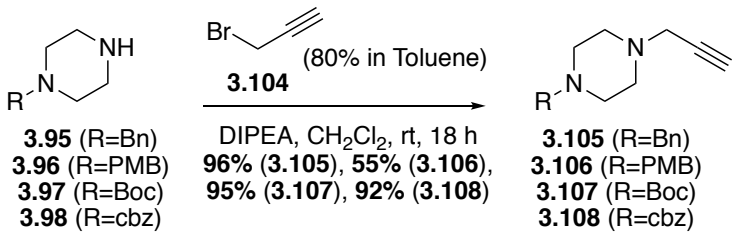

Scheme 3.39. Propargylation of protected piperazines (**3.95-3.98**)

Propargyl benzylpiperazines **3.100** and **3.105** were coupled to dehydroxylated pyridine oxime **3.9** using Sonogashira chemistry. The reaction was successful and ethynyl-linked benzyl piperazines **3.92** and **3.93** were obtained in yields of 37% and 6%, respectively (Scheme 3.40).

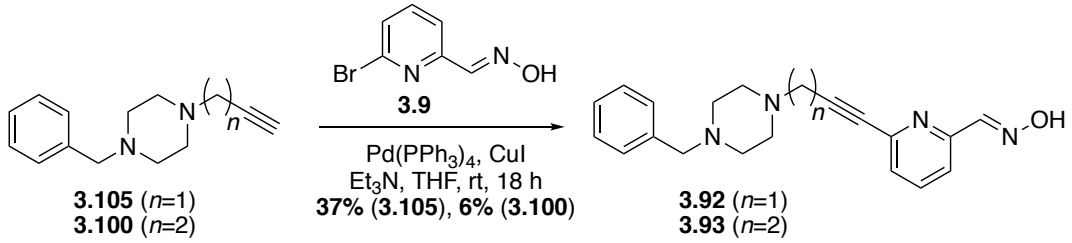

Scheme 3.40. Sonogashira coupling between benzyl piperazines **3.105** and **3.100** and dehydroxylated reactivator **3.9**

With ethynyl-linked compounds **3.92** and **3.93** in hand, hydrogenation was undertaken. Disappointingly, following Pearlman's catalyst-mediated hydrogenation of both compounds, the oxime functionality was reduced to corresponding primary amines **3.109** and **3.110** (Scheme 3.41). However, following hydrogenation, the benzyl group remained attached to the piperazine nitrogen, thus it was not necessary to continue with the previously mentioned protecting groups.

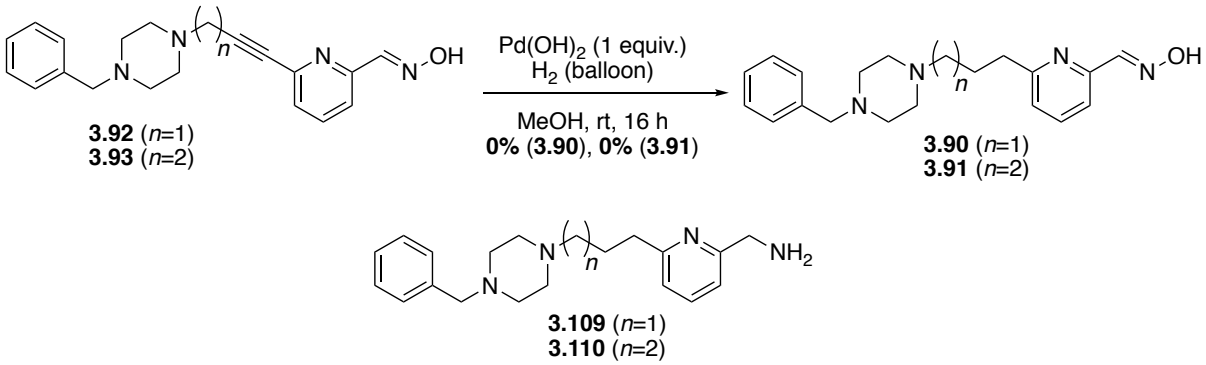

Scheme 3.41. Attempted non-selective hydrogenation of ethynyl-linked **3.92** and **3.93**, leading to the formation of corresponding primary amines **3.109** and **3.110**

Alternative hydrogenation methods were explored. Propargyl-linked benzylpiperazine **3.92** was treated under diimide reduction conditions (Scheme 3.42). Following 5 days at room temperature, by LCMS (ESI+), the reaction mixture showed only partially hydrogenated alkene **3.111** and no evidence of the desired propyl-linked benzylpiperazine **3.90**. This method of hydrogenation was abandoned and the reaction was next attempted with reduced equivalents of Pearlman's catalyst.

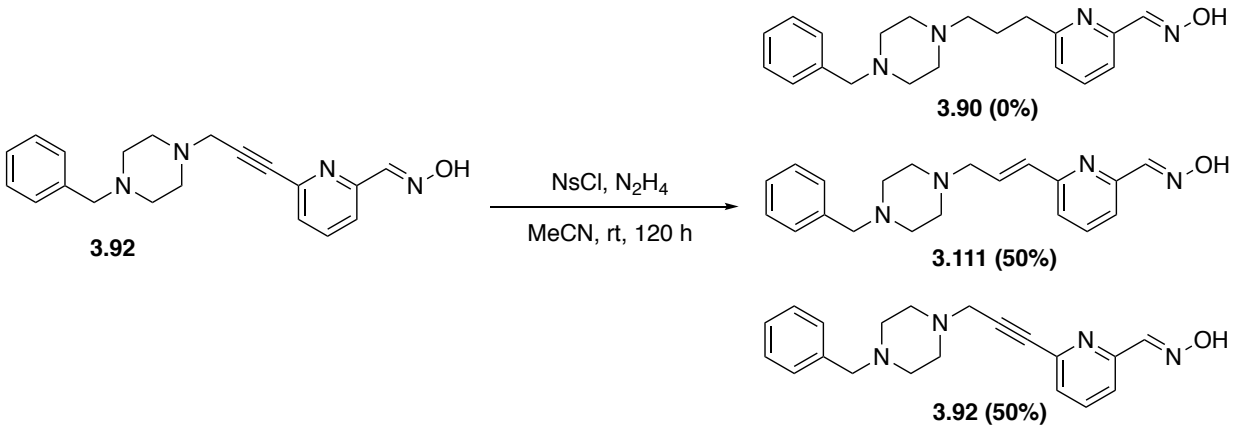

Scheme 3.42. Attempted diimide reduction of propargyl-linked benzylpiperazine **3.92**. Percent yields represent approximate values estimated from LCMS (ESI+) TIC peak integration

Hydrogenation of propargyl-linked benzylpiperazine **3.92**, using fewer equivalents of Pearlman's catalyst was tested (Scheme 3.43). The peaks corresponding to the starting material **3.92** and partially reduced alkene **3.111**, were overlapped on the LCMS TIC (ESI+) trace. However, gratifyingly this was not the case for the desired oxime **3.90** and the progress of the reaction was therefore conveniently monitored by LCMS (ESI+).

Following the addition of 0.5 equivalents of Pearlman's catalyst, the reaction was observed to proceed towards fully saturated oxime **3.90**. Unfortunately, LCMS analysis also revealed that it was not possible to push the reaction to complete conversion without risking overreduction towards primary amine **3.109**, therefore the reaction was repeated using only 0.5 equivalents of Pearlman's catalyst for two hours (Scheme 3.44).

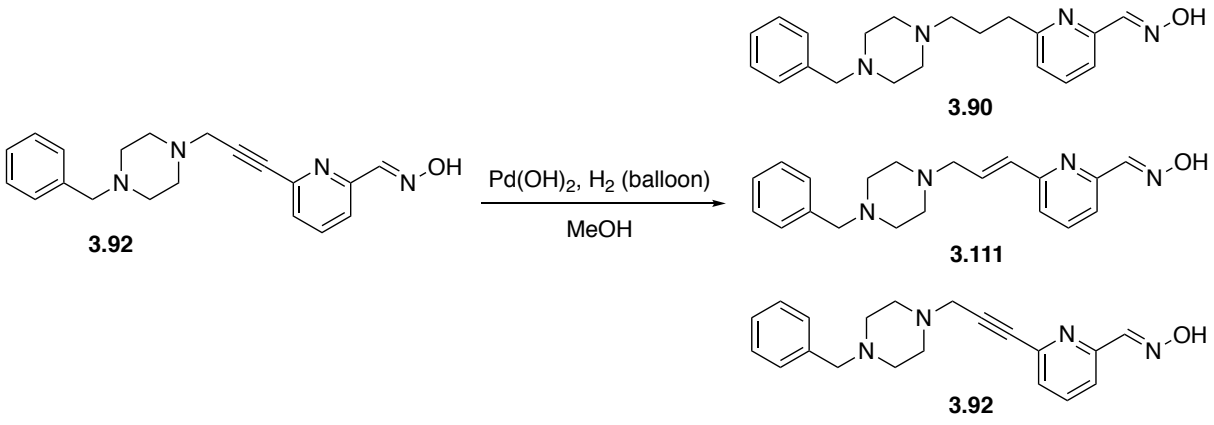

Scheme 3.43. Hydrogenation of alkyne **3.92** leading to a mixture of products

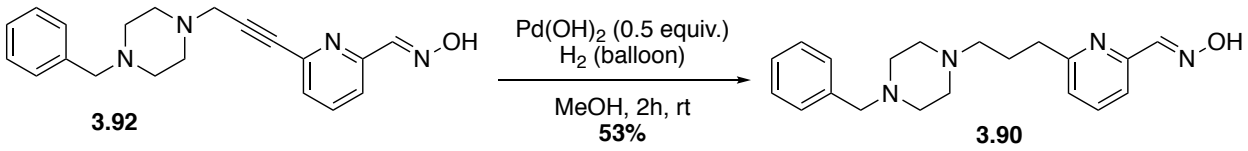

Scheme 3.44. Selective reduction of alkyne **3.92** to final hybrid reactivator **3.90**

Following the successful selective reduction of alkyne **3.92**, the same conditions were used for the reduction of homopropargyl-linked oxime **3.93** to saturated oxime **3.91**. This reaction was observed to result in the complete overreduction of the oxime (Scheme 3.45).

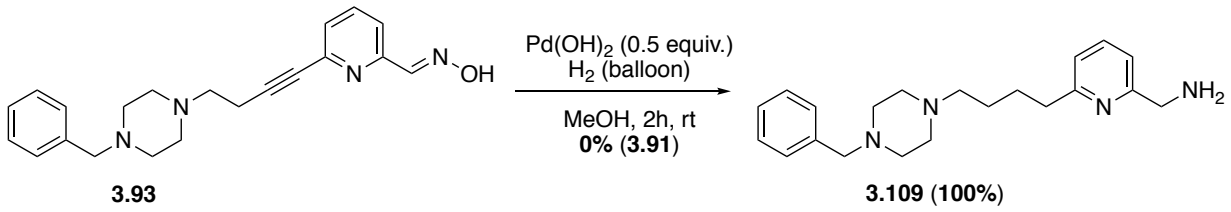

Scheme 3.45. Overreduction of alkyne **3.93** to primary amine **3.109.** Approximate yield of primary amine **3.109** was estimated from LCMS ESI+ TIC integration

Following the unsuccessful hydrogenation with 0.5 equivalents of Pearlman's catalyst, a weaker palladium catalyst was considered. Treatment of homopropargyl-linked benzylpiperazine **3.93** with 2 mol% of 10% palladium on carbon at room temperature for one hour afforded final hybrid reactivator **3.91** in 87% yield (Scheme 3.46).

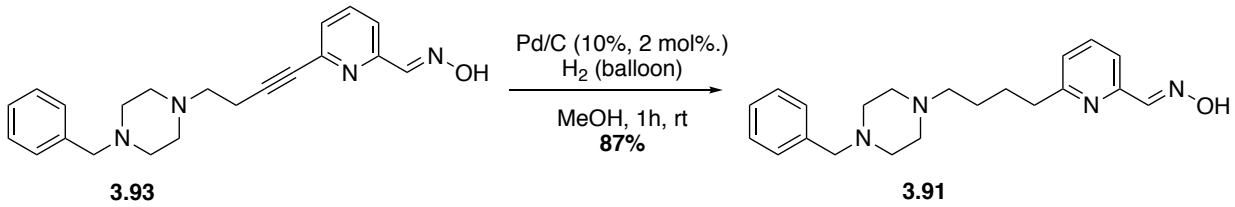

Scheme 3.46. Successful selective reduction of **3.93** to final hybrid reactivator **3.91**

Finally, Boc protected homopropargyl piperazine **3.102** was coupled with the protected hydroxypyridine using Sonogashira cross coupling to afford the alkynylpyridine **3.112** in modest 28% yield. This was followed by successful hydrogenation of the alkyne and hydrogenolysis of the *O*-benzyl functionality in 76% yield. Three-step TBS protection of the pseudo-phenolic hydroxy functionality, methyl ester reduction and TBS deprotection by DIBAL-H and oxime formation afforded final Boc protected piperazine hybrid reactivator **3.114** in unoptimised yield (Scheme 3.47).

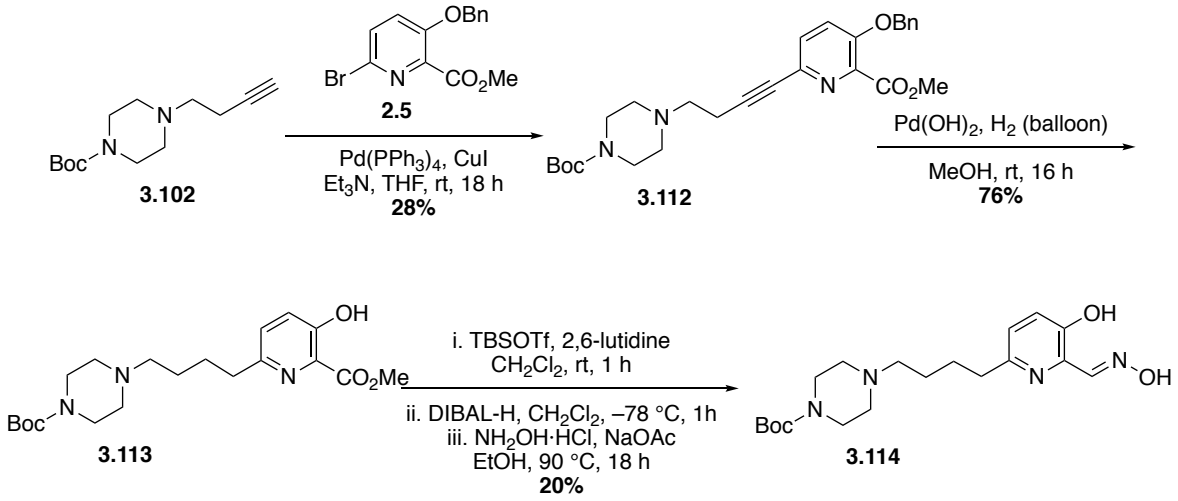

Scheme 3.47. Synthesis of Boc-piperazine hybrid reactivator **3.114**

Final benzylpiperazine **3.90**, **3.91**, **3.92**, **3.93** and Boc-piperazine **3.114** hybrid reactivators (Figure 3.12) were submitted for *in vitro* analysis to Dr José Dias at IRBA and the results will be discussed in Chapter 4.

3.4 Conclusions

During this chapter, the design and synthesis of a broader library of hybrid reactivators were discussed. The concepts of structural simplification and rigidification of existing hybrid reactivator scaffolds were explored in order to assess their effects *in vitro* as well as enabling synthetic route optimisation. Six dehydroxylated substituted quinoline-containing hybrid reactivators were synthesised (**3.6**, **3.7**, **3.10**, **3.11**, **3.12** and **3.13**, Figure 3.10), to enable comparative evaluation using *in vitro* data.

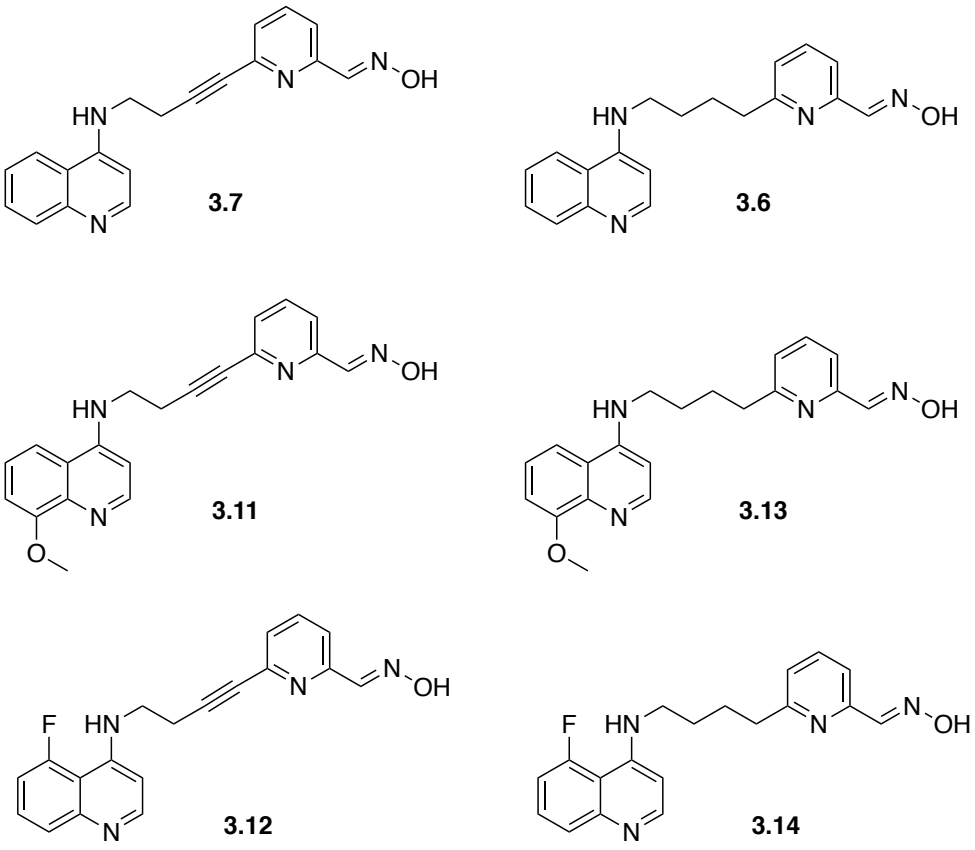

Figure 3.10. Dehydroxylated hybrid reactivators bearing quinoline PSLs

Two theobromine-containing reactivators **3.15** and **3.17** were synthesised (Figure 3.11) to investigate whether the theobromine scaffold would provide a new PSL for application in hybrid reactivators. Unfortunately difficulties encountered in purification and solubility due to the highly polar nature of the theobromine hybrids led us to abandon of this group of hybrid reactivators.

Given the impressive results previously reported by de Sousa from quinoline-containing hybrid reactivators,[186] two naphthylamine-containing hybrid reactivators **3.40** and **3.86** were synthesised (Figure 3.11), bearing a simplified dehydroxylated pyridine oxime reactivator.

Finally, a series of benzylpiperazine-containing hybrid reactivators **3.90**, **3.91**, **3.92** and **3.93** were designed and synthesised (Figure 3.12). These hybrid reactivator candidates featured flexible and

rigid three- and four-carbon linkers. In addition, a Boc-protected piperazine hybrid bearing a hydroxylated pyridine oxime reactivator **3.114** was also synthesised (Figure 3.12).

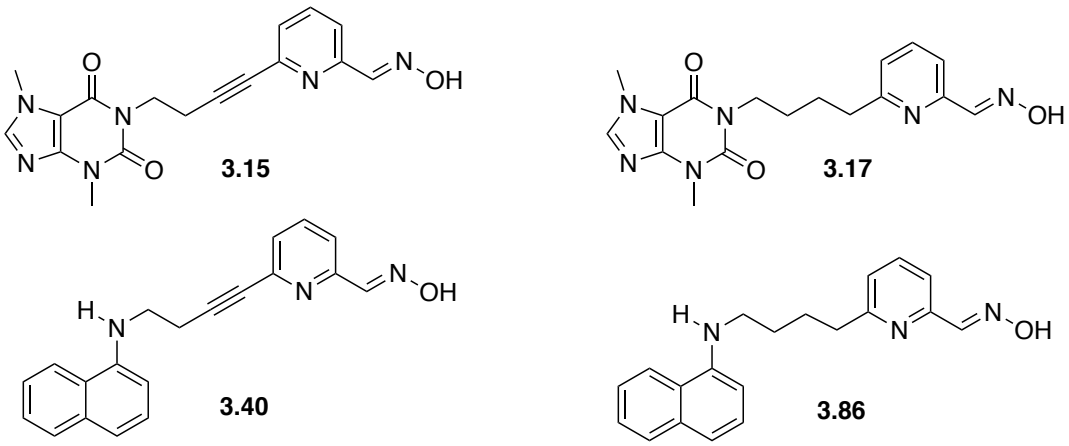

Figure 3.11. Dehydroxylated theobromine-bearing hybrid reactivators **3.15** and **3.17** and dehydroxylated butynyl-linked **3.40** and butyl-linked **3.86** naphthalene-bearing hybrid reactivators

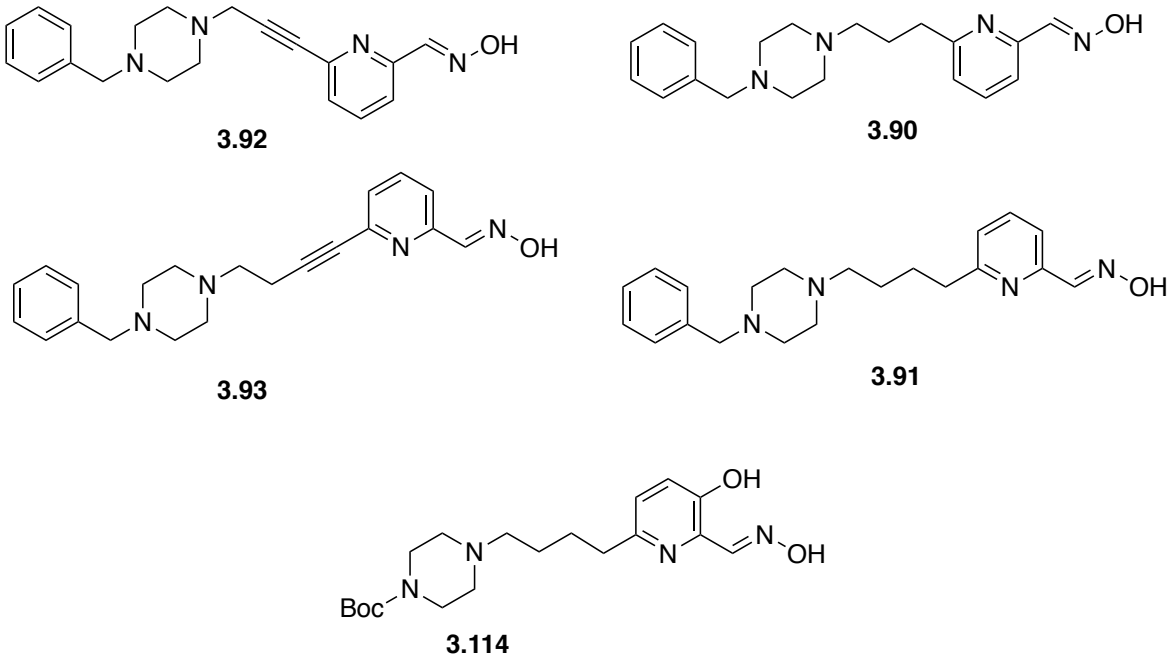

Figure 3.12. Dehydroxylated benzylpiperazine and *N*-Boc piperazine-containing hybrid reactivators

All fifteen novel hybrid reactivators were sent to our collaborator, Dr José Dias at IRBA, for *in vitro* evaluation and the results will be discussed in Chapter 4.

Chapter 4 Biological Evaluation of Hybrid Reactivators

4.1 *In Vitro* Evaluation

Due to the hazardous nature of handling OPNAs and OPNA surrogates, *in vitro* evaluation was undertaken within the Department of Toxicology and Chemical Risks in collaboration with Dr Florian Nachon and Dr José Dias at the Institut des Recherches Biomédicale des Armées (IRBA). Experimental studies were conducted by Dr José Dias, however, i*n vitro* evaluation of 7-trifluoromethylquinoline hybrid **2.46** against VX-inhibited *h*AChE was carried out by the author.

4.1.1 Enzyme Kinetics: Rate Constants

The *in vitro* reactivation assay determines three key metrics, which are used to assess the efficacy of hybrid reactivators. Firstly, K_D (dissociation constant) is inversely proportional to the affinity of the reactivator to inhibited *h*AChE. The reactivation rate constant (k_r) describes the velocity at which the OPNA is removed from the active site of *h*AChE.

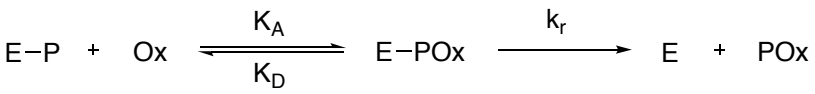

Scheme 4.1. Michaelis-Menten enzyme kinetics applied to the reactivation of phosphorylated AChE (E–P) by oximes (Ox), *via* the Michaelis-type complex (E–POx), to afford liberated AChE (E) and the phosphorylated oxime (POx)

Reactivation of OP-inhibited AChE (E–P) by an oxime (Ox) is analysed using Michaelis-Menten enzyme kinetics (Scheme 4.1), where E–POx represents the Michaelis-type phosphoryl-AChE-oxime complex, E represents the reactivated enzyme and POx represents the phosphorylated oxime. The dissociation constant, K_D, is calculated from the ratio of [E–P][Ox]/[E–POx]. Where $[E–P]_0 << [Ox]$ and complete reactivation is achieved, a pseudo-first order rate equation can be derived following Michaelis-Menten enzyme kinetics, k_{obs} (Equation 4.2), which represents the reactivation at a specific [Ox].[216] Where $K_D >> [Ox]$, the second order rate constant (k_{r2}) is defined as the ratio of k_r/K_D (Equation 4.2).

$$k_{obs} = \frac{k_r \times [Ox]}{K_D + [Ox]}$$

Equation 4.1. Pseudo-first order reactivation constant, k_{obs}

$$k_{r2} = \frac{k_r}{K_D}$$

Equation 4.2. Second order rate constant (k_{r2})

The three constants, k_r, K_D and k_{r2}, are useful in defining the reactivation potential of the hybrid reactivators. In addition, these constants facilitate quantitative comparison of candidates and will therefore be referred to during analysis of the compounds synthesised and evaluated in this thesis.

4.1.2 *In Vitro* Assay

The Ellman assay was used in this work to monitor the reactivation potential of the candidates. This assay depends upon a cascade of chemical reactions, which leads to a colour change. The colour change is monitored quantitatively by UV spectroscopy at 412 nm. The experimental procedure for the Ellman assay can be found in Chapter 7, Section 7.2 of this thesis.

The Ellman assay employs acetylthiocholine (ATC, **4.1**), an acetylcholine surrogate. ATC is hydrolysed in the same way as acetylcholine (ACh), resulting in the formation of acetic acid and thiol **4.2** (Scheme 4.2).

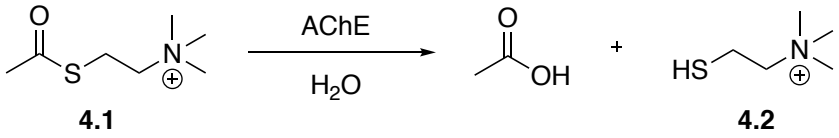

Scheme 4.2. Hydrolysis of ATC (**4.1**) by AChE to form AcOH and thiol **4.2**

The Ellman reagent, 5,5'-dithiobis-(2-nitrobenzoic acid) (**4.4**, $DTNB^{2-}$), present in the Ellman buffer contains a relatively weak disulfide bond (S–S), which is broken down in the presence of a nucleophile (Scheme 4.3). Thiolate **4.3**, generated from ATC hydrolysis, is deprotonated under physiological conditions and reacts with disulfide **4.4**. This chemical reaction results in the production of mixed disulfide **4.6** and 2-nitro-5-thiobenzoate (TNB^{2-}, **4.5**). The TNB^{2-} dianion has a vivid yellow colour, therefore, the extent of of TNB^{2-} production and hence intensity of yellow colour can be directly correlated with the degree of AChE reactivation. This is quantified by measurement of the absorbance of visible light at 412 nm.

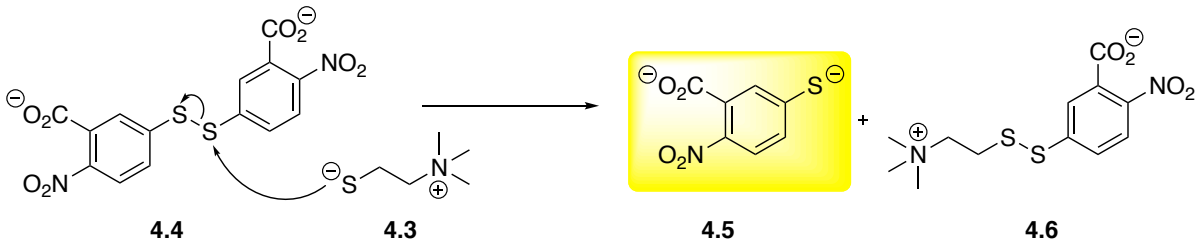

Scheme 4.3. Nucleophilic attack of $DTNB^{2-}$ by thiolate **4.4** leading to mixed disulfide **4.6** and TNB^{2-} (**4.5**)

Initially, before introduction of the oxime-containing hybrid reactivator to the OP-inhibited AChE, a calibration experiment is undertaken to measure the extent of oximolysis. Oximolysis describes the undesired breakdown of ATC (**4.1**) by the hybrid reactivator oximate anion, resulting in acylated oxime **4.7** (Scheme 4.4).

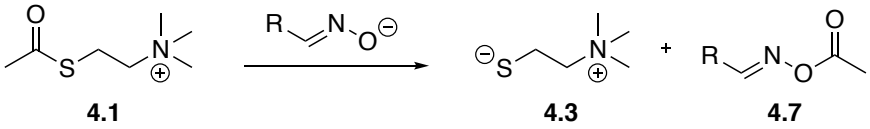

Scheme 4.4. Oximolysis of ATC (**4.1**) under physiological conditions resulting in the formation of thiolate **4.3** and acylated oxime **4.7**

Since the acylation of the oxime results in its complete deactivation, the hybrid reactivator is no longer able to liberate the OPNA from the inhibited enzyme. Additionally, thiolate **4.3** is generated, which could lead to false positive results. Thus, for an accurate representation of the reactivation efficiency of a compound, it is important to take into account the effect of oximolysis.

The apparent rate (k_{obs}), dissociation constant (K_D) and the reactivation rate constant (k_r) are calculated by non-linear fitting, using the ProFit software package (Quantumsoft). When plotting the apparent rate as a function of concentration, k_r appears at the maximal value of k_{obs} and the dissociation constant (K_D) is defined at the tangent of half maximal k_{obs} (Figure 4.1).

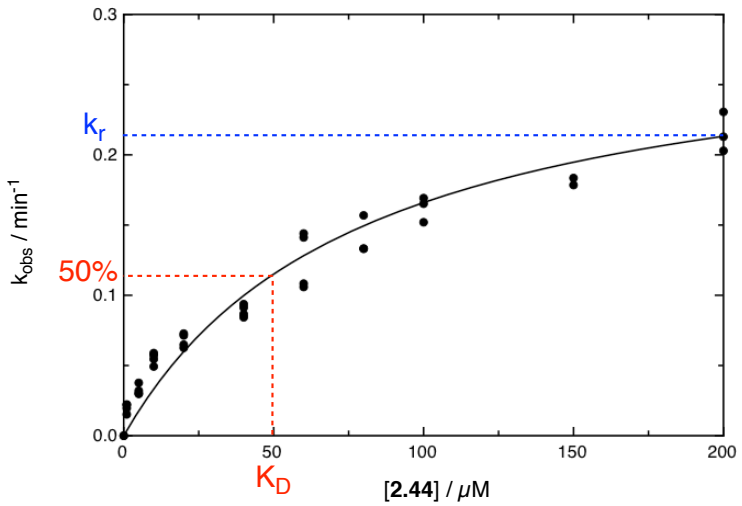

Figure 4.1. Reactivation plot to determine the reactivation constant for 7-trifluoromethylquinoline hybrid **2.46** for VX-inhibited *h*AChE

4.1.3 Pharmaceutical Salts

Aqueous solubility of the hybrid reactivator compounds is critical; without adequate solubility in physiological media, the reactivator is not carried within the bloodstream in sufficient concentration to reactivate OPNA-inhibited *h*AChE. Solubility is also key to evaluation of the reactivator candidates *in vitro*.

Various salt forms of 2-PAM have been synthesised since its initial development in 1955. 2-PAM chloride, iodide, methylsulfate and mesylate salts are all still in clinical use today[217] and 2-PAM mesylate (P_2S) has shown to be the most effective salt form for the reactivation of sarin and tabun-inhibited *h*AChE. [218,219]

It is estimated that half of all drug molecules used in clinical medicine are administered as a salt, as opposed to a free acid or base.[220] Advantages of delivering a pharmaceutical salt include; ease in production due to crystallisation of products; superior aqueous solubility and increased stability, ensuring prolonged drug shelf life.[221]

Figure 4.2 shows summary of the some of the factors affecting the salt selection process. In this work, all submitted oxime reactivators were evaluated as their corresponding hydrochloride salt. This salt was observed to give the reactivator compounds good solubility in water and is simple to prepare. All hybrid reactivator salts were formed by treatment of the free base with 2 M HCl and removing solvent *in vacuo*, to afford crystalline salts for evaluation.

Figure 4.2. Factors affecting salt selection of APIs (adapted from a figure by Wiedmann *et al.*[221])

4.1.4 *In Vitro* Results

Figure 4.4 displays the chemical structures of the 20 compounds developed, synthesised and evaluated *in vitro* during the course of this research. For comparison, the results of the *in vitro* evaluation will be presented alongside quinoline **2.1**, the lead compound previously synthesised by de Sousa,[186] as well as standard reactivators 2-PAM (**4.8**), Trimedoxime (**4.9**), Obidoxime (**4.10**) and Hi-6 (**4.11**) (Figure 4.3).

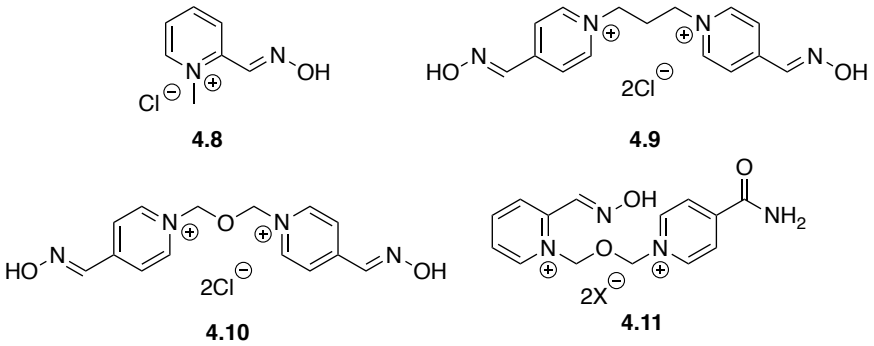

Figure 4.3. Chemical structures of standard reactivators; Pralidoxime, 2-PAM (**4.8**), Trimedoxime, TMB-4 (**4.9**), Obidoxime, LüH-6 (**4.10**) and Asisoxime, Hi-6 (**4.11**)

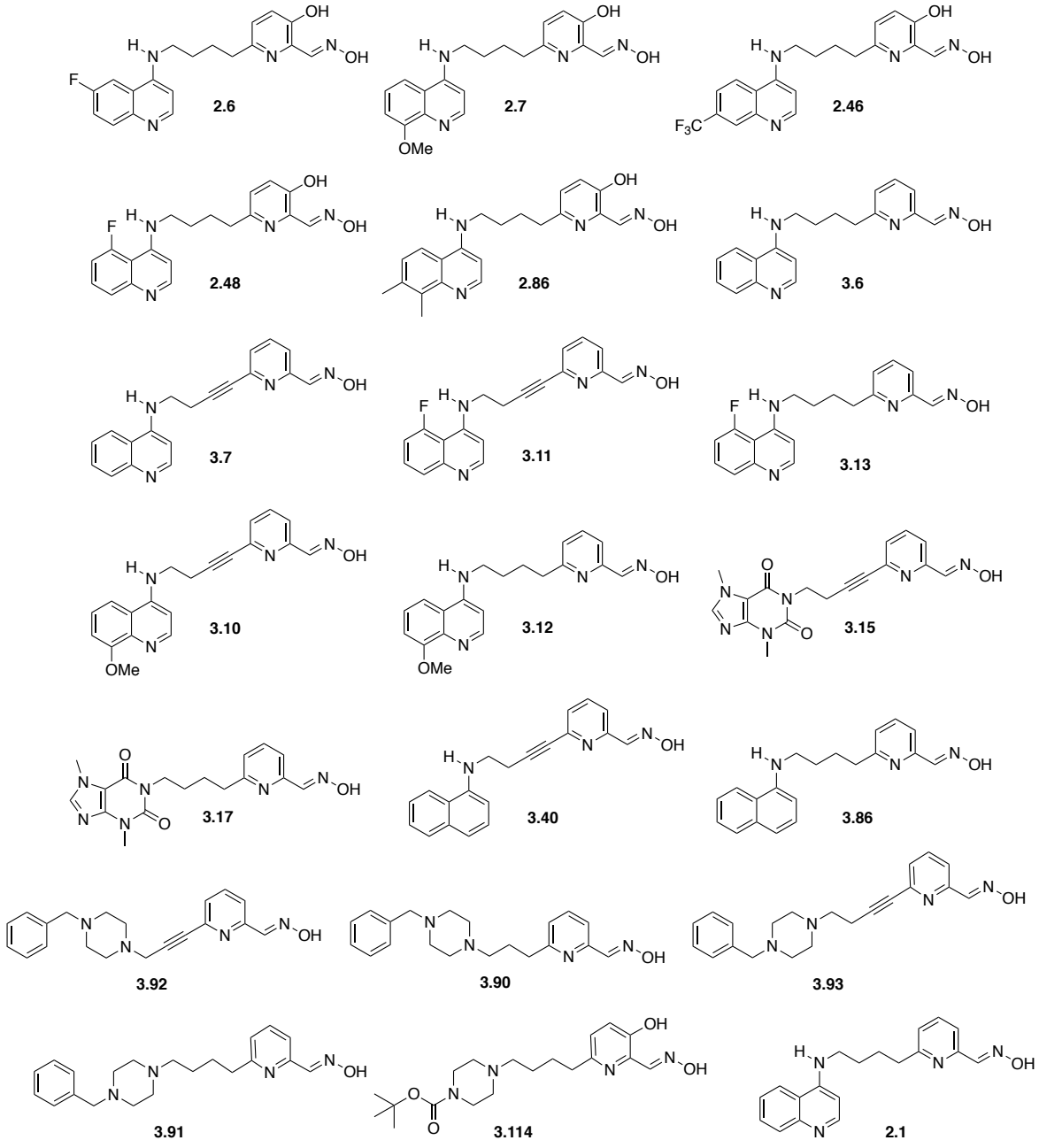

Figure 4.4. Chemical structures of lead quinoline **2.1** and novel hybrid reactivators synthesised and evaluated *in vitro*

Disappointingly, the hydrochloride salts of theobromine hybrid reactivators **3.15** and **3.17** and butynyl-linked naphthylamine **3.40** were not soluble in the *in vitro* assay medium; consequentially they are not included in the analyses. An efficient hybrid reactivator should demonstrate a good affinity towards the inhibited enzyme without inhibiting the native enzyme (characterised by a low value for K_D) and displace the phosphoryl moiety from the active site at a good rate (relatively high value for k_r). A high value of k_{r2} exemplifies an efficient hybrid reactivator.

Table 4.1. Kinetic constants for sarin-inhibited *h*AChE (n.d. denotes constants not determined due to linear dependence, however, $k_{r2} = k_r/K_D$ is given as the slope of the line, Ø denotes no reactivation up to 200 μM)

	sarin inhibited *h*AChE		
Reactivator	**K_D (μM)**	**k_r (min^{-1})**	**k_{r2} ($mM^{-1}min^{-1}$)**
2-PAM	26.7	0.25	9.1
TMB-4	n.d.[a]	n.d.[a]	n.d.[a]
LüH-6	31.3	0.94	29.9
Hi-6	50.1	0.68	13.5
2.1	30.0 ± 3	0.46 ± 0.016	18.3
2.6	22.0 ± 4	0.10 ± 0.0004	4.3
2.7	10.0 ± 2	0.11 ± 0.004	10.3
2.46	n.d.	n.d.	2.1
2.48	Ø	Ø	Ø
2.86	9.3 ± 1.4	0.03 ± 0.001	3.8
3.6	1.1 ± 0.1	0.03 ± 0.006	25
3.7	0.4 ± 0.1	0.03 ± 0.006	86
3.10	Ø	Ø	Ø
3.11	Ø	Ø	Ø
3.12	Ø	Ø	Ø
3.13	Ø	Ø	Ø
3.86	Ø	Ø	Ø
3.90	Ø	Ø	Ø
3.91	Ø	Ø	Ø
3.92	Ø	Ø	Ø
3.93	Ø	Ø	Ø
3.114	1 ± 0.3	0.2 ± 0.004	200

The results obtained from the *in vitro* analysis of the compounds synthesised in this work against sarin-inhibited *h*AChE are given in Table 4.1. 8-Methoxyquinoline **2.7 (**k_{r2} 10.3 $mM^{-1}min^{-1}$**)** demonstrated an elevated reactivation efficiency of sarin-*h*AChE comparable to that of 2-PAM (k_{r2} 9.1 $mM^{-1}min^{-1}$). However, 6-fluoroquinoline **2.6**, 7-trifluoromethylquinoline **2.46**, and 7,8-dimethylquinoline **2.86** exhibited inferior efficiency compared to 2-PAM. 5-Fluoroquinoline **2.48** was unable to reactivate sarin-*h*AChE. This outcome may indicate that the addition of substituents around the quinoline PSL has a detrimental effect on the final reactivator efficiency.

Dehydroxylated quinolines **3.6** (k_{r2} 25 $mM^{-1}min^{-1}$) and **3.7** (k_{r2} 85 $mM^{-1}min^{-1}$) appear to outperform all other tested reactivators, in terms of their overall reactivator efficiency. Interestingly, the dehydroxylated quinolines **3.6** and **3.7** demonstrate lower rates of displacement of sarin from the inhibited enzyme (k_r 0.03 min^{-1}) *cf.* lead quinoline **2.1** (k_r 0.46 min^{-1}). However, this loss in k_r is compensated by an increase in affinity of the butyl-linked dehydroxylated quinoline **3.6** (K_D 1.1 μM) and butynyl-linked dehydroxylated quinoline **3.7** (K_D 0.4 μM). The extremely high efficiency demonstrated by butynyl-linked dehydroxylated quinoline **3.7** (k_{r2} 85 $mM^{-1}min^{-1}$), seemingly originates from its excellent affinity to the enzyme, this may be related to the decreased flexibility of the reactivator, facilitating efficient entry into the gorge of the inhibited enzyme. The triple bond may also lower the pK_a of the oxime, increasing the relative proportion of the deprotonated oximate anion required for nucleophillic attack of the OPNA phosphorus electrophilic centre. The carbon atoms within the triple bond are sp hybridised and therefore possess higher s character offering better penetration and have a greater effective nuclear charge (Z_{eff}), resulting in better stabilisation of the oximate conjugate base.

Butyl-linked naphthalene **3.86**, whilst soluble in assay medium, did not elicit reactivation of sarin-inhibited *h*AChE. This is also true for dehydroxylated substituted quinolines **3.10-3.13** and the library of benzylpiperazines **3.90-3.93**. Contrastingly, compound **3.114**, bearing a *N*-Boc piperazine PSL proved exceptionally efficient compared to all other reactivators tested (k_{r2} 200 $mM^{-1}min^{-1}$). The combination of a high affinity to the enzyme (K_D 1 μM) and an impressive phosphoryl displacement rate (k_r 0.2 min^{-1}), gives rise to a high secondary reactivation rate constant (k_{r2}). The reactivator efficiency of *N*-Boc piperazine **3.114** exceeds the most efficient available reactivator of sarin-*h*AChE, LüH-6 (k_{r2} 29.9 $mM^{-1}min^{-1}$) seven-fold.

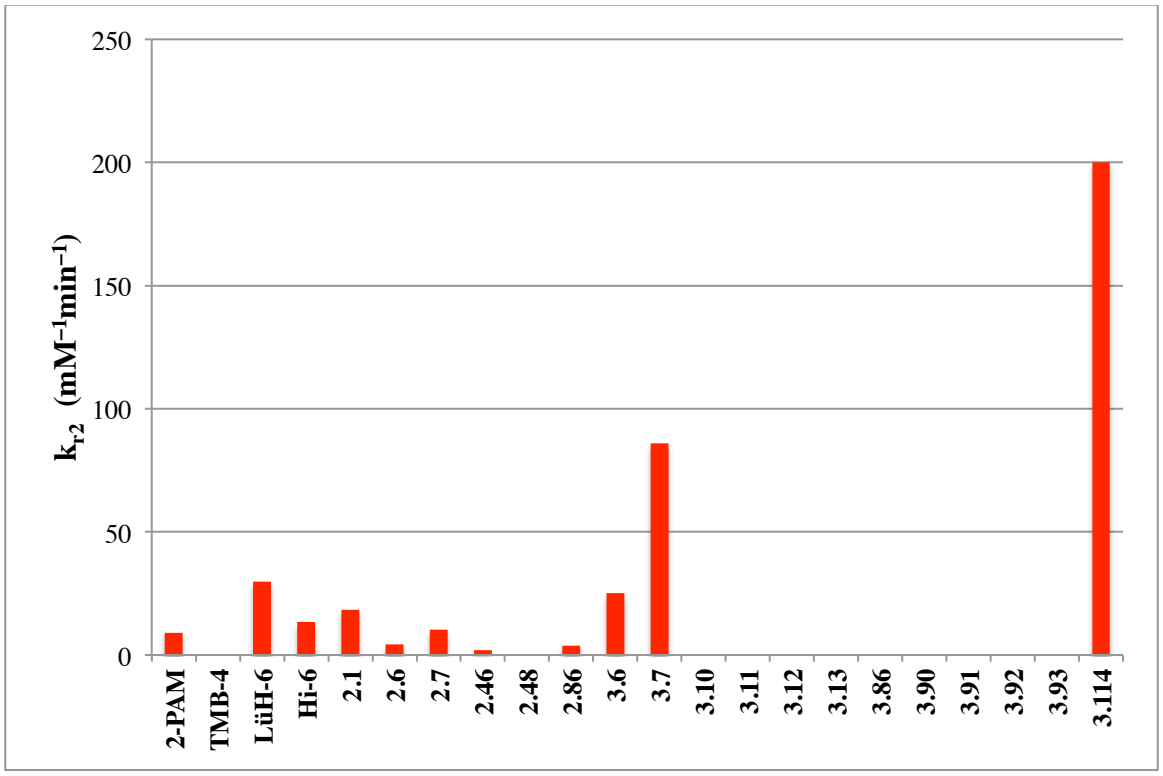

Figure 4.5. Second order reactivation rate constants of evaluated compounds against sarin-inhibited *h*AChE

Table 4.2. Kinetic constants for tabun-inhibited *h*AChE (Ø denotes no reactivation up to 200 μM)

	tabun inhibited *h*AChE		
Reactivator	**K_D (μM)**	**k_r (min^{-1})**	**k_{r2} ($mM^{-1}min^{-1}$)**
2-PAM	706	0.01	0.01
TMB-4	460	0.08	0.11
LüH-6	97.3	0.04	0.41
Hi-6	Ø	Ø	Ø
2.1	5.8 ± 1.9	0.36 ± 0.02	62.4
2.6	114 ± 22	0.23 ± 0.02	2
2.7	153 ± 19	0.29 ± 0.02	2
2.46	Ø	Ø	Ø
2.48	Ø	Ø	Ø
2.86	Ø	Ø	Ø
3.6	Ø	Ø	Ø
3.7	Ø	Ø	Ø
3.10	Ø	Ø	Ø
3.11	Ø	Ø	Ø
3.12	Ø	Ø	Ø
3.13	Ø	Ø	Ø
3.86	Ø	Ø	Ø
3.90	Ø	Ø	Ø
3.91	Ø	Ø	Ø
3.92	Ø	Ø	Ø
3.93	Ø	Ø	Ø
3.114	4.4 ± 0.3	0.23 ± 0.08	52

Data for tabun-inhibited *h*AChE reactivation is shown above in Table 4.2. Disappointingly, only 6-fluoroquinoline **2.6** (k_{r2} 2 $mM^{-1}min^{-1}$) and 8-methoxyquinoline **2.7** (k_{r2} 2 $mM^{-1}min^{-1}$) showed low efficiency reactivation compared to lead quinoline **2.1** (k_{r2} 62.4 $mM^{-1}min^{-1}$). 6-Fluoro and 8-methoxy-substituted quinolines **2.6** and **2.7** show similar rate of displacement of tabun from the enzyme (k_r 0.23 min^{-1} and 0.29 min^{-1}) compared to lead quinoline **2.1** (k_r 0.36 min^{-1}), however their overall efficiencies are dramatically limited by much lower affinity to the inhibited enzyme (K_D 114 μM and 153 μM).

5-Fluoroquinoline **2.48**, dehydroxylated substituted quinolines **3.10-3.13**, naphthalene **3.86** and benzylpiperazines **3.90-3.93** were unable to reactivate tabun-inhibited *h*AChE, up to a concentration of 200 µM. Gratifyingly, *N*-Boc piperazine **3.114** again demonstrated unprecedented reactivation of tabun-*h*AChE; a complex that is particularly challenging to reactivate due to the steric hindrance around the very weakly electrophilic target phosphorus atom. The affinity of *N*-Boc piperazine **3.114** (K_D 4.4 µM) towards tabun-*h*AChE is superior to that displayed by lead quinoline **2.1** (K_D 5.8 µM), though the dephosphorylation rate of *N*-Boc piperazine **3.114** remains slightly lower (k_r 0.23 min^{-1}) compared to quinoline **2.1** (k_r 0.36 min^{-1}). *N*-Boc piperazine **3.114** (k_{r2} 52 $mM^{-1}min^{-1}$) demonstrates reactivation efficiency far superior than any of the available reactivators for tabun-*h*AChE (2-PAM k_{r2} 0.01 $mM^{-1}min^{-1}$, TMB-4 k_{r2} 0.11 $mM^{-1}min^{-1}$ and LüH-6 k_{r2} 0.41 $mM^{-1}min^{-1}$)

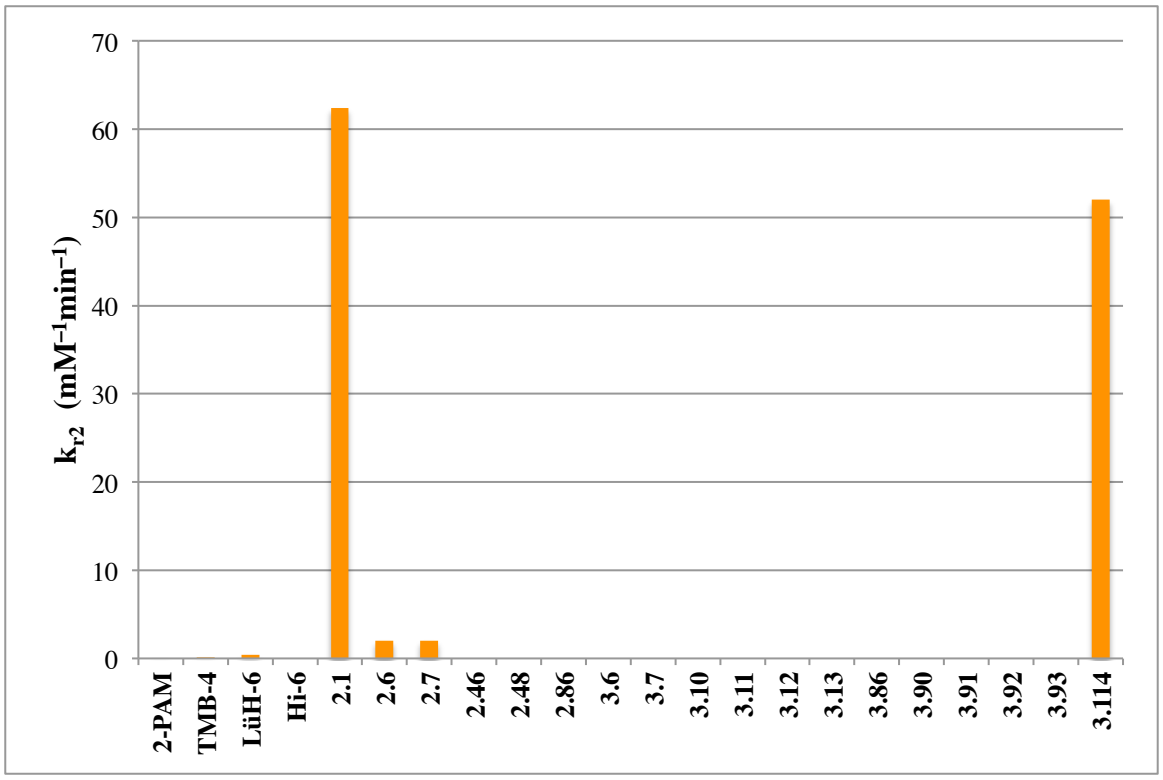

Figure 4.6. Second order reactivation rate constants of evaluated compounds against tabun-inhibited *h*AChE

Table 4.3. *In vitro* reactivation constants for VX-inhibited *h*AChE (Ø denotes no reactivation up to 200 μM)

	VX inhibited *h*AChE		
Reactivator	**K_D (μM)**	**k_r (min^{-1})**	**k_{r2} ($mM^{-1}min^{-1}$)**
2-PAM	215	0.06	0.28
TMB-4	159	0.13	0.89
LüH-6	54	0.60	11
Hi-6	50	0.44	9
2.1	3.9 ± 0.5	0.14 ± 0.003	94
2.6	175 ± 41	0.23 ± 0.03	1.3
2.7	39 ± 4	0.24 ± 0.02	6.2
2.46	66 ± 9	0.27 ± 0.02	4
2.48	Ø	Ø	Ø
2.86	7.1 ± 1.1	0.07 ± 0.002	10
3.6	3.2 ± 0.3	0.06 ± 0.001	21
3.7	1.2 ± 0.1	0.05 ± 0.0006	46
3.10	Ø	Ø	Ø
3.11	Ø	Ø	Ø
3.12	Ø	Ø	Ø
3.13	Ø	Ø	Ø
3.86	Ø	Ø	Ø
3.90	Ø	Ø	Ø
3.91	Ø	Ø	Ø
3.92	Ø	Ø	Ø
3.93	Ø	Ø	Ø
3.114	6.3 ± 1.2	0.23 ± 0.009	36.5

The results obtained from the *in vitro* analysis of the compounds synthesised in this work against sarin-inhibited *h*AChE are given in

Table 4.3. The reaction efficiencies of 6-fluoroquinoline **2.6** (k_{r2} 1.3 $mM^{-1}min^{-1}$), 8-methoxyquinoline **2.7** (k_{r2} 6.2 $mM^{-1}min^{-1}$), 7-trifluoromethylquinoline **2.46** (k_{r2} 4 $mM^{-1}min^{-1}$), and

7,8-dimethylquinoline **2.86** (k_{r2} 10 $mM^{-1}min^{-1}$) exceed standard reactivators 2-PAM (k_{r2} 0.28 $mM^{-1}min^{-1}$) and TMB-4 (k_{r2} 0.89 $mM^{-1}min^{-1}$) due to the latter's extremely poor affinity to VX-*h*AChE (K_D 215 μM and 159 μM). However, substituted quinolines **2.6, 2.7, 2.46** and **2.86** demonstrate weaker or comparable reactivation of VX-*h*AChE to standard reactivators LüH-6 (k_{r2} 11 $mM^{-1}min^{-1}$), and Hi-6 (k_{r2} 9 $mM^{-1}min^{-1}$). Quinoline **2.1** with a (k_{r2} 94 $mM^{-1}min^{-1}$) continues to offer superior reactivation efficiency compared to quinoline hybrid reactivators synthesised in this work. 5-Fluoroquinoline **2.48** was unable to reactivate the VX-inhibited *h*AChE in concentrations of up to 200 μM.

Dehydroxylated quinolines **3.6** (k_{r2} 21 $mM^{-1}min^{-1}$), and **3.7** (k_{r2} 46 $mM^{-1}min^{-1}$) display good reactivation efficiency, superior to all standard reactivators. Whilst the rate of OPNA displacement for the dehydroxylated quinolines **3.6** (k_r 0.06 min^{-1}), and **3.7** (k_r 0.05 min^{-1}) remains comparable to those of standard reactivator 2-PAM (k_r 0.06 min^{-1}), their greater affinities (dehydroxylated quinolines **3.6** K_D 3.2 μM and **3.7** 1.2 μM compared to K_D 2-PAM 215 μM) allow for increased overall efficiency. Interestingly, lead quinoline **2.1** displays a 2-fold increase in overall efficiency due to an increased dephosphorylation rate (k_r 0.14 min^{-1}) *cf.* dehydroxylated quinolines **3.6** and **3.7** (k_r 0.06 min^{-1} and 0.05 min^{-1})

For *h*AChE-VX, no reactivation was observed with 5-fluoroquinoline **2.48**, dehydroxylated substituted quinolines **3.10-3.13**, naphthylamine **3.86** and benzylpiperazines **3.90-3.93**, consistent with observations from other OPNA-inhibited *h*AChE. *N*-Boc piperazine **3.114** demonstrates good reactivation efficiency (k_{r2} 36.5 $mM^{-1}min^{-1}$), however due to lower affinity to the VX-*h*AChE complex (K_D 6.3 μM), it is outperformed by lead quinoline **2.1** (K_D 3.9 μM and k_{r2} 94 $mM^{-1}min^{-1}$). Despite a lower dephosphorylation rate, *N*-Boc piperazine **3.114** demonstrates an overall efficiency of more than 3-fold superior to LüH-6 (k_{r2} 11 $mM^{-1}min^{-1}$), the most efficient standard reactivator for VX-inhibited *h*AChE. *N*-Boc piperazine **3.114** demonstrates a greater rate of dephosphorylation (k_r 0.23 min^{-1}) compared to lead quinoline **2.1** (k_r 0.14 min^{-1}), however lead quinoline **2.1** shows a 1.7-fold increase in affinity (K_D 3.9 μM) compared to *N*-Boc piperazine **3.114** (K_D 6.3 μM).

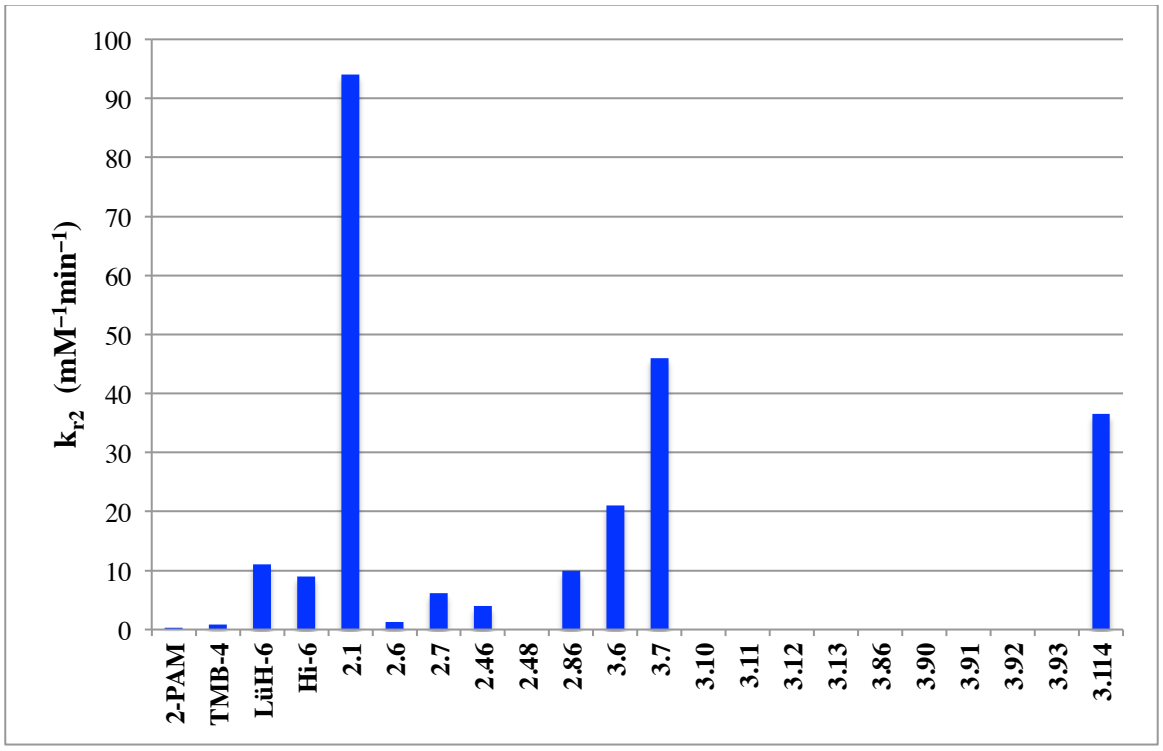

Figure 4.7. Second order reactivation rate constants of evaluated compounds against VX-inhibited *h*AChE

Table 4.4. *In vitro* reactivation constants for paraoxon-inhibited *h*AChE (Ø denotes no reactivation up to 200 μM)

	paraoxon inhibited *h*AChE		
Reactivator	**K_D (μM)**	**k_r (min^{-1})**	**k_{r2} ($mM^{-1}min^{-1}$)**
2-PAM	187	0.17	0.91
TMB-4	62	0.97	16
LüH-6	65	1.22	25
Hi-6	210	0.63	3
2.1	9.3 ± 1.38	0.19 ± 0.001	20
2.6	57 ± 9	0.36 ± 0.02	6
2.7	49 ± 10	0.48 ± 0.04	10
2.46	67 ± 6	0.2 ± 0.008	3
2.48	Ø	Ø	Ø
2.86	51 ± 7	0.1 ± 0.006	2.2
3.6	Ø	Ø	Ø
3.7	Ø	Ø	Ø
3.10	Ø	Ø	Ø
3.11	Ø	Ø	Ø
3.12	Ø	Ø	Ø
3.13	Ø	Ø	Ø
3.43	Ø	Ø	Ø
3.90	Ø	Ø	Ø
3.91	Ø	Ø	Ø
3.92	Ø	Ø	Ø
3.93	Ø	Ø	Ø
3.114	2.5 ± 0.3	0.2 ± 0.006	80

Data for paraoxon-inhibited *h*AChE reactivation is shown above in

Table 4.4. Lead quinoline **2.1** remains the most effective quinoline-containing hybrid reactivator of paraoxon-*h*AChE (k_{r2} 20 $mM^{-1}min^{-1}$). 6-Fluoroquinoline **2.6** (k_{r2} 6 $mM^{-1}min^{-1}$), 8-methoxyquinoline **2.7** (k_{r2} 10 $mM^{-1}min^{-1}$), 7-trifluoromethylquinoline **2.46** (k_{r2} 3 $mM^{-1}min^{-1}$) and 7,8-dimethylquinoline **2.86** (k_{r2} 2.2 $mM^{-1}min^{-1}$) were able to display reactivation, but suffering at least 2-fold reduction in efficiency compared to quinoline **2.1** (k_{r2} 20 $mM^{-1}min^{-1}$).

The reduced affinity of substituted 6-fluoroquinoline **2.6** (K_D 57 µM), 8-methoxyquinoline **2.7** (K_D 49 µM), 7-trifluoromethylquinoline **2.46** (K_D 67 µM) and 7,8-dimethylquinoline **2.86** (K_D 51 µM) appears to dramatically reduce overall efficiency of these substituted quinoline reactivators.

Interestingly, dehydroxylated quinolines **3.6** and **3.7** were unable to reactivate paraoxon-inhibited *h*AChE. Additionally, 5-fluoroquinoline **2.48**, dehydroxylated substituted quinolines **3.10-3.13**, theobromines **3.15** and **3.17**, naphthalene **3.86** and benzylpiperazines **3.90-3.93** do not demonstrate any reactivation against paraoxon-*h*AChE at concentrations of up to 200 µM.

N-Boc piperazine **3.114** demonstrated a k_{r2} of 80 $mM^{-1}min^{-1}$, outclassing existing reactivators; 2-PAM (k_{r2} 0.91 $mM^{-1}min^{-1}$), TMB-4 (k_{r2} 16 $mM^{-1}min^{-1}$), LüH-6 (k_{r2} 25 $mM^{-1}min^{-1}$) and Hi-6 (k_{r2} 3 $mM^{-1}min^{-1}$) and lead quinoline **2.1** (k_{r2} 20 $mM^{-1}min^{-1}$). The origins of this superior reactivation efficiency appear to come from the exceptional affinity of *N*-Boc piperazine **3.114** (K_D 2.5 µM) for the paraoxon-*h*AChE complex, with a 3.7-fold decrease in K_D compared to lead quinoline **2.1** (K_D 9.3 µM).

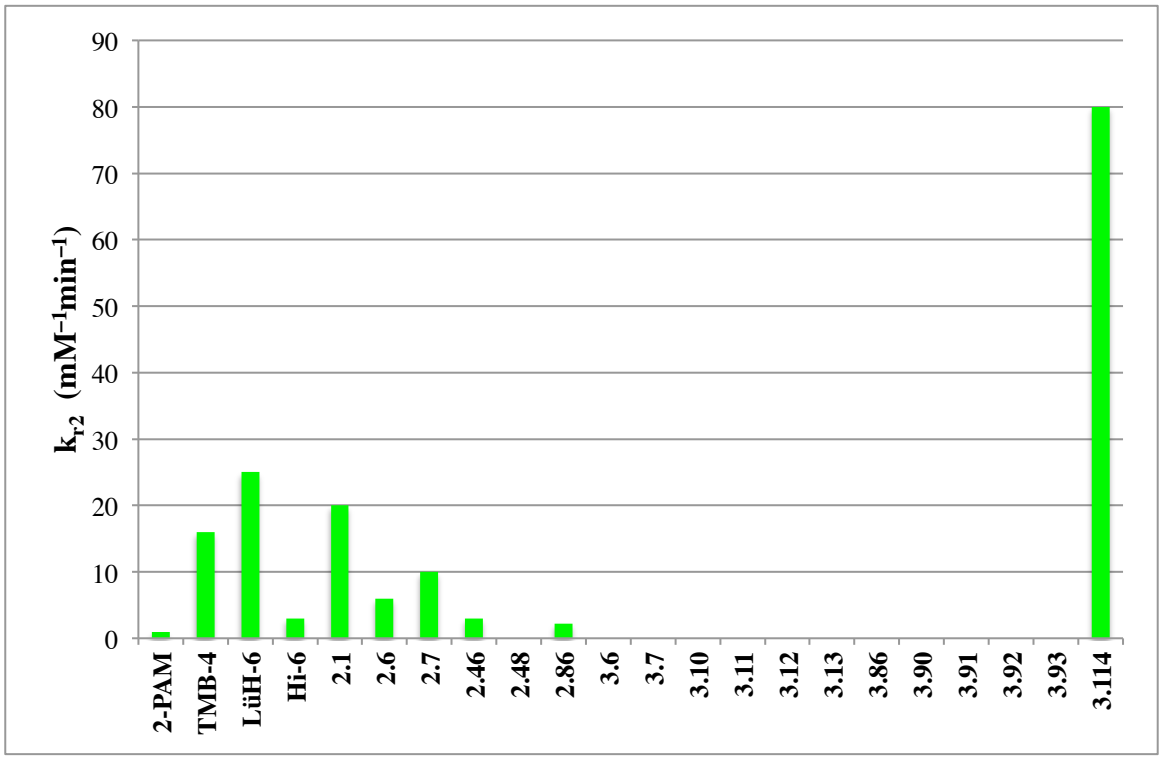

Figure 4.8. Second order reactivation rate constants of evaluated compounds against paraoxon-inhibited *h*AChE

4.1.5 Competitive Inhibition of *h*AChE by Hybrids: IC_{50} Data

The half maximal inhibitory concentration (IC_{50}) represents the potency of the hybrid reactivators to act as inhibitors of the native *h*AChE enzyme. The measurement quantifies the necessary concentration of reactivator required to inhibit the enzyme function by half of its original activity.

These measurements were taken *in vitro* and measured by spectrophotometry in a similar manner to the reactivation assay. Various concentrations of the reactivators in the Ellman solution described in Chapter 7, Section 7.2 were prepared and added to recombinant *h*AChE. The results were analysed by ProFit (Quantumsoft) and fitted using Equation 4.3.

$$\%\ Activity = 100\ \frac{IC_{50}}{(IC_{50} + [Reactivator])}$$

Equation 4.3. Equation used for reactivator concentration determination at IC_{50}

Table 4.5. Half maximal inhibitory concentration (IC_{50}) data

Reactivator	IC_{50} (μM)
2.1	1400 ± 100
2.6	18 ± 7
2.7	8 ± 3
2.46	25 ± 5
2.48	0.65 ± 0.08
2.86	19 ± 2
3.6	11 ± 2
3.7	4 ± 0.4
3.10	5.1 ± 0.6
3.11	1.8 ± 0.3
3.12	1.5 ± 0.1
3.13	0.4 ± 0.05
3.86	252 ± 37
3.90	4.3 ± 0.3
3.91	9 ± 1
3.92	18 ± 3
3.93	1 ± 0.08
3.114	156 ± 46

IC_{50} values from

Table 4.5 show that the lead quinoline **2.1** demonstrates a remarkably high IC_{50} at 1.4 ± 0.1 mM, proving it to be a relatively poor competitive inhibitor of *h*AChE. Conversely, 6-fluoroquinoline

2.6 (18 μM), 8-methoxyquinoline **2.7** (8 μM), 7-trifluoromethylquinoline **2.46** (25 μM) and 7,8-dimethylquinoline **2.86** (19 μM) all show relatively low IC_{50} values.

Their low IC_{50} values indicate a greater likelihood of competitively inhibiting the enzymes by blocking their active sites. This effect is emphasised by 5-fluoroquinoline **2.48** (0.65 μM) and dehydroxylated 5-fluoroquinolines **3.13** (0.4 μM), which demonstrate sub-micromolar competitive inhibition of *h*AChE. Both 5-fluoroquinoline **2.48** and dehydroxylated 5-fluoroquinoline **3.13** showed no reactivation of *h*AChE across the range of OPNAs tested against, suggesting that these compounds may exhibit such toxicity that they are extremely strong inhibitors of the enzyme.

Similarly, dehydroxylated quinolines **3.10-3.13**, were unable to reactivate *h*AChE inhibited with different nerve agents, demonstrate very low IC_{50} values. This may also indicate that these compounds have such a low concentration of inhibition that they themselves are acting in an inhibitory manner. Indeed, this may suggest that the addition of functionality around the quinoline, coupled with dehydroxylation of the reactivator moiety, may result in reactivation and then total inhibition of the enzyme.

The introduction of rigidification within the linker present in butynyl-linked dehydroxylated quinoline **3.7** demonstrates good affinity for OPNA-inhibited *h*AChE, however, does result in a relatively high toxicity (IC_{50} 4 μM). This conclusion could inspire the combination of particular characteristics of lead quinoline **2.1** with others from butynyl-linked dehydroxylated quinoline **3.7**, notably the triple bond (**3.7**) and the hydroxylated pyridine oxime reactivator functionality (**2.1**). Hydroxylated butynyl-linked quinoline **4.12** (Figure 4.9) would benefit from the increased affinity (lower K_D) ostensibly offered by the introduction of the triple bond within the linker, whilst maintaining good OPNA displacement rate (high k_r) demonstrated by the presence of the 3-hydroxyl pyridine oxime.

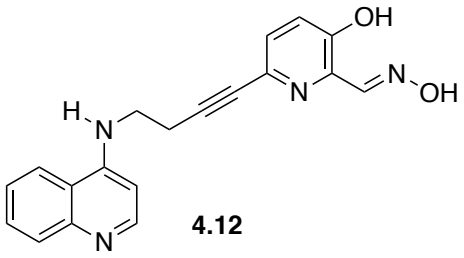

4.12

Figure 4.9. Potential new hybrid reactivator design, lead by *in vitro* data analysis

4.1.6 Determination of Drug Permeability

As discussed in Chapter 1, Section 1.5.1.1, existing reactivators of OPNA-inhibited *h*AChE demonstrate very poor blood-brain barrier permeability. Efficient passage of the reactivators through the BBB is essential for reactivation of inhibited AChE within the central nervous system. BBB permeability was evaluated for dehydroxylated quinolines **3.6** and **3.7**.

Studies of drug permeability were carried out by the Dehouck group of the Blood-Brain Barrier Laboratory at the University of Artois in Lens, France. The objective of these studies was to determine the propensity of absorption of the compounds through a BBB-like cell monolayer. The human colon carcinoma (Caco-2) cell line has been shown to provide good correlation *in vitro* to the BBB and is commonly used to predict drug transport *in vivo*.[222]

The protocol used was described by Artursson *et al.* (Figure 4.10).[223] Following cultivation of a monolayer of Caco-2 cells upon a filter support; a solution of the compound of interest is made up to a desired concentration at pH 7.4. This solution is termed the "donor solution" and is introduced into the apical side of the set up. The "acceptor solution" is introduced into the basal side of the apparatus and does not contain the compound of interest.

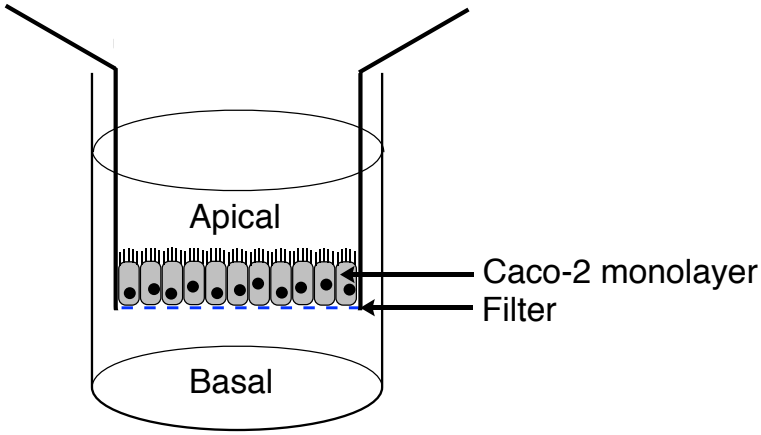

Figure 4.10. Diagram of basic set-up for permeability studies

By taking aliquots from both the apical and basal chambers and measuring concentrations of each, it is possible to calculate apparent permeability (P_{app}, units: cm s^{-1}) of the compound in question through the Caco-2 cell monolayer. Additionally, other compounds for which the passage across the BBB is known to be extremely facile and others which are particularly slow are tested to offer the opportunity to compare P_{app} values.

Following investigation into dehydroxylated quinolines **3.6** and **3.7**, Diazepam (a rapid penetrator of the BBB) and Lucifer Yellow (a poor BBB penetrator) were also tested. Figure 4.11 shows the initial findings from these experiments. Pleasingly, at both concentrations of 5 µM and 50 µM, both dehydroxylated quinolines **3.6** and **3.7** appear to display P_{app} values comparable or vastly surpassing that of the positive control, Diazepam. It was observed that butynyl-linked dehydroxylated quinoline **3.7**, at a concentration of 5 µM demonstrates apparent permeability 7.6 times superior to that of Diazepam. This indicated excellent permeability of dehydroxylated quinolines **3.6** and **3.7** through the Caco-2 monolayer and therefore their potential to effectively cross the BBB.

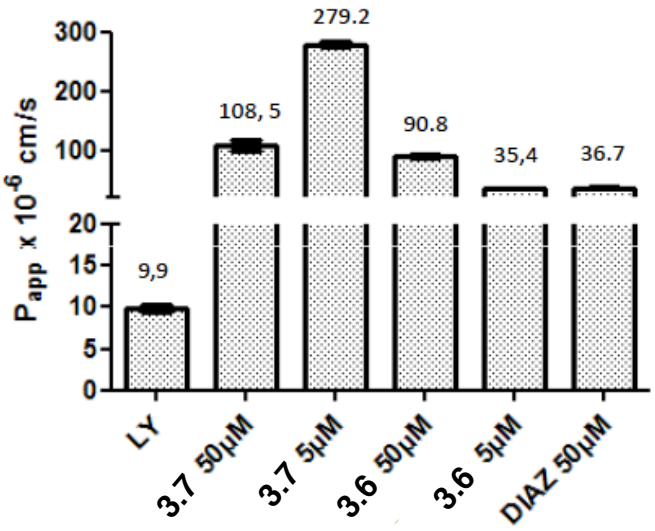

Figure 4.11. Results of BBB permeability assay (From the Dehouck BBB Laboratory, Unversité D'Artois)

4.2 Conclusions

Following biological evaluation of the hybrid reactivator candidates synthesised during this work (Figure 4.4), interesting outcomes were determined. Primarily, the novel substituted quinoline-containing compounds (**2.6**, **2.7**, **2.46**, **2.48** and **2.86**) appeared to demonstrate reduced activity as reactivators of OPNA-inhibited *h*AChE compared to lead quinoline **2.1**, suggesting that the effect of substitution of the quinoline PSL exclusively reduces reactivation potential. In terms of reactivation constants, the effect of substitution of the quinoline PSL increases the affinity of the compound towards the active site. Quinoline substitution also appears to have an unfavourable effect on the phosphoryl displacement rate constant (k_r). The overriding adverse effect on k_r for the substituted compounds results in an overall decrease in reactivator efficiency (k_{r2}) across all nerve agents tested, notably a 31-fold decrease in efficiency for tabun-inhibited *h*AChE. Toxicity studies of these compounds also highlighted relatively low IC_{50} values, indicating their ability to act as competitive inhibitors of *h*AChE.

Varied reactivation was also observed for compounds bearing the dehydroxylated pyridine oxime reactivator functionality (**3.6**, **3.7**, **3.10-3.13**). Dehydroxylated hybrid reactivators bearing the unsubstituted quinoline PSL (**3.6** and **3.7**) demonstrated exceptional reactivation efficiency compared to lead quinoline **2.1**. Whilst butynyl-linked dehydroxylated quinoline **3.7** was unable to reactivate tabun or paraoxon-inhibited *h*AChE, it demonstrated an impressive k_{r2} value of 86 $mM^{-1}min^{-1}$ (k_{r2} lead quinoline **2.1** 18.3 $mM^{-1}min^{-1}$) for sarin-inhibited *h*AChE. It may be concluded that the integration of a butynyl linker may assist in reducing the pK_a of the oxime and delivering increased reactivation rate and therefore overall efficiency.

Dehydroxylated hybrid reactivators bearing substituted quinolines (hybrid reactivators **3.10-3.13**) were unable to reactivate *h*AChE inhibited by all OPNAs tested. Measured IC_{50} values indicate that these compounds are effective inhibitors of *h*AChE at extremely low concentration.

Though the data obtained from the *in vitro* evaluation of the hybrid reactivators synthesised during this project were varied, fundamentals of hybrid reactivator design were investigated. Although it has been postulated that the presence of the 3-hydoxyl functionality on the pyridine oxime reactivator is necessary to illicit reactivation of OPNA-inhibited *h*AChE,[224] we have demonstrated unprecedented reactivation efficiency of sarin-*h*AChE by dehydroxylated butynyl-linked quinoline **3.7**. These dehydroxylated compounds allow for shorter and more efficient synthetic routes, with the prospect of high material output. This is important for the future development of reactivators as potential drug candidates as the need for greater quantities of compound increases with later stages of *in vivo* evaluation and clinical trials.

The effect of conformational restriction within the linker by the replacement of the flexible ethyl ($–CH_2CH_2–$) chain with an alkyne (–C≡C–) has been investigated. Gratifyingly, a positive effect was observed with respect to the affinity of dehydroxylated, alkyne-linked unsubstituted quinoline **3.7** towards the active site of sarin-*h*AChE. Consequently, a novel hybrid reactivator has been proposed (hydroxylated butynyl-linked quinoline **4.12**). Hydroxylated butynyl-linked quinoline **4.12** may combine the advantageous affinity (K_D) effects of the alkyne and the exceptional phosphoryl displacement rate (k_r) demonstrated by hydroxylated lead quinoline **2.1**.

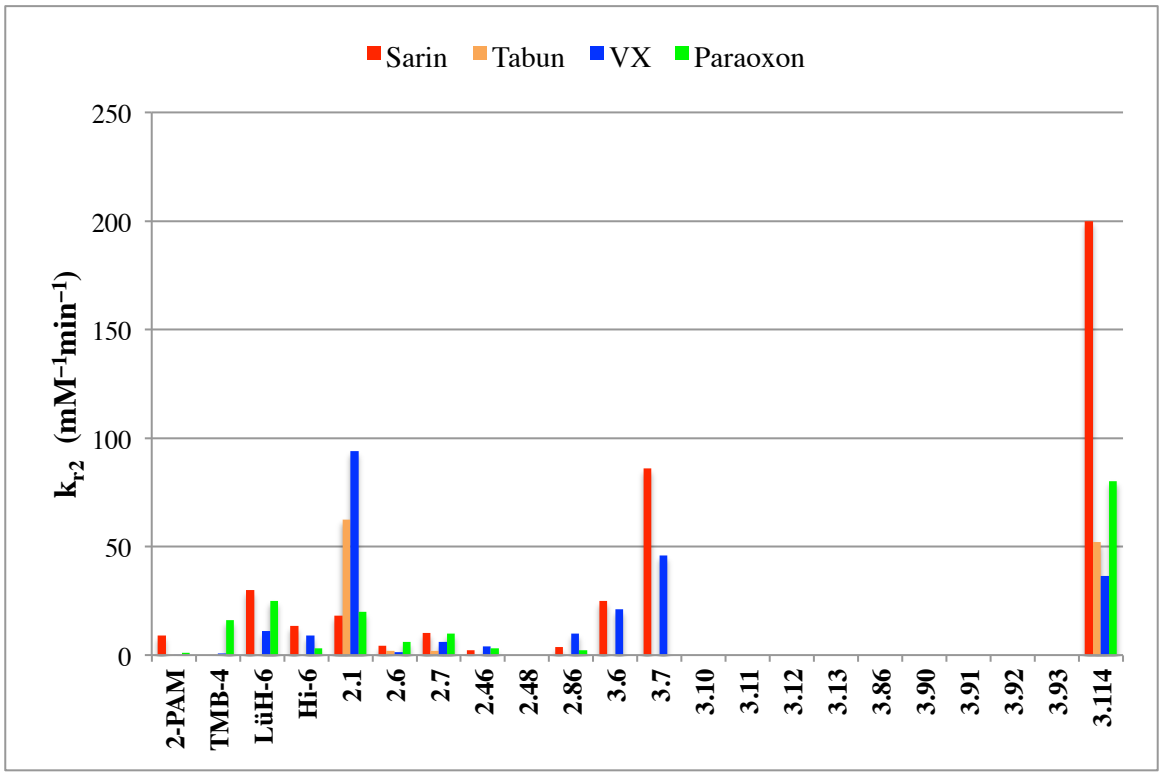

Figure 4.12. Combined second order reactivation rate constants of evaluated compounds against OPNA-inhibited *h*AChE

Dehydroxylated naphthalene, theobromine and benzylpiperazine-containing hybrids did not show reactivation at concentrations up to 200 μM. However, *N*-Boc piperazine **3.114** demonstrated unprecedented broad-spectrum reactivation of OPNA-inhibited *h*AChE, outperforming existing reactivators. *N*-Boc piperazine **3.114** was also observed to surpass reactivation efficiency of lead quinoline **2.1** against sarin and paraoxon.

N-Boc piperazine **3.114** has been identified as a new lead compound and the *N*-Boc piperazine PSL scaffold will be explored further in future developments of this project.

Chapter 5 Molecular Dynamics Simulations of Hybrid Reactivators

5.1 Introduction

This chapter will discuss the development of a new method for the future design of new generations of hybrid reactivators. Due to the time-consuming nature of synthetic chemistry, it was envisaged that an *in silico* model might be designed in order to undertake preliminary investigations into novel compounds. A computational model would allow for medium throughput *in silico* screening of potential reactivator libraries and enable more time-efficient drug design.

The model that was developed by the author in collaboration with Mabel Wong of the Essex Computational Chemistry Group at the University of Southampton is centred on the technique of molecular dynamics. The model uses existing data from x-ray crystallographic experiments undertaken on previously synthesised compounds, which have been co-crystallised inside of *Torpedo californica* AChE (pacific electric ray, *Tc*AchE). Using this information, it has been possible, alongside computational calculations to undertake "overlay" studies of similar compounds. Once the analogues are overlaid, it is possible to assess their likely interactions with AChE functionality, their potential affinity to the target enzyme and the distance between the reactivator and the site of reactivation. During the development of this model, the crystallographic data from three compounds within inhibited *Tc*AChE was used; quinoline **2.1**, tacrine **3.1** and 7-chlorotacrine **5.1** (Figure 5.1).

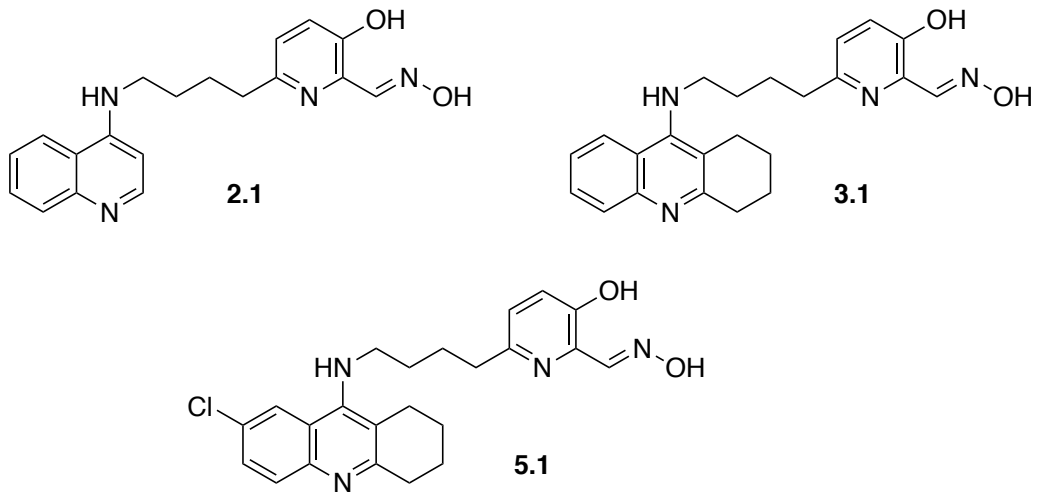

Figure 5.1. Compounds used for the development of *in silico* model

5.2 Molecular Dynamics

Molecular dynamics (MD) simulations were first developed in the late 1970s,[225] with the initial intention to overcome limitations encountered when calculating quantum-mechanical (QM) motions of large molecular systems. These calculations are much too complex and are far too computationally expensive for any supercomputer to undertake. Practically, these computational shortcomings can also be overcome by crystallographic studies, whereby one can credibly demonstrate molecular positions and orientations.[226] However, the effort and expense required to obtain such information can also be incredibly time and cost intensive. In addition, crystallographic data only represent the systems under 'crystallisation conditions', which are far from the conditions we observe *in vivo*.

MD simulations use simple approximations based on Newtonian physics to simulate atomic motions and generate the time evolution of a system. The simulation starts with an atomic model, prepared from *ab initio* homology modelling, crystallographic, cryo-electron microscopy or NMR data. The molecular forces acting upon each atom are then calculated. Each atom is moved according to the forces calculated and the simulation is advanced by 2 fsec. This process is repeated depending on the desired length of simulation.

The total energy contributed by bonded and non-bonded atomic interactions is calculated using an equation. The combination of these parameters is termed the "force field" and for this program of work, the AMBER force field was employed (Equation 5.1).[227]

$$\boldsymbol{E_{total}} = \sum_{bonds} K_b(r - r_0)^2 + \sum_{angles} K_\theta\,(\theta - \theta_0)^2 + \sum_{dihedrals} V_n[1 + \cos(n\phi - \gamma)] + \sum_{i=1}^{N-1}\sum_{j=i+1}^{N}\left[\frac{A_{ij}}{R_{ij}^{12}} - \frac{B_{ij}}{R_{ij}^{6}} + \frac{q_i q_j}{\varepsilon R_{ij}}\right]$$

Equation 5.1. AMBER force field Hamiltonian equation used to calculate the approximate forces between bonded and non-bonded atoms, which allow for estimation of molecular movement. Shown in red are bonded atomic forces, bonds and angles are modelled as balls on springs as harmonic oscillators and dihedral angles are modelled using a sinusoidal function, which approximates energy differences associated with staggered and eclipsed bond conformations. Non-bonding interactions, shown in green, arise from Van Der Waals forces and electrostatic interactions, which are modelled using the Lennard-Jones potential and Coulomb's Law respectively

Following the calculations given by the force field, the positions of each atom are moved according to Newton's laws of motion. Potential energy is that which results from position and its SI unit is the joule (or Newton × metre, hence describes an objects capacity for doing work as a result of its position). When force acting upon an object is a function of position only, it can be represented as a potential energy function. Force can therefore be expressed as the derivative of potential energy (Equation 5.2).

$$Force(x) = -\frac{\delta U}{dx}$$

Equation 5.2. Potential energy function where *U* represents potential energy and *x* represents position. The potential energy (*U*) is equal to the work you must do to move an object from *U*=0 to the point of position *x*. The force you exert to move an object must be equal and oppositely directed to move the object from its original position to position *x;* hence it exists as a negative function

The starting position of all atoms is obtained from the model generated experimentally (homology modelling, crystallography etc.) and their initial velocities are randomly assigned according to the Maxwell-Boltzmann distribution. Combining Equation 5.3 and Newton's second law of motion F=ma (force = mass × acceleration) allows us to relate potential energy with positions with respect to time.

$$Force\ (x) = ma = m\frac{dv}{dt} = m\frac{d^2r(t)}{dt^2}$$

Equation 5.3. Relationship between force, mass (m), acceleration (a), velocity (v), position (r) and time (t) using Newton's second law of motion. Hence, force is the second derivative of positions with respect to time

The combination of Equation 5.3 and a computational algorithm ("Leapfrog") enables us to calculate the time evolution of a system.[228] Since the potential energy is a function of the atomic positions of all atoms in the system, there is no possible analytical solution and hence we require an algorithm to solve them numerically. The algorithm firstly calculates the velocities of the atoms of the system at a time *t+1/2dt* (half a time-step), these velocities are then used to calculate the positions at time *t+dt* (one time-step). This leapfrogging continues until the entire length of the time evolution has been fully calculated. This process enables us to generate a time-evolved simulation of atomic motion of the ligand (hybrid reactivator) within the enzyme.

5.3 Parameterisation of Model Elements

5.3.1 Ligand Parameterisation

Before the MD simulation studies could be undertaken, work towards the preparation of the molecular models was required. This preparation is termed parameterisation. All crystallographic data in hand was novel and unpublished at the time of the development of the *in silico* model and hence needed to be parameterised such that the MD engine (AMBER) will recognise every element of the model. Firstly, quinoline **2.1**, tacrine **3.1** and 7-chloroquinoline **5.1** were parameterised. Atoms and bonds are defined as balls attached by springs and the parameters that were defined are as follows:

- size of each ball (atom)
- strength of each spring (bond)
- angles of dihedrals
- partial charges

To define these parameters, the ligand was first isolated from the crystallographic data and using OpenBabel (version 2.4.1), 1,000 conformers of the ligand were generated. Conformational clustering was performed on the 1,000 conformers to pull out three representative conformers (Figure 5.2).

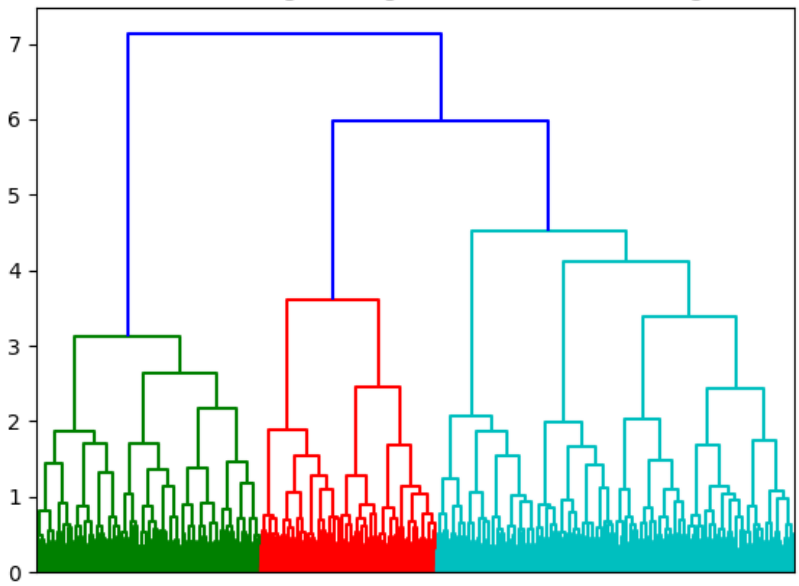

Figure 5.2. Hierarchical clustering of 1,000 conformers of quinoline **2.1** into three representative clusters (shown in green, red and turquoise)

The resulting PDB files for each representative cluster were converted to Gaussian input files. A Gaussian calculation, using Hartree-Fock (6–31G*) level of theory, was then run to define the molecular orbitals (MOs) of the ligand for each cluster. The electrostatic potential (ESP) data from the Gaussian calculations were extracted for each of the clusters and subsequently concatenated. This provided a QM calculation of the averaged ESP of the ligand being parameterised.

Using the QM calculation of ESP, it was then possible; using restrained electrostatic potential (RESP) to fit these charges to classical mechanics. A program called “respgen” was executed which uses the “Point Charge Model” to fit ESP data to RESP data. This process provides a prep file, which provides a description of both atom types and partial charges. The parameters of the prep file are then checked using a program called “Parmchk2”. “Parmchk2” reads the prep file against a large database and assigns correct parameters to the atoms.

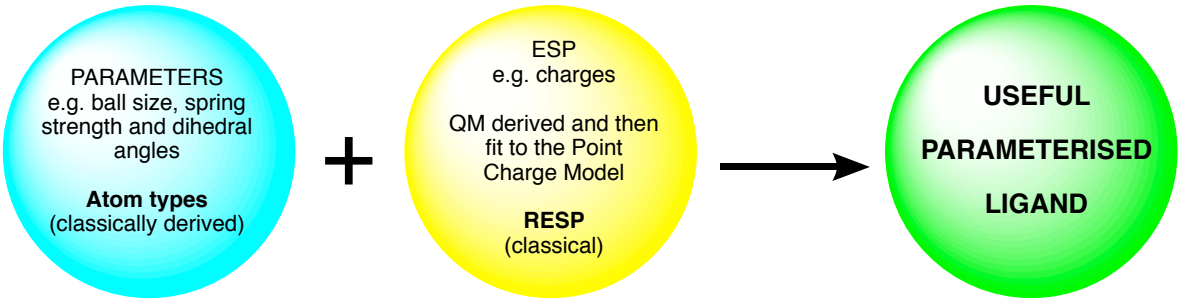

Figure 5.3. Combination of parameters derived from Parmchk2 (in cyan) and restrained electrostatic potential derived from fitting the QM output from Gaussian to the Point Charge Model (in yellow) can afford a prep file with correctly assigned parameters to a ligand (green)

Finally, using "tleap", a program that is responsible for setting up MD simulations, the predetermined coordinate file (from the original crystallographic data) and the parameterised ligand file are fed into the program. "Tleap" then generates a topology file (.prmtop) and a coordinate file (.rst), this ensures that the parameters have been set up correctly and that they can be used in a MD simulation.

Under physiological conditions, the hybrid reactivators exist as a mixture of their oxime/oximate forms, which is reliant on their oxime pK_a. Due to time constraints, the hybrid reactivator ligands were prepared in their neutral form and each oxime moiety was parameterised in its protonated state.

5.3.2 Protein Parameterisation

The X-ray crystallographic data used in this program of work were provided by Dr Gianluca Santoni from the European Synchotron Radiation Facility in Grenoble, France. X-ray data for tacrine **3.1** and 7-chlorotacrine **5.1** was provided within uninhibited *Tc*AChE and tabun (**5.3**) surrogate-*Tc*AChE complex, 4-nitrophenyl ethyl dimethylphosphoramidate (NEDPA) **5.2** (Figure 5.4). Data for quinoline **2.1** was provided within uninhibited *Tc*AChE only.

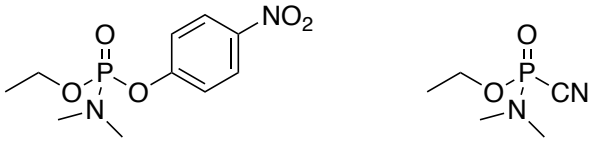

5.2 **5.3**

Figure 5.4. NEDPA (**5.2**) and tabun (**5.3**)

Since the AChE that was used in the crystallographic data originates from *Torpedo californicus*, some parameterisation of the protein was also necessary, such that the *in silico* model could best reflect the effect of the ligands upon human AChE. Since both NEDPA-inhibited *h*AChE and tabun-inhibited *h*AChE are not known within the literature, it was not possible to obtain data for the parameters for tabun-inhibited serine.

Mabel Wong of the Essex Computational Chemistry Group at the University of Southampton parameterised the inhibited serine residue with tabun by the same means as described in Section 5.3.1.

Some areas of missing residues of the enzyme were identified in the pdb file of sarin-inhibited *h*AChE (pdb: 5fpq). It is important to define all atoms within the system, such that an accurate representation of force experienced by the system can be calculated (as the force field calculation is a sum of all atoms, Equation 5.1). Fortunately, two areas of 'floppy loops', which are simple to model, represented the areas of missing residues.

The program, "MODELLER" (version 9.20), was fed the pdb files of *h*AChE without the missing residues and the sequence of the protein with the missing residues. The program then fills in the gaps between residues. The program generates twenty conformers, which are manually inspected and the average conformer is selected (Figure 5.5). Firstly, the conformers that appear as outliers were removed (such as the conformer represented in magenta, Figure 5.5a), then the conformer that appears to represent the average is then selected by eye.

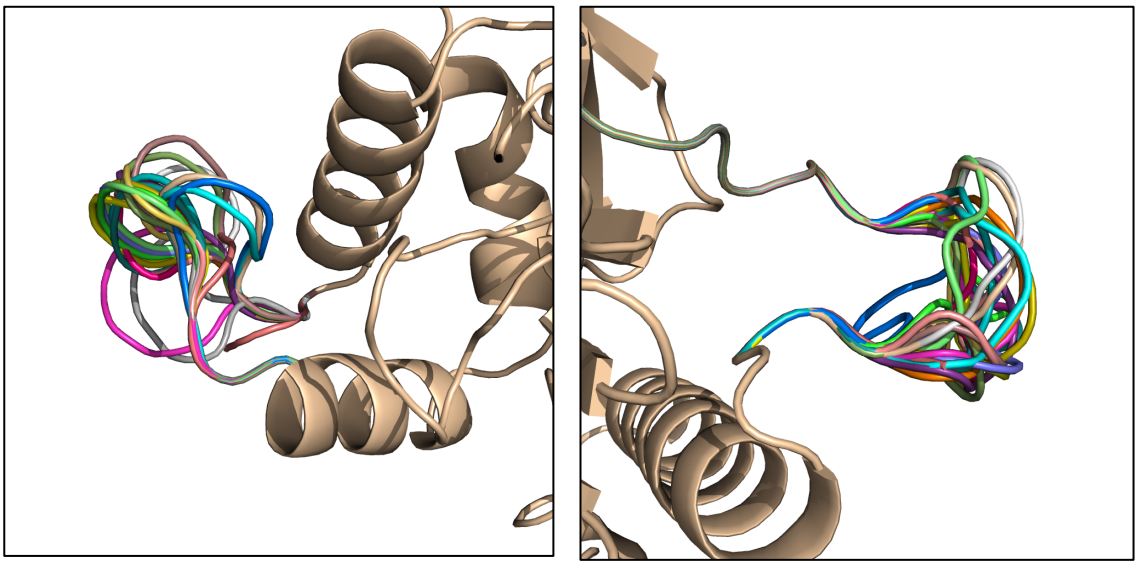

(a) **(b)**

Figure 5.5. Output pdb from "MODELLER" of *h*AChE (in beige) and areas of missing residues, filled in with twenty different conformations (show in various colours)

With a complete model of *h*AChE in hand, it was necessary to undertake alignment of this model with the *Tc*AChE, from the X-ray data. Mabel Wong of the Essex Computational Chemistry Group at the University of Southampton undertook this procedure. The sequence alignment of *Tc*AChE is similar to that of *h*AChE and hence the residues, particularly within the active site, are relatively similar. Therefore, it was possible to undertake alignment of the *Tc*AChE with the modelled pdb file of *h*AChE. This allowed visualisation of the relative position of the inhibited serine residue within the active site.

From the pair of aligned models, everything from the inhibited *Tc*AChE model was removed, except for the ligand and the phosphorylated serine. The uninhibited serine residue was removed from the human model. This treatment leaves only the aligned *h*AChE, the correct position and orientation of the ligand and the inhibited serine residue.

Similarly, to build an uninhibited model of *h*AChE from the data given from the uninhibited *Tc*AChE, the same alignment procedure was undertaken. However, the uninhibited serine residue was left and only the reactivator from the original crystallographic data was inserted into the model. Following this alignment technique, it was possible to obtain human models of inhibited and uninhibited AChE for use in MD simulations.

5.4 Preparation of Model for MD Simulation

With all six parameterised models (Table 5.1) in hand, it was then possible to begin the next phase of the model preparation.

Table 5.1. All parameterised models (*1*-*6*) ready for the next steps towards MD simulation

Model	Protein	Ligand	Inhibited/Uninhibited
1	*h*AChE	**2.1**	Inhibited
2	*h*AChE	**2.1**	Uninhibited
3	*h*AChE	**3.1**	Inhibited
4	*h*AChE	**3.1**	Uninhibited
5	*h*AChE	**5.1**	Inhibited
6	*h*AChE	**5.1**	Uninhibited

Using “tleap”, the models were individually loaded into a simulation environment. This includes the solvation of the model into a defined box of water molecules (12 Å around the protein and ligand complex) and the addition of sodium and chloride ions (Figure 5.6).

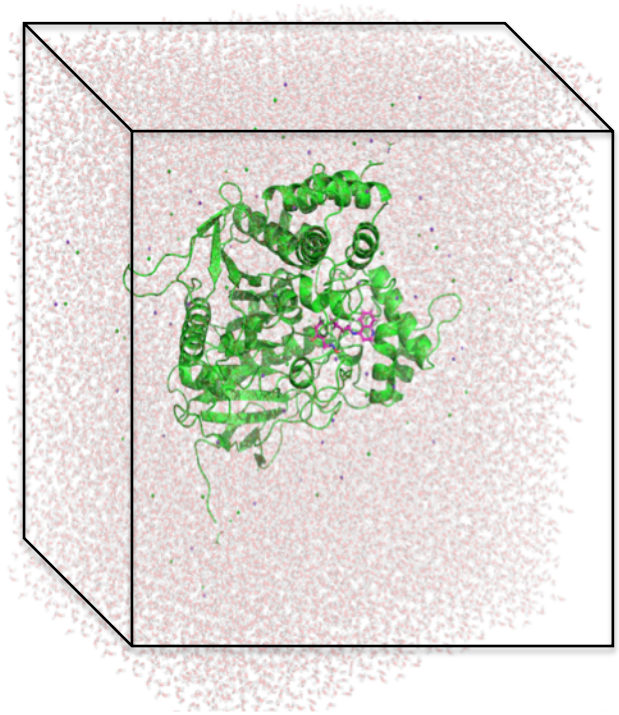

Figure 5.6. Model in simulation environment, shows a "box of waters" (red), including chloride ions (small green dots) and sodium ions (small purple dots) 12 Å around the centre, highlighted by a black cube. Inside the box is the *h*AChE (green) and ligand **2.1** (magenta)

Energy minimisation of each model was then undertaken. Richard Bradshaw, a past member of the Essex Computational Chemistry Group, wrote the original scripts that were adapted for this work.[229] Energy minimisation was undertaken in three stages and at every stage the protein was allowed to move towards its lowest energy conformation. During the first stage of minimisation everything in the model, except from the protein is allowed move towards its lowest energy conformation over 10,000 steps. Secondly, everything except from the protein backbone is allowed to move over 10,000 steps. Finally, all restrictions are lifted and the entire model is allowed to move towards its lowest energy conformation over 10,000 steps.

Following energy minimisation, three rounds of equilibration were undertaken. Equilibration is an integral step to achieve the model in the condensed phase compared to the solid phase taken from the x-ray data. It is necessary to allow the protein and ligand to equilibrate with the new conditions introduced (i.e. water and ion surroundings). The equilibration also consists of three individual stages:

1. The solvent and ions are heated to 300 K for 100 ps
2. NVT equilibration (constant number of particles, volume and temperature) where pressure is allowed to equilibrate for 100 ps
3. NPT (constant number of particles, pressure and temperature) equilibration where volume is allowed to equilibrate for 100 ps

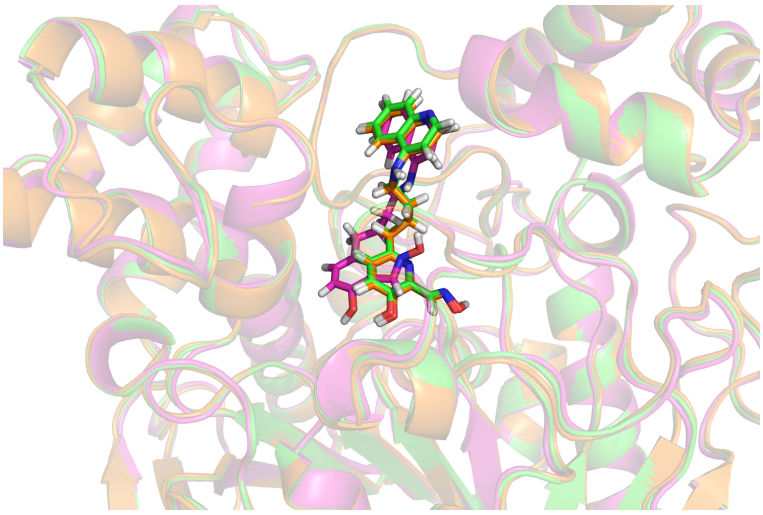

Figure 5.7. Overlaid structures of quinoline **2.1** bound within *h*AChE model. The magenta colour indicates the model after the first round minimisation. The green colour shows the model following the second minimisation and orange shows the final position of the model following the third minimisation step

After both energy minimisation and equilibration, the model is completely prepared for the MD simulation production run. The MD simulation runs for 100 ns at 300 K, over 50,000,000 steps, and is executed in triplicate. Each model, described in Table 5.1, was submitted to the MD simulation and their results will be discussed in Section 5.5.

5.5 MD Simulation Production Runs

The MD simulations output a restart file (.rst), which is converted into a pdb file using AMBPDB, such that it can be visualised using Pymol (version 1.8.4).

5.5.1 MD Simulation Analysis Scripts

A series of analysis scripts were run, written by Mabel Wong. The analysis scripts are listed below:

1. *Align trajectory*: this script aligns the protein of every frame to the protein backbone from the first frame, such that the trajectory is completely aligned and the movement of the ligand can be approximately monitored
2. *Skip 100 trajectory*: this script acts as a visual aid, taking every 100th frame from the MD simulation, it is possible to see the general trajectory of the ligand within the protein
3. *Reactivator RMSD*: this enables the calculation of the ligand's root-mean-square deviation (RMSD) in Ångström. This result allows for a general understanding of the extent of the ligand movement around the protein compared to its original position
4. *Reactivator-AChE Distance:* This script allows for a measurement of distance between the ligand and the protein over the length of the simulation. The measurement can be taken between two defined atoms from the model (Figure 5.8)

5. *Reactivator-AChE Angle:* This script allows for the measurement of an angle between three defined atoms within the model (Figure 5.8). This script was not used, due to the fact that no useful data was extracted from the information provided from the angles of approach.
6. *Reactivator-AChE Contacts:* This script selects atoms within 4 Å of the ligand, over the length of the MD simulation. This information is used to obtain 'b factor' data, which can be used to generate a heat map of areas of the protein where the ligand spends its time
7. *Get Average PDB:* This script is used to prepare a pdb file containing the averaged coordinates of the entire simulation for use in later scripts
8. *Average B Factor:* This script the average pdb file's coordinates (generated from script 7, above), to calculate b factor data to be used to calculate the root-mean-square fluctuation (RMSF). RMSF is a local measurement of atomic motion, measuring the mean fluctuation of atoms
9. *RMSF-B Factor:* This script replaces the b factor data in a pdb file with the RMSF data calculated in script 8, such that the data can be visualised

Figure 5.8. Distance (*l*) and angle (θ) measurements, described by scripts 4 and 5 respectively (X=H or tabun). n.b. the angle (θ) is only calculated for the inhibited enzyme

The distance between the oxygen atoms of the oxime reactivator and the inhibited serine is key. Here it is used as a quantitative metric to judge the reactivators ability to approach the phosphorylated serine residue in close enough proximity to allow for reactivation of the enzyme.

A series of data plotting scripts, also prepared by Mabel Wong, were employed for the presentation of data obtained in the above scripts. Each script was run on each of the MD simulations (Table 5.1), and the results from these analyses are summarised in Section 5.5.2.

5.5.2 Quinoline 2.1 Analysis

Biological evaluation of quinoline **2.1** showed excellent reactivation potency for all OPNA compounds tested (sarin, VX, tabun and paraoxon). In addition, the compound exhibited millimolar inhibition potency (IC_{50}), reducing the risk of competitive inhibition of the enzyme. This *in silico* simulation represents an opportunity to model a lead quinoline **2.1**.

Firstly, the ligand-protein model for the uninhibited AChE was developed as per the procedure described in Sections 5.3 and 5.4. Following the MD production run, the results were analysed using the scripts described in section 5.5.1.

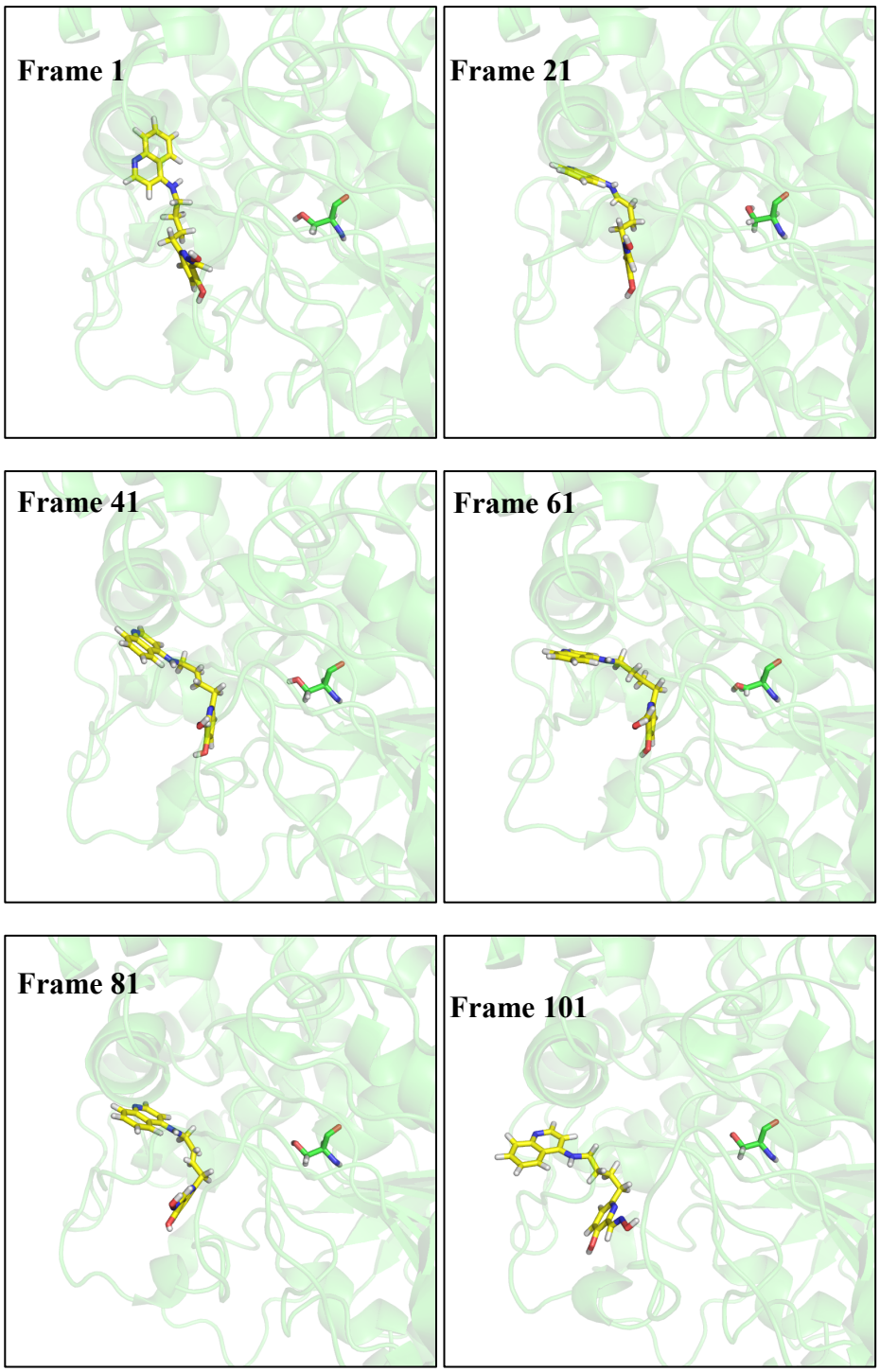

Figure 5.9. Six frames, taken over the MD simulation of ligand **2.1** (yellow) in uninhibited *h*AChE (green, the serine residue is shown as green sticks)

Generally, the simulation indicates the formation of strong interactions between the quinoline PSL and the peripheral site of the uninhibited enzyme (Figure 5.9). During the simulation, the quinoline remains anchored in the same general position, while the rest of the ligand is able to move around within the gorge. This observation is emphasised in Figure 5.10, where residues around 4 Å of the ligand are highlighted. Residues shown in red represent those that maintain the most contact with the ligand throughout the simulation, where the blue colour indicates the opposite.

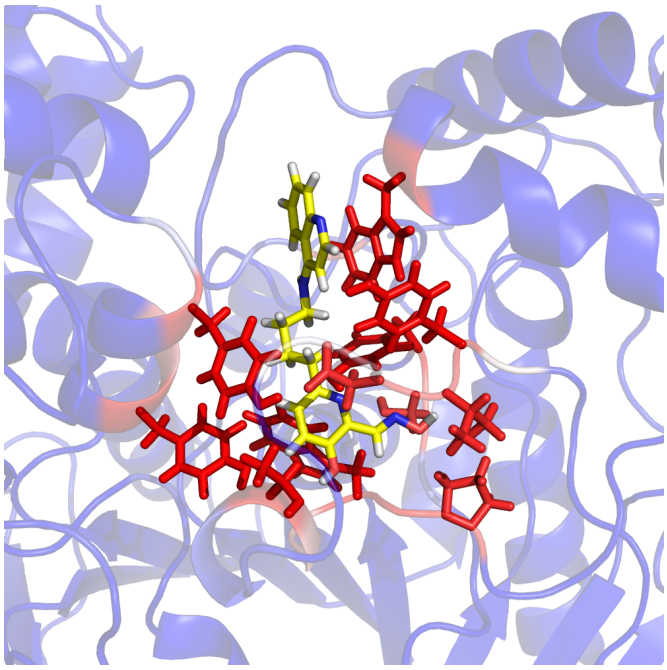

Figure 5.10. Heat map of MD simulation of quinoline **2.1** within uninhibited *h*AChE, residues within 4 Å are shown as sticks. Red areas represent parts of the model that spend most time within 4 Å of the ligand

Secondly, the tabun-inhibited *h*AChE model was developed as described in Section 5.3.2. Quinoline **2.1** was integrated into the energy-minimised model of tabun-*h*AChE, and the MD simulation was run.

Figure 5.11, showing six frames from the MD simulation of quinoline **2.1** within tabun-inhibited *h*AChE, demonstrates the high affinity of the ligand to the active site (containing tabun). After just 5 frames of the simulation, the quinoline-containing reactivator (yellow) moves from its 'starting' position, into a conformation that brings the oxime (highlighted by a pink asterisk) close in proximity to the tabun-inhibited serine residue (green, orange and red sticks).

Compared to the results obtained from the uninhibited *h*AChE, the distance between the oxygen atom of the oxime within the ligand and the oxygen atom of the serine residue in the active site of tabun-inhibited *h*AChE is much smaller. Highlighted in Figure 5.12, the vivid red line represents the distance measured and the pale red line represents one standard deviation. The blue lines represent the data from the uninhibited simulation. This may suggest that due to the close proximity of the reactivator oxime oxygen and the *h*AChE phosphorylated serine residue, the likelihood of reactivation is increased.

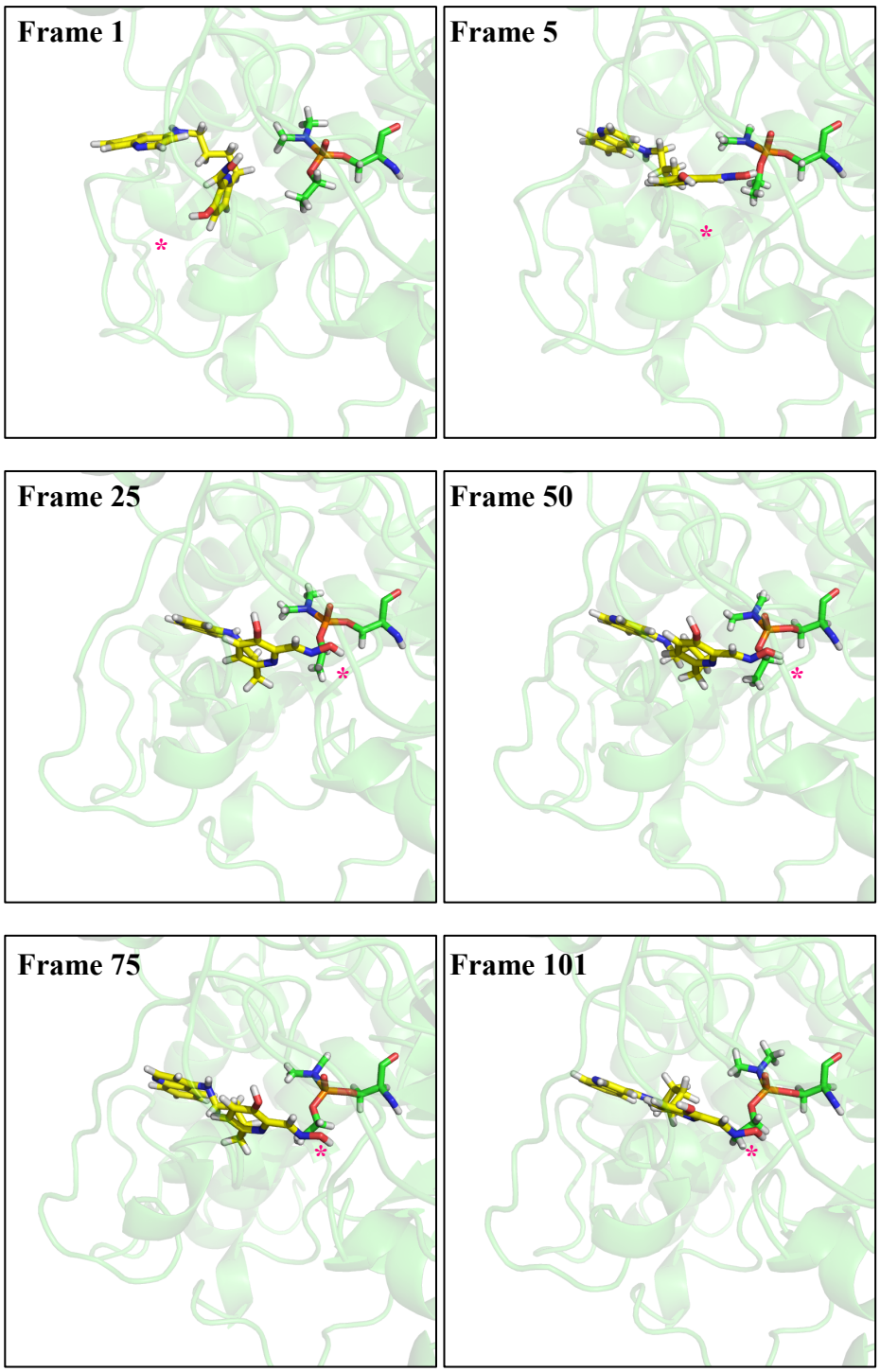

Figure 5.11. Six frames, taken over the MD simulation of quinoline **2.1** (yellow) in tabun-inhibited *h*AChE (green, the tabun-inhibited serine is shown as green sticks)

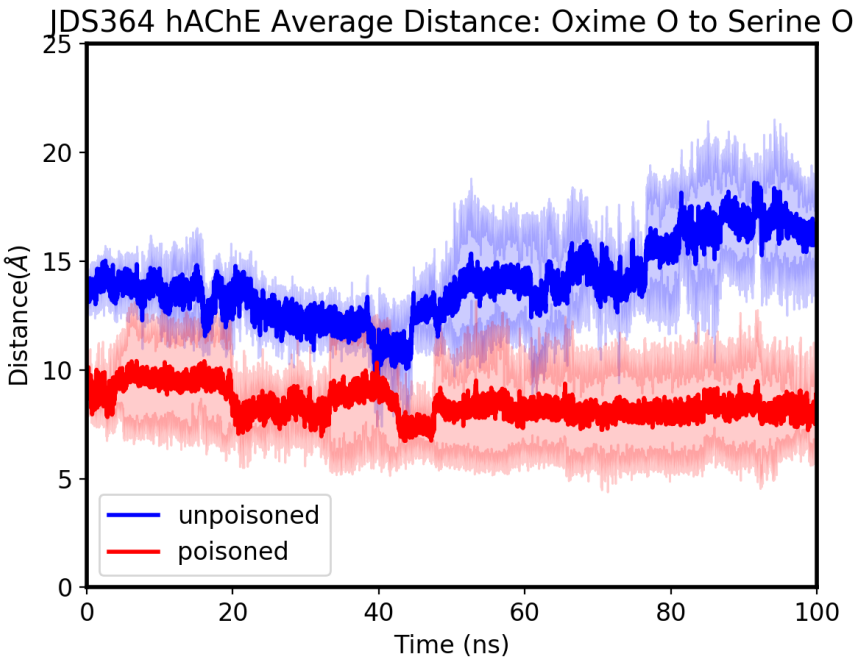

Figure 5.12. Mean distance between oxime oxygen of quinoline hybrid **2.1** and the oxygen of the serine residue of *h*AChE

Interestingly, the mean RMSD of the hybrid reactivator ligand within both inhibited and uninhibited *h*AChE seem to be very close in value (Figure 5.13). This suggests that, although the hybrid reactivator ligands adopt reasonably different conformations within the protein, their relative deviation from their starting position, post-equilibration remains reasonably consistent.

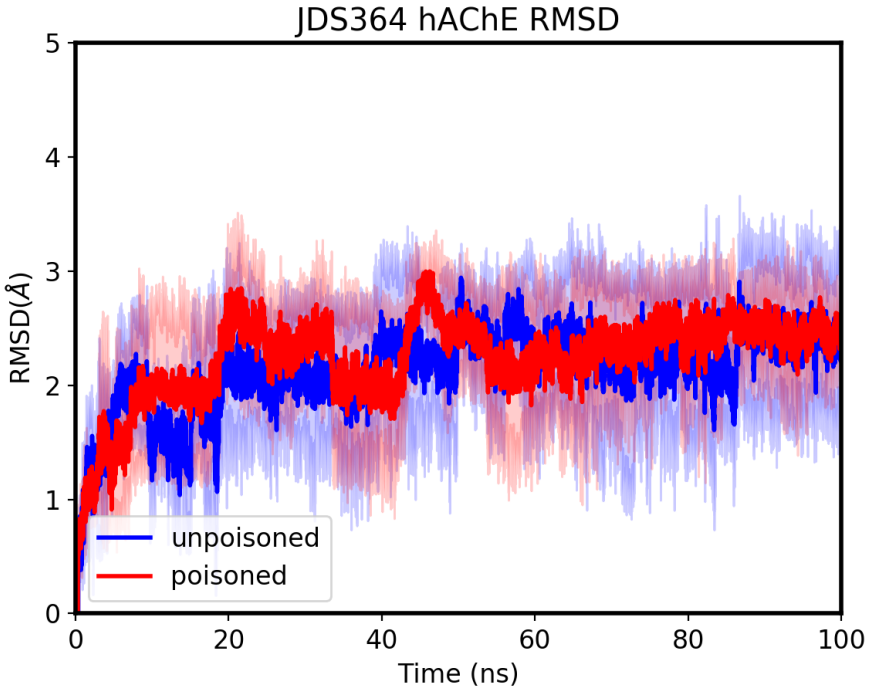

Figure 5.13.Mean RMSD of MD simulation of quinoline hybrid **2.1** within uninhibited (blue) and tabun-inhibited (red) *h*AChE

In vitro data of quinoline **2.1** indicates comparatively high affinity, good reactivation rate and thus very high reactivation efficiency. This appears to be mirrored by the *in silico* model that has been developed. During the simulation the quinoline PSL of quinoline **2.1** shows high affinity to the peripheral site, while the pyridine oxime reactivator remains in close proximity to the inhibited serine residue.

Table 5.2. Shows affinity (K_D), reactivation rate (k_r) and reactivator efficiency (k_{r2}) data of **2.1** for tabun-*h*AChE and other common commercially available reactivator compounds, from *in vitro* studies. [a]Data from[186]

	$\mathbf{K_D}$ (μM)	$\mathbf{k_r}$ (min^{-1})	$\mathbf{k_{r2}}$ ($mM^{-1}min^{-1}$)
2-PAM[a]	706 ± 76	0.010 ± 0.0005	0.01
HI-6[a]	no reaction	no reaction	0
Obidoxime[a]	250 ± 110	0.04 ± 0.006	0.16
Quinoline **2.1**[a]	6 ± 2	0.36 ± 0.02	62

5.5.3 Tacrine 3.1 and Chlorotacrine 5.1 Analysis

Tacrine **3.1** was subjected to the same parameterisation methods as described earlier in this chapter (section 5.3), energy minimisation (section 5.4) and the MD simulation was undertaken. Tacrine **3.1** (as well as chlorotacrine **5.1**) offers an opportunity to model the development of the tetrahydroacridine compounds. Following recent research (previously discussed in Chapter 2), Nachon and co-workers discovered that tacrine **3.1**, whilst displaying good reactivation efficiency of various OP-inhibited AChE, acted as a competitive inhibitor in sub-micromolar concentration (250 nM)[187]. Interestingly, the addition of a chlorine atom at the 7-position, giving chlorotacrine **5.1**, was observed to increase the concentration of competitive inhibition (2.3 μM) without adversely affecting the reactivation potential of the candidate.

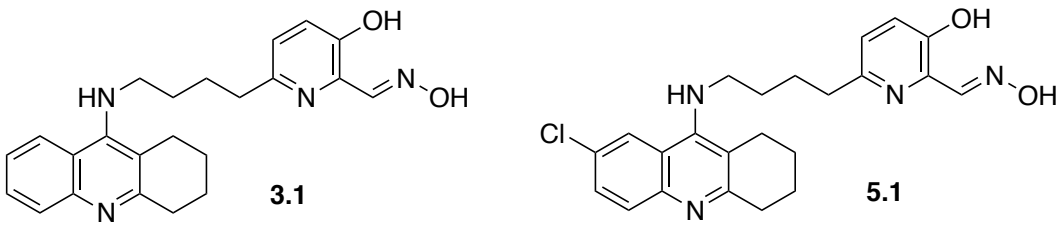

Figure 5.14. Chemical structures of tacrine **3.1** and chlorotacrine **5.1**

The competitive inhibition previously observed by Nachon and colleagues was shown to arise from a binding conformation whereby the tetrahydroacridine peripheral site ligand is bound in the active site of the enzyme, rather than the peripheral site. This is highlighted by the X-ray crystal structure (Figure 5.15).

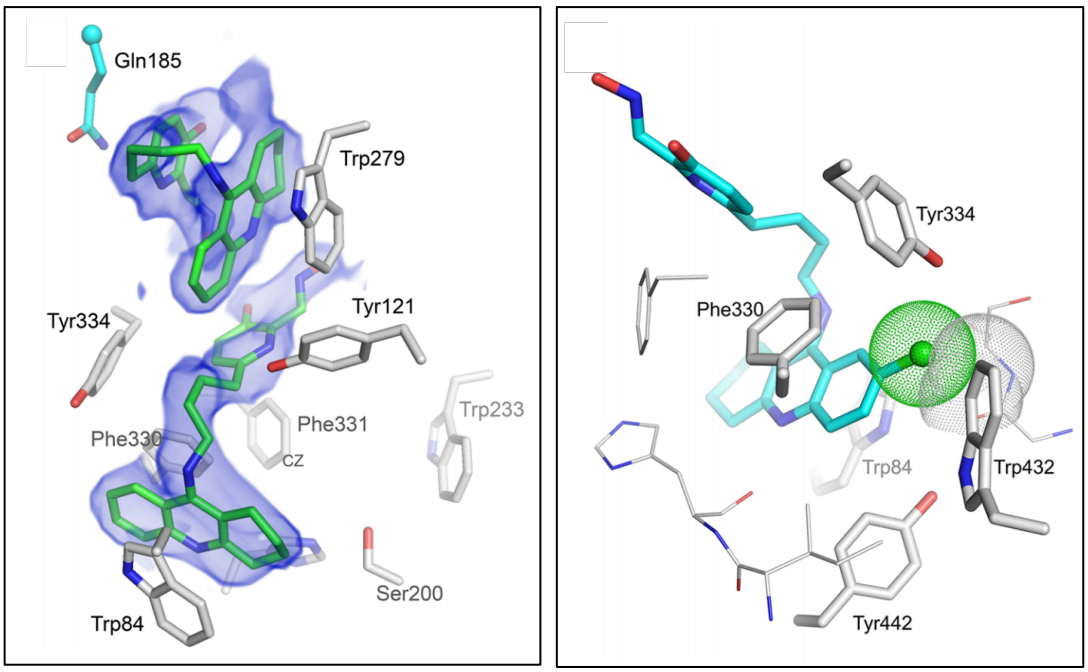

Figure 5.15a (left image) X-ray crystal data showing two equivalents of tacrine **3.1** (green sticks) bound within the enzyme gorge (highlighted in dark blue), demonstrating a binding conformation that leads to competitive inhibition[187] Figure 5.15b (right image) *In silico* model of chlorotacrine **5.1** (cyan sticks) in a similar binding configuration within the gorge. The green sphere shows steric clashing that prevents the binding conformation resulting in competitive inhibition[187]

It should be noted that the initial orientation of tacrine **3.1,** as seen in the available X-ray crystallography data and highlighted in frame 1 (Figure 5.16), shows the PSL bound correctly within the peripheral site. This is inconsistent with the published data shown in Figure 5.15. Following the MD simulation of tacrine **3.1** in uninhibited *h*AChE, the tetrahydroacridine moiety shows an excellent affinity to the peripheral site of the enzyme, as it appears to be consistently anchored in the same position throughout the simulation. However, the linker and reactivator portion of the ligand move more freely around the rotatable bonds of the linker. During the simulation, the reactivator portion does not appear to enter the gorge towards the serine residue (Figure 5.16).

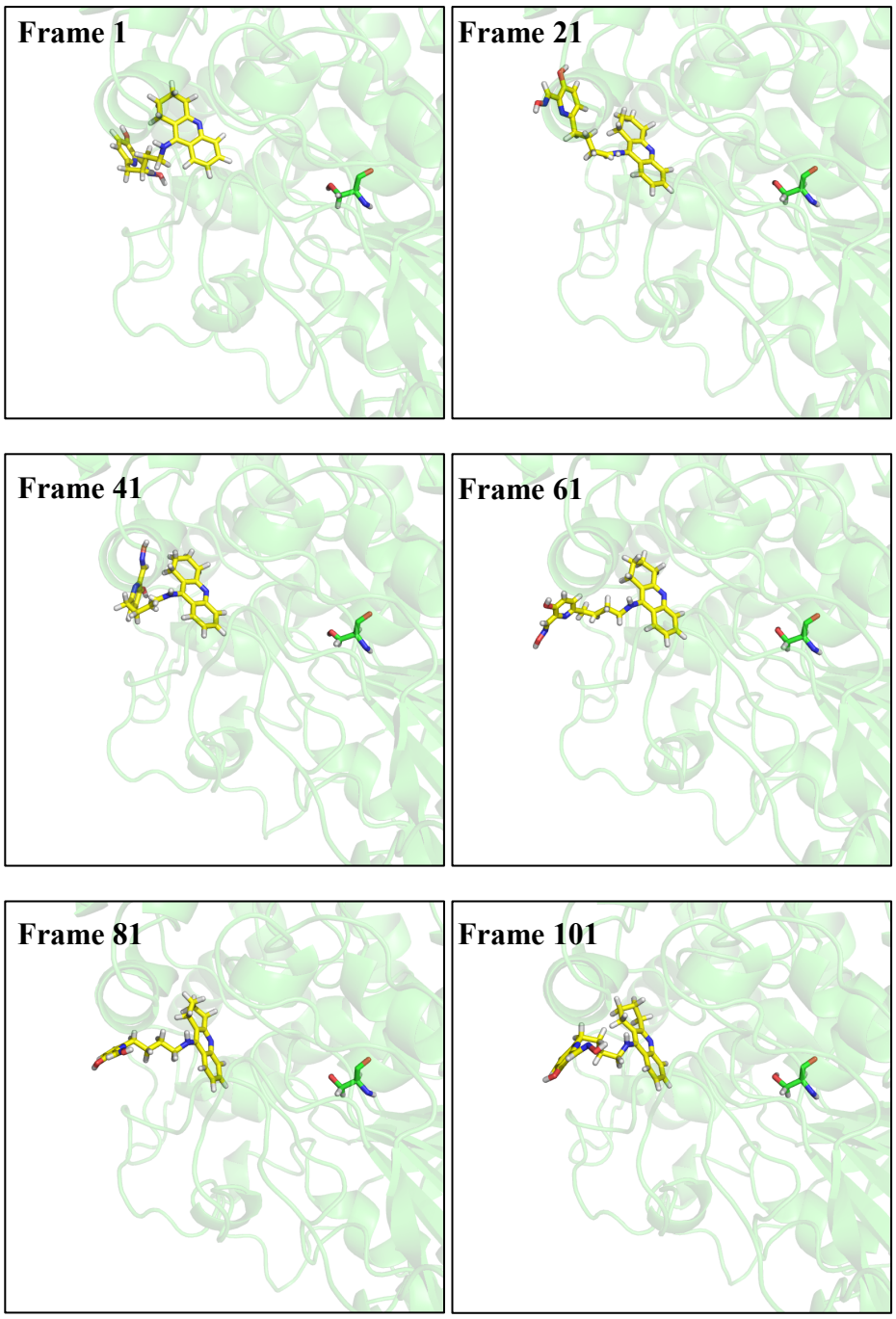

Figure 5.16. Six frames, taken over the MD simulation of tacrine **3.1** (yellow) in uninhibited *h*AChE (green, the serine residue is shown as green sticks)

Interestingly, following the MD simulation of tacrine **3.1** (Figure 5.17) within tabun inhibited-*h*AChE, the tacrine PLS retains its very high affinity for the peripheral site; however, the linker and reactivator continue to remain far in distance from the inhibited serine residue. By visual comparison, the two simulations appear to be very similar, yet the graphical comparison of the distances between the oxime oxygen atom of the ligand and the serine atom of the enzyme do show a difference (Figure 5.16).

It is undeniable that tacrine **3.1**, compared to quinoline **2.1**, appears to situate itself further away from the site of action, which is consistent with *in vitro* data obtained from biological studies of the two compounds. *In vitro*, tacrine **3.1** demonstrates a higher dissociation constant (K_D) and a much lower reactivation constant (k_r). The poor proximity of the pyridine oxime reactivator component of tacrine hybrid **3.1** to the active site, as observed in the *in silico* model, may result in a large distance between the reactivator oxime and the phosphorylated serine residue of the inhibited enzyme, such that reactivation rate is reduced dramatically.

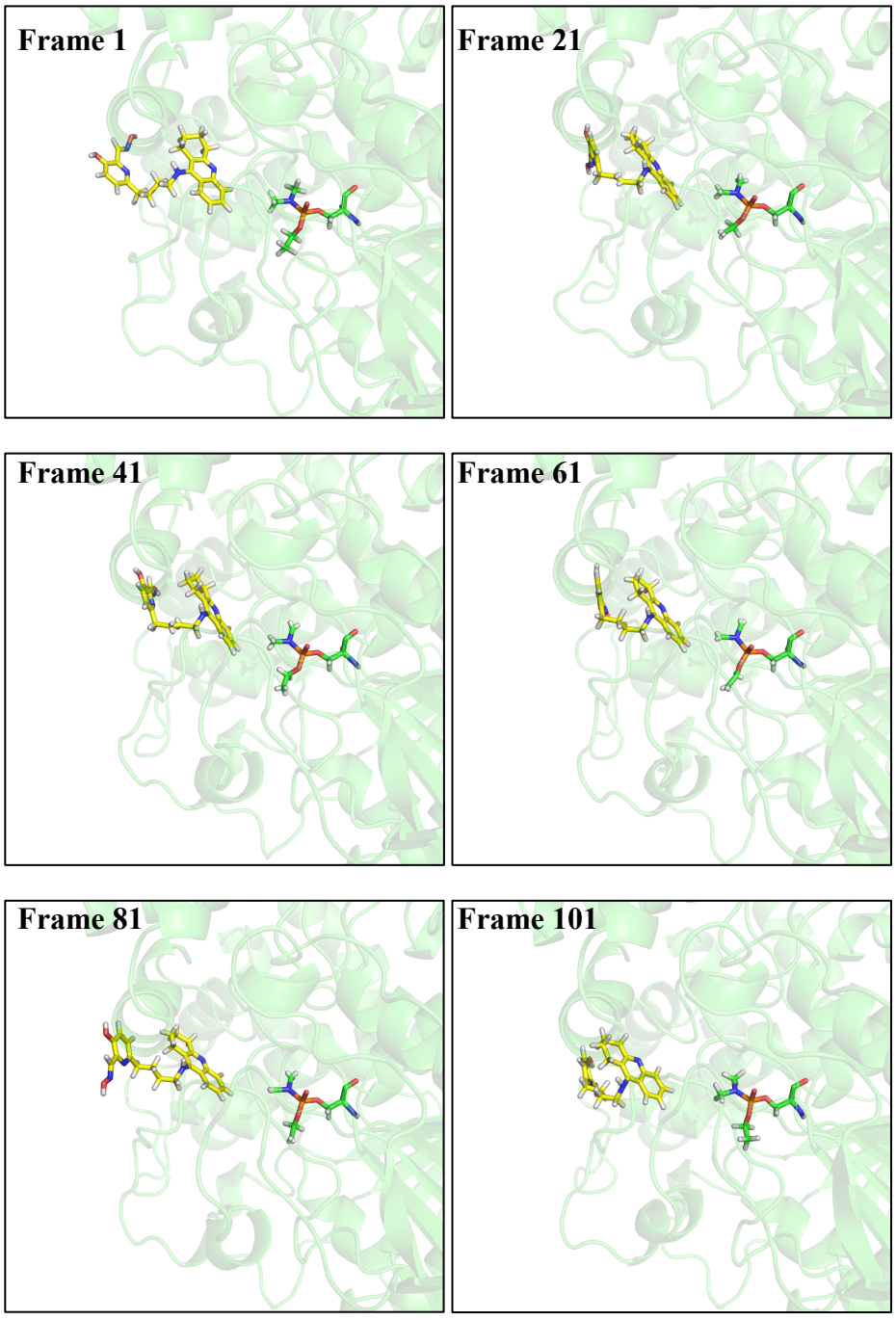

Figure 5.17. Six frames, taken over the MD simulation of tacrine **3.1** (yellow) in tabun-inhibited *h*AChE (green, the tabun-inhibited serine is shown as green sticks)

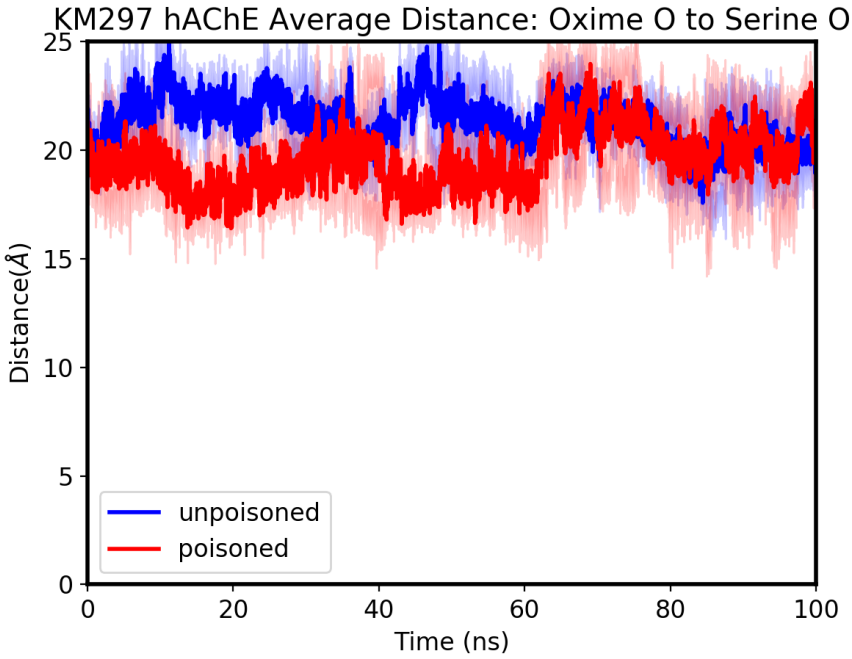

Figure 5.18. Combined average distances between the oxime oxygen atom of the ligand and the oxygen atom of the serine of the enzyme of tacrine **3.1** within tabun inhibited (red) and uninhibited (blue) *h*AChE

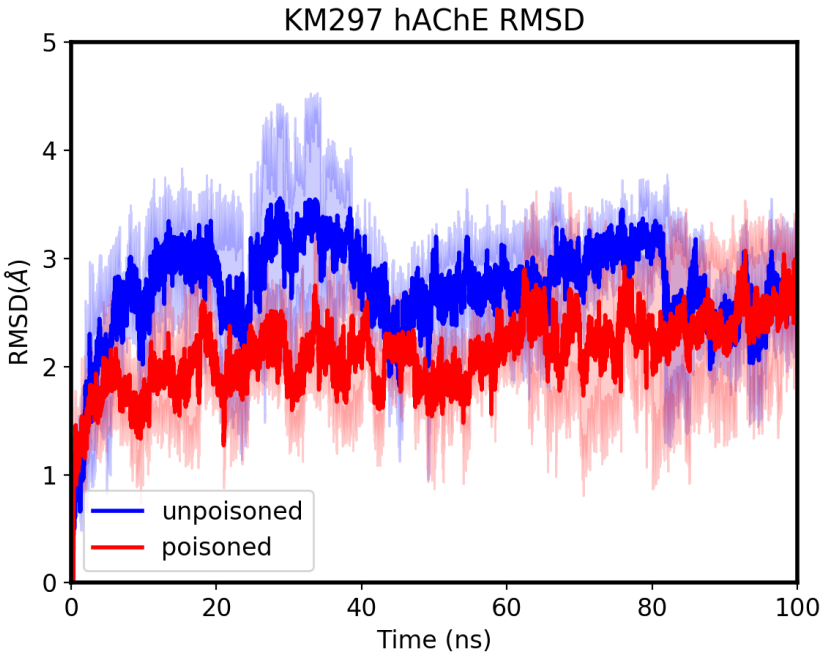

Figure 5.19. Combined RMSD of tacrine **3.1** within tabun inhibited (red) and uninhibited (blue) *h*AChE

In a similar vein to quinoline **2.1**, tacrine **3.1** within tabun inhibited-*h*AChE appears to deviate in a similar manner to that within the uninhibited enzyme (Figure 5.19). The notable increase in the RMSD at the beginning of the simulation (between 0 and 5 ns) is quite significant. However, this is characteristic of MD simulations as it represents an initial equilibration during the first stages of the simulation.

Otherwise, differences in RMSD between the two runs appear to arise regularly during the course of the simulations. Tacrine **3.1** in the uninhibited run appears to remain much more deviated from the initial frame compared to that of the tabun-inhibited run. This observation would continue to suggest that the presence of the OPNA within *h*AChE contributes towards the affinity of the ligand to the enzyme.

Finally, chlorotacrine **5.1** simulations were run, starting with the uninhibited *h*AChE (Figure 5.20).

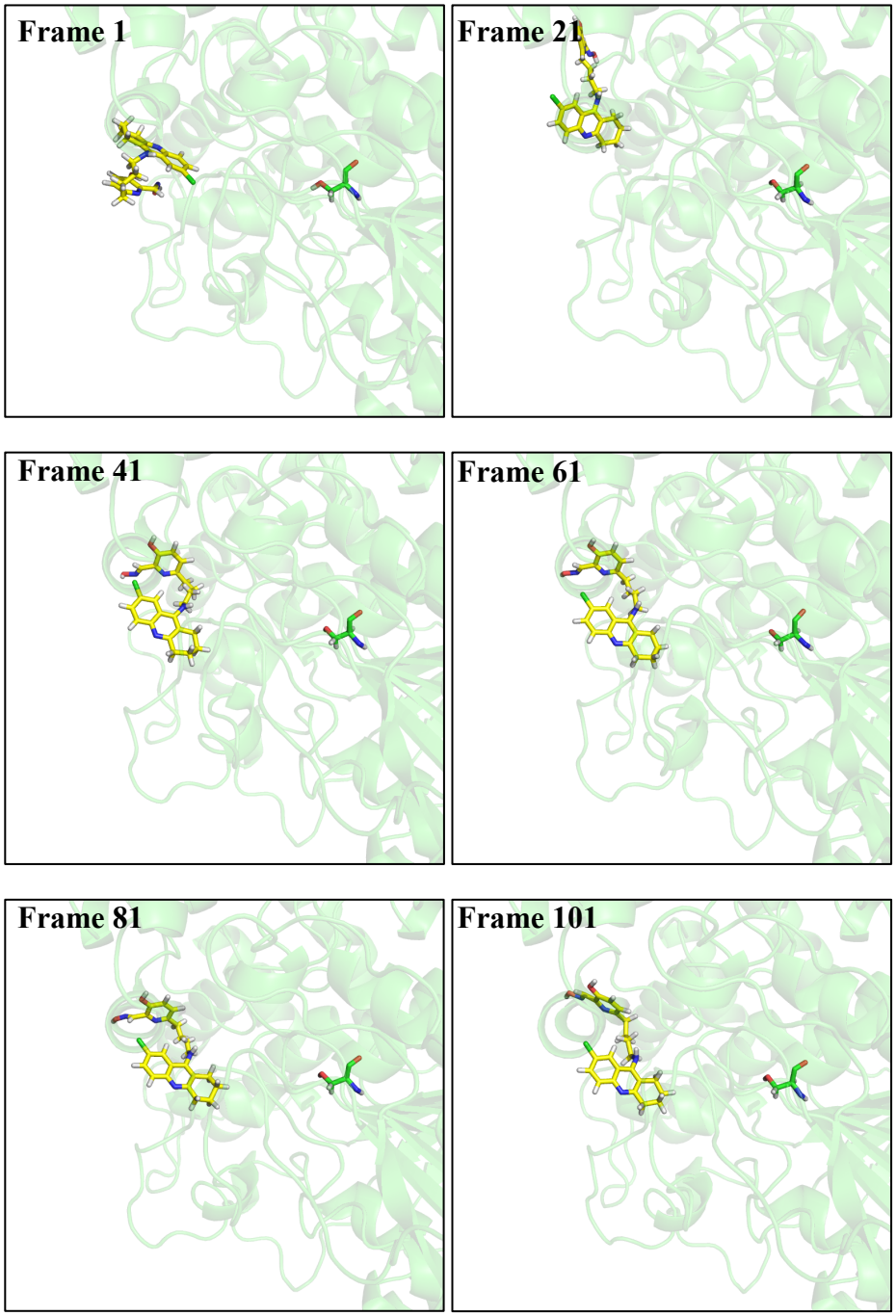

Figure 5.20. Six frames, taken over the MD simulation of chlorotacrine **5.1** (yellow) in uninhibited *h*AChE (green, the serine residue is shown as green sticks)

From the frames above, the simulation shows very similar movement to that of tacrine **3.1** within the uninhibited enzyme. It is clear that the 7-chlorotacrine maintains a very strong affinity for the peripheral site and the linker is free to rotate, but does not appear to enter the active site *via* the gorge. Chlorotacrine **5.1** appears to show less flexibility within the linker, perhaps due to steric clashing between the linker and the chlorine atom of the tetrahydroacridine PSL.

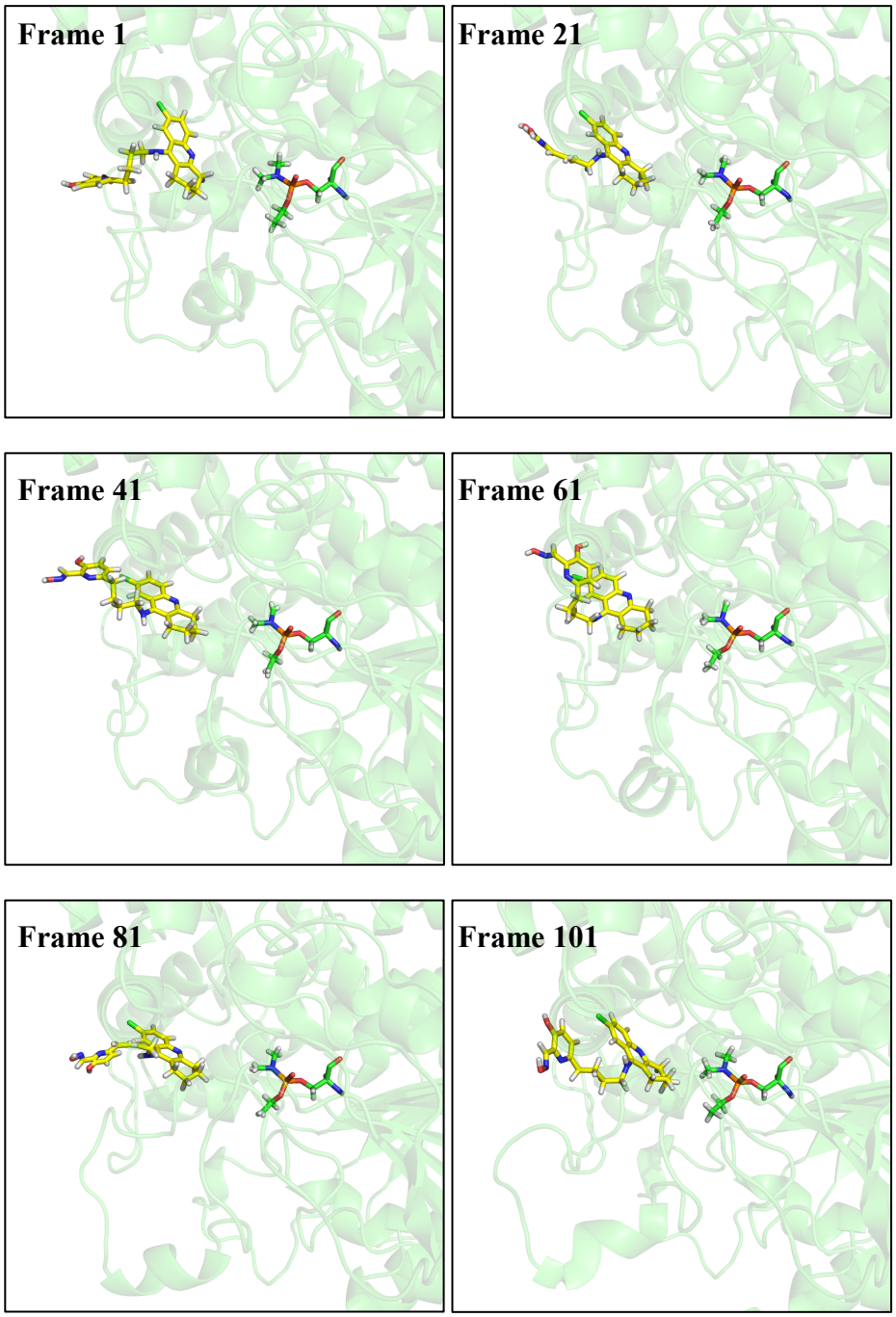

Figure 5.21. Six frames, taken over the MD simulation of chlorotacrine **5.1** (yellow) in tabun-inhibited *h*AChE (green, the tabun-inhibited serine is shown as green sticks)

Within tabun inhibited-*h*AChE, chlorotacrine **5.1** appears to display similar movements to tacrine **3.1** within the inhibited enzyme. Figure 5.22 demonstrates the distances between the two oxygen atoms; chlorotacrine **5.1** displays the greatest distance between the two atoms, indicating a lower probability of the reactivator oxime being in sufficient proximity to reactivate the phosphorylated serine residue of the inhibited *h*AChE.

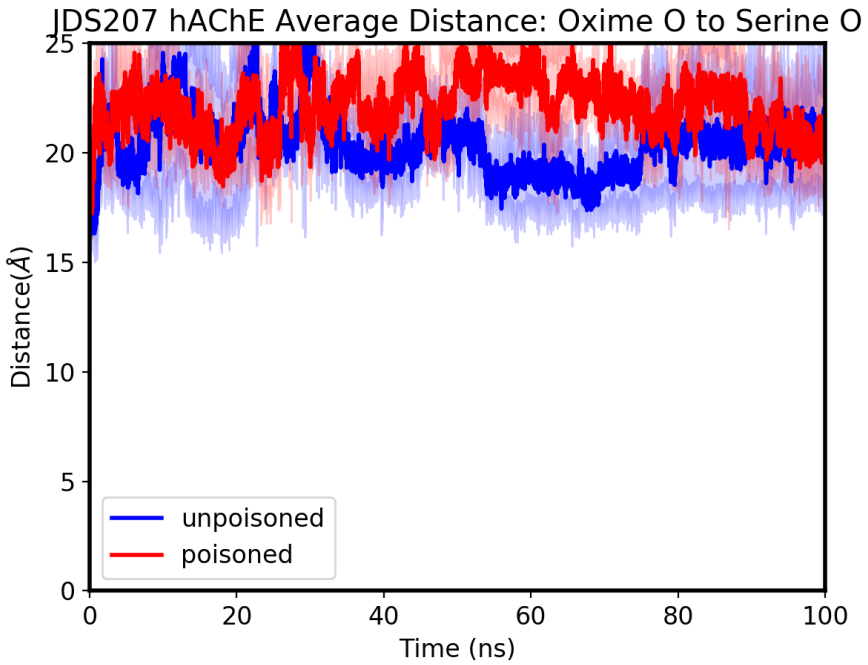

Figure 5.22. Combined average distances between the oxime oxygen atom of the ligand and the oxygen atom of the serine of the enzyme of chlorotacrine **5.1** within tabun inhibited (red) and uninhibited (blue) *h*AChE

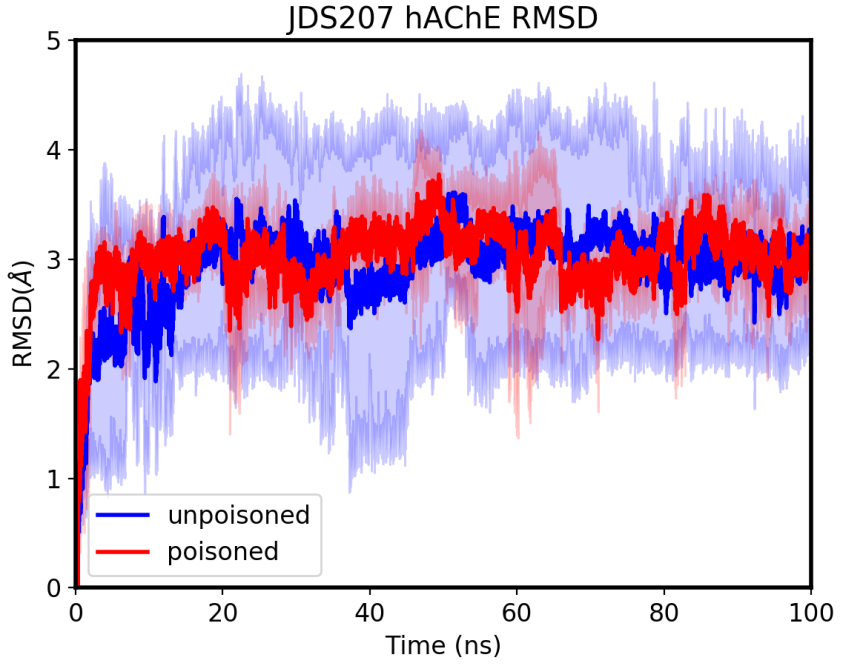

Figure 5.23. Combined RMSD of chlorotacrine **5.1** within tabun inhibited (red) and uninhibited (blue) *h*AChE

5.5.4 Conclusions: Quinoline 2.1, Tacrine 3.1 and Chlorotacrine 5.1

The *in silico* model appears to make some good correlations between the simulations and biological data obtained. Table 5.3 below highlights the combined *in vitro* and *in silico* data for the three ligands tested.

Table 5.3. Shows average distance between oxime oxygen and serine residue oxygen from uninhibited *in silico* models and affinity (K_D), reactivation rate (k_r) and reactivator efficiency (k_{r2}) data against tabun-inhibited AChE of quinoline **2.1**, tacrine **3.1** and chlorotacrine **5.1**, from *in vitro* studies. [a]Data from[186] [b]Data from Nachon *et al.*[187]

	Uninhibited average distance (Å)	**K_D** (μM)	**k_r** (min^{-1})	**k_{r2}** ($mM^{-1}min^{-1}$)
Quinoline **2.1**[a]	8.381	6 ± 2	0.36 ± 0.02	62
Tacrine **3.1**[b]	20.730	7.1 ± 1.5	0.021 ± 0.001	3
Chlorotacrine **5.1**[b]	20.317	10.4 ± 2.6	0.12 ± 0.01	12

All simulations suggest excellent affinity of the quinoline, tacrine and chlorotacrine PSL to the peripheral site, and this is reflected in their respective *in vitro* reactivator affinities (K_D). The reactivation rate (k_r) of quinoline **2.1** (0.36 min^{-1}) is shown to be the highest of the three ligands. The *in silico* model suggests that quinoline **2.1** is able to enter the *h*AChE gorge efficiently and place the oxime/oximate close in proximity to the inhibited serine residue, consistent with the high reactivation rate observed during biological assays. Conversely, both tacrine **3.1** and chlorotacrine **5.1** display reduced reaction rates *in vitro.* The *in silico* model shows that neither of the ligands' oxime functionality approaches the inhibited serine, which is consistent with the slower reactivation of OPNA-inhibited enzyme (tacrine **3.1** 0.021 min^{-1} and chlorotacrine **5.1** 0.12 min^{-1}**)** .

The X-ray data presents the initial orientation of tacrine **3.1** and chlorotacrine **5.1** with the tacrine PSL anchored at the peripheral site and the linker pointing away from the gorge. This presents a drawback for the simulations undertaken for tacrine **3.1** and chlorotacrine **5.1**. Since the *in vitro* affinity data of both ligands appears to be extremely high, it would seem unlikely that the favourable interactions between the PSL and the peripheral site would momentarily disengage for the ligand to re-orientate itself, such that the linker and pyridine oxime reactivator may enter the gorge and reach the active site. However, it is important to recognise that the X-ray data is already representative of the ligands favoured orientation. Nevertheless, for better understanding of tacrine **3.1** and chlorotacrine **5.1** behaviour within *h*AChE, X-ray data for the more desirable orientation of the ligands, may offer an opportunity to better simulate this.

5.6 Overlay Studies

Given the utility of the *in silico* study on quinoline **2.1**, tacrine **3.1** and chlorotacrine **5.1**, novel ligands were integrated into the model in order to run "overlay" simulations. This would offer the opportunity to model novel ligands within inhibited-*h*AChE to assess their orientation within the enzyme and compare the results to their *in vitro* data. The formerly developed ligand model for quinoline **2.1** was adapted such that the chemical structure of the new ligand could be integrated. Given the success of the dehydroxylated quinoline-containing hybrids **3.7** and **3.6**, these compounds were modelled into MD simulations.

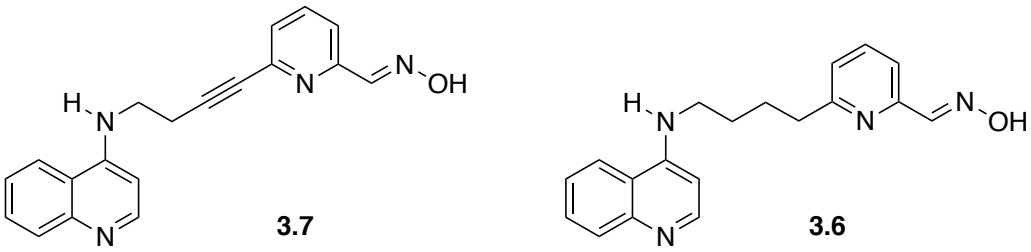

Figure 5.24. Dehydroxylated hybrid reactivators **3.7** and **3.6**

Due to their close structural similarity, dehydroxylated quinolines **3.7** and **3.6** could be altered in a chemical drawing software (Avogadro, version 1.2.0). Preparation of butyl-linked dehydroxylated quinoline **3.6** involved the removal of the hydroxyl group on the pyridine of quinoline **2.1**, whereas butynyl-linked dehydroxylated quinoline **3.7** was also prepared from quinoline **2.1** in the same way, while also integrating a triple bond within the linker.

The new ligands were subjected to the same parameterisation steps as highlighted in Section 5.3.1. Perhaps unsurprisingly, upon generation of conformers for butynyl-linked dehydroxylated quinoline **3.7**, it was not possible to generate more than 233 conformers. Due to the reduced conformational degrees of freedom when the butynyl linker of hybrid reactivator **3.7** replaces the butyl linker of hybrid reactivator **3.6**, a reduced number of conformers are available. The parameterisation was therefore undertaken on the average clusters of only 233 conformers compared to 1,000 conformers, for more rotationally flexible ligands. Upon the assignment of RESP for butynyl-linked dehydroxylated quinoline **3.7**, the Gaussian calculation failed upon approach of the triple bond angle to 180°. As an alternative method of ESP generation, an AM1bcc (AM1 bond charge correction) command was employed. AM1 produces atomic charges that emulate a similar level of theory as the Gaussian calculation's ESP of a molecule, using a semi-empirical method. The calculated charges are then corrected to best reproduce the QM ESP. However, these complications were not encountered when parameterising butyl-linked dehydroxylated quinoline **3.6**, so the original method of RESP was used. Following successful parameterisation, the ligands were integrated into the uninhibited and tabun-inhibited *h*AChE models in the same orientation found in the x-ray data of quinoline **2.1**, giving the first frame of the

simulation post-equilibration. Three MD simulations for both ligands were run in the inhibited and uninhibited models.

5.6.1 Butynyl-linked Dehydroxylated Quinoline 3.7 Analysis

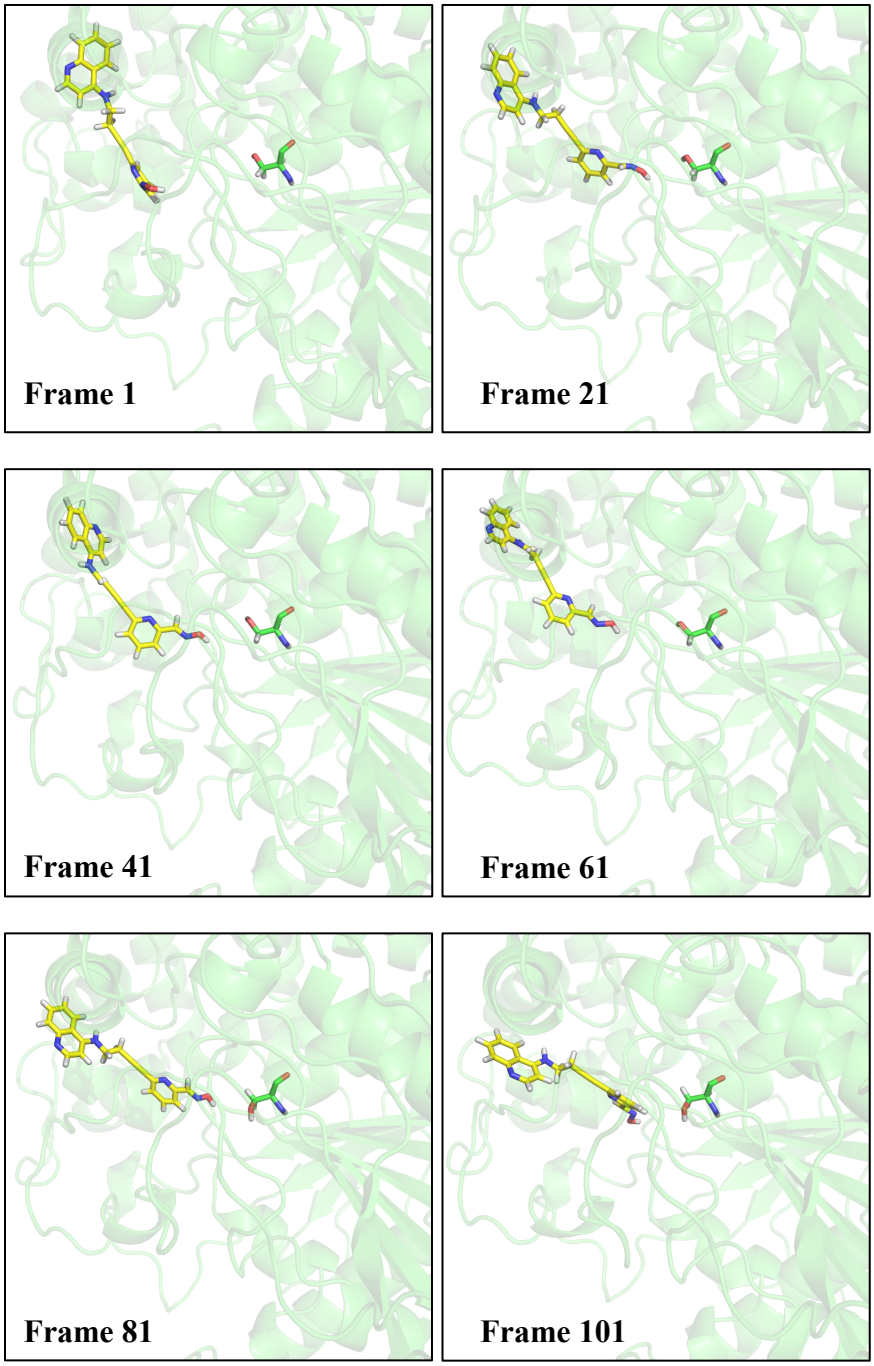

Figure 5.25. Six frames, taken over the MD simulation of butynyl-linked dehydroxylated quinoline **3.7** (yellow) in uninhibited *h*AChE (green, the serine residue is shown as green sticks)

The MD simulation for butynyl-linked dehydroxylated quinoline **3.7** (Figure 5.25), shows some flexibility within the interactions between the quinoline PSL and the peripheral site. The quinoline scaffold appears to be moving around the surface of the enzyme during the simulation. This however does not seem to cause a detrimental effect with respect to the distance between the oxime and the serine residue, as the linker and reactivator portions of the hybrid remain within the gorge throughout.

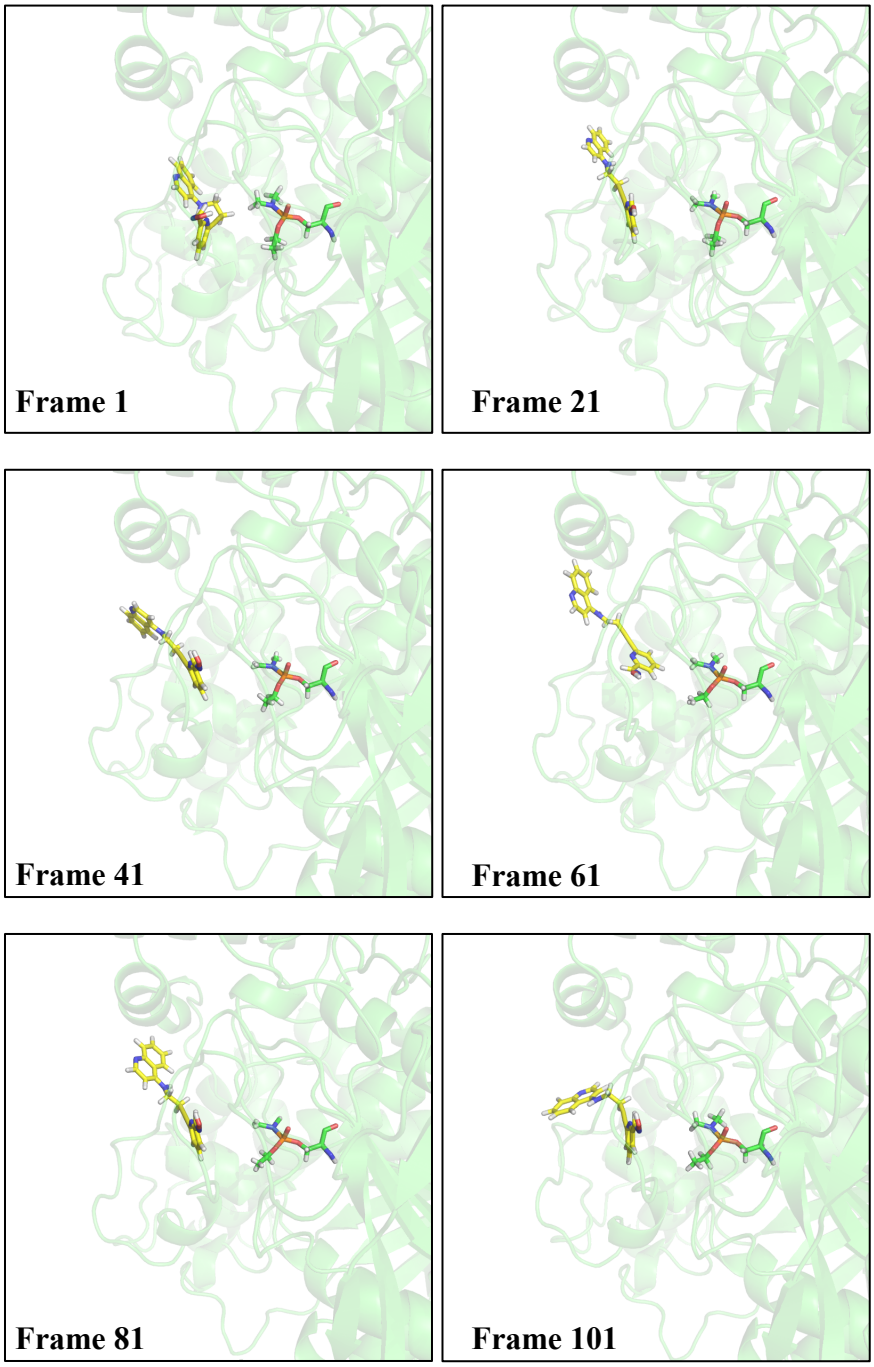

Figure 5.26. Six frames, taken over the MD simulation of butynyl-linked dehydroxylated quinoline **3.7** (yellow) in tabun-inhibited *h*AChE (green, the tabun-inhibited serine is shown as green sticks)

Simulation of butynyl-linked dehydroxylated quinoline **3.7** within tabun-inhibited *h*AChE (Figure 5.26), sees the ligand consistently docked within the enzyme gorge with the reactive oxime functionality close in proximity to the inhibited serine residue. The quinoline scaffold shows similar flexibility within the enzyme, as seen in the uninhibited model.

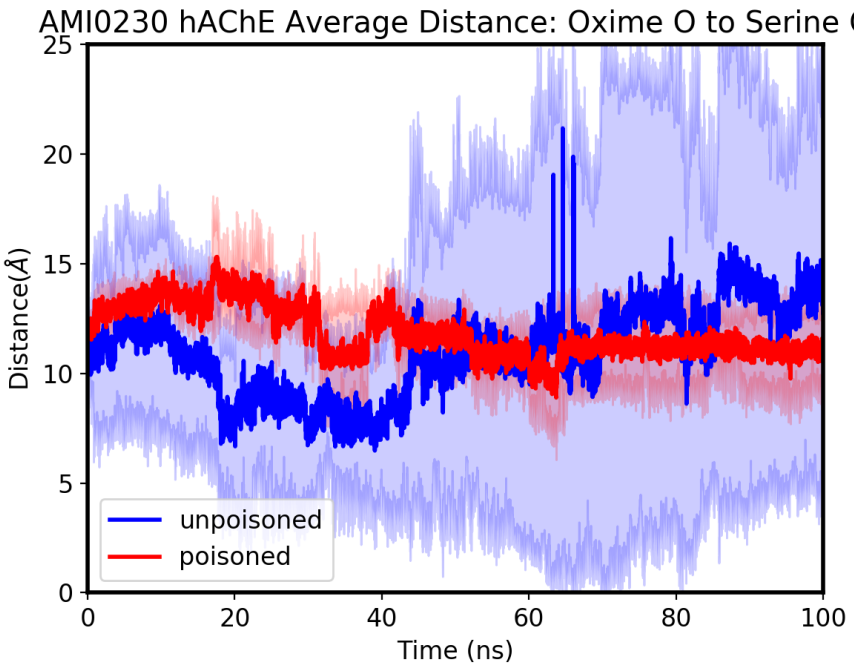

Figure 5.27. Combined average distances between the oxime oxygen atom of the ligand and the oxygen atom of the serine of the enzyme of butynyl-linked dehydroxylated quinoline **3.7** within tabun inhibited (red) and uninhibited (blue) *h*AChE

The uninhibited simulation shows much fluctuation of distance between the oxygen atom of the *h*AChE serine residue and the oxime oxygen of butynyl-linked dehydroxylated quinoline **3.7** (Figure 5.27), whereas the inhibited model (red) shows much less fluctuation. Intriguingly, the average standard deviation for the uninhibited enzyme production run is dramatically larger than that within the tabun-inhibited enzyme, this might suggest that the ligand is much more selectively bound within *h*AChE that has been inhibited by an OPNA.

The average RMSD of butynyl-linked dehydroxylated quinoline **3.7** in both inhibited and uninhibited models can be seen in Figure 5.28. The uninhibited model (blue) shows some fluctuation in RMSD from the initial frame, however, the inhibited model shows a much more consistent deviation from the initial frame. This may imply that the ligand finds a very favourable conformation within the inhibited enzyme, upon which an energy penalty is imposed when deviating from that orientation.

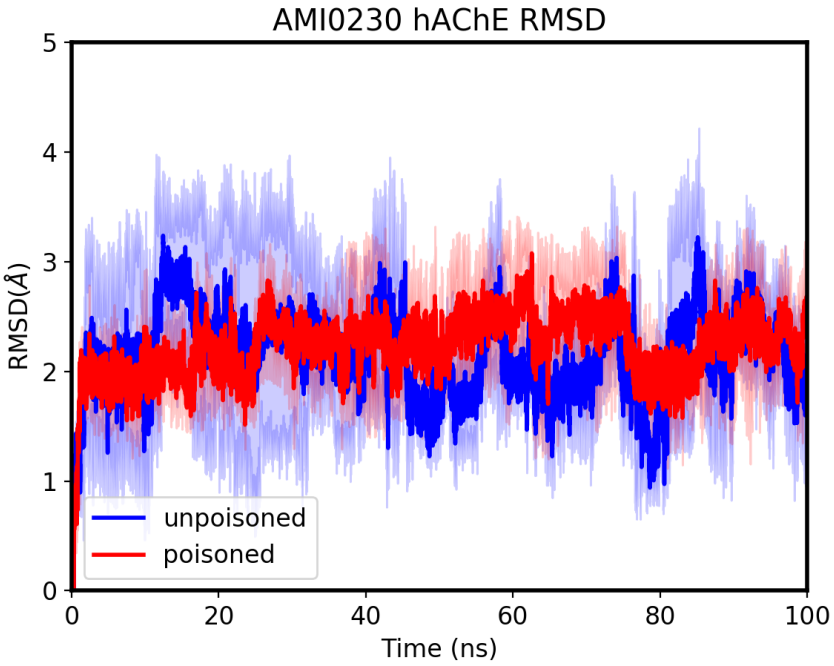

Figure 5.28. Combined RMSD of butynyl-linked dehydroxylated quinoline **3.7** within tabun inhibited (red) and uninhibited (blue) *h*AChE

5.6.2 Butyl-linked Dehydroxylated Quinoline 3.6 Analysis

Following the parameterisation and integration of butyl-linked dehydroxylated quinoline **3.6** into inhibited and uninhibited *h*AChE, MD simulations were run. Butyl-linked dehydroxylated quinoline **3.6** within the uninhibited model (Figure 5.29) was seen to remain fairly distant from the serine residue of *h*AChE. The rotational flexibility of the linker, in frames 81 and 101 of this simulation, appears to act to the detriment of extending the linker and pyridine oxime reactivator down the gorge, towards the serine residue. However, unlike simulations run for butynyl-linked dehydroxylated quinoline **3.7**, the quinoline PSL of butyl-linked dehydroxylated quinoline **3.6** appears to be bound at the peripheral site throughout the MD run. This may suggest that the rotational restriction from the triple bond may result in quinoline's failure to form successful π-π interactions with aromatic residues on the surface of the enzyme.

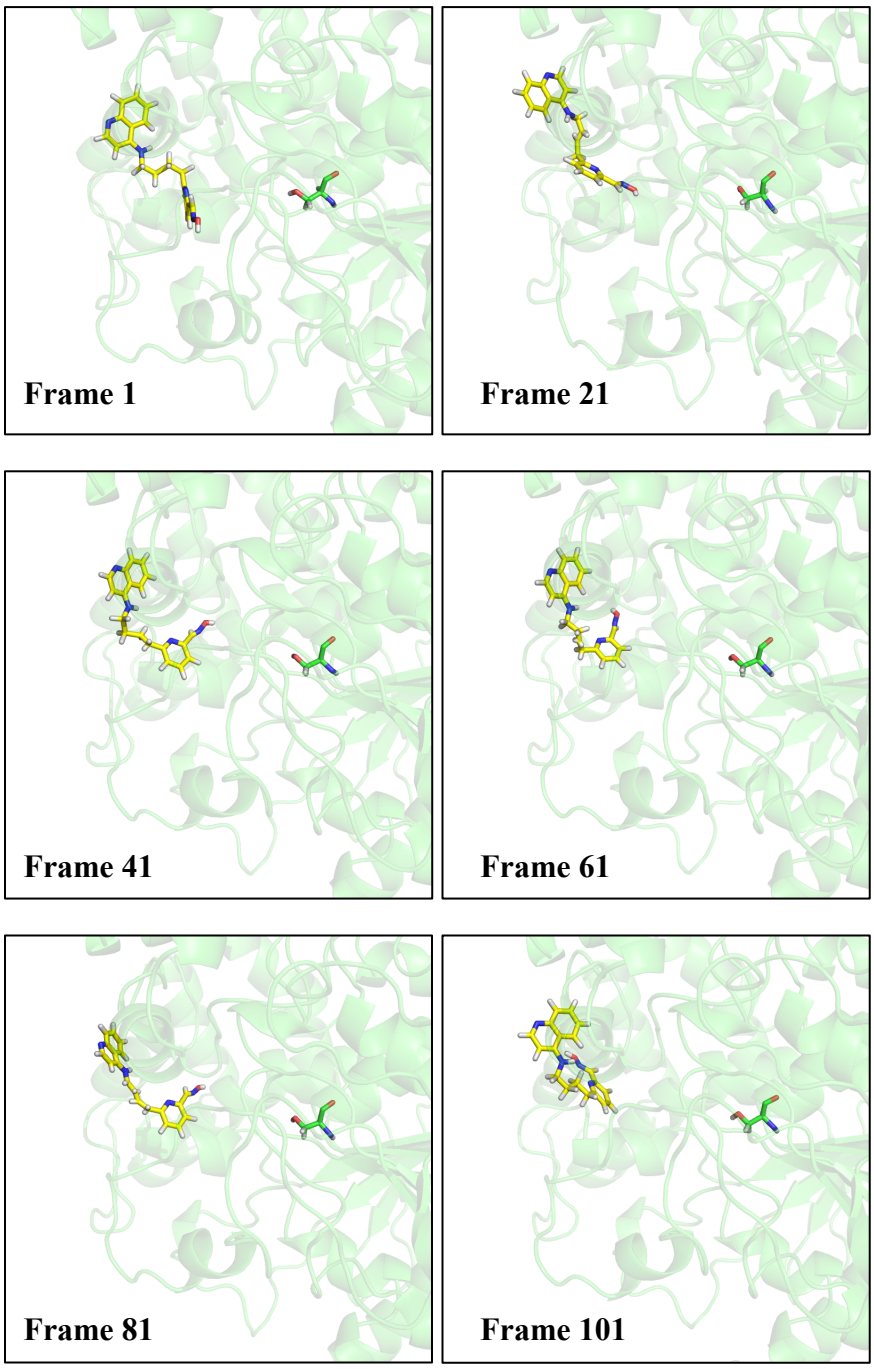

Figure 5.29. Six frames, taken over the MD simulation of butyl-linked dehydroxylated quinoline **3.6** (yellow) in uninhibited *h*AChE (green, the serine residue is shown as green sticks)

The MD simulation of butyl-linked dehydroxylated quinoline **3.6** within tabun-inhibited *h*AChE (Figure 5.30) shows a lot of movement of the ligand within the enzyme. Frames 1 to 21 show the PSL of the ligand at the peripheral site with oxime reactivator functionality very close to the tabun-inhibited serine residue of the enzyme. Conversely, following frame 41, the orientation of the ligand appears to change noticeably. The reactivating oxime appears to move up and away from the phosphorylated serine residue and frame 61 shows the ligand curled up – possibly indicating an intramolecular π-π stacking interaction between the quinoline PSL and pyridine reactivator moieties. This effect has been observed within some x-ray data of tetrahydroacridine hybrid

reactivators, as reported by Nachon *et al.*[187] (Figure 5.31). However, following frame 81, the ligand unfurls and approaches a similar position in frame 101 as that observed in frame 21.

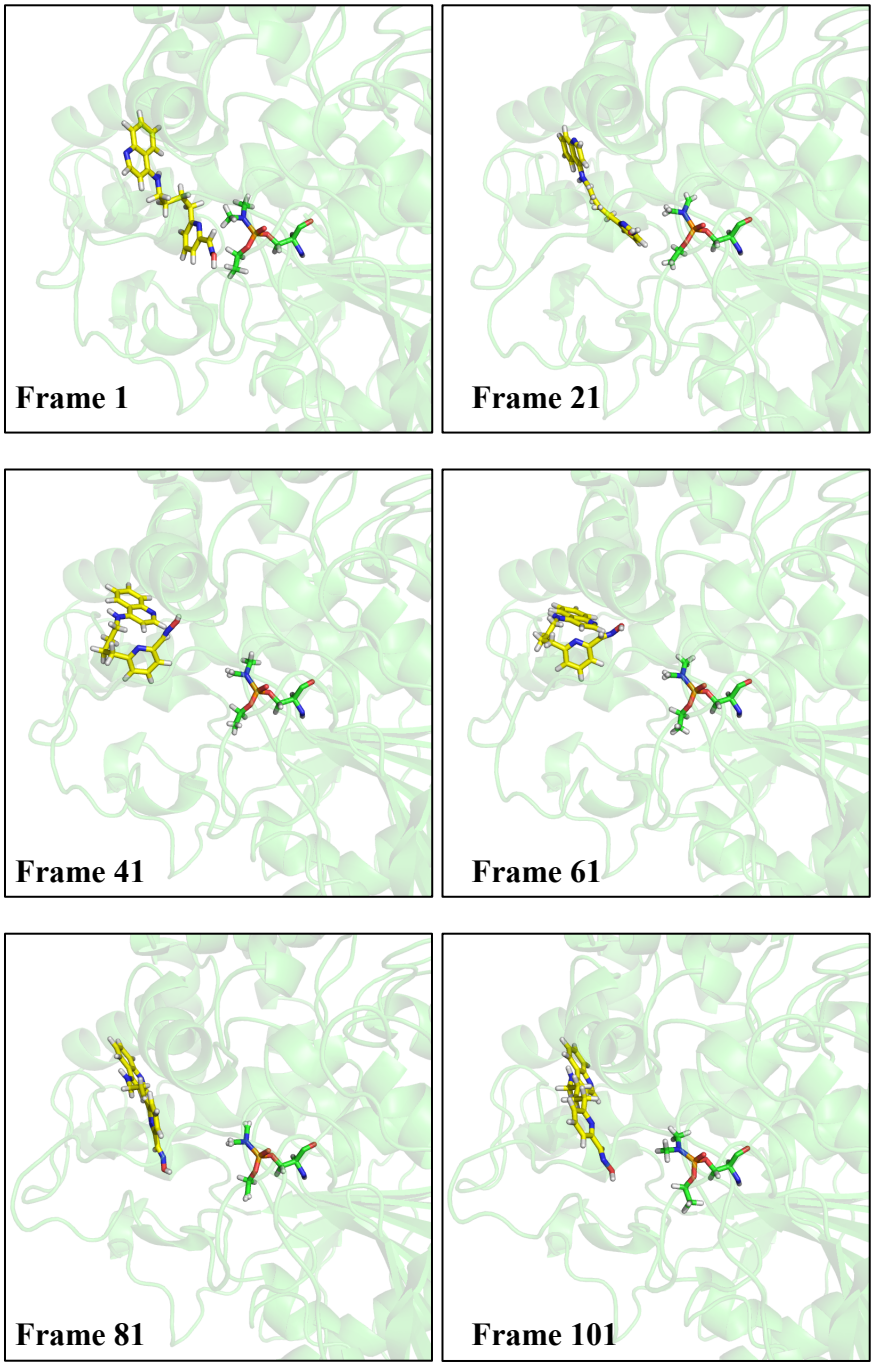

Figure 5.30. Six frames, taken over the MD simulation of butyl-linked dehydroxylated quinoline **3.6** (yellow) in tabun-inhibited *h*AChE (green, the tabun-inhibited serine is shown as green sticks)

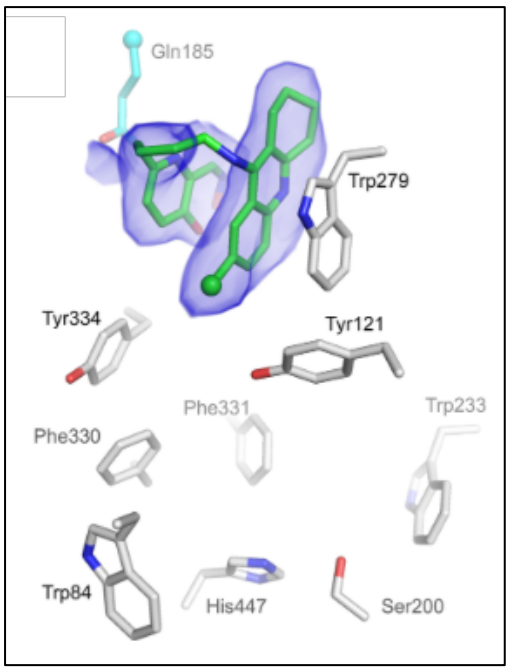

Figure 5.31. X-ray structure of chlorotacrine **5.1** within uninhibited *Tc*AChE (pdb: 6g4n) in a "curled-up" orientation[187]

The average distance between the oxime oxygen atom and the uninhibited *h*AChE serine oxygen atom, as demonstrated in all simulations, is consistently greater than that of the tabun-inhibited enzyme. This observation suggests the ligand has greater affinity for the inhibited enzyme active site compared to the uninhibited active site (Figure 5.32).

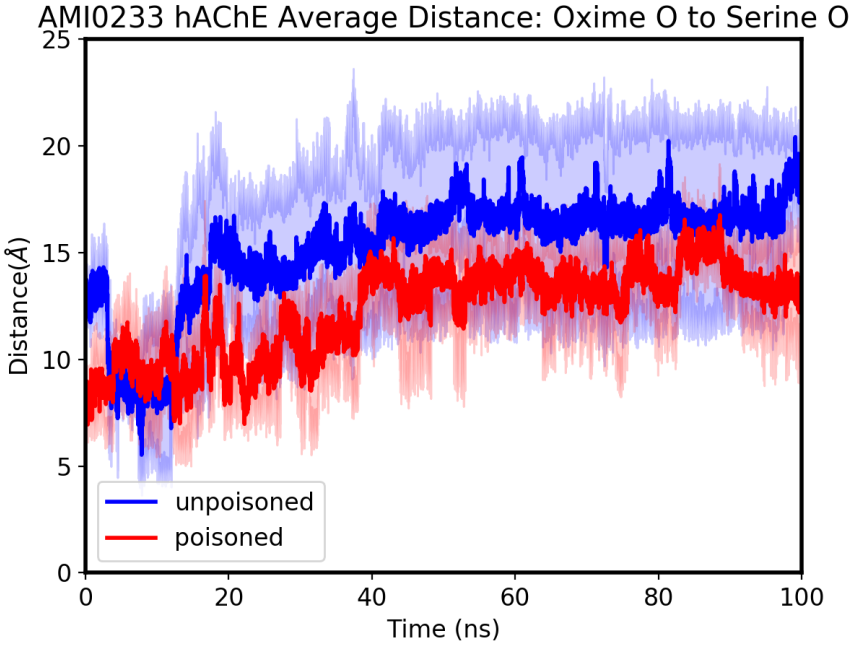

Figure 5.32. Combined average distances between the oxime oxygen atom of the ligand and the oxygen atom of the serine of the enzyme of butyl-linked dehydroxylated quinoline **3.6** within tabun inhibited (red) and uninhibited (blue) *h*AChE

The ligand within the tabun-inhibited model shows slightly greater RMSD (Figure 5.33) than that of the ligand in the uninhibited model. This too can be seen visually from the mobility of the ligand in the simulation.

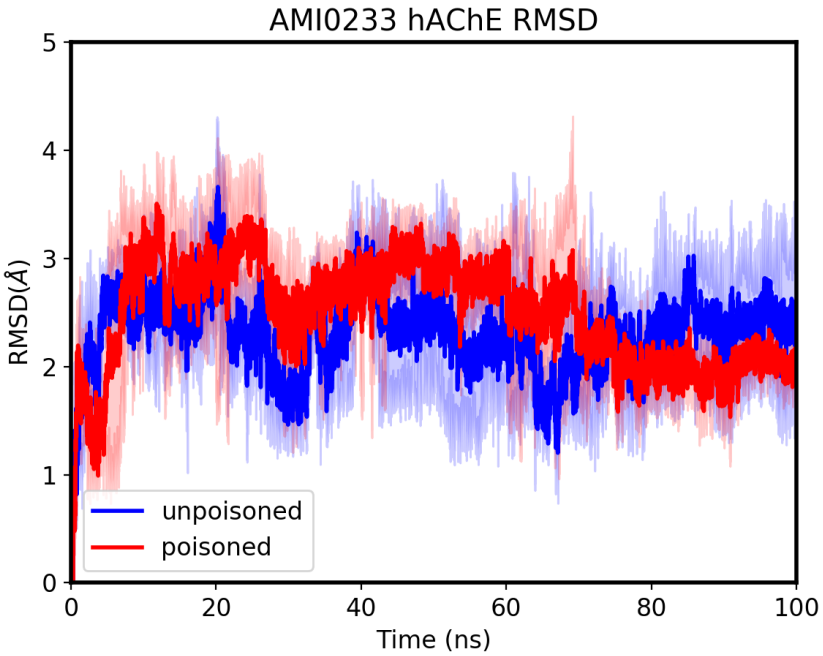

Figure 5.33. Combined RMSD of butyl-linked dehydroxylated quinoline **3.6** within tabun inhibited (red) and uninhibited (blue) *h*AChE

The increased mobility of butyl-linked dehydroxylated quinoline **3.6** within the tabun-inhibited *h*AChE could be due to possible intramolecular π-π stacking interactions observed during frames 41 to 61, this interaction could possibly be due to the flexibility of the fully saturated linker. The absence of the "curled up" orientation in simulation of butynyl-linked dehydroxylated quinoline **3.7** may support the proposition that conformational flexibility within the linker can result in intramolecular π-π stacking interactions and a subsequent "curled up" conformation.

5.6.3 Butynyl-linked dehydroxylated quinoline 3.7 and butyl-linked dehydroxylated quinoline 3.6: *In silico* and *In vitro* Comparison

Following the analysis of the *in silico* MD simulations and with the *in vitro* analyses of both butynyl-linked dehydroxylated quinoline **3.7** and butyl-linked dehydroxylated quinoline **3.6** in hand, it was possible to compare the data obtained from both computational and biological evaulation. Summarised in the table below are the collective *in vitro* data for ligands **3.7** and **3.6**, it is noteworthy that *in vitro*, both hybrid reactivators were not observed to reactivate tabun-inhibited AChE at reactivator concentrations up to 200 μM.

Table 5.4. Shows the [a]average distance between the serine oxygen and the oxime oxygen, taken from the final frame of each simulation for all compounds and their corresponding affinity (K_D), reactivation rate (k_r) and reactivator efficiency (k_{r2}) data of butynyl-linked dehydroxylated quinoline **3.7** and butyl-linked dehydroxylated quinoline **3.6**, from *in vitro* studies by José Dias at IRBA.[a] Ø represents no reactivation up to 200 μM

	Uninhibited average distance[a] (Å)	**OPNA**	**K_D** (μM)	**k_r** (min^{-1})	**k_{r2}** ($mM^{-1}min^{-1}$)
Butynyl-linked dehydroxylated quinoline **3.7**	10.790	*sarin*	0.35 ± 0.1	0.03 ± 0.0006	86
		VX	1.2 ± 0.1	0.05 ± 0.0006	46
		tabun	Ø [a]	Ø [a]	Ø [a]
		paraoxon	Ø [a]	Ø [a]	Ø [a]
Butyl-linked dehydroxylated quinoline **3.6**	12.881	*sarin*	1.1 ± 0.1	0.03 ± 0.0006	25
		VX	3.2 ± 0.3	0.06 ± 0.001	21
		tabun	Ø [a]	Ø [a]	Ø [a]
		paraoxon	Ø [a]	Ø [a]	Ø [a]

Although comparison of tabun-inhibited AChE is not possible as hybrid reactivators **3.6** and **3.7** were not observed to reactivate tabun-*h*AChE *in vitro*, it is still useful to draw comparisons between the results from other OPNA-inhibited AChE reactivation by both ligands. The *in vitro* data show that the butynyl-linked ligand **3.7** has a relatively higher affinity to both sarin-inhibited (0.35 μM) and VX-inhibited (1.2 μM) *h*AChE than the butyl-linked ligand **3.6** (1.1 μM and 3.2 μM, respectively). This effect was observed in the MD simulations, largely by the increased mobility of the quinoline PSL during the runs.

Both ligands **3.6** and **3.7** displayed almost identical reactivation rates against VX and sarin. Interestingly, their reactivator efficiency values (k_{r2}) differ considerably, which is due to the higher affinity of the unsaturated hybrid **3.7** for the enzyme.

Interestingly, the MD simulations demonstrate that the integration of the triple bond within the linker increases the affinity of the reactivator to the peripheral site and maintains it in place, with limited deviation from that position.

5.7 Conclusions

The development of an *in silico* model for the simulation of ligands' movement and behaviour within *h*AChE and tabun-inhibited *h*AChE has been discussed in this chapter. The model was developed from X-ray crystallographic data that was modified in a way that better represents human physiological conditions. Following MD simulations of the ligands that were available from crystallographic data, "overlay studies" were performed. By building and parameterising structurally similar compounds to those found in the x-ray data, it was possible to run molecular dynamics simulations to assess their behaviour *in silico.*

In vitro data allows for validation of the *in silico* model, which in turn allows for the study of intermolecular interactions and *in silico* evaluation of potential targets. Earlier in this chapter, quinoline **2.1** was shown, *in silico*, to bind immediately to the peripheral site *via* the quinoline PSL and direct the pyridine oxime reactivator towards the inhibited serine residue.

Table 5.5. Average distance between serine oxygen and oxime oxygen, [a]taken from the final frame of each simulation for all hybrid reactivators and their corresponding reactivation efficiencies against a range of OPNAs.[b]Data from[186] [c]Data for sarin reactivation with chlorotacrine **5.1** were obtained from AChE inhibited by an analogue of sarin (NIMP)[187]. [d]Ø represents no reactivation up to 200 μM

	Uninhibited average distance[a] (Å)	**k_{r2} ($mM^{-1}min^{-1}$)**			
		VX	*sarin*	*tabun*	*paraoxon*
Quinoline **2.1** [b]	8.381	34	18	51	20
Tacrine **3.1**	20.730	13	12	11	19
Chlorotacrine **5.1**[c]	20.317	22	16[c]	3	31
Butynyl-linked quinoline **3.7**	10.790	46	86	Ø[d]	Ø[d]
Butyl-linked quinoline **3.6**	12.881	10	4	Ø[d]	Ø[d]

Table 5.5 summarises *in vitro* kinetic reactivation constants (K_D, k_r and k_{r2}) and average distance between the serine oxygen of *h*AChE and the oxime oxygen of the hybrid reactivator compounds from the final frame findings from the simulations of all compounds. The results obtained from the *in silico* simulations appear to correlate with the *in vitro* findings. Both lead quinoline **2.1** and butynyl-linked dehydroxylated quinoline **3.7** show the lowest oxygen-oxygen distances and display the greatest reactivation efficiency. Conversely butyl-linked dehydroxylated quinoline **3.6** demonstrated lower affinity to the site of action during the simulation compared to compound **3.7**. This observation is also reflected in the lower *in vitro* reactivation efficiency of butyl-linked dehydroxylated quinoline **3.7** compared to butynyl-linked dehydroxylated quinoline **3.6**.

Following the analysis of all simulations, it is clear that there is a lot to learn from the computational model and great potential to lead further drug design in this area. There now exists a possibility of designing vast *in silico* libraries of analogues, in order to test their propensity to act well within the enzyme active site, with relatively high throughput. This opportunity means that more time may be spent developing syntheses towards more useful compounds with increased likelihood of developing effective and efficient reactivators.

This *in silico* model has the potential to accelerate work in this area towards understanding the structural modifications required of a hybrid reactivator to strike the balance between sufficient affinity for selective reactivation and competitive inhibitor of AChE. future work should be focussed on the development of further models containing other OPNAs, such as VX, sarin and paraoxon, such that the library of potential candidates may be screened for broad-spectrum activity.

Chapter 6 General Conclusions

The objectives of this research were to design, synthesise and evaluate a library of novel hybrid reactivators of organophosphorus nerve agent-inhibited human acetylcholinesterase. We have succeeded in the development and synthesis of nineteen novel reactivators based on diverse peripheral site ligand scaffolds. Initially, a range of differently substituted quinoline-based compounds were synthesised *via* a newly established route involving a Meldrum's Acid-mediated thermal cyclisation. An S_NAr step replaced the Buchwald-Hartwig microwave cross-coupling leading to increased yields, previously restricted by microwave apparatus size limitations. The improved route was also undertaken for the synthesis of lead quinoline **2.1** and demonstrated almost 2-fold improvement in yield over the final 6 steps.

Structural simplification of the pyridine oxime reactivator was investigated through the removal of the 3-hydroxyl functionality, which has previously been reported to drastically reduce the efficiency of reactivators. However, in this research, we demonstrate the development of butynyl-linked dehydroxylated quinoline **3.6** and butyl-linked dehydroxylated quinoline **3.7**. *In vitro* evaluation of butynyl-linked dehydroxylated quinoline **3.7** showed excellent reactivation efficiency for sarin-*h*AChE (k_{r2} 86 $mM^{-1}min^{-1}$) compared to lead quinoline **2.1** (k_{r2} 18.3 $mM^{-1}min^{-1}$). Whilst not demonstrating broad-spectrum reactivation, we have shown useful reactivation rates to be possible without the 3-hydroxy functionality. Butynyl-linked dehydroxylated quinoline **3.7** was designed to bear a triple bond within the linker, restricting rotational flexibility and decreasing oxime pK_a. According to *in vitro* data, this modification appears to deliver the most dramatic contribution to increased affinity of the reactivator to the site of action. In light of these SAR findings, a future hybrid reactivator (butynyl-linked hydroxylated quinoline **4.12**) has been proposed.

Various peripheral site ligands have been explored and investigated with the development of theobromine and naphthalene-containing compound. Solubility and polarity difficulties led to reduced synthetic success and difficulties attaining *in vitro* evaluation data. However, one naphthalene and a library of benzylpiperazine-containing hybrid reactivators have been synthesised and evaluated *in vitro*, disappointingly displaying no measurable reactivation.

Excitingly however, we have discovered a new lead compound, *N*-Boc piperazine **3.114**. This novel hybrid reactivator has been observed to outperform all existing reactivators and offers universally applicable reactivation across the range of OPNAs tested. Further exploration of synthetically accessible piperazine derivatives will be pursued.

Computational work has been described with the development of a novel approach towards *in silico* evaluation of potential hybrid reactivators. Based on x-ray crystallographic data of existing reactivators, it has been possible to replicate *in vivo* conditions and run molecular dynamics

simulations of ligand-enzyme complexes over 100 ns. The visualisation of a dynamic model, coupled with *in vitro* data may allow for informed reactivator design and identification of key interactions contributing to superior reactivation.

'Overlay studies' were also explored within the computational model, whereby novel reactivators were integrated into the existing model and molecular dynamics simulations were subsequently undertaken. This may enable future *in silico* screening of compound libraries, bypassing arduous synthetic efforts and time-consuming biological evaluation.

Future developments for this project lie in the *in vivo* evaluation of compound **3.7** in Swiss white mice by Dr Guilhem Calas at the Institut des Récherches Biomédicales des Armées, which are currently being undertaken. Synthetic work towards the development of proposed butynyl-linked hydroxylated quinoline **4.12** should also be assumed, such that SAR observations discussed in Chapter 4 (Section 4.1.4) may be combined into an improved reactivator.

Further synthetic efforts should be undertaken towards the synthetic route of compound **3.114** on a larger scale to facilitate the production of sufficient material for additional *in vivo* evaluation in Swiss white mice. Three compounds have been proposed to further develop SAR analysis of *N*-Boc piperazine **3.114**. Firstly, a dehydroxylated analogue (**6.1**) will allow understanding for whether the 3-hydroxyl functionality is integral in delivering useful reactivator efficiency. Secondly, the *N*-acetyl piperazine analogue (**6.2**) of compound **3.114** would provide information pertaining to the importance of the Boc protecting group and whether different substituent groups are tolerated at this position. Thirdly, the dehydroxylated analogue of compound **6.2**, should be prepared (**6.3**), this would offer an opportunity for direct comparison with its hydroxylated analogue.

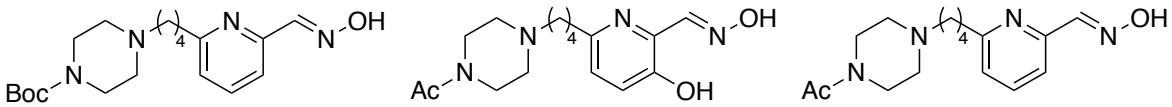

6.1 **6.2** **6.3**

Figure 6.1. Proposed future compounds for further SAR investigation

Finally, attempts towards the co-crystallisation of butynyl-linked dehydroxylated quinoline **3.7** within *h*AChE are also underway such that the crystallographic data may be compared to the *in silico* model. This would allow for direct comparison and precision evaluation of the model. Finally, further developments of the model should be considered, particularly in the modelling of the relevant ionised form of hybrid reactivators.

Chapter 7 Experimental Data

7.1 General Methods

All chemicals were purchased from Acros Organics, Alfa Aesar, Apollo Scientific, Fisher Scientific, Fluorochem, Merck or Sigma Aldrich. Air and moisture-sensitive reactions were undertaken under a positive flow of argon and anhydrous solvents, including THF, MeCN, Toluene, DMF, EtOAc, EtOH, MeOH and diethyl ether were obtained from Acros Organics as "Extra Dry 99+%, over molecular sieves", fitted with an AcroSeal. All anhydrous CH_2Cl_2 was obtained by distillation over CaH_2 before use. All TLC was undertaken on pre-coated SiO_2 or Al_2O_3 aluminium plates containing F_{254} indicator and were visualised under a UV lamp (254 nm) and/or by staining with cerium ammonium molybdate, potassium permanganate, potassium bismuth iodide, vanillin, iodine or phosphomolybdic acid. FCC was undertaken using high purity SiO_2 gel, Sigma Aldrich and Geduran, pore size 60 Å and mesh particle size 230-400 and 40 μm particle size. Microwave syntheses were undertaken in a sealed tube using a CEM Discover microwave reactor.

FTIR spectroscopy is reported in wavenumbers (cm^{-1}) was undertaken using a Nicolet iS5 Fourier Transform Infrared Spectrometer, fitted with the iD7 ATR attachment using the OMNIC software package. All samples were taken as neat solids or oils.

^{1}HNMR, ^{13}NMR and ^{19}FNMR were undertaken in deuterated solvents, purchased from Cambridge Isotope Laboratories or Sigma Aldrich at 298 K using Bruker DPX400, AVII400, AVIIHD400 (400, 101 and 376 MHz) and Bruker AVIIHD500 (500 and 126 MHz) spectrometers. Chemical shift (δ) is reported in ppm, relative to the residual solvent reference peak (δ 7.27 ppm in ^{1}HNMR and δ 77.00 ppm in ^{13}CNMR for $CDCl_3$, δ 2.50 ppm in ^{1}HNMR and δ 39.52 ppm in ^{13}CNMR for DMSO-d_6 and δ 3.31 ppm in ^{1}HNMR and δ 49.00 ppm in ^{13}CNMR for MeOD-d_4). All spectra were processed using ACDLabs NMR Spectrus Software (version 2015) or MestreNova (version 6.0.2-5475). Coupling constants (*J*) are reported in Hz and multiplicity is described by the following abbreviations; s (singlet), d (doublet), dd (double doublet), ddd (double doublet of doublets) dt (doublet of triplets), t (triplet), q (quartet), quin (quintet), sxt (sextet), sept (septet), m (multiplet), br (broad). Melting points were collected using a Stuart SMP20 instrument.

Electrospray low resolution mass spectrometry were analysed using a Waters (Manchester, UK) Acquity TQD mass tandem quadrupole mass spectrometer. Samples were introduced to the mass spectrometer *via* an Acquity H-Class quaternary solvent manager (with TUV detector at 254 nm, sample and column manager). Ultrahigh performance liquid chromatography was undertaken using Waters BEH C18 column (50 mm x 2.1 mm 1.7 μm).

Gradient elution from 20% acetonitrile (0.2% formic acid) to 100% acetonitrile (0.2% formic acid) was performed over five/ten minutes at a flow rate of 0.6 mL/min.

Electron impact mass spectrometry was recorded using a Thermo (Hemel Hempstead, UK) Trace GC-MS single quadrupole mass spectrometer. Gas chromatography was performed using a Phenomenex ZB5-MS 30 m x 0.25 mm 0.25 μm thickness non-polar column using helium as a carrier gas at 1.2 mL/min. The injector temperature was set at 240 °C and 1 μL of sample was injected in splitless mode. Low resolution positive ion electron ionisation (or chemical ionisation using ammonia as a reagent gas) mass spectra were recorded over a mass range of *m/z* 40-500 at 70 eV.

High resolution electrospray mass spectra were collected using a MaXis (Bruker Daltonics, Bremen, Germany) time of flight (TOF) mass spectrometer. Samples were introduced to the mass spectrometer *via* a Dionex Ultimate 3000 autosampler and uHPLC pump. Ultrahigh performance liquid chromatography was performed using a Waters UPLC BEH C18 (50 mm x 2.1 mm 1.7μm) column. Gradient elution from 20% acetonitrile (0.2% formic acid) to 100% acetonitrile (0.2% formic acid) was performed in five minutes at a flow rate of 0.6 mL/min. High resolution positive/negative ion electrospray ionisation mass spectra were recorded.

7.2 Ellman Assay Procedure

Recombinant *h*AChE was produced from Chinese Hamster Ovary cells.[230] A solution of 120 μM OP-inhibited *h*AChE was prepared with a five-fold excess of OP in 0.1% bovine serum albumin (BSA) in 20 mM tris(hydroxymethyl)aminomethane (Tris) buffer (pH 7.4) at 25 °C. *h*AChE was desalted and excess OPNA was removed by column chromatography (PD-10 column, GE Healthcare). The hybrid reactivator is added at specified concentrations (in solution, 0.1% BSA in 1 M phosphate-buffered saline, pH 7.4) and is incubated at 37 °C. 10 μL aliquots were transferred to a plate of cuvettes containing 1 mM acetylthiocholine and 1 mL Ellman's buffer at 25 °C.[177] The plate was transferred to a UV (412 nm) plate reader (Tecan, Spark 10M).

7.3 Characterisation Data

Methyl 3-hydroxypicolinate (2.3)

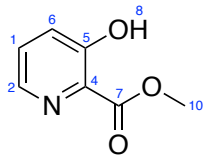

$C_7H_7NO_3$

MWt: 153.14 $gmol^{-1}$

Following a procedure by Louise-Leriche *et al.*,[231] concentrated sulphuric acid (5.75 mL, 107 mmol, 3 equiv.) was added dropwise to a suspension of 3-hydroxypicolic acid (5.00 g, 35.9 mmol, 1 equiv.) in MeOH (70 mL). The colourless mixture was heated to reflux for 24 h. Upon consumption of starting materials (TLC) the mixture was basified to pH 8.5 with an aqueous solution of K_2CO_3. The aqueous layer was extracted with EtOAc (3 × 20 mL). The organic layers were combined, dried ($MgSO_4$), filtered and concentrated *in vacuo*, to afford methyl 3-hydroxypicolinate (4.32 g, 28.2 mmol, 79%) as a colourless solid. Data was consistent to that reported in the literature.[231]

TLC R_f 0.43 (30% light petroleum ether in EtOAc, SiO_2)

^{1}HNMR (400 MHz, $CDCl_3$) δ 10.65 (br. s, 1H, O**H**), 8.30 (d, *J*=4.2 Hz, 1H, NC**H**), 7.47-7.38 (m, 2H, Ar**H**), 4.11 (s, 3H, O**CH$_3$**) ppm

^{13}CNMR (101 MHz, $CDCl_3$) δ 169.8 (**7**), 158.8 (**5**), 141.5 (**2**), 129.9 (**4**), 129.6 (**1**), 126.3 (**6**), 53.2 (**10**) ppm

IR (neat) ν_{max} 3029 (m), 2957 (m), 1668 (s) cm^{-1}

LRMS (ESI$^+$) m/z 154.1 $[M+H]^+$

Mpt 73-74 °C (lit: 72-73 °C)

Methyl 6-bromo-3-hydroxypicolinate (2.4)

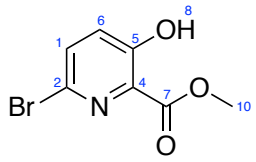

$C_7H_6BrNO_3$

MWt: 232.03 $gmol^{-1}$

Following a procedure by Louise-Leriche *et al.*,[231] to a colourless suspension of methyl 3-hydroxypicolinate (3.00 g, 19.6 mmol, 1 equiv.) in H_2O (100 mL) was added Br_2 (1.01 mL, 19.6 mmol, 1 equiv.) dropwise and portiowise (8 x 125 µL) over 2 h at 0 °C. The mixture was stirred at 0 °C for 2 h and at rt for an additional 15 min. The mixture was extracted with CH_2Cl_2 (2 × 20 mL). The organic layers were combined and washed with $Na_2S_2O_3$, brine, dried ($MgSO_4$), filtered and concentrated *in vacuo*. The crude pale yellow product was purified by column chromatography (SiO_2, 20% EtOAc in cyclohexane), to afford methyl 6-bromo-3-hydroxypicolinate (2.79 g, 12.0 mmol, 61%) as a colourless solid. Data was consistent to that reported in the literature.[231]

TLC R_f 0.81 (30% light petroleum ether in EtOAc, SiO_2)

^{1}HNMR (400 MHz, $CDCl_3$) δ 10.62 (s, 1H, **OH**), 7.49 (d, *J*=8.6 Hz, 1H, BrC**CH**), 7.23-7.18 (m, 1H, OHC**CH**), 4.03 (s, 3H, O**CH$_3$**) ppm

^{13}CNMR (101 MHz, $CDCl_3$) δ 169.0 (**7**), 158.5 (**5**), 136.7 (**2**), 134.4 (**1**), 130.6 (**4**), 129.4 (**6**), 53.4 (**10**) ppm

IR (neat) ν_{max} 3064 (m), 1666 (s) cm^{-1}

LRMS (ESI$^+$) m/z 232.0 $[M^{79}Br+H]^+$, 234.0 $[M^{81}Br+H]^+$

Mpt 115-116 °C (lit: 115-117 °C)

Methyl 3-benzyloxy-6-bromopicolinate (2.5)

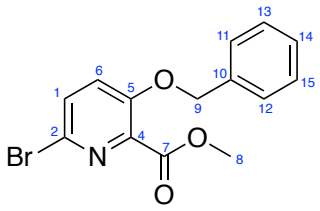

$C_{14}H_{12}BrNO_3$

MWt: 322.15 $gmol^{-1}$

Following a procedure by Louise-Leriche *et al.*,[231] benzyl bromide (3.80 mL, 31.8 mmol, 3 equiv.) was added slowly to a mixture of methyl 6-bromo-3-hydroxypicolinate (2.46 g, 10.6 mmol, 1 equiv.) and K_2CO_3 (6.59 g, 47.7 mmol, 4.5 equiv.) in acetone (150 mL). The colourless solution was heated to reflux for 18 h. The reaction mixture was filtered and concentrated *in vacuo*. Purification was undertaken by column chromatography (SiO_2, 10% EtOAc in cyclohexane), to afford methyl 3-benzyloxy-6-bromopicolinate (3.22 g, 10.5 mmol, 99%) as a colourless solid. Data was consistent to that reported in the literature.[231]

TLC R_f 0.29 (20% light petroleum ether in EtOAc, SiO_2)

^{1}HNMR (400 MHz, $CDCl_3$) δ 7.53-7.33 (m, 5H, BrC**C**H, Bn**H**), 7.30-7.25 (m, 2H, BnOC**C**H, Bn**H**), 5.23 (s, 2H, O**C**H**H**Ph), 3.99 (s, 3H, O**C**H_3) ppm

^{13}CNMR (101 MHz, $CDCl_3$) δ 164.0 (**7**), 154.0 (**5**), 140.0 (**4**), 135.3 (**10**), 131.3 (**1**), 131.2 (**4**), 128.8 (**15**, **13**), 128.4 (**11**, **12**), 127.0 (**14**), 125.0 (**2**), 71.3 (**9**), 52.8 (**8**) ppm

IR (neat) ν_{max} 3068 (m), 2952 (m), 1713 (s), 1261 (s), 1031 (s) cm^{-1}

LRMS (ESI^+) m/z 322.1 $[M^{79}Br+H]^+$, 324.1 $[M^{81}Br+H]^+$

Mpt 100-101 °C

Diethyl 2-(((4-fluorophenyl)amino)methylene)malonates (2.9)

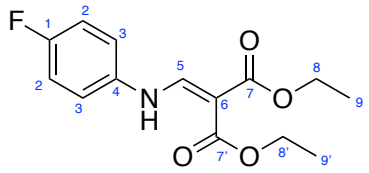

$C_{14}H_{16}FNO_4$

MWt: 281.28

Following a procedure by Dharmarajan *et al.*[232] for the addition of anilines to malonates, a mixture of *p*-fluoroaniline (0.43 mL, 4.50 mmol) and diethyl ethoxymethylmalonate (972 mg, 4.50 mmol) was heated to 110 °C for 4 h. The orange mixture was cooled to rt and light petroleum ether was added (20 mL), and the solution was stirred at rt for 15 min. An orange solid precipitated and was removed by filtration. The orange solid was recrystallised from EtOH to afford diethyl 2-(((4-fluorophenyl)amino)methylene)malonate (780 mg, 2.80 mmol, 62%) as a white crystalline solid. Data was consistent to that reported in the literature.[232]

TLC R_f	0.66 (30% light petroleum ether in EtOAc, SiO_2)
^{1}HNMR	(400MHz, $CDCl_3$) δ 11.01 (br. d, *J*=13.4 Hz, 1H, **NH**), 8.44 (d, *J*=13.4 Hz, 1H, NH**CH**), 7.20-7.00 (m, 4H, Ar**H**), 4.35-4.22 (m, 4H, CO_2**CH_2**CH_3), 1.42-1.30 (m, 6H, CO_2CH_2**CH_3**) ppm
IR (neat)	3139 (m), 2980 (m), 2939 (m), 2901 (m), 1680 (s), 1636 (s), 1214 (s) cm^{-1}
LCMS	(ESI$^+$) *m/z* 282.2 $[M+H]^+$
Mpt	68-69 °C (lit: 69-70 °C)

Ethyl 6-fluoro-4-hydroxyquinoline-3-carboxylate (2.10)

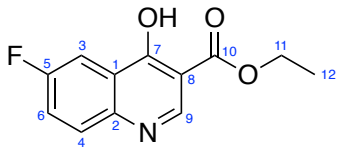

$C_{12}H_{10}FNO_3$

MWt: 235.21

Following a procedure by Dharmarajan *et al.*[232] for the Gould-Jacobs cyclisation towards quinolin-4-ols, a solution of diethyl 2-(((4-fluorophenyl)amino)methylene)malonate (700 mg, 2.50 mmol) in diphenyl ether (10 mL) was heated to 250 °C for 4 h. After 2 h, the colourless solution turned vivid orange. The cooled solution was diluted with hexanes (10 mL) and white solid precipitated out of solution. The solid was isolated by filtration and dried to afford ethyl 6-fluoro-4-hydroxyquinoline-3-carboxylate (210 mg, 0.90 mmol, 36%) as off-white crystals. Data was consistent to that reported in the literature.[232]

TLC R_f	0.16 (30% hexanes in EtOAc, SiO_2)
^{1}HNMR	(400MHz, DMSO-d_6) δ 12.44 (br. s, 1H, **OH**), 8.58 (s, 1H, NH**CH**), 7.80 (dd, *J*=9.3, 2.9 Hz, NC**CH**), 7.76-7.58 (m, 2H, NCCH**CH**, NCC**CH**), 4.22 (q, *J*=7.1 Hz, 2H, CO_2**CH_2**CH_3), 1.28 (t, *J*=7.1 Hz, 3H, CO_2CH_2**CH_3**) ppm
IR (neat)	3099 (m), 2905 (m), 1690 (s), 1615 (s), 1166 (s) cm^{-1}
LCMS	(ESI$^+$) *m/z* 236.1 $[M+H]^+$
Mpt	287-289 °C (lit: 288-290 °C)

6-Fluoro-4-hydroxyquinoline-3-carboxylic acid (2.11)

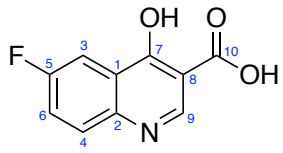

$C_{10}H_6FNO_3$

MWt: 207.16

Following a procedure from Dharmarajan *et al.,*[232] to an aqueous solution of NaOH (10% w/v, 1.75 mL) was added ethyl 6-fluoro-4-hydroxyquinoline-3-carboxylate (175 mg, 0.70 mmol). The colourless solution was heated to 100 °C for 2.5 h. The solution was allowed to cool to rt and HCl (2 M, 5 mL) was added. The white precipitate that formed was removed by filtration and dried, to afford 6-fluoro-4-hydroxyquinoline-3-carboxylic acid (120 mg, 0.70 mmol, 100%) as a cream solid. Data was consistent to that reported in the literature.[232]

TLC R_f	0.14 (EtOAc, SiO_2)
^{1}HNMR	(400MHz, DMSO-d_6) δ 15.12 (br. s, 1H, COO**H**), 13.25 (br. s, 1H, **OH**), 8.94 (s, 1H, NH**CH**), 8.01-7.87 (m, 3H, Ar**H**) ppm
IR (neat)	3250 (br), 3088 (m), 2833 (m), 1668 (s), 1480 (s), 822 (s) cm^{-1}
LCMS	(ESI^+) *m/z* 208.1 $[M+H]^+$
Mpt	286-289 °C (decomposed) (lit: 287 °C)

6-Fluoroquinolin-4-ol (2.14a)

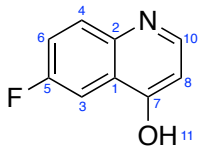

C_9H_8FNO

MWt: 163.20 $gmol^{-1}$

Following a procedure adapted from Margolis *et al.*,[233] to a solution of *p*-fluoroaniline (3.03 mL, 31.5 mmol, 1 equiv.) in EtOH (30 mL) was added Meldrum's acid (5.54 g, 38.4 mmol, 1.2 equiv.) and triethyl orthoformate (12.4 mL, 74.5 mmol, 2.4 equiv.). The pale beige mixture was heated to reflux for 2.5 h, the solution turned yellow and then brown. The brown reaction solution was cooled to 0 °C and the solid was filtered and washed with cold EtOH. The dried solid was added portiowise over 5 min to boiling diphenyl ether (100 mL). Reflux was maintained for an additional 3 min. The reaction was stirred at rt for 30 min before petroleum ether (25 mL) was added and the solid was filtered and dried. The crude product was purified by column chromatography (SiO_2, 5% MeOH in EtOAc), to afford 6-fluoroquinolin-4-ol (2.36 g, 14.5 mmol, 46%) as a pale brown solid. Data was consistent to that reported in the literature.[233]

TLC R_f 0.41 (25% MeOH in EtOAc, SiO_2)

^{1}HNMR (400MHz, DMSO-d^6) δ 11.90 (s, 1H, **OH**), 7.94 (d, *J*=7.5, 1H, N**CH**), 7.73 (m, 1H, NC**CH**), 7.53-7.67 (m, 2H, FC**CH**, FC**CH**), 6.04 (d, *J*=7.5, 1H, OHC**CH**) ppm

^{13}CNMR (101 MHz, DMSO-d^6) δ 158.7 (d, *J*=240 Hz, **5**), 140.0 (**7**), 137.3 (**10**), 127.3 (**4**), 122.2 (**1**), 122.0 (**2**), 121.0 (d, *J*=25 Hz, **3**), 109.2 (d, *J*=20 Hz, **6**), 108.3 (**8**) ppm

^{19}FNMR (376 MHz, DMSO-d^6) δ 117.7 ppm

IR (neat) ν_{max} 2768 (br), 1594 (m) cm^{-1}

LRMS (ESI$^+$) m/z 164.1 $[M+H]^+$

HRMS (ESI$^+$) *m/z calcd. for* C_9H_8FNO 164.0506 *m/z meas.* 164.0509 $[M+H]^+$

Mpt 227-228 °C (lit: 227-228 °C)

8-Methoxyquinolin-4-ol (2.14b)

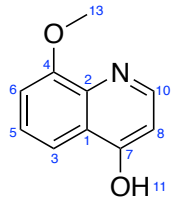

$C_{10}H_9NO_2$

MWt: 175.10 $gmol^{-1}$

Following a procedure adapted from Margolis *et al.*,[233] to a solution of *o*-anisidine (2.29 mL, 20.3 mmol, 1 equiv.) in EtOH (20 mL) was added Meldrum's acid (3.57 g, 24.8 mmol, 1.2 equiv.) and triethyl orthoformate (8.00 mL, 48.0 mmol, 2.4 equiv.). The beige mixture was heated to reflux for 2.5 h, the reaction mixture turned yellow and then brown. The brown reaction was cooled to 0 °C and the solid was filtered and washed with cold EtOH. The dried solid was added portiowise over 5 min to boiling diphenyl ether (100 mL). Reflux was maintained for an additional 3 min. The reaction was stirred at rt for 30 min before petroleum ether (25 mL) was added and the solid was filtered and dried. The crude product was purified by column chromatography (SiO_2, 5% MeOH in EtOAc), to afford 8-methoxyquinolin-4-ol (2.70 g, 15.4 mmol, 76%) as a pale orange solid.

TLC R_f 0.06 (5% MeOH in EtOAc, SiO_2)

^{1}HNMR (400 MHz, DMSO-d^6) δ 11.35 (s, 1H, **OH**), 7.70-7.58 (m, 1H, N**CH**), 7.43-7.38 (m, 1H, Ar**H**), 7.27-7.23 (m, 2H, OHCC**CH**, OMeC**CH**), 7.08-6.95 (m, 1H, OHC**CH**), 3.99 (s, 3H, O**CH$_3$**) ppm

^{13}CNMR (101 MHz, DMSO-d^6) δ 177.11 (**7**), 149.0 (**4**), 139.3 (**10**), 130.5 (**2**), 123.2 (**5**), 119.1 (**3**), 116.7 (**1**), 111.4 (**6**), 109.6 (**8**), 56.6 (**13**) ppm

IR (neat) ν_{max} 2921 (br), 2851 (m), 1272 (s), 1041 (s) cm^{-1}

LRMS (ESI$^+$) m/z 176.1 $[M+H]^+$

HRMS (ESI$^+$) *m/z calcd. for* $C_{10}H_9NO_2$ 176.0706 *m/z meas.* 176.0707 $[M+H]^+$

Mpt 168-169 °C (lit: 168-169 °C)

4-Bromo-6-fluoroquinoline (2.26a)

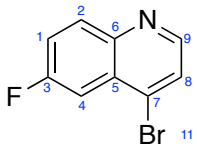

C_9H_5BrFN

MWt: 226.00 $gmol^{-1}$

Following a procedure adapted from Franzblau *et al.*,[234] to a solution of 6-fluoroquinolin-4-ol (2.30 g, 14.1 mmol, 1 equiv.) in DMF (20 mL) at 60 °C was added phosphorus tribromide (1.52 mL, 16.2 mmol, 1.2 equiv.). The dark orange mixture was cooled to 45 °C for 45 min. After cooling to rt, the reaction was diluted with H_2O (25 mL) and the solution was basified to pH 10 with saturated aqueous $NaHCO_3$. The resulting solid was washed in H_2O, filtered and taken up in EtOAc and concentrated *in vacuo*, to afford 4-bromo-6-fluoroquinoline (3.12 g, 13.8 mmol, 98%) as a pale brown solid.

TLC R_f 0.64 (20% MeOH in EtOAc, SiO_2)

^{1}HNMR (400MHz, DMSO-d^6) δ8.73 (d, *J*=4.6 Hz, 1H, NC**H**), 8.18 (m, 1H, NC**C**H), 8.00 (d, *J*=4.6 Hz, 1H, BrC**C**H), 7.77-7.88 (m, 2H, FC**C**H, FC**C**H) ppm

^{13}CNMR (101 MHz, DMSO-d^6) δ 158.7 (d, *J*=253 Hz, **3**), 150.5 (**7**), 146.0 (**6**), 133.0 (**2**), 128.6 (**7**), 128.5 (**8**), 126.6 (**5**), 121.3 (d, *J*=26 Hz, **4**), 110.5 (d, *J*=25 Hz, **1**) ppm

^{19}FNMR (376 MHz, DMSO-d^6) δ 110.2 ppm

IR (neat) ν_{max} 1585 (m) cm^{-1}

LRMS (ESI^+) m/z 227.0 $[M^{79}Br+H]^+$, 229.0 $[M^{81}Br+H]^+$

HRMS (ESI^+) *m/z calcd. for* C_9H_5BrFN 225.9662 *m/z meas.* 225.9662 $[M+H]^+$

Mpt 74-75 °C

4-Bromo-8-methoxyquinoline (2.26b)

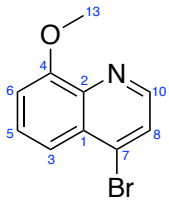

$C_{10}H_8BrNO$

MWt: 239.10 gmol-1

Following a procedure adapted from Franzblau *et al.*,[234] to a solution of 8-methoxyquinolin-4-ol (2.67 g, 15.2 mmol, 1 equiv.) in DMF (20 mL) at 60 °C was added phosphorus tribromide (1.65 mL, 17.5 mmol, 1.2 equiv.). The dark orange mixture was cooled to 45 °C for 45 min. After cooling to rt, the reaction was diluted with H_2O (25 mL) and the solution was basified to pH 10 with saturated aqueous $NaHCO_3$. The resulting solid was washed in H_2O, filtered and taken up in EtOAc and concentrated *in vacuo*, to afford 8-methoxy-4-bromoquinoline (2.44 g, 10.3 mmol, 67%) as a cream solid.

TLC R_f 0.51 (25% MeOH in EtOAc, SiO_2)

^{1}HNMR (400MHz, $CDCl_3$) δ 8.69 (d, *J*=4.7 Hz, 1H, NC**H**), 7.78 (d, *J*=8.1 Hz, 1H, BrCC**CH**), 7.75 (d, *J*=4.7 Hz, 1H, BrC**CH**), 7.58 (t, *J*=8.1 Hz, 1H, Ar**H**), 7.14 (d, *J*=8.1 Hz, 1H, Ar**H**), 4.12 (s, 3H, O**CH$_3$**) ppm

^{13}CNMR (101 MHz, $CDCl_3$) δ 155.5 (**4**), 148.5 (**10**), 134.1 (**2**), 129.0 (**7**), 128.0 (**1**), 125.8 (**5,8**), 118.5 (**3**), 108.5 (**6**), 56.3 (**13**) ppm

IR (neat) ν_{max} 1252 (s), 1085 (s) cm^{-1}

LRMS (ESI$^+$) m/z 238.0 $[M^{79}Br+H]^+$, 240.0 $[M^{81}Br+H]^+$

HRMS (ESI$^+$) *m/z calcd. for* $C_{10}H_8BrNO$ 237.9862 *m/z meas.* 237.9865 $[M+H]^+$

Mpt 99-101 °C (lit: 96-97 °C)

4-Chloro-6-fluoroquinoline (2.27a)

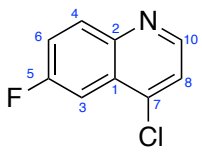

C_9H_5ClFN

MWt: 181.60 $gmol^{-1}$

Following an adapted procedure from Xu *et al.*[235] for the chlorination of quinolin-4-ols, a solution of 6-fluoroquinolin-4-ol (500 mg, 3.10 mmol) and phosphorus oxychloride (5.00 mL, 53.6 mmol) was heated to 100 °C for 3 hours. The colouress mixture was allowed to cool to rt, before being stirred overnight at that temperature. The reaction solution was concentrated *in vacuo* to remove excess phosphorus oxychloride and the residue was transferred to an ice water slurry. Using a saturated aqueous solution of K_2CO_3, the pH of the slurry was adjusted to 6-7. A white fluffy solid precipitated and was collected by filtration. The solid was dried to afford 4-chloro-6-fluoroquinoline (493 mg, 2.74 mmol, 89%) as pale cream crystals.

TLC R_f	0.70 (10% MeOH in EtOAc, SiO_2)
^{1}HNMR	(400MHz, $CDCl_3$) δ 8.86 (d, *J*=4.6 Hz, 1H, **NCH**), 8.21 (m, 1H, **NCCH**), 7.93 (m, 1H, **ClCCH**), 7.80-7.87 (m, 2H, **CHCFCH**) ppm
^{13}CNMR	(101 MHz, $CDCl_3$) δ 161.2 (d, *J*=241 Hz, **5**), 150.5 (**10**), 146.2 (**2**), 141.0 (**7**), 127.1 (**4**), 122.8 (**1**), 121.5 (d, *J*=26 Hz, **6**), 121.3 (**8**), 107.8 (d, *J*=20 Hz, **3**) ppm
IR (neat)	ν_{max} 2921 (m), 1222 (s), 675 (s) cm^{-1}
LCMS	(ESI^+) *m/z* 182.1 $[M+H]^+$
Mpt	76-77 °C (lit: 77-78 °C)

4-Chloro-8-methoxyquinoline (2.27b)

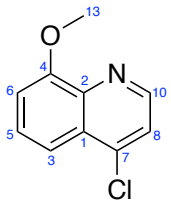

$C_{10}H_8ClNO$

MWt: 193.60 $gmol^{-1}$

Following an adapted procedure from Xu *et al.*[235] for the chlorination of quinolin-4-ols, a solution of 8-methoxyquinolin-4-ol (500 mg, 2.80 mmol) and phosphorus oxychloride (4.70 mL, 50.0 mmol) was heated to 100 °C for 3 hours. The colourless mixture was allowed to cool to rt, before being stirred overnight at that temperature. The colourless reaction solution was concentrated *in vacuo* to remove excess phosphorus oxychloride and the residue was transferred to an ice water slurry. Using an ammonium hydroxide solution (35% in H_2O), the pH of the slurry was adjusted to 6-7. The aqueous solution was extracted with CH_2Cl_2 (3 × 20 mL) and the organics were combined and washed (H_2O, 30 mL). The organic layer was separated, dried ($MgSO_4$), filtered and concentrated *in vacuo*, to afford 4-chloro-8-methoxyquinoline (553 mg, 2.80 mmol, 100%) as pale orange crystals.

TLC R_f	0.55 (15% MeOH in EtOAc, SiO_2)
^{1}HNMR	(400MHz, $CDCl_3$) δ 8.78 (d, *J*=4.6 Hz, 1H, N**CH**), 7.79 (d, *J*=4.6 Hz, 1H, NCH**CH**), 7.66-7.78 (m, 2H, ClCC**CHCH**), 7.37-7.46 (m, 1H, OMeCCH**CH**), 4.00 (s, 3H, **OMe**) ppm
^{13}CNMR	(101 MHz, $CDCl_3$) δ 156.0 (**4**), 149.2 (**10**), 141.4 (**2**), 141.0 (**7**), 130.5 (**1**), 129.0 (**8**), 122.6 (**3**), 119.1 (**5**), 110.0 (**6**), 56.4 (**13**) ppm
IR (neat)	ν_{max} 2922 (m), 1233 (s), 745 (s) cm^{-1}
LCMS	(ESI^+) *m/z* 194.1 $[M+H]^+$
Mpt	77-79 °C (lit: 79-80 °C)

_N_-Butyl-6-fluoroquinolin-4-amine (2.30)

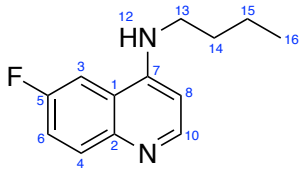

$C_{13}H_{15}FN_2$

MWt: 218.10

Following a procedure adapted from Musonda *et al.,*[236] 4-chloro-6-fluoroquinoline (100 mg, 0.40 mmol) was mixed with n-butylamine (161 mg, 2.20 mmol) to form a pale orange paste. The paste was heated to 80 °C for 1 h without stirring. The temperature was raised to 140 °C and the reaction was left for 15 h with stirring. The brown reaction mixture was cooled to room temperature and the organic product was basified with 10 % NaOH (2 mL) and extracted with EtOAc (5 × 5 mL), the combined organics were washed (H_2O, 10 mL) and dried ($MgSO_4$). The $MgSO_4$ was removed by filtration and the dried organic layer was concentrated *in vacuo* to afford *N*-butyl-6-fluoroquinolin-4-amine (80 mg, 0.34 mmol, 83 %) as an orange/brown solid.

TLC R_f	0.71 (20% MeOH in EtOAc, Al_2O_3)
^{1}HNMR	(400MHz, DMSO-d6) δ 8.38 (d, *J*=5.4 Hz, 1H, NC**H**), 8.08 (m, 1H, NCC**H**), 7.83 (m, 1H, FCC**H**), 7.40-7.66 (m, 1H, FCC**H**), 7.02 (br, t, *J*=5.1 Hz, 1H, **NH**), 6.46 (d, *J*=5.4 Hz, 1H, NHC**H**), 3.21-3.30 (m, 2H, NH**CH$_2$**), 1.66 (quin, *J*=7.3 Hz, 2H, NHCH$_2$**CH$_2$**), 1.43 (sxt, *J*= 7.3 Hz, 2H, NHCH$_2$CH$_2$**CH$_2$**), 0.95 (t, *J*=7.3 Hz, 3H, NHCH$_2$CH$_2$CH$_2$**CH$_3$**) ppm
^{13}CNMR	(101 MHz, DMSO-d6) δ 158.9 (d, *J*=207 Hz, 5), 150.7 (7), 146.0 (2), 132.2 (10), 132.1 (4), 118.7 (d, *J*=25 Hz, 6), 118.6 (1), 106.2 (d, *J*=22 Hz, 3), 98.8 (8), 42.6 (13), 30.4 (14), 20.3 (15), 14.3 (16) ppm
IR (neat)	3295 (m), 2949 (m), 2927 (m), 2867 (m), 1465 (m), 1374 (m) cm-1
LCMS	(ESI$^+$) *m/z* 219.1 $[M+H]^+$
Mpt	124-127 °C

***N*-Butyl-8-methoxyquinolin-4-amine (2.31)**

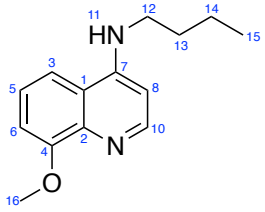

$C_{14}H_{18}N_2O$

MWt: 230.10

Following a procedure adapted from Musonda *et al.,*[236] 4-chloro-8-methoxyquinoline (100 mg, 0.40 mmol) was mixed with n-butylamine (135 mg, 2.20 mmol) to form a pale orange paste. The paste was heated to 80 °C for 1 h without stirring. The temperature was raised to 140 °C and the reaction was left for 15 h with stirring. The brown reaction mixture was cooled to room temperature and the organic product was basified with 10 % NaOH (2 mL) and extracted with EtOAc (5 × 5 mL), the combined organics were washed (H_2O, 10 mL) and dried ($MgSO_4$). The $MgSO_4$ was removed by filtration and the dried organic layer was concentrated *in vacuo* to afford *N*-butyl-6-fluoroquinolin-4-amine (80 mg, 0.34 mmol, 83 %) as an orange/brown solid.

TLC R_f	0.64 (20% MeOH in EtOAc, Al_2O_3)
^{1}HNMR	(400MHz, DMSO-d6) δ 8.21-8.43 (m, 1H, NC**H**), 7.61-7.82 (m, 1H, Ar**H**), 7.22-7.42 (m, 1H, NHCC**CH**), 6.94-7.15 (m, 2H, NH, MeOC**CH**), 6.39-6.54 (m, 1H, HNC**CH**), 3.89 (s, 3H, **Me**O), 3.22-3.29 (m, 2H, NH**CH$_2$**), 1.65 (quin, *J*=7.3 Hz, 2H, NHCH$_2$**CH$_2$**), 1.36-1.44 (m, 2H, NHCH$_2$CH$_2$**CH$_2$**), 0.95 (t, *J*= 7.3 Hz, 3H,NHCH$_2$CH$_2$CH$_2$**CH$_3$**) ppm
^{13}CNMR	(101 MHz, DMSO-d6) δ 155.8 (4), 150.3 (7), 140.6 (10), 124.2 (2), 120.1 (5), 118.0 (1), 113.7 (3), 108.5 (8), 99.1 (6), 56.0 (16), 42.6 (12), 30.5 (13), 20.3 (14), 14.3 (15) ppm
IR (neat)	3231 (m), 3071 (m), 2953 (m), 2928 (m), 2870 (m), 1466 (m),
LCMS	(ESI$^+$) *m/z* 231.1 $[M+H]^+$
Mpt	168-169 °C (lit: 172 °C)

***N*-(But-3-yn-1-yl)-6-fluoroquinolin-4-amine (2.34)**

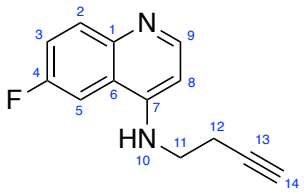

$C_{13}H_{11}FN_2$

MWt: 214.20 $gmol^{-1}$

Following a procedure adapted from Musonda *et al.*,[236] 3-butyn-1-amine (0.91 mL, 11.1 mmol, 5 equiv.) was mixed with 4-bromo-6-fluoroquinoline (500 mg, 2.21 mmol, 1 equiv.) to form a beige paste. The mixture was heated to 80 °C for 1 h without stirring. The temperature was raised to 140 °C and the reaction was left overnight, with stirring. The brown reaction solution was cooled to rt and NaOH (1M, 2 mL) was added. The organic product was basified with 10% NaOH and extracted with CH_2Cl_2 (3 × 15 mL), washed with H_2O and dried ($MgSO_4$). The product was concentrated *in vacuo*. The crude product was purified by column chromatography (Al_2O_3, 10% MeOH in EtOAc). This afforded *N*-(but-3-yn-1-yl)-6-fluoroquinolin-4-amine (465 mg, 2.17 mmol, 98%) as a cream solid.

TLC R_f 0.75 (10% MeOH in EtOAc, Al_2O_3)

^{1}HNMR (400MHz, DMSO-d^6) δ 8.41 (d, *J*=5.1 Hz, 1H, NC**H**), 8.08-7.89 (m, 1H, FCCH**CH**), 7.85 (dd, *J*=9.3, 5.1 Hz, 1H, FC**CH**CH), 7.53 (td, *J*=9.3, 2.8 Hz, 1H, FC**CH**C), 6.54 (d, *J*=5.1 Hz, 1H, NCH**CH**), 3.51-3.42 (m, 2H, **CH$_2$**CH$_2$CCH), 2.90 (t, *J*=2.6 Hz, 1H, CH$_2$CH$_2$C**CH**), 2.56 (td, *J*=7.1, 2.6 Hz, 2H, CH$_2$**CH$_2$**CCH) ppm

^{13}CNMR (101 MHz, DMSO-d^6) δ 159.1 (d, *J*=240 Hz, **4**), 150.2 (**7**), 149.1 (**9**), 140.0 (**1**), 124.6 (**2**), 118.8 (d, *J*=21 Hz, **3**), 113.6 (**6**), 106.3 (d, *J*=25 Hz, **5**), 99.4 (**8**), 82.8 (**14**), 72.9 (**13**), 41.8 (**11**), 18.3 (**12**) ppm

^{19}FNMR (376 MHz, DMSO-d^6) δ 110.0 ppm

IR (neat) ν_{max} 3387 (m), 2830 (m), 663 (s) cm^{-1}

LRMS (ESI$^+$) *m/z* 215.1 $[M+H]^+$

HRMS (ESI$^+$) *m/z calcd. for* $C_{13}H_{11}FN_2$ 215.0979 *m/z meas.* 215.0982 $[M+H]^+$

Mpt 148-150 °C

***N*-(But-3-yn-1-yl)-8-methoxyquinolin-4-amine (2.35)**

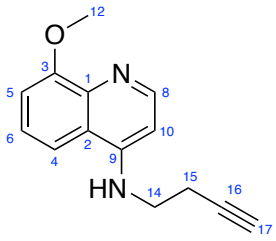

$C_{14}H_{14}N_2O$

MWt: 226.30 $gmol^{-1}$

Following a procedure adapted from Musonda *et al.*,[236] 3-butyn-1-amine (1.20 mL, 14.7 mmol, 5 equiv.) was mixed with 4-bromo-8-methoxyquinoline (700 mg, 2.94 mmol, 1 equiv.) to form a beige paste. The mixture was heated to 80 °C for 1 h without stirring. The temperature was raised to 140 °C and the reaction was left overnight, with stirring. The brown reaction was cooled to rt and 1 M aqueous NaOH (2 mL) was added. The organic product was basified with 10% aqueous NaOH and extracted with CH_2Cl_2 (3 × 15 mL), washed with H_2O and dried ($MgSO_4$). The product was concentrated *in vacuo*. The crude product was purified by column chromatography (Al_2O_3, 10% MeOH in EtOAc). This afforded *N*-(but-3-yn-1-yl)-6-fluoroquinolin-4-amine (652 mg, 2.88 mmol, 98%) as a pale orange solid.

TLC R_f 0.73 (10% MeOH in EtOAc, Al_2O_3)

^{1}HNMR (400MHz, DMSO-d^6) δ 8.36 (d, *J*=5.4 Hz, 1H, NC**H**), 7.73 (d, *J*=7.8 Hz, 1H, MeOCCHCH**CH**), 7.35 (t, *J*=7.8 Hz, 1H, MeOCCH**CH**), 7.10 (d, *J*=7.8 Hz, 1H, OMeC**CH**), 6.55 (d, *J*=5.4 Hz, 1H, NCH**CH**), 3.91 (s, 3H, **OCH_3**), 3.53-3.39 (m, 2H, **CH_2**CH_2CCH), 2.89 (t, *J*=2.6 Hz, 1H, CH_2CH_2C**CH**), 2.56 (td, *J*=7.1, 2.6 Hz, 2H, CH_2**CH_2**CCH) ppm

^{13}CNMR (101 MHz, DMSO-d^6) δ 155.2 (**3**), 149.9 (**9**), 148.8 (**8**), 139.6 (**1**), 124.3 (**4**), 119.6 (**6**), 113.3 (**2**), 108.5 (**5**), 99.1 (**10**), 82.4 (**17**), 72.6 (**16**), 55.8 (**12**), 41.5 (**14**), 18.0 (**15**) ppm

IR (neat) ν_{max} 3279 (m), 2938 (m), 753 (s) cm^{-1}

LRMS (ESI$^+$) *m/z* 227.1 $[M+H]^+$

HRMS (ESI$^+$) *m/z calcd. for* $C_{14}H_{14}N_2O$ *227.1179 m/z meas.* 227.1183 $[M+H]^+$

Mpt 154-155 °C

Methyl 3-(benzyloxy)-6-(4-((6-fluoroquinolin-4-yl)amino)but-1-yn-1-yl) picolinate (2.36)

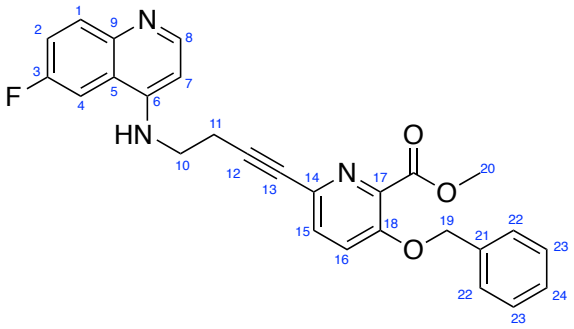

$C_{27}H_{22}FN_3O_3$

MWt: 455.50 $gmol^{-1}$

Following a procedure adapted from de Sousa,[186] to a degassed solution of methyl 3-(benzyloxy)-6-bromopyridine-2-carboxylate (497 mg, 1.54 mmol, 1.1 equiv.) in THF/Et_3N (7 mL/3 mL), tetrakis(triphenylphosphine) palladium (162 mg, 0.14 mmol, 10 mol%) and copper iodide (54.0 mg, 0.28 mmol, 20 mol%) were added. After bubbling the reaction mixture with argon for 5 minutes at rt, a degassed solution of *N*-(but-3-yn-1-yl)-6-fluoroquinolin-4-amine (300 mg, 1.40 mmol, 1 equiv.) in THF (3 mL) was added dropwise and the yellow reaction mixture was stirred for 16 h at rt. Upon consumption of starting materials (TLC) the reaction mixture was concentrated *in vacuo* and purified by column chromatography (SiO_2, EtOAc), affording methyl 3-(benzyloxy)-6-(4-((7-(trifluoromethyl)quinolin-4-yl)amino)but-1-yn-1-yl)picolinate (515 mg, 1.13 mmol, 81%) as a pale yellow solid.

TLC R_f 0.20 (10% MeOH in EtOAc, SiO_2)

^{1}HNMR (400MHz, DMSO-d^6) δ 8.14-8.00 (m, 1H, NC**H**), 7.69 (d, *J*=8.8 Hz, 1H, NCC**H**CHCF), 7.57 (d, *J*=8.8, 1H, NCC**H**), 7.52-7.29 (m, 8H, Ar**H**), 6.61 (m, 1H, NCH**CH**), 5.26 (s, 2H, Ph**CH$_2$**), 3.84 (s, 3H, CO_2**CH$_3$**), 3.61-3.53 (m, 2H, NH**CH$_2$**CH_2), 2.83 (t, *J*=7.0 Hz, 2H, $NHCH_2$**CH$_2$**) ppm

^{13}CNMR (101 MHz, DMSO-d^6) δ 165.2 (**19**), 160.3 (**18**), 159.1 (d, *J*=240 Hz, **3**), 152.5 (**6**), 150.7 (**9**), 149.7 (**8**), 140.6 (**17**), 136.5 (**14**), 134.3 (**22**), 130.4 (**15**), 129.0 (**5**), 127.7 (**24**), 123.0 (**16**), 119.0 (**2**), 118.7 (**23**), 106.4 (**4**), 106.1 (**7**), 88.0 (**12**), 80.8 (**13**), 70.4 (**21**), 52.8 (**20**), 41.7 (**10**), 19.0 (**11**) ppm

^{19}FNMR (376 MHz, DMSO-d^6) δ 115.9 ppm

IR (neat) ν_{max} 3255 (m), 2951 (m), 1725 (s), 721 (s) cm^{-1}

LRMS (ESI$^+$) *m/z* 456.2 $[M+H]^+$

HRMS (ESI$^+$) *m/z calcd. for* $C_{27}H_{22}FN_3O_3$ 456.1718 *m/z meas.* 456.1720 $[M+H]^+$

Mpt 156-157 °C

Methyl 3-(benzyloxy)-6-(4-((8-methoxyquinolin-4-yl)amino)but-1-yn-1-yl) picolinate (2.37)

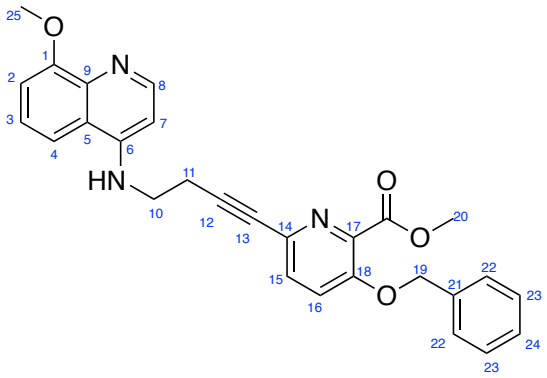

$C_{28}H_{25}N_3O_4$

MWt: 467.50 $gmol^{-1}$

Following a procedure adapted from de Sousa,[186] to a degassed solution of methyl 3-(benzyloxy)-6-bromopyridine-2-carboxylate (392 mg, 1.22 mmol, 1.1 equiv.) in THF/Et_3N (7 mL/3 mL), tetrakis(triphenylphosphine) palladium (128 mg, 0.11 mmol, 10 mol%) and copper iodide (42.0 mg, 0.22 mmol, 20 mol%) were added. After bubbling the reaction mixture with argon for 5 minutes at rt, a degassed solution of *N*-(But-3-yn-1-yl)-8-methoxyquinolin-4-amine (250 mg, 1.10 mmol, 1 equiv.) in THF (3 mL) was added dropwise and the yellow reaction mixture was stirred for 16 h at rt. Upon consumption of starting materials (TLC) the reaction mixture was concentrated *in vacuo* and purified by column chromatography (SiO_2, EtOAc), affording methyl 3-(benzyloxy)-6-(4-((7-(trifluoromethyl)quinolin-4-yl)amino)but-1-yn-1-yl)picolinate (515 mg, 1.13 mmol, 78%) as a dark yellow solid.

TLC R_f 0.80 (10% MeOH in EtOAc, Al_2O_3)

^{1}HNMR (400MHz, DMSO-d^6) δ 8.36 (br. d, *J*=5.1 Hz, 1H, NC**H**), 7.81-7.67 (m, 2H, NCC**CH**), 7.57 (d, *J*=7.6, 1H, NCC**CH**), 7.47-7.28 (m, 7H, Ar**H**), 7.08 (br. d, *J*=7.6 Hz, 1H, MeOC**CH**), 6.60 (br. d, *J*=5.1 Hz, 2H, NCH**CH**) 5.26 (s, 2H, Ph**CH_2**), 3.90 (s, 3H, CO_2**CH_3**), 3.84 (s, 3H, **OCH_3**), 3.60-3.50 (m, 2H, NH**CH_2**CH_2), 2.82 (br. t, *J*=7.1 Hz, 2H, NHCH_2**CH_2**) ppm

^{13}CNMR (101 MHz, DMSO-d^6) δ 165.2 (**19**), 152.6 (**1**), 141.4 (**18**), 136.6 (**6**), 134.8 (**8**), 132.3 (**17**), 132.0 (**22**), 131.9 (**14**), 130.1 (**9**), 129.1 (**4**), 129.0 (**24**), 128.9 (**5**), 128.4 (**15**), 127.7 (**16**), 126.0 (**23**), 123.4 (**3**), 111.6 (**2**), 101.2 (**7**), 88.0 (**12**), 81.4 (**13**), 71.2 (**21**), 57.0 (**25**), 52.5 (**20**), 42.3 (**10**), 19.3 (**11**) ppm

IR (neat) ν_{max} 2945 (m), 1722 (s), 695 (s) cm^{-1}

LRMS (ESI$^+$) *m/z* 468.2 $[M+H]^+$

HRMS (ESI$^+$) *m/z calcd. for* $C_{28}H_{25}N_3O_4$ 468.1931 *m/z meas.* 468.1930 $[M+H]^+$

Mpt 181-183 °C

Methyl 6-(4-((6-fluoroquinolin-4-yl)amino)butyl)-3-hydroxypicolinate (2.38)

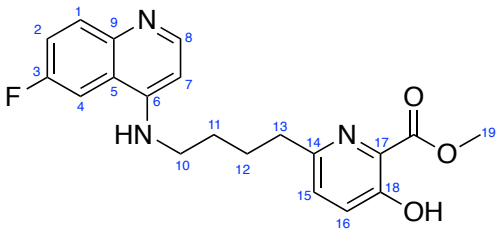

$C_{20}H_{20}FN_3O_3$

MWt: 369.40 $gmol^{-1}$

Following a procedure adapted from de Sousa,[186] to a degassed solution of methyl 3-(benzyloxy)-6-(4-((6-fluoroquinolin-4-yl)amino)but-1-yn-1-yl) picolinate (200 mg, 0.44 mmol, 1 equiv.) in anhydrous MeOH (25 mL), Pearlman's catalyst (13.0 mg, 0.08 mmol, 20 mol%) was added. After evacuating and flushing with H_2 five times, the black reaction mixture was stirred at rt under H_2 for 16 h. Upon consumption of starting materials (TLC) the catalyst was removed by filtration through Celite and the solvent was removed *in vacuo*. Methyl 6-{4-[(6-fluoroquinolin-4-yl)amino]butyl}-3-hydroxypyridine-2-carboxylate (160 mg, 0.43 mmol, 99 %) was obtained as a cream solid.

TLC R_f 0.14 (10% MeOH in EtOAc, Al_2O_3)

^{1}HNMR (400MHz, DMSO-d^6) δ 8.35 (d, *J*=5.4 Hz, 1H, NC**H**), 8.05 (dd, *J*=11.1, 5.9 Hz, 1H, NCC**H**), 7.81 (dd, *J*=8.7, 5.9 Hz, 2H, FC**C**H**C**H), 7.49 (td, *J*=11.1, 8.7 Hz, 1H, FCC**H**), 7.40-7.28 (m, 2H, NC**C**H**C**H**C**OH), 6.44 (d, *J*=5.4 Hz, 1H, NCH**CH**), 3.85 (s, 3H, CO2**CH$_3$**), 3.30-3.27 (m, 2H, HN**CH$_2$**CH$_2$CH$_2$CH$_2$), 2.78-2.67 (m, 2H, NHCH$_2$CH$_2$CH$_2$**CH$_2$**), 1.83-1.68 (m, 4H, NHCH$_2$**CH$_2$CH$_2$**CH$_2$) ppm

^{13}CNMR (101 MHz, DMSO-d^6) δ 169.2 (**19**), 159.4 (d, *J*=242 Hz, **3**), 158.2 (**14**), 157.2 (**18**), 153.2 (**6**), 150.9 (**8**), 144.5 (**9**), 130.0 (**17**), 129.0 (**15**), 127.1 (**1**), 124.7 (**16**), 118.6 (**2**), 105.2 (**5**), 105.0 (**4**), 98.0 (**7**), 51.8 (**20**), 42.3 (**10**), 35.9 (**13**), 29.3 (**11**), 27.3 (**12**) ppm

^{19}FNMR (376 MHz, DMSO-d^6) δ 116.4 ppm

IR (neat) ν_{max} 3240 (m), 2951 (m), 2860 (m), 2361 (s), 2342 (s), 1674 (s), 719 (s) cm^{-1}

LRMS (ESI$^+$) *m/z* 370.2 $[M+H]^+$

HRMS (ESI$^+$) *m/z calcd. for* $C_{20}H_{20}FN_3O_3^+$ 370.1561 *m/z meas.* 370.1568 $[M+H]^+$

Mpt 155-157 °C

Methyl 6-(4-((8-methoxyquinolin-4-yl)amino)butyl)-3-hydroxypicolinate (2.39)

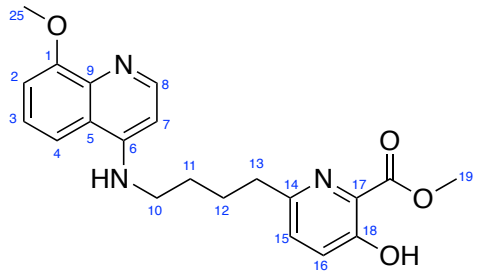

$C_{21}H_{23}N_3O_4$

MWt: 381.40 $gmol^{-1}$

Following a procedure adapted from de Sousa,[186] to a degassed solution of methyl 3-(benzyloxy)-6-(4-((8-methoxyquinolin-4-yl)amino)but-1-yn-1-yl) picolinate (200 mg, 0.43 mmol, 1 equiv.) in anhydrous MeOH (25 mL), Pearlman's catalyst (13.0 mg, 0.08 mmol, 20 mol%) was added. After evacuating and flushing with H_2 five times, the black reaction mixture was stirred at rt under H_2 for 16 h. Upon completion, the catalyst was removed by filtration through Celite and the solvent was removed *in vacuo*. Methyl 6-{4-[(6-fluoroquinolin-4-yl)amino]butyl}-3-hydroxypyridine-2-carboxylate (163 mg, 0.43 mmol, 100 %) was obtained as a cream solid.

TLC R_f 0.13 (20% MeOH in EtOAc, Al_2O_3)

^{1}HNMR (400MHz, $CDCl_3$) δ 8.50 (br. d, *J*=5.9 Hz, 1H, NC**H**), 7.41-7.23 (m, 4H, Ar**H**), 7.00 (d, *J*=7.8, 1H, MeOC**CH**), 6.42 (br. d, *J*=5.9 Hz, 1H, NCH**CH**), 3.98 (s, 3H, CO_2**CH_3**), 3.97 (s, 3H, **OMe**), 3.42 (br. s, 2H, NH**CH_2**CH_2CH_2), 2.88 (t, *J*=7.2 Hz, 2H, $NHCH_2CH_2$**CH_2**), 1.92-1.79 (m, 4H, NH**CH_2CH_2**CH_2) ppm

^{13}CNMR (101 MHz, $CDCl_3$) δ 169.9 (**19**), 157.2 (**14**), 153.5 (**18**), 153.2 (**1**), 151.6 (**6**), 146.7 (**8**), 136.5 (**9**), 129.3 (**4**), 128.7 (**17**), 126.9 (**15**), 125.1 (**16**), 119.0 (**3**), 112.6 (**5**), 108.6 (**2**), 98.6 (**7**), 55.9 (**25**), 53.0 (**20**), 43.3 (**10**), 36.7 (**13**), 27.6 (**12**), 27.5 (**11**) ppm

IR (neat) ν_{max} 2927 (m), 2359 (m), 1675 (s), 725 (s) cm^{-1}

LRMS (ESI$^+$) *m/z* 382.4 $[M+H]^+$

HRMS (ESI$^+$) *m/z calcd. for* $C_{21}H_{23}N_3O_4$ 382.1775 *m/z meas.* 382.1771 $[M+H]^+$

Mpt 156-159 °C

(*E*)-6-(4-((6-Fluoroquinolin-4-yl)amino)butyl)-3-hydroxypicolinaldehyde oxime (2.6)

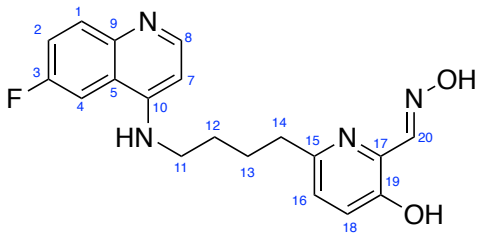

Mol. Wt. 354.4 $gmol^{-1}$

$C_{19}H_{19}FN_4O_2$

Following a procedure adapted from de Sousa,[186] to a degassed solution of methyl 6-(4-((6-fluoroquinolin-4-yl)amino)butyl)-3-hydroxypicolinate (100 mg, 0.27 mmol, 1 equiv.) in anhydrous CH_2Cl_2 (5 mL), was added 2,6-lutidine (0.09 mL, 0.81 mmol, 3 equiv.) and TBSOTf (0.12 mL, 0.54 mmol, 2 equiv.) successively and the pale yellow reaction solution was stirred at rt for 5 h under argon. The reaction mixture was concentrated *in vacuo*. To a solution of the residue in anhydrous CH_2Cl_2 (5 mL) at −78 °C was added DIBAL-H (1 M in CH_2Cl_2) (0.81 mL, 0.81 mmol, 3 equiv.) dropwise. The colourless reaction solution was stirred at −78 °C for 1 h and the reaction was quenched at −78 °C with MeOH (3 mL). The mixture was warmed to rt and the solvent was removed *in vacuo*. The white aluminium salts were removed by filtration in CH_2Cl_2. The colourless filtrate was concentrated *in vacuo* and the residue was dissolved in anhydrous EtOH (7 mL). Hydroxylamine hydrochloride (37.6 mg, 0.54 mmol, 2 equiv.) and sodium acetate (44.4 mg, 0.54 mmol, 2 equiv.) were added and the pale yellow solution was stirred at reflux for 16 h. After concentration *in vacuo*, the crude product was washed with CH_2Cl_2 (3 × 5 mL). The crude product was purified by column chromatography (SiO_2, 10% MeOH in CH_2Cl_2) to afford (*E*)-6-(4-((6-fluoroquinolin-4-yl)amino)butyl)-3-hydroxypicolinaldehyde oxime (80.0 mg, 0.27 mmol, 90%) as a beige solid.

(*E*)-6-(4-((6-Fluoroquinolin-4-yl)amino)butyl)-3-hydroxypicolinaldehyde oxime (10.0 mg, 0.03 mmol) was dissolved in 2 M HCl (3 mL). The colourless solution was stirred at rt for 10 mins. The reaction solution was concentrated *in vacuo* to afford (*E*)-6-(4-((6-fluoroquinolin-4-yl)amino)butyl)-3-hydroxypicolinaldehyde oxime hydrochloride (11.7 mg, 0.03 mmol, 100%) as a colourless solid.

TLC R_f 0.19 (10% MeOH in CH_2Cl_2, SiO_2)

^{1}HNMR (400MHz, MeOH-d^4) δ 8.33 (d, *J*=6.6 Hz, 1H, NC**H**), 8.21 (s, 2H, **CH_2**NOH), 8.05 (dd, *J*=10.3, 2.7 Hz, 1H, NC**C**H), 7.88 (dd, *J*=10.3, 5.0 Hz, 1H, FC**C**H**C**), 7.67 (m, 1H, FC**C**H**C**H), 7.30-7.09 (m, 2H, NC**C**H**C**H), 6.71 (d, *J*=6.6 Hz, 1H, NCH**C**H), 3.56-3.47 (m, 2H, NH**CH_2**CH_2), 2.80 (t, *J*=7.1 Hz, 2H, NHCH_2CH_2CH_2**CH_2**), 1.96-1.75 (m, 4H, NHCH_2**CH_2CH_2**CH_2) ppm

^{13}CNMR	(101 MHz, MeOH-d^4) δ 163.2 (**19**), 160.6 (d, *J*=220 Hz, **3**), 156.4 (**15**), 154.5 (**8**), 154.1 (**10**), 153.0 (**20**), 144.9 (**9**), 136.6 (**17**), 126.8 (**1**), 125.9 (**18**), 123.6 (**16**), 120.5 (**2**), 117.3 (**5**), 108.3 (**4**), 99.6 (**7**), 44.7 (**11**), 37.5 (**14**), 28.6 (**13**), 28.5 (**12**) ppm
^{19}FNMR	(376 MHz, MeOH-d^4) δ 79.6 ppm
IR (neat)	ν_{max} 3673 (br), 1602 (s), 1033 (s) cm^{-1}
LRMS	(ESI^+) *m/z* 355.3 $[M+H]^+$
HRMS	(ESI^+) *m/z calcd. for* $C_{19}H_{19}FN_4O_2$ 355.1561 *m/z meas.* 355.1561 $[M+H]^+$
Mpt	157-159 °C

(*E*)-3-Hydroxy-6-(4-((8-methoxyquinolin-4-yl)amino)butyl) picolinaldehyde oxime (2.7)

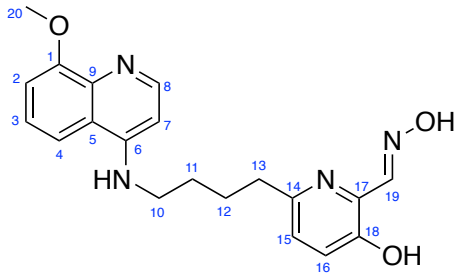

$C_{20}H_{22}N_4O_3$

Mol. Wt. 366.4 $gmol^{-1}$

Following a procedure adapted from de Sousa,[186] to a degassed solution of methyl 6-(4-((8-methoxyquinolin-4-yl)amino)butyl)-3-hydroxypicolinate (50 mg, 0.13 mmol, 1 equiv.) in anhydrous CH_2Cl_2 (5 mL), was added 2,6-lutidine (0.05 mL, 0.39 mmol, 3 equiv.) and TBSOTf (0.06 mL, 0.26 mmol, 2 equiv.) successively and the pale yellow reaction solution was stirred at rt for 5 h under argon. The reaction mixture was concentrated *in vacuo*. To a solution of the residue in anhydrous CH_2Cl_2 (5 mL) at −78 °C was added DIBAL-H (1 M in CH_2Cl_2) (0.40 mL, 0.40 mmol, 3 equiv.) dropwise. The reaction was stirred at −78 °C for 1 h and the reaction was quenched at −78 °C with MeOH (3 mL). The mixture was warmed to rt and the solvent was removed in vacuo. The white aluminium salts were removed by filtration in CH_2Cl_2. The filtrate was concentrated *in vacuo* and the residue was dissolved in anhydrous EtOH (7 mL). Hydroxylamine hydrochloride (18.0 mg, 0.26 mmol, 2 equiv.) and sodium acetate (22.0 mg, 0.26 mmol, 2 equiv.) were added and the colourless solution was stirred at reflux for 16 h. After concentration in vacuo, the crude product was washed with CH_2Cl_2 (3 × 5 mL). The crude product was purified by column chromatography (SiO_2, 10% MeOH in CH_2Cl_2) to afford (*E*)-3-hydroxy-6-(4-((8-methoxyquinolin-4-yl)amino)butyl) picolinaldehyde oxime (40.0 mg, 0.11 mmol, 83%) as a colourless solid.

(*E*)-3-Hydroxy-6-(4-((8-methoxyquinolin-4-yl)amino)butyl) picolinaldehyde oxime (10 mg, 0.03 mmol) was dissolved in 2 M HCl (3 mL). The colourless solution was stirred at rt for 10 mins. The reaction solution was concentrated *in vacuo* to afford (*E*)-3-hydroxy-6-(4-((8-methoxyquinolin-4-yl)amino)butyl) picolinaldehyde oxime hydrochloride (12.1 mg, 0.03 mmol, 100%) as a colourless solid.

TLC R_f 0.19 (10% MeOH in CH_2Cl_2, SiO_2)

^{1}HNMR (400MHz, MeOH-d^4) δ 8.16 (d, *J*=7.3 Hz, 1H, NC**H**), 8.10 (s, 2H, **CH_2**NOH), 7.78 (d, *J*=8.3 Hz, 1H, **C**HCOMe), 7.54 (t, *J*=8.3 Hz, 1H, **C**HCHCOMe), 7.38 (d, *J*=7.6 Hz, 1H, **C**HCHCHCOMe), 7.21-7.07 (m, 2H, NC**CHCH**), 6.76 (d, *J*=7.3 Hz, 1H, NCH**CH**), 4.07 (s, 3H, O**Me**), 3.54 (t, *J*=7.1 Hz, 2H, NH**CH_2**CH_2), 2.74 (t, *J*=7.1 Hz, 2H, NHCH_2CH_2CH_2**CH_2**), 1.88-1.73 (m, 4H, NHCH_2**CH_2CH_2**CH_2) ppm

^{13}CNMR	(101 MHz, MeOH-d^4) δ 157.4 (**1**), 154.2 (**19**), 153.9 (**6**), 152.8 (**14**), 151.1 (**18**), 142.1 (**8**), 136.4 (**17**), 128.5 (**9**), 126.1 (**15**), 125.7 (**16**), 123.5 (**3**), 120.3 (**2**), 114.6 (**5**), 113.3 (**4**), 99.7 (**7**), 57.4 (**20**), 44.5 (**10**), 37.3 (**13**), 28.3 (**12**), 28.5 (**11**) ppm
IR (neat)	ν_{max} 3451 (br), 1621 (s), 1043 (s) cm^{-1}
LRMS	(ESI$^+$) *m/z* 367.3 $[M+H]^+$
HRMS	(ESI$^+$) *m/z calcd. for* $C_{20}H_{22}N_4O_3$ 367.1765 *meas.* 367.1765 $[M+H]^+$
Mpt	157-159 °C

4-Bromo-7-(trifluoromethyl)quinoline (2.54)

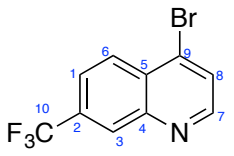

Mol. Wt. 276.1 $gmol^{-1}$

$C_{10}H_5BrF_3N$

Following a procedure adapted from Franzblau *et al.*,[234] to a solution of a mixture of 5-(trifluoromethyl)quinolin-4-ol (100 mg, 0.47 mmol, 0.05 equiv.) and 7-(trifluoromethyl)quinolin-4-ol (1.90 g, 8.91 mmol, 1 equiv.) in DMF (20 mL) at 60 °C was added phosphorus tribromide (0.97 mL, 10.3 mmol, 1.2 equiv.). The beige mixture was cooled to 45 °C for 45 min. After cooling to rt, the reaction was diluted with H_2O (10 mL) and the beige solution was basified to pH 10 with saturated aqueous $NaHCO_3$. The resulting solid was washed in H_2O, filtered and taken up in EtOAc and concentrated *in vacuo*, to afford a mixture, which was purified with column chromatography (SiO_2, EtOAc) to afford 4-bromo-7-(trifluoromethyl)quinoline (2.19 g, 7.93 mmol, 85%) as a colourless solid.

TLC R_f 0.73 (EtOAc, SiO_2)

^{1}HNMR (400MHz, DMSO-d^6) δ 8.87 (d, *J*=4.6 Hz, 1H, NC**H**), 8.41 (s, 1H, CF_3C**C**HC), 8.34 (d, *J*=8.8 Hz, 1H, CF_3C**C**HCH), 8.12 (d, *J*=4.6 Hz, 1H, NCH**C**H), 8.01 (d, *J*=8.8 Hz, 1H, CF_3CCH**C**H) ppm

^{13}CNMR (101 MHz, DMSO-d^6) δ 152.5 (**7**), 147.5 (**4**), 133.3 (**2**), 130.7 (**9**), 129.1 (**5**), 128.8 (**8**), 127.8 (**6**), 126.5 (q, *J*=254 Hz, **10**), 123.8 (**1**), 123.7 (**3**) ppm

^{19}FNMR (376 MHz, DMSO-d^6) δ 61.0 ppm

IR (neat) ν_{max} 2989 (br), 1287 (s), 1059 (s) cm^{-1}

LRMS (ESI^+) *m/z* 276.1 $[M^{79}Br+H]^+$, 277.9 $[M^{81}Br+H]^+$

HRMS (ESI^+) *m/z calcd. for* $C_{10}H_5BrF_3N$ 275.9634 *m/z meas.* 275.9636 $[M+H]^+$

Mpt 77-78 °C (lit: 72-73 °C)

***N*-(But-3-yn-1-yl)-7-(trifluoromethyl)quinolin-4-amine (2.55)**

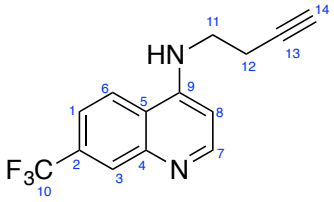

Mol. Wt. 264.1 $gmol^{-1}$

$C_{14}H_{11}F_3N_2$

Following a procedure adapted from Musonda *et al.*,[236] 3-butyn-1-amine (1.48 mL, 18.1 mmol, 5 equiv.) was mixed with 4-bromo-7-(trifluoromethyl)quinoline (1.00 g, 3.62 mmol, 1 equiv.) to form a paste. The paste was heated to 80 °C for 1 h without stirring. The temperature was then raised to 140 °C and the beige reaction was stirred overnight. The reaction was cooled to rt and 1 M aqueous NaOH (2 mL) was added. The organic product was basified with 10% aqueous NaOH and was extracted with CH_2Cl_2 (3 × 15 mL). The organic layers were combined, washed, dried ($MgSO_4$), filtered and concentrated *in vacuo*. The crude product was purified by column chromatography (SiO_2, EtOAc), affording *N*-(but-3-yn-1-yl)-7-(trifluoromethyl)quinolin-4-amine (900 mg, 3.41 mmol, 94%) as a cream solid.

TLC R_f 0.65 (EtOAc, SiO_2)

^{1}HNMR (400MHz, DMSO-d^6) δ 8.52 (d, *J*=5.4 Hz, 1H, NC**H**), 8.09 (s, 1H, CF_3C**C**H**C**), 7.70 (dd, *J*=8.8, 2.0 Hz, 1H, CF_3CCH**CH**), 7.58 (t, *J*=5.4 Hz, 1H, CF_3C**C**H**C**H), 6.64 (d, *J*=5.4 Hz, 1H, NCH**CH**), 3.43-3.52 (m, 2H, **C**$H_2$$CH_2$CCH), 2.89 (t, *J*=2.6 Hz, 1H, CH_2CH_2C**C**H), 2.57 (td, *J*=7.2, 2.6 Hz, 2H, CH_2CH_2CCH) ppm

^{13}CNMR (101 MHz, DMSO-d^6) δ 152.3 (**7**), 149.5 (**9**), 147.5 (**4**), 128.9 (**2**), 126.4 (**5**), 125.5 (q, *J*=250 Hz, **10**), 123.8 (**6**), 120.8 (**3**), 119.0 (**1**), 99.9 (**8**), 82.2 (**13**), 72.5 (**14**), 41.3 (**11**), 17.6 (**12**) ppm

^{19}FNMR (376 MHz, DMSO-d^6) δ 60.9 ppm

IR (neat) ν_{max} 3318 (m), 3077 (m), 738 (s) cm^{-1}

LRMS (ESI$^+$) *m/z* 265.2 $[M+H]^+$

HRMS (ESI$^+$) *m/z calcd. for* $C_{14}H_{11}F_3N_2$ 265.0945 *m/z meas.* 265.0945 $[M+H]^+$

Mpt 121-123 °C

Methyl 3-(benzyloxy)-6-(4-((7-(trifluoromethyl)quinolin-4-yl)amino)but-1-yn-1-yl) picolinate (2.56)

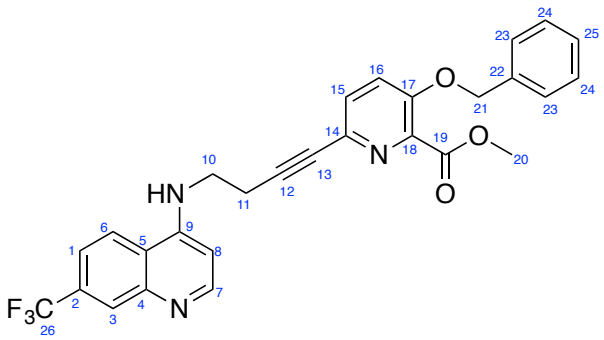

Mol. Wt. 505.5 gmol^{-1}

$C_{28}H_{22}F_3N_3O_3$

Following a procedure adapted from de Sousa,[186] to a degassed solution of methyl 3-(benzyloxy)-6-bromopyridine-2-carboxylate (671 mg, 2.08 mmol, 1.1 equiv.) in THF/Et_3N (7 mL/3 mL), tetrakis(triphenylphosphine) palladium (219 mg, 0.19 mmol, 10 mol%) and copper iodide (72.0 mg, 0.38 mmol, 20 mol%) were added. After bubbling the reaction mixture with argon for 5 minutes at rt, a degassed solution of N-(but-3-yn-1-yl)-7-(trifluoromethyl)quinolin-4-amine (500 mg, 1.89 mmol, 1 equiv.) in THF (3 mL) was added dropwise and the yellow reaction mixture was stirred for 16 h at rt. Upon consumption of starting materials (TLC) the reaction mixture was concentrated *in vacuo* and purified by column chromatography (SiO_2, EtOAc), affording methyl 3-(benzyloxy)-6-(4-((7-(trifluoromethyl)quinolin-4-yl)amino)but-1-yn-1-yl)picolinate (740 mg, 1.46 mmol, 77%) as pale orange/cream solid.

TLC R_f 0.27 (EtOAc, SiO_2)

^{1}HNMR (400MHz, $CDCl_3$) δ 8.65 (d, *J*=5.4 Hz, 1H, NC**H**), 8.28 (s, 1H, CF_3C**C**HC), 7.93 (d, *J*=8.8 Hz, 1H, CF_3CCH**C**H), 7.58 (d, *J*=8.8 Hz, 1H, CF_3C**C**HCH), 7.47-7.22 (m, 7H, Ar**H**), 6.54 (d, *J*=5.4 Hz, 1H, NCH**C**H), 5.21 (s, 2H, Ph**C**H_2O), 3.97 (s, 3H, CO_2**C**H_3), 3.61 (q, *J*=6.6 Hz, 2H, **C**H_2CH_2C), 2.88 (t, *J*=6.6 Hz, 1H, CH_2**C**H_2C) ppm

^{13}CNMR (101 MHz, $CDCl_3$) δ 164.8 (**19**), 153.3 (**17**), 152.3 (**7**), 149.1 (**9**), 147.8 (**4**), 140.4 (**18**), 135.3 (**22**), 134.5 (**14**), 131.1 (**2**), 130.8 (**1**), 130.0 (**15**), 128.8 (**23**), 128.3 (**24**) 127.8 (**25**), 126.9 (**6**), 125.3 (**5**), 121.8 (**16**), 121.0 (**3**), 120.4 (q, *J*=260 Hz, **26**), 100.3 (**8**), 86.0 (**12**), 81.7 (**13**), 70.9 (**21**), 52.8 (**20**), 41.4 (**10**), 19.6 (**11**) ppm

^{19}FNMR (376 MHz, $CDCl_3$) δ 63.0

IR (neat) ν_{max} 3205 (m), 2953 (m), 777 (s) cm^{-1}

LRMS (ESI$^+$) *m/z* 506.4 $[M+H]^+$

HRMS (ESI$^+$) *m/z calcd. for* $C_{28}H_{22}F_3N_3O_3$ 506.1686 *m/z meas.* 506.1688 $[M+H]^+$

Mpt 151-153 °C

Methyl 3-hydroxy-6-(4-((7-(trifluoromethyl)quinolin-4-yl)amino)butyl)picolinate

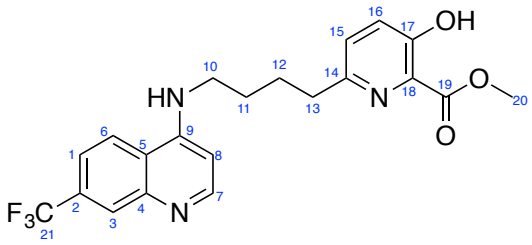

Mol. Wt. 419.4 gmol^{-1}

$C_{21}H_{20}F_3N_3O_3$

Following a procedure adapted from de Sousa,[186] to a degassed solution of methyl 3-(benzyloxy)-6-(4-((7-(trifluoromethyl)quinolin-4-yl)amino)but-1-yn-1-yl)picolinate (550 mg, 1.09 mmol, 1 equiv.) in anhydrous MeOH (40 mL), was added Pearlman's catalyst (30.0 mg, 0.38 mmol, 20 mol%). After evacuating and flushing with H_2 five times, the black reaction mixture was stirred at rt, under a H_2 atmosphere for 7 h. Upon completion, the catalyst was removed by filtration through Celite and the solvent was removed *in vacuo*, affording methyl 3-hydroxy-6-(4-((7-(trifluoromethyl)quinolin-4-yl)amino)butyl)picolinate (456 mg, 1.09 mmol, 100%) as a pale cream solid.

TLC R_f 0.22 (EtOAc, SiO_2)

^{1}HNMR (400MHz, MeOH-d^4) δ 8.30 (d, *J*=8.6 Hz, 1H, NC**H**), 8.07 (s, 1H, CF_3C**C**H**C**), 7.68-7.51 (m, 2H, CF_3C**C**H**CH**), 7.41 (d, *J*=1.0 Hz, 1H, NC**H**CH), 7.34 (d, *J*=1.0 Hz, 1H, NCH**CH**), 6.57 (d, *J*=8.6 Hz, 1H, NCH**CH**), 3.97 (s, 3H, CO_2**C**H_3), 3.41 (t, *J*=7.0 Hz, 2H, NH**C**$H_2$$CH_2CH_2CH_2$), 2.83 (t, *J*=7.0 Hz, 2H, $NHCH_2CH_2CH_2$**C**H_2), 2.57 (m, 4H, $NHCH_2$**C**H_2**C**H_2CH) ppm

^{13}CNMR (101 MHz, MeOD-d_4) δ 166.9 (**19**), 154.9 (**17**), 154.1 (**9**), 153.8 (**14**), 152.6 (**7**), 148.5 (**4**), 138.7 (**6**), 136.3 (**18**), 133.7 (**2**), 126.0 (q, *J*=240 Hz, **21**), 125.4 (**16**), 125.1 (**15**), 123.6 (**5**), 122.5 (**1**), 122.0 (**3**), 100.5 (**8**), 49.8 (**20**), 44.2 (**10**), 37.2 (**13**), 28.3 (**11, 12**) ppm

^{19}FNMR (376 MHz, MeOH-d^4) δ 63.9

IR (neat) ν_{max} 3222 (m), 2953 (m), 738 (s) cm^{-1}

LRMS (ESI$^+$) *m/z* 420.3 $[M+H]^+$

HRMS (ESI$^+$) *m/z calcd. for* $C_{21}H_{20}F_3N_3O_3$ 420.1534 *m/z meas.* 420.1535 $[M+H]^+$

Mpt 76-79 °C

(*E*)-3-Hydroxy-6-(4-((7-(trifluoromethyl)quinolin-4-yl)amino)butyl)picolinaldehyde oxime (2.46)

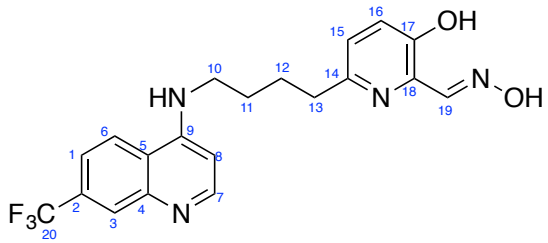

Mol. Wt. 404.1 gmol^{-1}

$C_{20}H_{19}F_3N_4O_2$

Following a procedure adapted from de Sousa,[186] To a degassed solution of methyl 3-hydroxy-6-(4-((7-(trifluoromethyl)quinolin-4-yl)amino)butyl)picolinate (150 mg, 0.36 mmol, 1 equiv.) in anhydrous CH_2Cl_2 (7.5 mL), was added 2,6-lutidine (0.13 mL, 1.07 mmol, 3 equiv.) and TBSOTf (0.16 mL, 0.72 mmol, 2 equiv.) successively and the pale yellow reaction solution was stirred at rt for 5 h under argon. The reaction mixture was concentrated *in vacuo*. To a solution of the residue in anhydrous CH_2Cl_2 (7.5 mL) at −78 °C was added DIBAL-H (1 M in CH_2Cl_2) (1.07 mL, 1.07 mmol, 3 equiv.) dropwise. The colourless reaction solution was stirred at −78 °C for 1 h and the reaction was quenched at −78 °C with MeOH (5 mL). The mixture was warmed to rt and the solvent was removed *in vacuo*. The white aluminium salts were removed by filtration in CH_2Cl_2. The filtrate was concentrated *in vacuo* and the residue was dissolved in anhydrous EtOH (10 mL). Hydroxylamine hydrochloride (49.7 mg, 0.72 mmol, 2 equiv.) and sodium acetate (59 mg, 0.72 mmol, 2 equiv.) were added and the beige solution was stirred at reflux for 16 h. After concentration *in vacuo*, the crude product was washed with CH_2Cl_2 (3 × 5 mL). The solution was concentrated *in vacuo* to afford ((*E*)-3-hydroxy-6-(4-((7-(trifluoromethyl)quinolin-4-yl)amino)butyl) picolinaldehyde oxime with good level of purity (100 mg, 0.25 mmol, 67%) as a cream solid.

((*E*)-3-Hydroxy-6-(4-((7-(trifluoromethyl)quinolin-4-yl)amino)butyl) picolinaldehyde oxime (20.0 mg, 0.04 mmol) was dissolved in 2 M HCl (3 mL). The colourless solution was stirred at rt for 10 mins. The reaction solution was concentrated *in vacuo* to afford ((*E*)-3-hydroxy-6-(4-((7-(trifluoromethyl)quinolin-4-yl)amino)butyl) picolinaldehyde oxime hydrochloride (16.2 mg, 0.04 mmol, 100%) as a colourless solid.

TLC R_f 0.19 (10% MeOH in CH_2Cl_2, SiO_2)

^{1}HNMR (400MHz, MeOH-d^4) δ 8.54 (d, *J*=8.8 Hz, 1H, CF_3CCHCH), 8.45 (d, *J*=6.8 Hz, 1H, NCH), 8.19 (s, 1H, CF_3CCHC), 8.15 (s, 1H, CH2NOH), 7.84 (dd, *J*=8.8, 1.7 Hz, 1H, CF_3CCHCH), 7.27-7.14 (m, 2H, NCCHCH), 6.83 (d, *J*=6.8 Hz, 1H, NCHCH), 3.36-3.56 (m, 2H, $NHCH_2CH_2$), 2.86-2.75 (m, 2H,

$NHCH_2CH_2CH_2\mathbf{CH_2}$), 1.78-1.94 (m, 4H, $NHCH_2\mathbf{CH_2}\mathbf{CH_2}CH_2$) ppm

^{13}CNMR (101 MHz, MeOH-d^4) δ 156.3 (**14**), 154.3 (**9**), 153.9 (**19**), 146.6 (**7**), 141.5 (**4**), 136.5 (**17**), 134.7 (**18**), 131.7 (**2**), 126.2 (**15**), 125.8 (**6**), 125.7 (**16**), 123.5 (**5**), 122.9 (**1**), 121.0 (**3**), 120.3 (q, *J*=262 Hz, **20**), 100.7 (**8**), 44.6 (**10**), 37.3 (**13**), 28.4 (**11**), 28.3 (**12**) ppm

^{19}FNMR (376 MHz, MeOH-d^4) 64.2

IR (neat) ν_{max} 3224 (br), 1603 (s), 1013 (s) cm^{-1}

LRMS (ESI^+) *m/z* 405.4 $[M+H]^+$

HRMS (ESI^+) *m/z calcd. for* $C_{20}H_{19}F_3N_4O_2$ 405.1531 *m/z meas.* 405.1531 $[M+H]^+$

Mpt 193-195 °C

4-Bromo-5-chloroquinoline (2.60)

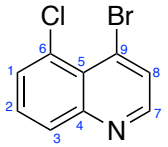

Mol. Wt. 242.5 $gmol^{-1}$

C_9H_5BrClN

Following a procedure adapted from Franzblau *et al.*,[234] to a solution of a mixture of 5-chloroquinolin-4-ol (0.6 g, 3.34, 1 equiv.) and 7-chloroquinolin-4-ol (0.6 g, 3.34 mmol, 1 equiv.) in DMF (10 mL) at 60 °C was added phosphorus tribromide (0.36 mL, 3.84 mmol, 1.2 equiv.). The beige mixture was cooled to 45 °C for 45 min. After cooling to rt, the reaction was diluted with H_2O (10 mL) and the solution was basified to pH 10 with saturated aqueous $NaHCO_3$. The resulting orange solid was washed in H_2O, filtered and taken up in EtOAc and concentrated *in vacuo*, to afford a mixture, which was purified with column chromatography (SiO_2, 25% EtOAc in hexanes) to afford 4-bromo-5-chloroquinoline (0.95 g, 3.92 mmol, 59%) as an orange solid.

TLC R_f 0.50 (25% EtOAc in hexanes, SiO_2)

^{1}HNMR (400MHz, DMSO-d^6) δ 8.76 (d, *J*=4.6 Hz, 1H, NC**H**), 8.22-8.13 (m, 2H, ClC**C**H**C**H**C**H), 7.98 (d, *J*=4.6 Hz, 1H, NCH**C**H), 7.84-7.77 (m, 1H, ClCCH**C**H) ppm

^{13}CNMR (101 MHz, DMSO-d^6) δ 151.8 (**7**), 148.5 (**4**), 135.3 (**9**), 133.0 (**6**), 128.9 (**1**), 128.4 (**8**), 128.2 (**2**), 125.9 (**3**), 125.8 (**5**) ppm

IR (neat) ν_{max} 2945 (m), 1292 (s), 1073 (s) cm^{-1}

LRMS (ESI$^+$) *m/z* 242.1 $[M^{79}Br+H]^+$, 244.1 $[M^{81}Br+H]^+$

HRMS (ESI$^+$) *m/z calcd. for* C_9H_5BrClN 241.9367 *m/z meas.* 241.9371 $[M+H]^+$

Mpt 104-105 °C

4-Bromo-7,8-dichloroquinoline (2.61)

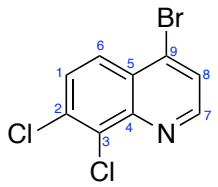

Mol. Wt. 275.9 $gmol^{-1}$

$C_9H_4BrCl_2N$

Following a procedure adapted from Franzblau *et al.*,[234] to a solution of 7,8-dichloroquinolin-4-ol (2.00 g, 9.34 mmol, 1 equiv.) in DMF (40 mL) at 60 °C was added phosphorus tribromide (2.91 mL, 10.7 mmol, 1.2 equiv.). The beige mixture was cooled to 45 °C for 45 min. After cooling to rt, the reaction was diluted with H_2O (20 mL) and the solution was basified to pH 10 with saturated aqueous $NaHCO_3$. The resulting orange solid was washed in H_2O, filtered and taken up in EtOAc and concentrated *in vacuo*, to afford 4-bromo-7,8-dichloroquinoline (2.54 g, 9.17 mmol, 98%) as an orange solid.

TLC R_f 0.86 (EtOAc, SiO_2)

^{1}HNMR (400MHz, DMSO-d^6) δ 8.85 (d, *J*=9.0 Hz, 1H, NC**H**), 8.21-8.05 (m, 2H, ClC**CHCH**), 7.92 (d, *J*=9.0 Hz, 1H, NCH**CH**) ppm

^{13}CNMR (101 MHz, DMSO-d^6) δ 152.0 (**7**), 145.0 (**4**), 134.1 (**9**), 133.6 (**3**), 131.0 (**2**), 129.3 (**6**), 126.8 (**5**), 126.6 (**8**), 126.4 (**1**) ppm

IR (neat) ν_{max} 2940 (br), 1273 (s), 1078 (s) cm^{-1}

LRMS (ESI$^+$) *m/z* 276.1 $[M^{79}Br+H]^+$, 278.1 $[M^{81}Br+H]^+$

HRMS (ESI$^+$) *m/z calcd. for* $C_9H_4BrCl_2N$ 275.8986 *m/z meas.* 275.8978 $[M+H]^+$

Mpt 113-114 °C

4-Bromo-6-chloroquinoline (2.62)

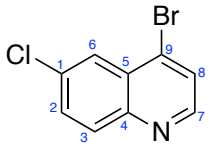

Mol. Wt. 241.5

C_9H_5BrClN

Following a procedure adapted from Franzblau *et al.*,[234] to a solution of 6-chloroquinolin-4-ol (2.00 g, 11.1 mmol, 1 equiv.) in DMF (30 mL) at 60 °C was added phosphorus tribromide (1.20 mL, 12.8 mmol, 1.2 equiv.). The beige mixture was cooled to 45 °C for 45 min. After cooling to rt, the reaction was diluted with H_2O (20 mL) and the solution was basified to pH 10 with saturated aqueous $NaHCO_3$. The resulting yellow solid was washed in H_2O, filtered and taken up in EtOAc and concentrated *in vacuo*, to afford 4-bromo-6-chloroquinoline (1.85 g, 7.63 mmol, 69%) as a pale yellow solid.

TLC R_f 0.70 (EtOAc, SiO_2)

^{1}HNMR (400MHz, $CDCl_3$) δ 8.68 (d, *J*=4.6 Hz, 1H, NC**H**), 8.20 (d, *J*=2.4 Hz, 1H, ClC**C**H**C**), 8.06 (d, *J*=8.8 Hz, 1H, NC**C**H), 7.76-7.68 (m, 2H, NCCH**CH,** NCH**CH**) ppm

^{13}CNMR (101 MHz, $CDCl_3$) δ 150.3 (**7**), 147.6 (**4**), 134.4 (**9**), 133.2 (**1**), 131.9 (**6**), 131.7 (**2**), 129.0 (**5**), 126.1 (**3**), 126.0 (**8**) ppm

IR (neat) ν_{max} 3073 (m), 1482 (s), 1081 (s) cm^{-1}

LRMS (ESI$^+$) *m/z* 242.1 $[M^{79}Br+H]^+$, 244.1 $[M^{81}Br+H]^+$

HRMS (ESI$^+$) *m/z calcd. for* C_9H_6BrClN 241.9367 *m/z meas.* 241.9370 $[M+H]^+$

Mpt 91-92 °C

***N*-(But-3-yn-1-yl)-5-chloroquinolin-4-amine (2.63)**

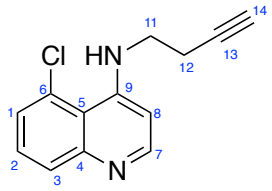

Mol. Wt. 230.1 $gmol^{-1}$

$C_{13}H_{11}ClN_2$

Following a procedure adapted from Musonda *et al.*,[236] 3-butyn-1-amine (0.81 mL, 9.90 mmol, 4 equiv.) was mixed with 4-bromo-5-chloroquinoline (600 mg, 2.47 mmol, 1 equiv.) to form a beige paste. The paste was heated to 80 °C for 1 h without stirring. The temperature was then raised to 140 °C and the reaction was stirred overnight. The brown reaction mixture was cooled to rt and 1 M aqueous NaOH (2 mL) was added. The organic product was basified to pH 10 with 10% aqueous NaOH and was extracted with CH_2Cl_2 (3 × 15 mL). The organic layers were combined, washed, dried ($MgSO_4$), filtered and concentrated *in vacuo*. The brown crude product was purified by column chromatography on silica gel (SiO_2, EtOAc), affording *N*-(but-3-yn-1-yl)-5-chloroquinolin-4-amine (380 mg, 1.65 mmol, 67%) as a colourless solid.

TLC R_f 0.59 (10% MeOH in EtOAc, SiO_2)

^{1}HNMR (400MHz, $CDCl_3$) δ 8.56 (d, *J*=5.4 Hz, 1H, NC**H**), 7.98 (d, *J*=2.1 Hz, 1H, ClC**CH**), 7.70 (d, *J*=9.0 Hz, 1H, NC**CH**), 7.38 (dd, *J*=9.0, 2.1 Hz, 1H, NCCH**CH**), 6.43 (d, *J*=5.4 Hz, 1H, NCH**CH**), 3.51 (q, *J*=6.5 Hz, 2H, **CH$_2$**CH$_2$CCH), 2.66 (td, *J*=6.5, 2.6 Hz, 2H, CH$_2$**CH$_2$**CCH), 2.13 (t, *J*=2.6 Hz, 1H, CH$_2$CH$_2$C**CH**) ppm

^{13}CNMR (101 MHz, $CDCl_3$) δ 152.0 (**9**), 149.3 (**4**), 149.2 (**7**), 135.0 (**6**), 128.9 (**2**), 125.5 (**3**), 120.9 (**1**), 117.3 (**5**), 99.2 (**8**), 80.7 (**13**), 71.0 (**14**), 41.4 (**11**), 18.7 (**12**) ppm

IR (neat) ν_{max} 3284 (m), 2961 (m), 782 (s) cm^{-1}

LRMS (ESI$^+$) *m/z* 231.2 $[M+H]^+$

HRMS (ESI$^+$) *m/z calcd. for* $C_{13}H_{11}ClN_2$ 231.0684 *m/z meas.* 231.0683 $[M+H]^+$

Mpt 162-163 °C

***N*-(But-3-yn-1-yl)-7,8-dichloroquinolin-4-amine (2.64)**

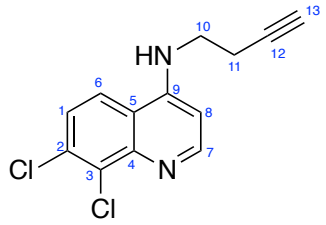

$C_{13}H_{10}Cl_2N_2$

MWt: 265.1 $gmol^{-1}$

Following a procedure adapted from Musonda *et al.*,[236] 3-butyn-1-amine (0.30 mL, 3.61 mmol, 5 equiv.) was mixed with 4-bromo-7,8-dichloroquinoline (200 mg, 0.72 mmol, 1 eq.) to form a beige paste. The paste was heated to 80 °C for 1 h without stirring. The temperature was then raised to 140 °C and the reaction was stirred overnight. The brown reaction mixture was cooled to rt and 1 M aqueous NaOH (2 mL) was added. The organic product was basified with 10% aqueous NaOH and was extracted with CH_2Cl_2 (3 × 15 mL). The organic layers were combined, washed, dried ($MgSO_4$), filtered and concentrated *in vacuo*. The crude product was purified by column chromatography (SiO_2, 10% MeOH in EtOAc), affording N-(but-3-yn-1-yl)-7,8-dichloroquinolin-4-amine (265 mg, 0.72 mmol, 100%) as an orange solid.

TLC R_f 0.79 (10% MeOH in EtOAc, SiO_2)

^{1}HNMR (400MHz, MeOH-d^4) δ 8.43 (d, *J*=5.6 Hz, 1H, NC**H**), 8.00 (d, *J*=9.0 Hz, 1H, ClCClC**CH**), 7.49 (d, *J*=9.0 Hz, 1H, ClCClCH**CH**), 6.62 (d, *J*=5.6 Hz, 1H, NCH**CH**), 3.65 (t, *J*=7.1 Hz, 2H, **CH$_2$**CH$_2$CCH), 2.60 (m, 2H, CH$_2$**CH$_2$**CCH), 2.35 (s, 1H, CH$_2$CH$_2$C**CH**) ppm

^{13}CNMR (101 MHz, MeOH-d^4) δ 151.4 (**7**), 151.3 (**9**), 145.3 (**4**), 133.7 (**2**), 129.9 (**3**), 124.9 (**1**), 120.6 (**6**), 118.3 (**5**), 99.1 (**8**), 80.7 (**12**), 69.8 (**13**), 41.6 (**10**), 17.6 (**11**) ppm

IR (neat) ν_{max} 3287 (m), 2946 (m), 772 (s) cm^{-1}

LRMS (ESI$^+$) *m/z* 215.1 $[M+H]^+$

HRMS (ESI$^+$) *m/z calcd. for* $C_{13}H_{10}Cl_2N_2$ 265.0294 *m/z meas.* 265.0291 $[M+H]^+$

Mpt 188-190 °C

_N_-(3-But-1-yn-1-yl)-6-chloroquin-4-amine (2.65)

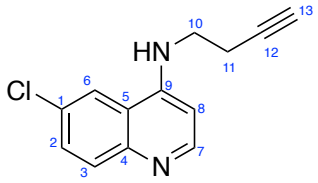

Mol. Wt. 230.7

$C_{13}H_{11}ClN_2$

Following a procedure adapted from Musonda *et al.*,[236] 3-butyn-1-amine (1.34 mL, 16.4 mmol, 4 equiv.) was mixed with 4-bromo-6-chloroquinoline (1.00 g, 4.09 mmol, 1 equiv.) to form a pale orange paste. The paste was heated to 80 °C for 1 h without stirring. The temperature was then raised to 140 °C and the reaction was stirred for 18 h. The reaction was cooled to rt and 1 M aqueous NaOH (2 mL) was added. The organic product was basified to pH 10 with 10% aqueous NaOH and was extracted (CH_2Cl_2). The organic layer was washed (H_2O), dried ($MgSO_4$), filtered and concentrated *in vacuo*. The crude product was purified by column chromatography (SiO_2, 20% MeOH in EtOAc), to afford *N*-(but-3-yn-1-yl)-6-chloroquinolin-4-amine (1.06 g, 4.95 mmol, 78%) as a cream solid.

TLC R_f 0.60 (20% MeOH in EtOAc, SiO_2)

^{1}HNMR (400MHz, DMSO-d_6) δ 8.41 (d, *J*=5.1 Hz, 1H, NC**H**), 8.35 (d, *J*=2.2 Hz, 1H, ClC**C**H**C**), 7.80 (d, *J*=8.9 Hz, 1H, NC**C**H), 7.61 (dd, *J*=8.9, 2.2 Hz, 1H, NCCH**C**H), 7.43-7.31 (m, 1H, **NH**), 6.54 (d, *J*=5.1 Hz, 1H, NCH**C**H), 3.44 (q, *J*=7.1 Hz, 2H, NH**C**$H_2$$CH_2$CCH), 2.88 (t, *J*=2.7 Hz, 1H, NHCH$_2$CH$_2$C**C**H), 2.56 (td, *J*=7.1, 2.7 Hz, 2H, NHCH$_2$**C**H_2CCH) ppm

^{13}CNMR (101 MHz, DMSO-d_6) δ 151.1 (**7**), 148.9 (**9**), 146.9 (**4**), 131.2 (**3**), 129.2 (**2**), 128.5 (**1**), 120.9 (**6**), 119.5 (**5**), 99.0 (**8**), 82.3 (**12**), 72.4 (**13**), 41.3 (**10**) 17.7 (**11**) ppm

^{19}FNMR (376 MHz, DMSO-d_6) δ 112.0 ppm

IR (neat) ν_{max} 3288 (s), 2968 (m), 2114 (s), 853 (s) cm^{-1}

LRMS (ESI$^+$) *m/z* 231.3 $[M+H]^+$

HRMS (ESI$^+$) *m/z calcd. for* $C_{13}H_{12}ClN_2^+$ 231.0684 *m/z meas.* 231.0682

Mpt 180-181 °C

Methyl 3-(benzyloxy)-6-(4-((5-chloroquinolin-4-yl)amino)but-1-yn-1-yl) picolinate (2.66)

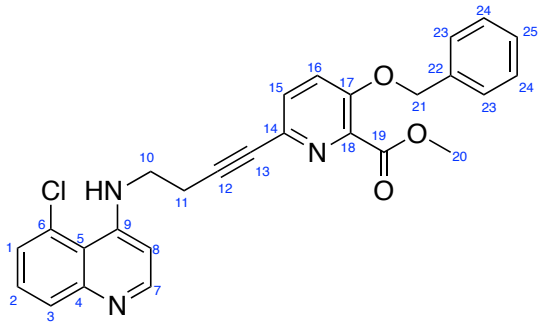

Mol. Wt. 471.1 $gmol^{-1}$

$C_{27}H_{22}ClN_3O_3$

Following a procedure adapted from de Sousa,[186] To a degassed solution of methyl 3-(benzyloxy)-6-bromopyridine-2-carboxylate (384 mg, 1.19 mmol, 1.1 equiv.) in THF/Et_3N (7 mL/3 mL), tetrakis(triphenylphosphine) palladium (125 mg, 0.11 mmol, 10 mol%) and copper iodide (41.0 mg, 0.22 mmol, 20 mol%) were added. After bubbling the reaction mixture with argon for 5 minutes at rt, a degassed solution of N-(but-3-yn-1-yl)-7-(trifluoromethyl)quinolin-4-amine (250 mg, 1.08 mmol, 1 equiv.) in THF (3 mL) was added dropwise and the yellow reaction mixture was stirred for 16 h at rt. Upon completion, the dark orange reaction mixture was concentrated *in vacuo* and purified by column chromatography (SiO_2, EtOAc), affording methyl 3-(benzyloxy)-6-(4-((5-chloroquinolin-4-yl)amino)but-1-yn-1-yl)picolinate (492 mg, 1.04 mmol, 96%) as a cream solid.

TLC R_f 0.14 (EtOAc, SiO_2)

^{1}HNMR (400MHz, $CDCl_3$) δ 8.55 (app. s, 1H, NC**H**), 7.96 (app. s, 1H, NCCH**CH**), 7.76 (d, *J*=8.8 Hz, 1H, NCC**H**), 7.48-7.23 (m, 8H, Ar**H**), 6.44 (br. d, *J*=5.1 Hz, 1H, NCH**CH**), 5.20 (s, 2H, **CH_2**Ph), 3.97 (s, 3H, CO_2**CH_3**), 3.67-3.50 (m, 2H, NH**CH_2**CH_2), 2.84 (t, *J*=6.5 Hz 2H, NHCH_2**CH_2**) ppm

^{13}CNMR (101 MHz, $CDCl_3$) δ 164.7 (**19**), 153.2 (**17**), 151.9 (**9**), 149.4 (**4**), 149.3 (**7**), 140.2 (**18**), 135.3 (**14**), 135.0 (**22**), 134.5 (**16**), 130.0 (**6**), 128.7 (**23**), 128.3 (**2**), 128.3 (**15**), 126.9 (**24**), 125.5 (**25**), 124.3 (**5**), 121.7 (**3**), 121.3 (**1**), 99.1 (**8**), 86.1 (**12**), 81.4 (**13**), 70.8 (**21**), 52.7 (**20**), 41.2 (**10**), 19.5 (**11**) ppm

IR (neat) ν_{max} 2984 (s), 1578 (s), 1000 (s) cm^{-1}

LRMS (ESI$^+$) *m/z* 472.4 $[M+H]^+$

HRMS (ESI$^+$) *m/z calcd. for* $C_{27}H_{22}ClN_3O_3$ 472.1422 *m/z meas.* 472.1428 $[M+H]^+$

Mpt 152-153 °C

Methyl 3-(benzyloxy)-6-(4-((7,8-dichloroquinolin-4-yl)amino)but-1-yn-1-yl)picolinate (2.67)

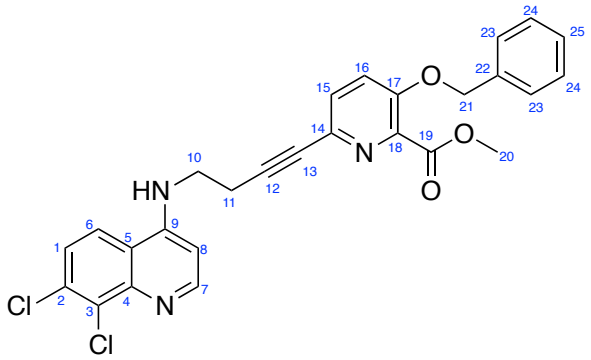

Mol. Wt. 505.4 $gmol^{-1}$

$C_{27}H_{21}Cl_2N_3O_3$

Following a procedure adapted from de Sousa,[186] to a degassed solution of methyl 3-(benzyloxy)-6-bromopyridine-2-carboxylate (668 mg, 2.07 mmol, 1.1 equiv.) in THF/Et_3N (7 mL/3 mL), tetrakis(triphenylphosphine) palladium (218 mg, 0.19 mmol, 10 mol%) and copper iodide (71.0 mg, 0.38 mmol, 20 mol%) were added. After bubbling the reaction mixture with argon for 5 minutes at rt, a degassed solution of N-(but-3-yn-1-yl)-7-(trifluoromethyl)quinolin-4-amine (500 mg, 1.89 mmol, 1 equiv.) in THF (3 mL) was added dropwise and the yellow reaction mixture was stirred for 16 h at rt. Upon consumption of starting materials (TLC) the reaction mixture was concentrated *in vacuo* and purified by column chromatography (SiO_2, EtOAc), affording methyl 3-(benzyloxy)-6-(4-((7,8-dichloroquinolin-4-yl)amino)but-1-yn-1-yl)picolinate (565 mg, 1.23 mmol, 96%) as a cream solid.

TLC R_f 0.57 (EtOAc, SiO_2)

^{1}HNMR (400MHz, $CDCl_3$) δ 8.66 (d, *J*=5.4 Hz, 1H, NC**H**), 7.73-7.67 (m, 1H, ClCClC**CH**), 7.53-7.31 (m, 7H, Ar**H**), 7.30-7.25 (m, 1H, ClCClCCH**CH**), 6.50 (d, *J*=5.4 Hz, 1H, NCH**CH**), 5.20 (s, 2H, **CH_2**Ph), 3.96 (s, 3H, CO_2**CH_3**), 3.58 (q, *J*=6.4 Hz, 2H, NH**CH_2**CH_2), 2.85 (t, *J*=6.4 Hz 2H, NHCH_2**CH_2**) ppm

^{13}CNMR (101 MHz, $CDCl_3$) δ 164.7 (**19**), 153.3 (**17**), 152.1 (**9**), 151.0 (**7**), 149.8 (**4**), 146.0 (**18**), 140.2 (**22**), 135.3 (**3**), 134.4 (**14**), 133.9 (**2**), 130.0 (**6**), 128.8 (**15**), 128.3 (**23**), 126.9 (**25**), 125.7 (**24**), 124.4 (**1**), 121.8 (**5**), 119.1 (**16**), 118.2 (**8**), 99.8 (**12**), 81.8 (**13**), 70.8 (**21**), 52.7 (**20**), 41.4 (**10**), 19.5 (**11**) ppm

IR (neat) ν_{max} 3124 (m), 1576 (s), 1018 (s) cm^{-1}

LRMS (ESI$^+$) *m/z* 506.4 $[M+H]^+$

HRMS (ESI$^+$) *m/z calcd. for* $C_{27}H_{21}Cl_2N_3O_3$ 506.1041 *m/z meas.* 506.1041 $[M+H]^+$

Mpt 145-147 °C

Methyl 3-(benzoyloxy)-6-bromopicolinate (2.68)

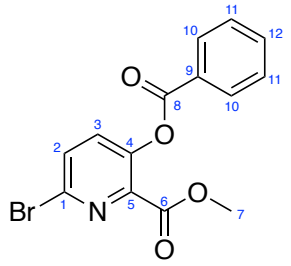

Mol. Wt. 334.9

$C_{14}H_{10}BrNO_4$

Following an adapted procedure from Winkler *et al.*[237] for the benzoylation of phenolic alcohols, to a solution of methyl 5-bromo-2-hydroxypicolinate (250 mg, 1.08 mmol, 1 equiv.) in CH_2Cl_2 (10 mL) at 0 °C was added Et_3N (1.50 mL, 10.82 mmol, 10 equiv.), DMAP (13.2 mg, 0.11 mmol, 10 mol%) and benzoyl chloride (0.38 mL, 3.25 mmol, 3 equiv.). The pale yellow solution was warmed to rt and was stirred for 30 min. The reaction mixture was concentrated *in vacuo* and the residue was purified by column chromatography (SiO_2, 20% EtOAc in light petroleum ether) to afford methyl 3-(benzoyloxy)-6-bromopicolinate (334 mg, 0.99 mmol, 92%) as a colourless solid.

TLC R_f 0.28 (10% MeOH in CH_2Cl_2, SiO_2)

^{1}HNMR (400MHz, $CDCl_3$) δ 8.24-8.18 (m, 2H, Ar**H**), 7.74 (d, *J*=8.6 Hz, 1H, NC(Br)**CH**CH), 7.70-7.66 (m, 1H, Ar**H**), 7.59-7.51 (m, 3H, Ar**H,** NC(Br)CH**CH**), 3.88 (s, 3H, CO_2**C**H_3) ppm

^{13}CNMR (101 MHz, $CDCl_3$) δ 164.5 (**8**), 162.7 (**6**), 147.7 (**4**), 141.6 (**5**), 137.6 (**1**), 135.2 (**2**), 134.2 (**12**), 132.5 (**3**), 130.5 (**10**), 128.8 (**11**), 128.4 (**9**), 53.1 (**7**) ppm

IR (neat) ν_{max} 3090 (m), 2954 (m), 1725 (s), 1430 (s), 1084 (s) cm^{-1}

LRMS (ESI$^+$) *m/z* 336.3 $[M^{79}Br+H]^+$ 338.3 $[M^{81}Br+H]^+$

HRMS (ESI$^+$) *m/z calcd. for* $C_{14}H_{11}BrNO_4^+$ 335.9866 *m/z meas.* 335.9872 $[M^{79}Br+H]^+$

Mpt 201-202 °C

Methyl 3-(benzoyloxy)-6-(4-((5-chloroquinolin-4-yl)amino)but-1-yn-1-yl)picolinate (2.69)

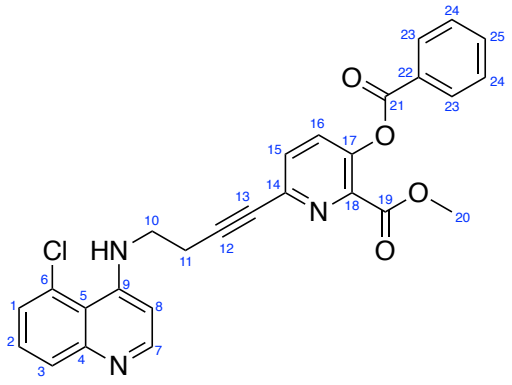

Mol. Wt. 485.9

$C_{27}H_{20}ClN_3O_4$

Following a procedure adapted from de Sousa,[186] To a degassed solution of methyl N-(but-3-yn-1-yl)-7-(trifluoromethyl)quinolin-4-amine (400 mg, 1.73 mmol, 1 equiv.) in THF/Et_3N (7 mL/3 mL), tetrakis(triphenylphosphine) palladium (200 mg, 0.17 mmol, 10 mol%) and copper iodide (66.0 mg, 0.34 mmol, 20 mol%) were added. After bubbling the reaction mixture with argon for 5 minutes at rt, a degassed solution of 3-(benzoyloxy)-6-bromopyridine-2-carboxylate (641 mg, 1.91 mmol, 1.1 equiv.) in THF (10 mL) was added dropwise and the yellow reaction mixture was stirred for 16 h at rt. Upon completion (TLC), the orange reaction mixture was concentrated *in vacuo* and purified by column chromatography (SiO_2, 20% MeOH in EtOAc), affording methyl 3-(benzoyloxy)-6-(4-((5-chloroquinolin-4-yl)amino)but-1-yn-1-yl)picolinate (754 mg, 1.55 mmol, 89%) as a yellow solid.

TLC R_f 0.39 (10% MeOH in EtOAc, SiO_2)

^{1}HNMR (400MHz, DMSO-d_6) δ 8.39-8.29 (app. br. s, 1H, NC**H**), 8.16-8.09 (m, 2H, Ar**H**), 7.99 (d, *J*=8.3 Hz, 1H, NCC**H**), 7.86-7.80 (m, 3H, Ar**H**), 7.68-7.58 (m, 3H, Ar**H**), 7.48 (d, *J*=9.0 Hz, 1H, NCCH**CH**), 6.69 (app. br. s, 1H, NCH**CH**), 3.74 (s, 3H, CO_2**CH_3**), 3.65-3.58 (m, 2H, NH**CH_2**CH_2), 2.95-2.85 (m, 2H, $NHCH_2$**CH_2**) ppm

^{13}CNMR (101 MHz, DMSO-d_6) δ 164.2 (**19**), 163.1 (**21**), 146.1 (**17**), 144.0 (**9**), 141.2 (**4**), 140.0 (**7**), 137.1 (**18**), 134.5 (**25**), 133.7 (**14**), 133.5 (**22**), 131.7 (**2**), 131.1 (**15**), 130.0 (**24**), 129.1 (**23**), 128.7 (**6**), 128.2 (**16**), 124.4 (**3**), 124.2 (**1**), 120.1 (**8**), 118.6 (**5**), 89.8 (**12**), 80.1 (**13**), 52.6 (**20**), 41.0 (**10**), 18.6 (**11**) ppm

IR (neat) ν_{max} 2950 (m), 2363 (s), 2233 (s), 1729 (s), 1575 (s), 1215 (s) cm^{-1}

LRMS (ESI^+) *m/z* 486.4 $[M+H]^+$

HRMS (ESI$^+$) *m/z calcd. for* $C_{27}H_{21}ClN_3O_4^+$ 486.1215 *m/z meas.* 486.1229 $[M+H]^+$

Mpt 94-95 °C

Methyl 3-(benzoyloxy)-6-(4-((7,8-dichloroquinolin-4-yl)amino)but-1-yn-1-yl)picolinate (2.70)

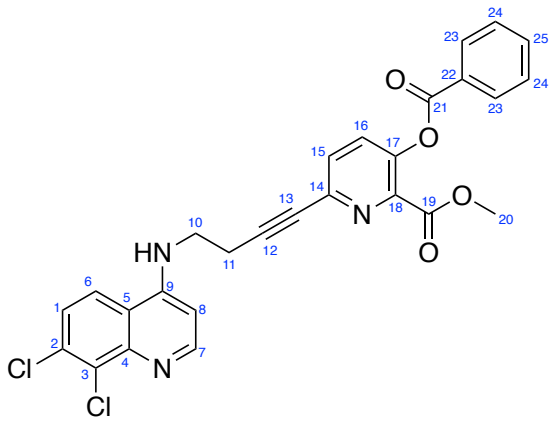

Mol.Wt. 520.4

$C_{27}H_{19}Cl_2N_3O_4$

Following a procedure adapted from de Sousa,[186] to a degassed solution of N-(but-3-yn-1-yl)-7,8-dichloroquinolin-4-amine (600 mg, 2.26 mmol, 1 equiv.) in anhydrous THF/Et_3N (12 mL/4 mL), tetrakis(triphenylphosphine) palladium (1.16 g, 0.23 mmol, 10 mol%) and copper iodide (190 mg, 0.45 mmol, 20 mol%) were added. After bubbling the reaction mixture with argon for 5 minutes at rt, a degassed solution of methyl 3-(benzoyloxy)-6-bromopicolinate (837 mg, 2.49 mmol, 1.1 equiv.) in anhydrous THF (10 mL) was added dropwise and the yellow reaction mixture was stirred for 16 h at rt. Upon completion, the reaction mixture was concentrated *in vacuo* and purified by column chromatography (SiO_2, EtOAc), to afford methyl 3-(benzoyloxy)-6-(4-((7,8-dichloroquinolin-4-yl)amino)but-1-yn-1-yl)picolinate (1.10 mg, 2.12 mmol, 94%) as a yellow solid.

TLC R_f 0.77 (EtOAc, SiO_2)

^{1}HNMR (400MHz, DMSO-d_6) δ 8.59-8.50 (br. s, 1H, **NH**), 8.26 (d, *J*=9.0 Hz, 1H, NC**H**), 8.16-8.09 (m, 2H, Ar**H**), 7.98 (d, *J*=8.3 Hz, 1H, Ar**H**), 7.83-7.71 (m, 3H, Ar**H**), 7.67-7.59 (m, 3H, Ar**H**), 6.74 (d, *J*=9.0 Hz, NCH**CH**), 3.74 (s, 3H, CO_2**CH_3**), 3.64 (q, *J*=7.1 Hz, 2H, NH**CH_2**CH_2), 2.91 (t, *J*=7.1 Hz, 2H, $NHCH_2$**CH_2**) ppm

^{13}CNMR (101 MHz, DMSO-d_6) δ 164.2 (**19**), 163.1 (**21**), 152.2 (**9**), 150.3 (**7**), 146.2 (**4**), 145.7 (**17**), 141.2 (**3**), 140.0 (**18**), 134.5 (**14**), 133.7 (**25**), 132.4 (**2**), 131.1 (**15**), 130.0 (**23**), 129.1 (**24**), 128.1 (**16**), 124.7 (**6**), 122.0 (**1**), 118.4 (**22**), 111.7 (**5**), 99.8 (**8**), 89.7 (**12**), 80.1 (**13**), 52.6 (**20**), 41.1 (**10**), 18.5 (**11**) ppm

IR (neat) ν_{max} 3455 (s), 3002 (m), 2954 (m), 2231 (s), 1725 (s), 1224 (s), cm^{-1}

LRMS (ESI^+) *m/z* 520.4 $[M+H]^+$

HRMS (ESI$^+$) *m/z calcd. for* $C_{27}H_{20}Cl_2N_3O_4^+$ 520.0825 *m/z meas.* 520.0827 $[M+H]^+$

Mpt 161-162 °C

Methyl 3-(benzoyloxy)-6-(4-((6-chloroquinolin-4-yl)amino)but-1-yn-1-yl)picolinate (2.71)

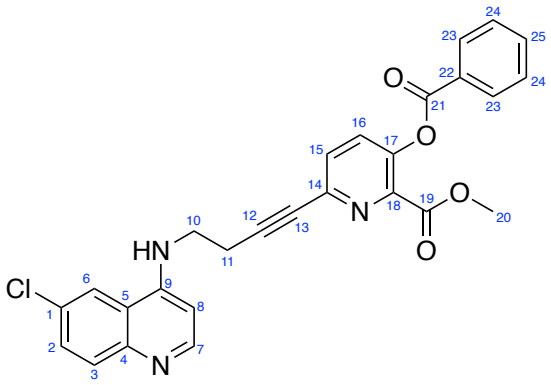

Mol. Wt. 485.9

$C_{27}H_{20}ClN_3O_4$

Following a procedure adapted from de Sousa,[186] To a degassed solution of methyl *N*-(but-3-yn-1-yl)-6-chloroquinolin-4-amine (350 mg, 1.52 mmol, 1 equiv.) in THF/Et_3N (7 mL/3 mL), tetrakis(triphenylphosphine) palladium (175 mg, 0.15 mmol, 10 mol%) and copper iodide (58.0 mg, 0.30 mmol, 20 mol%) were added. After bubbling the reaction mixture with argon for 5 minutes at rt, a degassed solution of 3-(benzoyloxy)-6-bromopyridine-2-carboxylate (561 mg, 1.67 mmol, 1.1 equiv.) in THF (10 mL) was added dropwise and the yellow reaction mixture was stirred for 16 h at rt. Upon completion (TLC), the orange reaction mixture was concentrated *in vacuo* and purified by column chromatography (SiO_2, 20% MeOH in EtOAc), affording methyl 3-(benzoyloxy)-6-(4-((6-chloroquinolin-4-yl)amino)but-1-yn-1-yl)picolinate (690 mg, 1.42 mmol, 94%) as a dark yellow solid.

TLC R_f 0.27 (10% MeOH in EtOAc, SiO_2)

^{1}HNMR (400MHz, MeOD-d_4) δ 8.26 (app. br. s, 1H, NC**H**), 8.21-8.16 (m, 2H, Ar**H**), 7.85-7.55 (m, 7H, Ar**H**), 6.70 (app. br. s, 1H, NCH**CH**), 3.80 (s, 3H, CO_2**CH_3**), 3.73 (t, *J*=6.7 Hz, 2H, NH**CH_2**CH_2), 2.92 (t, *J*=6.7 Hz, 2H, NHCH_2**CH_2**) ppm

^{13}CNMR (101 MHz, MeOD-d_4) δ 164.1 (**19**), 163.1 (**21**), 151.5 (**17**), 148.9 (**9**), 146.1 (**4**), 141.2 (**7**), 140.0 (**18**), 134.4 (**14**), 133.7 (**25**), 132.7 (**22**), 131.4 (**1**), 131.1 (**15**), 130.0 (**24**), 129.2 (**2**), 129.0 (**23**), 128.6 (**16**), 128.1 (**3**), 125.9 (**5**), 121.0 (**6**), 117.0 (**8**), 89.8 (**12**), 80.0 (**13**), 52.5 (**20**), 41.1 (**10**), 18.5 (**11**) ppm

IR (neat) ν_{max} 2950 (m), 2360 (s), 2234 (s), 1729 (s), 1573 (s), 1217 (s) cm^{-1}

LRMS (ESI$^+$) *m/z* 486.4 $[M+H]^+$

HRMS (ESI$^+$) *m/z calcd. for* $C_{27}H_{21}ClN_3O_4^+$ 486.1215 *m/z meas.* 486.1217 $[M+H]^+$

Mpt 103-104 °C

Methyl 3-(benzoyloxy)-6-(4-((6-chloroquinolin-4-yl)amino)butyl)picolinate (2.74)

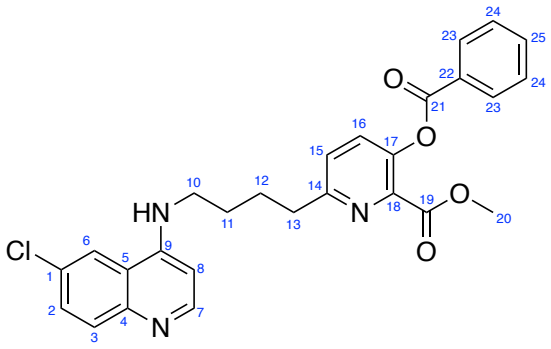

Mol. Wt. 489.9

$C_{27}H_{24}ClN_3O_4$

Following a procedure adapted from de Sousa,[186] to a solution of methyl 3-(benzoyloxy)-6-(4-((6-chloroquinolin-4-yl)amino)butyl)picolinate (50 mg, 0.10 mmol, 1 eq.) and tosyl hydrazine (114 mg, 0.62 mmol, 6 eq.) in anhydrous THF (3 mL) was added a solution of sodium acetate (51 mg, 0.62 mmol, 6 eq.) in H_2O (3 mL). The pale yellow mixture was heated to 80 °C for 18 h. The reaction was cooled to rt and a sat. aq. K_2CO_3 (5 mL) was added. The yellow reaction solution was stirred at rt for 1 h, before CH_2Cl_2 (10 mL) was added and the organic phase was separated. The aqueous phase was extracted (CH_2Cl_2, 2 × 10 mL) and the combined organics were dried ($MgSO_4$), filtered and concentrated *in vacuo*. The residue was purified by column chromatography (SiO_2, 10% MeOH in CH_2Cl_2) to afford methyl 3-(benzoyloxy)-6-(4-((6-chloroquinolin-4-yl)amino)butyl)picolinate (6.00 mg, 0.01 mmol, 12%) as a yellow solid.

TLC R_f 0.62 (10% MeOH in CH_2Cl_2, SiO_2)

^{1}HNMR (400MHz, $CDCl_3$) δ 8.54 (br. s, 1H, NC**H**), 8.25-8.20 (m, 2H, Ar**H**), 7.92 (d, *J*=8.8 Hz, 1H, NC**CH**), 7.87 (d, *J*=2.2 Hz, 1H, ClC**CH**C), 7.71-7.64 (m, 1H, NCCH**CH**), 7.62 (d, *J*=8.6 Hz, 1H, Py**H**), 7.58-7.52 (m, 3H, Ar**H**), 7.45 (d, *J*=8.6 Hz, 1H, Py**H**), 6.44 (d, *J*=5.4 Hz, 1H, NCH**CH**), 3.81 (s, 3H, CO_2**CH_3**), 3.40 (q, *J*=6.6 Hz, 2H, NH**CH_2**$CH_2CH_2CH_2$), 3.04 (t, *J*=7.3 Hz, 2H, $NHCH_2CH_2CH_2$**CH_2**), 2.02-1.85 (m, 4H, $NHCH_2$**CH_2CH_2**CH_2) ppm

^{13}CNMR (101 MHz, $CDCl_3$) δ 164.9 (**19**), 164.1 (**21**), 159.2 (**17**), 151.0 (**9**), 149.2 (**4**), 146.3 (**7**), 140.4 (**18**), 134.0 (**14**), 133.0 (**25**), 131.3 (**22**), 130.4 (**1**), 130.2 (**15**), 129.8 (**24**), 129.5 (**2**), 128.8 (**23**), 128.7 (**16**), 127.0 (**3**), 120.0 (**6**), 119.4 (**5**), 99.3 (**8**), 52.8 (**20**), 43.5 (**10**), 36.8 (**13**), 27.6 (**12**), 27.5 (**11**) ppm

IR (neat) ν_{max} 2949 (m), 2859 (s), 1719 (s), 1674 (s), 1538 (s), 1207 (s) cm^{-1}

LRMS (ESI^+) *m/z* 490.5 $[M+H]^+$

HRMS (ESI^+) *m/z calcd. for* $C_{27}H_{25}ClN_3O_4^+$ 490.1528 *m/z meas.* 490.1536 $[M+H]^+$

Mpt 68-69 °C

7,8-Dimethylquinolin-4-ol

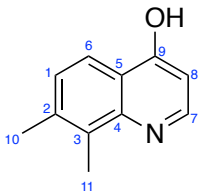

Mol. Wt. 173.1 $gmol^{-1}$

$C_{11}H_{11}NO$

Following a procedure adapted from Margolis *et al.*,[233] to a solution of 2,3-dimethylaniline (5.10 mL, 41.2 mmol, 1 equiv.) in EtOH (100 mL) were added Meldrum's acid (7.25 g, 50.4 mmol, 1.2 equiv.) and triethyl orthoformate (16.3 mL, 97.8 mmol, 2.4 equiv.). The beige mixture was heated to reflux for 2.5 h. The reaction was cooled to 0 °C and the beige solid was filtered and washed with cold EtOH. The dried solid was added portiowise over 5 min to boiling diphenyl ether (100 mL). Reflux was maintained for an additional 3 min. The brown reaction was stirred at rt for 30 min before petroleum ether (25 mL) was added and the yellow solid was filtered and dried. This afforded 7,8-dichloroquinolin-4-ol (5.45 g, 31.5 mmol, 76%) as a pale yellow solid.

TLC R_f 0.06 (10% MeOH in EtOAc, SiO_2)

^{1}HNMR (400MHz, MeOH-d^4) δ 8.01 (d, *J*=8.3 Hz, 1H, OHCC**CH**), 7.91 (d, *J*=7.3 Hz, 1H, N**CH**), 7.24 (d, *J*=8.3 Hz, 1H, OHCCCH**CH**), 6.31 (d, *J*=7.3 Hz, 1H, NCH**CH**), 2.47 (s, 3H, NC**CH$_3$**), 2.44 (s, 3H, NCCH$_3$C**CH$_3$**) ppm

^{13}CNMR (101 MHz, MeOH-d^4) δ 181.3 (**9**), 142.5 (**2**), 141.3 (**4**), 140.4 (**7**), 128.0 (**3**), 125.4 (**1**), 125.3 (**5**), 123.6 (**6**), 109.4 (**8**), 20.9 (**10**), 13.0 (**11**) ppm

IR (neat) ν_{max} 2953 (br), 1610 (s), 1066 (s) cm^{-1}

LRMS (ESI$^+$) *m/z* 174.1 $[M+H]^+$

HRMS (ESI$^+$) *m/z calcd. for* $C_{11}H_{11}NO$ 174.0913 *m/z meas.* 174.0915 $[M+H]^+$

Mpt 298-300 °C

5-Methylquinolin-4-ol

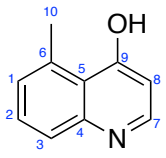

Mol. Wt. 159.1 $gmol^{-1}$

$C_{10}H_9NO$

Following a procedure adapted from Margolis *et al.*,[233] to a solution of *m*-toluidine (5.10 mL, 46.7 mmol, 1 equiv.) in EtOH (110 mL) were added Meldrum's acid (8.07 g, 56.0 mmol, 1.2 equiv.) and triethyl orthoformate (18.6 mL, 112 mmol, 2.4 equiv.). The mixture yellow was heated to reflux for 2.5 h. The reaction was cooled to 0 °C and the cream solid was filtered and washed with cold EtOH. The dried solid was added portiowise over 5 min to boiling diphenyl ether (100 mL). Reflux was maintained for an additional 3 min. The brown reaction was stirred at rt for 30 min before petroleum ether (25 mL) was added and the yellow solid was filtered and dried. This afforded 5-methylquinolin-4-ol (500 mg, 3.14 mmol, 7%) as a pale yellow solid.

TLC R_f 0.52 (EtOAc:MeOH 8:2, SiO_2)

^{1}HNMR (400MHz, MeOH-d^4) δ 7.75 (d, *J*=7.3 Hz, 1H, NC**H**), 7.49-7.40 (m, 1H, NC**CH**), 7.37-7.27 (m, 1H, NCCH**CH**), 7.12-7.02 (m, 1H, NCCHCH**CH**), 6.19 (d, *J*=7.3 Hz, 1H, NCH**CH**), 2.87 (s, 3H, **CH_3**) ppm

^{13}CNMR (101 MHz, MeOH-d^4) δ 158.7 (**9**), 141.4 (**4**), 139.6 (**7**), 132.4 (**6**), 130.8 (**2**), 127.5 (**1**), 119.7 (**5**), 117.3 (**3**), 111.5 (**8**), 23.9 (**10**) ppm

IR (neat) ν_{max} 2838 (br), 1609 (s), 1054 (s) cm^{-1}

LRMS (ESI$^+$) *m/z* 160.2 $[M+H]^+$

HRMS (ESI$^+$) *m/z calcd. for* $C_{10}H_9NO$ 160.0757 *m/z meas.* 160.0758 $[M+H]^+$

Mpt 161-162 °C 9 (lit: 157 °C)

4-Bromo-5-methylquinoline (2.79)

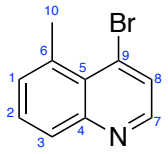

Mol. Wt. 221.0 $gmol^{-1}$

$C_{10}H_8BrN$

Following a procedure adapted from Franzblau *et al.*,[234] to a solution of 5-methylquinolin-4-ol (500 mg, 3.14 mmol, 1 equiv.) in DMF (15 mL) at 60 °C was added phosphorus tribromide (0.34 mL, 3.61 mmol, 1.2 equiv.). The mixture was cooled to 45 °C for 45 min. After cooling to rt, the dark orange reaction was diluted with H_2O (20 mL) and the solution was basified to pH 10 with saturated aqueous $NaHCO_3$. The resulting orange solid was washed in H_2O, filtered and taken up in EtOAc and concentrated *in vacuo*, to afford 4-bromo-5-methylquinoline (350 mg, 1.58 mmol, 50%) as an orange solid.

TLC R_f 0.90 (EtOAc:MeOH 8:2, SiO_2)

^{1}HNMR (400MHz, MeOH-d^4) δ 8.55 (d, *J*=4.6 Hz, 1H, NC**H**), 8.01 (d, *J*=8.1 Hz 1H, NC**CH**), 7.73 (d, *J*=4.6 Hz, 1H, NCH**CH**), 7.59 (dd, *J*=8.1, 7.1 Hz, 1H, NCCH**CH**), 7.42 (d, *J*=7.1 Hz, 1H, NCCHCH**CH**), 3.10 (s, 3H, **CH_3**) ppm

^{13}CNMR (101 MHz, MeOH-d^4) δ 150.9 (**4**), 148.8 (**7**), 135.7 (**6**), 131.0 (**9**), 129.7 (**1**), 129.5 (**2**), 127.7 (**5**), 127.0 (**8**), 118.9 (**3**), 25.6 (**10**) ppm

IR (neat) ν_{max} 2920 (br), 1595 (s), 1089 (s) cm^{-1}

LRMS (ESI$^+$) *m/z* 222.1 $[M^{79}Br+H]^+$, 224.1 $[M^{81}Br+H]^+$

HRMS (ESI$^+$) *m/z calcd. for* $C_{10}H_8BrN$ 221.9913 *m/z meas.* 221.9915 $[M+H]^+$

Mpt 76-79 °C

4-Bromo-7,8-dimethylquinoline (2.80)

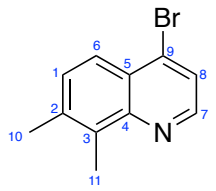

Mol. Wt. 235.0 $gmol^{-1}$

$C_{11}H_{10}BrN$

Following a procedure adapted from Franzblau *et al.*,[234] to a solution of 7,8-dimethylquinolin-4-ol (1.50 g, 8.66 mmol, 1 equiv.) in DMF (40 mL) at 60 °C was added phosphorus tribromide (0.94 mL, 9.96 mmol, 1.2 equiv.). The orange mixture was cooled to 45 °C for 45 min. After cooling to rt, the reaction was diluted with H_2O (20 mL) and the pH was adjusted to ~10 with saturated aqueous $NaHCO_3$. The resulting cream solid was washed in H_2O, filtered and taken up in EtOAc and concentrated *in vacuo*, to afford 4-bromo-7,8-dimethylquinoline (2.19 g, 7.93 mmol, 85%) as a colourless solid.

TLC R_f 0.94 (50% EtOAc in hexanes, SiO_2)

^{1}HNMR (400MHz, $CDCl_3$) δ 8.64 (d, *J*=4.6 Hz, 1H, NC**H**), 7.93 (d, *J*=8.6 Hz, 1H, BrCC**CH**), 7.61 (d, *J*=4.6 Hz, 1H, NCH**CH**), 7.44 (d, *J*=8.6 Hz, 1H, BrCCCH**CH**), 2.75 (s, 3H, NC**CH$_3$**), 2.52 (s, 3H, NCCH$_3$C**CH$_3$**) ppm

^{13}CNMR (101 MHz, $CDCl_3$) δ 148.4 (**4**), 148.1 (**7**), 138.3 (**2**), 134.9 (**9**), 134.2 (**3**), 130.6 (**1**), 126.2 (**5**), 123.9 (**6**), 123.7 (**8**), 20.8 (**10**), 13.7 (**11**) ppm

IR (neat) ν_{max} 2906 (m), 1298 (s), 1092 (s) cm^{-1}

LRMS (ESI^+) *m/z* 236.2 $[M^{79}Br+H]^+$, 238.2 $[M^{81}Br+H]^+$

HRMS (ESI^+) *m/z calcd. for* $C_{11}H_{10}BrN$ 236.0069 *m/z meas.* 236.0073 $[M+H]^+$

Mpt 66-68 °C

***N*-(But-3-yn-1-yl)-5-methylquinolin-4-amine (2.81)**

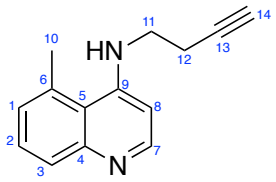

Mol. Wt. 210.1 $gmol^{-1}$

$C_{14}H_{14}N_2$

Following a procedure adapted from Musonda *et al.*,[236] 3-butyn-1-amine (0.60 mL, 6.75 mmol, 5 equiv.) was mixed with 4-bromo-5-methylquinoline (300 mg, 1.35 mmol, 1 equiv.) to form a orange paste. The paste was heated to 80 °C for 1 h without stirring. The temperature was then raised to 140 °C and the reaction was stirred overnight. The reaction was cooled to rt and 1 M aqueous NaOH (2 mL) was added. The organic product was basified to pH 10 with 10% aqueous NaOH and was extracted with CH_2Cl_2 (3 × 15 mL). The organic layers were combined, washed, dried ($MgSO_4$), filtered and concentrated *in vacuo*. The brown crude product was purified by column chromatography (SiO_2, 20% MeOH in EtOAc), to afford *N*-(but-3-yn-1-yl)-5-methylquinolin-4-amine (190 mg, 0.90 mmol, 67%) as a pale brown solid.

TLC R_f 0.20 (20% MeOH in EtOAc, SiO_2)

^{1}HNMR (400MHz, $CDCl_3$) δ 8.48 (d, *J*=5.4 Hz, 1H, NC**H**), 7.84 (d, *J*=8.3 Hz, 1H, NC**CH**), 7.45 (dd, *J*=8.3, 7.1 Hz, 1H, NCCH**CH**), 7.15 (d, *J*=7.1 Hz, 1H, NCCHCH**CH**), 6.37 (d, *J*=5.4 Hz, 1H, NCH**CH**), 3.48-3.38 (m, 2H, **CH_2**CH_2CCH), 3.00 (s, 3H, C**CH_3**), 2.69 (td, *J*=6.3, 2.7 Hz, 2H, CH_2**CH_2**CCH), 2.14 (t, *J*=2.6 Hz, 1H, CH_2CH_2C**CH**) ppm

^{13}CNMR (101 MHz, $CDCl_3$) δ 152.3 (**9**), 150.2 (**7**), 150.0 (**4**), 132.6 (**6**), 128.5 (**3**), 128.4 (**2**), 128.3 (**1**), 119.5 (**5**), 99.8 (**8**), 81.1 (**13**), 71.1 (**14**), 42.0 (**11**), 25.1 (**10**), 18.5 (**12**) ppm

IR (neat) ν_{max} 3224 (m), 2919 (m), 770 (s) cm^{-1}

LRMS (ESI$^+$) *m/z* 211.3 $[M+H]^+$

HRMS (ESI$^+$) *m/z calcd. for* $C_{14}H_{15}N_2$ 221.1230 *m/z meas.* 221.1233 $[M+H]^+$

Mpt 102–103 °C

_N_-(But-3-yn-1-yl)-7,8-dimethylquinolin-4-amine (2.82)

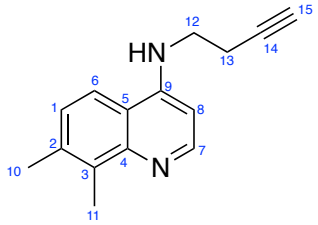

Mol. Wt. 224.3 $gmol^{-1}$

$C_{15}H_{16}N_2$

Following a procedure adapted from Musonda *et al.*,[236] 3-butyn-1-amine (1.30 mL, 15.9 mmol, 5 equiv.) was mixed with 4-bromo-7,8-dimethylquinoline (750 mg, 3.18 mmol, 1 equiv.) to form a colourless paste. The paste was heated to 80 °C for 1 h without stirring. The temperature was then raised to 140 °C and the reaction was stirred overnight. The brown reaction mixture was cooled to rt and 1 M aqueous NaOH (2 mL) was added. The organic product was basified to pH 10 with 10% aqueous NaOH and was extracted (CH_2Cl_2). The organic layers were combined, washed, dried ($MgSO_4$), filtered and concentrated *in vacuo*. The brown crude product was purified by column chromatography (SiO_2, EtOAc), affording *N*-(but-3-yn-1-yl)-7,8-dimethylquinolin-4-amine (429 mg, 1.91 mmol, 60%) as a pale brown solid.

TLC R_f 0.31 (MeOH:EtOAc 1:9, SiO_2)

^{1}HNMR (400MHz, $CDCl_3$) δ 8.61 (d, *J*=5.1 Hz, 1H, NC**H**), 7.54 (d, *J*=8.6 Hz, 1H, $CH_3CCH_3CCHC\mathbf{H}$), 7.28-7.31 (m, 1H, $CH_3CCH_3C\mathbf{C}H$), 6.42 (d, *J*=5.1 Hz, 1H, NCH**C**H), 3.51 (q, *J*=6.5 Hz, 2H, $\mathbf{CH_2}CH_2CCH$), 2.74 (s, 3H, $NCC\mathbf{CH_3}$), 2.66 (td, *J*=6.5, 2.7 Hz, 2H, $CH_2\mathbf{CH_2}CCH$), 2.49 (s, 3H, $NCCCH_3\mathbf{CH_3}$), 2.12 (t, *J*=2.7 Hz, 1H, $CH_2CH_2C\mathbf{C}H$) ppm

^{13}CNMR (101 MHz, $CDCl_3$) δ 149.7 (**9**), 149.5 (**4**), 147.4 (**7**), 136.9 (**2**), 134.8 (**6**), 127.5 (**3**), 116.9 (**1**), 116.1 (**5**), 98.3 (**8**), 81.0 (**14**), 70.8 (**15**), 41.5 (**12**), 20.7 (**13**), 18.8 (**10**), 13.9 (**11**) ppm

IR (neat) ν_{max} 3284 (m), 2915 (m), 780 (s) cm^{-1}

LCMS (ESI$^+$) *m/z* 225.3 $[M+H]^+$

HRMS (ESI$^+$) *m/z calcd. for* $C_{15}H_{16}N_2$ 225.1386 *m/z meas.* 225.1386 $[M+H]^+$

Mpt 183-185°C

Methyl 3-(benzyloxy)-6-(4-((5-methylquinolin-4-yl)amino)but-1-yn-1-yl)picolinate (2.83)

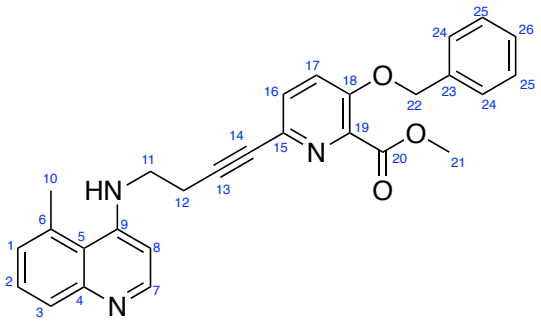

Mol. Wt. 451.2 $gmol^{-1}$

$C_{28}H_{25}N_3O_3$

Following a procedure adapted from de Sousa,[186] to a degassed solution of methyl 3-(benzyloxy)-6-bromopyridine-2-carboxylate (287 mg, 0.89 mmol, 1.1 equiv.) in THF/Et_3N (7 mL/3 mL), tetrakis(triphenylphosphine) palladium (93.0 mg, 0.08 mmol, 10 mol%) and copper iodide (31.0 mg, 0.16 mmol, 20 mol%) were added. After bubbling the reaction mixture with argon for 5 minutes at rt, a degassed solution of N-(but-3-yn-1-yl)-7-(trifluoromethyl)quinolin-4-amine (170 mg, 0.81 mmol, 1 equiv.) in THF (3 mL) was added dropwise and the yellow reaction mixture was stirred for 16 h at rt. Upon completion (TLC), the reaction mixture was concentrated *in vacuo* and purified by column chromatography (SiO_2, 20% MeOH in EtOAc), affording methyl 3-(benzyloxy)-6-(4-((5-methylquinolin-4-yl)amino)but-1-yn-1-yl)picolinate (270 mg, 0.88 mmol, 74%) as a cream solid.

TLC R_f 0.80 (20% MeOH in EtOAc, SiO_2)

^{1}HNMR (400MHz, MeOD-d_4) δ 8.31 (br. d, *J*=5.9 Hz, 1H, NC**H**), 7.70-7.18 (m, 10H, Ar**H**), 6.68 (d, *J*=5.9 Hz, 1H, NCH**CH**), 5.22 (s, 2H, Ph**CH$_2$**), 3.91 (s, 3H, CO_2**CH$_3$**), 3.67 (t, *J*=6.6 Hz, 2H, NH**CH$_2$**CH_2), 2.98 (s, 3H, C**CH$_3$**), 2.93 (t, *J*=6.6 Hz, 2H, $NHCH_2$**CH$_2$**) ppm

^{13}CNMR (101 MHz, MeOD-d_4) δ 166.6 (**20**), 155.7 (**18**), 154.4 (**9**), 148.1 (**7**), 148.0 (**4**), 141.5 (**19**), 137.2 (**15**), 135.8 (**6**), 135.6 (**23**), 131.3 (**24**), 131.1 (**25**), 129.9 (**16**), 129.7 (**17**), 129.2 (**26**), 128.3 (**2**), 125.3 (**5**), 125.2 (**1**), 123.8 (**3**), 100.7 (**8**), 88.1 (**13**), 81.8 (**14**), 71.9 (**22**), 53.0 (**21**), 43.1 (**11**), 24.6 (**12**), 19.6 (**10**) ppm

IR (neat) 3423 (m), 3192 (m), 2944 (m), 2300 (s), 1719 (s), 1090 (s)

LRMS (ESI$^+$) *m/z* 452.45 $[M+H]^+$

HRMS (ESI$^+$) *m/z calcd. for* $C_{28}H_{26}N_3O_3^+$ 452.1985 *m/z meas.* 452.1978 $[M+H]^+$

Mpt 176-178 °C

Methyl 3-(benzyloxy)-6-(4-((7,8-dimethylquinolin-4-yl)amino)but-1-yn-1-yl) picolinate (2.84)

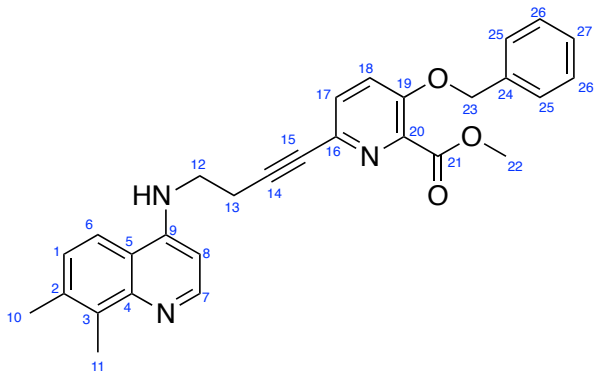

Mol. Wt. 465.2 $gmol^{-1}$

$C_{29}H_{27}N_3O_3$

Following a procedure adapted from de Sousa,[186] to a degassed solution of methyl 3-(benzyloxy)-6-bromopyridine-2-carboxylate (316 mg, 0.98 mmol, 1.1 equiv.) in THF/Et_3N (7 mL/3 mL), tetrakis(triphenylphosphine) palladium (103 mg, 0.09 mmol, 10 mol%) and copper iodide (34.0 mg, 0.18 mmol, 20 mol%) were added. After bubbling the reaction mixture with argon for 5 minutes at rt, a degassed solution of N-(but-3-yn-1-yl)-7-(trifluoromethyl)quinolin-4-amine (200 mg, 0.89 mmol, 1 equiv.) in THF (3 mL) was added dropwise and the black reaction mixture was stirred for 16 h at rt. Upon completion, the reaction mixture was concentrated *in vacuo* and purified by column chromatography on silica gel (20% MeOH in EtOAc), to afford methyl 3-(benzyloxy)-6-(4-((7,8-dimethylquinolin-4-yl)amino)but-1-yn-1-yl)picolinate (410 mg, 0.88 mmol, 99%) as a cream solid.

TLC R_f 0.36 (20% MeOH in EtOAc, SiO_2)

^{1}HNMR (400MHz, $CDCl_3$) δ 8.40 (d, *J*=5.9 Hz, 1H, NC**H**), 8.05 (br. d, *J*=8.6 Hz, 1H, $CH_3CCH_3CCHC\mathbf{H}$), 7.68 (d, *J*=8.8 Hz, 1H, NC**H**CH), 7.56 (d, *J*=8.8 Hz, 1H, N**H**CH), 7.46-7.30 (m, 6H, $CH_3CCH_3C\mathbf{H}CH$, Ar**H**), 6.66 (d, *J*=5.9 Hz, 1H, NCH**CH**), 5.26 (s, 2H, Ph$\mathbf{CH_2}$), 3.83 (s, 3H, $CO_2\mathbf{CH_3}$), 3.71-3.54 (m, 2H, NH$\mathbf{CH_2}CH_2$), 2.92-2.79 (m, 2H, $NHCH_2\mathbf{CH_2}$), 2.57 (s, 3H, NCC$\mathbf{CH_3}$) , 2.43 (s, 3H, $NCCCH_3C\mathbf{CH_3}$) ppm

^{13}CNMR (101 MHz, $CDCl_3$) δ 165.2 (**21**), 152.4 (**19**), 147.7 (**4**), 146.1 (**7**), 143.7 (**3**), 143.3 (**9**), 140.6 (**20**), 136.4 (**16**), 134.2 (**2**), 131.8 (**24**), 130.4 (**27**), 128.9 (**25**), 128.4 (**17**), 127.6 (**26**), 122.9 (**18**), 119.3 (**6**), 117.9 (**1**), 116.7 (**5**), 98.2 (**8**), 87.8 (**14**), 80.8 (**15**), 70.4 (**23**), 52.7 (**22**), 41.8 (**12**), 20.7 (**10**), 19.0 (**13**), 13.9 (**11**) ppm

IR (neat) ν_{max} 3192 (m), 1578 (s), 1012 (s) cm^{-1}

LRMS (ESI^+) *m/z* 466.5 $[M+H]^+$

HRMS (ESI$^+$) *m/z calcd. for* $C_{29}H_{28}N_3O_3$ 466.2125 *m/z meas.* 466.2125 $[M+H]^+$

Mpt 197-200 °C

Methyl 3-hydroxy-6-(4-((5-methylquinolin-4-yl)amino)butyl)picolinate (2.85)

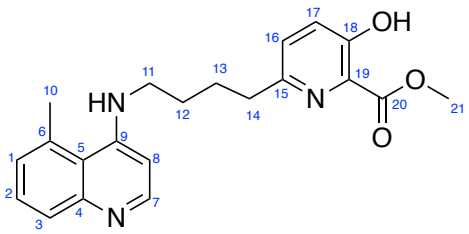

Mol. Wt. 365.2

$C_{21}H_{23}N_3O_3$

Following a procedure adapted from de Sousa,[186] to a degassed solution of methyl 3-(benzyloxy)-6-(4-((5-methylquinolin-4-yl)amino)but-1-yn-1-yl)picolinate (270 mg, 0.60 mmol, 1 equiv.) in anhydrous MeOH (20 mL), was added Pearlman's catalyst (90.0 mg, 0.64 mmol, 1 equiv.). After evacuating and flushing with hydrogen five times, the black reaction mixture was stirred at rt, under a hydrogen atmosphere for 7 h. Upon completion (TLC), the catalyst was removed by filtration through Celite and the solvent was removed *in vacuo*, affording methyl 3-hydroxy-6-(4-((5-methylquinolin-4-yl)amino)butyl)picolinate (205 mg, 0.56 mmol, 94%) as a pale cream solid.

TLC R_f 0.06 (20% MeOH in EtOAc, SiO_2)

^{1}HNMR (400MHz, MeOD-d_4) δ 8.24 (d, *J*=5.9 Hz, 1H, NC**H**), 7.67-7.18 (m, 5H, Ar**H**), 6.52 (d, *J*=5.9 Hz, 1H, NCH**CH**), 3.97 (s, 3H, CO_2**C**H_3), 3.38 (br. t, *J*=6.7 Hz, 2H, NH**C**$H_2$$CH_2$), 2.92 (s, 3H, C**C**H_3), 2.88-2.80 (m, 2H, NHCH_2CH_2CH_2**C**H_2), 1.92-1.77 (m, 4H, NHCH_2**C**H_2**C**H_2CH_2) ppm

^{13}CNMR (101 MHz, MeOD-d_4) δ 170.5 (**20**), 158.3 (**18**), 155.8 (**15**), 154.6 (**9**), 148.4 (**7**), 148.2 (**4**), 135.6 (**6**), 130.7 (**17**), 130.6 (**19**), 130.2 (**1**), 129.6 (**2**), 128.3 (**16**), 125.5 (**3**), 120.0 (**5**), 100.5 (**8**), 53.2 (**21**), 44.3 (**11**), 37.2 (**14**), 28.5 (**12**), 28.4 (**13**), 24.5 (**10**) ppm

IR (neat) 3369 (m), 2932 (m), 1617 (s), 1217 (s), 1083 (s)

LRMS (ESI$^+$) *m/z* 366.3 $[M+H]^+$

HRMS (ESI$^+$) *m/z calcd. for* $C_{21}H_{24}N_3O_3^+$ 366.1812 *m/z meas.* 366.1817 $[M+H]^+$

Mpt 64-66 °C

Methyl 6-(4-((7,8-dimethylquinolin-4-yl)amino)butyl)-3-hydroxypicolinate (2.88)

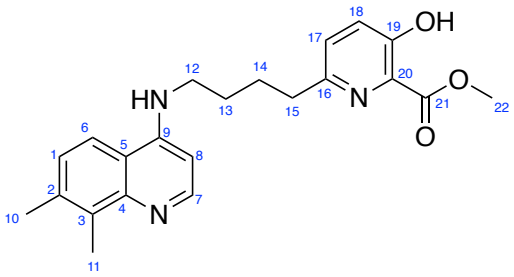

Mol. Wt. 379.2 $gmol^{-1}$

$C_{22}H_{25}N_3O_3$

Following a procedure adapted from de Sousa,[186] to a degassed solution of methyl 3-(benzyloxy)-6-(4-((7,8-dimethylquinolin-4-yl)amino)but-1-yn-1-yl) picolinate (300 mg, 0.64 mmol, 1 equiv.) in anhydrous MeOH (10 mL) was added Pearlman's catalyst (91.0 mg, 0.64 mmol, 1 equiv.). After evacuating and flushing with hydrogen five times, the black reaction mixture was stirred at rt, under a hydrogen atmosphere for 18 h. Upon completion, the catalyst was removed by filtration through Celite and the solvent was removed *in vacuo*, affording methyl 6-(4-((7,8-dimethylquinolin-4-yl)amino)butyl)-3-hydroxypicolinate (245 mg, 0.64 mmol, 100%) as a pale cream solid.

TLC R_f 0.08 (20% MeOH in EtOAc, SiO_2)

^{1}HNMR (400MHz, DMSO-d_6) δ 8.34 (d, *J*=6.4 Hz, 1H, NC**H**), 8.18-8.09 (m, 1H, NCC(CH_3)C(CH_3)CH**CH**), 7.44-7.32 (m, 3H, Ar**H**), 6.60 (d, *J*=6.4 Hz, 1H, NCH**CH**), 3.86 (s, 3H, CO_2**CH_3**), 3.44-3.38 (m, 2H, NH**CH_2**CH_2), 2.76-2.68 (m, 2H, $NCH_2CH_2CH_2$**CH_2**), 2.54 (s, 3H, NCC(CH_3)C(**CH_3**)), 2.43 (s, 3H, NCC(**CH_3**)C(CH_3)), 1.79-1.63 (m, 4H, $NHCH_2$**CH_2CH_2**CH_2) ppm

^{13}CNMR (101 MHz, DMSO-d_6) δ 168.0 (**21**), 156.2 (**16**), 153.9 (**9**), 153.2 (**4**), 152.4 (**19**), 145.6 (**7**), 135.8 (**2**), 133.0 (**18**), 131.6 (**20**), 128.1 (**3**), 127.5 (**17**), 126.0 (**1**), 119.4 (**6**), 115.9 (**5**), 97.5 (**8**), 52.3 (**22**), 42.5 (**12**), 36.0 (**15**), 27.3 (**14**), 26.8 (**13**), 20.2 (**10**), 13.5 (**11**) ppm

IR (neat) 3430 (m), 3223 (m), 2951 (m), 2859 (m), 1615 (s), 1219 (s)

LRMS (ESI$^+$) *m/z* 380.45 $[M+H]^+$

HRMS (ESI$^+$) *m/z calcd. for* $C_{22}H_{26}N_3O_3$ 380.1969 *m/z meas.* 380.1974 $[M+H]^+$

Mpt 69-72 °C

(*E*)-6-(4-((7,8-Dimethylquinolin-4-yl)amino)butyl)-3-hydroxypicolinaldehyde oxime (2.86)

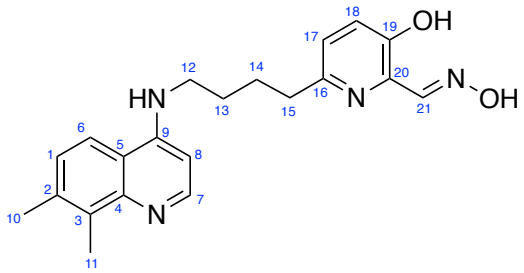

Mol. Wt. 364.4 gmol^{-1}

$C_{21}H_{24}N_4O_2$

Following a procedure adapted from de Sousa,[186] to a degassed solution of methyl 6-(4-((7,8-dimethylquinolin-4-yl)amino)butyl)-3-hydroxypicolinate (200 mg, 0.52 mmol, 1 equiv.) in anhydrous CH_2Cl_2 (20 mL), was added 2,6-lutidine (0.18 mL, 1.58 mmol, 3 equiv.) and TBSOTf (0.24 mL, 1.05 mmol, 2 equiv.) successively and the pale yellow reaction was stirred at rt for 5 h under argon. The reaction mixture was concentrated *in vacuo*. To a solution of the residue in anhydrous CH_2Cl_2 (20 mL) at −78 °C was added DIBAL-H (1 M in CH_2Cl_2) (1.60 mL, 1.58 mmol, 3 equiv.) dropwise. The reaction was stirred at −78 °C for 1 h and the reaction was quenched at −78 °C with MeOH (5 mL). The colourless mixture was warmed to rt and the solvent was removed *in vacuo*. The white aluminium salts were removed by filtration in CH_2Cl_2. The filtrate was concentrated *in vacuo* and the residue was dissolved in anhydrous EtOH (40 mL). Hydroxylamine hydrochloride (73.0 mg, 1.05 mmol, 2 equiv.) and sodium acetate (87.0 mg, 1.05 mmol, 2 equiv.) were added and the solution was stirred at reflux for 16 h. After concentration *in vacuo*, the off white crude product was washed with CH_2Cl_2 (3 × 10 mL). The solution was concentrated *in vacuo* and purified by column chromatography (SiO_2, 10% MeOH in CH_2Cl_2), to afford (*E*)-6-(4-((7,8-dimethylquinolin-4-yl)amino)butyl)-3-hydroxypicolinaldehyde oxime (140 mg, 0.38 mmol, 73%) as a cream solid.

(*E*)-6-(4-((7,8-Dimethylquinolin-4-yl)amino)butyl)-3-hydroxypicolinaldehyde oxime (20.0 mg, 0.05 mmol) was dissolved in 2 M HCl (3 mL). The cream solution was stirred at rt for 10 mins. The reaction solution was concentrated *in vacuo* to afford (*E*)-6-(4-((7,8-dimethylquinolin-4-yl)amino)butyl)-3-hydroxypicolinaldehyde oxime hydrochloride (20.0 mg, 0.05 mmol, 100%) as a colourless solid.

TLC R_f 0.18 (10% MeOH in CH_2Cl_2, SiO_2)

^{1}HNMR (400MHz, MeOD-d_4) δ 8.22 (d, *J*=7.1 Hz, 1H, NC**H**), 8.11 (s, 1H, **CH**NOH), 8.07 (d, *J*=8.8 Hz, 1H, NCC(CH3)C(CH3)CH**CH**), 7.52 (d, *J*=8.8 Hz, 1H, NCC(CH3)C(CH3)**CH**CH), 7.22 (d, *J*=8.3 Hz, 1H, NC**CH**CH), 7.16 (d, *J*=8.3 Hz, 1H, NCCH**CH**), 6.77 (d, *J*=7.1 Hz, NCH**CH**), 3.62-3.56 (m, 2H, NH**CH$_2$**CH$_2$CH$_2$CH$_2$), 2.83-2.74 (s, 2H, NHCH$_2$CH$_2$CH$_2$**CH$_2$**), 2.57 (s, 3H,

	NCC(CH_3)C(**CH_3**)), 2.56 (s, 3H, NCC(**CH_3**)C(CH_3)), 1.94-1.75 (m, 4H, $NHCH_2$**CH_2CH_2**CH_2) ppm
^{13}CNMR	(101 MHz, MeOD-d_4) δ 158.0 (**10**), 154.2 (**9**), 153.9 (**16**), 152.8 (**21**), 144.4 (**4**), 142.6 (**7**), 136.5 (**20**), 130.7 (**3**), 127.5 (**2**), 126.1 (**1**), 125.7 (**17**), 123.5 (**18**), 121.3 (**5**), 120.8 (**6**), 98.9 (**8**), 44.5 (**12**), 37.3 (**15**), 28.2 (**13**), 28.1 (**14**), 21.0 (**10**), 13.3 (**11**) ppm
IR (neat)	3271 (m), 2488 (m), 2361 (m), 1619 (s), 1466 (s), 1030 (s)
LRMS	(ESI$^+$) *m/z* 365.40 $[M+H]^+$
HRMS	(ESI$^+$) *m/z calcd. for* $C_{21}H_{25}N_4O_2^+$ 365.1972 *m/z meas.* 365.1977 $[M+H]^+$
Mpt	202 °C (decomposed)

Bromo-5-fluoroquinoline (2.90)

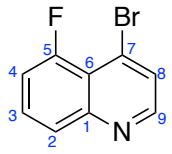

Mol. Wt. 226.0 $gmol^{-1}$

C_9H_5BrFN

Following a procedure adapted from Franzblau *et al.*,[234] to a solution of a mixture of 5-fluoroquinolin-4-ol (2.60 g, 15.9 mmol, 1.86 equiv.) and 7-fluoroquinolin-4-ol (1.40 g, 8.58 mmol, 1 equiv.) in DMF (30 mL) at 60 °C was added phosphorus tribromide (1.86 mL, 19.7 mmol, 2.3 equiv.). The orange mixture was cooled to 45 °C and stirred for 45 min. After cooling to rt, the reaction was diluted with H_2O (20 mL) and the solution was basified with saturated aqueous $NaHCO_3$ to pH 10. The resulting pale yellow solid was washed with H_2O, filtered and taken up in EtOAc and concentrated *in vacuo*. The crude product was purified by column chromatography (SiO_2, 30% hexane in EtOAc) to afford 4-bromo-7,8-dimethylquinoline (2.50 g, 11.1 mmol, 69%) as a cream solid.

TLC R_f 0.74 (30% hexane in EtOAc, SiO_2)

^{1}HNMR (400MHz, $CDCl_3$) δ 8.67 (d, *J*=4.6 Hz, 1H, NC**H**), 8.22 (dd, *J*=9.2, 5.9 Hz, 1H, CC**H**CH), 7.75 (dd, *J*=9.2, 2.7 Hz, 1H, FC**C**H), 7.68 (d, *J*=4.6 Hz, 1H, NCH**C**H), 7.44 (ddd, *J*=9.2, 5.9, 2.7 Hz, 1H, CCH**C**H ppm

^{13}CNMR (101 MHz, MeOD-d_4) δ 163.4 (d, *J*=251 Hz, **5**), 150.6 (**9**), 149.6 (**1**), 133.7 (**7**), 128.9 (**3**), 124.7 (**8**), 124.1 (**2**), 118.0 (d, *J*=25 Hz, **6**), 113.1 (d, *J*=20 Hz, **4**) ppm

^{19}FNMR (376 MHz, $CDCl_3$) δ 108.7 ppm

IR (neat) ν_{max} 3091 (m), 3041 (m), 1298 (s), 1057 cm^{-1}

LRMS (ESI$^+$) *m/z* 227.1 $[M^{79}Br+H]^+$, 229.1 $[M^{81}Br+H]^+$

HRMS (ESI$^+$) *m/z calcd. for* $C_9H_5BrFN^+$ 225.9658 *m/z meas.* 225.9662

Mpt 89-90 °C

***N*-(But-3-yn-1-yl)-5-fluoroquinolin-4-amine (2.91)**

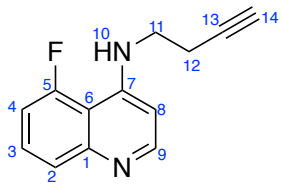

Mol. Wt. 214.2 $gmol^{-1}$

$C_{13}H_{11}FN_2$

Following a procedure adapted from Musonda *et al.*,[236] 3-butyn-1-amine (0.60 mL, 6.64 mmol, 1 equiv.) was mixed with 4-bromo-5-fluoroquinoline (1.50 g, 6.64 mmol, 1 equiv.) to form a beige paste. The paste was heated to 80 °C for 1 h without stirring. The temperature was then raised to 120 °C and the reaction was stirred for 16 h. The reaction was cooled to rt and 1 M aqueous NaOH (2 mL) was added. The brown organic product was basified to pH 10 with 10% aqueous NaOH and was extracted (CH_2Cl_2). The organic layers were combined, washed, dried ($MgSO_4$), filtered and concentrated *in vacuo*. The brown crude product was purified by column chromatography (SiO_2, 20% MeOH in EtOAc), to afford N-(but-3-yn-1-yl)-5-fluoroquinolin-4-amine (1.06 g, 4.95 mmol, 75%) as a cream solid.

TLC R_f 0.59 (20% MeOH in EtOAc, SiO_2)

^{1}HNMR (400MHz, DMSO-d_6) δ 8.39 (d, *J*=5.4 Hz, 1H, NC**H**), 8.27 (dd, *J*=10.8, 8.3 Hz, 1H, CC**H**CH), 7.47 (dd, *J*=10.8, 2.5 Hz, 1H, FC**CH**), 7.44-7.39 (m, 1H, N**H**), 7.35 (ddd, *J*=10.8, 8.3, 2.5 Hz, 1H, CCH**CH**), 6.49 (d, *J*=5.6 Hz, 1H, NCH**CH**), 3.45 (q, *J*=7.1 Hz, 2H, NH**CH$_2$**CH$_2$CCH), 2.88 (t, *J*=2.7 Hz, 1H, NHCH$_2$CH$_2$C**CH**), 2.55 (td, *J*=7.1, 2.7 Hz, 2H, NHCH$_2$**CH$_2$**CCH) ppm

^{13}CNMR (101 MHz, DMSO-d_6) δ 163.4 (**9**), 160.9 (d, *J*=245 Hz, **5**), 151.9 (**7**), 149.7 (**1**), 124.5 (**3**), 115.8 (**2**), 113.5 (d, *J*=25 Hz, **4**), 112.2 (d, *J*=20 Hz, **6**), 98.2 (**8**), 82.2 (**13**), 72.4 (**14**), 41.2 (**11**) 17.7 (**12**) ppm

^{19}FNMR (376 MHz, DMSO-d_6) δ 112.0 ppm

IR (neat) ν_{max} 3080 (m), 2912 (m), 2240 (s), 785 (s) cm^{-1}

LRMS (ESI$^+$) *m/z* 215.3 $[M+H]^+$

HRMS (ESI$^+$) *m/z calcd. for* $C_{13}H_{11}FN_2^+$ 215.0983 *m/z meas.* 215.0979

Mpt 225-226 °C

Methyl 3-(benzyloxy)-6-(4-((5-fluoroquinolin-4-yl)amino)but-1-yn-1-yl)picolinate (2.92)

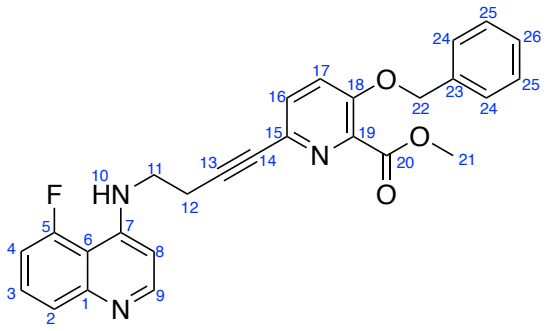

Mol. Wt. 455.5 $gmol^{-1}$

$C_{27}H_{22}FN_3O_3$

Following a procedure adapted from de Sousa,[186] to a degassed solution of N-(but-3-yn-1-yl)-5-fluoroquinolin-4-amine (300 mg, 1.40 mmol, 1 equiv.) in anhydrous THF/Et_3N (7 mL/3 mL), tetrakis(triphenylphosphine) palladium (161 mg, 0.14 mmol, 10 mol%) and copper iodide (54.0 mg, 0.28 mmol, 20 mol%) were added. After bubbling the reaction mixture with argon for 5 minutes at rt, a degassed solution of methyl 3-(benzyloxy)-6-bromopyridine-2-carboxylate (497 mg, 1.54 mmol, 1.1 equiv.) in anhydrous THF (3 mL) was added dropwise and the yellow reaction mixture was stirred for 16 h at rt. Upon completion (TLC), the orange reaction mixture was concentrated *in vacuo* and purified by column chromatography (SiO_2, EtOAc to 20% MeOH in EtOAc), to afford methyl 3-(benzyloxy)-6-(4-((5-fluoroquinolin-4-yl)amino)but-1-yn-1-yl)picolinate (485 mg, 1.07 mmol, 76%) as a cream solid.

TLC R_f 0.55 (20% MeOH in EtOAc, SiO_2)

^{1}HNMR (400MHz, DMSO-d_6) δ 8.44 (br. s, 1H, NH), 8.33 (br. dd, *J*=9.0, 4.4 Hz, 1H, NCH), 7.69 (d, *J*=8.8 Hz, 1H, NCCHCHC), 7.65-7.52 (m, 2H, ArH), 7.51-7.26 (m, 7H, ArH), 6.56 (br. d, *J*=4.4 Hz, 1H, NCHCH), 5.26 (s, 2H, $PhCH_2$), 3.84 (s, 3H, CO_2CH_3), 3.57 (q, *J*=6.7 Hz, 2H, $NHCH_2CH_2$), 2.83 (t, *J*=6.7 Hz, 2H, $NHCH_2CH_2$) ppm

^{13}CNMR (101 MHz, DMSO-d_6) δ 165.2 (20), 163.8 (9), 161.4 (d, *J*=250 Hz, 5), 152.4 (18), 150.2 (7), 140.6 (19), 136.5 (16), 134.3 (23), 132.0 (1), 130.4 (3), 129.3 (8), 129.0 (24), 128.7 (15), 127.8 (25), 127.7 (26) 125.1 (2) 122.9 (17), 114.0 (d, *J*=21 Hz, 4), 112.7 (d, *J*=22 Hz, 6), 88.0 (13), 80.7 (14), 70.4 (22), 52.8 (21), 41.6 (11), 19.0 (12) ppm

^{19}FNMR (376 MHz, DMSO-d_6) δ 112.1 ppm

IR (neat) ν_{max} 3293 (m), 2232 (s), 1580 (s), 1007 (s) cm^{-1}

LRMS (ESI$^+$) *m/z* 456.4 $[M+H]^+$

HRMS (ESI$^+$) *m/z calcd. for* $C_{27}H_{22}FN_3O_3^+$ 456.1724 *m/z meas.* 456.1723

Mpt 65-66 °C

Methyl 6-(4-((5-fluoroquinolin-4-yl)amino)butyl)-3-hydroxypicolinate (2.93)

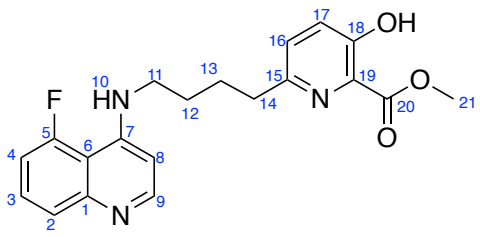

Mol. Wt. 369.4 gmol^{-1}

$C_{20}H_{20}FN_3O_3$

Following a procedure adapted from de Sousa,[186] to a degassed solution of methyl 3-(benzyloxy)-6-(4-((5-fluoroquinolin-4-yl)amino)but-1-yn-1-yl)picolinate (400 mg, 0.88 mmol, 1 equiv.) in anhydrous MeOH (20 mL) was added Pearlman's catalyst (123 mg, 0.88 mmol, 1 equiv.). After evacuating and flushing with hydrogen five times, the black reaction mixture was stirred at rt, under a hydrogen atmosphere for 7 h. Upon completion, the catalyst was removed by filtration through Celite and the solvent was removed *in vacuo*, affording methyl 6-(4-((5-fluoroquinolin-4-yl)amino)butyl)-3-hydroxypicolinate (324 mg, 0.88 mmol, 100%) as a pale cream solid.

TLC R_f 0.25 (20% MeOH in EtOAc, SiO_2)

^{1}HNMR (400MHz, DMSO-d_6) δ 8.38-8.28 (m, 2H, **OH,** N**CH**), 7.65-7.52 (m, 1H, NC**CH**), 7.43 (dd, *J*=10.9, 2.6 Hz, 1H, NCCH**CH**), 7.37-7.25 (m, 2H, **NH,** NCCHCH**CH**), 7.12 (d, *J*=8.6 Hz, 1H, NC**C**HCHCOH), 7.04 (br. d, *J*=8.6 Hz, 1H, NCCH**CH**COH), 6.41 (d, *J*=5.6 Hz, 1H, NCH**CH**), 3.75 (s, 3H, CO_2**C**H_3), 3.27 (q, *J*=6.1 Hz, 2H, NH**C**$H_2$$CH_2CH_2CH_2$), 2.62 (t, *J*=6.6 Hz, 2H, $NHCH_2CH_2CH_2$**C**H_2), 1.76-1.58 (m, 4H, $NHCH_2$**C**H_2**C**$H_2$$CH_2$) ppm

^{13}CNMR (101 MHz, DMSO-d_6) δ 167.9 (**20**), 163.3 (d, *J*=250 Hz, **7**), 151.9 (**5**), 150.2 (**1**), 149.5 (**9**), 149.7 (**18**), 146.8 (**15**), 131.5 (**19**), 128.8 (**3**), 127.0 (**16**), 124.7 (**17**), 115.9 (**2**), 113.3 (d, *J*=23 Hz, **4**), 112.2 (d, *J*=20 Hz, **6**), 98.0 (**8**) 51.3 (**21**) 42.3 (**11**), 36.1 (**14**), 27.4 (**12**), 27.3 (**13**) ppm

^{19}FNMR (376 MHz, DMSO-d_6) δ 112.4 ppm

IR (neat) ν_{max} 3077 (m), 1581 (s), 1034 (s) cm^{-1}

LRMS (ESI$^+$) *m/z* 370.4 $[M+H]^+$

HRMS (ESI$^+$) *m/z calcd. for* $C_{20}H_{20}FN_3O_3^+$ 370.1566 *m/z meas.* 370.1566

Mpt 154-156 °C (decomposed)

(E)-6-(4-((5-Fluoroquinolin-4-yl)amino)butyl)-3-hydroxypicolinaldehyde oxime (2.48)

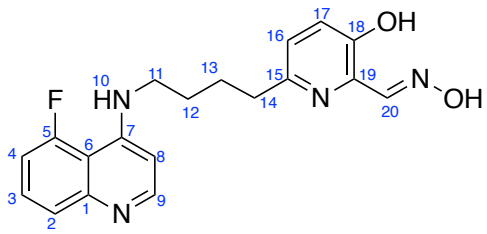

Mol. Wt. 354.4 $gmol^{-1}$

$C_{19}H_{19}FN_4O_2$

Following a procedure adapted from de Sousa,[186] to a degassed solution of methyl 6-(4-((5-fluoroquinolin-4-yl)amino)butyl)-3-hydroxypicolinate (45.0 mg, 0.12 mmol, 1 equiv.) in anhydrous CH_2Cl_2 (2 mL), was added 2,6-lutidine (0.04 mL, 0.37 mmol, 3 equiv.) and TBSOTf (0.06 mL, 0.24 mmol, 2 equiv.) successively and the pale yellow reaction was stirred at rt for 5 h under argon. The reaction mixture was concentrated *in vacuo*. To a colourless solution of the residue in anhydrous CH_2Cl_2 (2 mL) at −78 °C was added DIBAL-H (1 M in CH_2Cl_2) (0.37 mL, 0.37 mmol, 3 equiv.) dropwise. The reaction was stirred at −78 °C for 1 h and the reaction was quenched at −78 °C with MeOH (3 mL). The mixture was warmed to rt and the solvent was removed *in vacuo*. The white aluminium salts were removed by filtration in CH_2Cl_2. The filtrate was concentrated *in vacuo* and the residue was dissolved in anhydrous EtOH (5 mL). Hydroxylamine hydrochloride (17.0 mg, 0.24 mmol, 2 equiv.) and sodium acetate (20.0 mg, 0.24 mmol, 2 equiv.) were added and the solution was stirred at reflux for 16 h. After concentration *in vacuo*, the orange crude product was washed with CH_2Cl_2. The crude product was purified by column chromatography (SiO_2, 10% MeOH in CH_2Cl_2) to afford (*E*)-6-(4-((5-fluoroquinolin-4-yl)amino)butyl)-3-hydroxypicolinaldehyde oxime (40 mg, 0.11 mmol, 93%) as a pale orange solid.

(*E*)-6-(4-((5-Fluoroquinolin-4-yl)amino)butyl)-3-hydroxypicolinaldehyde oxime (10.0 mg, 0.03 mmol) was dissolved in 2 M HCl (3 mL). The orange solution was stirred at rt for 10 mins. The reaction solution was concentrated *in vacuo* to afford (*E*)-6-(4-((5-fluoroquinolin-4-yl)amino)butyl)-3-hydroxypicolinaldehyde oxime hydrochloride (11.7 mg, 0.03 mmol, 100%) as a beige solid.

TLC R_f 0.28 (10% MeOH in CH_2Cl_2, SiO_2)

^{1}HNMR (400MHz, MeOH-d^4) δ 8.33 (d, *J*=7.1 Hz, 1H, NC**H**), 8.18 (s, 1H, N**OH**), 7.70-7.62 (m, 1H, N**H**), 7.55-7.46 (m, 3H, NCC**H**C**H**C**H**), 7.24 (d, *J*=8.6 Hz, 1H, NCCHC**H**C(OH)), 7.17 (d, *J*=8.6 Hz, 1H, NC**H**CHC(OH)), 6.80 (d, *J*=7.1 Hz, 1H, NCHC**H**), 3.26-3.16 (m, 2H, NH**CH$_2$**CH$_2$), 2.84-2.77 (m, 2H, NHCH$_2$CH$_2$CH$_2$**CH$_2$**), 1.93-1.77 (m, 4H, NHCH$_2$**CH$_2$CH$_2$**CH$_2$) ppm

^{13}CNMR (101 MHz, MeOH-d^4) δ 167.1 (d, *J*=250 Hz, **5**), 156.3 (**7**), 153.3 (**20**), 151.6 (**1**), 149.3 (**18**), 146.0 (**9**), 142.4 (**15**), 132.8 (**19**), 127.3 (**3**), 124.7 (**16**), 122.0 (**17**), 118.8 (**2**), 116.3 (d, *J*=25 Hz, **4**), 104.5 (**8**), 98.2 (d, *J*=19 Hz, **6**), 46.6 (**14**), 43.0 (**11**), 27.1 (**13**), 26.5 (**12**) ppm

^{19}FNMR (376 MHz, MeOH-d^4) δ 79.7 ppm

IR (neat) ν_{max} 2956 (m), 2853 (s), 2360 (s), 1734 (s), 1457 (s) cm^{-1}

LRMS (ESI^+) *m/z* 355.5 $[M+H]^+$

HRMS (ESI^+) *m/z calcd. for* $C_{19}H_{19}FN_4O_2^+$ 355.1565 *m/z meas.* 355.1565 $[M+H]^+$

Mpt 201-202 °C

4-Bromoquinoline (2.26)

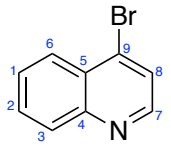

Mol. Wt. 207.1

C_9H_6BrN

Following the procedure from Margolis *et al.*[233] for the synthesis of bromoquinolines, to a solution of 4-quinolinol (5.00 g, 34.4 mmol, 1 equiv.) in DMF (50 mL) at 60 °C was added dropwise PBr_3 (3.34 mL, 35.5 mmol, 1.03 equiv.). Upon addition, a colour change was observed from yellow to vivid orange, with effervescence. The orange reaction mixture was stirred at 45 °C for 45 min. The solution was cooled to rt and diluted with H_2O (20 mL) and a saturated solution of aqueous $NaHCO_3$ was slowly added to basify the reaction mixture to pH 10. The solution was extracted with CH_2Cl_2 (5 × 20 mL), then the organic solutions were combined and washed with H_2O (20 mL), dried ($MgSO_4$), filtered and concentrated *in vacuo*. Column chromatography (SiO_2, EtOAc) afforded 4-bromoquinoline (5.56 g, 26.7 mmol, 78%) as a cream solid. Data was consistent to that reported in the literature.[233]

TLC R_f 0.76 (EtOAc, SiO_2)

^{1}HNMR (400MHz, DMSO-d_6) δ 8.68 (d, *J*=4.6 Hz, 1H, NC**H**), 8.20 (dd, *J*=8.4, 0.9 Hz, 1H, NC**C**H**C**H**C**H**C**H), 8.11 (d, *J*=8.4 Hz, 1H, NCCHCHCH**C**H), 7.78 (ddd, *J*=8.4, 7.0, 1.4 Hz, 1H, NCCH**C**H), 7.71 (d, *J*=4.6 Hz, 1H, NCH**C**H), 7.66 (ddd, *J*=8.4, 7.0, 1.4 Hz, 1H, NCCHCH**C**H**C**H) ppm

^{13}CNMR (101 MHz, DMSO-d_6) δ 149.9 (**7**), 149.0 (**4**), 134.2 (**9**), 130.4 (**2**), 129.9 (**1**), 127.9 (**3**), 127.8 (**5**), 126.8 (**6**), 125.1 (**8**) ppm

IR (neat) ν_{max} 3062 (m), 1615 (s), 1058 (s) cm^{-1}

LRMS (ESI$^+$) *m/z* 208.1 $[M^{79}Br+H]^+$ 210.1 $[M^{81}Br+H]^+$

Mpt 28-29 °C (lit: 29-30 °C)

_N_-(But-3-yn-1-yl)quinolin-4-amine (2.25)

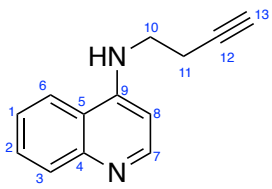

Mol. Wt. 196.2

$C_{13}H_{12}N_2$

Following a procedure adapted from Musonda *et al.*,[236] 3-butyn-1-amine (4.72 mL, 57.7 mmol, 4 equiv.) was added to 4-bromoquinoline (3.00 g, 14.4 mmol, 1equiv.) to form a cream-coloured paste. The paste was heated to 80 °C for 1 h without stirring. The temperature was increased to 140 °C and the paste was heated for 18 h with stirring. The viscous, brown reaction mixture was cooled to rt and purified by chromatography on (SiO_2, 20% MeOH in EtOAc) to afford *N*-(but-3-yn-1-yl)quinolin-4-amine (2.82 g, 14.4 mmol, 100%) as a cream solid.

TLC R_f 0.27 (20% MeOH in EtOAc, SiO_2)

^{1}HNMR (400MHz, DMSO-d_6) δ 8.45 (d, *J*=5.9 Hz, 1H, NC**H**), 8.30 (dd, *J*=8.3, 1.2 Hz, 1H, NC**C**H**C**HCHCH), 7.93 (br. s, 1H, **NH**), 7.82 (dd, *J*=8.3, 1.2 Hz, 1H, NCCHCHCH**C**H), 7.71 (ddd, *J*=8.3, 7.0, 1.2 Hz, 1H, NCCH**C**H**C**HCH), 7.51 (ddd, *J*=8.3, 7.0, 1.2 Hz, 1H, NCCHCH**C**H**C**H), 6.63 (d, *J*=5.9 Hz, 1H, NCH**C**H), 3.54 (q, *J*=7.0 Hz, 2H, NH**C**$H_2$$CH_2$CCH), 2.91 (t, *J*=2.7 Hz, 1H, NHCH$_2$CH$_2$C**C**H), 2.58 (td, *J*=6.8, 2.7 Hz, 2H, NHCH$_2$**C**H_2CCH) ppm

^{13}CNMR (101 MHz, DMSO-d_6) δ 151.3 (**9**), 148.2 (**7**), 145.1 (**4**), 130.2 (**2**), 126.4 (**5**), 124.7 (**3**), 122.1 (**6**), 118.1 (**1**), 98.3 (**8**), 82.1 (**12**), 72.6 (**13**), 41.4 (**10**), 17.8 (**11**) ppm

IR (neat) ν_{max} 3281 (s), 3169 (m), 3067 (s), 1918 (s), 1151 (s) cm^{-1}

LRMS (ESI$^+$) *m/z* 197.2 $[M+H]^+$

HRMS (ESI$^+$) *m/z calcd. for* $C_{13}H_{13}N_2^+$ 197.1073 *m/z meas.* 197.1072 $[M+H]^+$

Mpt 165-166 °C

Methyl 3-(benzyloxy)-6-(4-(quinolin-4-ylamino)but-1-yn-1-yl)picolinate (2.44)

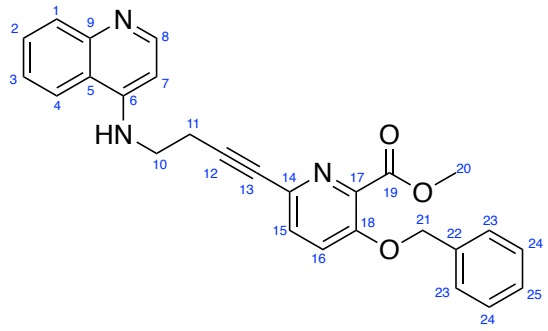

Mol. Wt. 437.2

$C_{27}H_{23}N_3O_3$

Following a procedure adapted from de Sousa,[186] to a degassed solution of *N*-(but-3-yn-1-yl)quinoline-4-amine (500 mg, 2.55 mmol, 1 equiv.) in THF/Et_3N (50 mL/15 mL) was added $Pd(PPh_3)_4$ (294 mg, 0.25 mmol, 10 mol%) and CuI (97.0 mg, 0.51 mmol, 20 mol%). To the resulting yellow reaction mixture was added dropwise a degassed solution of methyl 3-(benzyloxy)-6-bromopyridine-2-carboxylate (902 mg, 2.80 mmol, 1.1 equiv.) in THF (20 mL). The brown solution was stirred for 18 h at rt. The orange reaction was concentrated *in vacuo*. Column chromatography (SiO_2, 20% MeOH in EtOAc) afforded methyl 3-(benzyloxy)-6-(4-(quinolin-4-ylamino)but-1-yn-1-yl)picolinate (825 mg, 1.89 mmol, 74%) as a cream solid. Data was consistent to that reported in the literature.[186]

TLC R_f 0.07 (10% MeOH in EtOAc, SiO_2)

^{1}HNMR (400MHz, DMSO-d_6) δ 8.28 (br d, *J*=5.9 Hz, 1H, NC**H**), 7.85-7.29 (m, 11H, Ar**H**), 6.66 (d, *J*=5.9 Hz, NCH**CH**), 5.26 (s, 2H, Ph**CH$_2$**), 3.83 (s, 3H, CO_2**CH$_3$**), 3.62 (q, *J*=7.1 Hz, 2H, NH**CH$_2$**CH_2), 2.85 (t, *J*=7.1 Hz, 2H, $NHCH_2$**CH$_2$**) ppm

^{13}CNMR (101 MHz, DMSO-d_6) δ 164.7 (**19**), 155.9 (**6**), 151.9 (**18**), 150.5 (**8**), 149.6 (**9**), 140.1 (**17**), 135.9 (**14**), 133.8 (**22**), 130.4 (**16**), 129.9 (**2**), 129.6 (**15**), 128.5 (**23**), 128.0 (**25**), 127.5 (**5**), 127.2 (**24**), 124.4 (**1**), 122.5 (**4**), 121.9 (**3**), 113.4 (**7**), 87.4 (**12**), 80.3 (**13**), 70.0 (**21**), 52.3 (**20**), 41.2 (**10**), 18.5 (**11**) ppm

IR (neat) ν_{max} 3292 (b), 2948 (s), 2235 (s), 1727 (s), 1581 (s) cm^{-1}

LRMS (ESI$^+$) *m/z* 438.4 $[M+H]^+$

HRMS (ESI$^+$) *m/z calcd. for* $C_{27}H_{24}N_3O_3^+$ 438.1812 *m/z meas.* 438.1815 $[M+H]^+$

Mpt 69-70 °C (decomposed)

Methyl 3-hydroxy-6-(4-(quinolin-4-ylamino)butyl)picolinate (2.45)

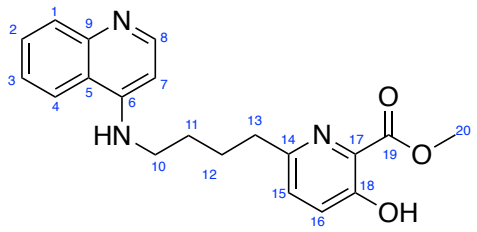

Mol. Wt. 351.4

$C_{20}H_{21}N_3O_3$

Following a procedure adapted from de Sousa,[186] to a degassed suspension of methyl 3-(benzyloxy)-6-(4-(quinoline-4-ylamino)but-1-yn-1-yl)picolinate (420 mg, 0.96 mmol, 1 equiv.) in anhydrous MeOH (25 mL), was added Pearlman's catalyst (135 mg, 0.96 mmol, 1 equiv.). The reaction vessel was evacuated and flushed with hydrogen gas five times. The black reaction mixture was stirred for 18 h at rt. The catalyst was removed by filtration through Celite and the solvent was removed *in vacuo* to afford Methyl 3-hydroxy-6-(4-(quinolin-4-ylamino)butyl)picolinate (336 mg, 0.96 mmol, 100%) as a pale yellow solid.

TLC R_f 0.26 (50% MeOH in EtOAc, SiO_2)

^{1}HNMR (400MHz, DMSO-d_6) δ 8.39 (d, *J*=5.9 Hz, 1H, NC**H**), 8.29 (d, *J*=8.3, 1H, NC**C**HCHCHCH), 7.79 (d, *J*=8.3 Hz, 1H, NCCHCHCH**CH**), 7.69-7.58 (m, 2H, NCCH**CH**CHCH, **NH**$CH_2CH_2CH_2CH_2$), 7.48-7.33 (m, 3H, NCCHCH**CH**CH, Py**H**), 6.50 (d, *J*=5.9 Hz, NCH**CH**), 3.86 (s, 3H, CO_2**CH_3**), 3.34 (q, *J*=6.0 Hz, 2H, NH**CH_2**$CH_2CH_2CH_2$), 2.74 (t, *J*=7.2 Hz, 2H, $NHCH_2CH_2CH_2$**CH_2**), 1.82-1.62 (m, 4H, $NHCH_2$**CH_2CH_2**CH_2CH_2) ppm

^{13}CNMR (101 MHz, DMSO-d_6) δ 168.0 (**19**), 154.0 (**18**), 152.5 (**6**), 151.0 (**9**), 148.8 (**14**), 146.0 (**8**), 131.6 (**17**), 129.6 (**2**), 128.1 (**1**), 127.0 (**15**), 126.0 (**4**), 124.2 (**16**), 122.0 (**3**), 118.4 (**5**), 98.1 (**7**), 52.3 (**20**), 42.3 (**10**), 36.1 (**13**), 27.3 (**11**), 26.9 (**12**) ppm

IR (neat) ν_{max} 3234 (b), 2929 (s), 1716 (s), 1582 (s) cm^{-1}

LRMS (ESI$^+$) *m/z* 352.4 $[M+H]^+$

HRMS (ESI$^+$) *m/z calcd. for* $C_{20}H_{22}N_3O_3^+$ 352.1656 *m/z meas.* 352.1659 $[M+H]^+$

Mpt 92-93 °C

(*E*)-3-Hydroxy-6-(4-(quinolin-4-ylamino)butyl)picolinaldehyde oxime (2.1)

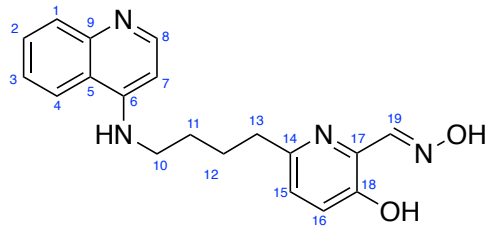

Mol. Wt. 336.4

$C_{19}H_{20}N_4O_2$

Following a procedure adapted from de Sousa,[186] to a solution of methyl 3-hydroxy-6-(4-(quinoline-4-ylamino)butyl)picolinate (200 mg, 0.57 mmol, 1 equiv.) in anhydrous CH_2Cl_2 (20 mL), was added 2,6-lutidine (0.20 mL, 1.71 mmol, 3 equiv.) and TBSOTf (0.26 mL, 1.14 mmol, 2 equiv.), and the yellow solution was stirred at rt, under an Ar atmosphere for 5 h. The solvent was removed *in vacuo*, and the crude ester was taken up in anhydrous CH_2Cl_2 (10 mL), then cooled to –78 °C. DIBAL-H (1 M in CH_2Cl_2, 1.71 mL, 1.71 mmol, 3 equiv.) was added dropwise and the yellow reaction was stirred at –78 °C for 1 h. MeOH (3 mL) was added and the reaction mixture was allowed to warm to rt. The solvent was removed *in vacuo*, CH_2Cl_2 (35 mL) was added, and the white aluminium salts were removed by filtration. The filtrate was concentrated *in vacuo* and anhydrous EtOH (20 mL), hydroxylamine hydrochloride (79 mg, 1.14 mmol, 2 equiv.) and NaOAc (93 mg, 1.14 mmol, 2 equiv.) were added. The yellow reaction solution was heated to reflux for 18 h and upon cooling to rt, the solvent was removed *in vacuo* to afford (*E*)-3-hydroxy-6-(4-(quinolin-4-ylamino)butyl)picolinaldehyde oxime (106 mg, 0.32 mmol, 55%) as a cream solid.

(*E*)-3-Hydroxy-6-(4-(quinolin-4-ylamino)butyl)picolinaldehyde oxime (10.0 mg, 0.03 mmol) was dissolved in 2 M HCl (3 mL). The colourless solution was stirred at rt for 10 mins. The reaction solution was concentrated *in vacuo* to afford (*E*)-3-hydroxy-6-(4-(quinolin-4-ylamino)butyl)picolinaldehyde oxime hydrochloride (11.2 mg, 0.03 mmol, 100%) as a beige solid.

TLC R_f 0.14 (20% MeOH in EtOAc, SiO_2)

^{1}HNMR (400MHz, DMSO-d_6) δ 8.42 (d, *J*=8.6 Hz, 1H, NC**C**H), 8.34 (d, *J*=7.1 Hz, 1H, N**C**H), 8.19 (s, 1H, **C**HNOH), 7.93 (ddd, *J*=8.3, 7.0, 1.0 Hz, 1H, NCCHCH**C**HCH), 7.87 (d, *J*=7.8 Hz, 1H, NCCHCHCH**C**H), 7.69 (ddd, *J*=8.3, 7.0, 1.0 Hz, 1H, NCCH**C**HCHCH), 7.24 (d, *J*=8.6 Hz, 1H, NCCH**C**HC(OH)), 7.18 (d, *J*=8.6 Hz, 1H, NC**C**HCHC(OH)), 6.82 (d, *J*=7.1 Hz, 1H,NCH**C**H), 3.63 (t, *J*=6.4 Hz, 2H, NH**C**$H_2$$CH_2CH_2CH_2$), 2.80 (br t, *J*=7.0 Hz, 2H, $NHCH_2CH_2CH_2$**C**H_2), 1.87-1.83 (m, 4H, $NHCH_2$**C**H_2**C**H_2CH_2) ppm

^{13}CNMR (101 MHz, DMSO-d_6) δ 154.3 (**6**), 152.5 (**14**), 151.5 (**19**), 150.4 (**8**), 143.6 (**9**),

139.8 (**18**), 135.5 (**17**), 125.8 (**1**), 124.2 (**2**), 123.9 (**16**), 123.3 (**15**), 121.7 (**4**), 119.1 (**6**), 117.1 (**3**), 99.6 (**7**), 42.6 (**10**), 36.0 (**13**), 27.2 (**11**), 26.8 (**12**) ppm

IR (neat) ν_{max} 3145 (b), 2953 (s), 1255 (s), 1167 (s) cm^{-1}

LRMS (ESI^+) *m/z* 337.4 $[M+H]^+$

HRMS (ESI^+) *m/z calcd. for* $C_{19}H_{21}N_4O_2^+$ 337.1659 *m/z meas.* 337.1661 $[M+H]^+$

Mpt 214-215 °C

1,8-Naphthyridin-4-(*8H*)-one (2.102)

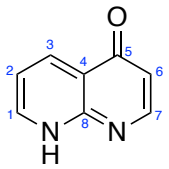

Mol. Wt. 146.0

$C_8H_6N_2O$

Following an adapted procedure from Narender *et al.*[192] for the thermal cyclisation of aminopyridines, 2-aminopyridine (2.00 g, 21.3 mmol, 1 equiv.) was dissolved in anhydrous EtOH (50 mL) and ethyl propiolate (3.23 mL, 31.9 mmol, 1.5 equiv.) was added dropwise at rt. The brown mixture was stirred at rt for 18 h. The solvent was removed *in vacuo* and the brown residue was recrystallised from EtOAc in hexanes. The yellow crystals were taken up in diphenyl ether (40 mL) and the yellow solution was heated to 250 °C for 1 h. The reaction was cooled to rt and poured into hexanes (200 mL). The brown solid was filtered and washed twice with hexanes. The resulting brown solid was recrystallised from EtOH to afford 1,8-naphthyridin-4-(*8H*)-one (1.60g, 10.9 mmol, 52%) as a brown solid.

TLC R_f 0.08 (10% MeOH in EtOAc, SiO_2)

^{1}HNMR (400MHz, DMSO-d_6) δ 8.33 (d, *J*=7.8 Hz, 1H, NC**H**), 8.17 (d, *J*=6.6 Hz, 1H, NCC**CH**), 7.68 (ddd, *J*=9.1, 6.6, 1.7 Hz, 1H, NH**CH**), 7.13 (d, *J*=9.1 Hz, 1H, **NH**), 6.95 (td, *J*=6.6, 1.7 Hz, 1H, NHCH**CH**), 6.41 (d, *J*=7.8 Hz, 1H, NCH**CH**) ppm

^{13}CNMR (101 MHz, DMSO-d_6) δ 167.4 (**5**), 151.4 (**8**), 139.7 (**7**), 136.8 (**1**), 134.3 (**3**), 122.9 (**4**), 115.6 (**6**), 112.6 (**2**) ppm

IR (neat) ν_{max} 3041 (m), 2964 (s), 1690 (s) cm^{-1}

LRMS (ESI$^+$) *m/z* 169.2 $[M+Na]^+$

Mpt 239-241 °C (lit: 241-242 °C)

1-Tosyl-*1H*-indole (2.107)

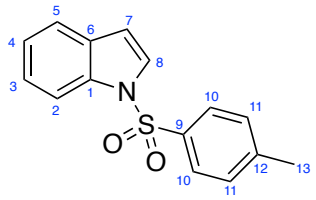

Mol. Wt. 271.1 $gmol^{-1}$

$C_{15}H_{13}NO_2S$

Following a procedure by Wang *et al.*,[238] tetrabutyl hydrogensulfate (0.61 g, 1.20 mmol, 0.07 equiv.), potassium hydroxide (50% aqueous solution, 25 mL) and a solution of tosyl chloride (3.91 g, 20.5 mmol, 1.2 equiv.) in toluene (30 mL) were added to a solution of indole (2.00 g, 17.1 mmol, 1 equiv.) in toluene (20 mL). After stirring for 4 h at rt, H_2O (40 mL) was added and the layers were separated. The organic layer was washed with H_2O and brine, dried ($MgSO_4$) and concentrated *in vacuo*. The brown crude product was purified by column chromatography (SiO_2, 20% EtOAc in hexanes) to afford 1-tosyl-*1H*-indole (4.63 g, 17.1 mmol, 100%) as a pink solid. Data was consistent to that reported in the literature.[238]

TLC R_f 0.60 (20% EtOAc in hexanes, SiO_2)

^{1}HNMR (400MHz, $CDCl_3$) δ 8.02 (d, *J*=8.3 Hz, 1H, NC**C**H), 7.78 (d, *J*=8.6 Hz, 2H, Ar**H**), 7.58 (d, *J*=3.7 Hz, 1H, N**C**H), 7.54 (d, *J*=7.8 Hz, 1H, NCCHCHCH**C**H), 7.37-7.28 (m, 1H, NCCHCH**C**H), 7.26-7.18 (m, 3H, NCCH**C**H, Ar**H**), 6.67 (d, 1H, *J*=3.7 Hz, NCH**C**H), 2.33 (s, 3H, Ar**C**H_3) ppm

^{13}CNMR (101 MHz, $CDCl_3$) δ 144.9 (**12**), 135.3 (**1**), 134.8 (**9**), 130.7 (**6**), 129.8 (**11**), 126.8 (**10**), 126.3 (**3**), 124.5 (**8**), 123.2 (**4**), 121.3 (**5**), 113.5 (**2**), 109.0 (**7**), 21.5 (**13**) ppm

IR (neat) ν_{max} 3120 (s), 1307 (s), 1119 (s) cm^{-1}

LRMS (ESI^+) *m/z* 272.3 $[M+H]^+$

Mpt 82-85 °C (lit: 81-83 °C)

3-Nitro-1-tosyl-*1H*-indole (2.108)

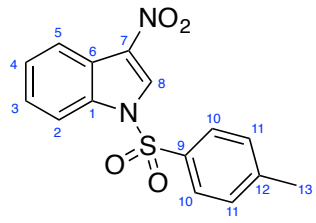

Mol. Wt. 316.1 $gmol^{-1}$

$C_{15}H_{12}N_2O_4S$

Following a procedure adapted from Li *et al.,*[239] acetyl nitrate was formed *in situ* by the dropwise addition of nitric acid (0.92 mL, 22.1 mmol, 3 equiv.) to an excess of acetic anhydride (20 mL) at 0 °C. The mixture was left to stand at rt for 10 min. This solution was added to a stirred solution of 1-tosyl-*1H*-indole (2.00 g, 7.37 mmol, 1 equiv.) at −70 °C, dropwise over 30 minutes. The mixture was allowed to warm to rt and was stirred for 16 h. The pale yellow solution was poured over ice with external cooling. The aqueous solution was extracted with EtOAc (3 × 20 mL) and the combined organic extracts were washed with brine and dried ($MgSO_4$). The dried solution was concentrated *in vacuo* to give 3-nitro-1-tosyl-1*H*-indole (600 mg, 1.90 mmol, 26%) as a pale yellow solid. Data was consistent to that reported in the literature. Data was consistent to that reported in the literature.[239]

TLC R_f	0.62 (20% EtOAc in hexanes, SiO_2)
^{1}HNMR	(400MHz, $CDCl_3$) δ 8.57 (s, 1H, NC**H**), 8.25-8.19 (m, 1H, (NO_2)CC**CH**), 8.04-7.98 (m, 1H, NCC**H**), 7.92-7.86 (m, 2H, Ar**H**), 7.41-7.51 (m, 2H, Ar**H**), 7.34 (d, *J*=8.1 Hz, 2H, Ar**H**), 2.40 (s, 3H, Ar**CH$_3$**) ppm
^{13}CNMR	(101 MHz, $CDCl_3$) δ 146.4 (**12**), 133.5 (**7**), 133.2 (**9**), 130.2 (**11**), 129.9 (**1**), 127.5 (**8**), 127.1 (**4**), 126.4 (**3**), 125.5 (**10**), 121.4 (**6**), 120.9 (**5**), 113.2 (**2**), 21.4 (**13**) ppm
IR (neat)	ν_{max} 3140 (s), 1541 (s), 1358 (s), 1309 (s), 1133 (s) cm^{-1}
LRMS	(ESI$^+$) *m/z* 317.2 $[M+H]^+$
HRMS	(ESI$^+$) *m/z calcd. for* $C_{15}H_{12}N_2O_4S$ 339.0400 *m/z meas.* 339.0402 $[M+H+Na]^+$
Mpt	171-173 °C (lit: 168-169 °C)

1-Tosyl-*1H*-indol-3-amine (2.109)

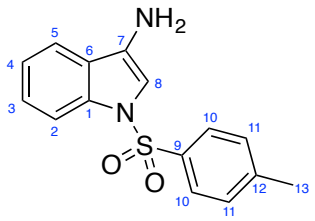

Mol. Wt. 286.1 $gmol^{-1}$

$C_{15}H_{14}N_2O_2S$

Following a procedure adapted from Bahekar *et al.,*[240] palladium on carbon (10%, 41.2 mg, 0.39 mmol, 35 mol%) was added to 3-nitro-1-tosyl-1*H*-indole (350 mg, 1.11 mmol, 1 equiv.) under an atmosphere of argon at 0 °C in anhydrous MeOH (100 mL). The flask was repeatedly evacuated and flushed with H_2 gas and allowed to warm to rt. The reaction was stirred for 72 h. The black solution was filtered through Celite and concentrated *in vacuo* to afford 1-tosyl-*1H*-indol-3-amine (310 mg, 1.08 mmol, 98%) as a pale yellow solid. Data was consistent to that reported in the literature.[240]

TLC R_f 0.10 (25% EtOAc in hexanes, SiO_2)

^{1}HNMR (400MHz, $CDCl_3$) δ 8.02 (d, *J*=8.3 Hz, 1H, NC**H**), 7.69 (d, *J*=8.1 Hz, 2H, Ar**CH**), 7.40-7.29 (m, 2H, NCCH**CH**, NCCHCH**CH**), 7.26-7.20 (m, 1H, NC**CH**), 7.16 (d, *J*=8.1 Hz, 2H, Ar**H**), 6.94 (s, 1H, N**CH**), 3.43 (br. s, 2H, **NH_2**), 2.31 (s, 3H, Ar**CH_3**) ppm

^{13}CNMR (101 MHz, $CDCl_3$) δ 144.4 (**12**), 134.9 (**9**), 134.8 (**1**), 129.9 (**7**), 129.5 (**10**), 126.7 (**11**), 126.4 (**3**), 125.1 (**4**), 122.9 (**5**), 117.6 (**6**), 114.4 (**2**), 107.8 (**8**), 21.5 (**13**) ppm

IR (neat) ν_{max} 3351 (m), 3145 (s), 2933 (s), 1294 (s), 1090 (s) cm^{-1}

LRMS (ESI^+) *m/z* 287.3 $[M+H]^+$

HRMS (ESI^+) *m/z calcd. for* $C_{15}H_{14}N_2O_2S$ 287.0849 *m/z meas.* 287.0848 $[M+H+Na]^+$

Mpt 142-143 °C

3-Bromo-1-tosyl-1*H*-indole (2.113)

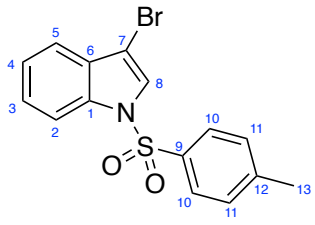

Mol. Wt. 350.0

$C_{15}H_{12}BrNO_2S$

Following a procedure by Chen-Hsu *et al.*[241] for the bromination of 1-tosyl-*1H*-indole, a solution of bromine (0.23 mL, 4.42 mmol, 1.2 equiv.), in CH_2Cl_2 (30 mL) was added to a stirred solution of 1-tosyl-*1H*-indole (1.00 g, 3.68 mmol, 1 equiv.) in CH_2Cl_2 (30 mL) at 0 °C under an inert argon atmosphere. The pink solution turned a deep shade of orange and was stirred for 1 h at 0 °C. The solution was washed (saturated aqueous $Na_2S_2O_3$, 30 mL). The organic phase was washed (brine, 30 mL), dried ($MgSO_4$), filtered and concentrated *in vacuo*. This afforded 3-bromo-1-tosyl-*1H*-indole (1.29 g, 3.69 mmol, 100%) as a pale lilac solid. Data was consistent to that reported in the literature.[241]

TLC R_f 0.63 (20% EtOAc in hexanes, SiO_2)

^{1}HNMR (400MHz, $CDCl_3$) δ 8.00 (dt, *J*=8.3, 0.8 Hz, 1H, NC**C**H), 7.78 (d, *J*=8.1 Hz, 2H, Ar**H**), 7.63 (s, 1H, N**C**H), 7.50 (br. dt, *J*=7.8, 0.8 Hz, 1H, NCCHCHCH**C**H), 7.39 (td, *J*=7.8, 1.3 Hz, 1H, NCCHCH**C**H), 7.35-7.29 (m, 1H, NCCH**C**H), 7.24 (d, *J*=8.1 Hz, 2H, Ar**H**), 2.36 (s, 3H, Ar**C**H_3) ppm

^{13}CNMR (101 MHz, $CDCl_3$) δ 145.3 (**12**), 134.8 (**9**), 134.2 (**1**), 130.0 (**10**), 129.7 (**6**), 126.9 (**11**), 125.7 (**8**), 124.7 (**3**), 123.8 (**4**), 120.0 (**5**), 113.6 (**2**), 99.6 (**7**), 21.6 (**13**) ppm

IR (neat) ν_{max} 2941 (s), 1590 (s), 1264 (s), 1190 (s) cm^{-1}

LRMS (EI) *m/z* 350.8445 $[M^{79}Br]^+$ 352.8582 $[M^{81}Br]^+$

Mpt 122-124 °C (lit: 122-123 °C)

(*E*)-6-Bromopicolinaldehyde oxime (3.9)

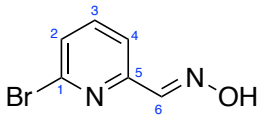

Mol. Wt. 200.0

$C_6H_5BrN_2O$

Following an adapted procedure adapted from de Sousa,[186] for the synthesis of oximes from aldehydes, to a solution of 6-bromopicolinaldehyde (3.00 g, 16.1 mmol, 1 equiv.) in anhydrous EtOH (50 mL) at rt was added hydroxylamine hydrochloride (2.24 g, 32.3 mmol, 2 equiv.) and sodium acetate (2.65 g, 32.3 mmol, 2 equiv.). Upon addition, the colourless solution with a white suspension was stirred at 90 °C for 3 h. The solution was cooled to rt and concentrated *in* vacuo. The resulting white solid was dissolved in EtOAc (50 mL). The organic layer was washed with H_2O (5 × 20 mL), dried ($MgSO_4$), filtered and concentrated *in vacuo* to afford (E)-6-bromopicolinaldehyde oxime (3.21 g, 16.0 mmol, 99%) as a white solid.

TLC R_f 0.79 (EtOAc, SiO_2)

^{1}HNMR (400MHz, DMSO-d_6) δ 11.90 (s, 1H, CHN**OH**), 8.04 (s, 1H, **CH**NOH), 7.82-7.74 (m, 2H, NC**CH**CHCH, NCCH**CH**CH), 7.63 (dd, *J*=6.8, 1.7 Hz, 1H, NCCHCH**CH**) ppm

^{13}CNMR (101 MHz, DMSO-d_6) δ 153.3 (5), 147.5 (6), 141.0 (3), 140.1 (1), 128.1 (2), 119.3 (4) ppm

IR (neat) ν_{max} 3203 (m), 3084 (m), 2912 (s), 1546 (s), 1119 (s), 704 (s) cm^{-1}

LRMS (ESI$^+$) *m/z* 201.1 $[M^{79}Br+H]^+$ 203.1 $[M^{81}Br+H]^+$

HRMS (ESI$^+$) *m/z calcd. for* $C_6H_6BrN_2O^+$ 200.9658 *m/z meas.* 200.9657 $[M+H]^+$

Mpt 168-170 °C (lit: 164-166 °C)

(*E*)-6-(4-(Quinolin-4-ylamino)but-1-yn-1-yl)picolinaldehyde oxime (3.7)

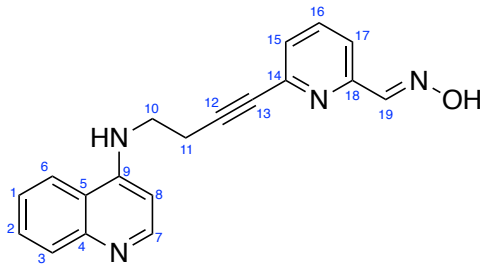

Mol. Wt. 316.4

$C_{19}H_{16}N_4O$

Following a procedure adapted from de Sousa,[186] to a degassed solution of *N*-(but-3-yn-1-yl)quinoline-4-amine (1.00 g, 5.10 mmol, 1 equiv.) in anhydrous THF/Et_3N (50 mL/15 mL) was added $Pd(PPh_3)_4$ (588 mg, 0.51 mmol, 10 mol%) and CuI (194 mg, 1.02 mmol, 20 mol%). To the resulting orange reaction mixture was added dropwise a degassed solution of (E)-6-bromopicolinaldehyde oxime (1.13 g, 5.61 mmol, 1.1 equiv.) in anhydrous THF (20 mL). The brown solution was stirred for 18 h at rt. The reaction was concentrated *in vacuo*. Chromatography (SiO_2, 20% MeOH in EtOAc) afforded (*E*)-6-(4-(quinolin-4-ylamino)but-1-yn-1-yl)picolinaldehyde oxime (1.55 g, 4.92 mmol, 96%) as an orange solid.

(*E*)-6-(4-(Quinolin-4-ylamino)but-1-yn-1-yl)picolinaldehyde oxime (100 mg, 0.32 mmol) was dissolved in 2 M HCl (7 mL). The orange solution was stirred at rt for 10 mins. The reaction solution was concentrated *in vacuo* to afford (*E*)-6-(4-(quinolin-4-ylamino)but-1-yn-1-yl)picolinaldehyde oxime hydrochloride (113 mg, 0.32 mmol, 100%) as a yellow solid.

TLC R_f 0.08 (10% MeOH in EtOAc, SiO_2)

^{1}HNMR (400MHz, DMSO-d_6) δ 11.90-11.69 (br. s, 1H, CHN**OH**), 8.43 (br d, *J*=5.4 Hz, 1H, N**CH**), 8.23 (d, *J*=8.3 Hz, 1H, NC**CH**), 8.03 (s, 1H, **CH**NOH), 7.85-7.65 (m, 3H, **NH**, Ar**H**), 7.52-7.38 (m, 3H, Ar**H**), 6.60 (d, *J*=5.4 Hz, 1H, NCH**CH**), 3.61 (q, *J*=6.7 Hz, 2H, NH**CH$_2$**CH$_2$), 2.88 (t, *J*=6.7 Hz, 2H, NHCH$_2$**CH$_2$**) ppm

^{13}CNMR (101 MHz, DMSO-d_6) δ 152.5 (**9**), 150.3 (**18**), 149.8 (**4**), 148.4 (**7**), 147.8 (**19**), 142.4 (**14**), 137.8 (**16**), 129.0 (**15**), 128.6 (**2**), 126.8 (**3**), 124.1 (**6**), 121.7 (**1**), 118.9 (**5**), 118.7 (**17**), 98.5 (**8**), 88.7 (**12**), 81.1 (**13**), 48.6 (**10**), 18.6 (**11**) ppm

IR (neat) ν_{max} 3331 (b), 3068 (m), 2947 (s), 2241 (s), 1617 (s) cm^{-1}

LRMS (ESI$^+$) *m/z* 317.1 $[M+H]^+$

HRMS (ESI$^+$) *m/z calcd. for* $C_{19}H_{17}N_4O^+$ 317.1397 *m/z meas.* 317.1396 $[M+H]^+$

Mpt 69-70 °C

(*E*)-6-(4-(Quinolin-4-ylamino)butyl)picolinaldehyde oxime (3.6)

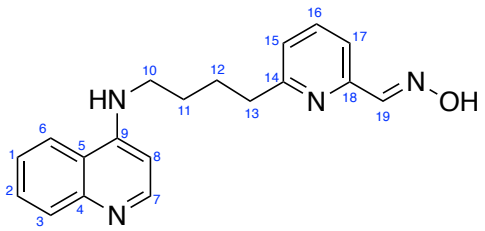

Mol. Wt. 320.4

$C_{19}H_{20}N_4O$

Following a procedure adapted from de Sousa,[186] to a degassed suspension of (E)-6-(4-(quinolin-4-ylamino)but-1-yn-1-yl)picolinaldehyde oxime (575 mg, 1.80 mmol, 1 equiv.) in anhydrous MeOH (20 mL), was added Pearlman's catalyst (255 mg, 1.80 mmol, 1 equiv.). The reaction vessel was evacuated and flushed with hydrogen gas five times. The black reaction mixture was stirred for 18 h at rt. The catalyst was removed by filtration through Celite and the solvent was removed *in vacuo* to afford (*E*)-6-(4-(quinolin-4-ylamino)butyl)picolinaldehyde oxime (550 mg, 1.74 mmol, 94%) as a cream solid.

(*E*)-6-(4-(Quinolin-4-ylamino)butyl)picolinaldehyde oxime (100 mg, 0.32 mmol) was dissolved in 2 M HCl (7 mL). The colourless solution was stirred at rt for 10 mins. The reaction solution was concentrated *in vacuo* to afford (*E*)-6-(4-(quinolin-4-ylamino)butyl)picolinaldehyde oxime hydrochloride (114 mg, 0.32 mmol, 100%) as a beige solid.

TLC R_f 0.20 (50% MeOH in EtOAc, SiO_2)

^{1}HNMR (400MHz, D_2O) δ 8.15 (s, 1H, **CH**NOH), 8.01 (d, *J*=7.1 Hz, 1H, N**CH**), 7.89-7.49 (m, 7H, Ar**H**), 6.62 (d, *J*=7.1 Hz, 1H, NCH**CH**), 3.54 (t, *J*=6.6 Hz, 2H, NH**CH$_2$**CH$_2$CH$_2$CH$_2$), 3.09 (t, *J*=7.2 Hz, 2H, NHCH$_2$CH$_2$CH$_2$**CH$_2$**), 1.99-1.76 (m, 4H, NHCH$_2$**CH$_2$CH$_2$**CH$_2$) ppm

^{13}CNMR (101 MHz, D_2O) δ 156.1 (**14**), 146.7 (**19**), 145.0 (**9**), 142.7 (**7**), 141.7 (**18**), 137.6 (**4**), 134.1 (**16**), 127.5 (**3**), 127.4 (**6**), 123.2 (**1**), 122.3 (**15**), 122.1 (**2**), 120.2 (**17**), 116.8 (**5**), 98.2 (**8**), 42.9 (**10**), 33.1 (**13**), 26.1 (**11**), 17.2 (**12**) ppm

IR (neat) ν_{max} 3145 (b), 3026 (s), 2985 (s), 1593 (s), 1224 (s), 658 (s) cm^{-1}

LRMS (ESI$^+$) *m/z* 321.1 $[M+H]^+$

HRMS (ESI$^+$) *m/z calcd.* $C_{19}H_{21}N_4O^+$ calculated 321.1710 *m/z meas.*

321.1713 $[M+H]^+$

Mpt 218-219 °C

(*E*)-6-(4-((8-Methoxyquinolin-4-yl)amino)but-1-yn-1-yl)picolinaldehyde oxime (3.10)

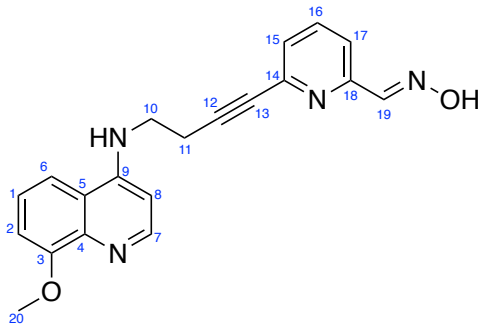

Mol. Wt. 346.1

$C_{20}H_{18}N_4O_2$

Following a procedure adapted from de Sousa,[186] to a degassed solution of *N*-(but-3-yn-1-yl)-8-methoxyquinoline-4-amine (1.00 g, 4.42 mmol, 1 equiv.) in anhydrous THF/Et_3N (30 mL/12 mL) was added $Pd(PPh_3)_4$ (511 mg, 0.44 mmol, 10 mol%) and CuI (190 mg, 0.88 mmol, 20 mol%). To the resulting orange reaction mixture was added dropwise a degassed solution of (E)-6-bromopicolinaldehyde oxime (977 g, 4.86 mmol, 1.1 equiv.) in anhydrous THF (30 mL). The brown solution was stirred for 18 h at rt. The reaction was concentrated *in vacuo*. Purification by column chromatography (Al_2O_3, 10% MeOH in EtOAc) afforded (E)-6-(4-(8-methoxyquinolin-4-ylamino)but-1-yn-1-yl)picolinaldehyde oxime (400 mg, 1.16 mmol, 26%) as an orange solid.

(*E*)-6-(4-(Quinolin-4-ylamino)butyl)picolinaldehyde oxime (100 mg, 0.29 mmol) was dissolved in 2 M HCl (7 mL). The orange solution was stirred at rt for 10 mins. The reaction solution was concentrated *in vacuo* to afford (*E*)-6-(4-(quinolin-4-ylamino)butyl)picolinaldehyde oxime hydrochloride (111 mg, 0.29 mmol, 100%) as a cream solid.

TLC R_f 0.46 (10% MeOH in EtOAc, Al_2O_3)

^{1}HNMR (400MHz, DMSO-d_6) δ 11.91-11.70 (br. s, 1H, CHN**OH**), 8.66-8.48 (m, 1H, N**H**), 8.35 (d, *J*=6.1 Hz, 1H, N**CH**), 7.98-7.97 (m, 2H, **CH**NOH, NCC(OCH$_3$)CHCH**CH**), 7.78 (t, *J*=7.8 Hz, 1H, NCCH**CH**CH), 7.72 (d, *J*=7.8 Hz, 1H, NCCHCH**CH**), 7.49 (t, *J*=8.1 Hz, 1H, NCC(OCH$_3$)CH**CH**CH), 7.39 (d, *J*=7.8 Hz, 1H, NC**CH**CHCH), 7.29 (d, *J*=8.1 Hz, 1H, NCC(OCH$_3$)**CH**CHCH), 6.84 (d, *J*=6.1 Hz, 1H, NCH**CH**), 3.99 (s, 3H, O**CH$_3$**) 3.61 (br. t, *J*=7.0 Hz, 2H, NH**CH$_2$**CH$_2$), 2.90 (t, *J*=7.0 Hz, 2H, NHCH$_2$**CH$_2$**) ppm

^{13}CNMR (101 MHz, DMSO-d_6) δ 152.6 (**3**), 152.5 (**18**), 152.1 (**9**), 148.3 (**19**), 145.1 (**7**), 142.3 (**14**), 137.3 (**4**), 134.2 (**16**), 126.8 (**15**), 125.4 (**1**), 119.0 (**6**), 118.5 (**5**), 113.7 (**17**), 110.3 (**2**), 99.0 (**8**), 88.3 (**12**), 81.3 (**13**), 56.1 (**20**), 48.5 (**10**), 18.7 (**11**) ppm

IR (neat) ν_{max} 3084 (b), 2236 (s), 1617 (s), 1277 (s) cm^{-1}

LRMS (ESI^+) *m/z* 347.4 $[M+H]^+$

HRMS (ESI^+) *m/z calcd. for* $C_{20}H_{19}N_4O_2^+$ 347.1503 *m/z meas.* 347.1506 $[M+H]^+$

Mpt 171-172 °C

(*E*)-6-(4-((5-Fluoroquinolin-4-yl)amino)but-1-yn-1-yl)picolinaldehyde oxime (3.11)

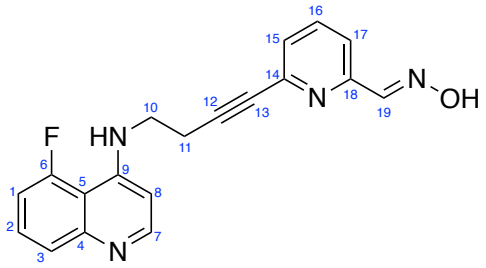

Mol. Wt. 334.1

$C_{19}H_{15}FN_4O$

Following a procedure adapted from de Sousa,[186] to a degassed solution of *N*-(but-3-yn-1-yl)-5-fluoroquinolin-4-amine (500 mg, 2.33 mmol, 1 equiv.) in anhydrous THF/Et_3N (7 mL/3 mL) was added $Pd(PPh_3)_4$ (270 mg, 0.23 mmol, 10 mol%) and CuI (89 mg, 0.47 mmol, 20 mol%). To the resulting orange reaction mixture was added dropwise a degassed solution of (E)-6-bromopicolinaldehyde oxime (516 mg, 2.57 mmol, 1.1 equiv.) in anhydrous THF (20 mL). The brown solution was stirred for 16 h at rt. The reaction was concentrated *in vacuo*. Purification by column chromatography (SiO_2, EtOAc to 20% MeOH in EtOAc) afforded (*E*)-6-(4-((5-fluoroquinolin-4-yl)amino)but-1-yn-1-yl)picolinaldehyde oxime (140 mg, 0.42 mmol, 18%) as pale cream solid.

(*E*)-6-(4-((5-Fluoroquinolin-4-yl)amino)but-1-yn-1-yl)picolinaldehyde oxime (10 mg, 0.03 mmol) was dissolved in 2 M HCl (3 mL). The cream solution was stirred at rt for 10 mins. The reaction solution was concentrated *in vacuo* to afford (*E*)-6-(4-((5-fluoroquinolin-4-yl)amino)but-1-yn-1-yl)picolinaldehyde oxime hydrochloride (11.1 mg, 0.03 mmol, 100%) as a colourless solid.

TLC R_f 0.49 (20% MeOH in EtOAc, SiO_2)

^{1}HNMR (400MHz, DMSO-d_6) δ 11.79 (s, 1H, CHN**OH**), 8.42 (d, *J*=5.4 Hz, 1H, N**C**H**C**H), 8.30 (dd, *J*=9.2, 7.1 Hz, 1H, NCCH**C**H**C**HCF), 8.02 (s, 1H, **C**H**C**NOH), 7.83-7.69 (m, 2H, Ar**H**), 7.53 (t, *J*=5.6 Hz, 1H, **NH**CH_2CH_2), 7.48 (dd, *J*=10.8, 2.7 Hz, 1H, NCCH**C**H**C**H), 7.41 (d, *J*=7.1 Hz, 1H, NCCHCH**C**H**C**F), 7.35 (td, *J*=8.7, 2.7 Hz, 1H, NC**C**H**C**HCH), 6.58 (d, *J*=5.4 Hz, 1H, NCH**C**H), 3.66-3.51 (m, 2H, NH**C**$H_2$$CH_2$), 2.86 (t, *J*=7.0 Hz, 2H, $NHCH_2$**C**H_2) ppm

^{13}CNMR (101 MHz, DMSO-d_6) δ 163.4 (**4**), 160.9 (d, *J*=220 Hz, **6**), 152.4 (**7**), 151.9 (**18**), 149.8 (**19**), 148.4 (**9**), 142.4 (**14**), 137.3 (**16**), 126.9 (**5**), 124.5 (**3**), 119.0 (**15**), 115.9 (**17**), 113.5 (**1**), 112.2 (**2**), 98.4 (**8**), 88.7 (**12**), 81.1 (**13**), 41.0 (**10**), 18.6 (**11**) ppm

^{19}FNMR (376 MHz, DMSO-d_6) δ 112.0 ppm

IR (neat) ν_{max} 3500 (s), 3435 (s), 3034 (b), 2239 (s), 1622 (s), 1234 (s) cm^{-1}

LRMS (ESI^+) *m/z* 335.4 $[M+H]^+$

HRMS (ESI^+) *m/z calcd. for* $C_{19}H_{16}FN_4O^+$ 335.1303 *m/z meas.* 335.1298 $[M+H]^+$

Mpt 168-169 °C

(*E*)-6-(4-((8-Methoxyquinolin-4-yl)amino)but-1-yn-1-yl)picolinaldehyde oxime (3.12)

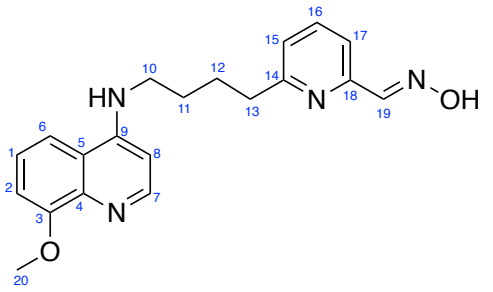

Mol. Wt. 350.2

$C_{20}H_{22}N_4O_2$

Following a procedure adapted from de Sousa,[186] to a degassed suspension of (E)-6-(4-((8-methoxyquinolin-4-yl)amino)but-1-yn-1-yl)picolinaldehyde oxime (110 mg, 0.32 mmol, 1 equiv.) in anhydrous MeOH (10 mL), was added Pearlman's catalyst (9.00 mg, 0.06 mmol, 0.2 equiv.). The reaction vessel was evacuated and flushed with hydrogen gas five times. The black reaction mixture was stirred for 18 h at rt. The catalyst was removed by filtration through Celite and the solvent was removed *in vacuo* to afford (*E*)-6-(4-((8-methoxyquinolin-4-yl)amino)but-1-yn-1-yl)picolinaldehyde oxime (40.0 mg, 0.11 mmol, 36%) as a cream solid.

(*E*)-6-(4-((8-Methoxyquinolin-4-yl)amino)but-1-yn-1-yl)picolinaldehyde oxime (10 mg, 0.03 mmol) was dissolved in 2 M HCl (3 mL). The colourless solution was stirred at rt for 10 mins. The reaction solution was concentrated *in vacuo* to afford (*E*)-6-(4-((8-methoxyquinolin-4-yl)amino)but-1-yn-1-yl)picolinaldehyde oxime hydrochloride (11.6 mg, 0.03 mmol, 100%) as a colourless solid.

TLC R_f 0.28 (20% MeOH in CH_2Cl_2, SiO_2)

^{1}HNMR (400MHz, MeOD-d_4) δ 8.29 (d, *J*=5.6 Hz, 1H, NC**H**CH), 8.08 (s, 1H, **CH**NOH), 7.71-7.57 (m, 3H, Ar**H**), 7.34 (t, *J*=8.2 Hz, 1H, NCC(OMe)CH**CH**CH), 7.24-7.19 (m, 1H, NCC(OMe)CHCH**CH**), 7.08 (d, *J*=7.8 Hz, 1H, NC**CH**CHCH), 6.48 (d, *J*=5.6 Hz, NCH**CH**), 3.98 (s, 3H, O**CH$_3$**), 3.36 (t, *J*=7.1 Hz, 2H, NH**CH$_2$**CH$_2$CH$_2$CH$_2$), 2.83 (t, *J*=7.1 Hz, 2H, NHCH$_2$CH$_2$CH$_2$**CH$_2$**), 1.94-1.66 (m, 4H, NHCH$_2$**CH$_2$CH$_2$**CH$_2$) ppm

^{13}CNMR (101 MHz, MeOD-d_4) δ 163.2 (**14**), 156.2 (**3**), 153.3 (**9**), 152.7 (**18**), 150.0 (**19**), 149.6 (**7**), 140.4 (**4**), 138.8 (**16**), 125.8 (**6**), 124.5 (**15**), 121.1 (**1**), 119.3 (**5**), 113.8 (**17**), 109.3 (**2**), 99.9 (**8**), 56.4 (**20**), 43.8 (**10**), 38.4 (**13**), 28.9 (**11**), 28.7 (**12**) ppm

IR (neat) ν_{max} 3084 (b), 2236 (s), 1617 (s), 1277 (s) cm^{-1}

LRMS (ESI^+) *m/z* 351.1 $[M+H]^+$

HRMS (ESI$^+$) *m/z calcd. for* $C_{20}H_{23}N_4O_2^+$ 351.1816 *m/z meas.* 351.1817 $[M+H]^+$

Mpt 107-108 °C

(*E*)-6-(4-((5-Fluoroquinolin-4-yl)amino)butyl)picolinaldehyde oxime (3.13)

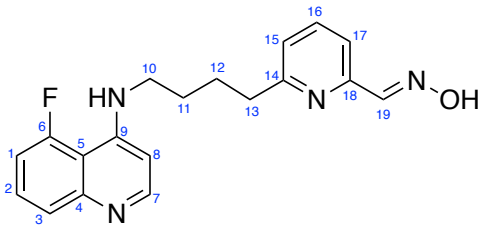

Mol. Wt. 338.4

$C_{19}H_{19}FN_4O$

Following a procedure adapted from de Sousa,[186] to a degassed suspension of (E)-6-(4-((5-fluoroquinolin-4-yl)amino)but-1-yn-1-yl)picolinaldehyde oxime (50.0 mg, 0.15 mmol) in anhydrous MeOH (5 mL), was added Pearlman's catalyst (21.0 mg, 0.15 mmol). The reaction vessel was evacuated and flushed with hydrogen gas five times. The black reaction mixture was stirred for 18 h at rt. The catalyst was removed by filtration through Celite and the solvent was removed *in vacuo* to afford (*E*)-6-(4-((5-fluoroquinolin-4-yl)amino)butyl)picolinaldehyde oxime (50.0 mg, 0.15 mmol, 100%) as a cream solid.

(*E*)-6-(4-((5-Fluoroquinolin-4-yl)amino)butyl)picolinaldehyde oxime (10 mg, 0.03 mmol) was dissolved in 2 M HCl (3 mL). The colourless solution was stirred at rt for 10 mins. The reaction solution was concentrated *in vacuo* to afford (*E*)-6-(4-((5-fluoroquinolin-4-yl)amino)butyl)picolinaldehyde oxime hydrochloride (11.2 mg, 0.03 mmol, 100%) as a colourless solid.

TLC R_f 0.31 (20% MeOH in EtOAc, SiO_2)

^{1}HNMR (400MHz, D_2O) δ 8.44 (t, *J*=8.1 Hz, 1H, NCCH**C**HCH), 8.19 (d, *J*=7.3 Hz, 1H, N**C**HCH), 8.16-8.13 (m, 2H, **C**HNOH, **NH**$CH_2CH_2CH_2CH_2$), 7.91-7.81 (m, 2H, NC**C**HCHCHCF, NCCH**C**HCHCF), 7.70 (d, *J*=8.1 Hz, 1H, NC**C**HCHCH), 7.42-7.32 (m, 2H, NCCHCH**C**H), 6.70 (d, *J*=7.3 Hz, NCH**C**H), 3.58 (t, *J*=6.8 Hz, 2H, NH**C**$H_2CH_2CH_2CH_2$), 3.12 (t, *J*=7.7 Hz, 2H, $NHCH_2CH_2CH_2$**C**H_2), 2.01-1.76 (m, 4H, $NHCH_2$**C**H_2**C**H_2CH_2) ppm

^{13}CNMR (101 MHz, D_2O) δ 166.0 (**18**), 163.5 (**14**), 161.5 (d, *J*=235 Hz, **6**), 159.1 (**19**), 155.8 (**9**), 146.5 (**7**), 141.9 (**4**), 139.0 (**5**), 127.0 (**16**), 125.6 (**3**), 124.0 (**15**), 116.2 (**2**), 113.5 (**17**), 105.1 (**1**), 98.0 (**8**), 42.8 (**10**), 39.9 (**13**), 26.9 (**11**), 25.9 (**12**) ppm

^{19}FNMR (376 MHz, DMSO-d_6) δ 103.3 ppm

IR (neat) ν_{max} 3247 (s), 2935 (s), 2859 (b), 1622 (s), 1584 (s) cm^{-1}

LRMS (ESI^+) *m/z* 339.2 $[M+H]^+$

HRMS (ESI$^+$) *m/z calcd. for* $C_{19}H_{20}FN_4O^+$ 339.1980 *m/z meas.* 339.1980 $[M+H]^+$

Mpt 206-207 °C

1-(But-3-yn-1-yl)-3,7-dimethyl-3,7-dihydro-1*H*-purine-2,6-dione (3.19)

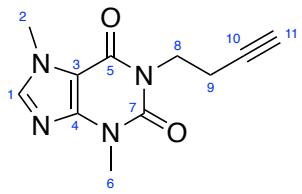

Mol. Wt. 232.1

$C_{11}H_{12}N_4O_2$

Following a procedure adapted from Tsunoda *et al.*,[202] to a yellow suspension of 3-butyn-1-ol (0.11 mL, 1.40 mmol, 1 equiv.), theobromine (500 mg, 2.78 mmol, 2 equiv.) and PPh_3 (728 g, 2.78 mmol, 2 equiv.) in anhydrous THF (80 mL) was added ADDP (700 mg, 2.78 mmol, 2 equiv.) dropwise at rt. The yellow reaction mixture was stirred for 24 h at 60 °C. H_2O (60 mL) was added and the aqueous layer was extracted (EtOAc, 3 × 30 mL). The combined organics were washed (brine, 30 mL). The organic layer was separated, dried ($MgSO_4$), filtered and concentrated *in vacuo*. The crude product was purified by column chromatography (SiO_2, EtOAc), to afford 1-(but-3-yn-1-yl)-3,7-dimethyl-3,7-dihydro-1*H*-purine-2,6-dione (120 mg, 0.52 mmol, 37%) as a colourless solid.

TLC R_f	0.25 (EtOAc, SiO_2)
^{1}HNMR	(400MHz, DMSO-d_6) δ 8.00 (s, 1H, NC**H**N), 3.99 (t, *J*=7.6 Hz, 1H, N**CH_2**CH_2CCH), 3.87 (s, 3H, NCHN(**CH_3**)), 3.40 (s, 3H, NCOCN(**CH_3**)), 2.84 (t, *J*=2.7 Hz, 1H, NCH_2CH_2C**C**H), 2.45 (td, *J*=7.6, 2.7 Hz, 2H, NCH_2**CH_2**CCH) ppm
^{13}CNMR	(101 MHz, DMSO-d_6) δ 154.6 (**7**), 151.1 (**5**), 148.7 (**4**), 143.5 (**1**), 107.0 (**3**), 81.5 (**10**), 73.0 (**11**), 40.6 (**8**), 33.6 (**2**), 29.8 (**6**), 17.3 (**9**) ppm
IR (neat)	ν_{max} 3228 (s), 1651 (s), 1018 (s), 761 (s) cm^{-1}
LCMS	(ESI) *m/z* 233.2 $[M+H]^+$
HRMS	(ESI$^+$) *m/z calcd. for* $C_{11}H_{13}N_4O_2^+$ 233.1033 *m/z meas.* 233.1035
MPt	192-193 °C

Methyl 3-(benzyloxy)-6-(4-(3,7-dimethyl-2,6-dioxo-2,3,6,7-tetrahydro-1*H*-purin-1-yl)but-1-yn-1-yl)picolinate (3.23)

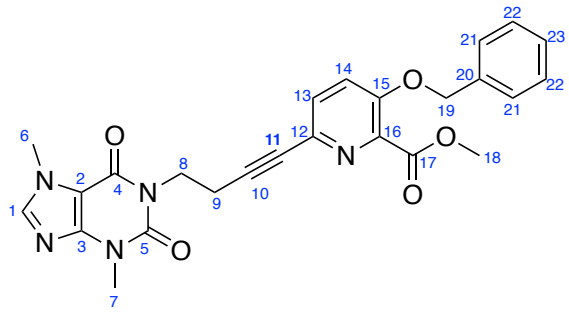

Mol. Wt. 473.5

$C_{25}H_{23}N_5O_5$

Following a procedure adapted from de Sousa,[186] to a degassed solution of 1-(but-3-yn-1-yl)-3,7-dimethyl-3,7-dihydro-1*H*-purine-2,6-dione (400 mg, 1.72 mmol, 1 equiv.) in anhydrous THF/Et_3N (7 mL/3 mL), tetrakis(triphenylphosphine) palladium (199 mg, 0.17 mmol, 10 mol%) and copper iodide (66.0 mg, 0.34 mmol, 20 mol%) were added. After bubbling the reaction mixture with argon for 5 minutes at rt, a degassed solution of methyl 3-(benzyloxy)-6-bromopyridine-2-carboxylate (610 mg, 1.90 mmol, 1.1 equiv.) in anhydrous THF (7 mL) was added dropwise and the yellow reaction mixture was stirred for 16 h at rt. Upon completion, the orange reaction mixture was concentrated *in vacuo* and purified by column chromatography (SiO_2, EtOAc to 20% MeOH in EtOAc), to methyl 3-(benzyloxy)-6-(4-(3,7-dimethyl-2,6-dioxo-2,3,6,7-tetrahydro-1*H*-purin-1-yl)but-1-yn-1-yl)picolinate (500 mg, 1.06 mmol, 61%) as a cream solid.

TLC R_f 0.24 (EtOAc, SiO_2)

^{1}HNMR (400MHz, DMSO-d_6) δ 7.51 (s, 1H, NC**H**N(CH_3)), 7.32 (d, *J*=8.8 Hz, 1H, NC**CH**), 7.22-7.16 (m, 3H, Ar**H,** NCCH**CH**), 7.12-7.01 (m, 3H, Ar**H**), 4.97 (s, 2H, **CH_2**Ph), 3.92 (t, *J*=7.5 Hz, 1H, N**CH_2**CH_2), 3.67 (s, 3H, NCHN(**CH_3**)), 3.59-3.54 (m, 3H, NCON(**CH_3**)), 3.17 (m, 3H, CO_2**CH_3**), 2.48-2.45 (m, 2H, NCH_2**CH_2**) ppm

^{13}CNMR (101 MHz, DMSO-d_6) δ 164.8 (**17**), 154.9 (**5**), 153.0 (**4**), 151.3 (**15**), 148.9 (**3**), 141.5 (**16**), 140.0 (**1**), 135.5 (**12**), 135.2 (**20**), 130.1 (**13**), 128.7 (**21**), 128.2 (**23**), 126.9 (**21**), 121.7 (**14**), 107.6 (**2**), 86.7 (**10**), 80.5 (**11**), 70.8 (**19**), 52.7 (**18**), 39.4 (**8**), 33.6 (**6**), 29.7 (**7**), 18.6 (**9**) ppm

IR (neat) ν_{max} 3228 (s), 1651 (s), 1018 (s) cm^{-1}

LCMS (ESI) *m/z* 474.5 $[M+H]^+$

HRMS (ESI$^+$) *m/z calcd. for* $C_{25}H_{24}N_5O_5^+$ 474.1772 *m/z meas.* 474.1772

MPt 190-191 °C

(*E*)-6-(4-(3,7-Dimethyl-2,6-dioxo-2,3,6,7-tetrahydro-1*H*-purin-1-yl)but-1-yn-1-yl)picolinaldehyde oxime (3.15)

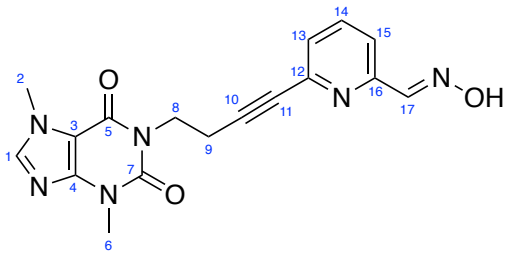

Mol . Wt. 352.1

$C_{17}H_{16}N_6O_3$

Following a procedure adapted from de Sousa,[186] to a degassed solution of 1-(but-3-yn-1-yl)-3,7-dimethyl-3,7-dihydro-1*H*-purine-2,6-dione (500 mg, 2.15 mmol, 1 equiv.) in anhydrous THF/Et_3N (7 mL/3 mL), tetrakis(triphenylphosphine) palladium (249 mg, 0.21 mmol, 10 mol%) and copper iodide (82.0 mg, 0.43 mmol, 20 mol%) were added. After bubbling the reaction mixture with argon for 5 minutes at rt, a degassed solution of (E)-6-bromopicolinaldehyde oxime (476 mg, 2.37 mmol, 1.1 equiv.) in anhydrous THF (7 mL) was added dropwise and the yellow reaction mixture was stirred for 16 h at rt. Upon completion, the brown reaction mixture was concentrated *in vacuo* and purified by column chromatography (SiO_2, EtOAc to 20% MeOH in EtOAc), to afford (*E*)-6-(4-(3,7-dimethyl-2,6-dioxo-2,3,6,7-tetrahydro-1*H*-purin-1-yl)but-1-yn-1-yl)picolinaldehyde oxime (230 mg, 0.65 mmol, 30%) as a yellow solid.

(*E*)-6-(4-(3,7-Dimethyl-2,6-dioxo-2,3,6,7-tetrahydro-1*H*-purin-1-yl)but-1-yn-1-yl)picolinaldehyde oxime (10 mg, 0.03 mmol) was dissolved in 2 M HCl (3 mL). The yellow solution was stirred at rt for 10 mins. The reaction solution was concentrated *in vacuo* to afford (*E*)-6-(4-(3,7-dimethyl-2,6-dioxo-2,3,6,7-tetrahydro-1*H*-purin-1-yl)but-1-yn-1-yl)picolinaldehyde oxime hydrochloride (11.6 mg, 0.03 mmol, 100%) as a yellow solid.

TLC R_f 0.41 (10% MeOH in EtOAc, SiO_2)

^{1}HNMR (400MHz, DMSO-d_6) δ 11.80-11.70 (s, 1H, N**OH**), 8.03 (s, 1H, N**CH**N(CH_3)), 8.00 (s, 1H, **CH**NOH), 7.79 (t, *J*=8.1 Hz, 1H, NCCH**CH**CH), 7.73 (dd, *J*=8.1, 1.0 Hz, 1H, NCCHCH**CH**), 7.39 (dd, *J*=8.1, 1.0 Hz, NC**CH**CHCH), 4.12 (t, *J*=7.5 Hz, 1H, N**CH$_2$**CH_2), 3.88 (s, 3H, NCHN(**CH_3**)), 3.42 (s, 3H, NCON(**CH_3**)), 2.75 (t, *J*=7.5 Hz, 2H, NCH_2**CH_2**) ppm

^{13}CNMR (101 MHz, DMSO-d_6) δ 154.2 (**7**), 152.4 (**5**), 150.7 (**16**), 148.4 (**17**), 148.3 (**4**), 143.1 (**12**), 142.3 (**1**), 137.3 (**14**), 126.8 (**13**), 119.0 (**3**), 106.5 (**15**), 87.4 (**10**), 81.3 (**11**), 40.3 (**8**), 33.2 (**2**), 29.4 (**6**), 17.7 (**9**) ppm

IR (neat) ν_{max} 3178 (b), 3087 (s), 2872 (s), 2230 (s), 1700 (s), 1647 (s), 739 (s) cm^{-1}

LCMS (ESI) *m/z* 353.4 $[M+H]^+$

HRMS (ESI^+) *m/z calcd. for* $C_{17}H_{17}N_6O_3^+$ 353.1357 *m/z meas.* 353.1358

MPt 210-211 °C

Methyl 6-(4-(3,7-dimethyl-2,6-dioxo-2,3,6,7-tetrahydro-1*H*-purin-1-yl)butyl)-3-hydroxypicolinate (3.24)

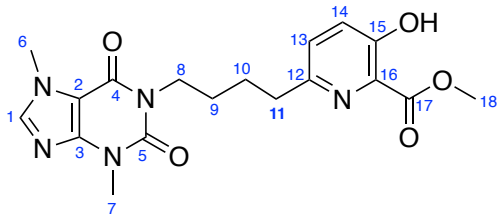

Mol. Wt. 387.4

$C_{18}H_{21}N_5O_5$

Following a procedure adapted from de Sousa,[186] to a degassed solution of methyl 3-(benzyloxy)-6-(4-(3,7-dimethyl-2,6-dioxo-2,3,6,7-tetrahydro-1*H*-purin-1-yl)but-1-yn-1-yl)picolinate (200 mg, 0.42 mmol, 1 equiv.) in anhydrous MeOH (10 mL), was added Pearlman's catalyst (60.0 mg, 0.42 mmol, 1 equiv.). After evacuating and flushing with hydrogen five times, the black reaction mixture was stirred at rt, under a hydrogen atmosphere for 16 h. Upon completion, the catalyst was removed by filtration through Celite and the solvent was removed *in vacuo*, affording methyl 6-(4-(3,7-dimethyl-2,6-dioxo-2,3,6,7-tetrahydro-1*H*-purin-1-yl)butyl)-3-hydroxypicolinate (130 mg, 0.34 mmol, 79%) as a colourless solid.

TLC R_f	0.37 (10% MeOH in EtOAc, SiO_2)
^{1}HNMR	(400MHz, DMSO-d_6) δ 8.00 (s, 1H, NC**H**N), 7.37 (d, *J*=8.6 Hz, 1H, NCC**H**), 7.34 (d, *J*=8.6 Hz, 1H, NCCH**CH**), 3.90-3.80 (m, 8H, N**CH$_2$**CH$_2$, CO$_2$**CH$_3$**, COCN(**CH$_3$**)), 3.40 (s, 3H, NCHN(**CH$_3$**)), 2.71-2.36 (m, 2H, NCH$_2$CH$_2$CH$_2$**CH$_2$**), 1.68-1.49 (m, 4H, NCH$_2$**CH$_2$CH$_2$**CH$_2$) ppm
^{13}CNMR	(101 MHz, DMSO-d_6) δ 168.1 (**17**), 154.4 (**15**), 153.5 (**12**), 152.3 (**4**), 150.8 (**5**), 148.2 (**3**), 142.9 (**1**), 131.5 (**13**), 128.2 (**16**), 126.1 (**14**), 106.6 (**2**), 52.3 (**18**) 41.0 (**8**), 36.2 (**6**), 33.1 (**7**), 29.3 (**9**), 27.2 (**10**), 26.8 (**11**) ppm
IR (neat)	ν_{max} 3245 (m), 2954 (s), 1652 (s), 1098 (s) cm^{-1}
LCMS	(ESI) *m/z* 388.4 $[M+H]^+$
HRMS	(ESI$^+$) *m/z calcd. for* $C_{18}H_{22}N_5O_5^+$ 388.1617 *m/z meas.* 388.1615
MPt	150-151 °C

(*E*)-6-(4-(3,7-Dimethyl-2,6-dioxo-2,3,6,7-tetrahydro-1*H*-purin-1-yl)butyl) picolinaldehyde oxime (3.16)

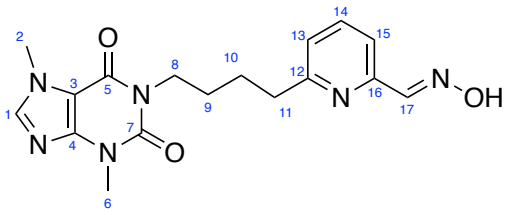

Mol. Wt. 365.4

$C_{17}H_{20}N_6O_3$

Following a procedure adapted from de Sousa,[186] to a degassed solution of methyl (*E*)-6-(4-(3,7-dimethyl-2,6-dioxo-2,3,6,7-tetrahydro-1*H*-purin-1-yl)but-1-yn-1-yl)picolinaldehyde oxime (60.0 mg, 0.17 mmol, 1 equiv.) in anhydrous MeOH (6 mL), was added Pearlman's catalyst (24.0 mg, 0.17 mmol, 1 equiv.). After evacuating and flushing with hydrogen five times, the black reaction mixture was stirred at rt, under a hydrogen atmosphere for 16 h. Upon completion, the catalyst was removed by filtration through Celite and the solvent was removed *in vacuo*, affording (*E*)-6-(4-(3,7-dimethyl-2,6-dioxo-2,3,6,7-tetrahydro-1*H*-purin-1-yl)butyl)picolinaldehyde oxime (56.0 mg, 0.16 mmol, 92%) as a yellow oil.

(*E*)-6-(4-(3,7-Dimethyl-2,6-dioxo-2,3,6,7-tetrahydro-1*H*-purin-1-yl)butyl)picolinaldehyde oxime (10 mg, 0.02 mmol) was dissolved in 2 M HCl (3 mL). The yellow solution was stirred at rt for 10 mins. The reaction solution was concentrated *in vacuo* to afford (*E*)-6-(4-(3,7-dimethyl-2,6-dioxo-2,3,6,7-tetrahydro-1*H*-purin-1-yl)butyl)picolinaldehyde oxime hydrochloride (8.0 mg, 0.02 mmol, 100%) as a yellow solid.

TLC R_f 0.12 (20% MeOH in EtOAc, SiO_2)

^{1}HNMR (400MHz, DMSO-d_6) δ 8.10 (s, 1H, NC**H**N), 7.49 (s, 1H, **CH**NOH), 7.46 (t, *J*=7.5 Hz, 1H, NCCH**CH**CH), 7.01 (d, *J*=7.5 Hz, 1H, NCCHCH**CH**), 6.99 (d, *J*=7.5 Hz, 1H, NC**CH**CHCH), 4.05 (t, *J*=7.2 Hz, N**CH$_2$**CH$_2$CH$_2$CH$_2$), 3.98 (s, 3H, NCHN(**CH$_3$**)), 3.57 (s, 3H, NCON(**CH$_3$**)), 2.82 (t, *J*=7.2 Hz, 2H, NCH$_2$CH$_2$CH$_2$**CH$_2$**), 1.88-1.65 (m, 4H, NCH$_2$**CH$_2$CH$_2$**CH$_2$) ppm

^{13}CNMR (101 MHz, DMSO-d_6) δ 161.5 (**7**), 161.2 (**5**), 155.3 (**16**), 151.5 (**12**), 148.8 (**4**), 141.4 (**1**), 136.8 (**17**), 136.6 (**15**), 120.8 (**14**), 118.4 (**13**), 107.7 (**3**), 41.2 (**8**), 38.0 (**11**), 33.6 (**2**), 29.7 (**6**), 27.8 (**9**), 27.3 (**10**) ppm

IR (neat) ν_{max} 3113 (m), 2947 (s), 1698 (s), 909 (s) cm^{-1}

LCMS (ESI) *m/z* 357.4 $[M+H]^+$

HRMS (ESI$^+$) *m/z calcd. for* $C_{17}H_{21}N_6O_3^+$ 357.2020 *m/z meas.* 357.2021

Methyl 3-((*tert*-butyldimethylsilyl)oxy)-6-(4-(3,7-dimethyl-2,6-dioxo-2,3,6,7-tetrahydro-1*H*-purin-1-yl)butyl)picolinate (3.25)

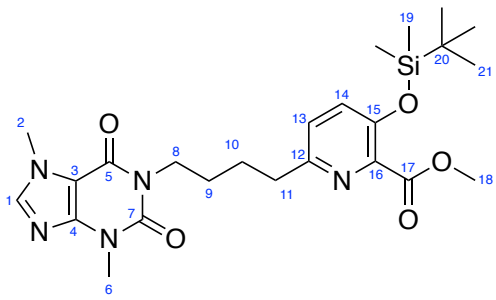

Mol. Wt. 501.2

$C_{24}H_{35}N_5O_5Si$

Following a procedure adapted from de Sousa,[186] to a solution of methyl 6-(4-(3,7-dimethyl-2,6-dioxo-2,3,6,7-tetrahydro-1*H*-purin-1-yl)butyl)-3-hydroxypicolinate (100 mg, 0.26 mmol, 1 equiv.) in anhydrous CH_2Cl_2 (5 mL) was added 2,6-lutidine (0.09 mL, 0.77 mmol, 3 equiv.) and TBSOTf (0.12 mL, 0.52 mmol, 2 equiv.) successively and the pale yellow reaction mixture was stirred for 24 h at rt under an inert argon atmosphere. The reaction solution was concentrated *in vacuo* an the residue was purified by column chromatography (SiO_2, EtOAc) to afford methyl 3-((*tert*-butyldimethylsilyl)oxy)-6-(4-(3,7-dimethyl-2,6-dioxo-2,3,6,7-tetrahydro-1*H*-purin-1-yl)butyl)picolinate (105 mg, 0.21 mmol, 81%) as a colourless oil.

TLC R_f 0.17 (EtOAc, SiO_2)

^{1}HNMR (400MHz, $CDCl_3$) δ 7.05 (s, 1H, NC**H**N), 6.95 (d, *J*=8.3 Hz, 1H, NC**CH**), 6.92 (d, *J*=8.3 Hz, 1H, NCCH**CH**), 3.83 (br. t, *J*=6.8 Hz 2H, N**CH$_2$**CH$_2$CH$_2$CH$_2$), 3.76 (s, 3H, NCHN(**CH$_3$**)), 3.69 (s, 3H, CO$_2$**CH$_3$**), 3.35 (s, 3H, COCN(**CH$_3$**)), 2.59 (br. t, *J*=7.5 Hz, 2H, NCH$_2$CH$_2$CH$_2$**CH$_2$**), 1.59-1.47 (m, 4H, NCH$_2$**CH$_2$CH$_2$**CH$_2$), 0.77 (s, 9H, Si(CH$_3$)$_2$C(**CH$_3$**)$_3$), –0.01 (s, 6H, Si(**CH$_3$**)$_2$C(CH$_3$)$_3$) ppm

^{13}CNMR (101 MHz, $CDCl_3$) δ 166.1 (**17**), 155.3 (**7**), 154.4 (**12**), 151.5 (**5**), 149.2 (**15**), 148.7 (**4**), 141.3 (**1**), 141.0 (**16**), 128.8 (**14**), 125.7 (**13**), 107.7 (**3**), 52.4 (**18**) 41.1 (**8**), 37.2 (**11**), 33.6 (**2**), 29.7 (**6**), 27.8 (**9**), 27.4 (**10**), 25.5 (**21**), 18.1 (**20**), –4.5 (**19**) ppm

IR (neat) ν_{max} 3323 (m), 3060 (s), 2956 (s), 2359 (s), 1699 (s), 774 (s) cm^{-1}

LCMS (ESI) *m/z* 502.4 $[M+H]^+$

HRMS (ESI$^+$) *m/z calcd. for* $C_{24}H_{36}N_5O_5Si^+$ 502.2480 *m/z meas.* 502.2472

1-Naphthyl triflate (3.33)

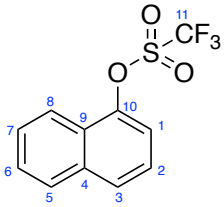

Mol. Wt. 276.2

$C_{10}H_8F_3SO_3$

Following a procedure from Glorius *et al.*[242] for the triflation of aromatic alcohols, to a solution of 1-naphthol (4.33 g, 30.0 mmol, 1 equiv.) in CH_2Cl_2 (30 mL) was added pyridine (4.86 mL, 60.1 mmol, 2 equiv.). The solution was cooled to 0 °C and Tf_2O (5.98 mL, 36.0 mmol, 1.2 equiv.) was added dropwise and the ice bath was removed. The colourless reaction was stirred at rt for 5 min. Et_2O (20 mL) was added and HCl (1 M, 20 mL). The organic layer was removed and washed (sat. aq. $NaHCO_3$, 20 mL), brine (20 mL), dried ($MgSO_4$), filtered and concentrated *in vacuo* to afford 1-naphthyl triflate (8.15 g, 29.5 mmol, 98%) as a colourless oil. Data was consistent with that reported in the literature.[242]

TLC R_f	0.89 (10% EtOAc in light petroleum ether, SiO_2)
^{1}HNMR	(400MHz, $CDCl_3$) δ 7.99 (d, *J*=8.5 Hz, 1H, 8-Ar**H**), 7.84-7.72 (m, 2H, 4-Ar**H**, 5-Ar**H**), 7.58-7.46 (m, 2H, 6-Ar**H**, 7-Ar**H**), 7.42-7.34 (m, 2H, 2-Ar**H**, 3-Ar**H**) ppm
^{13}CNMR	(101 MHz, $CDCl_3$) δ 145.7 (**10**), 134.9 (**4**), 128.5 (**5**), 128.1 (**7**), 127.9 (**9**), 127.4 (**2**), 126.4 (**8**), 125.1 (**6**), 120.8 (**3**), 118.8 (q, *J*=250 Hz, **11**), 117.8 (**1**) ppm
^{19}FNMR	(376 MHz, $CDCl_3$) δ 73.6 ppm
IR (neat)	ν_{max} 3069 (m), 1417 (s), 1205 (s), 1004 (s), 892 (s) cm^{-1}
LCMS	(ESI^+) *m/z* 277.2 $[M+H]^+$

N-Boc-naphthylamine (3.34)

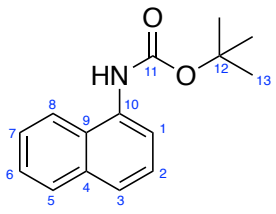

Mol. Wt. 243.1

$C_{15}H_{17}NO_2$

Following a procedure from Garg *et al.*[243] for the Boc protection of aromatic amines, to a solution of naphthylamine (3.00 g, 21.0 mmol, 1 equiv.) in EtOH (35 mL) was added Boc_2O (16.0 g, 73.3 mmol, 3.5 equiv.) and the pale purple reaction was stirred at 50 °C for 18 h. The solvent was removed *in vacuo* and the residue was triturated by the addition of light petroleum ether (approx. 5 mL). The resulting colourless solid was collected by vacuum filtration to afford N-Boc-naphthylamine (4.26 g, 17.5 mmol, 84%) as a colourless solid. Data was consistent with that reported in the literature.[243]

TLC R_f	0.63 (20% EtOAc in light petroleum ether, SiO_2)
^{1}HNMR	(400MHz, $CDCl_3$) δ 7.96-7.80 (m, 3H, 4-Ar**H**, 5-Ar**H**, 8-Ar**H**), 7.65 (d, *J*=8.2 Hz, 1H, 3-Ar**H**), 7.56-7.43 (m, 3H, 6-Ar**H**, 7-Ar**H**, 2-Ar**H**), 6.88 (br. s, 1H **NH**), 1.58 (s, 9H, C(**CH$_3$**)$_3$) ppm
^{13}CNMR	(101 MHz, $CDCl_3$) δ 153.5 (**11**), 134.1 (**10**), 133.0 (**4**), 128.8 (**5**), 126.5 (**2**), 126.0 (**6**), 125.9 (**9**), 125.8 (**7**), 124.5 (**8**), 120.5 (**3**), 118.7 (**1**), 80.7 (**12**), 28.4 (**13**) ppm
IR (neat)	ν_{max} 3255 (s), 3050 (m), 2972 (s), 1681 (s), 1154 (s), 764 (s) cm^{-1}
LCMS	(ESI$^+$) *m/z* 244.2 $[M+H]^+$
MPt	96-98 °C (lit: 96-99 °C)

2-Bromo-*N*-(naphthalen-1-yl)acetamide (3.37)

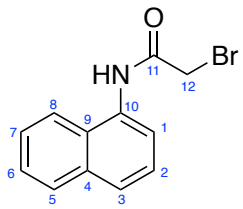

Mol. Wt. 263.0

$C_{12}H_{10}BrNO$

Following a procedure from Zhong-Xing *et al.*[244] for the substitution of naphthylamine, to a solution of naphthylamine (2.00 g, 14.0 mmol, 1 equiv.) and Et_3N (2.14 mL, 15.4 mmol, 1.1 equiv.) in CH_2Cl_2 (30 mL) at 0 °C was added bromoacetyl bromide (1.34 mL, 15.4 mmol, 1.1 equiv.) over 15 min. The pale purple mixture was stirred at 0 °C for 1 h. The mixture was diluted with CH_2Cl_2 (20 mL), washed with 2 M HCl (2 × 20 mL), H_2O (20 mL), sat. aq. $NaHCO_3$ (20 mL), brine (20 mL), dried (Na_2SO_4), filtered and concentrated *in vacuo* leaving 2-bromo-*N*-(naphthalene-1-yl)acetamide (3.58 g, 13.6 mmol, 97%) as a pale brown solid. Data was consistent with that reported in the literature.[244]

TLC R_f	0.43 (20% EtOAc in light petroleum ether, SiO_2)
^{1}HNMR	(400MHz, $CDCl_3$) δ 8.69 (br. s, 1H, **NH**), 7.97 (d, *J*=7.6 Hz, 1H, 8-Ar**H**), 7.93-7.87 (m, 2H, 2-Ar**H**, 5-Ar**H**), 7.76 (d, *J*=8.3 Hz, 1H, 4-Ar**H**), 7.61-7.48 (m, 3H, 3-Ar**H**, 6-Ar**H**, 7-Ar**H**), 4.20 (s, 2H NHCO**C**$\mathbf{H_2}$) ppm
^{13}CNMR	(101 MHz, $CDCl_3$) δ 163.8 (**11**), 134.1 (**10**), 131.4 (**4**), 128.9 (**5**), 127.0 (**9**), 126.7 (**6**), 126.5 (**2**), 126.2 (**8**), 125.7 (**3**), 120.5 (**7**), 120.2 (**1**), 30.0 (**12**) ppm
IR (neat)	ν_{max} 3250 (s), 3050 (m), 2962 (s), 1657 (s), 1392 (s), 797 (s) cm^{-1}
LCMS	(ESI^+) *m/z* 264.1 $[M^{79}Br+H]^+$ 266.1 $[M^{81}Br+H]^+$
MPt	153-156 °C (lit: 151-154 °C)

***N*-(2-Bromoethyl)naphthalen-1-amine (3.36)**

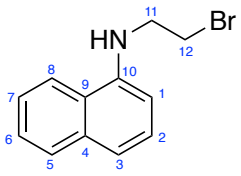

Mol. Wt. 249.0

$C_{12}H_{12}BrN$

Following a procedure by Brondsted *et al.*[245] for the reduction of aromatic amides, to a solution of 2-bromo-*N*-(naphthalene-1-yl)acetamide (1.00 g, 3.79 mmol, 1 equiv.) in THF (20 mL) was added $BH_3 \cdot SMe_2$ (0.72 g, 9.47 mmol, 2.5 eq) slowly at rt. The pale brown mixture was heated to 80 °C for 1 h. After cooling to rt, the orange reaction mixture was further cooled to 0 °C, MeOH (10 mL) was added and the solution was stirred for 10 min at 0 °C. The pH of the solution was adjusted to 2 by addition of c. HCl and the reaction was heated to 80 °C for 30 min. Sat. aq. NaOH (20 mL) was added and the aqueous solution was extracted (EtOAc, 3 × 40 mL). The organic layers were combined, dried ($MgSO_4$), filtered and concentrated *in vacuo*. The brown residue was purified by column chromatography (SiO_2, hexanes to 20% EtOAc in hexanes) to afford *N*-(2-bromoethyl)naphthalene-1-amine (489 mg, 1.95 mmol, 52%) as a yellow oil. Data was consistent with that reported in the literature.[245]

TLC R_f	0.80 (20% EtOAc in hexanes, SiO_2)
^{1}HNMR	(400MHz, $CDCl_3$) δ 7.91-7.79 (m, 2H, 5-Ar**H**, 8-Ar**H**), 7.52-7.45 (m, 2H, 4-Ar**H**, 7-Ar**H**), 7.39-7.33 (m, 2H, 3-Ar**H**, 6-Ar**H**), 6.67 (d, *J*=7.1 Hz, 1H, 2-Ar**H**), 3.85-3.68 (m, 4H NHCO**CH_2CH_2**) ppm
^{13}CNMR	(101 MHz, $CDCl_3$) δ 137.0 (**10**), 134.4 (**4**), 128.7 (**2**), 126.3 (**5**), 126.0 (**8**), 125.3 (**6**), 123.8 (**3**), 119.9 (**7**), 119.2 (**9**), 107.0 (**1**), 46.0 (**11**), 31.5 (**12**) ppm
IR (neat)	ν_{max} 2895 (m), 2706 (m), 2458 (s), 1606 (s), 763 (s) cm^{-1}
LCMS	(ESI^+) *m/z* 250.0 $[M^{79}Br+H]^+$ 252.0 $[M^{81}Br+H]^+$

(*E*)-6-((Trimethylsilyl)ethynyl)picolinaldehyde oxime (3.39)

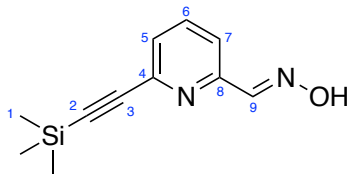

Mol. Wt. 218.1

$C_{11}H_{14}N_2OSi$

Following a procedure adapted from Yamanaka *et al.*[246] for the addition of TMS acetylene to aryl bromides, to a solution of (E)-6-bromopicolinaldehyde oxime (2.00 g, 9.95 mmol, 1 equiv.), dichlorobis(triphenylphosphine) palladium (140 mg, 0.20 mmol, 2 mol%), copper iodide (40.0 mg, 0.20 mmol, 2 mol%) and triphenyl phosphine (105 mg, 0.40, 4 mol%) in toluene (10 mL) was added DIPEA (3.32 mL, 23.5 mmol, 2.4 equiv.). The reaction was stirred at rt for 5 min before TMS acetylene (1.70 mL, 11.9 mmol, 1.2 equiv.) was added. The yellow reaction solution was stirred at 80 °C for 16 h. To the brown reaction mixture was added sat. aq. NH_4Cl (50 mL), the aqueous phase was separated and extracted (CH_2Cl_2, 3 × 50 mL). The combined organics were dried ($MgSO_4$), filtered and concentrated *in vacuo* and the residue was purified by column chromatography (SiO_2, 20% EtOAc in hexanes) to afford (*E*)-6-((trimethylsilyl)ethynyl)picolinaldehyde oxime (1.45 g, 6.64 mmol, 67%) as an orange solid.

TLC R_f	0.36 (50% EtOAc in hexanes, SiO_2)
^{1}HNMR	(400MHz, $CDCl_3$) δ 8.35 (s, 1H, N**OH**), 8.30 (s, 1H, **CH**NOH), 7.80 (dd, *J*=8.1, 1.0 Hz, 1H, NC**CH**CHCH), 7.67 (t, *J*=8.1 Hz, 1H, NCCH**CH**CH), 7.45 (dd, *J*=8.1, 1.0 Hz, 1H, NCCHCH**CH**), 0.28 (s, 9H, Si(**CH$_3$**)$_3$) ppm
^{13}CNMR	(101 MHz, $CDCl_3$) δ 152.1 (**8**), 150.6 (**9**), 142.8 (**4**), 136.7 (**6**), 127.7 (**5**), 119.9 (**7**), 103.0 (**3**), 95.8 (**2**), 0.2 (**1**) ppm
IR (neat)	ν_{max} 3194 (m), 2958 (s), 2360 (s), 2170 (s), 1564 (s), 1247 (s) cm^{-1}
LCMS	(ESI) *m/z* 219.2 $[M+H]^+$
HRMS	(ESI$^+$) *m/z calcd. for* $C_{11}H_{15}N_2OSi^+$ 219.0948 *m/z meas.* 219.0953
MPt	112-113 °C

(*E*)-6-Ethynylpicolinaldehyde oxime (3.38)

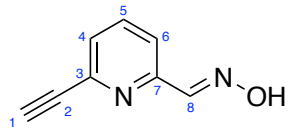

Mol. Wt. 146.1

$C_8H_6N_2O$

Following a procedure by Jarowski *et al.*[247] for TMS deprotection of terminal alkynes, to a solution of (*E*)-6-((trimethylsilyl)ethynyl)picolinaldehyde oxime (1.00 g, 4.58 mmol, 1 equiv.) in MeOH (20 mL) was added slowly potassium hydroxide (1 M in H_2O, 283 mg, 5.04 mmol, 1.1 equiv.) and the orange solution was stirred at rt for 30 min. The solvent was removed in vacuo and H_2O (10 mL) was added. The aqueous phase was extracted (3 × CH_2Cl_2, 30 mL), the organic layers were combined, dried ($MgSO_4$), filtered and concentrated *in vacuo*. The orange residue was purified by column chromatography (SiO_2, 20% EtOAc to 50% EtOAc in hexanes) to afford (*E*)-6-ethynylpicolinaldehyde oxime (320 mg, 2.19 mmol, 48%) as a pale yellow solid.

TLC R_f	0.70 (50% EtOAc in hexanes, SiO_2)
^{1}HNMR	(400MHz, MeOD-d_4) δ 8.07 (s, 1H, **CH**NOH), 7.89-7.77 (m, 2H, NCCH**CHCH**), 7.51 (dd, *J*=7.6, 1.2 Hz, 1H, NC**CH**CHCH), 3.76 (s, 1H, C**CH**) ppm
^{13}CNMR	(101 MHz, MeOD-d_4) δ 154.5 (**7**), 149.3 (**8**), 143.3 (**3**), 138.9 (**5**), 128.9 (**4**), 121.4 (**6**), 83.1 (**2**), 79.9 (**1**) ppm
IR (neat)	ν_{max} 3238 (s), 3091 (m), 2784 (m), 2360 (s), 2110 (s), 1562 (s) cm^{-1}
LCMS	(ESI) *m/z* 147.1 $[M+H]^+$
MPt	167-169 °C (lit: 169-171 °C)

1-(Naphthalen-1-yl)aziridine (3.41)

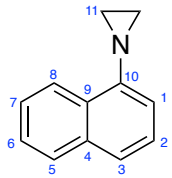

Mol. Wt. 169.1

$C_{12}H_{11}N$

Following a procedure from Zhou *et al.*[248] for the formation of aromatic aziridines, to a solution of *N*-(2-bromoethyl)naphthalen-1-amine (600 mg, 2.40 mmol, 1 equiv.) in THF (20 mL) at rt was added sodium hydride (146 mg, 6.12 mmol, 2.55 equiv.) and the pale brown reaction mixture was stirred at rt for 16 h. H_2O (35 mL) was added and the aqueous phase was extracted (Et_2O, 45 mL). The organic phase was separated and washed with 2 M HCl (45 mL), H_2O (45 mL), brine (45 mL). The organic phase was dried ($MgSO_4$), filtered and concentrated *in vacuo* and the residue was purified by column chromatography (SiO_2, 20% EtOAc in hexanes) to afford 1-(naphthalen-1-yl)aziridine (275 mg, 1.63 mmol, 68%) as a pale brown oil.

TLC R_f	0.53 (20% EtOAc in hexanes, SiO_2)
^{1}HNMR	(400MHz, $CDCl_3$) δ 8.37 (d, *J*=7.8 Hz, 4-Ar**H**), 7.88-7.81 (m, 1H, 5-Ar**H**), 7.58-7.43 (m, 3H, 8-Ar**H**, 7-Ar**H**, 6-Ar**H**), 7.36 (t, *J*=7.8 Hz, 1H, 3-Ar**H**), 6.96 (d, *J*=7.8 Hz, 1H, 2-Ar**H**), 2.30 (br. s, 4H, **CH_2CH_2**) ppm
^{13}CNMR	(101 MHz, $CDCl_3$) δ 150.5 (**10**), 134.5 (**4**), 128.6 (**9**), 126.3 (**5**), 126.1 (**8**), 126.0 (**7**), 125.7 (**6**), 123.1 (**2**), 123.0 (**3**), 114.9 (**1**), 28.6 (**11**) ppm
IR (neat)	ν_{max} 3048 (m), 2965 (s), 2883 (s), 1398 (s), 773 (s) cm^{-1}
LCMS	(ESI^+) *m/z* 170.2 $[M+H]^+$

3-Butynoic acid (3.42)

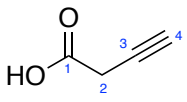

Mol. Wt. 84.1

$C_4H_4O_2$

Following a procedure from Loh *et al.*[249] for the oxidation of 3-butyn-1-ol, a solution of c. HNO_3 (0.11 mL, 2.50 mmol, 5 mol%), sodium dichromate (148 mg, 0.50 mmol, 1 mol%) and sodium periodate (23.5 g, 109 mmol, 2.2 equiv.) was stirred vigorously at 0 °C for 15 min. 3-Butyn-1-ol (3.78 mL, 49.9 mmol, 1 equiv.) was dissolved in cold water (45 mL) and was added slowly to the first solution at 0 °C. The reaction mixture was stirred at rt for 18 h. A colour change was observed from orange to blue. The product was extracted into Et_2O (6 × 80 mL) and the combined organics were dried ($MgSO_4$) and filtered. CH_2Cl_2 (10 mL) was added to the resulting red oil and the solvent was removed *in vacuo*. This process was repeated 10 times to give 3-butynoic acid (3.00 g, 35.7 mmol, 71%) as a pale yellow solid. Data was consistent with that reported in the literature.[249]

TLC R_f	0.10 (EtOAc, SiO_2)
^{1}HNMR	(400MHz, $CDCl_3$) δ 10.57 (br. s, 1H, CO_2**H**), 3.39 (d, *J*=2.8 Hz, 2H, **C**H_2CCH), 2.25 (t, *J*=2.8 Hz, 1H, CH_2C**C**H) ppm
^{13}CNMR	(101 MHz, $CDCl_3$) δ 173.8 (**1**), 74.4 (**3**), 72.1 (**4**), 25.5 (**2**) ppm
IR (neat)	ν_{max} 3295 (s), 3210 (w), 2910 (s), 2205 (s), 1685 (s), 1233 (s) cm^{-1}
LCMS	(EI) *m/z* 84.0 $[M]^+$
MPt	80-82 °C (lit: 83-84 °C)

_N_-(Naphthalen-1-yl)but-3-ynamide (3.43)

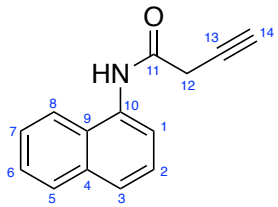

Mol. Wt. 209.1

$C_{14}H_{11}NO$

Following a procedure from Lam *et al.*[250] for the substitution of aminonaphthalene, a solution of 3-butynoic acid (2.00 g, 23.8 mmol, 1 equiv.) and DMF (0.02 mL, 0.31 mmol, 1 mol%) in CH_2Cl_2 (10 mL) was cooled to 0 °C and oxalyl chloride (2.66 mL, 30.9 mmol, 1.3 equiv.) was added dropwise. The reaction mixture was allowed to warm slowly to rt and stirred for 2 h until the pale yellow solution turned dark orange and the evolution of gas stopped. The solvent and excess oxalyl chloride were removed *in vacuo* and the resulting dark red residue was dissolved in CH_2Cl_2 (10 mL). The resulting red solution was cooled to 0 °C, followed by the addition of naphthylamine (8.52 g, 59.5 mmol, 2.5 equiv.). The reaction mixture was warmed to rt and stirred for 2 h. The solution was diluted with CH_2Cl_2 (20 mL), washed (sat. aq. $NaHCO_3$, 2 × 20 mL), brine (20 mL), dried ($MgSO_4$), filtered and concentrated *in vacuo*. The resulting orange residue was purified by column chromatography (SiO_2, 20% EtOAc in hexanes) to afford *N*-(naphthalen-1-yl)but-3-ynamide (850 mg, 4.06 mmol, 17%) as a yellow oil.

TLC R_f 0.16 (20% EtOAc in hexanes, SiO_2)

^{1}HNMR (400MHz, $CDCl_3$) δ 8.79 (br. s, 1H, **NH**), 8.03 (d, *J*=7.3 Hz, 1H, 8-Ar**H**), 7.93-7.86 (m, 2H, 4-Ar**H**, 5-Ar**H**), 7.74 (d, *J*=8.3 Hz, 1H, 2-Ar**H**), 7.60-7.48 (m, 3H, 3-Ar**H**, 6-Ar**H**, 7-Ar**H**), 3.54 (d, *J*=2.8 Hz, 2H NHCO**CH_2**CH), 2.64 (t, *J*=2.8 Hz, 1H, NHCOCH_2**CH**) ppm

^{13}CNMR (101 MHz, $CDCl_3$) δ 164.4 (**11**), 134.1 (**10**), 131.7 (**4**), 128.9 (**2**), 126.9 (**9**), 126.5 (**8**), 126.1 (**7**), 126.0 (**6**), 125.8 (**5**), 120.3 (**3**), 120.2 (**1**), 77.6 (**13**), 75.4 (**14**), 28.4 (**12**) ppm

IR (neat) ν_{max} 3302 (s), 3286 (s), 3030 (m), 2902 (s), 1656 (s), 1545 (s) cm^{-1}

LCMS (ESI^+) *m/z* 210.2 $[M+H]^+$

Ethyl 3-(naphthalen-1-ylamino)propanoate (3.51)

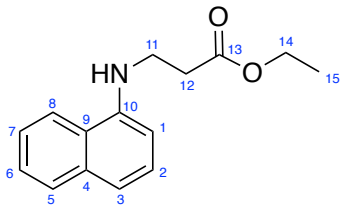

Mol. Wt. 243.1

$C_{15}H_{17}NO_2$

Following a procedure from Moura *et al.*[251] for the substitution of 1-aminonaphthalene, to a solution of 1-aminonaphthalene (2.00 g, 14.0 mmol, 1 equiv.) in EtOH (5 mL) was added ethyl 3-bromopropionate (1.87 mL, 14.7 mmol, 1.05 equiv.). The resulting purple mixture was heated 90 °C for 16 h. A colour change to a deep red was observed and the reaction mixture was allowed to cool to rt and the solvent was removed *in vacuo*. The red residue was purified by column chromatography (SiO_2, $CHCl_3$) to afford ethyl 3-(naphthalen-1-ylamino)propanoate (1.23 g, 5.06 mmol, 36%) as a yellow oil. Data was consistent with that reported in the literature.[251]

TLC R_f	0.74 ($CDCl_3$, SiO_2)
^{1}HNMR	(400MHz, $CDCl_3$) δ 7.95-7.71 (m, 2H, 5-Ar**H**, 8-Ar**H**), 7.52-7.43 (m, 2H, 6-Ar**H**, 7-Ar**H**), 7.38 (t, *J*=7.8 Hz, 1H, 3-Ar**H**), 7.29 (d, *J*=7.8 Hz, 1H, 4-Ar**H**), 6.69 (d, *J*=7.8 Hz, 1H, 2-Ar**H**), 4.21 (q, *J*=7.1 Hz, 2H, $OC\mathbf{H_2}CH_3$), 3.64 (t, *J*=6.3 Hz, 2H, $NHC\mathbf{H_2}CH_2$), 2.79 (t, *J*=6.3 Hz, 2H, $NHCH_2C\mathbf{H_2}$), 1.31 (t, *J*=7.1 Hz, 3H, $OCH_2C\mathbf{H_3}$) ppm
^{13}CNMR	(101 MHz, $CDCl_3$) δ 172.5 (**13**), 142.3 (**10**), 134.4 (**4**), 128.6 (**8**), 126.4 (**2**), 125.9 (**6**), 125.0 (**7**), 123.9 (**9**), 120.0 (**5**), 118.5 (**3**), 105.6 (**1**), 60.8 (**14**), 40.3 (**11**), 33.5 (**12**), 14.2 (**15**) ppm
IR (neat)	ν_{max} 3433 (b), 3051 (m), 2980 (m), 1723 (s), 767 (s) cm^{-1}
LCMS	(ESI^+) *m/z* 244.2 $[M+H]^+$

4-(Naphthalen-1-ylamino)butanenitrile (3.54)

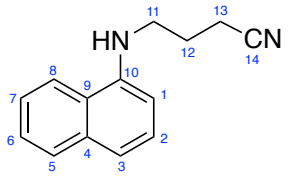

Mol. Wt. 210.1

$C_{14}H_{14}N_2$

Following a procedure from Liliana *et al.*[252] for the substitution of naphthylamine, a solution of 4-chlorobutyronitrile (2.68 mL, 27.9 mmol, 1 equiv.) in DMF (10 mL) was added over 90 min to a solution of 1-naphthylamine (4.00 h, 27.9 mmol, 1 equiv.), cesium carbonate (9.10 g, 27.9 mmol, 1 equiv.) and potassium iodide (9.27 g, 55.9 mmol, 2 equiv.) in DMF (10 mL). The purple reaction mixture was stirred at 105 °C for 2.5 h. The mixture was treated with Et_2O (100 mL) and H_2O (30 mL) and the aqueous phase was separated and extracted (Et_2O, 30 mL). The combined organics were dried (Na_2SO_4), filtered and concentrated *in vacuo*, the brown residue was purified by column chromatography (SiO_2, 30% EtOAc in hexanes) to afford 4-(naphthalen-1-ylamino)butanenitrile (3.00 g, 14.3 mmol, 51%) as a pink oil. Data was consistent with that reported in the literature.[252]

TLC R_f 0.24 (30% EtOAc in hexanes, SiO_2)

^{1}HNMR (400MHz, $CDCl_3$) δ 7.85-7.79 (m, 2H, 5-Ar**H**, 8-Ar**H**), 7.52-7.28 (m, 4H, 3-Ar**H**, 4-Ar**H**, 6-Ar**H**, 7-Ar**H**), 6.67 (d, *J*=7.6 Hz, 1H, 2-Ar**H**), 3.52 (t, *J*=6.8 Hz, 2H, NH**CH_2**CH_2CH_2), 2.56 (t, *J*=6.8 Hz, 2H, $NHCH_2CH_2$**CH_2**), 2.14 (quin, *J*=6.8 Hz, 2H, $NHCH_2$**CH_2**CH_2) ppm

^{13}CNMR (101 MHz, $CDCl_3$) δ 134.8 (**10**), 134.6 (**4**), 129.1 (**2**), 128.3 (**5**), 127.8 (**6**), 127.4 (**8**), 125.7 (**1**), 125.2 (**7**), 122.0 (**9**), 121.0 (**3**), 118.0 (**14**), 30.9 (**11**), 22.0 (**12**), 15.1 (**13**) ppm

IR (neat) ν_{max} 3437 (s), 3392 (s), 3045 (m), 2945 (m), 2249 (s), 1582 (s) cm^{-1}

LCMS (ESI^+) *m/z* 211.2 $[M+H]^+$

(*E*)-*N*-Pentyl-3,4-dihydronaphthalen-1(2*H*)-imine (3.71)

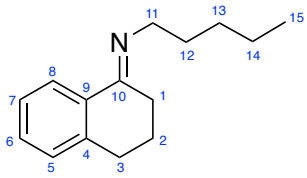

Mol. Wt. 215.2

$C_{15}H_{21}N$

Following a procedure from Marples *et al.*[253] for the formation of imines from α-tetralone, to a yellow solution of α-tetralone (0.91 mL, 6.84 mmol, 1 equiv.), pentylamine (4.13 mL, 35.6 mmol, 5.2 equiv.) and PTSA (24 mg, 0.14 mmol, 2 mol%) in toluene (50 mL) was heated to 110 °C for 18 h under a Dean and Stark water separator. The organic phase was separated and washed (sat. aq. $NaHCO_3$, 2 × 50 mL) and concentrated *in vacuo* to afford (*E*)-*N*-pentyl-3,4-dihydronaphthalen-1(2*H*)-imine (1.20 g, 5.57 mmol, 81%) as a brown oil. Data was consistent with that reported in the literature.[253]

TLC R_f	0.75 (20% EtOAc in hexanes, SiO_2)
^{1}HNMR	(400MHz, $CDCl_3$) δ 8.18 (dd, =7.8, 1.5 Hz, 1H, 8-Ar**H**), 7.31-7.27 (m, 1H, 7-Ar**H**), 7.27-7.20 (m, 1H, 6-Ar**H**), 7.16-7.11 (m, 1H, 5-Ar**H**), 3.45 (t, *J*=7.2 Hz, 2H, N**CH_2**$CH_2CH_2CH_2CH_3$), 2.82 (t, *J*=6.3 Hz, 2H, **CH_2**CH_2CH_2C=N), 2.58 (t *J*=6.3 Hz, 2H, CH_2CH_2**CH_2**C=N), 1.95 (quin, *J*=6.3 Hz, 1H, CH_2**CH_2**CH_2C=N), 1.76 (quin, *J*=7.2 Hz, 2H, NCH_2**CH_2**$CH_2CH_2CH_3$), 1.50-1.34 (m, 4H, NCH_2CH_2**CH_2CH_2**CH_3), 0.94 (t, *J*=6.6 Hz, 3H, $NCH_2CH_2CH_2CH_2$**CH_3**) ppm
^{13}CNMR	(101 MHz, $CDCl_3$) δ 164.0 (**10**), 140.3 (**4**), 135.0 (**9**), 129.4 (**6**), 128.2 (**5**), 126.3 (**8**), 125.5 (**7**), 51.1 (**11**), 30.8 (**1**), 30.0 (**12**), 29.8 (**13**), 27.7 (**3**), 22.7 (**14**), 22.6 (**2**), 14.1 (**15**) ppm
IR (neat)	ν_{max} 3430 (m), 3051 (s), 2926 (s), 2856 (s), 1581 (s), 763 (s) cm^{-1}
LCMS	(EI) *m/z* 215.1 $[M]^+$

_N_-Pentylnaphthalen-1-amine (3.72)

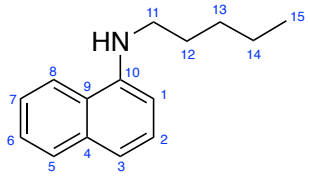

Mol. Wt. 213.2

$C_{15}H_{19}N$

Following a procedure from Yoshikai *et al.*[210] for the oxidation of imines to aromatic amines, to a flame-dried Schlenk flask containing a solution of (*E*)-*N*-pentyl-3,4-dihydronaphthalen-1(2*H*)-imine (1.00 g, 4.64 mmol, 1 equiv.), palladium diacetate (104 mg, 0.46 mmol, 10 mol%), TBAB (3.00 g, 9.29 mmol, 2 equiv.) and 3Å molecular sieves (2.50 g) in toluene (20 mL) was added DMSO (2.5 mL). The flask was evacuated under vacuum and refilled with oxygen. The resulting mixture was heated to 90 °C for 16 h. Upon cooling to rt, EtOAc (20 mL) was added and the brown solution was filtered through a pad of silica gel. The filtrate was concentrated *in vacuo* and purified by column chromatography (SiO_2, 10% EtOAc in hexanes) to afford *N*-pentylnaphthalen-1-amine (615 mg, 2.88 mmol, 62%) as a yellow oil. Data was consistent with that reported in the literature.[210]

TLC R_f 0.57 (10% EtOAc in hexanes, SiO_2)

^{1}HNMR (400MHz, $CDCl_3$) δ 7.85-7.77 (m, 2H, 7-Ar**H**, 8-Ar**H**), 7.49-7.40 (m, 2H, 3-Ar**H**, 4-Ar**H**), 7.36 (t, *J*=8.6 Hz, 1H, 6-Ar**H**), 7.23 (d, *J*=8.6 Hz, 1H, 5-Ar**H**), 6.62 (d, *J*=7.6 Hz, 1H, 2-Ar**H**), 4.32 (br. s, 1H, **NH**), 3.29 (t, *J*=7.1 Hz, 2H, $NHC\mathbf{H_2}CH_2CH_2CH_2CH_3$), 1.80 (quin, *J*=7.1 Hz, 1H, $NHCH_2\mathbf{CH_2}CH_2CH_2CH_3$), 1.58-1.37 (m, 4H, $NCH_2CH_2\mathbf{CH_2CH_2}CH_3$), 0.97 (t, *J*=7.6 Hz, 3H, $NCH_2CH_2CH_2CH_2\mathbf{CH_3}$) ppm

^{13}CNMR (101 MHz, $CDCl_3$) δ 143.6 (**10**), 134.3 (**4**), 128.7 (**9**), 126.7 (**2**), 125.6 (**5**), 124.6 (**6**), 123.3 (**8**), 119.7 (**7**), 117.0 (**3**), 104.1 (**1**), 44.2 (**11**), 29.5 (**12**), 29.1 (**13**), 22.6 (**14**), 14.1 (**15**) ppm

IR (neat) ν_{max} 3429 (m), 3053 (m), 2926 (s), 2856 (s), 1581 (s), 763 (s) cm^{-1}

LCMS (EI) *m/z* 213.4 $[M]^+$

(*E*)-*N*-(But-3-yn-1-yl)-3,4-dihydronaphthalen-1(2*H*)-imine (3.73)

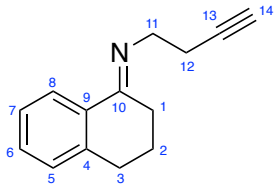

Mol. Wt. 197.1

$C_{14}H_{15}N$

Following a procedure from Marples *et al.*[253] for the formation of imines from α-tetralone, to a solution of α-tetralone (0.91 mL, 6.84 mmol, 1 equiv.), 3-butyn-1-amine (2.91 mL, 35.6 mmol, 5.2 equiv.) and PTSA (24 mg, 0.14 mmol, 2 mol%) in toluene (50 mL) was heated to 110 °C for 18 h under Dean and Stark water separator. The organic phase was separated and washed (sat. aq. $NaHCO_3$, 2 × 50 mL). Activated charcoal was added and the solution was passed through a silica gel plug and concentrated in vacuo to afford (*E*)-*N*-(but-3-yn-1-yl)-3,4-dihydronaphthalen-1(2*H*)-imine (750 mg, 3.80 mmol, 56%) as a yellow oil.

TLC R_f	0.59 (20% EtOAc in hexanes, SiO_2)
^{1}HNMR	(400MHz, $CDCl_3$) δ 8.05 (dd, =7.5, 1.5 Hz, 1H, 8-Ar**H**), 7.48 (t, *J*=7.5 Hz, 1H, 7-Ar**H**), 7.35-7.29 (m, 1H, 6-Ar**H**), 7.16-7.11 (m, 1H, 5-Ar**H**), 3.62 (t, *J*=7.5 Hz, 2H, N**CH_2**CH_2CCH), 2.98 (t, *J*=6.1 Hz, 2H, **CH_2**CH_2CH_2C=N), 2.87-2.80 (m, 2H, NCH_2**CH_2**CCH), 2.71-2.65 (m, 2H, CH_2CH_2**CH_2**C=N), 2.16 (quin, *J*=6.3 Hz, 1H, CH_2**CH_2**CH_2C=N), 1.96 (quin, *J*=6.3 Hz, 1H, NCH_2CH_2**CH**) ppm
^{13}CNMR	(101 MHz, $CDCl_3$) δ 165.4 (**10**), 140.5 (**4**), 133.4 (**9**), 128.7 (**5**), 128.3 (**6**), 127.2 (**8**), 126.4 (**7**), 83.3 (**13**), 68.8 (**14**), 49.9 (**11**), 29.8 (**1**), 28.0 (**3**), 22.5 (**2**), 21.0 (**12**) ppm
IR (neat)	ν_{max} 3293 (m), 2933 (s), 2117 (s), 1680 (s), 760 (s) cm^{-1}
LCMS	(EI) *m/z* 197.1 $[M]^+$

2-(Naphthalen-1-ylamino)ethan-1-ol (3.76)

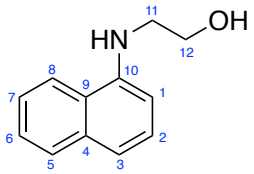

Mol. Wt. 187.1

$C_{12}H_{13}NO$

Following a procedure from Couty *et al.*[211] for the substitution of 1-iodonaphthalene, to mixture of 1-iodonaphthalene (2.50 g, 9.84 mmol, 1 equiv.), 2-aminoethanol (1.78 mL, 29.5 mmol, 3 equiv.), copper chloride (132 mg, 0.98 mmol, 10 mol%) and freshly crushed potassium hydroxide (1.10 g, 19.7 mmol, 2 equiv.) was added DMSO (2 mL). The maroon solution was stirred at rt for 16 h. Sat. aq. NH_4Cl (5 mL) was added and the yellow reaction mixture was extracted (EtOAc, 3 × 20 mL). The combined organics were washed (brine, 20 mL), dried ($MgSO_4$), filtered and concentrated *in vacuo*. The residue was purified by column chromatography (SiO_2, 30% EtOAc in light petroleum ether) to afford 2-(naphthalen-1-ylamino)ethan-1-ol (1.68 g, 8.97 mmol, 91%) as a pale beige oil. Data was consistent with that reported in the literature.[211]

TLC R_f	0.08 (30% EtOAc in light petroleum ether, SiO_2)
^{1}HNMR	(400MHz, $CDCl_3$) δ 7.93-7.76 (m, 2H, 5-Ar**H**, 8-Ar**H**), 7.52-7.29 (m, 4H, 3-Ar**H**, 4-Ar**H**, 6-Ar**H**, 7-Ar**H**), 6.67 (d, *J*=7.3 Hz, 1H, 2-Ar**H**), 4.01 (t, *J*=5.1 Hz, 2H, $NHCH_2\mathbf{CH_2}$), 3.49 (t, *J*=5.1 Hz, 2H, $NH\mathbf{CH_2}CH_2$) ppm
^{13}CNMR	(101 MHz, $CDCl_3$) δ 142.8 (**10**), 134.4 (**4**), 128.7 (**5**), 126.4 (**2**), 125.8 (**6**), 125.0 (**7**), 123.9 (**9**), 123.1 (**2**), 120.0 (**8**), 118.5 (**3**), 105.5 (**1**), 61.0 (**12**), 46.6 (**11**) ppm
IR (neat)	ν_{max} 3404 (w), 3051 (m), 2973 (s), 2869 (m), 1581 (s), 766 (s) cm^{-1}
LCMS	(ESI$^+$) *m/z* 188.1 $[M+H]^+$

2-((2-Hydroxyethyl)(naphthalen-1-yl)amino)acetonitrile (3.77)

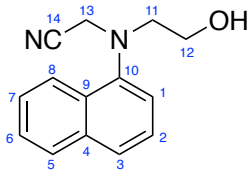

Mol. Wt. 226.1

$C_{14}H_{14}N_2O$

Following a procedure from Couty *et al.*[211] for the *N*-cyanomethylation of 2-(naphthalen-1-ylamino)ethan-1-ol, to a colourless solution of 2-(naphthalen-1-ylamino)ethan-1-ol (745 mg, 3.98 mmol, 1 equiv.) and paraformaldehyde (7.16 mg, 7.96 mmol, 2 equiv.) in MeCN (20 mL) was heated to 90 °C for 16 h. After cooling the solution to rt, to the reaction was added TMSCN (789 mg, 7.96 mmol, 2 equiv.) and AcOH (0.46 mL, 7.96 mmol, 2 equiv.) and the reaction mixture was heated to 90 °C for a further 16 h. After cooling to rt, H_2O (40 mL) was added to the white suspension and the aqueous solution was extracted (CH_2Cl_2, 10 mL) and the organic phase was washed with 1 M NaOH (20 mL) and brine (20 mL). The organic phase was dried ($MgSO_4$), filtered and concentrated *in vacuo* and the pale cream residue was purified by column chromatography (SiO_2, 30% EtOAc in light petroleum ether) to afford 2-((2-hydroxyethyl)(naphthalen-1-yl)amino)acetonitrile (850 mg, 3.76 mmol, 94%) as a colourless solid. Data was consistent with that reported in the literature. [211]

TLC R_f	0.08 (30% EtOAc in light petroleum ether, SiO_2)
^{1}HNMR	(400MHz, $CDCl_3$) δ 8.17 (d, *J*=8.3 Hz, 2H, 8-Ar**H**), 7.91 (d, *J*=7.6 Hz, 1H, 2-Ar**H**), 7.75 (d, *J*=7.6 Hz, 1H, 4-Ar**H**), 7.61-7.42 (m, 4H, 5-Ar**H**, 6-Ar**H**, 7-Ar**H**, 3-Ar**H**), 4.17 (s, 2H, **CH$_2$**CN), 2.78 (br. t, *J*=5.0 Hz, 2H, NHCH$_2$**CH$_2$**), 3.54 (t, *J*=5.0 Hz, 2H, NH**CH$_2$**CH$_2$) ppm
^{13}CNMR	(101 MHz, $CDCl_3$) δ 145.8 (**10**), 134.8 (**4**), 129.7 (**5**), 128.5 (**9**), 126.2 (**6**), 126.1 (**8**), 125.8 (**3**), 125.7 (**2**), 122.9 (**7**), 119.1 (**1**), 116.0 (**14**), 61.1 (**12**), 55.1 (**11**), 44.7 (**13**) ppm
IR (neat)	ν_{max} 3422 (w), 2956 (s), 2236 (s), 1705 (s), 1046 (s), 775 (s) cm^{-1}
LCMS	(ESI$^+$) *m/z* 227.2 $[M+H]^+$
MPt	70-71 °C (lit: 71-73 °C)

1-(Naphthalen-1-yl)azetidine-2-carbonitrile (3.78)

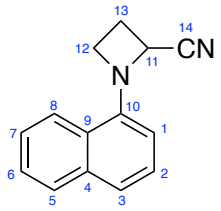

Mol. Wt. 208.1

$C_{14}H_{12}N_2$

Following a procedure from Couty *et al.*[211] for the cyclisation of 2-((2-hydroxyethyl)(naphthalen-1-yl)amino)acetonitrile, to a colourless solution of 2-((2-hydroxyethyl)(naphthalen-1-yl)amino)acetonitrile (500 mg, 2.21 mmol, 1 equiv.) and Et_3N (0.77 mL, 5.52 mmol, 2.5 equiv.) in CH_2Cl_2 (10 mL), cooled to 0 °C, was added dropwise MsCl (0.21 mL, 2.65 mmol, 1.2 equiv.) and the reaction mixture was stirred at 0 °C for 30 min, warmed to rt and stirred for another 30 min. H_2O (20 mL) was added and extracted (CH_2Cl_2, 3 × 10 mL). The combined organic layers were washed (2 M HCl, 20 mL) and brine (20 mL) before being dried ($MgSO_4$), filtered and concentrated *in vacuo*. The resulting mesylate was directly dissolved in anhydrous THF (15 mL) and the solution was cooled to 0 °C. KO^{t}Bu (297 mg, 2.65 mmol, 1.2 equiv) was added and the solution was allowed to warm to rt. H_2O (20 mL) was added and the aqueous solution was extracted (EtOAc, 3 × 20 mL). The combined organics were washed (brine, 20 mL), dried ($MgSO_4$), filtered and concentrated *in vacuo* and the residue was purified by column chromatography (SiO_2, 10% EtOAc in light petroleum ether) to afford 1-(naphthalen-1-yl)azetidine-2-carbonitrile (330 mg, 1.58 mmol, 72%) as a colourless solid. Data was consistent with that reported in the literature.[211]

TLC R_f	0.18 (10% EtOAc in light petroleum ether, SiO_2)
^{1}HNMR	(400MHz, $CDCl_3$) δ 7.96-7.82 (m, 2H, 5-Ar**H**, 8-Ar**H**), 7.56-7.38 (m, 4H, 3-Ar**H**, 4-Ar**H**, 6-Ar**H**, 7-Ar**H**), 6.75 (d, *J*=7.3 Hz, 1H, 2-Ar**H**), 4.93 (dd, *J*=8.3, 6.8 Hz, 1H, $NCH_2CH_2C\mathbf{H}CN$), 4.51 (ddd, *J*=8.3, 6.8, 4.9 Hz, 1H, $NC\mathbf{H}HCH_2C\mathbf{H}CN$), 3.88 (dt, *J*=8.3, 6.8 Hz, 1H, $NCH\mathbf{H}CH_2C\mathbf{H}CN$), 2.91-2.80 (m, 1H, $NCH_2C\mathbf{H}HC\mathbf{H}CN$), 2.78-2.66 (m, 1H, $NCH_2CH\mathbf{H}C\mathbf{H}CN$) ppm
^{13}CNMR	(101 MHz, $CDCl_3$) δ 145.0 (**10**), 134.7 (**4**), 128.6 (**5**), 126.1 (**9**), 125.6 (**6**), 125.2 (**7**), 125.1 (**2**), 122.9 (**8**), 122.5 (**3**), 118.4 (**14**), 109.5 (**1**), 54.3 (**12**), 51.0 (**11**), 22.7 (**13**) ppm
IR (neat)	ν_{max} 3433 (m), 3049 (s), 2958 (m), 2248 (s), 1577 (s), 766 (s) cm^{-1}
LCMS	(ESI$^+$) *m/z* 209.2 $[M+H]^+$
MPt	129-131 °C (lit: 130-132 °C)

***N*-(3-Butyn-1-yl)naphthylamine (3.28)**

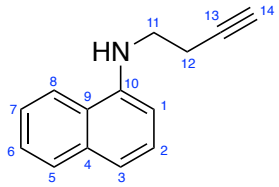

Mol. Wt. 195.1

$C_{14}H_{13}N$

Following a procedure from Couty *et al.*[212] for the synthesis of homopropargylamines from 2-cyanoazetidines, to colourless solution of 1-(naphthalen-1-yl)azetidine-2-carbonitrile (1.00 g, 4.80 mmol, 1 equiv.) in toluene (15 mL) was added dibutyltin oxide (298 mg, 1.20 mmol, 25 mol%) and $TMSN_3$ (0.95 mL, 7.20 mmol, 1.5 equiv.). The colourless solution was stirred at 60 °C for 96 h. The reaction mixture was cooled to rt and concentrated *in vacuo*. The brown residue was purified by column chromatography (SiO_2, 2% EtOAc in light petroleum ether) to afford *N*-(3-butyn-1-yl)naphthylamine (454 mg, 2.33 mmol, 48%) as a colourless oil. Data was consistent with that reported in the literature.[212]

TLC R_f	0.19 (2% EtOAc in hexanes, SiO_2)
^{1}HNMR	(400MHz, $CDCl_3$) δ 7.90-7.79 (m, 2H, 5-Ar**H**, 8-Ar**H**), 7.57-7.29 (m, 4H, 3-Ar**H**, 4-Ar**H**, 6-Ar**H**, 7-Ar**H**), 6.66 (d, *J*=7.3 Hz, 1H, 2-Ar**H**), 3.50 (t, *J*=6.5 Hz, 2H, NH**CH_2**CH_2CCH), 2.69 (td, *J*=6.5, 2.7 Hz, 2H, NHCH_2**CH_2**CCH), 2.11 (t, *J*=2.7 Hz, 1H, NHCH_2CH_2C**C**H) ppm
^{13}CNMR	(101 MHz, $CDCl_3$) δ 146.7 (**10**), 134.4 (**4**), 128.7 (**2**), 126.4 (**8**), 125.9 (**6**), 125.0 (**5**), 123.8 (**9**), 121.0 (**1**), 119.9 (**7**), 118.3 (**3**), 85.2 (**13**), 70.4 (**14**), 27.4 (**11**), 18.9 (**12**) ppm
IR (neat)	ν_{max} 3293 (s), 3050 (m), 2975 (m), 2117 (s), 1690 (s), 767 (s) cm^{-1}
LCMS	(ESI^+) *m/z* 196.2 $[M+H]^+$

(*E*)-6-(4-(Naphthalen-1-ylamino)but-1-yn-1-yl)picolinaldehyde oxime (3.40)

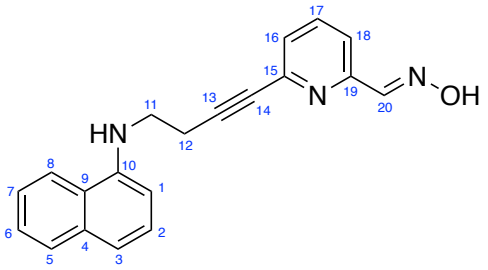

Mol. Wt. 315.1

$C_{20}H_{17}N_3O$

Following a procedure adapted from de Sousa,[186] to a degassed solution of *N*-(but-3-yn-1-yl)naphthylamine (400 mg, 2.05 mmol, 1 equiv.) in THF/Et_3N (7 mL/3 mL) was added $Pd(PPh_3)_4$ (237 mg, 0.20 mmol, 10 mol%) and CuI (78.0 mg, 0.41 mmol, 20 mol%). To the resulting orange reaction mixture was added dropwise a degassed solution of (E)-6-bromopicolinaldehyde oxime (452 mg, 2.25 mmol, 1.1 equiv.) in THF (10 mL). The brown solution was stirred for 18 h at rt. The reaction was concentrated *in vacuo*. The brown residue was purified by column chromatography (SiO_2, hexanes to 10% EtOAc in hexanes) to afford (*E*)-6-(4-(naphthalen-1-ylamino)but-1-yn-1-yl)picolinaldehyde oxime (350 mg, 1.11 mmol, 54%) as an orange solid.

(*E*)-6-(4-(Naphthalen-1-ylamino)but-1-yn-1-yl)picolinaldehyde oxime (10 mg, 0.03 mmol) was dissolved in 2 M HCl (3 mL). The orange solution was stirred at rt for 10 mins. The reaction solution was concentrated *in vacuo* to afford (*E*)-6-(4-(naphthalen-1-ylamino)but-1-yn-1-yl)picolinaldehyde oxime hydrochloride (10.5 mg, 0.03 mmol, 100%) as a orange solid.

TLC R_f 0.55 (20% EtOAc in hexanes, SiO_2)

^{1}HNMR (400MHz, $CDCl_3$) δ 8.28 (s, 1H, **CH**NOH), 7.95-7.73 (m, 4H, Ar**H**), 7.67 (t, *J*=7.8 Hz, 1H, 3-Ar**H**), 7.53-7.33 (m, 4H, Ar**H**), 6.70 (d, *J*=7.8 Hz, 1H, 2-Ar**H**), 3.66 (t, *J*=6.7 Hz, 2H, NH**CH_2**CH_2), 2.96 (t, *J*=6.7 Hz, 2H, NHCH_2**CH_2**) ppm

^{13}CNMR (101 MHz, $CDCl_3$) δ 151.96 (**19**), 150.5 (**20**), 143.1 (**10**), 142.1 (**15**), 136.8 (**17**), 134.4 (**4**), 128.7 (**16**), 127.8 (**5**), 127.3 (**2**), 126.4 (**6**), 125.9 (**7**), 125.0 (**8**), 123.8 (**9**), 120.0 (**3**), 119.8 (**18**), 105.2 (**1**), 88.6 (**13**), 81.4 (**14**), 42.6 (**11**), 19.8 (**12**) ppm

IR (neat) ν_{max} 3350 (b), 3047 (m), 2864 (m), 2190 (s), 1628 (s), 1013 (s) cm^{-1}

LRMS (ESI$^+$) *m/z* 316.4 $[M+H]^+$

HRMS (ESI$^+$) *m/z calcd. for* $C_{20}H_{18}N_3O^+$ 316.1444 *m/z meas.* 316.1445 $[M+H]^+$

MPt 143-144 °C

(*E*)-6-(4-(Naphthalen-1-ylamino)butyl)picolinaldehyde oxime (3.86)

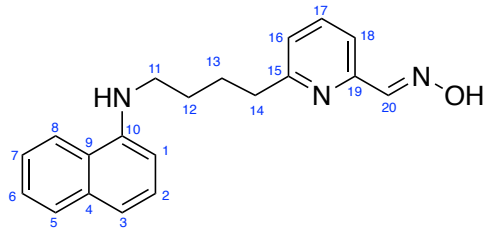

Mol. Wt. 319.2

$C_{20}H_{21}N_3O$

Following a procedure adapted from de Sousa,[186] to a degassed suspension of (*E*)-6-(4-(naphthalen-1-ylamino)but-1-yn-1-yl)picolinaldehyde oxime (173 mg, 0.55 mmol, 1 equiv.) in anhydrous MeOH (10 mL), was added Pearlman's catalyst (154 mg, 1.10 mmol, 2 equiv.). The reaction vessel was evacuated and flushed with hydrogen gas five times. The black reaction mixture was stirred for 18 h at rt. The catalyst was removed by filtration through Celite and the solvent was removed *in vacuo*. The residue was purified by column chromatography (SiO_2, 50% EtOAc in hexanes) to afford (*E*)-6-(4-(naphthalen-1-ylamino)butyl)picolinaldehyde oxime (60.0 mg, 0.19 mmol, 34%) as a white solid.

(*E*)-6-(4-(Naphthalen-1-ylamino)butyl)picolinaldehyde oxime (10 mg, 0.03 mmol) was dissolved in 2 M HCl (3 mL). The orange solution was stirred at rt for 10 mins. The reaction solution was concentrated *in vacuo* to afford (*E*)-6-(4-(naphthalen-1-ylamino)but-1-yn-1-yl)picolinaldehyde oxime hydrochloride (10.6 mg, 0.03 mmol, 100%) as a colourless solid.

TLC R_f 0.06 (20% EtOAc in hexanes, SiO_2)

^{1}HNMR (400MHz, $CDCl_3$) δ 8.21 (s, 1H, **CH**NOH), 7.77-7.67 (m, 2H, Ar**H**), 7.60-7.49 (m, 2H, Ar**H**), 7.41-7.30 (m, 2H, Ar**H**), 7.26 (t, *J*=8.2 Hz, 1H, NCCH**CH**CH), 7.15 (d, *J*=8.2 Hz, 1H, NC**CH**CHCH), 7.09 (dd, *J*=7.1, 1.7 Hz, 1H, 7-Ar**H**), 6.53 (d, *J*=7.5 Hz, 1H, 2-Ar**H**), 3.26 (t, *J*=6.9 Hz, 2H, NH**CH$_2$**CH$_2$CH$_2$CH$_2$), 2.85 (t, *J*=6.7 Hz, 2H, NHCH$_2$CH$_2$CH$_2$**CH$_2$**), 2.00-1.65 (m, 4H, NHCH$_2$**CH$_2$CH$_2$**CH$_2$) ppm

^{13}CNMR (101 MHz, $CDCl_3$) δ 162.0 (**19**), 151.1 (**20**), 150.9 (**10**), 143.4 (**15**), 137.1 (**17**), 134.3 (**4**), 128.6 (**5**), 126.6 (**2**), 125.7 (**16**), 124.7 (**6**), 123.4 (**9**), 123.3 (**7**), 119.9 (**8**), 118.8 (**3**), 117.3 (**18**), 104.4 (**1**), 44.1 (**11**), 37.7 (**14**), 28.8 (**12**), 27.6 (**13**) ppm

IR (neat) ν_{max} 3351 (b), 3047 (b), 2867 (m), 1628 (s), 1014 (s) cm^{-1}

LRMS (ESI^+) *m/z* 320.5 $[M+H]^+$

HRMS (ESI$^+$) *m/z calcd. for* $C_{20}H_{22}N_3O^+$ 320.1757 *m/z meas.* 320.1759 $[M+H]^+$

MPt 151-152 °C

1-Benzylpiperazine (3.95)

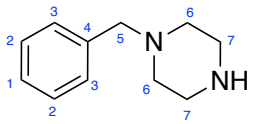

Mol. Wt. 176.1

$C_{11}H_{16}N_2$

Following a procedure from Bozell *et al.*[254] for the benzyl protection of piperazine, benzyl bromide (3.56 mL, 29.8 mmol, 1 equiv.) was added dropwise to a solution of piperazine (12.9 g, 149 mmol, 5 equiv.) in anhydrous CH_2Cl_2 (100 mL) at 0 °C and the pale yellow reaction solution was stirred for 1 h at 0°C. The reaction mixture was washed with sat. aq. $NaHCO_3$ (2 × 50 mL), dried (Na_2SO_4), filtered and concentrated *in vacuo*. Absolute EtOH (50 mL) was added and the white precipitate was removed by filtration. The filtrate was concentrated *in vacuo* to afford 1-benzylpiperazine (22.5 g, 127 mmol, 85%) as a viscous yellow oil. Data was consistent with that reported in the literature.[254]

TLC R_f 0.05 (20% MeOH in CH_2Cl_2, SiO_2)

^{1}HNMR (400MHz, $CDCl_3$) δ 7.36-7.28 (m, 5H, Ar**H**), 3.50 (s, 2H, Ph**CH_2**), 2.90 (t, *J*=4.9 Hz, 4H, (**CH_2**)$_2$NH), 2.55-2.30 (br. s, 5H, BnN(**CH_2**)$_2$, **NH**) ppm

^{13}CNMR (101 MHz, $CDCl_3$) δ 138.1 (**4**), 129.2 (**3**), 128.2 (**2**), 127.0 (**1**), 63.7 (**5**), 54.5 (**6**), 46.1 (**7**) ppm

IR (neat) ν_{max} 3277 (b), 3026 (m), 2947 (m), 2804 (m), 696 (s) cm^{-1}

LRMS (ESI$^+$) *m/z* 177.3 $[M+H]^+$

1-(4-Methoxybenzyl)piperazine (3.96)

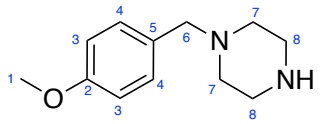

Mol. Wt. 206.1

$C_{12}H_{18}N_2O$

Following a procedure from Brown *et al.*[255] for the formation of *p*-methoxybenzyl chloride, *p*-methoxybenzyl alcohol (3.73 mL, 30.0 mmol, 1 equiv.) was dissolved in anhydrous Et_2O (50 mL) and stirred under an inert argon atmosphere at rt, to this solution was slowly added thionyl chloride (4.35 mL, 60.0 mmol, 2 equiv.) via dropping funnel over 20 min, with a 2 M NaOH gas scrubber. Upon complete addition, the pale yellow reaction was stirred at rt for 1 h. The reaction was quenched by slow addition of H_2O (10 mL) at 0 °C. The organic phase was extracted (CH_2Cl_2, 3 × 50 mL) and the combined organic phases were washed (H_2O, 50 mL), dried ($MgSO_4$), filtered and concentrated *in vacuo*. The residue was treated with THF (50 mL) and piperazine (15.5 g, 180 mmol, 6 equiv.) and the reaction mixture was heated to 90 °C for 2.5 h. The white solid was removed by filtration and the filtrate was concentrated *in vacuo*. The crude white gum was purified by column chromatography (EtOAc to 50% MeOH in EtOAc) to afford 1-(4-methoxybenzyl)piperazine (5.80 g, 28.1 mmol, 94%) as a colourless oil. Data was consistent with that reported in the literature.[255]

TLC R_f 0.20 (EtOAc, SiO_2)

^{1}HNMR (400MHz, $CDCl_3$) δ 7.24 (d, *J*=8.6 Hz, 2H, Ar**H**), 6.86 (d, *J*=8.6 Hz, 2H, Ar**H**), 3.81 (s, 3H, O**CH$_3$**), 3.44 (s, *2*H, Ph**CH$_2$**), 2.89 (t, *J*=4.9 Hz, 4H, PMBN(**CH$_2$**)$_2$), 2.40 (br. s, 4H, (**CH$_2$**)$_2$NH), 1.55 (br. s, 1H, **NH**) ppm

^{13}CNMR (101 MHz, $CDCl_3$) δ 158.8 (**2**), 130.5 (**4**), 130.2 (**5**), 113.6 (**3**), 63.2 (**8**), 55.3 (**1**), 54.6 (**6**), 46.2 (**7**) ppm

IR (neat) ν_{max} 2936 (m), 2806 (m), 1736 (s), 1238 (s) cm^{-1}

LRMS (ESI$^+$) *m/z* 207.2 $[M+H]^+$

But-3-yn-1-yl 4-methylbenzenesulfonate (3.99)

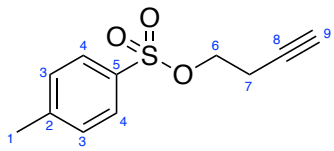

Mol. Wt. 224.0

$C_{11}H_{12}SO_3$

Following a procedure by Larouche-Gauthier *et al.*[256] for the tosyl protection of aliphatic alcohols, to a colourless solution of 3-butyn-1-ol (3.24 mL, 42.8 mmol, 1 equiv.), DMAP (522 mg, 4.28 mmol, 10 mol%) and Et_3N (7.73 mL, 55.6 mmol, 1.3 equiv.) in CH_2Cl_2 (15 mL) at 0 °C was added a solution of TsCl (8.98 g, 47.1 mmol, 1.1 equiv.) in CH_2Cl_2 (15 mL). The yellow solution was allowed to warm and was stirred at rt for 2 h. H_2O (30 mL) was added and the reaction was stirred for a further 20 min. The organic layer was separated and the aqueous layer was extracted (CH_2Cl_2, 5 × 40 mL). The organic layers were combined, dried (Na_2SO_3), filtered and concentrated *in vacuo* to afford but-3-yn-1-yl 4-methylbenzenesulfonate (9.60 g, 42.8 mmol, 100%) as a red/brown oil. Data was consistent with that reported in the literature.[256]

TLC R_f	0.58 (50% EtOAc in hexanes, SiO_2)
^{1}HNMR	(400MHz, $CDCl_3$) δ 7.81 (d, *J*=8.3 Hz, 2H, **ArH**), 7.36 (d, *J*=8.3 Hz, 2H, **ArH**), 4.11 (t, *J*=7.1 Hz, 2H, TsO**CH_2**CH_2CCH), 2.56 (td, *J*=7.1, 2.7 Hz, 2H, TsOCH_2**CH_2**CCH), 2.46 (s, 3H, Ar(**CH_3**)), 1.98 (t, *J*=2.7 Hz, 1H, TsOCH_2CH_2C**C**H) ppm
^{13}CNMR	(101 MHz, $CDCl_3$) δ 145.0 (**2**), 132.8 (**5**), 129.9 (**3**), 128.0 (**4**), 78.3 (**8**), 70.7 (**9**), 67.4 (**6**), 21.6 (**7**), 19.4 (**1**) ppm
IR (neat)	ν_{max} 3289 (m), 2960 (s), 2120 (s), 1355 (s), 1120 (s) cm^{-1}
LCMS	(ESI) *m/z* 225.2 $[M+H]^+$

1-Benzyl-4-(but-3-yn-1-yl)piperazine (3.100)

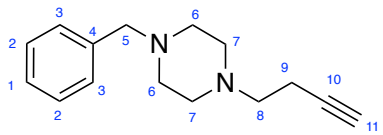

Mol. Wt. 228.2

$C_{15}H_{20}N_2$

Following a procedure from Guarna *et al.*[257] for the substitution of piperazine, to a solution of but-3-yn-1-yl *p*-toluenesulfonate (2.31 g, 10.3 mmol, 1 equiv.) in DMF (60 mL) was added Na_2CO_3 (1.20 g, 11.3 mmol, 1.1 mmol) and 1-benzylpiperazine (2.00 g, 11.3 mmol, 1.1 equiv.). The yellow reaction mixture was stirred at 80 °C for 18 h. H_2O (10 mL) and Et_2O (10 mL) were added and the organic layer was separated and washed (brine, 20 mL). The organic layer was dried ($MgSO_4$), filtered and concentrated *in vacuo*. The crude brown residue was purified by column chromatography (SiO_2, CH_2Cl_2 to 10% MeOH in CH_2Cl_2) to afford 1-benzyl-4-(but-3-yn-1-yl)piperazine (1.69 g, 7.40 mmol, 72%) as an orange oil.

TLC R_f 0.67 (10% MeOH in CH_2Cl_2, SiO_2)

^{1}HNMR (400MHz, $CDCl_3$) δ 7.35-7.28 (m, 5H, Ar**H**), 3.52 (s, 2H, Ph**CH_2**), 2.61 (t, *J*=7.6 Hz, 2H, N**CH_2**CH_2CCH), 2.58-2.42 (m, 8H, Piz(**CH_2**)$_4$), 2.41-2.34 (dt, *J*=7.6, 2.7 Hz, 2H, NCH_2**CH_2**CCH), 1.97 (t, *J*=2.7 Hz, 1H, NCH_2CH_2C**CH**) ppm

^{13}CNMR (101 MHz, $CDCl_3$) δ 138.1 (**4**), 129.2 (**3**), 128.2 (**2**), 127.0 (**1**), 82.8 (**10**), 69.0 (**11**), 63.0 (**5**), 57.0 (**8**), 52.9 (**7**), 52.8 (**6**), 16.8 (**9**) ppm

IR (neat) ν_{max} 3291 (b), 3026 (m), 2939 (m), 2807 (s), 2119 (s), 697 (s) cm^{-1}

LRMS (ESI^+) *m/z* 229.3 $[M+H]^+$

HRMS (ESI^+) *m/z calcd. for* $C_{15}H_{21}N_2^+$ 229.1699 *m/z meas.* 229.1695 $[M+H]^+$

1-(But-3-yn-1-yl)-4-(4-methoxybenzyl)piperazine (3.101)

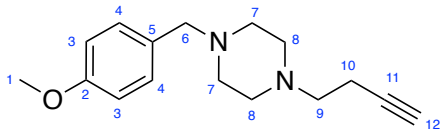

Mol. Wt. 258.2

$C_{16}H_{22}N_2O$

Following a procedure from Guarna *et al.*[257] for the substitution of piperazine, to a solution of but-3-yn-1-yl *p*-toluenesulfonate (1.98 g, 8.81 mmol, 1 equiv.) in DMF (50 mL) was added Na_2CO_3 (1.03 g, 9.70 mmol, 1.1 mmol) and 1-(4-methoxybenzyl)piperazine (2.00 g, 9.70 mmol, 1.1 equiv.). The colourless reaction solution was stirred at 80 °C for 18 h. H_2O (10 mL) and Et_2O (10 mL) were added and the organic layer was separated and washed (brine, 20 mL). The organic layer was dried ($MgSO_4$), filtered and concentrated *in vacuo*. The crude orange residue was purified by column chromatography (SiO_2, 50% EtOAc in hexanes) to afford 1-(but-3-yn-1-yl)-4-(4-methoxybenzyl)piperazine (900 mg, 3.48 mmol, 40%) as a yellow oil.

TLC R_f 0.19 (50% EtOAc in hexanes, SiO_2)

^{1}HNMR (400MHz, $CDCl_3$) δ 7.23 (d, *J*=8.7 Hz, 2H, Ar**H**), 6.86 (d, *J*=8.7 Hz, 2H, Ar**H**), 3.80 (s, 3H, O**CH$_3$**), 3.45 (s, *2*H, Ph**CH$_2$**), 2.61 (t, *J*=7.7 Hz, 2H, N**CH$_2$**CH$_2$CCH), 2.42-2.34 (m, 8H, Piz(**CH$_2$**)$_4$), 2.38 (td, *J*=7.7, 2.7 Hz, 2H, NCH$_2$**CH$_2$**CCH), 1.98 (t, *J*=2.7 Hz, 1H, NCH$_2$CH$_2$C**C**H) ppm

^{13}CNMR (101 MHz, $CDCl_3$) δ 158.8 (**2**), 130.4 (**3**), 130.2 (**5**), 113.6 (**4**), 82.8 (**11**), 69.1 (**12**), 62.5 (**9**), 57.1 (**7**), 55.3 (**8**), 52.9 (**1**), 52.8 (**6**), 16.8 (**10**) ppm

IR (neat) ν_{max} 3291 (m), 2938 (m), 2808 (m), 2100 (s) 1510 (s), 1006 (s) cm^{-1}

LRMS (ESI$^+$) *m/z* 259.3 $[M+H]^+$

HRMS (ESI$^+$) *m/z calcd. for* $C_{16}H_{23}N_2O^+$ 259.1805 *m/z meas.* 259.1799 $[M+H]^+$

***Tert*-butyl 4-(but-3-yn-1-yl)piperazine-1-carboxylate (3.102)**

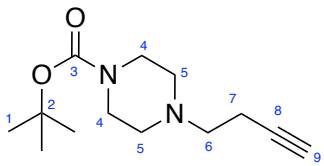

Mol. Wt. 238.2

$C_{13}H_{22}N_2O_2$

Following a procedure adapted from Guarna *et al.*[257] for the substitution of piperazine, to a solution of 1-Boc-piperazine (2.00 g, 10.7 mmol, 1 equiv.) in EtOH (25 mL) was added DIPEA (5.32 mL, 32.2 mmol, 3 equiv.) and but-3-yn-1-yl *p*-toluenesulfonate (2.65 g, 11.8 mmol, 1.1 equiv.). The colourless reaction solution was stirred at 60 °C for 18 h. The volatiles were removed *in vacuo* and CH_2Cl_2 (15 mL) was added. The organic phase was washed (sat. aq. Na_2CO_3, 20 mL), dried ($MgSO_4$), filtered and concentrated *in vacuo*. The crude brown residue was purified by column chromatography (SiO_2, 10% MeOH in CH_2Cl_2) to afford benzyl 4-(but-3-yn-1-yl)piperazine-1-carboxylate (2.03 g, 8.51 mmol, 79%) as a yellow oil.

TLC R_f 0.67 (10% MeOH in CH_2Cl_2, SiO_2)

^{1}HNMR (400MHz, $CDCl_3$) δ 3.44 (t, *J*=5.1 Hz, 4H, BocN(**CH_2**)$_2$), 2.60 (t, *J*=7.4 Hz, 2H, N**CH_2**CH_2CCH), 2.48-2.32 (m, 6H, (**CH_2**)$_2$NCH_2**CH_2**CCH), 1.99 (t, *J*=2.7 Hz, 1H, NCH_2CH_2**C**C**H**), 1.46 (s, 9H, C(**CH_3**)$_3$) ppm

^{13}CNMR (101 MHz, $CDCl_3$) δ 154.7 (**3**), 82.5 (**8**), 79.7 (**2**), 77.2 (**9**), 69.1 (**6**), 57.0 (**5**), 52.7 (**4**), 28.4 (**1**), 16.8 (**7**) ppm

IR (neat) ν_{max} 3299 (b), 2975 (m), 2813 (s), 2119 (s), 1688 (s), 1166 (s) cm^{-1}

LRMS (ESI$^+$) *m/z* 239.3 $[M+H]^+$

HRMS (ESI$^+$) *m/z calcd. for* $C_{13}H_{23}N_2O_2^+$ 239.1754 *m/z meas.* 239.1755 $[M+H]^+$

Benzyl 4-(but-3-yn-1-yl)piperazine-1-carboxylate (3.103)

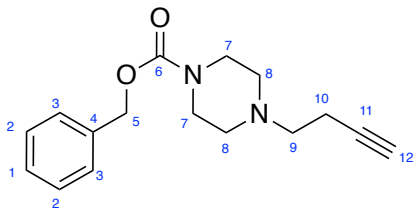

Mol. Wt. 272.2

$C_{16}H_{20}N_2O_2$

Following a procedure from Guarna *et al.*[257] for the substitution of piperazine, to a solution of but-3-yn-1-yl *p*-toluenesulfonate (1.50 g, 6.69 mmol, 1 equiv.) in DMF (40 mL) was added Na_2CO_3 (780 mg, 7.36 mmol, 1.1 mmol) and 1-Cbz-piperazine (1.62 g, 7.36 mmol, 1.1 equiv.). The colourless reaction solution was stirred at 80 °C for 18 h. H_2O (10 mL) and Et_2O (10 mL) were added and the organic layer was separated and washed (brine, 20 mL). The organic layer was dried ($MgSO_4$), filtered and concentrated *in vacuo*. The crude yellow residue was purified by column chromatography (SiO_2, 50% EtOAc in hexanes) to afford benzyl 4-(but-3-yn-1-yl)piperazine-1-carboxylate (1.41 g, 5.19 mmol, 78%) as a colourless oil.

TLC R_f 0.42 (50% EtOAc in hexanes, SiO_2)

^{1}HNMR (400MHz, $CDCl_3$) δ 7.40-7.29 (m, 5H, Ar**H**), 5.14 (s, 2H, Ph**CH_2**), 3.53 (br. t, *J*=4.9 Hz, 4H, CbzN(**CH_2**)$_2$), 2.61 (t, *J*=7.4 Hz, 2H, N**CH_2**CH_2CCH), 2.50-2.42 (m, 4H, (**CH_2**)$_2$NCH_2CCH), 2.39 (td, *J*=7.4 Hz, 2.7 Hz, 2H, NCH_2**CH_2**CCH), 1.99 (t, *J*=2.7 Hz, 1H, NCH_2CH_2C**C**H) ppm

^{13}CNMR (101 MHz, $CDCl_3$) δ 155.2 (**6**), 136.7 (**4**), 128.5 (**3**), 128.0 (**1**), 127.9 (**2**), 82.5 (**11**), 69.2 (**12**), 67.1 (**5**), 56.9 (**9**), 52.6 (**8**), 43.7 (**7**), 16.8 (**10**) ppm

IR (neat) ν_{max} 3245 (b), 2929 (m), 1667 (s), 1236 (s) cm^{-1}

LRMS (ESI$^+$) *m/z* 273.3 $[M+H]^+$

HRMS (ESI$^+$) *m/z calcd. for* $C_{16}H_{21}N_2O_2^+$ 273.1598 *m/z meas.* 273.1599 $[M+H]^+$

1-Benzyl-4-(prop-2-yn-1-yl)piperazine (3.105)

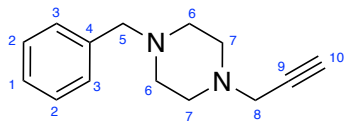

Mol. Wt. 214.2

$C_{14}N_{18}N_2$

Following a procedure from Dambacher *et al.*[258] for the substitution of piperazine, a pale yellow solution of 1-benzylpiperazine (1.75 g, 9.93 mmol, 1 equiv.), propargyl bromide (1.28 mL, 14.9 mmol, 1.5 equiv.) and DIPEA (3.28 mL, 19.9 mmol, 2 equiv.) in CH_2Cl_2 (50 mL) was stirred at rt for 18 h. H_2O (50 mL) was added and the aqueous phase was separated and extracted (CH_2Cl_2, 3 × 20 mL). The combined organics were washed (brine, 20 mL), dried ($MgSO_4$), filtered and concentrated *in vacuo*. The residue was purified by column chromatography (SiO_2, 50% EtOAc in hexanes to EtOAc) to afford 1-benzyl-4-(prop-2-yn-1-yl)piperazine (2.04 g, 9.53 mmol, 96%) as an orange oil.

TLC R_f 0.71 (10% MeOH in CH_2Cl_2, SiO_2)

^{1}HNMR (400MHz, $CDCl_3$) δ 7.37-7.28 (m, 5H, Ar**H**), 3.56 (s, 2H, Ph**CH_2**), 3.30 (d, *J*=2.5 Hz, 2H, N**CH_2**CCH), 2.73-2.44 (m, 8H, Piz(**CH_2**)$_4$), 2.25 (t, *J*=2.5 Hz, 1H, NCH$_2$C**C**H) ppm

^{13}CNMR (101 MHz, $CDCl_3$) δ 129.5 (**4**), 129.3 (**3**), 128.3 (**2**), 127.2 (**1**), 78.9 (**9**), 73.2 (**10**), 62.8 (**5**), 52.8 (**7**), 51.8 (**6**), 46.8 (**8**) ppm

IR (neat) ν_{max} 3290 (b), 3026 (m), 2933 (m), 2807 (m), 2117 (s), 697 (s) cm^{-1}

LRMS (ESI$^+$) *m/z* 215.2 $[M+H]^+$

HRMS (ESI$^+$) *m/z calcd. for* $C_{14}H_{19}N_2^+$ 215.1543 *m/z meas.* 215.1542 $[M+H]^+$

1-(4-Methoxybenzyl)-4-(prop-2-yn-1-yl)piperazine (3.106)

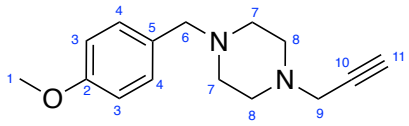

Mol. Wt. 244.2

$C_{15}H_{20}N_2O$

Following a procedure from Dambacher *et al.*[258] for the substitution of piperazine, a pale yellow solution of 1-(4-methoxybenzyl)piperazine (2.00 g, 9.70 mmol, 1 equiv.), propargyl bromide (1.25 mL, 14.5 mmol, 1.5 equiv.) and DIPEA (3.20 mL, 19.4 mmol, 2 equiv.) in CH_2Cl_2 (50 mL) was stirred at rt for 18 h. H_2O (50 mL) was added and the aqueous phase was separated and extracted (CH_2Cl_2, 3 × 20 mL). The combined organics were washed (brine, 20 mL), dried ($MgSO_4$), filtered and concentrated *in vacuo*. The yellow residue was purified by FCC (SiO_2, 50% EtOAc in hexanes to EtOAc) to afford 1-(4-methoxybenzyl)-4-(prop-2-yn-1-yl)piperazine (1.30 g, 5.32 mmol, 55%) as a pale yellow oil.

TLC R_f 0.15 (50% EtOAc in hexanes, SiO_2)

^{1}HNMR (400MHz, $CDCl_3$) δ 7.25 (d, *J*=8.7 Hz, 2H, Ar**H**), 6.87 (d, *J*=8.7 Hz, 2H, Ar**H**), 3.82 (s, 3H, O**CH$_3$**), 3.48 (s, *2*H, Ph**CH$_2$**), 3.32 (d, *J*=2.5 Hz, 2H, N**CH$_2$**CCH), 2.62 (br. s, 4H, PMBN(**CH$_2$**)$_2$), 2.52 (br. s, 4H, (**CH$_2$**)$_2$NCH$_2$CCH), 2.26 (t, *J*=2.5 Hz, 1H, NCH$_2$C**CH**) ppm

^{13}CNMR (101 MHz, $CDCl_3$) δ 158.7 (**2**), 130.3 (**3**), 130.1 (**5**), 113.6 (**4**), 79.0 (**10**), 73.1 (**11**), 62.3 (**7**), 55.3 (**1**), 52.8 (**9**), 52.0 (**6**), 46.8 (**8**) ppm

IR (neat) ν_{max} 3289 (m), 2933 (m), 2808 (m), 2360 (s) 1510 (s), 1010 (s) cm^{-1}

LRMS (ESI$^+$) *m/z* 245.2 $[M+H]^+$

HRMS (ESI$^+$) *m/z calcd. for* $C_{15}H_{21}N_2O^+$ 245.1648 *m/z meas.* 245.1643 $[M+H]^+$

***Tert*-butyl 4-(prop-2-yn-1-yl)piperazine-1-carboxylate (3.107)**

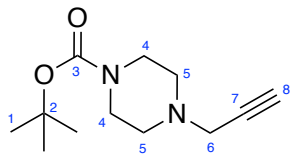

Mol. Wt. 224.2

$C_{12}H_{20}N_2O_2$

Following a procedure from Dambacher *et al.*[258] for the substitution of piperazine, a pale yellow solution of 1-Boc-piperazine (2.00 g, 10.7 mmol, 1 equiv.), propargyl bromide (1.39 mL, 16.1 mmol, 1.5 equiv.) and DIPEA (3.55 mL, 21.5 mmol, 2 equiv.) in CH_2Cl_2 (50 mL) was stirred at rt for 18 h. H_2O (50 mL) was added and the aqueous phase was separated and extracted (CH_2Cl_2, 3 × 20 mL). The combined organics were washed (brine, 20 mL), dried ($MgSO_4$), filtered and concentrated *in vacuo*. The residue was purified by column chromatography (SiO_2, 50% EtOAc in hexanes to EtOAc) to afford *tert*-butyl 4-(prop-2-yn-1-yl)piperazine-1-carboxylate (2.30 g, 10.3 mmol, 95%) as a pale brown oil.

TLC R_f 0.30 (EtOAc, SiO_2)

^{1}HNMR (400MHz, $CDCl_3$) δ 3.48 (t, *J*=5.4 Hz, 4H, BocN(**CH_2**)$_2$), 3.33 (d, *J*=2.5 Hz, 2H, N**CH_2**CCH), 2.53 (t, *J*=5.4 Hz, 4H, (**CH_2**)$_2$NCH_2CCH), 2.27 (t, *J*=2.5 Hz, 1H, NCH_2C**C**H), 1.48 (s, 9H, C(**CH_3**)$_3$) ppm

^{13}CNMR (101 MHz, $CDCl_3$) δ 154.7 (**3**), 79.7 (**2**), 78.4 (**7**), 73.4 (**8**), 60.4 (**6**), 51.6 (**5**), 47.0 (**4**), 28.4 (**1**) ppm

IR (neat) ν_{max} 3291 (b), 2975 (m), 2815 (s), 1687 (s), 1119 (s) cm^{-1}

LRMS (ESI$^+$) *m/z* 225.3 $[M+H]^+$

HRMS (ESI$^+$) *m/z calcd. for* $C_{12}H_{21}N_2O_2^+$ 225.1598 *m/z meas.* 225.1597 $[M+H]^+$

Benzyl 4-(prop-2-yn-1-yl)piperazine-1-carboxylate (3.108)

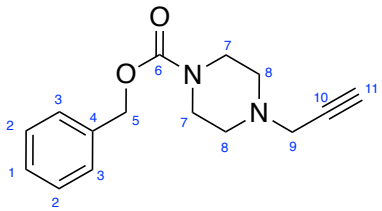

Mol. Wt. 258.9

$C_{15}H_{18}N_2O_2$

Following a procedure from Dambacher *et al.*[258] for the substitution of piperazine, a pale yellow solution of 1-Cbz-piperazine (3.00 g, 13.6 mmol, 1 equiv.), propargyl bromide (1.76 mL, 20.4 mmol, 1.5 equiv.) and DIPEA (4.50 mL, 27.2 mmol, 2 equiv.) in CH_2Cl_2 (60 mL) was stirred at rt for 18 h. H_2O (50 mL) was added and the aqueous phase was separated and extracted (CH_2Cl_2, 3 × 20 mL). The combined organics were washed (brine, 20 mL), dried ($MgSO_4$), filtered and concentrated *in vacuo*. The residue was purified by column chromatography (SiO_2, 50% EtOAc in hexanes) to afford benzyl 4-(prop-2-yn-1-yl)piperazine-1-carboxylate (3.24 g, 12.6 mmol, 92%) as a colourless oil.

TLC R_f 0.30 (50% EtOAc in hexanes, SiO_2)

^{1}HNMR (400MHz, $CDCl_3$) δ 7.41-7.29 (m, 5H, Ar**H**), 5.15 (s, 2H, Ph**CH_2**), 3.57 (br. t, *J*=5.1 Hz, 4H, CbzN(**CH_2**)$_2$), 3.33 (d, *J*=2.4 Hz, 2H, N**CH_2**CCH), 2.58-2.50 (m, 4H, (**CH_2**)$_2$NCH_2CCH), 2.27 (t, *J*=2.4 Hz, 1H, NCH_2C**C**H) ppm

^{13}CNMR (101 MHz, $CDCl_3$) δ 155.2 (**6**), 136.7 (**4**), 128.5 (**3**), 128.0 (**1**), 127.9 (**2**), 78.3 (**10**), 73.5 (**11**), 67.2 (**5**), 51.5 (**8**), 47.0 (**7**), 43.7 (**9**) ppm

IR (neat) ν_{max} 3288 (b), 2937 (m), 2815 (s), 1693 (s), 1232 (s) cm^{-1}

LRMS (ESI$^+$) *m/z* 259.2 $[M+H]^+$

HRMS (ESI$^+$) *m/z calcd. for* $C_{15}H_{19}N_2O_2^+$ 259.1141 *m/z meas.* 259.1140 $[M+H]^+$

(*E*)-6-(3-(4-Benzylpiperazin-1-yl)prop-1-yn-1-yl)picolinaldehyde oxime (3.92)

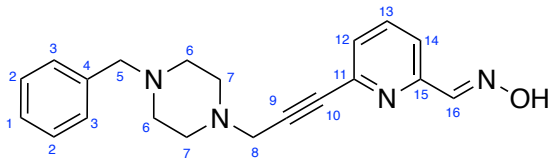

Mol. Wt. 334.2

$C_{20}H_{22}N_4O$

Following a procedure adapted from de Sousa,[186] to a degassed solution of 1-benzyl-4-(prop-2-yn-1-yl)piperazine (1.30 g, 6.07 mmol, 1 equiv.) in THF/Et_3N (7 mL/3 mL) was added $Pd(PPh_3)_4$ (700 mg, 0.61 mmol, 10 mol%) and CuI (231 mg, 1.21 mmol, 20 mol%). To the resulting orange reaction mixture was added dropwise a degassed solution of (E)-6-bromopicolinaldehyde oxime (1.34 g, 6.67 mmol, 1.1 equiv.) in THF (10 mL). The brown solution was stirred for 18 h at rt. The reaction was concentrated *in vacuo*. The residue was purified by column chromatography (SiO_2, EtOAc) to afford (*E*)-6-(3-(4-benzylpiperazin-1-yl)prop-1-yn-1-yl)picolinaldehyde oxime (750 mg, 2.24 mmol, 37%) as a cream solid.

(*E*)-6-(3-(4-Benzylpiperazin-1-yl)prop-1-yn-1-yl)picolinaldehyde oxime (10 mg, 0.03 mmol) was dissolved in 2 M HCl (3 mL). The beige solution was stirred at rt for 10 mins. The reaction solution was concentrated *in vacuo* to afford (*E*)-6-(3-(4-benzylpiperazin-1-yl)prop-1-yn-1-yl)picolinaldehyde oxime hydrochloride (11.1 mg, 0.03 mmol, 100%) as a colourless solid.

TLC R_f 0.47 (10% MeOH in CH_2Cl_2, SiO_2)

^{1}HNMR (400MHz, $CDCl_3$) δ 12.20 (s, 1H, **OH**), 7.99 (s, 1H, **CH**NOH), 7.71 (d, *J*=8.0 Hz, 1H, NCCHCH**CH**), 7.53 (t, *J*=8.0 Hz, 1H, NCCH**CH**CH), 7.43-7.20 (m, 6H, NC**CH**CHCH, Ar**H**), 3.70 (s, 2H, Ph**CH$_2$**), 3.63 (s, 2H, N**CH$_2$**CC), 3.08-2.36 (m, 8H, PMBN(**CH$_2$**)$_2$, N(**CH$_2$**)$_2$) ppm

^{13}CNMR (101 MHz, $CDCl_3$) δ 152.7 (**15**), 149.0 (**16**), 142.2 (**11**), 136.3 (**4**), 136.2 (**13**), 129.9 (**12**), 128.4 (**3**), 127.6 (**2**), 127.1 (**1**), 119.1 (**14**), 85.3 (**10**), 84.3 (**9**), 63.2 (**5**), 52.9 (**7**), 50.5 (**6**), 47.1 (**8**) ppm

IR (neat) ν_{max} 3150 (m), 3048 (m), 2944 (m), 2808 (s), 2364 (s), 1578 (s), 1136 (s) cm^{-1}

LRMS (ESI^+) *m/z* 335.5 $[M+H]^+$

HRMS (ESI^+) *m/z calcd. for* $C_{20}H_{23}N_4O^+$ 335.1866 *m/z meas.* 335.1863 $[M+H]^+$

MPt 143-145 °C

(*E*)-6-(4-(4-Benzylpiperazin-1-yl)but-1-yn-1-yl)picolinaldehyde oxime (3.93)

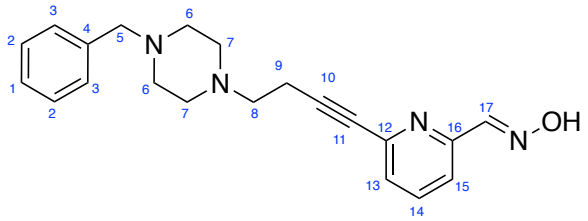

Mol. Wt. 348.2

$C_{21}H_{24}N_4O$

Following a procedure adapted from de Sousa,[186] to a degassed solution of 1-benzyl-4-(but-3-yn-1-yl)piperazine (1.55 g, 6.79 mmol, 1 equiv.) in THF/Et_3N (7 mL/3 mL) was added $Pd(PPh_3)_4$ (784 mg, 0.68 mmol, 10 mol%) and CuI (258 mg, 1.36 mmol, 20 mol%). To the resulting orange reaction mixture was added dropwise a degassed solution of (E)-6-bromopicolinaldehyde oxime (1.50 g, 7.47 mmol, 1.1 equiv.) in THF (10 mL). The brown solution was stirred for 18 h at rt. The reaction was concentrated *in vacuo*. The residue was purified by column chromatography (SiO_2, 50% EtOAc in hexanes to EtOAc) to afford (*E*)-6-(4-(4-benzylpiperazin-1-yl)but-1-yn-1-yl)picolinaldehyde oxime (150 mg, 0.43 mmol, 6%) as a cream solid.

(*E*)-6-(4-(4-Benzylpiperazin-1-yl)but-1-yn-1-yl)picolinaldehyde oxime (10 mg, 0.03 mmol) was dissolved in 2 M HCl (3 mL). The colourless solution was stirred at rt for 10 mins. The reaction solution was concentrated *in vacuo* to afford (*E*)-6-(4-(4-benzylpiperazin-1-yl)but-1-yn-1-yl)picolinaldehyde oxime hydrochloride (11.5 mg, 0.03 mmol, 100%) as a colourless solid.

TLC R_f 0.47 (10% MeOH in CH_2Cl_2, SiO_2)

^{1}HNMR (400MHz, $CDCl_3$) δ 11.48 (s, 1H, **OH**), 8.20 (s, 1H, **CH**NOH), 7.76 (d, *J*=8.0 Hz, 1H, NCCHCH**CH**), 7.59 (t, *J*=8.0 Hz, 1H, NCCH**CH**CH), 7.35-7.27 (m, 6H, NC**CH**CHCH, Ar**H**), 3.56 (s, 2H, Ph**CH_2**), 2.82-2.41 (m, 12H, PMBN(**CH_2**)$_2$, N(**CH_2**)$_2$, N**CH_2CH_2**) ppm

^{13}CNMR (101 MHz, $CDCl_3$) δ 152.9 (**16**), 149.7 (**17**), 143.1 (**12**), 137.4 (**4**), 136.5 (**14**), 129.5 (**3**), 128.3 (**2**), 127.3 (**13**), 126.7 (**1**), 119.1 (**15**), 89.1 (**10**), 80.8 (**11**), 63.0 (**5**), 56.6 (**8**), 52.6 (**7**), 52.5 (**6**), 17.4 (**9**) ppm

IR (neat) ν_{max} 3161 (m), 3060 (m), 2954 (m), 2808 (s), 2231 (s), 1576 (s), 1202 (s) cm^{-1}

LRMS (ESI$^+$) *m/z* 349.5 $[M+H]^+$

HRMS (ESI$^+$) *m/z calcd. for* $C_{21}H_{25}N_4O^+$ 349.2023 *m/z meas.* 349.2018 $[M+H]^+$

MPt 134-136 °C

(*E*)-6-(3-(4-Benzylpiperazin-1-yl)propyl)picolinaldehyde oxime (3.90)

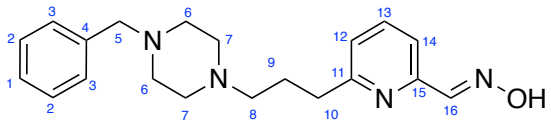

Mol. Wt. 338.2

$C_{20}H_{26}N_4O$

Following a procedure adapted from de Sousa,[186] to a degassed suspension of (*E*)-6-(3-(4-benzylpiperazin-1-yl)prop-1-yn-1-yl)picolinaldehyde oxime (200 mg, 0.60 mmol, 1 equiv.) in anhydrous MeOH (20 mL), was added Pearlman's catalyst (44 mg, 0.30 mmol, 1 equiv.). The reaction vessel was evacuated and flushed with hydrogen gas five times. The black reaction mixture was stirred for 2 h at rt. The catalyst was removed by filtration through Celite and the solvent was removed *in vacuo*. The residue was purified by column chromatography (SiO_2, CH_2Cl_2 to 10% MeOH in CH_2Cl_2) to afford (*E*)-6-(3-(4-benzylpiperazin-1-yl)propyl)picolinaldehyde oxime (107 mg, 0.32 mmol, 53%) as a pale yellow oil.

(*E*)-6-(3-(4-Benzylpiperazin-1-yl)propyl)picolinaldehyde oxime (10 mg, 0.03 mmol) was dissolved in 2 M HCl (3 mL). The pale yellow solution was stirred at rt for 10 mins. The reaction solution was concentrated *in vacuo* to afford (*E*)-6-(3-(4-benzylpiperazin-1-yl)propyl)picolinaldehyde oxime hydrochloride (11.2 mg, 0.03 mmol, 100%) as a colourless solid.

TLC R_f 0.43 (10% MeOH in CH_2Cl_2, SiO_2)

^{1}HNMR (400MHz, $CDCl_3$) δ 8.19 (s, 1H, **CH**NOH), 7.58-7.51 (m, 2H, NCCHCH**CH**, NCCH**CH**CH), 7.36-7.27 (m, 5H, Ar**H**), 7.10 (d, *J*=6.5 Hz, 1H, NC**CH**CHCH), 3.55 (s, 2H, Ph**CH$_2$**), 2.82 (t, *J*=7.8 Hz, 2H, N**CH$_2$**CH_2CH_2), 2.72-2.35 (m, 10H, PMBN(**CH$_2$**)$_2$, N(**CH$_2$**)$_2$, NCH_2CH_2**CH$_2$**), 2.02 (quin, *J*=7.8 Hz, 2H, NCH_2**CH$_2$**CH_2) ppm

^{13}CNMR (101 MHz, $CDCl_3$) δ 161.2 (**15**), 151.8 (**11**), 150.3 (**16**), 137.6 (**4**), 136.6 (**13**), 129.4 (**3**), 128.3 (**2**), 127.2 (**1**), 122.8 (**12**), 118.0 (**14**), 62.9 (**8**), 57.7 (**5**), 52.8 (**7**), 52.5 (**6**), 35.8 (**10**), 26.3 (**9**) ppm

IR (neat) ν_{max} 3162 (m), 3057 (m), 2939 (m), 2816 (s), 1584 (s), 1153 (s) cm^{-1}

LRMS (ESI$^+$) *m/z* 339.5 $[M+H]^+$

HRMS (ESI$^+$) *m/z calcd. for* $C_{20}H_{27}N_4O^+$ 339.2179 *m/z meas.* 339.2176 $[M+H]^+$

(*E*)-6-(4-(4-Benzylpiperazin-1-yl)butyl)picolinaldehyde oxime (3.91)

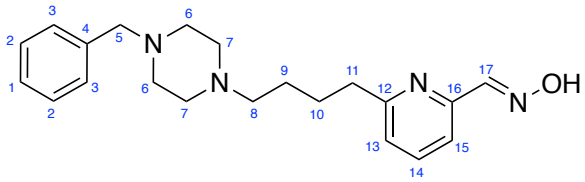

Mol. Wt. 352.2

$C_{21}H_{28}N_4O$

Following a procedure adapted from de Sousa,[186] to a degassed suspension of (*E*)-6-(3-(4-benzylpiperazin-1-yl)prop-1-yn-1-yl)picolinaldehyde oxime (60 mg, 0.17 mmol, 1 equiv.) in anhydrous MeOH (5 mL), was added Pd/C (10%, 4 mg, 0.04 mmol, 2 mol%). The reaction vessel was evacuated and flushed with hydrogen gas five times. The black reaction mixture was stirred for 1.5 h at rt. The catalyst was removed by filtration through Celite and the solvent was removed *in vacuo* to afford (*E*)-6-(4-(4-benzylpiperazin-1-yl)butyl)picolinaldehyde oxime (53 mg, 0.15 mmol, 87%) as a yellow oil.

(*E*)-6-(4-(4-Benzylpiperazin-1-yl)butyl)picolinaldehyde oxime (10 mg, 0.03 mmol) was dissolved in 2 M HCl (3 mL). The yellow solution was stirred at rt for 10 mins. The reaction solution was concentrated *in vacuo* to afford (*E*)-6-(4-(4-benzylpiperazin-1-yl)butyl)picolinaldehyde oxime hydrochloride (11.6 mg, 0.03 mmol, 100%) as a beige solid.

TLC R_f 0.17 (10% MeOH in EtOAc, SiO_2)

^{1}HNMR (400MHz, $CDCl_3$) δ 8.18 (s, 1H, **CH**NOH), 7.62-7.50 (m, 2H, NCCHCH**CH**, NCCH**CH**CH), 7.34-7.29 (m, 5H, Ar**H**), 7.11 (d, *J*=7.3 Hz, 1H, NC**CH**CHCH), 5.31 (s, 2H, Ph**CH$_2$**), 2.82 (t, *J*=7.3 Hz, 2H, N**CH$_2$**$CH_2CH_2CH_2$), 2.59-2.31 (m, 10H, PMBN(**CH$_2$**)$_2$, N(**CH$_2$**)$_2$, $NCH_2CH_2CH_2$**CH$_2$**), 1.76 (quin, *J*=7.3 Hz, 2H, NCH_2**CH$_2$**CH_2CH_2), 1.58 (br. s, 2H, NCH_2CH_2**CH$_2$**CH_2) ppm

^{13}CNMR (101 MHz, $CDCl_3$) δ 161.9 (**16**), 151.5 (**12**), 150.6 (**17**), 136.7 (**4**), 136.6 (**14**), 129.3 (**3**), 128.2 (**2**), 127.1 (**1**), 122.9 (**13**), 118.1 (**15**), 63.0 (**8**), 58.4 (**5**), 53.0 (**7**), 52.7 (**6**), 37.9 (**11**), 27.6 (**10**), 26.1 (**9**) ppm

IR (neat) ν_{max} 3181 (m), 3060 (m), 2938 (m), 2818 (m), 1586 (s), 1154 (s) cm^{-1}

LRMS (ESI$^+$) *m/z* 353.6 $[M+H]^+$

HRMS (ESI$^+$) *m/z calcd. for* $C_{21}H_{29}N_4O^+$ 353.2336 *m/z meas.* 353.2332 $[M+H]^+$

***Tert*-butyl 4-(4-(5-(benzyloxy)-6-(methoxycarbonyl)pyridin-2-yl)but-3-yn-1-yl)piperazine-1-carboxylate (3.112)**

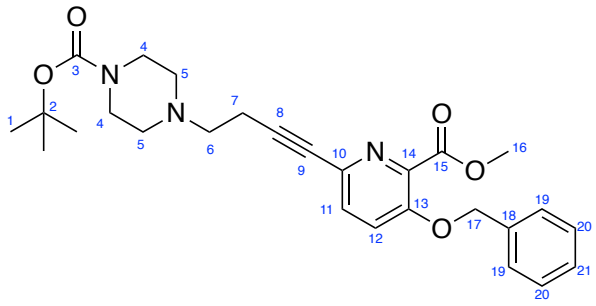

Mol. Wt. 479.2

$C_{27}H_{33}N_3O_5$

Following a procedure adapted from de Sousa,[186] to a degassed solution of benzyl 4-(but-3-yn-1-yl)piperazine-1-carboxylate (1.00 g, 4.20 mmol, 1 equiv.) in THF/Et_3N (7 mL/3 mL) was added $Pd(PPh_3)_4$ (485 mg, 0.42 mmol, 10 mol%) and CuI (160 mg, 0.84 mmol, 20 mol%). To the resulting orange reaction mixture was added dropwise a degassed solution of methyl 3-(benzyloxy)-6-bromopyridine-2-carboxylate (1.49 g, 4.62 mmol, 1.1 equiv.) in THF (10 mL). The brown solution was stirred for 18 h at rt. The reaction was concentrated *in vacuo*. The residue was purified by column chromatography (SiO_2, 50% EtOAc in hexanes to EtOAc) to afford *tert*-butyl 4-(4-(5-(benzyloxy)-6-(methoxycarbonyl)pyridin-2-yl)but-3-yn-1-yl)piperazine-1-carboxylate (564 mg, 1.18 mmol, 28%) as an orange oil.

TLC R_f 0.32 (EtOAc, SiO_2)

^{1}HNMR (400MHz, $CDCl_3$) δ 7.68-7.29 (m, 7H, Ar**H**), 5.19 (s, 2H, Ph**CH$_2$**), 3.94 (s, 3H, CO_2**CH$_3$**), 3.42 (t, *J*=7.9 Hz, 2H, N**CH$_2$**CH_2CC), 2.71-2.38 (m, 6H, BocN(**CH$_2$**)$_2$,NCH_2**CH$_2$**CC), 2.05 (br. s, 4H, (**CH$_2$**)$_2$$NCH_2CC$), 1.39 (s, 9H, C(**CH$_3$**)$_3$) ppm

^{13}CNMR (101 MHz, $CDCl_3$) δ 170.1 (**15**), 153.0 (**3**), 135.5 (**13**), 132.2 (**18**), 132.0 (**14**), 131.9 (**10**), 129.9 (**19**), 128.8 (**11**), 128.6 (**21**), 128.4 (**20**), 128.3 (**12**), 126.9 (**2**), 121.8 (**9**), 88.2 (**8**), 80.1 (**17**), 70.9 (**6**), 60.4 (**5**), 56.8 (**16**), 52.7 (**4**), 52.6 (**7**), 28.4 (**1**) ppm

IR (neat) ν_{max} 2974 (m), 2814 (m), 2232 (s), 1687 (s), 741 (s) cm^{-1}

LRMS (ESI$^+$) *m/z* 480.4 $[M+H]^+$

HRMS (ESI$^+$) *m/z calcd. for* $C_{27}H_{34}N_3O_5^+$ 480.2493 *m/z meas.* 480.2493 $[M+H]^+$

***Tert*-butyl 4-(4-(5-hydroxy-6-(methoxycarbonyl)pyridin-2-yl)butyl)piperazine-1-carboxylate (3.113)**

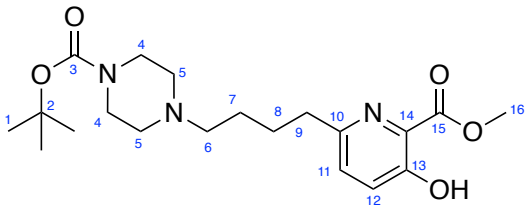

Mol. Wt. 393.2

$C_{20}H_{31}N_3O_5$

Following a procedure adapted from de Sousa,[186] to a degassed suspension of *tert*-butyl 4-(4-(5-(benzyloxy)-6-(methoxycarbonyl)pyridin-2-yl)but-3-yn-1-yl)piperazine-1-carboxylate (500 mg, 1.04 mmol, 1 equiv.) in anhydrous MeOH (20 mL), was added Pearlman's catalyst (146 mg, 1.04 mmol, 1 equiv.). The reaction vessel was evacuated and flushed with hydrogen gas five times. The black reaction mixture was stirred for 18 h at rt. The catalyst was removed by filtration through Celite and the solvent was removed *in vacuo*. The residue was purified by column chromatography (SiO_2, EtOAc) to afford *tert*-butyl 4-(4-(5-hydroxy-6-(methoxycarbonyl)pyridin-2-yl)butyl)piperazine-1-carboxylate (310 mg, 0.79 mmol, 76%) as a yellow oil.

TLC R_f 0.08 (EtOAc, SiO_2)

^{1}HNMR (400MHz, $CDCl_3$) δ 10.61 (s, 1H, **OH**), 7.35-7.29 (m, 2H, Ar**H**), 4.06 (s, 3H, $CO_2\mathbf{CH_3}$), 3.44 (t, *J*=5.1 Hz, 4H, BocN($\mathbf{CH_2}$)$_2$), 2.83 (t, *J*=7.6 Hz, 2H, N$\mathbf{CH_2}$$CH_2CH_2CH_2$), 2.41-2.34 (m, 6H, ($\mathbf{CH_2}$)$_2$$NCH_2CC$, $NCH_2CH_2CH_2\mathbf{CH_2}$), 1.80-1.68 (m, 2H, $NCH_2\mathbf{CH_2}CH_2CH_2$), 1.63-1.51 (m, 2H, $NCH_2CH_2\mathbf{CH_2}CH_2$), 1.48 (s, 9H, C($\mathbf{CH_3}$)$_3$) ppm

^{13}CNMR (101 MHz, $CDCl_3$) δ 170.2 (**15**), 157.2 (**3**), 154.8 (**13**), 153.8 (**14**), 129.1 (**11**), 128.8 (**10**), 126.7 (**12**), 79.6 (**2**), 58.5 (**4**), 53.2 (**5**), 53.1 (**16**), 37.5 (**6**), 30.9 (**7**), 28.4 (**9**), 27.9 (**8**), 26.4 (**1**) ppm

IR (neat) ν_{max} 3161 (m), 2932 (m), 2808 (m), 1689 (s), 1166 (s) cm^{-1}

LRMS (ESI$^+$) *m/z* 394.4 $[M+H]^+$

HRMS (ESI$^+$) *m/z calcd. for* $C_{20}H_{32}N_3O_5^+$ 394.2336 *m/z meas.* 394.2340 $[M+H]^+$

***Tert*-butyl (*E*)-4-(4-(5-hydroxy-6-((hydroxyimino)methyl)pyridin-2-yl)butyl)piperazine-1-carboxylate (3.114)**

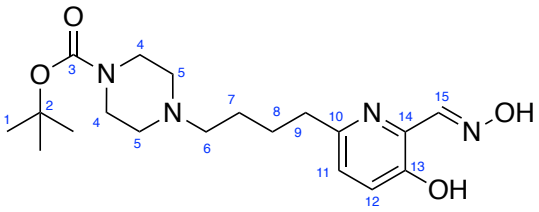

Mol. Wt. 378.2

$C_{19}H_{30}N_4O_4$

Following a procedure adapted from de Sousa,[186] to a solution of *tert*-butyl 4-(4-(5-hydroxy-6-(methoxycarbonyl)pyridin-2-yl)butyl)piperazine-1-carboxylate (200 mg, 0.51 mmol, 1 equiv.) in anhydrous CH_2Cl_2 (5 mL), was added 2,6-lutidine (0.18 mL, 1.52 mmol, 3 equiv.) and TBSOTf (0.23 mL, 1.02 mmol, 2 equiv.), and the yellow solution was stirred at rt, under an Ar atmosphere for 5 h. The solvent was removed *in vacuo*, and the crude ester was taken up in anhydrous CH_2Cl_2 (5 mL), then cooled to –78 °C. DIBAL-H (1.0 M in CH_2Cl_2, 1.53 mL, 1.52 mmol, 3 equiv.) was added dropwise and the reaction was stirred at –78 °C for 1 h. MeOH (5 mL) was added and the reaction mixture was allowed to warm to rt. The solvent was removed *in vacuo*, CH_2Cl_2 (35 mL) was added, and the white aluminium salts were removed by filtration. The filtrate was concentrated *in vacuo* and anhydrous EtOH (10 mL), NH_2OH•HCl (71 mg, 1.02 mmol, 2 equiv.) and NaOAc (83 mg, 1.02 mmol, 2 equiv.) were added. The yellow reaction solution was heated to reflux for 18 h and upon cooling to rt, the solvent was removed *in vacuo* to afford *tert*-butyl (*E*)-4-(4-(5-hydroxy-6-((hydroxyimino)methyl)pyridin-2-yl)butyl)piperazine-1-carboxylate (38 mg, 0.10 mmol, 20%) as an orange solid.

Tert-butyl (*E*)-4-(4-(5-hydroxy-6-((hydroxyimino)methyl)pyridin-2-yl)butyl)piperazine-1-carboxylate (10 mg, 0.03 mmol) was dissolved in 2 M HCl (3 mL). The orange solution was stirred at rt for 10 mins. The reaction solution was concentrated *in vacuo* to afford *tert*-butyl (*E*)-4-(4-(5-hydroxy-6-((hydroxyimino)methyl)pyridin-2-yl)butyl)piperazine-1-carboxylate hydrochloride (12.4 mg, 0.03 mmol, 100%) as a pale orange solid.

TLC R_f 0.15 (EtOAc, SiO_2)

^{1}HNMR (400MHz, MeOD-d_4) δ 8.30 (s, 1H, **CH**NOH), 7.30 (d, *J*=8.5 Hz, 1H, NCCH**CH**), 7.19 (d, *J*=8.5 Hz, 1H, NC**CH**CH), 3.33 (d, *J*=3.3 Hz, 4H, BocN(**CH$_2$**)$_2$), 2.77 (t, *J*=7.5 Hz, 2H, N**CH$_2$**CH$_2$CH$_2$CH$_2$), 2.56-2.43 (m, 6H, (**CH$_2$**)$_2$NCH$_2$CC, NCH$_2$CH$_2$CH$_2$**CH$_2$**), 1.79-1.68 (m, 2H, NCH$_2$**CH$_2$**CH$_2$CH$_2$), 1.65-1.53 (m, 2H, NCH$_2$CH$_2$**CH$_2$**CH$_2$), 1.47 (s, 9H, C(**CH$_3$**)$_3$) ppm

^{13}CNMR (101 MHz, MeOD-d_4) δ 154.9 (**3**), 153.0 (**13**), 152.4 (**14**), 151.4 (**15**), 134.9

(**10**), 124.6 (**11**), 124.0 (**12**), 80.0 (**2**), 57.8 (**6**), 52.4 (**5**), 52.2 (**4**), 36.1 (**9**), 27.5 (**7**), 27.2 (**1**), 25.3 (**8**) ppm

IR (neat) ν_{max} 3490 (b), 2974 (m), 2951 (m), 2863 (m), 1700 (s), 1166 (s) cm^{-1}

LRMS (ESI$^+$) *m/z* 379.4 $[M+H]^+$

HRMS (ESI$^+$) *m/z calcd. for* $C_{19}H_{31}N_4O_4^+$ 379.2340 *m/z meas.* 379.2341 $[M+H]^+$

MPt 130-131 °C

[1] G. A. Petroianu *et al.*, *Die Pharmazie* 2009, **64**, 269-275

[2] J. Pelouze *et al.*, *J. Chim. Med. Pharm. Toxicol*. 1833, **9**, 129-147

[3] F. Voegeli *et al.*, *Ann. Physik. Chem.* 1848, **75**, 282-319

[4] J. L. de Bleecker *et al.*, *Clin. Neurol. Neurosurg.* 1992, **94**, 93-103

[5] W. Lange *et al.*, *Ber. Dtsch. Chem. Ges.* 1932, **65**, 1598-1601

[6] B. Holmstedt, in *On Cholinesterases and Anticholinesterase Agents*, Springer, 1963, pp. 428-485

[7] J. Timbrell, in *Introduction to Toxicology*, CRC Press, 2002, pp. 90

[8] M. W. Aktar *et al.*, *Interdiscip. Toxicol.* 2009, **2**, 1-12

[9] C. D. S. Tomlin, in *The Pesticide Manual: A World* Compendium, British Crop Protection Council, Hampshire, UK, 13 edn, 2003, pp. 1344

[10] C. Karunakaran *et al.*, *J. Indian Med. Assoc.* 1958, **31**, 204-207

[11] W. H. Rodgers *et al.*, *Colum. L. Rev.* 1970, **70**, 567-611

[12] E. Marquez *et al.*, *Salud Púb. Méx.* 1968, **10**, 293-300

[13] A. Wishahi *et al.*, *Arch. Pediatr.* 1958, **75**, 387

[14] A. Wiercinski *et al.*, in *Nerve Agents*, 2018, StatPearl Publishing, Florida, US

[15] J. Jeyaratnam *et al.*, *Br. J. Ind. Med.* 1985, **42**, 505

[16] T. Stock *et al.*, in *The Challenge of Old Chemical Munitions and Toxic Armament Wastes,* 1997*,* vol. 16, Oxford University Press on Demand, Oxford, UK, ch. 2, pp. 15-34

[17] S. M. Somani, in *Chemical Warfare Agents*, Academic Press, London, UK, 1992, pp. 71

[18] F. Schmaltz *et al.*, *J. Hist. Neurosci.* 2006, **15**, 186-209

[19] G. Reiter *et al.*, *J. Chromatogr. B.* 2007, **859**, 9-15

[20] U. Ivarsson *et al.*, in *A FOA Briefing Book on Chemical Weapons: Threat, Effects and Protection*, Forsvarets Forskningsanstalt, 1992

[21] J. Misik *et al.*, *Drug Chem. Toxicol.* 2015, **38**, 32-36.

[22] M. Pianka *et al.*, *J. Soc. Chem. Ind.* 1955, **5**, 109-120

[23] M. J. A. Joosen *et al.*, *Chem. Biol. Interact.* 2017**, 267**, 48-56

[24] J. B. Tucker, War of Nerves: Chemical Warfare from World War I to Al-Qaeda, Anchor, New York, 2007

[25] J. Borkin, in *The Crime and Punishment of I.G. Farben*, The Free Press, New York, US, 1978

[26] F. Rajaee, *The Iran-Iraq War: The Politics of Aggression*, University Press of Florida, Florida, US, 1993

[27] C. Macilwain *et al.*, *Nature* 1993, **363**, 3

[28] A. A. Alwaely *et al.*, *Int. J. Sci. Eng. Res.* 2015, **6**, 40-44

[29] T. Nakajima *et al.*, *Occup. Environ. Med.* 1997, **54**, 697-701

[30] H. Okudera *et al.*, *J. Clin. Neurosci.* 2002, **9**, 17-21

[31] K. Yokoyama *et al.*, *Neurotoxicol.* 2007, **28**, 364-373

[32] T. Okumura *et al.*, *Ann. Emerg. Med.* 1996, **28**, 129-135

[33] R. Pita *et al.*, *Toxics* 2014, **2**, 391-402

[34] E. Dolgin *et al.*, *Nat. Med.* 2013, **19**, 1194-1195

[35] BBC News Website, https://www.bbc.co.uk/news/world-asia-38971655, (accessed: November 2018)

[36] BBC News Website, https://www.bbc.co.uk/news/uk-43315636, (accessed: November 2018)

[37] BBC News Website, https://www.bbc.co.uk/news/uk-43506232, (accessed: November 2018)

[38] V. S. Mirzayanov, in State Secrets: An Insider's Chronicle of the Russian Chemical Weapons Program, Outskirts Press, US, 2008

[39] BBC News Website, https://www.bbc.co.uk/news/uk-44721558, (accessed: November 2018)

[40] K. Coleman, in *A History of Chemical Warfare*, Palgrave, New York, US, 2005

[41] R. Thakur, in *The Chemical Weapons Convention: Implementation, Challenges, Opportunities*, United Nations University Press, Tokyo, Japan, 2006

[42] OPCW Website, https://www.opcw.org/news-publications/publications/facts-and-figures, (accessed: November 2018)

[43] J. E. Casida *et al.*, *Chem. Biol. Interact.* 2005, **157–158**, 277-283.

[44] E. Giacobini, in Cholinesterases and Cholinesterase Inhibitors: Basic Preclinical and Clinical Aspects, Martin Dunitz Ltd., London, UK, 2000

[45] D. M. Quinn *et al.*, *Chem. Rev.* 1987, **87**, 955-979

[46] E. S. Valenstein *et al.*, *Brain Cogn.* 2002, **49**, 73-95

[47] D. Grisaru *et al.*, *Eu. J. Biochem.* 1999, **264**, 672-686

[48] P. Allderdice *et al.*, *Genomics* 1991, **11**, 452-454

[49] A. Saxena *et al.*, *Biochem.* 1997, **36**, 14642-14651

[50] D. C. Vellom *et al.*, *Biochemistry* 1993, **32**, 12-17

[51] P. Masson *et al.*, *Protein Pept. Letts.* 2009, **16**, 1215-1224

[52] Z. Kovarik *et al.*, *Chem. Biol. Interact.* 2010, **187**, 167-171

[53] P. Masson *et al.*, *Biochim. Biophys. Acta* 1998, **1387**, 41-52

[54] P. Masson *et al.*, *J. Neurochem.,* 2017, **142** (Suppl. 2), 26-40

[55] D. E. Lenz *et al.*, *Chem. Biol. Interact*., **157-158**, 205-210

[56] O. Lockridge *et al.*, *Pharmacol. Ther.*, **148**, 34-46

[57] A. Saxena *et al.*, *Process Biochem.*, **45**, 1313-1318

[58] T. Wille *et al., Arch. Toxicol.,* **91**, 1309-1318

[59] G. M. Simon *et al.*, *J. Biol. Chem.* 2010, **285**, 11051-11055

[60] P. Taylor *et al.*, *Annu. Rev. Pharmacol. Toxicol.* 1994, **34**, 281-320

[61] I. B. Wilson *et al.*, *Ann. N.Y. Acad. Sci.* 1966, **135**, 177-183

[62] M. Schumacher *et al.*, *Nature* 1986, **319**, 407-409

[63] H. Soreq *et al.*, *PNAS* 1990, **87**, 9688-9692

[64] J. L. Sussman *et al.*, *Science* 1991, **253**, 872-879

[65] D. Nachmansohn *et al.*, *Adv. Enzymol. Relat. Subj. Biochem.* 1951, **12**, 259-339.

[66] P. Taylor *et al.*, *Biochemistry* 1975, **14**, 1989-1997

[67] Y. Bourne *et al.*, *EMBO J.* 2003, **22**, 1-12

[68] T. L. Rosenberry *et al.*, Chem. *Biol. Interact.* 2005, **157–158**, 181-189.

[69] D. Barak *et al.*, *Biochemistry* 1995, **34**, 15444-15452

[70] P. H. Axelsen *et al.*, *Protein Sci.* 1994, **3**, 188-197

[71] J. P. Colletier *et al., EMBO J.* 2006, **25**, 2746-2756

[72] M. Harel *et al.*, *JACS* 1996, **118**, 2340-2346

[73] L. Pezzementi *et al.*, *PLoS ONE* 2011, **6**, e17396

[74] P. Masson *et al.*, *Arch. Biochem. Biophys.* 2010, **494**, 107

[75] B. Holmstedt *et al.*, *Pharmacol. Rev.* 1959, **11**, 567-688

[76] M. Jokanović *et al.*, *Toxicology* 2001, **166**, 139-160

[77] J. A. Vale *et al.*, *Toxicol. Letts.* 1998, **102–103**, 649-652

[78] M. Jokanovic *et al.*, *Curr. Med. Chem.* 2009, **16**, 2177-2188

[79] H. Benschop *et al.*, *Biochim. Biophys. Acta* 1966, **128**, 586-588

[80] G. S. Sirin *et al.*, *J. Phys. Chem. B* 2012, **116**, 12199-12207

[81] F. Worek *et al.*, *Toxicology* 2008, **244**, 35-41

[82] J. V. Peter *et al.*, *Indian J. Crit. Care Med.* 2014, **18**, 735-745

[83] R. S. Wadia *et al.*, *J. Neurol. Neurosurg. Psychiatry* 1974, **37**, 841-847

[84] D. Grob *et al.*, *J. Clin. Invest.* 1958, **37**, 350-368

[85] T. Namba *et al.*, *Am. J. Med.* 1971, **50**, 475-492

[86] B. Holmstedt *et al.*, *Pharmacol. Rev.* 1959, **11**, 567-688

[87] S. Mohapatra *et al.*, *J. Neurosci. Rural Pract.* 2014, **5**, S86-S87

[88] B. H. Hsieh *et al.*, *Neurotoxicology* 2001, **22**, 423-427

[89] C.-C. Yang *et al., J. Chinese Med. Assoc.* 2007, **70**, 467-472

[90] F. Worek *et al.*, *Biochem. Pharmacol.* 2004, **68**, 2237-2248

[91] G.B. Koelle, in *Cholinesterases and Anticholinesterase Agents*, Springer-Verlag, Berlin, Germany, 1963

[92] F. Worek *et al., Toxicol. Appl. Pharmacol.,* 2007, **219**, 226

[93] F. Worek *et al.*, *Biochem. Pharmacol.* 2007, **73**, 1807-1817

[94] C.-T. Su *et al.*, *Toxicol. Sci.* 1986, **6**, 506-514

[95] Y. Ren *et al.*, *J. Org. Chem.,* 2007, **72**, 5660-5667

[96] C. M. Timperley *et al., J. Fluor. Chem.,* 2011, **132**, 541-547

[97] I. B. Wilson *et al.*, *J. Biol. Chem.* 1951, **190**, 111-117

[98] G. A. Petroianu *et al.*, *Die Pharmazie* 2012, **67**, 874-879

[99] I. B. Wilson *et al.*, *Biochim. Biophys. Acta* 1955, **18**, 168-170

[100] D. Nachmansohn *et al.*, US Pat., 2 816 113, 1957

[101] R. K. Plumb, in *New York Times*, New York, 1958, pp. 31

[102] T. A. Alston *et al.*, *Anesth. Analg.* 2005, **101**, 926

[103] I. B. Wilson *et al.*, *Biochem. Pharmacol.* 1959, **1**, 200-206

[104] F. Hobbiger *et al.*, *Nature* 1958, **182**, 1672-1673

[105] R. Sharma *et al.*, *Mini-Rev. Med. Chem.* 2015, **15**, 58-72

[106] J. G. Clement *et al.*, *Toxicol. Sci.* 1981, **1**, 193-202

[107] M. Jokanović *et al.*, *Arch. Toxicol.* 1995, **70**, 119-123

[108] A. Luttringhaus *et al.*, *Forsch.* 1964, **14**, 1

[109] D. Malinak *et al.*, *Curr. Org. Chem.* 2018**, 22**, 1619-1648

[110] F. Hobbiger *et al.*, *Biochem. Pharmacol.* 1966, **15**, 1677-1690

[111] T. C. Marrs *et al.*, Adverse Drug React. Toxicol. Rev. 1990, **10**, 61-73

[112] M.P. Stojiljković *et al.*, *Arh. Hig. Rada Toksikol.* 2006, **57**, 435-443

[113] H. Oldiges *et al.*, *Arch. Toxikolog.* 1970, **26**, 293-305

[114] M. Maksimovic *et al.*, *Acta Pharm. Jugoslav* 1980, **30**, 151-160

[115] R. H. Inns *et al.*, *J. Pharm. Pharmacol.* 1983, **35**, 427-433

[116] J. G. Clement *et al.*, *Biochem. Pharmacol.* 1982, **31**, 1283-1287

[117] S. Ćetković *et al.*, *Fundam. Appl. Toxicol.* 1984, **4**, S116-S123

[118] P. M. Lundy *et al.*, *Toxicology* 2005, **208**, 399-409

[119] M. Löffler, PhD Thesis, Univerity of Freiburg, 1986

[120] L. P. de Jong *et al.*, *Biochem. Pharmacol.* 1989, **38**, 633-640

[121] F. Worek *et al.*, *Toxicology* 1995, **95**, 123-133

[122] P. M. Lundy *et al.*, *Toxicology* 1992, **72**, 99-105

[123] F. Worek *et al.*, *Arch. Toxicol.* 1994, **68**, 231-239

[124] F. Worek *et al.*, *Pharmacol. Toxicol.* 1994, **75**, 302-309

[125] P. Alberts *et al.*, *Eu. J. Pharmacol.* 1990, **184**, 191-194

[126] J. Kassa *et al.*, *Mini-Rev. Med. Chem.* 2012, **12**, 24-34

[127] K. Kuca *et al.*, *Basic Clin. Pharmacol. Toxicol.* 2006, **98**, 389-394

[128] J. Cabal *et al., Basic Clin. Pharmacol. Toxicol.* 2004, **95**, 81-86

[129] K. Kuca *et al.*, *Clin. Toxicol.* 2007, **45**, 512-515

[130] F. Worek *et al.*, *Pharmacol. Ther.* 2013, **139**, 249-259

[131] C. Luo *et al.*, *Chem. Biol. Interact.* 2010, **187**, 185-190

[132] F. Worek *et al.*, *Biochem. Pharmacol.* 2012, **83**, 1700-1706

[133] C. Luo *et al.*, *Biochemistry* 2007, **46**, 11771-11779

[134] H. Ohta *et al.*, *Pharm. Res.* 2006, **23**, 2827-2833

[135] S. Okuno *et al.*, *Toxicol. Appl. Pharmacol.* 2008, **227**, 8-15

[136] K. Musilek *et al., Bioorg. Med. Chem.* 2011, **19**, 754-762

[137] J. Acharya *et al., Med. Chem. Res.* 2013, **22**, 1277-1286

[138] K. Musilek *et al., Bioorg. Med. Chem. Lett.* 2006, **16**, 5673-5676

[139] J. Cabal *et al.*, *Basic Clin. Pharmacol. Toxicol.* 2004, **95**, 81-86.

[140] K. Musilek *et al.*, *Bioorg. Med. Chem.* 2011, **19**, 754-762

[141] J. Acharya *et al.*, *Toxicol. in Vitro* 2008, **22**, 525-530.

[142] K. Musilek *et al.*, *J. Med. Chem.* 2007, **50**, 5514-5518

[143] E. Artursson *et al., Toxicology* 2009, **265**, 108-114

[144] K. Kuca et al., BMC Pharmacol. Toxicol. 2018, **19**, 8-18

[145] K. Musilek *et al.*, *J. Enzyme Inhib. Med. Chem.* 2005, **20**, 409-415

[146] A. Hörnberg *et al.*, *Biochem. Pharmacol.* 2010, **79**, 507-515

[147] T. C. Marrs *et al.*, *Toxicol. Rev.* 2003, **22**, 75-81

[148] J. Bajgar *et al.*, *Mini-Rev. Med. Chem.* 2007, **7**, 461-466

[149] M. Jokanović *et al.*, *Eu. J. Pharmacol.* 2006, **553**, 10-17

[150] M. Eddleston *et al.*, *Lancet*, 2007, **371**, 597-607

[151] D. D. Johnson *et al.*, *Can. J. Physiol. Pharmacol.* 1970, **48**, 625-630

[152] F. R. Sidell *et al.*, in *Medical Aspects of Chemical and Biological Warfare*, The Office of the Surgeon General, Washington DC, US, 1997

[153] M. Murphy *et al.*, *Aviat. Space Environ. Med.* 1993, **64**, 110-115

[154] E. W. Dickson *et al.*, *Acad. Emerg. Med.* 2003, **10**, 1303-1306

[155] F. Worek *et al.*, *Biochem. Pharmacol.* 2007, **73**, 1807-1817

[156] Z. Wei *et al.*, *Toxicol. Lett.* 2016, **246**, 1-6

[157] J. Korabecny *et al.*, *Mini-Rev. Med. Chem.* 2014, **14**, 215-221

[158] K. L. Kirk *et al.*, *J. Fluorine Chem.* 2006, **127**, 1013-1029

[159] H. C. Jeong *et al.*, *Bioorg. Med. Chem. Lett.* 2009, **19**, 1214-1217

[160] E. S. Rachaman *et al.*, *Arzneimittelforsch. Drug Res.* 1976, **29**, 875-876

[161] E. Heldman *et al.*, *Carbohydr. Res.* 1986, **151**, 337-347

[162] G. E. Garcia *et al.*, *Chem. Biol. Interact.* 2010, **187**, 199-206

[163] M. V. Rajapurkar *et al.*, *J. Pharmacol. Exp. Ther.* 1958, **123**, 247-253

[164] T.-M. Shih *et al.*, *Adv. Stud. Biol.* 2009, **1**, 155-196

[165] J. W. Skovira *et al.*, *Chem. Biol. Interact.* 2010, **187**, 318-324

[166] G. Saint-André *et al.*, *Tetrahedron* 2011, **67**, 6352-6361.

[167] Y. Ashani *et al.*, *J. Med. Chem.,* 1971, **14**, 621-626

[168] M. C. de Koning *et al.*, *Toxicol. Lett.* 2011, **206**, 54-59.

[169] M. C. de Koning *et al.*, *Bioorg. Med. Chem.* 2011, **19**, 588-594

[170] W. G. Lewis *et al.*, *Angew. Chem. Int. Ed.* 2002, **41**, 1053-1057

[171] M. Kilachyna *et al.*, *Eu. J. Med. Chem.,* 2014, **78**, 455-467

[172] P-Y. Renard *et al., Chem. Commun.,* 2014, **50**, 3947

[173] N. Bodor *et al.*, *J. Med. Chem.* 1976, **19**, 102-107

[174] J. J. Marty *et al.*, *Pharm. Acta Helv.* 1978, **53**, 17-23

[175] K. Langer *et al.*, *Int. J. Pharm.* 2003, **257**, 169-180

[176] A. M. Cook *et al.*, *Pharmacotherapy* 2009, **29**, 832-845

[177] K. Hynynen *et al.*, *NeuroImage* 2005, **24**, 12-20

[178] W. G. Bradley *et al.*, *J. Am. Coll. Radiol.* 2009, **6**, 510-513

[179] F. S. Katz *et al.*, *ChemBioChem*, 2015, **16**, 2205-2215

[180] K. A. Neftel *et al.*, *Br. Med. J*., 1986, **292**, 721-723

[181] M.C. de Koning *et al.*, *Eu. J. Med. Chem.* 2018, **157**, 151-160

[182] C.L. Cadieux *et al.*, *Chem. Biol. Interact.* 2016, **259**, 133-141

[183] F.S. Katz *et al.*, *Chem. Bio. Chem*. 2015, **16**, 2205-2215

[184] P-Y. Renard *et al.*, *Chem. Eu. J.* 2018, **24**, 9675-9691

[185] Y-S. Jung *et al.*, *Bioorg. Med. Chem. Letts.,* 2018, **28**, 3784-3786

[186] J. de Sousa, PhD Thesis, Université de Strasbourg and University of Southampton, 2015

[187] F. Nachon *et al*, *J. Med. Chem.* 2018, **61**, 7630-7639

[188] J. de Sousa *et al.*, *Eu. J. Org. Chem* 2014, **16**, 3468-3474

[189] H. Miyamoto *et al.*, *Org. Process Res. Dev.* 2015, **19**, 1054-106

[190] S. E. Denmark *et al.*, *J. Am. Chem. Soc.,* 2004, **126**, 12432-12440

[191] G. A. Patani *et al.*, *Chem. Rev.,* 1996, **96**, 3147-3176

[192] A. Narender *et al.*, *J. Chil. Chem. Soc.* 2009, **54**, 473-474

[193] P-Y. Renard *et al.*, *Chem. Bio. Interact.* 2013, **203**, 81-84

[194] G. Prance *et al.* in *The Cultural History of Plants*, Routledge, New York, US, 2004

[195] N. Niemenak *et al.*, *S Afr. J. Bot.* 2008, **74**, 629-638

[196] D. Nachmansohn *et al., J. Biol. Chem.* 1945, **159**, 239-240

[197] O. Mitsunobu, *Synthesis*, 1981, 1

[198] K. C. Kumara Swamy *et al.*, *Chem. Rev.*, 2009, **109**, 2551-2651

[199] S. Fletcher *et al.*, *Org. Chem. Front.,* 2015, **2**, 739

[200] G. Kortum *et al.*, in Dissociation Constants of Organic Acids in Aqueous Solution, Butterworths, London, UK, 1961

[201] D. M. Wilhite *et al.*, *Bielstein J. Org. Chem.* 2006, **2**, 21

[202] T. Tsunoda *et al.*, *Tetrahedron Lett.* 1995, **36**, 2531-2534

[203] J-A. García-López *et al.*, *Chem. Soc. Rev.* 2016, **45**, 6766-6798

[204] D. Seyfirth *et al.*, *J. Org. Chem.*, 1971, **36**, 1379-1386

[205] J. M. J. Williams *et al.*, *Adv. Synth. Catal.* 2007, **349**, 1555-1575

[206] J. M. J. Williams *et al.*, *Dalton Trans.* 2009, **5**, 753-762

[207] M. J. Krische *et al.*, *Angew. Chem. Int. Ed.* 2009, **48**, 34-46

[208] Y Wanatabe *et al.*, *J. Org. Chem.* 1984, **49**, 3359-3363

[209] M. H. S. A. Hamid *et al.*, *J. Am. Chem. Soc.* 2009, **131**, 1766-1774

[210] N. Yoshikai *et al.*, *Org. Lett.* 2012, **14**, 5488-5491

[211] F. Couty *et al.*, *J. Org. Chem.* 2016, **81**, 2899-2910

[212] F. Couty *et al.*, *Chem. Commun.* 2016, **52**, 10072-10075

[213] A. Mohammadi-Farani *et al.*, *DARU J. Pharm. Sci.* 2013, **21**, 47-56

[214] *G.* Wágner *et al., Bioorg. Med. Chem. Lett. 2010*, **20**, 3737–3741

[215] W. Lui *et al.*, *Bioorg. Med. Chem. Lett.* 2017, **27**, 5046-5052

[216] M-T. Wu et al., Fundam. Appl. Toxicol., 1986, **6**, 506-514

[217] J. F. O'Leary *et al., J. Pharmacol. Exp. Ther.,* 1961, **132**, 50-57

[218] O. L. Wolthius *et al.*, *Biochem. Pharmacol.,* 1967, **16**, 361-367

[219] B. Harvey *et al., Biochem. Pharmacol.,* 1984, **33**, 3499-3501

[220] P. H. Stahl, in *Handbook of Pharmaceutical Salts*, Wiley-VCH, Weinheim, Germany, 2002

[221] T. S. Wiedmann *et al.*, *Asian J. Pharm. Sci.,* 2016, **11**, 722-734

[222] H. J. Galla *et al., J. Drug Target.,* 2002, **10**, 263-276

[223] P. Artursson *et al.*, *Nat. Protoc.,* 2007*,* **2**, 2111-2119

[224] A. Wagner *et al., Tetrahedron,* 2011, **67**, 6352-6361

[225] J. A. McCammon *et al.*, *Nature* 1977, **117**, S179-S197

[226] J. D. Durrant *et al.*, *BMC Biol.* 2011, **9**, 71-80

[227] W. D. Cornell *et al.*, *J. Am. Chem. Soc.* 1995, **117**, 5179-5197

[228] R. D. Skeel *et al.*, *BIT Num. Maths.,* 1993, **33**, 172-175

[229] Adapted scripts originally written by R. Bradshaw, University of Southampton

[230] F. Nachon *et al., J. Am. Chem. Soc.,* 2008, **130**, 16011-16020

[231] L. Louise-Leriche *et al.*, *Chem. Eu. J.* 2010, **16**, 3510-3523

[232] S. Dharmarajan *et al., Eu. J. Med. Chem.*, 2015, **103**, 1-16

[233] Margolis. B. J. *et al.*, *J. Org. Chem.,* 2007, **72**, 2232-2235

[234] S. G. Franzblau *et al.*, *J. Med. Chem.*, 2009, **52**, 6966-6978

[235] Y-G. Xu *et al., Eu. J. Med. Chem.,* 2014, **84**, 698-707

[236] C. C. Musonda *et al.*, *Bioorg. Med. Chem. Letts.*, 2007, **17**, 4733-4736

[237] Winkler *et al.*, *J. Am. Chem. Soc.,* 2002, **124**, 9726-9728

[238] K. Wang *et al.*, Synth. Communs. 2009, **40**, 144-150.

[239] Y. Li *et al., Angew. Chim. Int. Ed.,* 2016, **55**, 1020-1024

[240] R. H. Bahekar *et al.*, *Bioorg. Med. Chem*., 2007, **15**, 3248-3265

[241] Y. Chun-Hsu *et al., Eur. J. Med. Chem.,* 2012, **55**, 32-37

[242] F. Glorius *et al., Angew. Chim. Int. Ed.,* 2011, **50**, 4983-4987

[243] N. K. Garg *et al., J. Am. Chem. Soc.,* 2009, **131**, 17748-17749

[244] J. Zhong-Xing *et al., Med. Chem. Commun.,* 2016, **7**, 1672-1680

[245] M. Brondsted *et al., J. Org. Chem.,* 2011, **76**, 245-263

[246] H. Yamanaka *et al. Synthesis,* 1983*,* **4**, 312-314

[247] P. D. Jarowski *et al., Angew. Chim. Int. Ed.,* 2015, **127**, 8060-8064

[248] Q. Zhou *et al., Angew. Chim. Int. Ed.,* 2018, **57**, 11146-11150

[249] T-P. Loh *et al., Angew. Chim. Int. Ed.,* 2014, **53**, 7491-7494

[250] Y. Lam *et al., Chem. Eur. J.,* 2012, **18**, 1476

[251] J. C. V. P. Moura *et al., Tett. Letts.,* 2005, **46**, 4949-4952

[252] R. Liliana *et al., Synlett,* 2009, **5**, 751-754

[253] G. P. Marples *et al., J. Chem. Soc. Perkin Trans. 1*, 1988, 3399-3406

[254] J. J. Bozell *et al., Org. Letts.,* 2013, **15**, 2730-2733

[255] R. C. D. Brown *et al., Org. Letts.,* 2017, **19**, 2050-2053

[256] R. Larouche-Gauthier *et al., J. Org. Chem.,* 2012, **77**, 3215-3221

[257] A. Guarna *et al., J. Med. Chem.,* 2010, **53**, 7119-7128

[258] C. M. Dambacher *et al.*, Wo. Pat., 184 996, 2017